Biological Evaluation of Synergistic Drug Combinations, Design and Synthesis of Potent and Selective PI3K Inhibitors and the Design of Bifunctional Ligands Incorporating Pictilisib & Ceritinib for the Treatment of EML4-ALK Positive Lung Cancer

Aimie Elizabeth Garces

MSci (Hons)

Thesis submitted to the University of Nottingham
for the degree of Doctor of Philosophy

April 2019

Acknowledgements

There are so many people to acknowledge it is difficult to know where to begin! Firstly, I would like to thank and acknowledge my family, for without their love and support I would not have had the strong foundations built during my early years to have made it this far. For as long as I can remember they have always been there for me, encouraging me to do my best. I would like to thank my grandparents, Alan and Joyce, who feature in my earliest memories, which were of playing at their house: usually Tiddly winks and Snakes & Ladders with Grandad, or playing shop with Gran, after she had kept all the empty packaging to make a pretend shop. Their house is the family base and they are the solid rock and foundation of the family. I would also like to thank my Stepdad, Joe, who has always encouraged me to be my best and reach further; whenever I came home with my school report he would recognise my achievements, but would always remind me that I could reach further. I would like to thank my husband, David, who always supports me through the tough times ; including unsuccessful experiments or thesis writing, when I may not have been in the best of moods! I would also like to acknowledge my dad, Peter, who passed away of metastatic throat cancer during my PhD. One of the last things he was able to tell me was that he was proud of me, and I'm sure he would be proud that I have completed this thesis. Lastly, but most certainly the most important, I cannot possibly give enough thanks and acknowledgement to my Mum, Margaret. She is the strongest and most determined woman on the planet and her outlook on life and rationality is what has made me who I am today. Her ability to tackle real problems head-on and her resilience have taught me so much, and the example she has set has given me the tools to navigate life. I cannot thank her enough for this, and for all the love and encouragement she gives me.

Next I would like to thank the friends, who know who they are, who have helped guide and shape me into who I am, and where I have got to. In particular Karrie Hennessey, who when I was deciding which university to attend, convinced me that The University of Nottingham was the place for me - she was right! Guillaume Gimond,

who always is there to give his support. Andrew Valentine, who has been with me for the whole university journey, and for taking good photos. Eleonora Comeo for always making my day a happy one. Dr. Fadi Soukarieh for his advice, particularly for molecular modelling, and his great sense of humour. Dr. Cristophe Fromont for looking after the LCMS and Dr. Divneet Kaur for her insightful conversations. Dr. Sean Conroy for teaching me how to use the HPLC. The C-floor staff and students who give the department its excellent community. Last but definitely not least, Dr. Nicholas Kindon who not only had taught me so much through his mentorship, but has also been there for me as friend. I've lost count how many times he has been there for me when I have received bad news, particularly during the times of my fathers suffering and my gran being diagnosed with Guillain-Barre syndrome. I cannot thank him enough for his emotional support, his friendship, and mentorship.

Next I would like to thank collaborators. Firstly, MSc students Inaki Pickering Montoya and Jiaxin Li, both of who are exceptional students and a pleasure to have bench supervised. Inaki and Jiaxin performed most of the MTT assays throughout this thesis under my supervision. Additionally, Jiaxin performed the clonogenic assays and flow cytometric assays in Chapter II, also under my supervision and direction. Their assistance is greatly acknowledged and appreciated. I cannot thank them enough and wish them all the best for there future endeavours. I would also like to thank Dr Mohammed Al-Hayali, for expert immunoblots. Mohammed performed the immunoblotting in chapter II. I would also like to thank Dr. Jong Bong Lee who assisted with the plasma and buffer stability studies of the prodrugs in chapter IV. I would also like to thank Dr James Rowedder for testing the PI3K compounds at GSK, and Prof. Simon MacDonald for his input. I would also like to thank Dr Huw Williams for assistance using the high field NMR spectrometers and teaching me how to analyse large datasets in TopSpin.

Next I would like to thank my supervisors. Firstly, Dr. Michael Stocks who is very approachable and always has an open door to discuss any issues. He is a fantastic mentor and often shares his knowledge gained from his many years experience. His help, support and advice for both academia and my career is greatly appreciated and I cannot

thank him enough for this. He always has good banter, and has an excellent sense of humour. It has been an honour to have been supervised by him. Next is Dr Tracey Bradshaw, who is not only is full of knowledge about her field, but is the kindest and most warm hearted person I know. She always has time to hear you out, and always has an open door for a chat. I cannot thank her enough for the emotional support and academic support throughout my PhD.

Next I would like to thank The University of Nottingham. I had always had trouble feeling like I belong somewhere until I came to university. Nottingham has become my home, all thanks to the atmosphere and sense of belonging I feel on campus. I am so grateful to everyone who makes the university feel this way - Thank you. I would also like to thank the university for enabling me to complete my PhD in a fantastic school, The School of Pharmacy. I would also like to thank the Medicines Research Council for the funding for my PhD, as well as funding to go on a conference trip to the ACS in San Franscisco.

Abstract

Lung cancer remains the leading cause of cancer death in the United Kingdom. Non-small cell lung cancer makes up the majority of all lung cancers, approximately 80-85%. Of these non-small cell lung cancers, 3-7% possess chromosomal rearrangements of anaplastic lymphoma kinase (ALK). These lead to constitutively active ALK fusion proteins such as the fusion of the echinoderm microtubule-associated protein-like 4 (EML4) and ALK genes to give the EML4-ALK fusion gene. This activates downstream signals of the Ras/Raf/MEK/ERK1/2, JAK/STAT and PI3K/AKT/mTOR pathways.

Chapter 1 gives an introduction into lung cancer, and, in particular, EML4-ALK positive lung cancer. The chapter explores the current FDA approved inhibitors (crizotinib, ceritinib, alectinib, and brigatinib) for the treatment of EML4-ALK positive lung cancer, and discusses that, although efficacious, resistance rapidly emerges. The mechanisms of resistance are discussed, where it is suggested that the use of up-front combination therapies is a strategy for overcoming resistance, where the benefit is the synergistic response of the combined therapy vs the response of the single agent. In addition, combination therapies targeting one or more signalling nodes suppress the survival and emergence of resistant tumour cells.

Chapter 2 goes on to explore 1:1 molar ratio combinations with ceritinib, one of the approved ALK inhibitors. Combinations were explored using an MTT cell viability assay against an isogenic pair of human lung carcinoma cell lines, A549 and A549 EML4-ALK+. Combinations include P2Y2, VEGFR, dual mTOR/PI3K, AKT, PI3K, and JAK inhibitors. It was seen that the pan PI3K inhibitor, pictilisib, exhibited excellent synergy with ceritinib, thus this combination was evaluated further. The combination of ceritinib and pictilisib was investigated using immunoblot analysis, where it was found that the combination perturbs the JAK/STAT pathway. Additionally, cell cycle analysis was used to examine the effects of pictilisib, ceritinib and their combination on

the cell cycle, where it was found that the combination induced G1 arrest. Clonogenic assays were performed on the combination, and it was seen that after 24 h exposure, there was no significant reduction in colonies. However, after 72 h exposure a significant reduction in colony formation was observed. An annexin-V FITC/PI apoptosis assay showed that after 72 h exposure neither ceritinib, pictilisib, nor their combination induce apoptosis, which is indicative of cytostasis.

Chapter 3 brings the focus towards PI3K inhibitors, due to the success of the pan PI3K inhibitor pictilisib in combination with ceritinib. The chapter provides an in-depth introduction to PI3K, and a review of the literature around the design and synthesis of selective inhibitors to the four Class I isoforms of PI3K (α, β, δ, and γ). Following this introduction, an array of PI3Kδ inhibitors with a thienopyrimidine core were designed and synthesised. The chemical synthesis of the series, the structure activity relationships and the physicochemical properties are discussed in detail. The highlight of the series is compound 3, a highly potent and highly selective PI3Kδ inhibitor, which was tested in combination with ceritinib by MTT cell viability assay. A further two series of benzothiazole containing inhibitors were designed and synthesised, where their chemical synthesis, structure activity relationships, and physicochemical properties are discussed in detail. The highlight of these series' is compound 28, a potent and selective PI3Kγ inhibitor, which was tested in combination with ceritinib by MTT cell viability assay. Additionally, a PI3Kα inhibitor, alpelisib, was evaluated in combination with ceritinib by MTT cell viability assay. The combinations of the selective α, δ, and γ PI3K inhibitors did not exhibit the same level of synergy as observed with the pan PI3K inhibitor pictilisib, and thus, the combination with pictilisib was selected to be incorporated into a bifunctional ligand.

Chapter 4 discusses the design of bifunctional inhibitors. The chapter begins with a brief introduction to bifunctional ligands, linked together via a linker, although all examples in the current literature are of covalent linkers. With anti-cancer therapies, including ceritinib and pictilisib, exhibiting severe side effects, a reduction of dose is highly desirable. One strategy for lowering dosage is through drug delivery to the site of

action via controlled release i.e. in the form of a prodrug. In this chapter, the combination therapy of ceritinib and pictilisib were brought together into a bifunctional ligand, where the inhibitors are linked via a pH dependent cleavable linker, introducing a tunable method for controlled release, since cancer cells can have a range of pH states (5.7 - 7.8), mainly due to hypoxia. The design of these prodrugs began with model systems of ceritinib and pictilisib linked together with novel linkers . The synthesis and kinetic studies of these systems are discussed in detail. Additionally, a mechanism of release is proposed. Following this, synthesis progressed to linking pictilisib and ceritinb to give AEG-118, which was shown to simultaneously release the active pay-loads, ceritinib and pictilisb, in a pH dependant manner.

Table of Contents

1. EML4-ALK Lung Cancer **1**

1.1 Introduction 2

1.1.1 Lung Cancer 2

1.1.1.1 EML4-ALK positive non-small cell lung cancer . . 3

1.1.1.2 Anaplastic lymphoma kinase 4

1.1.1.3 ALK Inhibitors 5

1.1.1.4 Combating Resistance 8

2. Combination Therapies and Synergy **9**

2.1 Introduction 10

2.1.1 Combination Therapy 10

2.1.2 Synergy Determination 10

2.1.2.1 Webb Method 10

2.1.2.2 Chou & Talalay Method 11

2.2 Results and Discussion 15

2.2.1 Potential Signalling Nodes to Target 15

2.2.2 P2Y2 Inhibition 17

2.2.2.1 Combination of Ceritinib with AR-C118925 . . . 17

2.2.3 VEGFR inihibition 18

2.2.3.1 Combination of Ceritinib and Linifanib 18

2.2.4 PI3K/AKT/mTOR Pathway Inhibitors 21

2.2.4.1 Combination of Ceritinib and Uprosertib 21

2.2.4.2 Combination of Ceritinib and Gedatolisib 24

2.2.4.3 Combination of Ceritinib and Pictilisib 27

2.2.4.4 Combination of Ruxolitnib and Ceritinib 45

2.3 Chapter Conclusions 48

3. Homing in on Synergy with PI3K Inhibitors **51**

3.1 Introduction 52

3.1.1 Phosphoinositide 3-kinase (PI3K) 52

3.1.1.1 General design of PI3K inhibitors 55

3.1.2 “Flat” PI3K Inhibitors 57

3.1.2.1 Thienopyrimidines and their Derivatives 57

3.1.2.2 Triazines and their derivatives 78

3.1.3 Benzoxepins 90
3.1.3.1 Benzothiazoles and derivatives 96
3.1.3.2 Copanlisib 106
3.1.4 So-called “Propellar” Inhibitors 107
3.2 Aims and Objectives 109
3.3 Results and Discussion 111
3.3.1 PI3Kδ Inhibition 111
3.3.1.1 Inhibitor Design 111
3.3.1.2 Inhibitor Synthesis. 113
3.3.1.3 Assay details. 117
3.3.1.4 Biological Results 118
3.3.1.5 Discussion of Biological Results 122
3.3.1.6 Discussion of Physicochemical properties . . . 132
3.3.1.7 Series Conclusion 138
3.3.1.8 Synergy with Ceritinib 139
3.3.2 PI3Kα Inhibition 142
3.3.2.1 Inhibitor Design 142
3.3.2.2 Scaffold synthesis 145
3.3.2.3 Inhibitor design 162
3.3.2.4 Synthesis. 165
3.3.2.5 Biological Results 171
3.3.2.6 Discussion of Biological Results 174
3.3.2.7 Amide compounds. 181
3.3.2.8 Discussion of Physicochemical properties . . . 183
3.3.2.9 Series conclusion 184
3.3.2.10 Synergy with Ceritinib 185
3.3.3 Iteration 2 PI3K α inhibition 187
3.3.3.1 Inhibitor design 187
3.3.3.2 Synthesis. 187
3.3.3.3 Biological Results 199
3.3.3.4 Synergy with Ceritinib 201
3.4 Chapter Conclusion. 203
4. Bifunctional Ligands. 207

4.1 Introduction . . . 208
4.1.1 Linked Bifunctional Compounds . . . 209
4.2 Aims and Objectives . . . 213
4.3 Results and Discussion . . . 214
4.3.1 Prodrug Model Systems . . . 214
4.3.1.1 Model Prodrug Design . . . 214
4.3.1.2 Model Prodrug Synthesis . . . 217
4.3.1.3 Prodrug Model Kinetic Study . . . 218
4.3.2 Ceritinib/Pictilisib Prodrug, AEG-118 . . . 230
4.3.2.1 Synthesis of AEG-118 . . . 230
4.3.2.2 In vitro Stability studies of AEG-118 . . . 235
4.3.2.3 Plasma Stability of AEG-118 . . . 238
4.3.3 Analogues of AEG-118 . . . 240
4.3.3.1 Synthesis of Analogues of AEG-118 . . . 240
4.3.3.2 In vitro Stability of Analogues of AEG-118 . . . 246
4.3.4 Summary of Pharmacokinetics . . . 250
4.3.5 Biological evaluation of AEG-118 . . . 252
4.4 Chapter Conclusion . . . 258
5. Conclusions and Future Work 259
5.1 Conclusion . . . 260
5.2 Future Work . . . 262
6. Experimental 263
6.1 Pharmacological Protocols . . . 264
6.1.1 Protocols for Chapter II . . . 264
6.1.1.1 Mammalian Cell Tissue Culture and Equipment 264
6.1.1.2 MTT Assay . . . 265
6.1.1.3 Clonogenic Assay . . . 265
6.1.1.4 Cell Cycle Analysis Assay . . . 266
6.1.1.5 Apoptosis Annexin V (FIT-C/PI) Assay . . . 266
6.1.1.6 Pharmacological Data Analysis . . . 267
6.1.2 Protocols for Chapter III . . . 268
6.1.2.1 HTRF PI3K assay . . . 268
6.1.2.2 Lipophilicty determination ($mLogD_{7.4}$) . . . 268

6.1.2.3 Aqueous solubility determination. 268
6.2 Molecular Modelling 270
6.2.1 Modelling for Chapter III 270
6.3 Pharmacokinetic Protocols 271
6.3.1 Pharmacokinetics for Chapter IV 271
6.3.1.1 NMR Kinetic Studies 271
6.3.1.2 HPLC Kinetic studies 272
6.4 Chemical Synthesis 273
6.4.1 General 273
6.4.2 Nuclear Magnetic Resonance 273
6.4.3 Mass Spectrometry 273
6.4.4 Chromatography 274
6.4.5 Synthesis 274
6.4.5.1 Synthesis for Chapter III 274
6.4.5.2 Synthesis for Chapter IV 331
7. References **377**
7.1 Bibliography 378

List of Abbreviations

NSCLC	Non-small cell lung cancer
MRI	Magnetic Resonance Imaging
CT	Computed Tomography
PET	Positron Emission Tomography
ALK	Anaplastic Lymphoma Kinase
EML4	Echinoderm Microtubule-Associated Protein-like 4
RAF	Rapidly Accelerated Fibrosarcoma
MEK	Mitogen-activated Protein Kinase
ERK	Extracellular Signal–Regulated Kinases
JAK	Janus kinase
STAT	Signal Transducer and Activator of Transcription
PI3K	Phosphatidylinositol-4,5-bisphosphate 3-kinase
AKT	Protein Kinase B
mTOR	Mammalian Target of Rapamycin
FDA	Federal Drug Agency
D_m	Dose Median
Fa	Fractional Effect
CI	Combination Index
GI_{50}	Conc. required to inhibit 50% of maximal cell proliferation
MTT	3-(4,5-dimethylthiazol-2-yl)-2,5-diphenyltetrazolium bromide
SEM	Standard Error of the Mean
S-Phase	Synthesis Phase
G1	Growth Phase 1
G2	Growth Phase 2
PI	Propidium Iodide
DNA	Deoxyribonucleic acid
FITC	Fluorescein isothiocyante

PIP2	Phosphatidylinositol 4,5-bisphosphate
PIP3	Phosphatidylinositol (3,4,5)-trisphosphate
PI4P	Phosphatidylinositol 4-phosphate
PI3P	Phosphatidylinositol 3-phosphate
ATM	Ataxia Telangiectasia Mutated
ATR	Ataxia Telangiectasia and Rad3 Related
DNA-PK	DNA-Dependent Protein Kinase
ICR	Institute for Cancer Research
PDB	Protein Data Bank
CYP3A4	Cytochrome P450 3A4
CYP2C19	Cytochrome P450 2C19
CYP2D6	Cytochrome P450 2D6
BBB	Blood Brain Barrier
P-gp	P-Glycoprotein
B-crp1	Breast Cancer Resistance Protein 1
CNS	Central Nervous System
TPSA	Total Polar Surface Area
MPO	Multi-Parameter Optimisation
MDCK	Madin-Darby Canine Kidney
MNT	Micronucleus Test
HCA	Human Chromosome Aberration
SAR	Structure Activity Relationship
HDAC	Histone Deacetylase
ADME	Absorption, Distribution, Metabolism and Excretion
ADMET	Absorption, Distribution, Metabolism, Excretion and Toxicity
PK	Pharmacokinetic
ADP	Adenosine Diphosphate
ATP	Adenosine Triphosphate
hERG	Human Ether-à-go-go-Related Gene

PAMPA	Parallel Artificial Membrane Permeability Assay
HTS	High Throughput Screen
DMA	Dimethyl acetal
DMF	Dimethylformamide
NMM	N-methylmorpholine
HATU	1-[Bis(dimethylamino)methylene]-1H-1,2,3-triazolo[4,5-b] pyridinium 3-oxid hexafluorophosphate
TFA	Trifluoroacetic acid
MeOH	Methanol
FBS	Foetal Bovine Serum
PBS	Phosphate Buffered Saline
EDTA	Ethylenediaminetetraacetic acid
EtOAc	Ethyl Acetate
THF	Tetrahydrofuran
TLC	Thin Layer Chromatography
HPLC	High Performance Liquid Chromatography
LCMS	Liquid Chromatography Mass Spectrometry
MS	Mass Spectrometry
NMR	Nuclear Magnetic Resonance
DIPEA	N,N-Diisopropylethylamine
DMAP	Dimethylamino Pyridine
BINAP	2,2′-bis(diphenylphosphino)-1,1′-binaphthyl
mCPBA	Meta-Chloroperoxybenzoic acid
IPA	Isopropyl alcohol
Et_2O	Diethyl Ether
THP	Tetrahydropyran
Boc	N-tert-butoxycarbonyl
EtOH	Ethanol
DMSO	Dimethylsulfoxide

ACE-Cl	1-chloroethyl chloroformate
AcOH	Acetic Acid
TsOH	Tosic Acid
TMS-Cl	Trimethylsilyl chloride
DBU	1,8-Diazabicyclo(5.4.0)undec-7-ene
MsCl	Mesyl Chloride
DCM	Dichloromethane
GSK	GlaxoSmithKline
NBS	N-Bromosuccinimide
NIS	N-Iodosuccinamide
TR-FRET	Time-Resolved Fluorescence Resonance Energy Transfer
HTRF	Homogeneous Time Resolved Fluorescence
MW	Molecular Weight
BEI	Binding Efficiency Index
HBA	Hydrogen Bond Acceptor
HBD	Hydrogen Bond Donor
HSA	Human Serum Albumin
PPB	Plasma Protein Binding
SEI	Surface-Binding Efficiency Index
HAC	Heavy Atom Count
LE	Lipophilic Efficiency
LLE	Lipophilic Ligand Efficiency
ARC	Aromatic Ring Count
PFI	Property Forecast Index
RB	Rotatable Bonds
PMA	Phosphomolybdic Acid
UV	Ultra Violet
RPMI	Roswell Park Memorial Institute
ANOVA	Analysis of variance

Publications

1 Schwehm, C.; Kellam, B.; Garces, A. E.; Hill, P. S. J.; Kindon, N. D.; Bradshaw, T. D.; Li, J.; Macdonald, S. J. F.; Rowedder, J. E.; Stoddart, L. A.; Stocks M. J. Design and Elaboration of a Tractable Tricyclic Scaffold to Synthesise Drug-like Inhibitors of Dipeptidyl Peptidase-4 (DPP-4), Antagonists of the C-C Chemokine Receptor Type 5 (CCR5), and Highly Potent and Selective Phosphoinositol-3 Kinase δ (PI3Kδ) Inhibitors. *Journal of Medicinal Chemistry*, **2017**, 60 (4), pp 1534–1554.

2 Lee, J. B.; Zgair, A.; Malec, J.; Kim, T. H.; Kim, M. G.; Ali, J.; Qin, C.; Feng, W.; Chiang, M.; Gao, X.; V, Gregory; Garces, A. E. et al. Lipophilic Activated Ester Prodrug Approach for Drug Delivery to the Intestinal Lymphatic System. *Journal of Controlled Release*, **2018**, 286, 10–19.

3 Garces, A. E.; Stocks, M. J.; Class 1 PI3K Clinical Candidates and Recent Inhibitor Design Strategies - A Medicinal Chemistry Perspective. *Journal of Medicinal Chemistry*, **2018**, (Accepted, In Press).

1. EML4-ALK Lung Cancer

1.1 Introduction

1.1.1 Lung Cancer

Lung cancer remains the leading cause of cancer death in the UK, where approximately 35 400 people died from lung cancer in 2012 and a further 46 400 people were diagnosed in 2014[1].

There are two main types of lung cancer, namely, non-small cell lung cancer (NSCLC) and small cell lung cancer. NSCLC makes up the majority of all lung cancers (approximately 80-85%) and can be divided into subcategories based on the histology of the cells. These are adenocarcinoma, squamous cell carcinoma and large cell carcinoma[2].

Here we focus in on NSCLC which is often insidious, and patients experience no symptoms until the disease is well progressed. Patients present with symptoms that include cough, chest pain, shortness of breath, wheezing, hoarseness, coughing up blood, recurring infections such as bronchitis and pneumonia, weight-loss, fatigue, and loss of appetite. Signs that indicate metastasis include headache, weakness or numbness of limbs, dizziness, seizures, bone pain and spinal cord impingement[3].

Current methods of diagnosis include a physical examination by a physician, where an X-ray is often the first test performed. Diagnosis can be confirmed by a range of methods including various other imaging techniques (magnetic resonance imaging (MRI), computed tomography (CT), positron emission tomography (PET), bone scan or ultra sound), or biopsy (sputum cytology, thoracentesis, needle biopsy, or bronchoscopy). Staging, which refers to the extent of cancer progression, is confirmed with a CT scan[4].

The prognosis for patients diagnosed with NSCLC depends on factors including the stage of the cancer, the type of NSCLC, whether there are mutations within certain genes[5], and the general health of the patient. Unfortunately, in the vast majority of cases, current treatments do not cure the cancer, and treatment regimens generally only extend the life of the patient by a short amount of time. It is therefore of great impor-

tance to extend research in this area[4].

1.1.1.1 EML4-ALK positive non-small cell lung cancer

Of the NSCLCs, 3-7% possess chromosomal rearrangements of ALK (anaplastic lymphoma kinase), [6],[7] which lead to constitutively active ALK fusion proteins[8]. In this work the focus is an inversion occurring in the p-arm of chromosome 2, leading to the fusion of the echinoderm microtubule-associated protein-like 4 (EML4)[9] and ALK genes. This fusion protein, ALK-EML4, is found mainly in younger, non-smoking female patients. All ALK-EML4 fusion genes[10] observed in NSCLCs contain exons of ALK that code for the intracellular kinase domain of ALK and eight EML4 exons, all of which activate downstream signals of the Ras/Raf/MEK/ERK1/2, JAK/STAT and PI3K/AKT/mTOR pathways[11] (Figure 1). Thus the EML4-ALK fusion protein constitutively activates signalling pathways that participate in cell proliferation and propagation of cell survival, ultimately leading to uncontrolled cell growth and thus its onco-

genic nature.

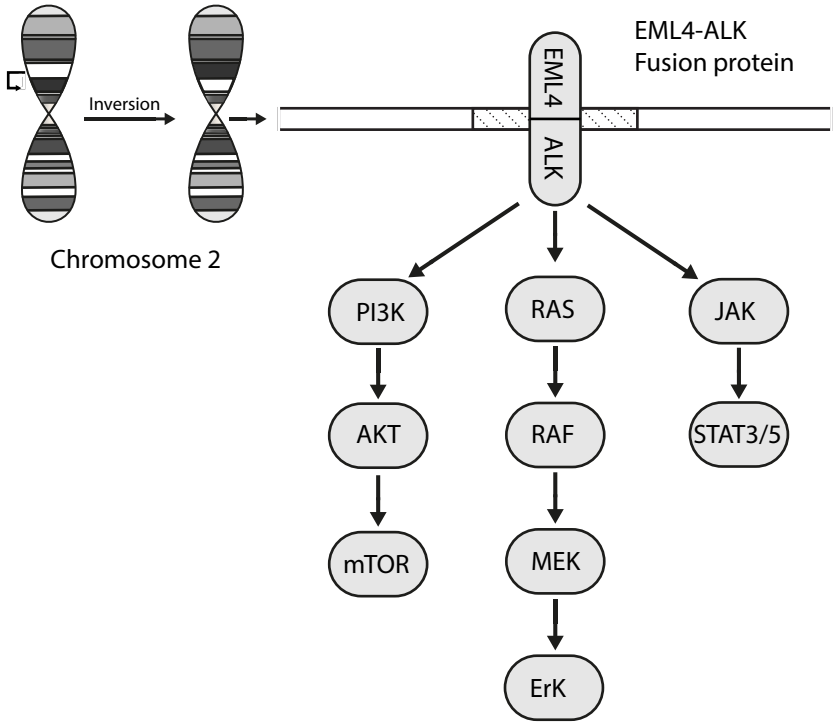


Figure 1. Downstream signalling of the EML4-ALK oncogene: This constitutively active EML4-ALK fusion protein, a result of an inversion on chromosome 2, inappropriately activates the ALK signalling pathways, resulting in uncontrolled tumour growth and proliferation.

1.1.1.2 Anaplastic lymphoma kinase

ALK is a type-I transmembrane receptor tyrosine kinase and is a member of the insulin receptor super family. ALK has all of the classical features of a receptor tyrosine kinase, with an extracellular ligand-binding domain, a transmembrane spanning region and an intracellular tyrosine kinase domain (Figure 2)[12].

Mammalian ALK has been proposed to play a role in the normal development and function of the nervous system (during embryogenesis) and it has also been shown in mature human tissues that ALK has very little activity and is maintained only at low levels. It is currently thought that under normal physiological conditions an unknown endogenous ligand binds to the extracellular domain of the kinase and subsequently induces dimerisation of ALK. Dimerisation allows for autophosphorylation resulting in activation of the intracellular domain and downsteam signalling[13].

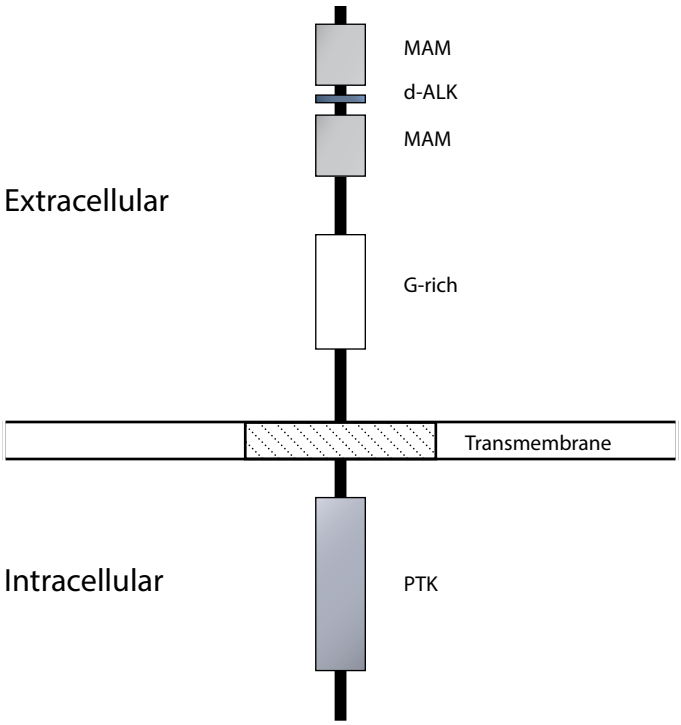


Figure 2. Structure of ALK: ALK comprises of two meprin, A5 protein and receptor protein tyrosine phosphatase mu (MAM) domains, a glycine-rich region, and a transmembrane spanning region, which connects the extracellular region to the intracellular region containing the protein tyrosine kinase (PTK) domain.

1.1.1.3 ALK Inhibitors

As ALK is required for oncogenic activity, ALK inhibitors have been developed as targeted anti-tumour therapies. Crizotinib (PF-023410660)[14],[15] (Figure 3), a first generation ALK inhibitor developed by Pfizer, has recently featured in numerous phase III clinical trails for ALK+ patients with NSCLC adenocarcinoma. Crizotinib was shown to exhibit anti-tumour activity leading to approval by the FDA (November 2013) [16]. Unfortunately, despite the initial response, patients relapsed due to the emergence of acquired resistance, a common occurrence in cancer therapy[17]. To overcome this, a second generation of ALK inhibitors was developed.

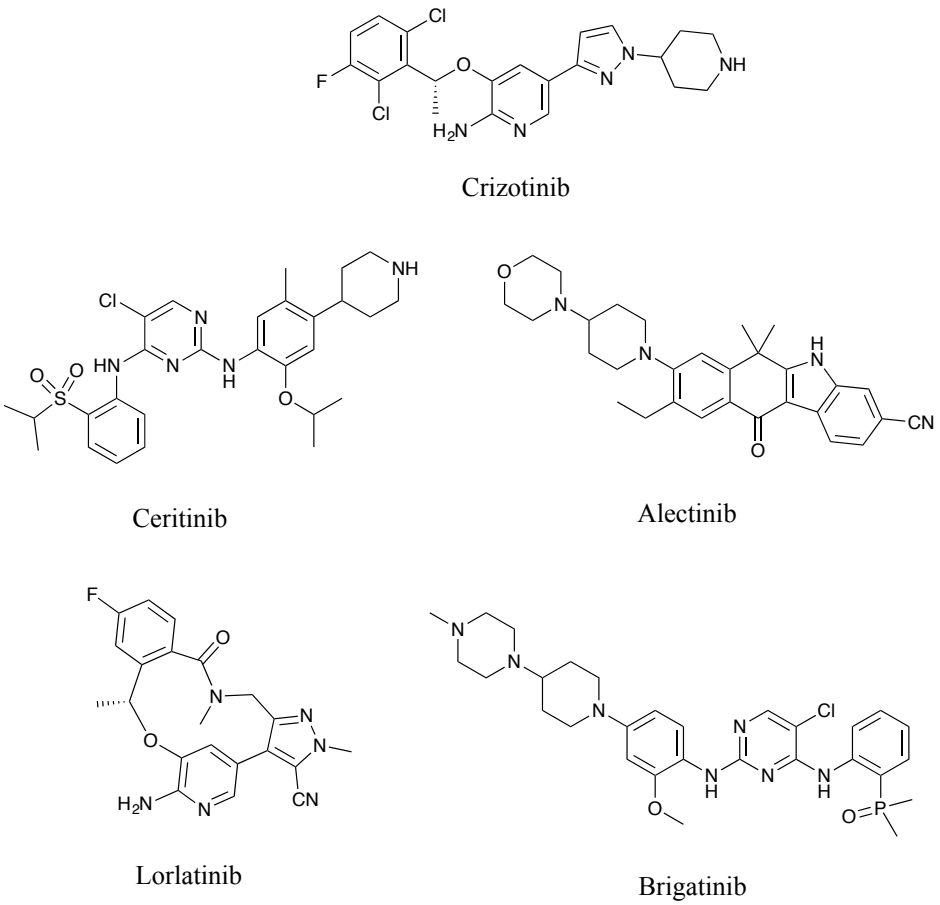


Figure 3. Current 1st, 2nd and 3rd generation ALK inhibitors. Crizotinib, ceritinib and alcetinib have been approved by the FDA for ALK+ NSCLC. Lorlatinib and brigatinib are currently in phase I and II clinical trails.

Ceritinib[18],[19],[20],[21] (Figure 3), developed by Novartis, has recently been approved by the FDA (April 2014)[22] and is featured in numerous phase III clinical trials including both crizotinib "naive" patients and patients that have relapsed on crizotinib. Ceritinib was shown to exhibit anti-tumour activity and with the vast majority of patients tumours were reduced considerably (Figure 4). Interestingly, although some patients had developed resistance to crizotinib, ceritinib was still effective. Although, as with crizotinib, patients quickly develop resistance and brain metastases are common.

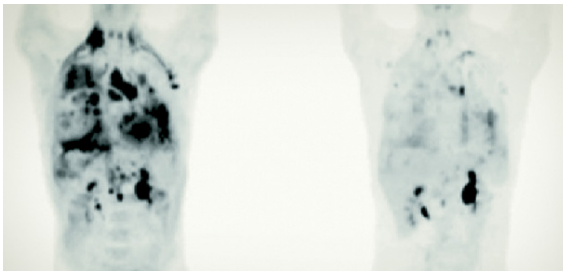


Figure 4. PET scans of a patient on ceritinib: Scans were taken at baseline (left) and after 3.5 weeks of ceritinib treatment (right) in a patient with crizotinib-resistant disease. Ceritinib is very effective at reducing tumour burden, however resistance quickly develops and patients relapse.

Alectinib[23] (Figure 3), another second generation ALK inhibitor, developed by the Roche group, was found in clinical trials to result in far fewer metastases to the brain due to its ability to penetrate the blood brain barrier. Alectinib has a 76% progression free survival rate at 2 years, which is considerably higher than that of 1st generation ALK inhibitors, where patients relapse after approximately 10.5 months. Alectinib was approved by the FDA (December 2015)[24] to treat patients with advanced metastatic ALK+ NSCLC.

More recently, third generation ALK inhibitors (Figure 3), lorlatinib[20] (PF-06463922), developed by Pfizer, and brigatinib[26] (AP26113), developed by Takeda, have been put through phase I and II clinical trials. With lorlatinib, patients were reported to show stable disease and lorlatinib was awarded breakthrough therapy in April 2017 and the FDA granted priority review in early 2018. Brigatinib was approved by the FDA in April 2017.

Mechanisms of acquired resistance

Acquired clinical resistance to ALK Inhibitors[27] can be divided into 2 categories as described by Doebele *et al*[28][29]: ALK dominant and ALK non-dominant. ALK dominant resistance has been described as having an "addiction to the ALK signalling pathway" This resistance is associated with secondary mutations in the ALK gene, namely of gatekeeper residues that are found in the ATP binding pocket of the kinase. Bulky res-

idues block the binding of the ALK inhibitor to the receptor. It is thought that these point mutations can be temporarily overcome by treatment with a more potent ALK inhibitor and hence why crizotinib resistance can be treated with ceritinib, which is 20-fold more potent[30]. Common mutations include L1196M, G1269A, C1156Y, F1174L, 1151Tins, L1152R, S1206Y, I1171T, G1202R, D1203N, and V1180L[31]. ALK non-dominant resistance, "activation of bypass tracks", are resistance mechanisms where alternate signalling pathways are activated, leading to cell growth, proliferation, and survival.

1.1.1.4 Combating Resistance

In addition to using ALK inhibitors in succession, as resistance is acquired, another strategy for overcoming resistance to ALK inhibitors is to use upfront combination therapies[32], targeting one or more signalling nodes, that suppress the survival and emergence of resistant tumour cells[33],[34]. It is, however, unclear which effector is most critical for EML4-ALK driven cell survival. Herein, in Chapter 2 we explore drug combinations and assess for synergy between an ALK inhibitor and these drugs.

2. Combination Therapies and Synergy

2.1 Introduction

2.1.1 Combination Therapy

Combination therapy[35],[36] is a widely used approach in cancer therapy and infection where there are many known combination regimens. The benefit, of course, is the synergistic response of the combined therapy vs the response of single agent therapies. There is, however, an issue when it comes to the definition of synergy. A crude definition is that to exhibit synergy between a combination of drugs, the effect should be greater than their individual effects. If this effect is equal, then the effect is said to be "additive" and if this effect is less than the individual effects, then the effect is said to be "antagonistic".

There have been many proposed methods over the years to assess whether drug combinations display a synergistic, additive or antagonistic response, the two used in this work are detailed below.

2.1.2 Synergy Determination

2.1.2.1 Webb Method

A common method, the fractional product method, proposed by Webb *et al*[37] is quite simplistic. The Webb method calculates an "expected" effect (Equation 1), which represents an additive response. The expected response is then compared to the "observed" effect. If the observed effect is significantly greater than the "expected" effect, the response is said to be synergistic and an "observed" response less than the "expected" effect is antagonistic. An "observed" response similar to the "expected" effect is said to be additive. An example is as follows: If drug A exhibits a 50% response and drug B exhibits a 60% response, then the additive effect of these drugs should be (0.5 x 0.6) x 100 = 30%. If the observed effect is greater than 30%, the response is said to be synergistic and a response less than 30% is antagonistic.

Equation 1:

$$Additive\ Response\ (\text{"Expected"}) = [(F_a)_A \times (F_a)_B] \times 100$$

The fractional product method assumes that the drugs are mutually non-exclusive

and that they follow first order dynamics, i.e. the Hill coefficient is equal to 1 and there are no cooperative effects in terms of the ligand binding. The Webb method is utilised with a bar-graph giving the "expected" response (The expected response if the response was additive, from the fractional product equation) vs the observed response. The statistical significance between the observed and expected response is then determined by calculation of the p-value, which allows determination of an additive response or a synergic/antagonistic response.

2.1.2.2 Chou & Talalay Method

Another method, the Chou and Talalay method[38],[39],[40][41], is widely used as it is based on the median-effect equation (equation 2) and can be used in any system that follows the physiochemical principle of the mass action law, regardless of the dynamics, whether it be first or higher order, i.e. regardless of the mechanism of action. Synergy is ultimately determined by calculation of the Combination Index (CI), where a CI of 1 is considered additive, a CI greater than 1 is antagonistic, and a CI less than 1 is synergistic. Chou and Talalay recommend that the combination assay be performed in constant ratio as this allows for a range of CI index values to be computed.

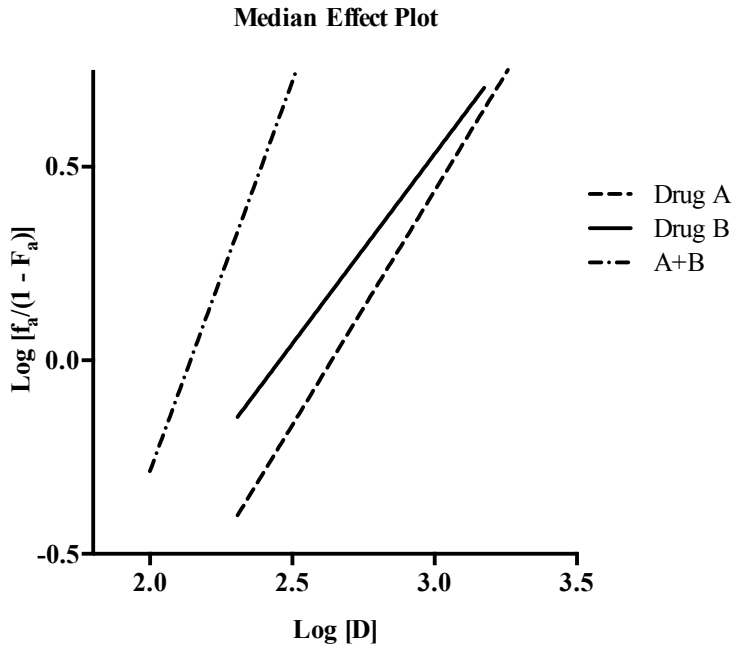


Figure 5. An example median effect plot.

As mentioned above, the median effect equation is at the heart of the Chou and Talalay method. The median effect equation is used to linearise dose-response curves, the result being the median-effect plot (Figure 5), a plot of Log [Dose] vs Log [Fa/(1-Fa)]. The anti-log of the x-intercept gives the median dose (D_m) value, the dose required to achieve 50% effect) and the gradient gives the m value, a Hill-type coefficient, describing the shape of the dose-response curve. When m = 1, the dose-response curve is hyperbolic, where m is greater than 1 the dose-response curve is sigmoidal and the greater the value, the greater its sigmoidicity. When the dose-effect relationships of drug A, drug B and the combination are all parallel in the median-effect plot, the effects of drug A and drug 2 are mutually exclusive. If the plots of drugs A and B are parallel but the plot of the combination tends to intersect the plot of the more potent of the two drugs, their effects are mutually non-exclusive. If the plots for drugs A and B and the combination are not parallel to one another, then the exclusivity effects cannot be determined.

Equation 2:

$$\frac{F_a}{(1-F_a)} = \left(\frac{D}{D_m}\right)^m \quad \Longrightarrow \quad Log\left(\frac{F_a}{(1-F_a)}\right) = mLog(D) - mLog(D_m)$$

Once the m-value and the D_m value have been obtained from the median-effect plot, D_x values can be calculated (equation 3) for each drug and drug combination at different Fa values. These are the doses of each drug required to achieve the desired percentage effect. From this, the D_A, D_B... values can be obtained by factoring in the ratio (A : B) of the individual drug concentrations in the drug combinations (Equation 4).

Equation 3:

$$D_x = D_m\left(\frac{F_a}{(1-F_a)}\right)^{m^{-1}}$$

Equation 4:

$$(D)_A = (D_x)_{A,B} \times \left(\frac{A}{A+B}\right) \qquad (D)_B = (D_x)_{A,B} \times \left(\frac{B}{A+B}\right)$$

Once the D_A and D_B doses are known to cause a % effect, Fa, it is then possible to calculate the combination index, and plot the CI plot. Equation 5 and 6 calculate the CI for mutually exclusive and mutually non-exclusive combinations respectively.

Equation 5:

$$CI = \left(\frac{(D)_A}{(D_x)_A}\right) + \left(\frac{(D)_B}{(D_x)_B}\right)$$

Equation 6:

$$CI = \left(\frac{(D)_A}{(D_x)_A}\right) + \left(\frac{(D)_B}{(D_x)_B}\right) + \frac{(D)_A(D)_B}{(D_x)_A(D_x)_B}$$

The combination index for each fractional effect is represented on a CI plot (Figure 6) where a CI of 1 is additive, >1 is antagonisstic, and <1 is synergic

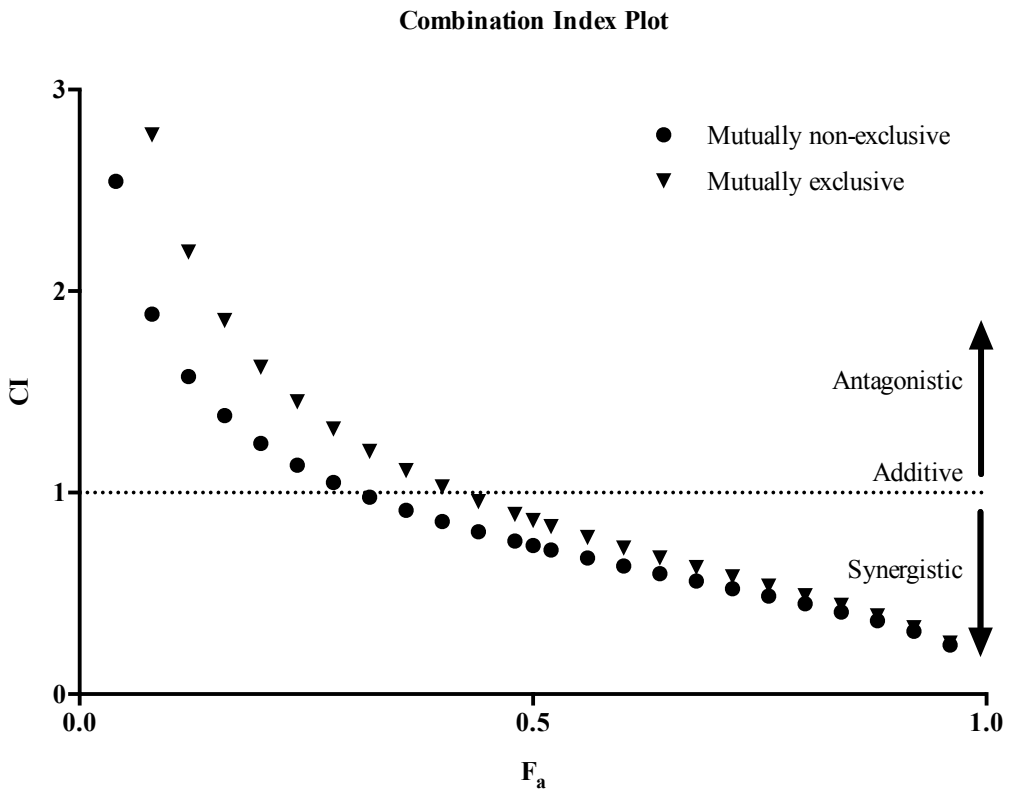


Figure 6. An example CI plot. A CI of 1 is additive, > 1 is antagonistic, and <1 is synergic.

2.2 Results and Discussion

2.2.1 Potential Signalling Nodes to Target

In chapter 1, the mechanisms of acquired resistance in EML4-ALK+ NSCLC were introduced, namely ALK dominant and ALK non-dominant resistance, and in order to address acquired resistance, it was proposed to employ an upfront combination therapy approach. With current research it is not clear which effector is most critical for EML4-ALK driven cell survival; herein drug combinations are explored to assess for synergy between the ALK inhibitor ceritinib and a range of inhibitors of signalling nodes that may be important to EML4-ALK driven cell survival.

Recently, alternate receptor tyrosine kinase activation pathways have been identified as being involved in EML4-ALK+ driven cell survival: Yang and Li *et al* [42] have been exploring the Ras/ERK1/2, JAK/STAT and PI3K/AKT pathways[43], and more recently Tanizaki *et al* [44] have looked at ALK inhibitors in combination with MEK inhibitors. Ras signalling has also been shown to be of great importance in ALK+ NSCLC[45],[46]. Additionally, Wilson *et al* [47], have identified that P2Y receptors mediate ALK inhibitor resistance in part by Protein Kinase C (PKC) potentially by activation of PKC by P2Y2. They have also shown that EGFR, HER2 and P2Y gene signatures are enriched in ALK-inhibitor resistant tumours. Gower *et al* [48]have shown that HSP90 inhibitors[49] may be effective to combat resistance.

Based on the literature precedence above, the search for synergy began. The following discussion will describe the *in vitro* effects (measured by MTT assay) of combinations with ceritinib, the ALK inhibitor, against an isogenic pair of human lung carcinoma cell lines, A549 and A549 EML4-ALK, which will be referred to as the ALK- and ALK+ respectively in the following discussion. The human lung carcinoma cell lines used in this study, and their respective known muations are listed in Table 1.

Table 1. Cell lines used in assays

Cell Line	EML4-ALK	PI3KCA	Other Mutations
Current cell lines			
A549	-	wt	CDKN2A, KRAS
CCL-185IG (A549 isogenic cell line)	+	wt	CDKN2A, KRAS

MTT Assay

Firstly, a note on the definition of GI_{50} and D_m values: The GI_{50} value is defined as the concentration of drug required to inhibit 50% of maximal cell proliferation, where the control is considered to be 100% growth and the T_{zero} value is considered to be 0% growth. The GI_{50} value, calculated by equations 7 and 8, considers growth inhibition, where a response below the Tzero value indicates cytotoxicity. The D_m value, however does not consider the T_{zero} value, and is relative to the total number of viable cells. This is necessary, as often in combination, the effect can be below the T_{zero} value and if this data was normalised to the T_{zero} value, the effect would be negative and it is not possible to take logarithms of negative numbers. On dose-response curves the Tzero value is indicated on the graph as a dotted horizontal line where points below this line may indicate cytotoxicity of the agent. Note that MTT asssays were performed a minimum of n = 3.

Equation 7:

$$Abs.of\ GI_{50} = \left[\frac{Abs.of\ Control - Abs.of\ Tzero}{2}\right] + Abs.of\ Tzero$$

Equation 8:

$$GI_{50} = \left[\frac{\left(\begin{matrix}Highest\ Abs.\\ where\ GI_{50}\ falls\end{matrix}\right) - (Abs.of\ GI_{50})}{\left(\begin{matrix}Highest\ Abs.\\ where\ GI_{50}\ falls\end{matrix}\right) - \left(\begin{matrix}Lowest\ Abs.\\ where\ GI_{50}\ falls\end{matrix}\right)}\right] \times \left[\left(\begin{matrix}Highest\ Conc.\\ where\\ GI_{50}\ falls\end{matrix}\right) - \left(\begin{matrix}Lowest\ Conc.\\ where\\ GI_{50}\ falls\end{matrix}\right)\right] + \left[\begin{matrix}Lowest\ Conc.\\ where\\ GI_{50}\ falls\end{matrix}\right]$$

Drug ratios

The aim of this work is to identify a drug combination that exhibits synergy in a 1:1 molar ratio since it is the overall aim to identify a bivalent inhibitor where 2 drugs are linked together with a cleavable linker: This is further discussed in Chapter 4. In the following discussion the drug combinations are deliberately tested in a 1:1 molar ratio for this reason.

2.2.2 P2Y2 Inhibition

2.2.2.1 Combination of Ceritinib with AR-C118925

An interesting combination to explore is that of a P2Y2 antagonist with an ALK inhibitor as there is evidence to support that P2Y receptors mediate ALK inhibitor resistance in part by PKC, potentially by activation of PKC by P2Y2 activation. AR-C118925[50] (Figure 7), a non nucleotide P2Y2 antagonist, developed by Astrazeneca, was identified as a suitable P2Y2 inhibitor to be used in the study. AR-C118925 is reported to have a PA_2 of 7.8 and was synthesised in-house.

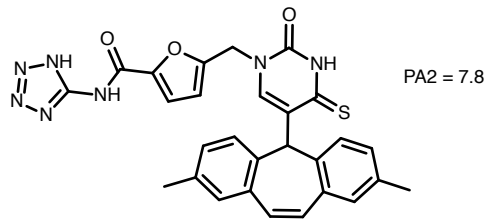


Figure 7. Chemical structure of AR-C118925.

In vitro evaluation by MTT assay of AR-C118925 against the ALK- and ALK+ cell lines showed that AR-C118925 had no growth inhibitory effects against either tested cell line. The dose response curves against both cell lines are shown in Figure 8. Additionally, treatment in combination with ceritinib showed no statistically significant synergistic or antagonistic effects as calculated by the Webb method, Figure 9. Chou and Talalay combination indices cannot be calculated for this combination as it is not possible to constuct a median-effect plot for an inactive compound.

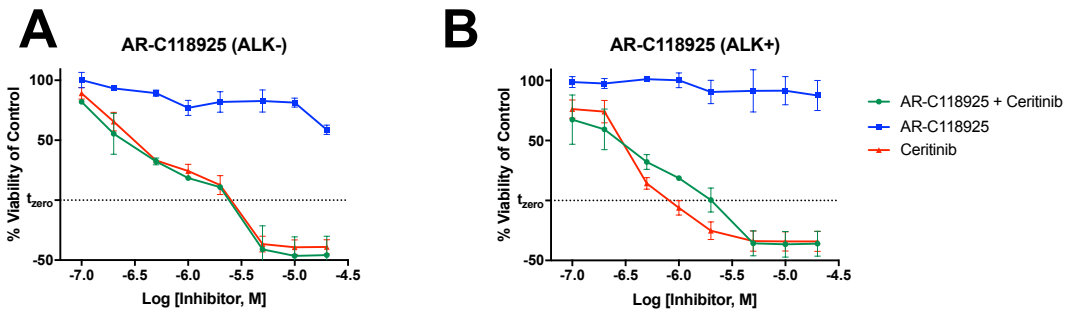


Figure 8. The Dose-response curves for ceritinib, AR-C118925 and their combination against the ALK- cell line (A) and ALK+ cell line (B). Points are given as the mean ± the standard error of the mean (minimum 3 internal replicates). The dotted line shows the T_{zero} value (0% growth), and points below this line may indicate that an agent is cytotoxic. Growth is represented as percentage viability of the control, which has been normalised to 100%, where 0% is the T_{zero}.

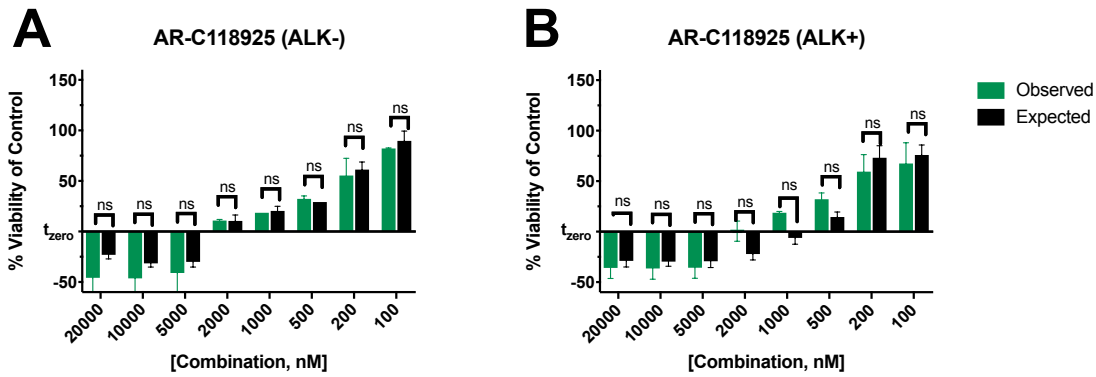


*Figure 9. Combination assay data of ceritinib and AR-C118925 against the ALK- cell line (A) and ALK+ cell line (B), analysed by the Webb fractional product method, comparing the expected (additive) effect against the observed effect. Where the observed % viability is less than the expected, synergy can be assumed. Statistical significance has been determined by calculation of the p-value using t-tests where: *** $P \leq 0.001$, ** $P \leq 0.01$, * $P \leq 0.05$, ns $P > 0.05$. Error bars shown represent the standard error of the mean.*

2.2.3 VEGFR inihibition

2.2.3.1 Combination of Ceritinib and Linifanib

Linifanib (ABT-869), Figure 10, is a potent VEGFR/PDGFR inhibitor for KDR, CSF-1R, Flt-1/3 and PDGFRβ with IC_{50} of 4 nM, 3 nM, 3 nM/4 nM and 66 nM respectively.

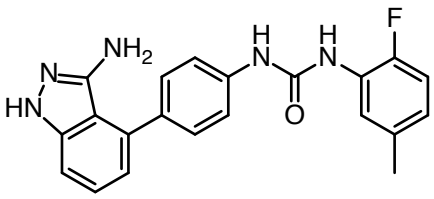


Figure 10. Chemical structure of linifanib.

In vitro evaluation by MTT assay of linifanib against the ALK- and ALK+ cell lines showed that linifanib had a GI_{50} of 10.5 µM ± 7.6 against the ALK- cell line and had a GI_{50} of 10.6 µM ± 0.2 against the ALK+ cell line. The dose response curves for linifanib and its combination with ceritinib are shown in Figure 11. Linifanib mainly showed a growth inhibitory effect, however it began to show potentially cytotoxic effects at higher concentrations.

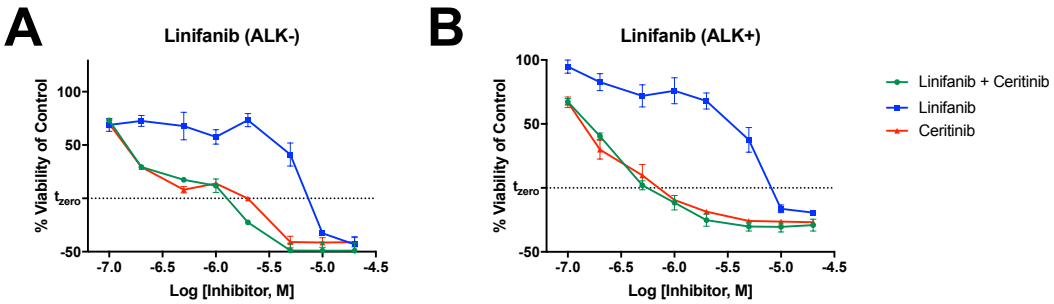


Figure 11. The Dose-response curves for ceritinib, linifanib and their combination against the ALK- cell line (A) and ALK+ cell line (B). Points are given as the mean ± the standard error of the mean (minimum 3 internal replicates). The dotted line shows the T_{zero} value (0% growth), and points below this line may indicate that an agent is cytotoxic. Growth is represented as percentage viability of the control, which has been normalised to 100%, where 0% is the T_{zero}.

In terms of evaluating synergy for the combination, the Webb method indicated that there was no statistical significance between the expected and observed effects at concentrations <1000 nM in both cell lines. However, at higher concentrations >1000 nM, there was statistical significance suggesting a synergistic effect for the combination, Figure 12.

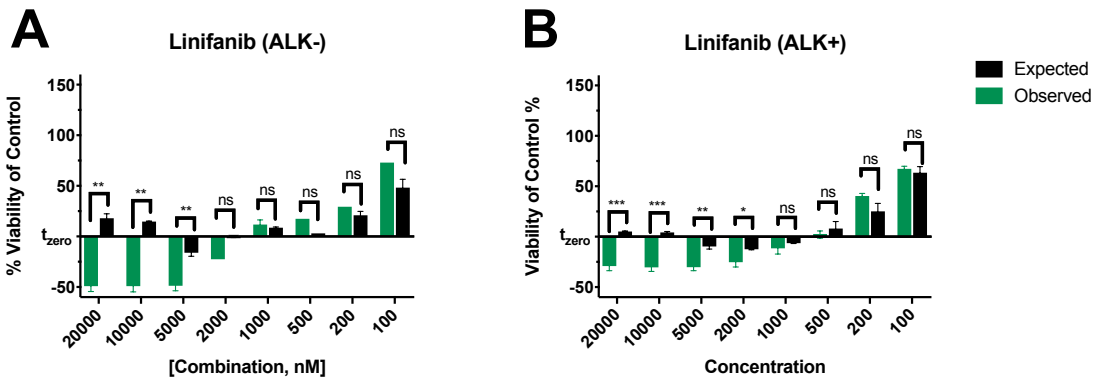


*Figure 12. Combination assay data of ceritinib and linifanib against the ALK- cell line (A) and ALK+ cell line (B), analysed by the Webb fractional product method, comparing the expected (additive) effect against the observed effect. Where the observed % viability is less than the expected, synergy can be assumed. Statistical significance has been determined by calculation of the p-value using t-tests where: *** $P \leq 0.001$, ** $P \leq 0.01$, * $P \leq 0.05$, ns $P > 0.05$. Error bars shown represent the standard error of the mean*

For the Chou and Talalay method, linearisation of the dose respose curves by generation of the median effect plot gave linifanib D_m values of 11.8 µM ± 6.3 against the ALK- cell line and 15.5 µM ± 11.0 against the ALK+ cell line. Additionally, an m-value for linifanib of 1.23 ± 0.25 was obtained for the ALK- cell line, and an m-value of 0.83 ± 0.36 was obtained for the ALK+ cell line. For the combination of ceritinib and linifanib D_m values of 2.1 µM ± 1.7 and 0.53 µM ± 0.49 were obtained for the ALK- and ALK+ cell lines respectively. The corresponding m-values were found to be 0.9 ± 2.05 and 1.30 ± 0.22 for the ALK- and ALK+ cell lines respectively. These D_m and m-values allowed for the calculation of the combination indices across a range of concentrations. The combination indices at a fractional effect (Fa) of 0.5 (effectively at the IC_{50}) were found to be 2.03 and 0.55 for the ALK- and ALK+ cell lines respectively. At higher concentration, at a fractional effect of 0.96, the combination indices were 3.35 and 0.47 against the ALK- and ALK+ cell lines respectively. The combination index plots for both cell lines are shown in Figure 13. Against the ALK+ cell line, the linifanib/ceritinib combination shows synergy across the whole range of fractional effects. However, against the ALK- cell line, the combination is very antagonistic.

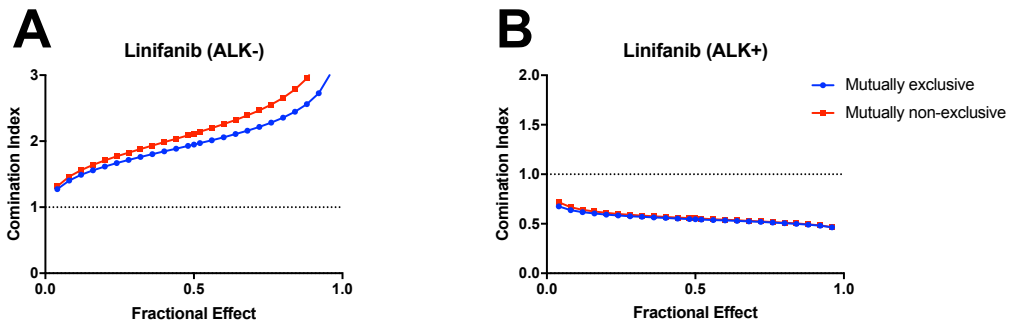


Figure 13. Combination index plots generated using the Chou and Talalay method for a 1:1 molar ratio of linifanib and ceritinib against the ALK- cell line (A) and the ALK+ cell line (B). A combination index at a given fractional effect of 1 is an additive effect,>1 is antagonistic and <1 is synergistic.

Looking at the dose-response curves in isolation, without considering the mathematical models for evaluating synergy, the activity of the combination appears to be similar to the activity of ceritinib alone. This suggests that there is in fact no synergy observed at these tested doses. With linifanib being less potent that ceritinib it may be that this combination may not be suitable in a 1:1 ratio and a higher ratio of linifanib may be required to show a synergisic effect. Although the mathematical models predict a synergistic response, with this 1:1 ratio we opted not to persue this combination further.

2.2.4 PI3K/AKT/mTOR Pathway Inhibitors

2.2.4.1 Combination of Ceritinib and Uprosertib

With the PI3K/Akt/mTOR pathway being downstream of EML4-ALK, exploring combinations with ceritinib and inhibitors of this pathway is interesting. Uprosertib[54] (GSK2141795), Figure 14, is a selective AKT inhibitor with activities of 180 nM, 328 nM, and 38 nM for AKT 1, 2 and 3, respectively. Due to its selectivity to AKT, uprosertib was selected as a suitable AKT inhibitor to be used in the study.

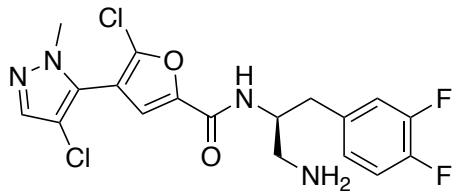


Figure 14. Chemical structure of uproserib.

In vitro evaluation by MTT assay of uprosertib against the ALK- and ALK+ cell lines showed that uprosertib had a GI_{50} of 2.5 µM ± 0.9 against the ALK- cell line and had a GI_{50} of 10.6 µM ± 0.2 against the ALK+ cell line. The dose response curves for uprosertib and its combination with ceritinib are shown in Figure 15 . Uprosertib mainly showed a growth inhibitory effect, however it began to show potentially cytotoxic effects at higher concentration.

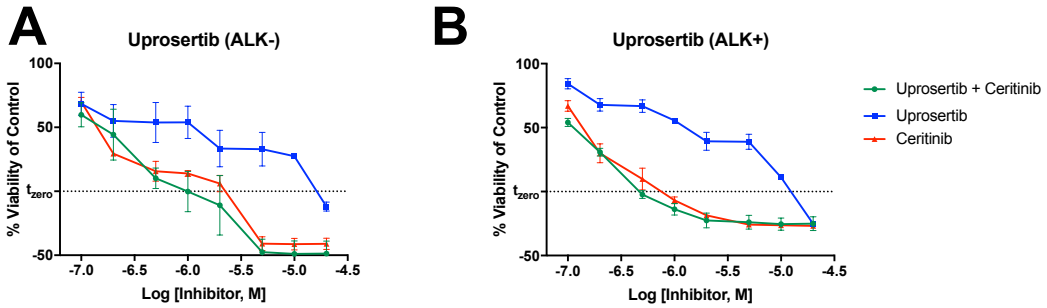


Figure 15. The Dose-response curves for ceritinib, uprosertib and their combination against the ALK- cell line (A) and ALK+ cell line (B). Points are given as the mean ± the standard error of the mean (minimum 3 internal replicates). The dotted line shows the T_{zero} value (0% growth), and points below this line may indicate that an agent is cytotoxic. Growth is represented as percentage viability of the control, which has been normalised to 100%, where 0% is the T_{zero}.

In terms of evaluating synergy for the combination, the Webb method indicated that there was no statistical significance between the expected and observed effects at concentration above 500 nM in both cell lines. However, at lower concentrations <500 nM, there was statistical significance suggesting an antagonistic effect for the combi-

nation (Figure 16).

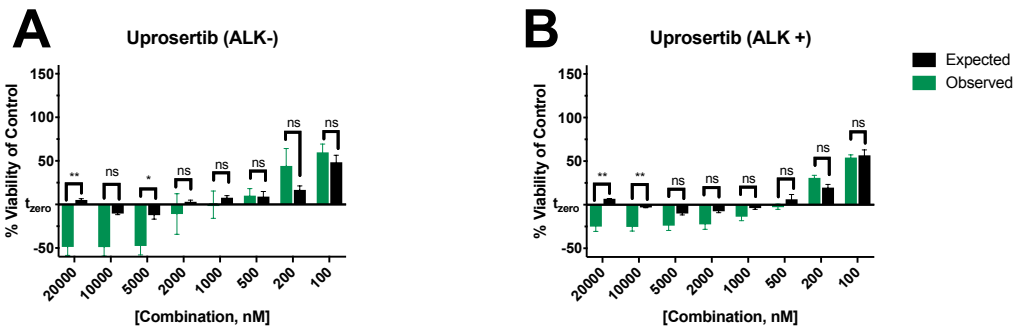


*Figure 16. Combination assay data of ceritinib and uprosertib against the ALK- cell line (A) and ALK+ cell line (B), analysed by the Webb fractional product method, comparing the expected (additive) effect against the observed effect. Where the observed % viability is less than the expected, synergy can be assumed. Statistical significance has been determined by calculation of the p-value using t-tests where: *** $P \leq 0.001$, ** $P \leq 0.01$, * $P \leq 0.05$, ns $P > 0.05$. Error bars shown represent the standard error of the mean.*

For the Chou and Talalay method, linearisation of the dose respose curves by generation of the median effect plot gave uprosertib D_m values of 12.3 µM ± 6.3 against the ALK- cell line and 4.2 µM ± 1.3 against the ALK+ cell line. Additionally, an m-value for uprosertib of 0.33 ± 0.02 was obtained for the ALK- cell line, and an m-value of 0.60 ± 0.12 was obtained for the ALK+ cell line. For the combination of ceritinib and uprosertib D_m values of 1.2 µM ± 0.5 and 0.4 µM ± 0.04 were obtained for the ALK- and ALK+ cell lines respectively. The corresponding m-values were found to be 1.18 ± 0.60 and 1 ± 0.17 for the ALK- and ALK+ cell lines respectively. These D_m and m-values allowed for the calculation of the combination indices across a range of concentrations. The combination indices at a fractional effect (Fa) of 0.5 (effectively at the IC_{50}) were found to be 1.12 and 0.42 for the ALK- and ALK+ cell lines respectively. At higher concentration, at a fractional effect of 0.96, the combination indices were 0.68 against both the ALK- and ALK+ cell lines. The combination index plots for both cell lines is shown in Figure 17. Against the ALK+ cell line, for the uprosertib/ceritinib combination, shows synergy across the whole range of fractional effects. However, against the ALK- cell line, it is only at a fractional effect requiring higher concentrations where the

combination becomes synergistic. At concentrations lower than this the combination can be seen to be quite antagonistic, with very high combination indices.

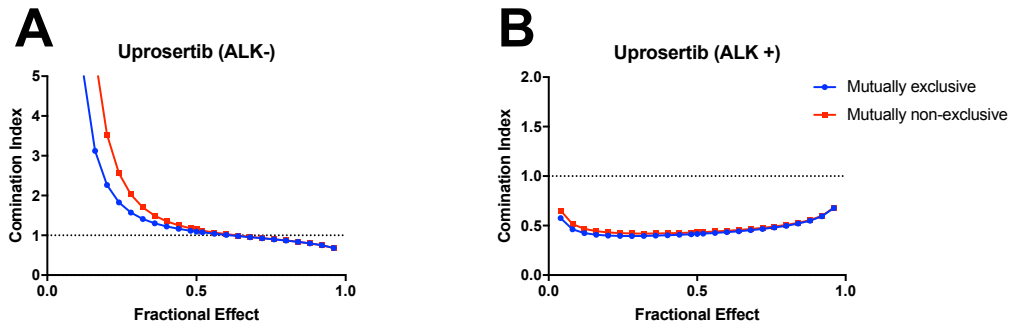


Figure 17. Combination index plots generated using the Chou and Talalay method for a 1:1 molar ratio of uprosertib and ceritinib against the ALK- cell line (A) and the ALK+ cell line (B). A combination index at a given fractional effect of 1 is an additive effect,>1 is antagonistic and <1 is synergistic.

This initial observation of good synergy against the ALK+ cell line for the uprosertib/ceritinb combination, using the Chou and Talalay method, could be an indication that the PI3K/AKT/mTOR pathway is important for EML4-ALK cell survival. On the other hand, however, looking at the dose response curves for the combination the activity appears to mimic that of ceritinib alone. With uprosertib being less potent that ceritinib it may be that this combination may not be suitable in a 1:1 ratio and a higher ratio of linifanib may be required to show a synergisic effect. Although the mathematical models predict a synergistic response, with this 1:1 ratio we opted not to persue this combination further.

2.2.4.2 Combination of Ceritinib and Gedatolisib

Gedatolisib[52] (PF-05212384), Figure 18, is a highly potent dual pan-PI3K/mTOR inhibitor developed by Wyeth then Pfizer. Gedatolisib is active against the 4 class I PI3Ks (α = 0.6 nM β = 6 nM, δ = 6 nM, γ = 8 nM) and is highly potent against mTOR which an activity of 1.6 nM making it a suitable candidate inhibitor for this study. Gedatolisib is discussed in more detail in Chapter 3.

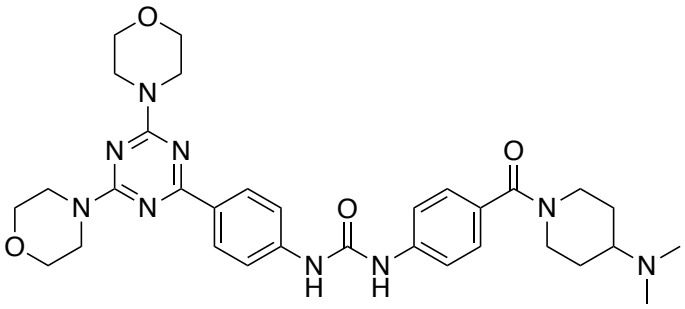


Figure 18. Chemical structure of gedatolisib

In vitro evaluation by MTT assay of gedatolisib against the ALK- and ALK+ cell lines showed that gedatolisib had a GI_{50} of 23 nM ± 2 against the ALK- cell line and had a GI_{50} of 13 µM ± 3 against the ALK+ cell line. The dose response curves for uprosertib and its combination with ceritinib are shown in Figure 19. Gedatolisib mainly showed a growth inhibitory effect, however it began to show potentially cytotoxic effects at higher concentrations in the ALK+ cell line at the highest concentration tested. Additionally, upon initial inspection it can be seen that the combination of ceritinib with gedatolisib shows a more active effect against the ALK+ cell line, suggesting the possiblity of synergism.

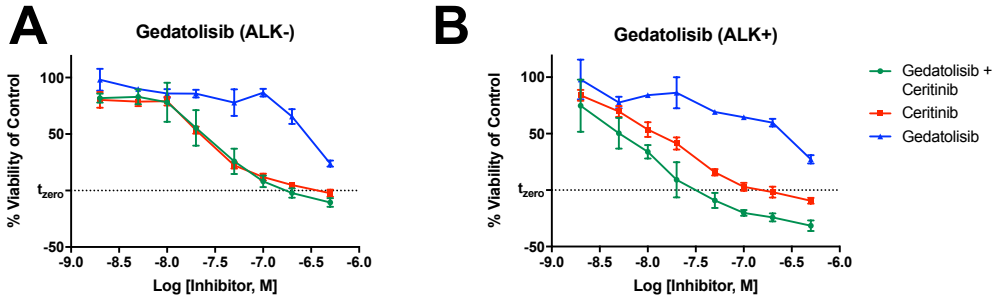


Figure 19. The Dose-response curves for ceritinib, gedatolisib and their combination against the ALK- cell line (A) and ALK+ cell line (B). Points are given as the mean ± the standard error of the mean (minimum 3 internal replicates). The dotted line shows the T_{zero} value (0% growth), and points below this line may indicate that an agent is cytotoxic. Growth is represented as percentage viability of the control, which has been normalised to 100%, where 0% is the T_{zero}.

In terms of evaluating synergy for the combination, the Webb method (Figure 20) indicated that there was no statistical significance between the expected and observed

effects against the ALK- cell line. Against the ALK+ cell line there was statistically significant differences at concentrations below 10 nM, however this suggested an antagonistic effect.

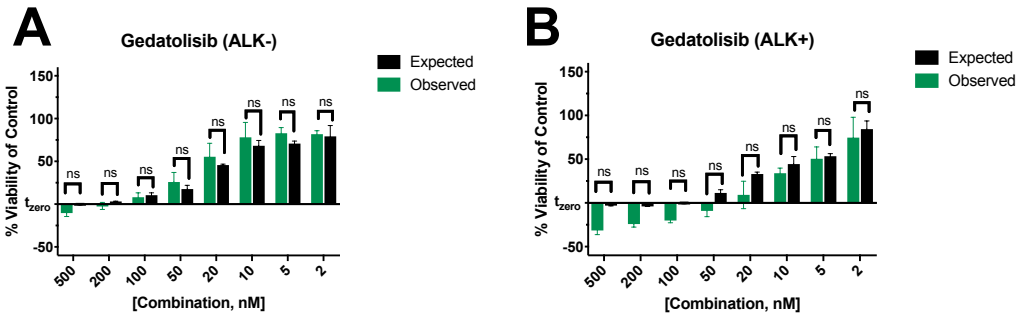


*Figure 20. Combination assay data of ceritinib and gedatolisib against the ALK- cell line (A) and ALK+ cell line (B), analysed by the Webb fractional product method, comparing the expected (additive) effect against the observed effect. Where the observed % viability is less than the expected, synergy can be assumed. Statistical significance has been determined by calculation of the p-value using t-tests where: *** $P \leq 0.001$, ** $P \leq 0.01$, * $P \leq 0.05$, ns $P > 0.05$. Error bars shown represent the standard error of the mean.*

For the Chou and Talalay method (Figure 21), linearisation of the dose respose curves by generation of the median effect plot gave gedatolisib D_m values of 53 nM ± 3 against the ALK- cell line and 23 nM ± 4 against the ALK+ cell line. Additionally, an m-value for gedatolisib of 0.81 ± 0.05 was obtained for the ALK- cell line, and an m-value of 0.82 ± 0.09 was obtained for the ALK+ cell line. For the combination of ceritinib and gedatolisib D_m values of 97 nM ± 40 and 34 nM ± 7 were obtained for the ALK- and ALK+ cell lines respectively. The corresponding m-values were found to be 0.86 ± 0.19 and 1.04 ± 0.25 for the ALK- and ALK+ cell lines respectively. These D_m and m-values allowed for the calculation of the combination indices across a range of concentrations. The combination indices at a fractional effect (Fa) of 0.5 (effectively at the IC_{50}) were found to be 0.44 and 0.78 for the ALK- and ALK+ cell lines respectively. At higher concentration, at a fractional effect of 0.96, the combination indices were 0.38 against both the ALK- and ALK+ cell lines. The combination index plots for both cell lines are shown in Figure 20. Against the ALK- cell line the combination index indicates synergy across the whole range of concentrations, however, against the ALK+ cell

line a synergistic response is only observed at concentrations higher than the concentration required to achieve a fractional effect of approximately 0.25.

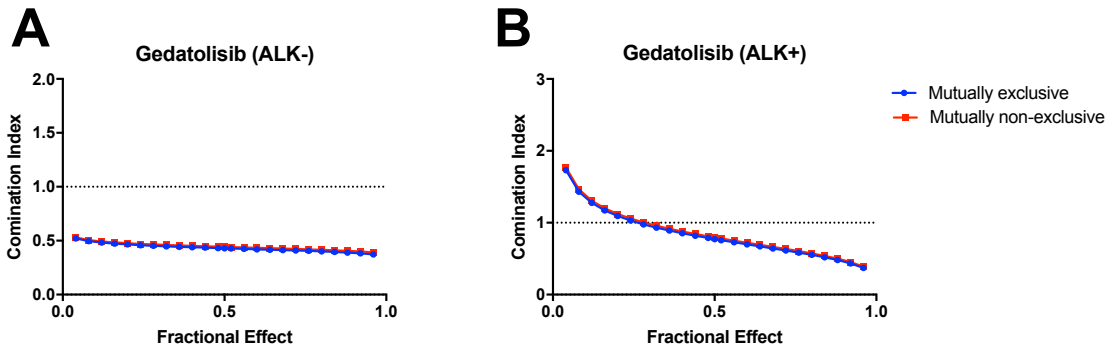


Figure 21. Combination index plots generated using the Chou and Talalay method for a 1:1 molar ratio of gedatolisib and ceritinib against the ALK- cell line (A) and the ALK+ cell line (B). A combination index at a given fractional effect of 1 is an additive effect,>1 is antagonistic and <1 is synergistic.

This initial observation of good synergy against the ALK+ cell line for the gedatolisib/ceritinb combination, using the Chou and Talalay method, could be an indication that the PI3K/AKT/mTOR pathway is important for EML4-ALK cell survival

2.2.4.3 Combination of Ceritinib and Pictilisib

Pictilisib[52][53] (GDC-0941), Figure 22, is a pan-PI3K inhibitor developed by Genentech. Pictilisib is highly potent against the class I PI3Ks (α = 3 nM, β = 33 nM, δ = 3 nM, γ = 75 nM) and weakly inhibits mTOR at 0.58 μM. Its selectivity over mTOR and high activity towards PI3K make it a good candidate for this study. Pictilisib is discussed in more detail in chapter 3.

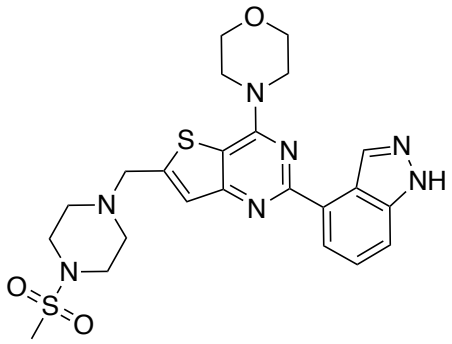


Figure 22. Chemical structure of Pictilisib

In vitro evaluation of pictilisib against the ALK- and ALK+ cell lines showed that pictilisib had a GI_{50} of 1217 nM ± 85 against the ALK- cell line and had a GI_{50} of 1175 nM ± 141 against the ALK+ cell line. The dose response curves for pictilisib and its combination with ceritinib are shown in Figure 23.

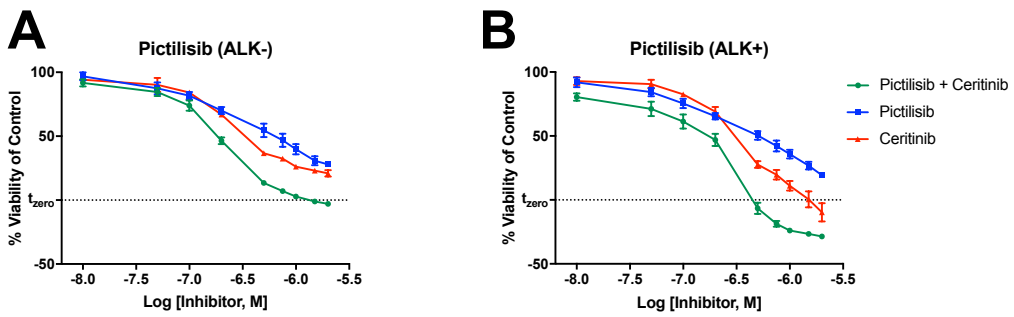


Figure 23. The Dose-response curves for ceritinib, pictilisib and their combination against the ALK- cell line (A) and ALK+ cell line (B). Points are given as the mean ± the standard error of the mean (minimum 3 internal replicates). The dotted line shows the T_{zero} value (0% growth), and points below this line may indicate that an agent is cytotoxic. Growth is represented as percentage viability of the control, which has been normalised to 100%, where 0% is the T_{zero}.

Evaluating for synergy using the Webb method (Figure 24) showed that there was no statistical significance bewteen the observed and expected effects across the whole range of concentrations, in ALK- cells. Conversely, against the ALK+ cell line there was good statistical significance at concentrations >500 nM.

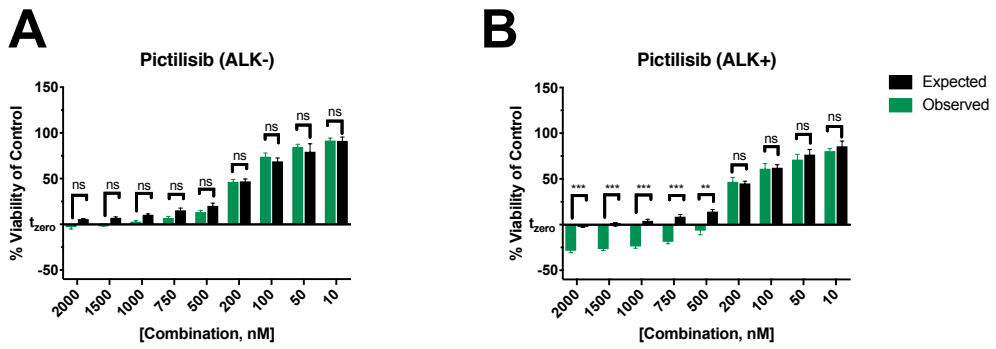


*Figure 24. Combination assay data of ceritinib and gedatolisib against the ALK- cell line (A) and ALK+ cell line (B), analysed by the Webb fractional product method, comparing the expected (additive) effect against the observed effect. Where the observed % viability is less than the expected, synergy can be assumed. Statistical significance has been determined by calculation of the p-value using t-tests where: *** $P \leq 0.001$, ** $P \leq 0.01$, * $P \leq 0.05$, ns $P > 0.05$. Error bars shown represent the standard error of the mean.*

Using the Chou and Talalay method (Figure 25), linearisation of the dose response curve by generation of the median-effect plot for pictilisib gave a D_m value of 1.2 µM ± 0.09 for the ALK- cell line, and a D_m value of 1.2 µM ± 0.1 for the ALK+ cell line. Additionally, the m-value obtained for pictilisib against the ALK- cell line was 0.72 ± 0.09, and the m-value obtained for pictilisib was 0.64 ± 0.08. For the combination of pictilisib with ceritinib, the D_m value obtained was 0.67 µM ± 0.05 against the ALK- cell line and was 0.28 µM ± 0.05 against the ALK- cell line. The corresponding m-values were 0.88 ± 0.07 and 1.0 ± 0.05 for the ALK- and ALK+ cell lines respectively. These D_m and m-values allowed for the calculation of the combination indices across a range of concentrations. The combination indices at a fractional effect (Fa) of 0.5 (effectively at the IC_{50}) were found to be 0.72 and 0.37 for the ALK- and ALK+ cell lines respectively. At higher concentration, at a fractional effect of 0.35, the combination indices were 0.24 against both the ALK- and ALK+ cell lines. The combination index plots for both cell lines is shown in Figure 25. Against the ALK- cell line, the Chou and Talalay method indicates synergy at concentrations above a fractional effect of 0.25, but at lower concentrations, shows additive and even anatgonistic effects. Conversely, the synergy

observed against the ALK+ cell line is greater and is observed at even lower concentrations. In conclusion, greater synergy between pictilisib and ceritinib is observed against the ALK+ cell line.

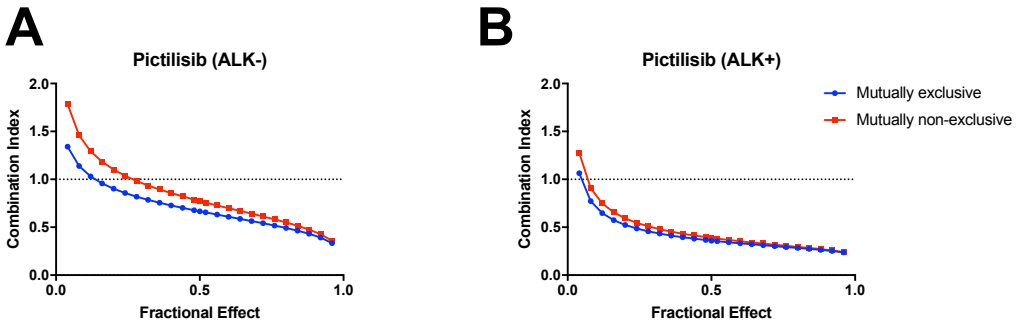


Figure 25. Combination index plots generated using the Chou and Talalay method for a 1:1 molar ratio of pictilisib and ceritinib against the ALK- cell line (A) and the ALK+ cell line (B). A combination index at a given fractional effect of 1 is an additive effect,>1 is antagonistic and <1 is synergistic.

Immunoblot Analysis

Seeing excellent synergy with inhibitors of the PI3K pathway, the investigation progressed to the exploration of the pictilisib/ceritinib combination with immunoblot analysis. Cell were treated with ceritinib (500 nM, 24 h), pictilisib (500 nM, 24 h), and their combination (500 nM of each inhibitor, 24 h). The treatment was consistent for all analyses, and for the following discussion, for simplicity, this will simply be referred to as treatment with ceritinib, pictilisib, or the combination.

The PI3K/AKT/mTOR pathway was explored using immunoblot analysis, looking at the phosphorylation of AKT (Figure 26). Total AKT expression was observed in both the ALK+ and ALK- cell lines, and was seen to be unaffected by treatment with ceritinib, pictilisib, or the combination. Phosphorylation of AKT however, was observed to be only slightly inhibited upon treatment with ceritinib, likely due to the EML4-ALK fusion protein preceding PI3K and AKT in the signalling cascade, however the pathway could still be triggered through crosslinks. Additionally, as expected, pictilisib as a single agent and its combination with ceritinib inhibited phosphorylation of AKT, thus completely preturbing the PI3K/AKT/mTOR pathway.

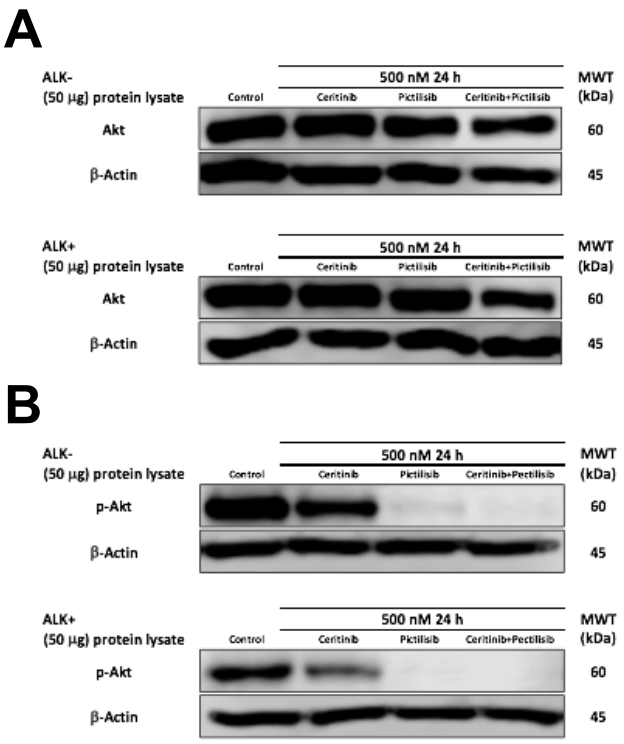


Figure 26. Immunoblot analysis of total AKT (A) and phosphorylated AKT (B) against the ALK+ and ALK- cell lines after 24 h treatment of pictilisib, ceritinib and their combination.

Examination of the Ras/Raf/MEK/ERK pathway (Figure 27) showed total ERK expression (ERK1 and ERK2) in ALK- cells to be expressed and unaffected by treatment with ceritinib, pictilisib, or the combination. However, it was noted that the total ERK1 expression was significantly less than ERK2 expression. In the ALK+ cell line however, there was more ERK1 expression than that of the A549 parent cell line, and it was seen to be slightly affected upon treatment with ceritinib, pictilisib, and the combination. Phosphorylation of ERK1 and ERK2 in the ALK+ cell line was seen to be unaffected by treatment with ceritinib, pictilisib, or the combination. However, in the ALK- cell line, both p-ERK1 and p-ERK2 were inhibited by ceritinib, pictilisib, and the combination.

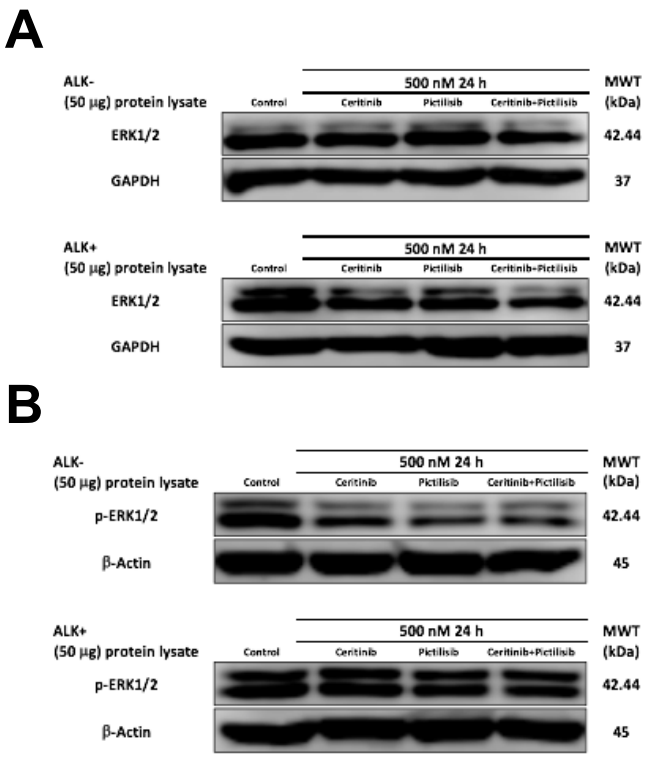


Figure 27. Immunoblot analysis of total ERK1/2 (A) and phosphorylated ERK1/2 (B) against the ALK+ and ALK- cell lines after 24 h treatment of pictilisib, ceritinib and their combination.

Investigating the total STAT3 in the JAK/STAT pathway (Figure 28) showed that total STAT3 was expressed and unaffected by treatment with ceritinib, pictilisib, or the combination. However, most interestingly, no phosphorylated STAT3 was observed in ALK- cells at all, even in the untreated control sample. Conversely, in the ALK+ cell line, phosphorylation of STAT3 was observed in the untreated control sample. This is likely due to the constitutive nature of signal transduction, a consequence of the EML4-ALK fusion. Additionally, treatment with ceritinib pictilisib, and the combination showed a reduction in p-STAT3, where there was almost complete inhibition of the JAK/STAT signal trasnduction with the combination.

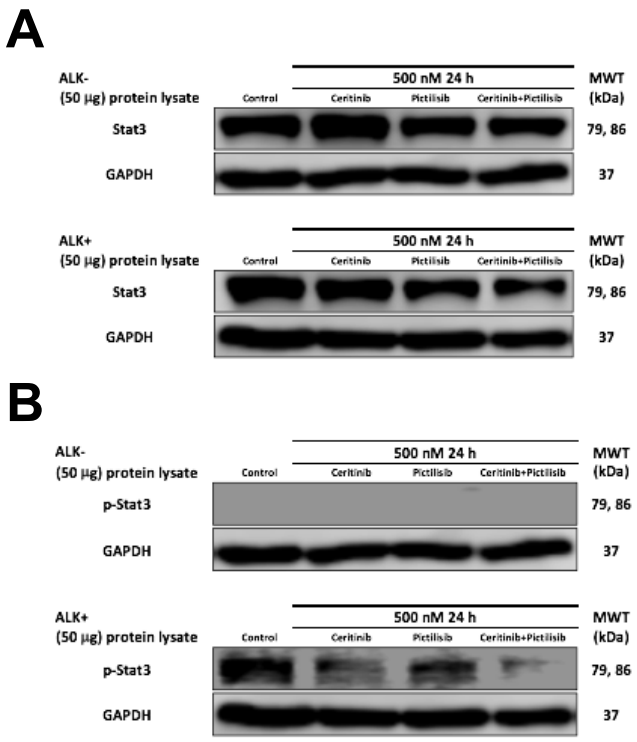


Figure 28. Immunoblot analysis of total ERK1/2 (A) and phosphorylated ERK1/2 (B) against the ALK+ and ALK- cell lines after 24 h treatment of pictilisib, ceritinib and their combination.

Immunoblot analysis confirmed the presence of the EML4-ALK fusion protein (Figure 29).

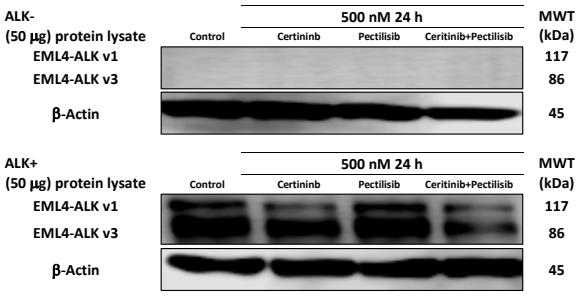


Figure 29. Immunoblot analysis confirming the pressence of EML4-ALK in the ALK+ cell line.

Clonogenic assays

The effects on colony formation of pictilisib, ceritinib and their combination were assessed by clonogenic assay. ALK- and ALK+ cells were plated at 400 cells per well, and treated with 500 nM or 1 μM of test agent, and in the case of the combination, treated with a the concentration of each agent in a 1:1 molar ratio. Images of colonies are illustrated in Figure 30 and Figure 31. The results of the 24 h clonogenic assays are summarised in Figure 32, where there is no significant reduction in the ability to form colonies except upon treatment of the ALK- cell line with 1 μM ceritinib.

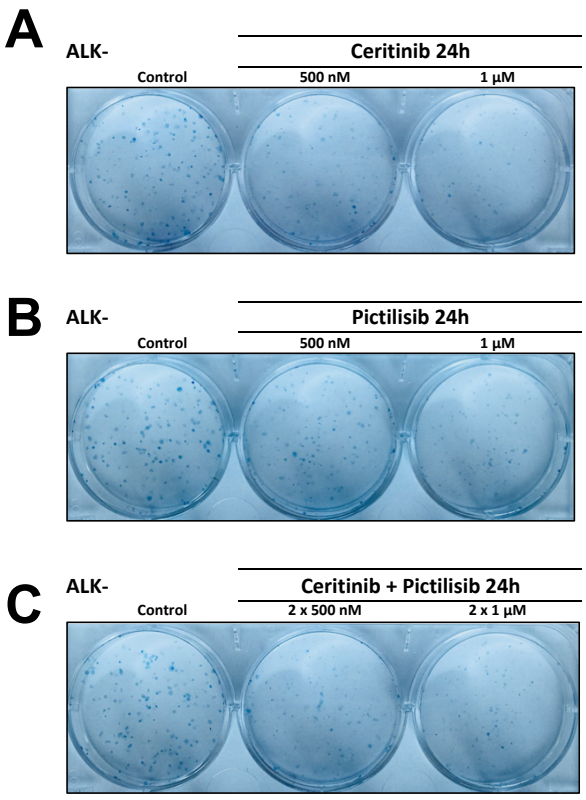


Figure 30. Representative clonogenic assay plates assesing the ability of cells to form colonies following 24 h treatment of (A) ceritinib, (B) pictilisib, and (C) ceritinib + pictilisib against the ALK- cell line. Cells are stained with methylene blue.

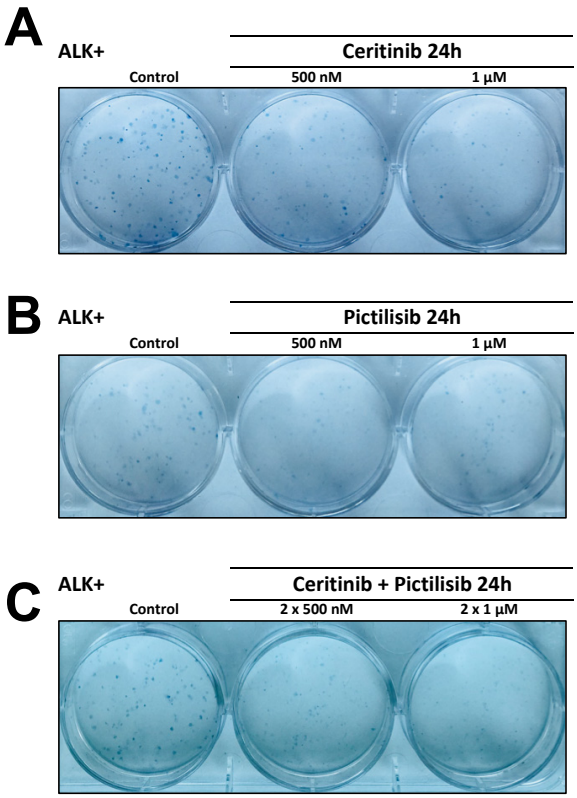


Figure 31. Representative clonogenic assay plates assesing the ability of cells to form colonies following 24 h treatment of (A) ceritinib, (B) pictilisib, and (C) ceritinib + pictilisib against the ALK+ cell line. Cells are stained with methylene blue.

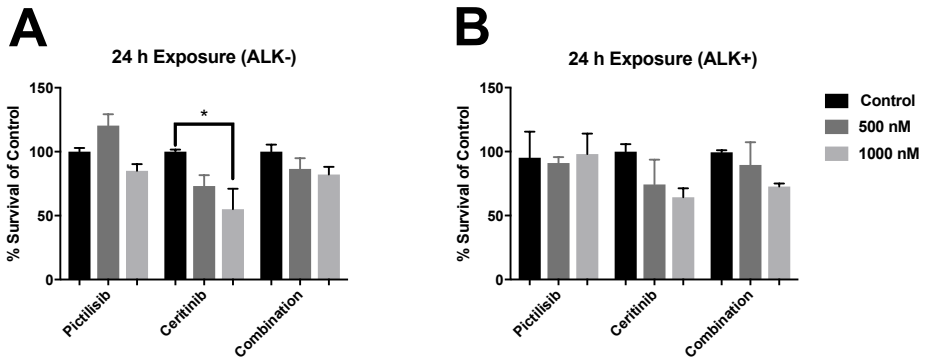


*Figure 32. Effect of ceritinib, pictilisib and their combination on colony formation after 24 h against (A) the ALK- and (B) ALK+ cell lines. Mean survival fraction as a % of control is represented as the mean and SEM of 3 independent samples, where *p < 0.05.*

Since there was no great reduction in the ability to form colonies, indicating test agents were cytostatic rather than cytotoxic at the concentrations selected after 24 h exposure, the exposure time to the drugs was increased to 72 h. The results of this ex-

periment are shown in Figure 33 and Figure 34.

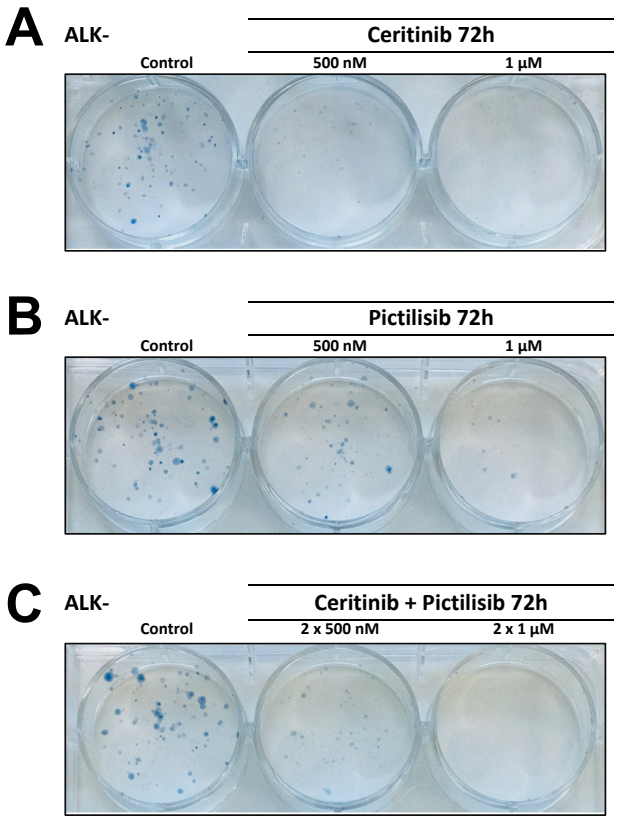


Figure 33. representative clonogenic assay plates assessing the ability of cells to form colonies following 72 h treatment of (A) ceritinib, (B) pictilisib, and (C) ceritinib + pictilisib against the ALK- cell line. Cells are stained with methylene blue.

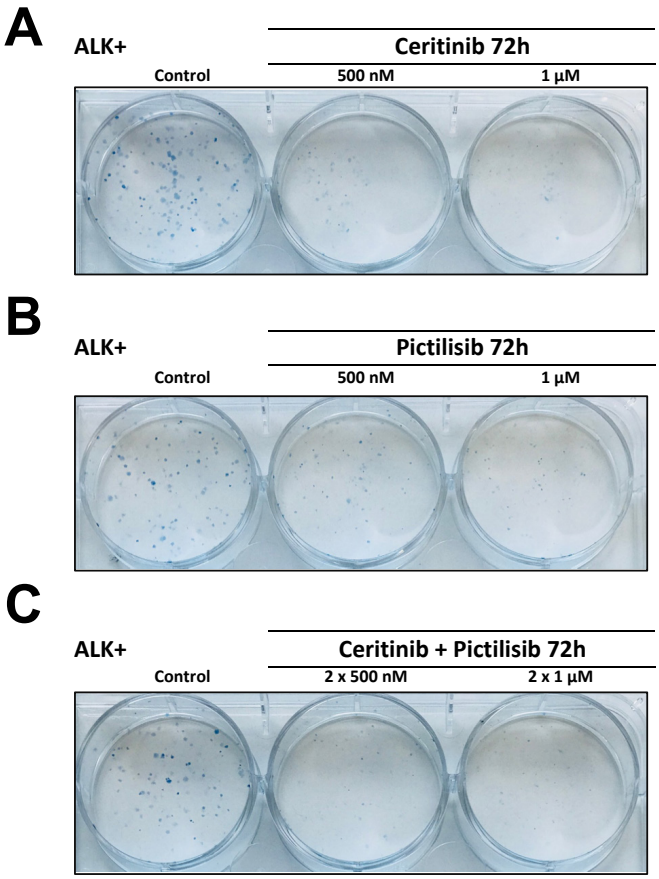


Figure 34. Representative clonogenic assay plates assesing the ability of cells to form colonies following 72 h treatment of (A) ceritinib, (B) pictilisib, and (C) ceritinib + pictilisib against the ALK+ cell line. Cells are stained with methylene blue.

The results of the 72 h exposure clonogenic asssays are summarised in Figure 35, where a significant reduction in colony formation was observed, particularly in the ALK+ cell line where ceritinib and the combination showed an excellent reduction in the ability to form colonies. Since the number of colonies have been reduced after 72h exposure this suggests that at this dose and exposure time the drugs may no longer be cytostatic but we may start to be seeing cytotoxicity occuring since in the clonogenic assay, a purely cytostatic agent will not reduce the number of colonies, only the size of the colonies. Cancer cells possessing an oncogene driver mutation such as EML4-ALK, that are addicted to a particular oncogenic cascade, inhibiting that cascade in the short term may stop proliferation, which is seen here. In the mid-long term inhibition of the pathway might cause apoptotis, but in the long term (from the patients' view) acquired

resistance will emerge as compensatory signalling cascades are activated/ further mutations evolve.

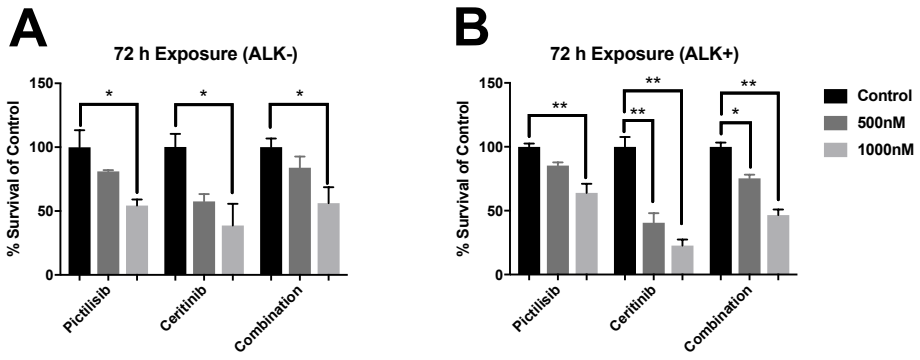


*Figure 35. Effect of ceritinib, pictilisib and their combination on colony formation after 72 h against (A) the ALK- and (B) ALK+ cell lines. Mean survival fraction as a % of control is represented as the mean and SEM of 3 independent samples, where *p < 0.05, **p < 0.01.*

Cell cycle

Cell cycle analysis was used to examine the effects of pictilisib, ceritinib and their combination on the cell cycle. Figure 36 and Figure 37 shows representative histograms from these experiments, where cells were stained with propidium iodide, which intercalates DNA. The number of events were counted, and DNA content per event was analysed and by flow cytometry. The percentage of gated events in each cell cycle phase is shown in Figure 38 (ALK-) and Figure 39 (ALK+). After 24 h exposure, against the ALK- cell line, there was significant accumulation in the G1 phase and decline in S phase events for the combination. Against the ALK+ cell line there was great accumulations in the G1 phase and decline in S phase events for both pictilisib alone and its combination with ceritinib. Likewise, after 72 h exposure, pictilisib and its combination showed significant accumulations in G1. In conclusion, the combination of ceritinib and pictilisib induce G1 arrest. This may be expected in the short term as there is inhibition/ interruption of the proliferative signals. In the longer term this could cause a crisis and tip the cells into apoptosis. This may be the case as indicated in clonogenic assays as there were fewer colonies which is an indication of loss of viability.

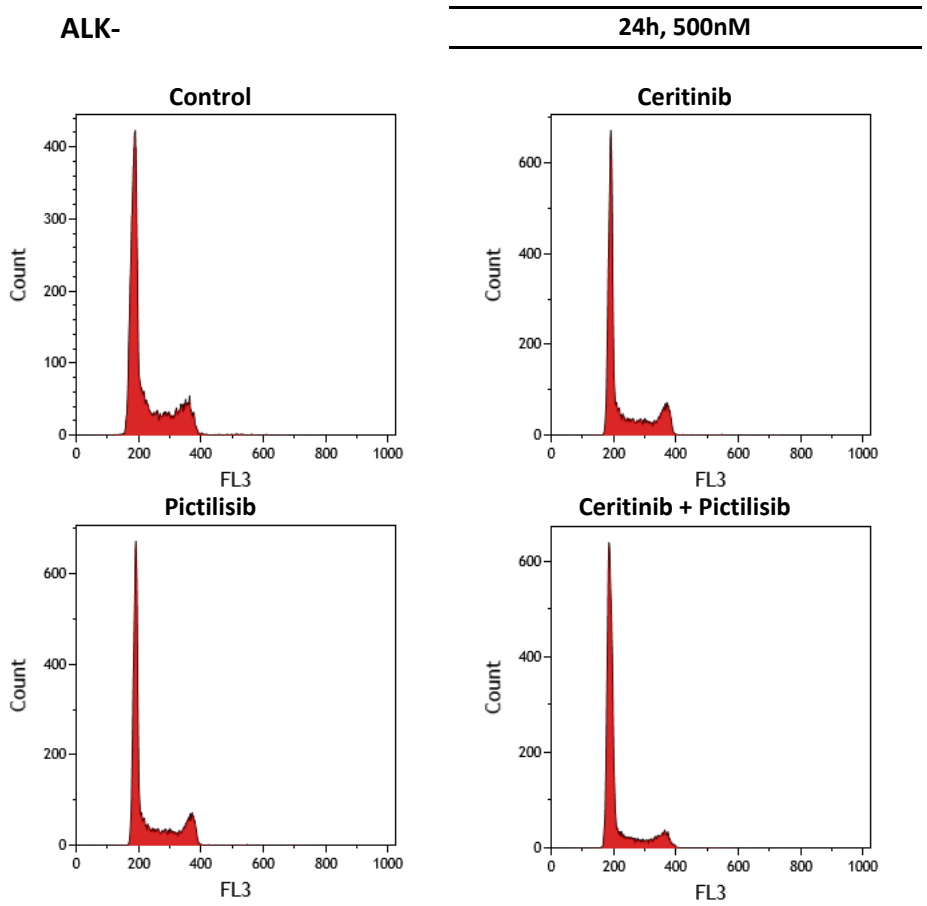


Figure 36. Cell cycle analysis histograms against the ALK- cell line after 24 h exposure of 500 nM test agent for single agents and 500 nM of each test agent in the case of the combination. Cells were stained with propidium iodide, which intercalates DNA, and analysed by flow cytometry. A minimum of 10,000 events were recorded. Experiments were repeated ≥ 3 times.

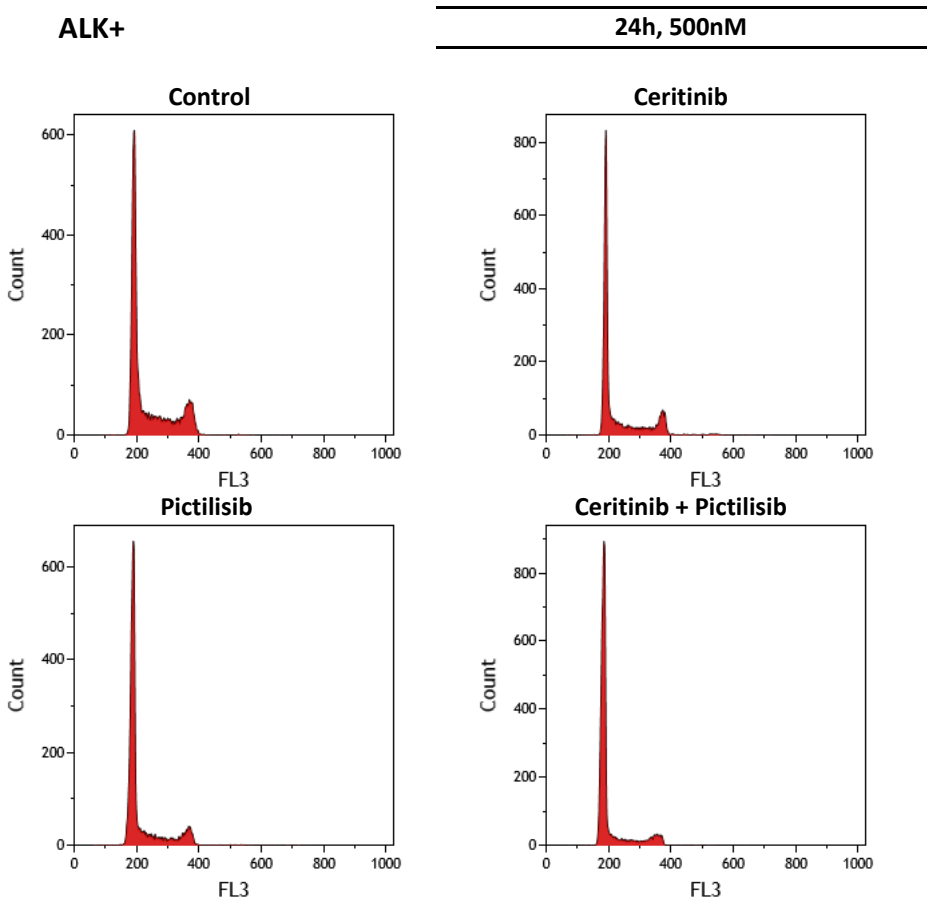


Figure 37. Cell cycle analysis histograms against the ALK+ cell line after 24 h exposure of 500 nM test agent for single agents and 500 nM of each test agent in the case of the combination. Cells were stained with propidium iodide, which intercalates DNA, and analysed by flow cytometry. A minimum of 10,000 events were recorded. Experiments were repeated ≥ 3 times

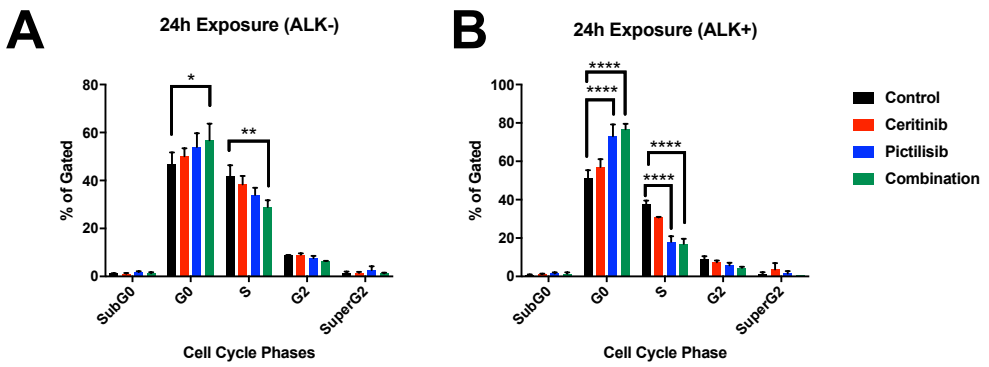


*Figure 38. Effect of ceritinib, pictilisib and their combination against the (A) ALK- and (B) ALK+ cell lines at 500 nM after 24 h exposure. A minimum of 10,000 events were recorded. Experiments were repeated ≥ 3 times. *p < 0.05; **p < 0.01; ***p < 0.001; ****p < 0.000.*

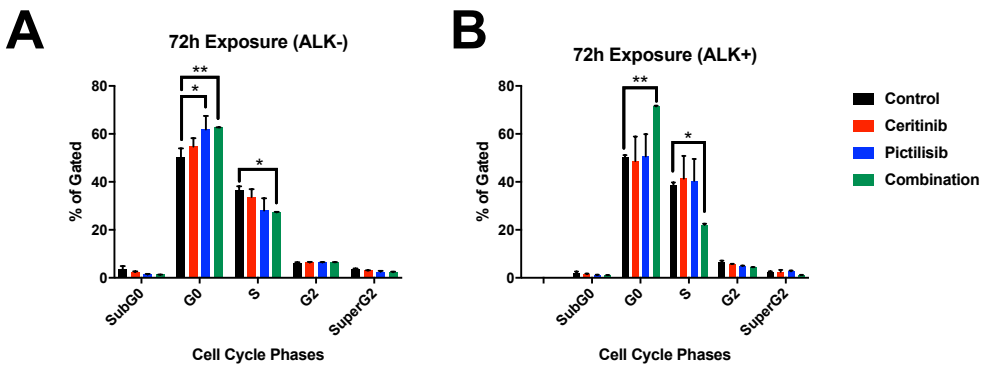


*Figure 39. Effect of ceritinib, pictilisib and their combination against the (A) ALK- and (B) ALK+ cell lines at 500 nM after 72 h exposure. A minimum of 10,000 events were recorded. Experiments were repeated ≥ 3 times. *p < 0.05; **p < 0.01; ***p < 0.001; ****p < 0.000.*

Apoptosis

The ability of ceritinib and pictilisib (either alone or in combination) to induce cellular apoptosis was evaluated by flow cytometry following dual annexin-V FITC and PI staining of cells. Representative dot plots for the experiments are shown in Figure 40 (ALK -) and Figure 41 (ALK+). A summary of the results for this experiment are shown in Figure 42, which shows that after 72 h exposure neither ceritinib, pictilisib, nor their combination induce apoptosis, again indicative of cytostasis at the concentrations examined.

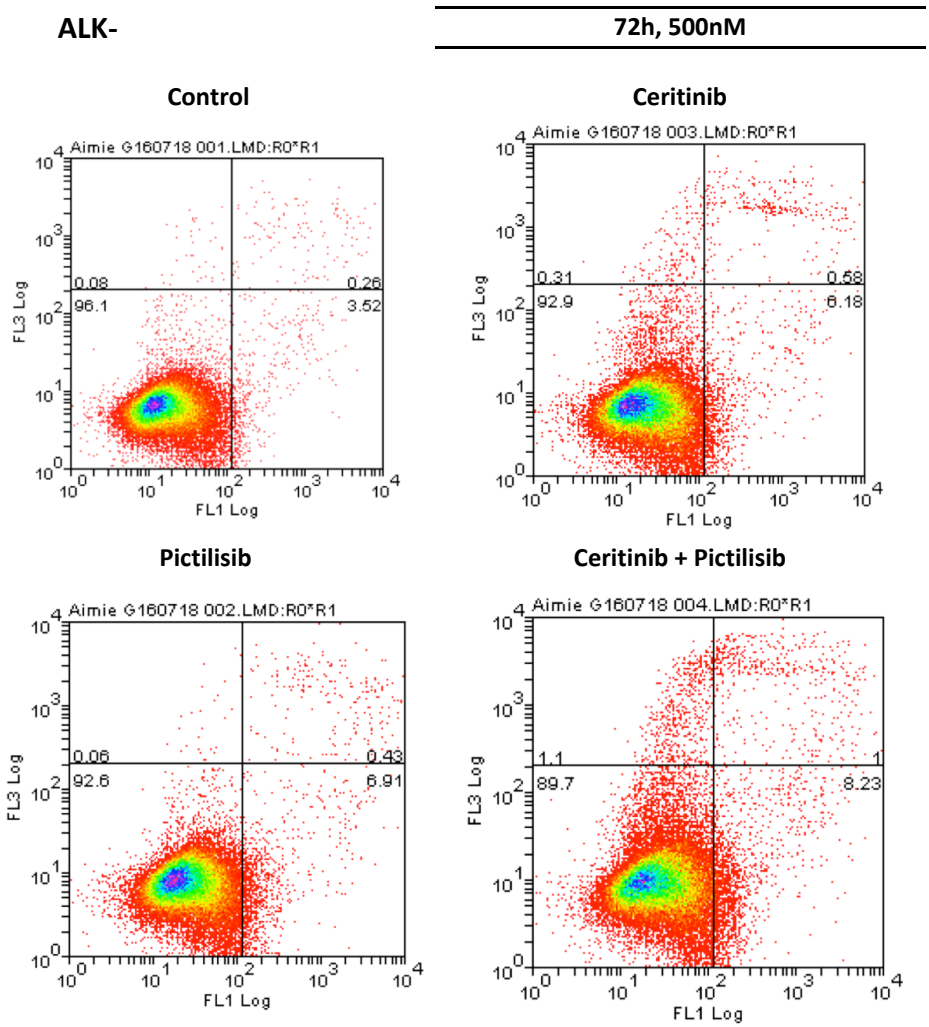


Figure 40. Representative dot plots of ceritinib, pictilisib and their combination at 500 nM after 72 h exposure against the ALK- cell line. Events in the lower left (LL) quadrant show cells not undergoing apoptosis, events in the lower right (LR) quadrant show cells undergoing early apoptosis, events in the upper right (UR) quadrant show cells undergoing late apoptosis, and events in the upper left (UL) show necrotic cells. A minimum of 20,000 events were recorded. Experiments were repeated 2 times.

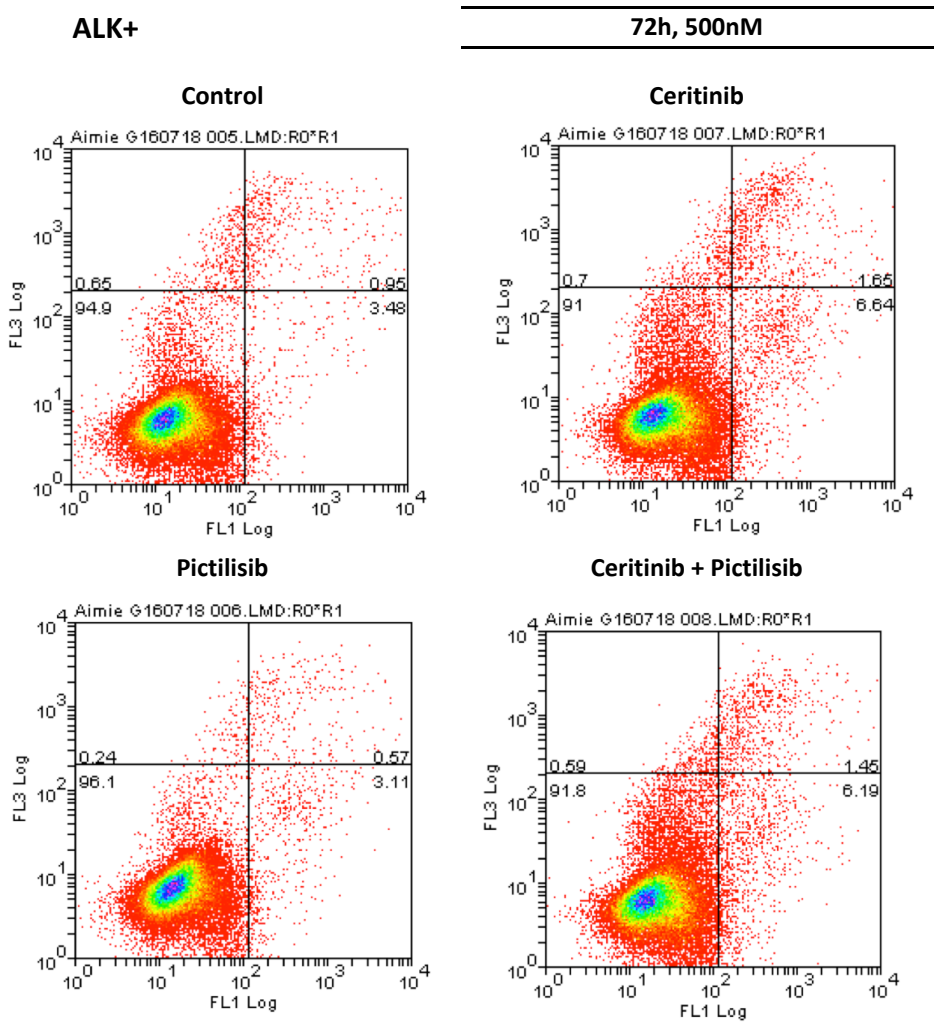


Figure 41. Representative dot plots of ceritinib, pictilisib and their combination at 500 nM after 72 h exposure against the ALK+ cell line. Events in the lower left (LL) quadrant show cells not undergoing apoptosis, events in the lower right (LR) quadrant show cells undergoing early apoptosis, events in the upper right (UR) quadrant show cells undergoing late apoptosis, and events in the upper left (UL) show necrotic cells. A minimum of 20,000 events were recorded. Experiments were repeated 2 times.

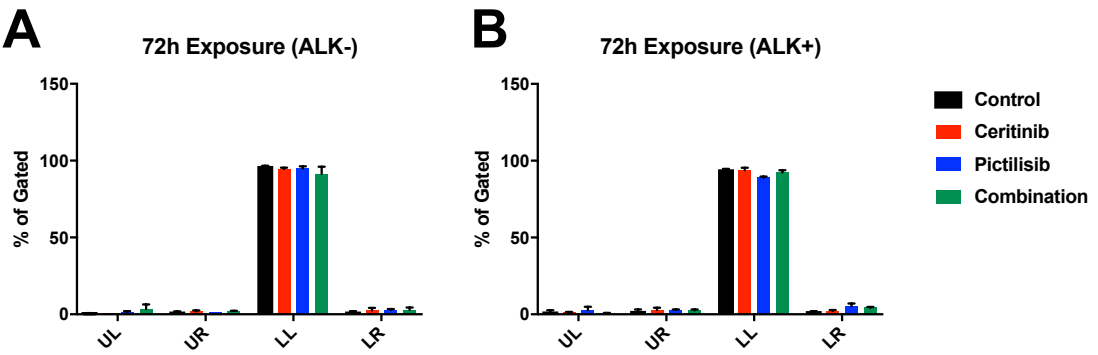


Figure 42. Effect of ceritinib, pictilisib and their combination against the ALK- cell line (A) and ALK+ cell line (B) at 500 nM after 72 h exposure. Cellular annexin V-FITC/PI stained DNA content was analysed by flow cytometry. A minimum of 20,000 events were recorded. Experiments were repeated 2 times.

2.2.4.4 Combination of Ruxolitnib and Ceritinib

Ruxolitinib (INCB018424), Figure 43, is the first potent, selective, JAK1/2 inhibitor to enter the clinic with IC_{50} of 3.3 nM/2.8 nM in cell-free assays, >130-fold selectivity for JAK1/2 versus JAK3.

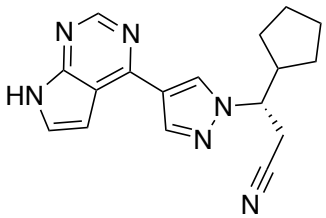


Figure 43. Structure of ruxolitnib (INCB018424).

In vitro evaluation by MTT assasy of ruxolitnib against the ALK- and ALK+ cell lines showed that Ruxolitinib had a GI_{50} of 36.5 µM ± 14.2 against the ALK- cell line and had a GI_{50} of 12.8 µM ± 3.6 against the ALK+ cell line. The dose response curves for ruxolitnib and its combination with ceritinib are shown in Figure 44. Ruxolitnib showed a growth inhibitory effect at higher concentration, and is signifcantly less potent that ceritinib.

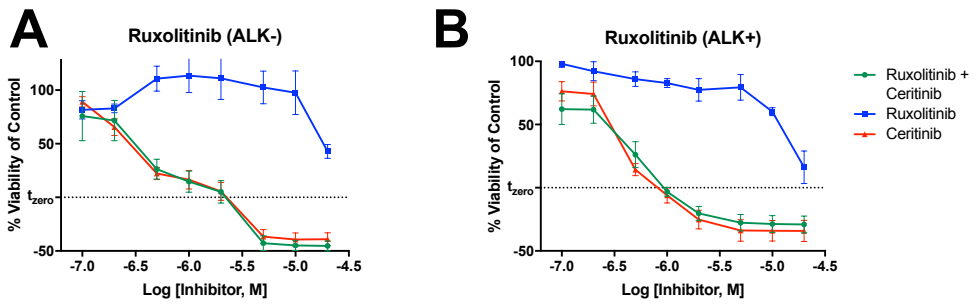


Figure 44. The Dose-response curves for ceritinib, ruxolitnib and their combination against the ALK- cell line (A) and ALK+ cell line (B). Points are given as the mean ± the standard error of the mean. The dotted line shows the Tzero value (0% growth), and points below this line may indicate that an agent is cytotoxic.

Evaluating for synergy using the Webb method (Figure 45) showed that there was no statistical significance between the observed and expected effects across the whole range of concentrations.

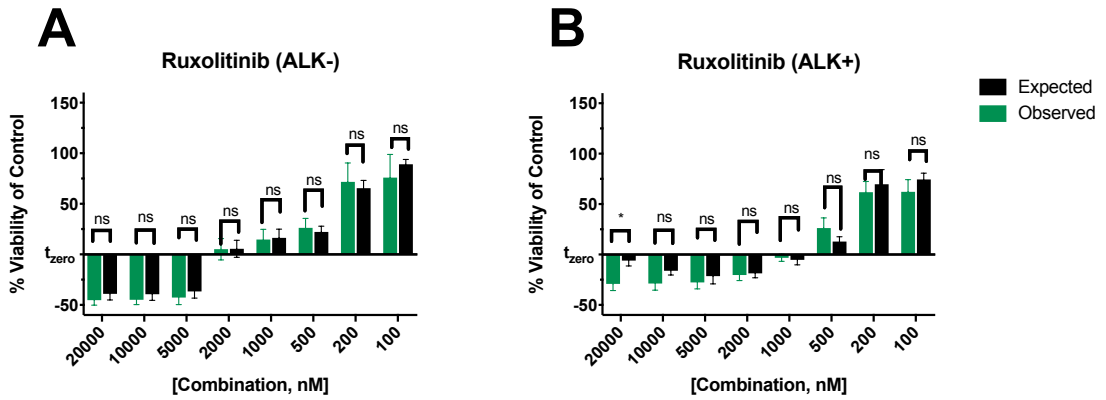


*Figure 45. Combination assay data of ceritinib and ruxolitnib against the ALK- cell line (A) and ALK+ cell line (B), analysed by the Webb fractional product method, comparing the expected (additive) effect against the observed effect. Where the observed % viability is less than the expected, synergy can be assumed. Statistical significance has been determined by calculation of the p-value using t-tests where: *** $P \leq 0.001$, ** $P \leq 0.01$, * $P \leq 0.05$, ns $P > 0.05$. Error bars shown represent the standard error of the mean.*

For the Chou and Talalay method (Figure 46), linearisation of the dose respose curves by generation of the median effect plot gave ruxolitnib D_m values of 36.5 µM ± 14.2 against the ALK- cell line and 12.8 µM ± 3.6 against the ALK+ cell line. Addition-

ally, an m-value for ruxolitnib of 3.12 ± 2.51 was obtained for the ALK- cell line, and an m-value of 1.40 ± 0.38 was obtained for the ALK+ cell line. For the combination of ceritinib and ruxolitnib D_m values of 14.9 µM ± 0.58 and 1.51 µM ± 0.86 were obtained for the ALK- and ALK+ cell lines respectively. The corresponding m-values were found to be 0.97 ± 0.28 and 1.05 ± 0.14 for the ALK- and ALK+ cell lines respectively. These D_m and m-values allowed for the calculation of the combination indices across a range of concentrations. The combination indices at a fractional effect (Fa) of 0.5 (effectively at the IC_{50}) were found to be 1.34 and 1.60 for the ALK- and ALK+ cell lines respectively. At higher concentration, at a fractional effect of 0.96, the combination indices were 1.87 and 2.60 against the ALK- and ALK+ cell lines respectively. The combination index plots for both cell lines is shown in figure 45. Against the ALK+ cell line, the ruxolitnib/ceritinib combination shows antagonism across the whole range of fractional effects.

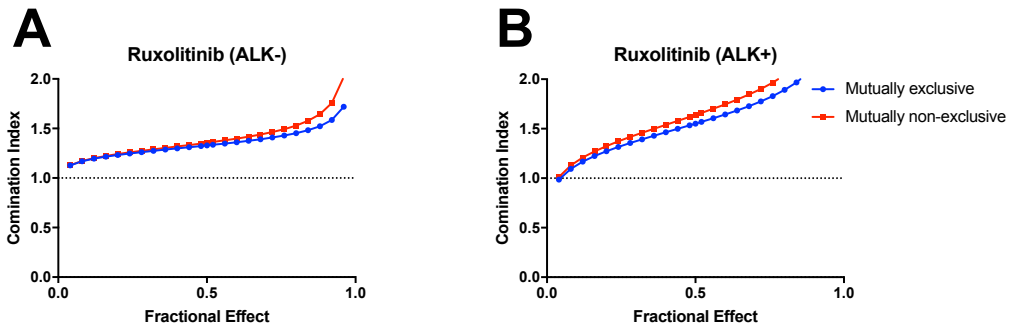


Figure 46. Combination index plots generated using the Chou and Talalay method for a 1:1 molar ratio of ruxolitnib and ceritinib against the ALK- cell line (A) and the ALK+ cell line (B). A combination index at a given fractional effect of 1 is an additive effect,>1 is antagonistic and <1 is synergistic.

2.3 Chapter Conclusions

Table 2 summarises the Chou and Talalay *in vitro* data for the various combinations discussed in this chapter.

Table 2. The parameters used to calculate the Combination Index of combinations against the ALK- (grey) and ALK+ cell lines . The combination index is given as an average of the mutually exclusive and mutually non-exclusive combination indexes.

	m-value (± SEM)	**D_m value (± SEM)/μM**	**Combination Index**			
			$(Fa)_{25}$	**$(Fa)_{50}$**	**$(Fa)_{76}$**	**$(Fa)_{96}$**
Ceritinib	1.02 ± 0.01	0.57 ± 0.5				
Linifanib	1.23 ± 0.25	11.8 ± 6.3	1.72	2.03	2.42	3.35
Combination	0.9 ± 2.05	2.1 ± 1.7				
Ceritinib	1.23 ± 0.14	0.51 ± 0.5				
Linifanib	0.83 ± 0.36	15.5 ± 11.0	0.59	0.55	0.52	0.47
Combination	1.30 ±0.22	0.53 ± 0.49				
Ceritinib	1.02 ± 0.01	0.57 ± 0.5				
Uprosertib	0.33 ± 0.02	12.3 ± 6.3	2.19	1.12	0.90	0.68
Combination	1.18 ± 0.60	1.2 ± 0.49				
Ceritinib	1.23 ± 0.14	0.51 ± 0.5				
Uprosertib	0.60 ± 0.12	4.2 ± 1.3	0.41	0.42	0.46	0.68
Combination	1.00 ± 0.17	0.37 ± 0.04				
Ceritinib	1.02 ± 0.01	0.57 ± 0.5				
Gedatolisib	0.81 ± 0.05	0.05 ± 0.003	0.46	0.44	0.41	0.38
Combination	0.86 ± 0.19	0.10 ± 0.04				
Ceritinib	1.23 ± 0.14	0.51 ± 0.5				
Gedatolisib	0.82 ± 0.09	0.023 ± 0.004	1.04	0.78	0.60	0.38
Combination	1.04 ± 0.25	0.034 ± 0.007				
Ceritinib	0.76 ± 0.07	0.85 ± 0.09				
Pictilisib	0.72 ± 0.09	1.22 ± 0.09	0.95	0.72	0.55	0.35
Combination	0.88 ± 0.07	0.67 ± 0.05				
Ceritinib	0.76 ± 0.07	0.57 ± 0.1				
Pictilisib	0.64 ± 0.08	1.12 ± 0.1	0.52	0.37	0.30	0.24
Combination	0.28 ± 0.05	0.60 ± 0.22				
Ceritinib	1.02 ± 0.01	0.57 ± 0.5				
Ruxolitnib	3.12 ± 2.51	36.5 ± 14.2	1.25	1.34	1.46	1.87
Combination	0.97 ± 0.28	14.9 ± 0.58				
Ceritinib	1.23 ± 0.14	0.51 ± 0.5				
Ruxolitnib	1.40 ± 0.38	12.8 ± 3.6	1.34	1.60	1.90	2.60
Combination	1.05 ± 0.14	1.51 ± 0.86				

From the above it can be concluded that a synergistic effect is not observed between ceritinb and the P2Y2 inhibitor AR-C118925, and therefore this combination was not considered further. Combination of ceritinib and the VEGF inhibitor linifanib showed synergy in the Chou and Talalay method, however the Webb method was not in agreement and the dose response curve from the MTT assay did not appear to shift for the combination therefore this combination was occluded from further investigation. Combination of Uprosertib, the AKT inhibitor, and Ceritinb showed synergy against the ALK+ cell line by the Chou and Talalay method, however the Webb method did not agree and the dose response curve did not shift. It was therefore decided not to investigate this combination further. The combination of gedatolisib, the dual PI3K/mTOR inhibitor and ceritinib also was synergistic using the Chou and Talalay method, with the Webb method not in agreement, therefore this combination was also occluded from further study. Likewise was the combination of ruxolitnib, the JAK inhibitor, and ceritinib. The combination of the pan PI3K inhibitor, pictilisib, and ceritinib was the most interesting combination since both methods of synergy determination were in agreement. This combination was studied further; the ability for the combination to reduce colony formation was assesed by clonogenic assay, the ability for the combination to induce apoptosis was assessed with the Annexin V assay, and the ability for the combination to perturb the cell cycle was assessed through cell cycle analysis. Clonogenic assays determined that the combination of pictilisib and ceritinib reduced the ability of the cells to form colonies after treatment of 500 nM of test agents with 72 h exposure. An annexin V assay showed that 500 nM treatment of test agents and the combination did not induce apoptosis, and cell cycle analysis showed that 500 nM of each test agent after both 24 h and 72 h exposure lead to G1 arrest. Immunoblot analysis showed inhibition of the PI3K pathway and the JAK/STAT pathway. The combination with the pan PI3K inhibitor showed excellent synergy, which prompted further investigation of PI3K, which is the topic of the next chapter, where isoform selective PI3K inhibitors will be evaluated.

3. Homing in on Synergy with PI3K Inhibitors

3.1 Introduction

3.1.1 Phosphoinositide 3-kinase (PI3K)

Phosphatidylinositol-3-kinases[55] (PI3K) are a family of lipid kinases that phosphorylate phosphoinositides specifically at the 3-position of the inositide ring[57][58]. The PI3K family is divided into three classes (I, II, and III) on the basis of sequence homology, structure, binding partners, mode of activation and substrate preference[56].

In Class I of the PI3Ks, which exist as heterodimers consisting of a regulatory and a catalytic subunit, there are four structural isoforms (PI3Kα, PI3Kβ, PI3Kδ, and PI3Kγ), divided into 2 classes, class IA and IB. Class IA PI3Ks (PI3Kα, PI3Kβ, and PI3Kδ), which are activated by receptor tyrosine kinases (RTKs), consist of a p110 catalytic subunit, of which there are 3 variants (p110α, p110β, and p110δ), and a regulatory subunit, of which there are 5 variants (p85α, p55α, p50α, p85β, and p55γ, where p85 variants are the most highly expressed). Class IB PI3Ks (PI3Kγ), which are activated by G-protein-coupled receptors (GPCRs), consist of a p110γ catalytic subunit and either a p101 or p84 regulator subunit. As a whole, class I PI3Ks are primarily responsible for the phosphorylation of the phospholipid phosphatidylinositol 4,5-bisphosphate (PI(4,5) P_2 or PIP2) to phosphatidylinositol (3,4,5)-trisphosphate (PI(3,4,5)P_3 or PIP3). PIP3 functions to activate downstream signalling, primarily the activation of protein kinase B (AKT). Once activated, AKT can go on to activate numerous substrates including the mammalian target of rapamycin (mTOR), which functions, among others, to regulate

cell growth/migration/proliferation/survival and transcripton.

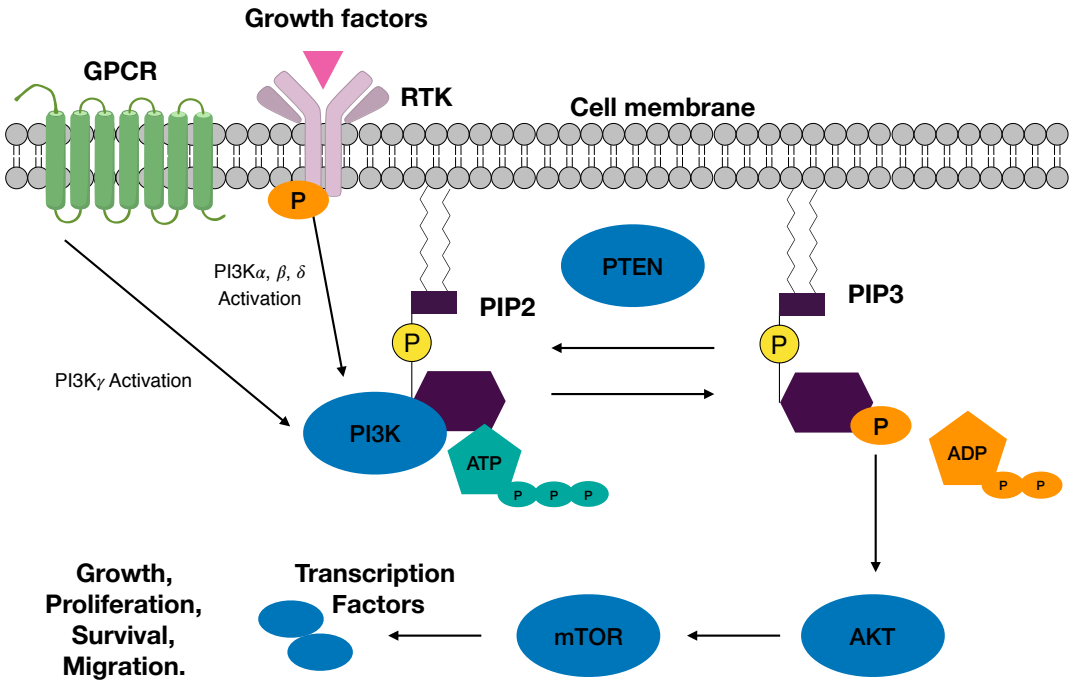


Figure 47. Signalling cascade of PI3K.

In terms of expression, the PI3Kα and PI3Kβ isoforms are ubiquitous, whereas the PI3Kδ and PI3Kγ isoforms are found predominantly in leukocytes[59]. The effect of knock-out in mice proves lethal in the case of the α and β isoforms, but viable in the case of the δ and γ isoforms[60].

The class II PI3Ks, unlike the Class I PI3Ks exist only as the catalytic isoforms (i.e. they have no regulatory proteins). There are 3 catalytic isoforms C2α, C2β, and C2γ, and thus 3 class II PI3Ks (PI3KC2α, PI3KC2β, and PI3KC2γ), which share a common domain structure to the catalytic subunits of the Class I PI3Ks. The class II PI3Ks are primarily responsible for the phosphorylation of phosphatidylinositol 4-phosphate (PI4P) to phosphatidylinositol 3,4-bisphosphate ($PI(3,4)P_2$). Recent studies have shown that $PI(3,4)P_2$ may play a significant role in cell migration through its binding protein, lamellipodin (Lpd)[61].

There is only 1 known class III PI3K, PI3K Vps34[62], and it is even more similar in structure to the class I PI3Ks than the class II PI3Ks. PI3K Vps34 also exists as a het-

erodimer, comprising of the Vps34 catalytic subunit, and the p150 regulatory subunit. PI3K Vps34 is primarily responsible for the phosphorylation of phosphatidylinositol (PI) to form phosphatidylinositol 3-phosphate (PI3P). The role of PI3K Vps34 is not yet fully understood.

Another class of more distantly related protein serine/threonine kinases exist that are similar in structure to the PI3Ks. These are commonly referred to as class IV PI3Ks and include ataxia telangiectasia mutated (ATM)[63], ataxia telangiectasia and Rad3 related (ATR), DNA-dependent protein kinase (DNA-PK) and mammalian target of rapamycin (mTOR).

In this work, the focus is on the class I PI3Ks and from here on referral to PI3K and its isoforms, refers only to the class I PI3Ks (PI3Kα, PI3Kβ, PI3Kδ, and PI3Kγ). In the previous chapter pictilisib, a pan Class I PI3K inhibitor and was used as the representative PI3K inhibitor. However, recently there has been a lot of effort from both industry and academia to develop inhibitors that are selective for the different isoforms of PI3K due to their differing biological roles.

The PI3Kδ isoform plays a crucial role in B-cell regulation, including proliferation and survival. Additionally, PI3Kδ is hyperactivated in different B-cell cancers, and as such the FDA has recently approved[66] the PI3Kδ inhibitor, Idelalisib[67], (July 2014) for the treatment of relapsed chronic lymphocytic leukemia, relapsed follicular B-cell non-Hodgkin lymphoma or relapsed small lymphocytic lymphoma.

The PI3Kδ isoform has also been shown to be required for cytokine production and proliferation in T-cells and allergen induced de-granulation of mast cells via the IgE, ultimately leading to inflammation[64]. This has put PI3Kδ inhibitors in the position as a treatment for inflammatory respiratory diseases such as allergic asthma and chronic obstructive pulmonary disease.

PI3Kγ, similarly to PI3Kδ is found in leukocytes[65], PI3Kγ has been shown to be involved in many immune functions such as granulocyte migration, activation of mast cells and dendritic cells, as well as the development and differentiation of lymphocytes. This role suggests that inhibition of PI3Kγ may be beneficial for the treatment of both

inflammatory diseases as well as autoimmune conditions[68].

PI3Kα is the most extensively studied isoform for its role in oncology. Recent preclinical studies have shown that cancers exhibiting the PIK3CA mutation, which codes for the p110a catalytic subunit of PI3K, are more sensitive to PI3Kα inhibitors[69], and as such there are many inhibitors in development .

PI3Kβ is the least understood of the Class I PI3Ks, however, recently there has been evidence to suggest that PTEN-deficient tumours have been shown to depend on PI3Kβ activity [70][71].

3.1.1.1 General design of PI3K inhibitors

PI3K inhibitors act on the active conformation of the kinase, where the binding interactions mimic the adenine interactions of the ATP cofactor, blocking access to other substrates. Figure 48 shows a generalised pharmacophore model introduced by Traxler *et al* [72], often used to describe the binding of Type I PI3K inhibitors.

Generally, inhibitors have a central scaffold in the adenine pocket, and form hydrogen bonds with the hinge region, taking advantage of nearby hydrophobic regions to increase affinity. Most importantly, the specificity pocket is where key interactions can be made to gain selectivity over the other isoforms. Additionally, there is often a

solubilising group that extends out into solvent.

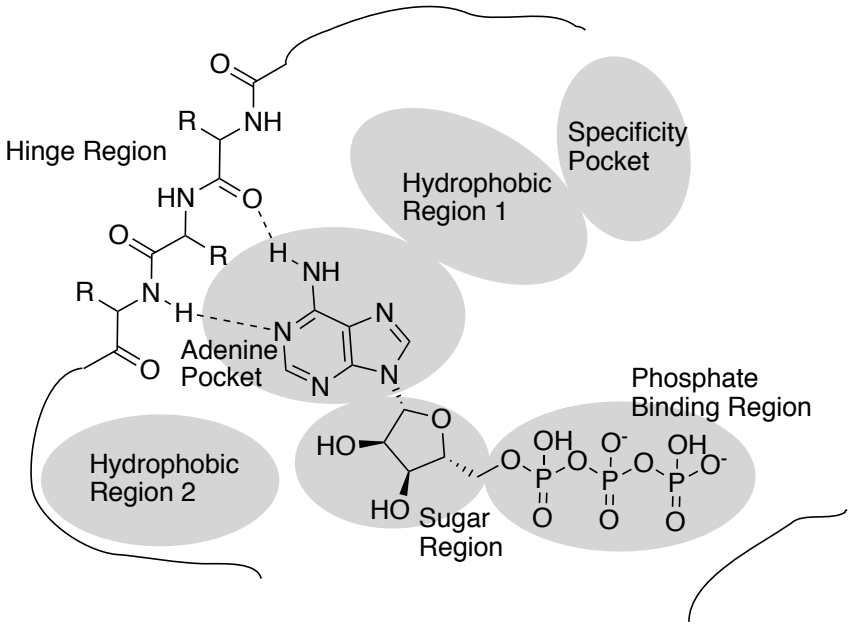


Figure 48. A generalised pharmacophore for PI3K inhibitors.

Early PI3K inhibitors include LY294002[73] and wortmannin[74] (Figure 48). Although these inhibitors are potent PI3K inhibitors, IC_{50} = 1.4 μM and 5 nM respectively, these compounds are unselective, and show similar activity against members of the whole PIK family (Class I, II, and III). Additionally, these compounds are generally considered tool compounds since they do not exhibit drug-like properties.

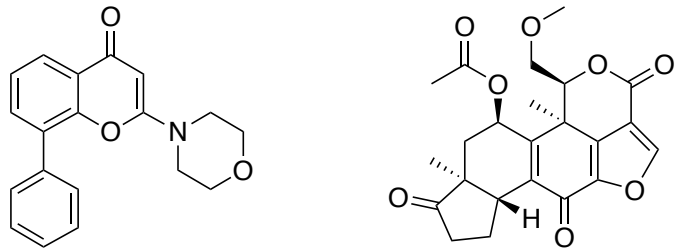


Figure 49. Early non-selective inhibitors of PI3K, LY294002 and Wortmannin.

In recent years there has been a huge effort from both industry and academia towards the development of drug-like and isoform specific PI3K inhibitors. There has been three main classes of compounds developed; namely the "flat" inhibitors, the "propeller type" and the "distorted propeller-shape". The following section will examine the

current literature in this field, focusing on the so-called "flat" inhibitors, that do not provoke any conformational rearrangements to the kinase, although the "propeller type', will be briefly discussed for completeness.

3.1.2 "Flat" PI3K Inhibitors

The following introduction is written to follow chronological order of the literature of a given scaffold type. Some exceptions exist across different scaffolds in order to maintain a coherent flow. For ease, drawn structures have been orientated so as to place the hinge binder pointing up on the page, groups in the sovent exposed region are always to the left hand side, and groups on the right hand side interact with the activity pocket.

3.1.2.1 Thienopyrimidines and their Derivatives

Genentech's efforts: Pan PI3K inhibition (GDC-0941), dual PI3K/mTOR Inhibition (GDC-0980), and PI3K δ-selective inhibition (GDC-0984).

In 2008 Genentech disclosed the synthesis and biological evaluation of a series of thieno[3,2-d]pyrimidines that demonstrate potent inhibition of PI3Kα, culminating in the discovery of pictilisib (GDC-0941), a pan PI3K inhibitor (Figure 50)[55]. Pictilisib was initially discovered by the Institute for Cancer Research (ICR) and Piramed then licenced to Genentech.

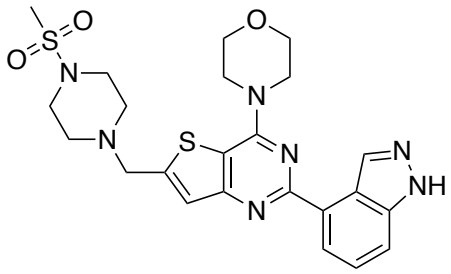


Figure 50. Structure of pictilisib (GDC-0941), a pan-PI3K inhibitor, disclosed by Genentech in 2008.

A crystal structure of Pictilisib bound to PI3Kγ was obtained (PDB 3DBS), Figure 51, showing that it demonstrated a binding mode that mimics ATP. The morpholine oxygen forms a pivotal hydrogen bond to the hinge region of the kinase via the amide of Val 882 and the indazole moiety points towards the affinity pocket, where the indazole

nitrogens make key interactions with the carboxyl group of Asp 841 and the phenol oxygen of Tyr 867. Finally, the 4-methanesulfonyl-piperazin-1-ylmethyl group extends out to solvent where the piperazine ring packs against the side chain of Met 804 (not shown for clarity), and the sulfonyl group oxygens are within hydrogen bond distance of the side chain of Lys802 and the amide nitrogen of Ala 805.

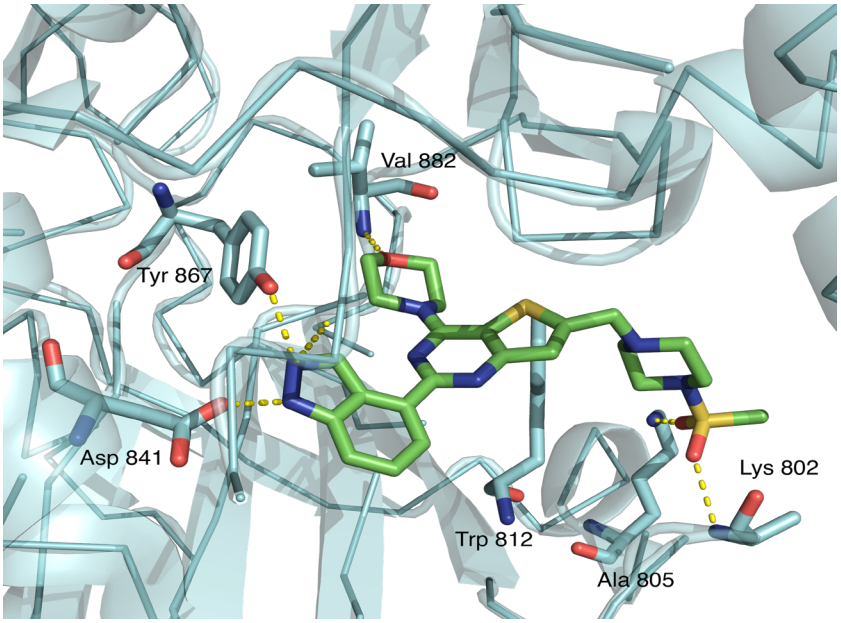


Figure 51. Crystal Structure of pictilisib bound to p110γ (p110γ numbering displayed) showing key interactions. PDB 3DBS.

For their design, Genentech utilised a thienopyrimidine core identified by Hayakawa *et al.* [76] (PI-249, Figure 52), which was shown to be potent against PI3Kα, and showed significant anti-proliferative activity *in vitro*. However, the PK profile of PI-249 was poor, with a half-life of less than 10 mins after inter-peritoneal administration in mice and at the onset of the project, Genentech's aim was to improve upon physico-

chemical properties, metabolic stability, and potency of PI-249.

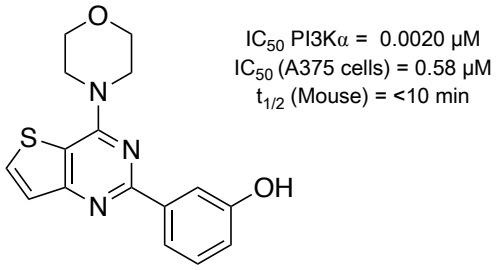


Figure 52. Structure of PI-249, an early potent inhibitor of PI3Kα in vitro, however, PI-249 has a poor PK profile with a half-life of less than 10 mins after inter-peritoneal administration in mice.

Initially, the importance of the morpholine group for P13K activity was shown when its substitution resulted in large reductions in potency, leading to Genentech retaining the morpholine group on all further derivatives. Methyl substitutions at the 6- and 7- position on the thienopyrimidine ring were investigated showing that 6-Me substitution was well tolerated but 7-Me substitution showed a decrease in potency. Upon considering the potential to block metabolism at the 6-position, coupled with the decrease in potency, efforts were focussed on the 6-position, finding that the 6-position could tolerate a large range of substituents. An interesting substitution at the 6-position were those of tertiary amines, offering the potential for salt formation to aid kinetic solubility, dissolution rates, as well as *in vivo* absorption and tumour exposure. Piperazine analogues, such as the example in Figure 53, displayed enhanced metabolic stability in human and mouse microsomes (85 - 90%) relative to other analogues in the series. However, they exhibited low bioavailability (F = 0-11%) in mouse and rat, mainly due to glucuronidation of the phenol.

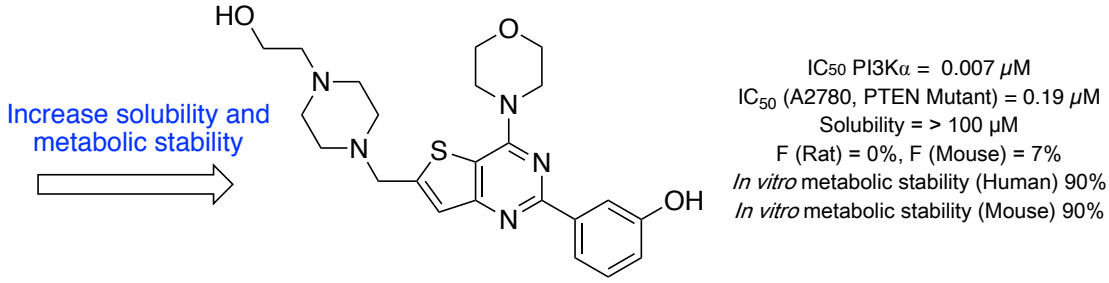


Figure 53. Improvements to PI-249 Increased aqueous solubility and metabolic stability, however the phenol still posed a metabolic liability due to glucuronidation.

The metabolic liability of glucuronidation of the phenol, led to the search for suitable bioisosteres of the phenol; investigating heterocyclic groups with the potential to act as a hydrogen bond donor. These changes led to the discovery of Pictilisib (PI3Kα = 0.003 μM, PI3Kβ = 0.033 μM, PI3Kδ = 0.003 μM, PI3Kγ = 0.075 μM, mTOR = 0.58 μM). Acceptable oral bioavailability was achieved in all species tested; mouse (77%), rat (30%), dog (71%), and monkey (20%). See Figure 54.

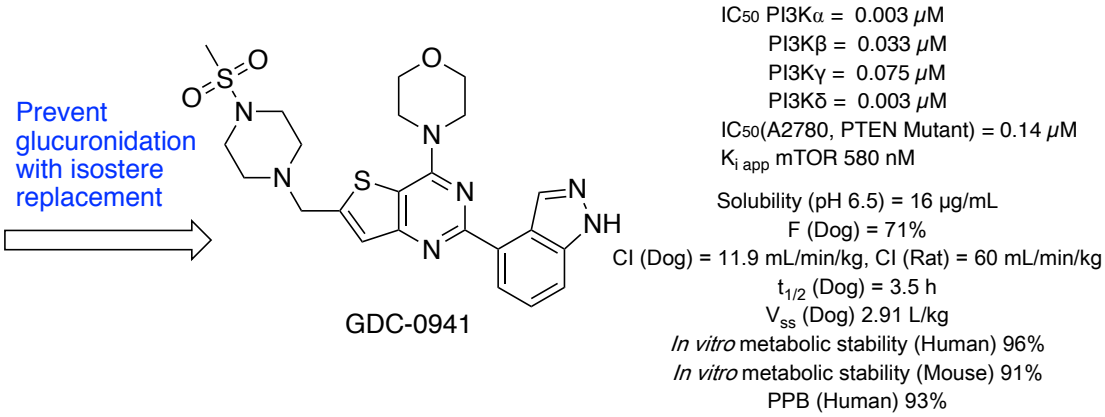
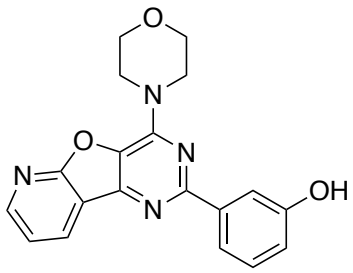


Figure 54. Bioisosteric replacement of the phenol group with an indazole group led to the discovery of Pictilisib (GDC-0941), which was progressed into the clinic.

Good levels of selectivity are observed for Pictilisib when tested against members of PI3K classes II, III, and IV, including C2β (0.670 μM), Vps34 (>10 μM), DNA-PK (1.23 μM), and mTOR (0.58 μM). Additionally, Pictilisib displayed outstanding selectivity for the PIK family kinases over a panel of 228 kinases in the KinaseProfiler panel from Millipore (formerly Upstate Biotechnologies). Only two displayed greater than 50% inhibition at 1 μM. Flt3 displayed 59% inhibition and TrkA displayed 61% inhibition by 1 μM, (IC_{50} 2.85 μM). Pictilisib shows minimal inhibition of the six principal cytochrome P450 isoforms, and at a concentration of 25 μM, there is negligible induction of CYP1A and CYP3A4. There was also no significant blockade of the hERG channel for 1 (IC_{50} 64 μM) in the patch clamp assay. Pictilisib was progressed to *in vivo* studies and it was found that it exhibits a strong inhibitory effect on the growth of human U87MG glioblastoma xenografts in athymic mice (tumour growth inhibition of 83%). Pictilisib progressed to phase I and II clinical trials in human, and as of the time

of writing trials appear to have been terminated.

Following the discovery of Pictilisib in 2009, with increasing evidence of clinical need for a dual mTOR/PI3K inhibitor, Genentech set out to build in mTOR activity into Pictilisib. They used Piramed's PI-103 (Figure 55) as a tool compound as it also contains the morpholino-pyrimidine core and was known to inhibit mTOR and the PI3Ks.



PI-103

Figure 55. Structure of PI-103, developed by Piramed. PI-103 was used in the design of a dual PI3K/mTOR inhibitor as it was known to inhibit both PI3K and mTOR.

Genentech aimed to improve clearance of the scaffold whilst also maintaining or improving on the potency and solubility. Additionally, Genentech had also published a library of previous analogues[77][78] (GNE-477)] containing a methyl group on the thienopyrimidine core; this showed that it was possible to inhibit both mTOR and the class 1 PI3K's simultaneously.

When the indazole group (from Pictilisib), across a range of analogues, was replaced with 2-aminopyrimidine, they observed a 10-fold increase in mTOR potency on average. Interestingly, when the indazole of Pictilisib was replaced with 2-aminopyrimidine (Figure 56) they observed a 20-fold increase in mTOR potency (from 580 nM to 29 nM). This change didn't dramatically change the proliferation potencies of

the inhibitors.

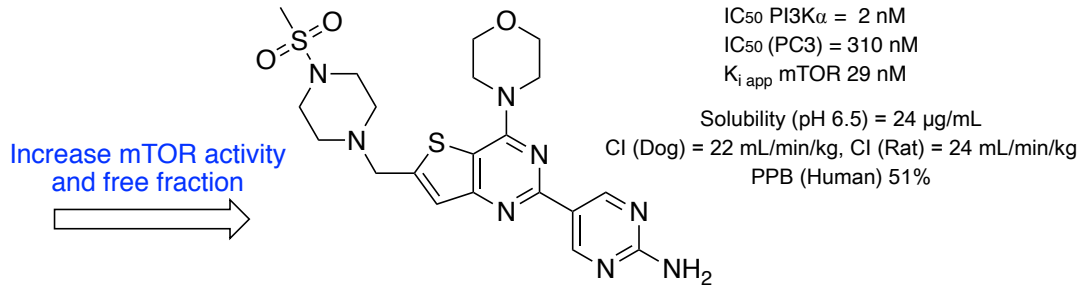


Figure 56. Substitution of pictilisib's indazole group with a 2-aminopyrimidine led to a 20-fold increase in mTOR activity.

The indazole substitution also lowered the cLogP by 1.9 (from logD of 2.4 to 1.3), which consequently increased the free fraction and *in vitro* stability across species, including human. The microsomal stability data correlated well with *in vivo* data, except for in dogs, where a methyl substitution on the core (Figure 57) was required improve dog clearance.

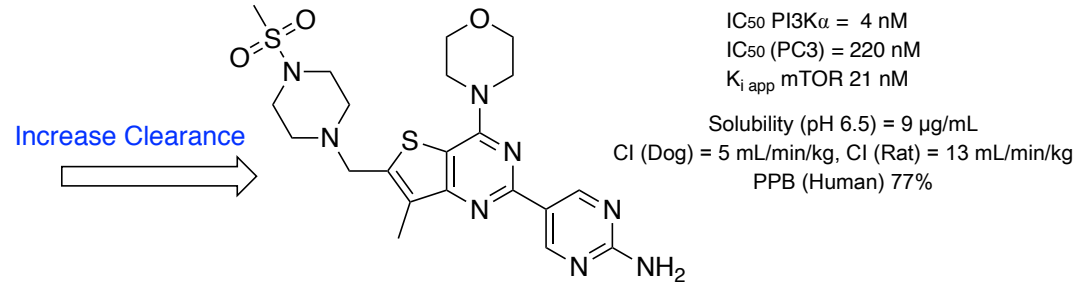


Figure 57. A methyl substitution on the thienopyrimidine core was required to improve clearance in dogs.

This change, however, caused solubility issues, and the focus then moved to improve solubility, whilst maintaining acceptable biological and pharmacokinetic properties. This was achieved by considering modification to the solvent exposed sulfonamide. Piperazine amides were explored to maintain the neutral charge of the distal amine, using both amino and hydroxy acids, with and without substitution at the α-position to modulate metabolic stabilities. Amine based, α-amino analogues all had good potency (0.7 – 2.1 nM) and showed a good improvement to solubility (0.69 – 1.0 mg/mL pH 6.5) but they observed *in vivo* clearance at or above liver blood flow, rendering the drugs

not orally bioavailable (F% = 0-6%). The alcohol-based α-hydroxy analogues, such as apitolisib, Figure 58, showed much better PK properties, showing increased solubility (0.084 – 0.6 mg/mL pH 6.5), low to moderate predicted human clearance (3.1 - 7.2 mg/min/kg), and thus good oral bioavailability (F% = 71 – 100%). The enantiomer of apitolisib showed biochemical activities and microsomal stabilities less preferred so was not progressed further. Apitolisib, (GDC-0980) was primarily chosen for further study due to its low predicted clearance in human (3.1 ml/min/kg), its low *in vivo* clearance in rat (15 ml/min/kg), and thus its maximised oral bioavailability (F% = 100%).

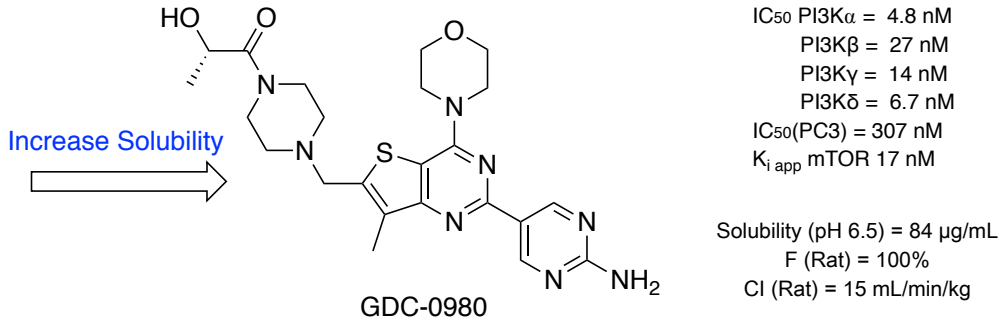


Figure 58. Modification of the solvent exposed sulfonamide to a hydroxy acids improved solubility, whist retaining good PK properties and potency. This led to the discovery of apitolisib (GDC-0980) which was advanced to phase I and II clinical trials.

The *in vivo* profile of apitolisib was characterised through PK studies conducted in several different species. Clearance was low (predicted Cl_h 33 mL/min/kg, Cl_p 9.2 mL/min/kg), PPB was low (71%), solubility was good (0.084 mg/mL pH 6.5), and volume of distribution was 1.7 L/kg. The maximum tolerated dose of apitolosib was found to be 7.5 mg/kg and at this dose tumour stasis or regression was observed in PC-3 and MCF-7 neo/HER2 mouse xenograft models. This is likely due to the high cellular potency, low plasma clearance, and relatively high free-fraction of the drug *in vivo*. Apitolisib was found to show a high degree of selectivity over off-target kinases even while maintaining dual inhibition of mTOR and the PI3K isoforms. This was confirmed by Invitrogen's SelectScreen panel. Of the 240 kinases in the panel, only 5 other kinases consistently showed greater than 60% inhibition when treated with 1 µM (Fgr 697 nM, Mlk1 232 nM, PAK4, Syk 134 nM, and Yes1). Apitolisib was highly selective over

closely related PI3K family kinases: C2α (1300 nM), C2β 794 nM, VPS34 2000 nM, PI4Kα >10 μM, PI4Kβ >10 μM, and DNA-PK 623 nM. Apitolisib was advanced into development, where it is currently in phase I and II clinical trials.

Following the disclosure of Pictilisib, a pan-PI3K inhibitor and apitolisib, a pan PI3K/mTOR inhibitor, in 2012, using the thienopyrimidine core, Genentech disclosed the development of a series of PI3Kδ-selective compounds[79], including the example in Figure 59, (PI3Kδ = 1.8 nM, δ/α = 129, δ/β = 104, δ/γ = 1444), utilising 4-substituted indole as the phenol bioisostere replacement.

It was hypothesised that although the residues in the affinity pocket are highly conserved between the PI3K isoforms, disruption of the strong hydrogen bond between the indazole nitrogen and Tyr867, could radiate and extend past the conserved affinity pocket, resulting in undesirable conformational changes for the antitargets (α, β, γ); thereby providing PI3Kδ specificity when indazole is replaced with indole.

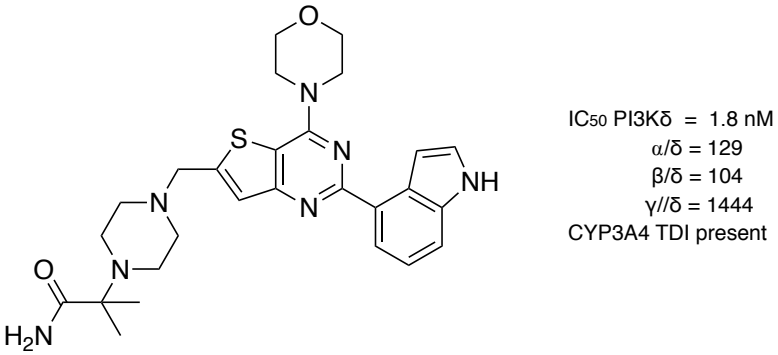


Figure 59. By utilising 4-substituted indole as the phenol bioisostere replacement, PI3Kδ selectivity was introduced.

Although this bioisosteric replacement led to great improvements in selectivity, they observed dramatic differences in time-dependent CYP3A4 inhibition, which could lead to autoinhibition and poor drug-drug interactions. They employed several strategies to reduce this time-dependant inhibition to develop the example in Figure 60, (PI3Kδ = 2.3 nM, δ/α = 50, δ/β = 815, δ/γ = 112), such as: introduction of metabolic soft-spots to divert metabolism from the indole, modification of physicochemical prop-

erties, and blocking potential sites of metabolism.

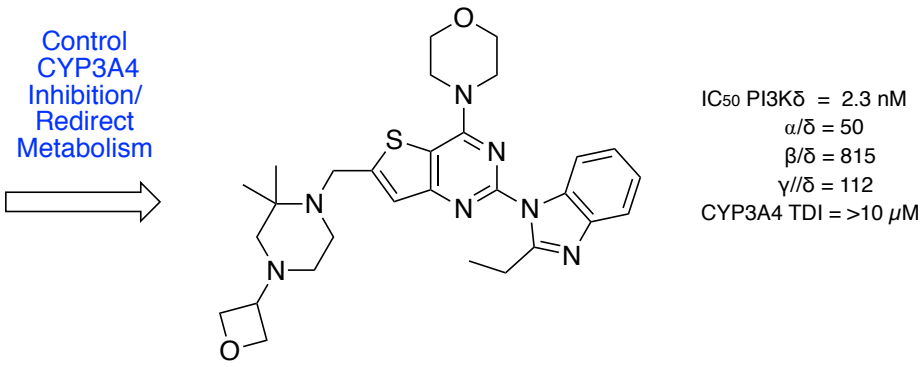


Figure 60. Diverting metabolism and replacing the indole with a benzimidazole controlled CYP3A4 inhibition.

Ultimately, however, although controlling autoinhibition, they were unsuccessful in identifying a compound with combined acceptable potency, selectivity, and drug-like properties to progress the PI3K δ-selective compounds further.

Following their previous programs, in 2012 Genentech extended their study towards brain penetrant inhibitors[80]. Pictilisib ([brain]u/[Plasma]u = <0.05), and apitolisib ([brain]u/[Plasma]u = <0.05) were found to poorly penetrate the blood-brain-barrier (BBB), where this lack of BBB penetration was attributed to efflux by the two most prevalent transporters in the BBB, P-glycoprotein (P-gp) and breast cancer resistance protein (Bcrp1). The properties of these compounds are markedly different from marketed drugs that target the central nervous system (CNS), where the median values are: MW = 305, HBD = 1, TPSA = 45, and cLogP = 2.8. In order to bring these properties in-line with the median, they initially truncated the solvent exposed regions of the compounds, showing that they retained activity. Additionally, using a central nervous system multi-parameter optimisation (CNS MPO) scoring system (a score of 0-6), which has been shown to display a correlation between higher CNS MPO score and low P-gp efflux, they prioritised the synthesis of compounds that have a CNS MPO score of ≥4.5 for their study. Of the molecules they made prior to implementing an in silico evaluation, 53% had high efflux mediated by P-gp and 66% by Bcrp1. After employing the CNS MPO score of ≥4.5 as a filter, new compounds were more than twice as likely as

those made before using this filter to have low efflux as a result of either P-gp or Bcrp1 efflux. All of the compounds studied maintained the aminopyrimidine at the 2-position of the thienopyrimidine core, essentially every compound made also had acceptable biochemical and cellular potency. This technique lead to the discovery of the examples in Figure 61. Figure 61 (Top) ([brain]u/[Plasma]u = 0.5, PI3Kα = 1 nM, mTOR = 10 nM) and Figure 61 (Bottom) ([brain]u/[Plasma]u = 0.4, PI3Kα = 2 nM, mTOR = 9 nM), both highly potent brain penetrant PI3K/mTOR inhibitors.

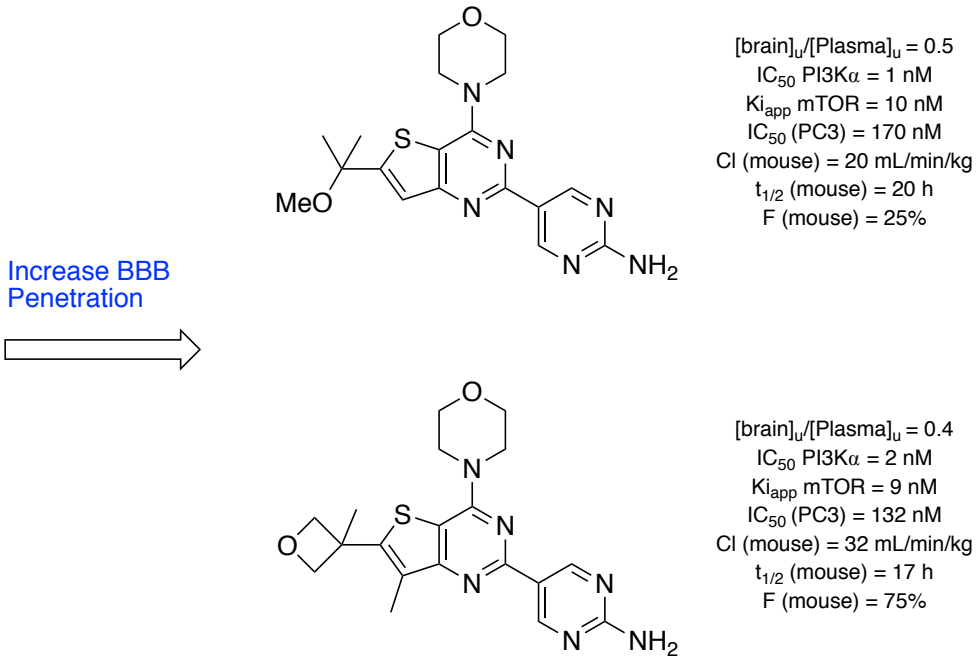
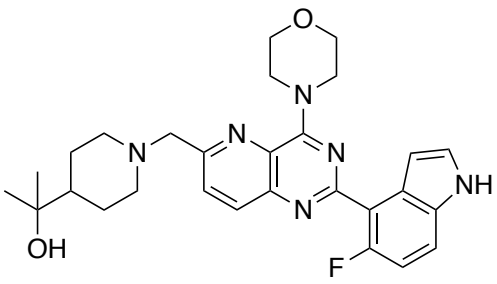


Figure 61. Through implementation of a CNS MPO scoring system BBB penetration was greatly improved by reducing efflux by the P-Gp and Bcrp1 transporters.

Furthermore, the examples in Figure 61 were evaluated in a panel of 59 kinases provided by Invitrogen's SelectScreen service. Only Figure 61 (bottom) inhibited any kinase in the panel by >75% at 1 μM concentration (PI3KC2β, 77%). However, at the time of writing, none of the reported brain penetrant compounds have been reported to have entered the clinic

Later in 2012, Genentech reported further on their δ-selective program. By utilising the highly selective indole group as a bioisostere for the phenol group, but deviating from the thienopyrimidine core, Genentech reported the highly selective PI3Kδ compound in Figure 62, (PI3Kδ = 3.8 nM, δ/α = 340, δ/β = 200, δ/γ = 410)[81].



IC_{50} PI3Kδ = 3.8 nM
α/δ = 340
β/δ = 200
γ//δ = 410
Cl (mouse) = 53 mg/min/kg
Cl (rat) = 59 mg/min/kg
$t_{1/2}$ (mouse) = 2.6 - 5 h
$t_{1/2}$ (rat) = 2.6 - 4 h
F (mouse) = 80%
F (rat) = 90%

Figure 62. Deviation from the thienopyrimidine core and utilisation of the indole group produced a δ-selective compound.

Additionally, a crystal structure of a representative inhibitor of the series co-crystallised with a mutated (K802T) PI3Kγ was reported, showing that the methyl groups of the tertiary alcohol of the compound in Figure 62 could form hydrophobic contacts with the face of Trp760 (δ-numbering). This interaction would allow them to specifically target the space created by the Thr750 side chain in PI3Kδ, which is electronically and structurally distinct from the residues found in PI3Kα, β, and γ (Arg770, Lys771, and Lys802, respectively). This hydrophobic region in PI3Kδ is often referred to as the "tryptophan shelf" (Figure 63).

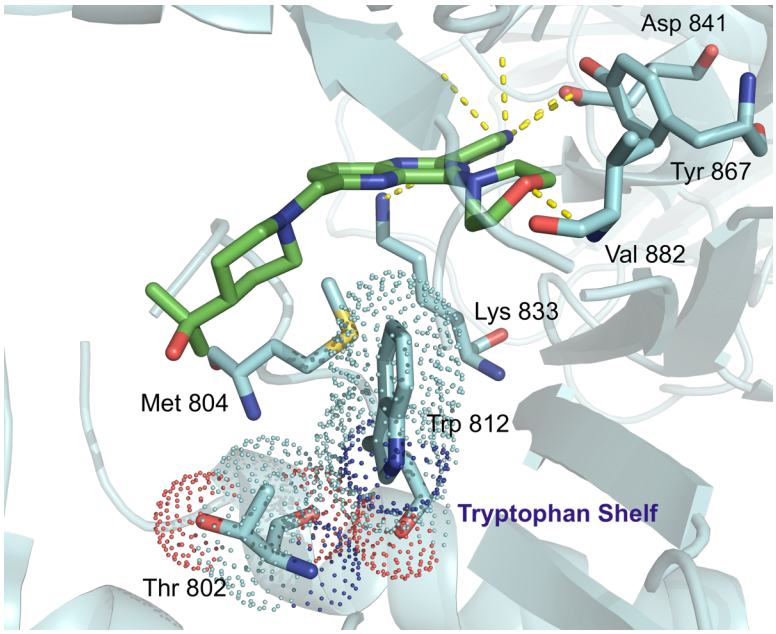


Figure 63. A representative δ-selective PI3K inhibitor bound to mutated (K802T) PI3Kγ (PDB 4EZL) showing that the methyl groups of the tertiary alcohol could form hydrophobic contacts with the face of the "tryptophan shelf" formed by Trp 812 and Thr 802.

The compound in Figure 62 was progressed to *in vivo* studies in mouse and rat, and showed moderate hepatic clearance (53 mL/min/kg and 59 mL/min/kg respectively). Reasonable half lives were observed upon oral dosing (2.6 - 5 h and 2.6 - 4 h respectively) as well as good oral bioavailability (80% and 90% respectively). At the time of writing it appears to be that none of the reported compounds from the series have progressed into the clinic.

After controlling CYP3A4 inhibition with benzimidazoles (Figure 60) as a replacement for the highly δ-selective indole group that sits in the activity pocket, in 2012 Genentech aimed to identify benzimidazole-based inhibitors of PI3Kδ with improved selectivity against other PI3K isoforms as well as improved *in vitro* and *in vivo* pharmacokinetic properties [82]. Initially modification of the central heterocycle was considered, which was hypothesised would allow attunement of the interaction of the solvent region of the inhibitors with the 'tryptophan shelf'. Heterocyclic replacements were investigated and it was found that purines were interesting replacements for the thienopyrimidine since inhibitors were inactive against PI3Kγ, and only weak inhibitors of PI3Kβ. The calculated ground state conformation of the purines indicated that a low-energy conformation is adopted in which the purine and benzimidazole rings are coplanar. Further optimisation of PI3Kδ selectivity was achieved by optimising interactions with Trp760 through substitution of the solvent exposed group with alternative sterically demanding amines, compounds containing a hydrophobic groups attached to the piperazine ring, bulky amine groups, and azetidines. Although, substitution with the 4-methanesulfonylpiperazine of Pictilisib resulted in a significant increase in activity versus PI3Kα and PI3Kγ. Figure 64 shows a representative example of the series (PI3Kδ = 2 nM, δ/α = 100, δ/γ = 260); exhibiting good solubility in aqueous solution (sol. at pH 6.5 = 338 μg/mL) and has good permeability in a standard MDCK assay (Papp = 16 × 10−6 cm/s). Rat (90%) and human (91%) plasma protein binding was good. There was no reversible or time-dependent CYP inhibition associated with the compound in testing against five CYP isoforms.

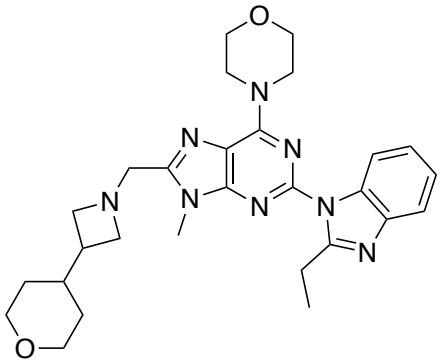


Figure 64. Replacing the thienopyrimidine core with a purine core results in a planar-conformation. Planarity, coupled with hydrophobic contacts with the tryptophan shelf and retention of the benzimidazole ring resulted in a series of δ-selective inhibitors.

Additionally, very weak inhibition with (less than 25% inhibition at 1 μM) was observed in testing against a panel of 55 diverse kinases. Pharmacokinetic profiling indicates that it has moderate to low clearance, Cl (rat) = 34 mL/min/kg, with a Vss of 6.5 L/kg, and T1/2 = 2.6 h. At the time of writing there are no reports of any of the series progressing to the clinic.

In 2013, Genentech reported[83] that inhibitors from their benzimidazole purine containing series, were found to induce micronuclei formation in both the micronucleus test (MNT) and human chromosome aberration (HCA) *in vitro* assays in the absence of compound metabolism using the liver S9 fraction (-S9). However, it was determined to be non-genotoxic in the Ames test, suggesting that neither the MNT or HCA result was directly due to DNA mutation. They reported that the genotoxicity SAR suggested that it is the combination of the purine core with the benzimidazole moiety that was responsible for the observed genotoxicity. Initially, compounds that tested negative in the MNT assay were successfully identified through modifications of the molecular volume of the 2-benzimidazole, however, whilst they were exploring the conformational preferences required for selectivity towards PI3Kδ they simultaneously explored the effects of substitution and conformational restriction on genotoxicity. They designed analogues that altered the dihedral angle between the amine group and the purine N7, mainly by

substitution of the methylene carbon with heteroatoms. Through crystallographic and docking studies, the preferred dihedral angle was determined to be 10–30 °C. This led to the discovery of the example in Figure 65, where an isopropyl group increases the molecular volume of the 2-benzimidazole, and an oxygen linker favours a torsional angle of <30 °C. The compound tested negative in the HCA assay and exhibited excellent PI3K isoform selectivity (PI3K δ = 0.47 nM, δ/α = 256, δ/β = 420, δ/γ = 219) and broad kinase selectivity through Invitrogen's 239 kinase panel at 1 μM, only B-Raf was inhibited at 61% and PI4Kβ at 71%. Additionally the compound possessed favourable pharmacokinetic properties, with low predicted hepatic clearance in human (1.7 mL/min/kg), moderate permeability (MDCK Papp A to B 8.23 x 10^{-6}) led to high oral absorption across species (F% = 82–100%) and acceptable half-lives ($T_{1/2}$ = 2.59–11.6 h).

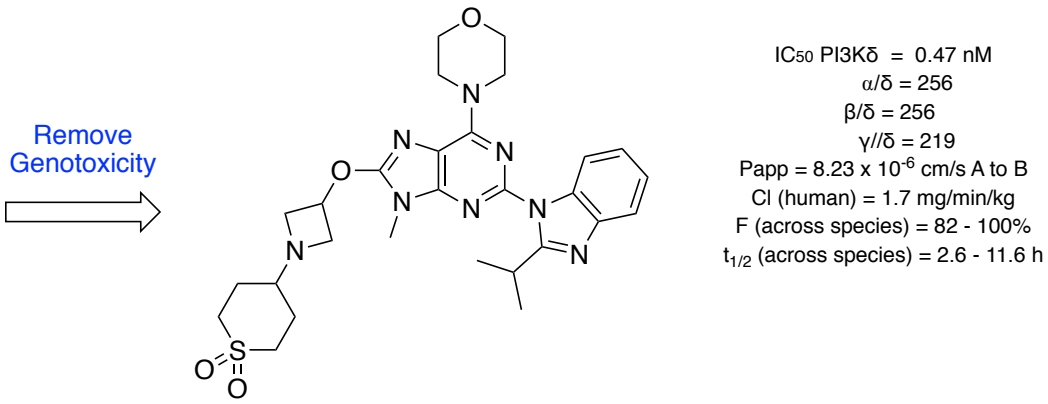
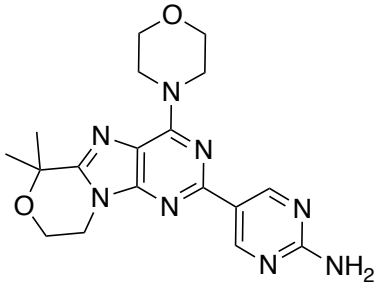


Figure 65. Tuning the purine-azetidine oxygen linked dihedral angle removed genotoxicity.

Following up on their identification of a series thienopyrimide containing brain penetrant PI3K inhibitors (discussed above, Figure 61), which were ultimately deemed not suitable for clinical development due to projected poor metabolic stability in humans, in 2016 Genentech utilised their knowledge of purine containing cores to move forward[84]. With the knowledge that desirable metabolic stability was attainable with a purine scaffold, they evaluated purine-based analogues of their previous thienopyrimidine series, ultimately resulting in GDC-0084 (PI3Kα = 2nM, mTOR = 0.07 μM), Figure 66, exhibiting excellent human metabolic stability in microsomal and hepatocyte incubations (Cl (mouse) = 19 mL/min/kg) and exhibits good oral bioavailability

in mouse (F = 75%). GDC-0084 was able to penetrate the BBB through determination of the brain-to-plasma ratio in mouse, where [Brain]u/[Plasma]u = 0.4. Additionally, GDC-0084 was studied in a subcutaneous U87 tumour xenograft model of glioblastoma in mice, showing a dose-dependent tumour growth inhibition. GDC-0084 was progressed to clinical development.



GDC-0084

$[brain]_u/[Plasma]_u = 0.4$
IC_{50} PI3Kα = 2 nM
Ki_{app} mTOR = 9 nM
Cl (mouse) = 19 mL/min/kg
F (mouse) = 75%

Figure 66. GDC-0084, Genentech's most recent PI3K clinical candidate to date.

Additional Efforts by Micellaneous Companies and Institutions: Dual PI3K/ HDAC Inhibition (CUDC-907), Dual PI3K/mTOR Inhibition (VS-5584)

Curis observed synergistic effects between PI3K inhibitors and HDAC inhibitors [85] and therefore synthesised a novel series of dual-acting PI3K and histone deacetylase (HDAC) inhibitors by incorporating HDAC inhibitory functionality into a PI3K inhibitor pharmacophore. They incorporated the morpholine-pyrimidine core from PI-103 (Figure 55), Pictilisib (Figure 54), and Buparlisib (discussed later, Figure 82) for PI3K inhibition and the hydroxamic acid from SAHA (Vorinostat), LBH-589 (Panobinostat) and JNJ-16241199 for HDAC inhibition to produce CUDC-907 (PI3Kα = 19 nM, PI3Kβ = 54 nM, PI3Kδ = 39 nM, PI3Kγ = 311 nM, HDAC = 1.7 - 674 nM (across 11 HDACs)), Figure 67. They reported potent anticancer activity in both cultured cancer cells and xenograft models and may offer therapeutic benefits in multiple cancers through broad signalling network disruption. CUDC-907 is currently in phase I and II clinical trials.

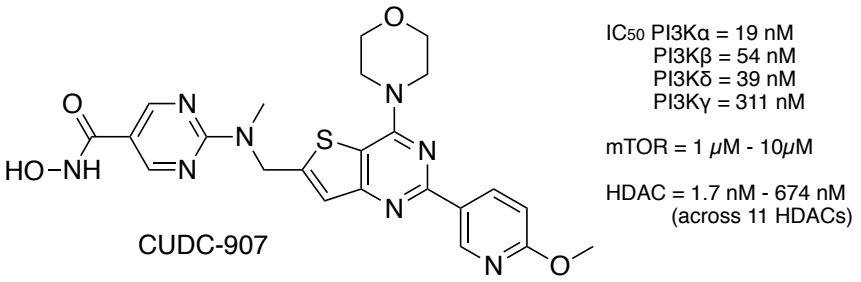


Figure 67. Curis incorperated hydroxamic functionality in order to introduce HDAC activity, leading to CUDC-907.

Scientists at the Chinese Academy of Sciences[86] utilised the structural information of PI-103 (Figure 55) to design a series of 4-(2-arylpyrido[30,20:3,4]pyrrolo[1,2-f][1,2,4]triazin-4-yl)morpholine derivatives. Their compounds had comparable PI3Kα activity with PI-103. All of the compounds showed selectivity over 15 tested protein kinases and anti-proliferative activity at micromolar concentration against several cancer cell lines. Figure 68 shows an example of the series (PI3Kα = 33.6 nM).

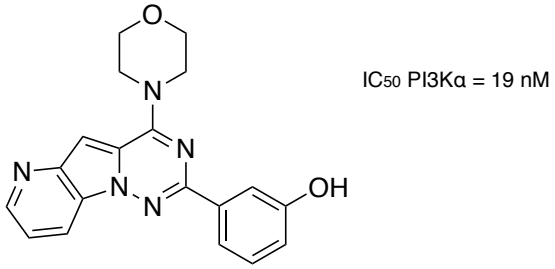


Figure 68. An example of a series of compounds developed by the Chinese Academy of Sciences.

The Spanish National Cancer Research Centre developed ETP-46321, Figure 69, employing a similar strategy to the Genentech team in the development of Pictilisb. Through a rational design exercise they replaced the C-C unit between the pyrimidine ring and the thiophene with a C-N unit. In an effort to optimise potency and *in vivo* properties a variety of heteroaryls at the imidazo [1,2-a] pyrazine C6 position were explored, leading to the discovery of ETP-46321 (PI3Kα = 2.3 nM, PI3Kβ = 170 nM, PI3Kγ = 179 nM, PI3Kδ =14.2 nM). ETP-46321 was shown to be a potent PI3K α/δ inhibitor that is highly selective over mTOR (4.88 μM) and 288 representative kinas-

es. ETP-46321 demonstrated a good pharmacokinetic profile in mice (Cl = 0.6 L/h/kg and F = 90%,) and was selected for preliminary *in vivo* evaluation in a lung tumour mouse model driven by a K-Ras G12V oncogenic mutation, showing significant tumour growth inhibition (ca. 51%).

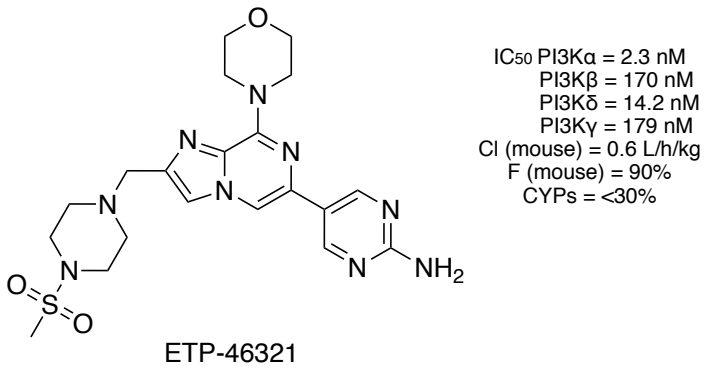


Figure 69. Stucture of ETP-46321

In a later publication[87] they applied a conformational restriction strategy to enable the exploration of the solvent-exposed region. Figure 70 (PI3Kα = 0.5 nM) is an example of the series. The compound was progressed to a preliminary *in vivo* PK study and showed similar results to ETP-46321.

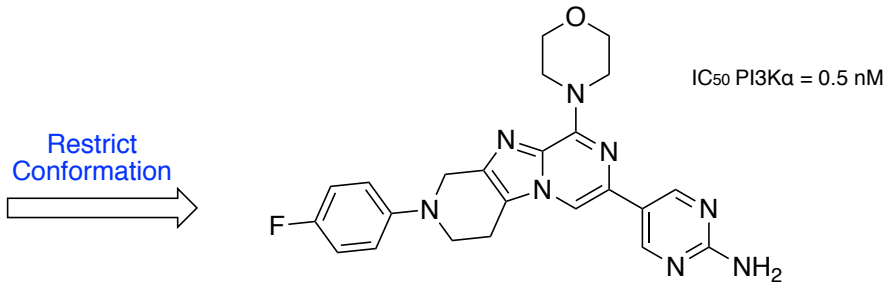


Figure 70. The Spanish National Cancer Research Centre employed a conformational restriction strategy to expore the solvent exposed region.

Additionally they have reported[88] a scaffold hopping strategy to replace the core moiety of ETP-46321 to produce compounds such as the example in Figure 71 (PI3Kα = 1.52 nM, PI3Kβ = 155 nM).

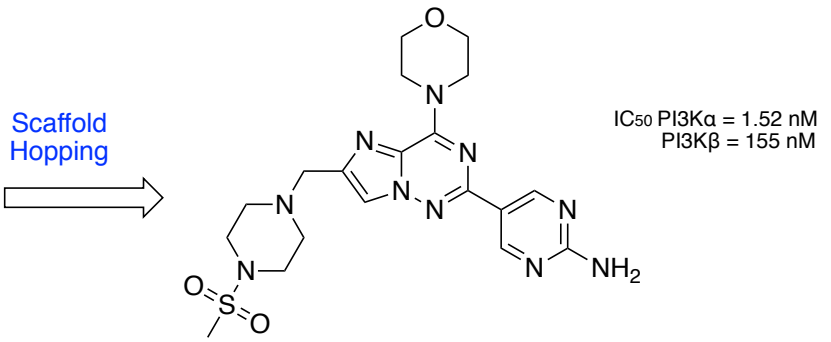
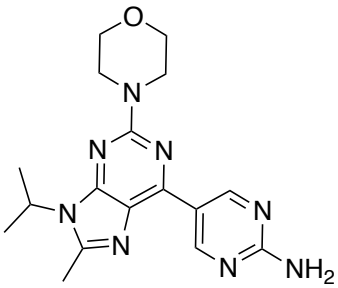


Figure 71. The Spanish National Cancer Research Centre employed a scaffold hopping strategy to change the central core of ETP-46321.

With the goal of developing a dual mTOR/PI3K inhibitor, which would equipotently inhibit the 4 isoforms of PI3K and mTOR, Verastem used structure and ligand based design to develop VS-5584 (SB2343)[89], Figure 72. They used PI-103, LY294002, and ZSTK474, and through scaffold hopping, developed their lead structure possessing a purine core substituted with a morpholine, a phenol headgroup, and a hydrophobic substituent. The lead compound showed good potency against PI3K*α* (89 nM) and mTOR (400 nM), however a phenol group posed a metabolic liability through glucoronidation *in vivo*. In order to overcome the metabolic liability, bioisoteric replacement of the phenol was employed resulting in substitution of the phenol for an amino-pyrimidine head group. The amino-pyrimidine head group was found to be equipotent with the phenol in inhibiting mTOR (300 nM) but introduced an imbalance in the inhibitory activity between mTOR and PI3Kα being 10 times more potent toward PI3Kα (34 nM). Optimisation of the 8 and 9-position side chains led to the discovery of VS-5584 with improved mTOR potency (37 nM) and PI3K activity (PI3K*α* =16 nM, PI3Kβ = 68 nM, PI3Kδ = 42 nM, and PI3Kγ = 25 nM).



VS-5584

IC_{50} PI3Kα = 16 nM
PI3Kβ = 68 nM
PI3Kγ = 25 nM
PI3Kδ = 42 nM
mTOR = 37 nM

Figure 72. Structure of VS-5584, a dual PI4K/mTOR inhibitor developed by Vertastem. VS-5584 progressed to phase I trials in patients with advanced non-hematologic malignancies or lymphoma.

VS-5584 was progressed and was selected for further profiling and found to have excellent PK and ADME properties as well as being active in animal models. VS-5584 progressed to phase I trials in patients with advanced non-hematologic malignancies or lymphoma.

Celgene Avilomics Research have described CNX-1351 [90], Figure 73, the first example of a targeted covalent inhibitor of the lipid kinase family that is an isoform-selective inhibitor of PI3Kα (Apparent IC_{50}s: PI3Kα = 6.8 nM, PI3Kβ = 166 nM, PI3Kδ = 3020 nM, PI3Kγ = 240.3 nM). After examining the ATP binding site and nearby residues of PI3Kα to identify opportunities for selective covalent modification, they identified Cys862, which is unique to PI3Kα, as a promising amino acid to target for covalent inhibition. Using the core of Pictilisib and through a series of design cycles exploring both linker spacing and electrophilic functional groups they identified CNX-1351, and although useful as a tool compound, the pharmacokinetic properties are suboptimal, and thus they are currently focusing their efforts on improving the oral bioavailability.

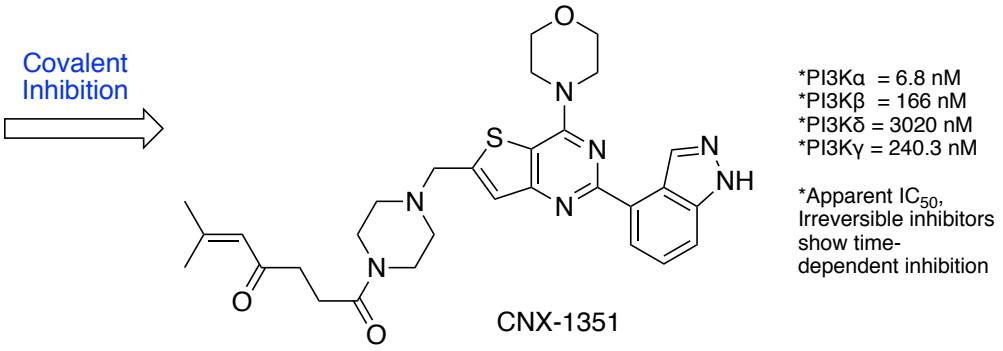


Figure 73. Structure of CNX-1351, a covalent PI3Kα inhibitor through Cys 862, a residue unique to the PI3Kα isoform.

Saurat et. al.[91] Have described a series of dual mTOR/PI3K inhibitors based on a pyridopyrimidine scaffold that have nanomolar enzymatic and cellular activities with an acceptable kinase selectivity profile. Figure 74 shows a representative example of the series (PI3Kα = 58 nM, mTOR = 5 nM).

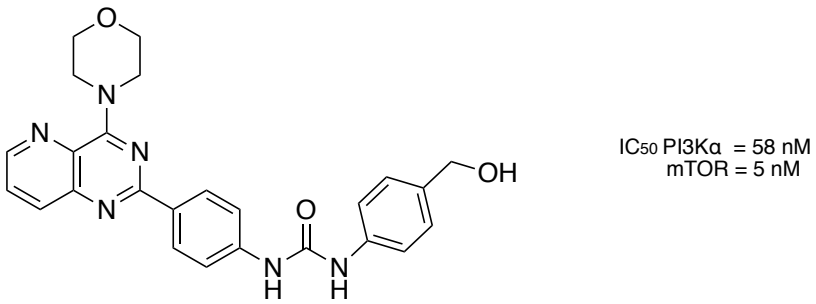


Figure 74. A representative of a series of dual PI3K/mTOR inhibitors reported by Saurat et. al.

Scientists at Sphaera Pharma Pte. Ltd began the discovery of their pre-clinical compound from a morpholino-pyrrolotriazine heterocyclic lead[92]. Through introduction of the aminopyrimidine into the affinity pocket, and a sulfonamide to the solvent exposed region they obtained the example illustrated in Figure 75. An interesting observation was that installing an (S)-methyl group *α*-to the nitrogen on the morpholine group had little effect on the potency compared to an (R)-methyl group, which induced a ~50-fold reduction in potency. Using modelling tools they observed that only 2 configurations fit; where the methyl group on the morpholine ring was equatorial for

(S)-methyl and axial for (R)-methyl. The requirement for the (R)-methyl group to be in the axial position to bind to the receptor requires a higher energy conformation relative to the (S)-methyl analogue, resulting in the (R)-methyl analogue being a much weaker binder energetically. The better compound, however, was without methyl substitution on the morpholine: The example in Figure 75 (PI3Kα = 20 nM) was found to be inactive against all of the kinases in a panel of close homology kinases, except for other isoforms of PI3K (PI3Kβ 54% inhibition at 1 μM, PI3Kδ 67% inhibition at 1 μM) and mTOR (85% inhibition at 1 μM).

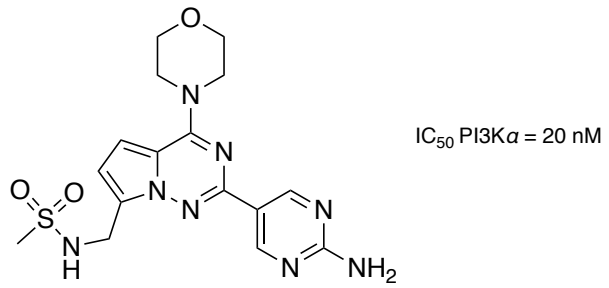


Figure 75. A representative of a series of inhibitors reported by Sphaera Pharma.

Wang et. al.[93] have described a series of compounds based on a quinazoline scaffold. Figure 76 is representative of the series (PI3Kα =96 nM, PI3Kβ = 128 nM, PI3Kδ = 330 nM, and PI3Kγ = 465 nM). The compound showed anti-proliferative effects *in vitro* and was found to induce apoptosis. Western blots suggested that the compound can block the PI3K/AKT/mTOR pathway. Additionally, it inhibited tumour growth on a mouse S180 homograft model.

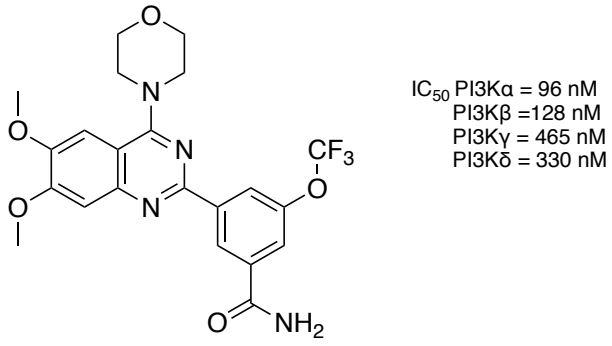


Figure 76. A representative of a series of compounds reported by Wang et. al.

Wang et. al. synthesised a series of inhibitors based on a thiopyrano-pyrimidine

core. Figure 77 (A) is an example of the series (PI3Kα = 8.38 μM), showing cytotoxicity against four cancer cell lines (6.02–10.27 μM). In a later publication [94] a series of compounds were produced, where Figure 77 (B) (PI3Kα = 1.25 μM) is representative of the series.

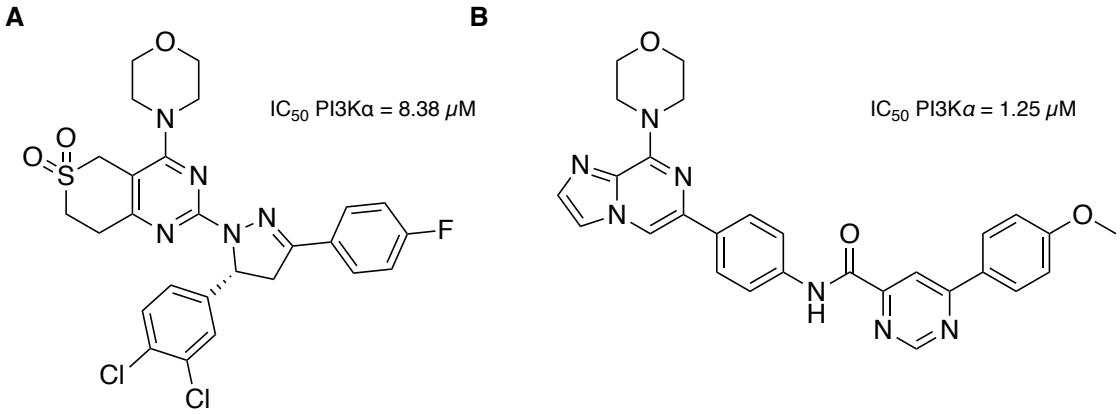


Figure 77. Structures of inhibitors synthesised by Wang et. al.

3.1.2.2 Triazines and their derivatives

Efforts from the Japansese Foundation for Cancer Research, Novartis, and The University of Basel: Pan PI3K Inhibition (ZSTK474, NVP-BKM120, and PQR-309) and dual PI3K/mTOR inhibition (PKI-402 and PKI-586).

ZSTK474 (Figure 78), was discovered as a library hit by the Japanese Foundation for Cancer Research that showed strong anti-proliferative activity[95]. However, its molecular target or its potential for a novel anticancer drug was unknown and they set about to elucidate its molecular target. They initially observed that the cellular potencies of ZSTK474 against a panel of cell-lines closely correlated with the cellular potencies of LY294002 (Figure 49) so they examined the ability of ZSTK474 to inhibit PI3K, observing that ZSTK474 was 20-fold more active (PI3Kα = 8.9 nM, PI3Kβ = 17 nM, PI3Kγ = 53 nM, PI3Kδ = 16 nM) than LY294002 against PI3K. ZSTK474 did not substantially inhibit the activity of 139 other protein kinases. A crystal structure of ZSTK474 bound to PI3Kδ[96] has been obtained and is shown in Figure 79.

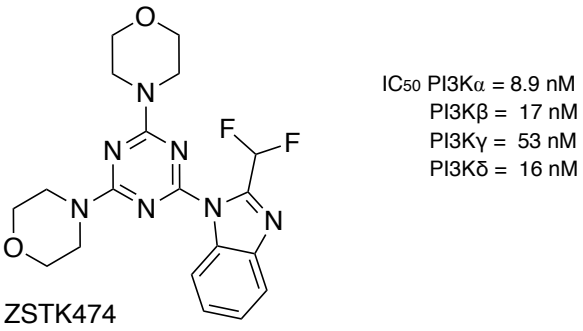


Figure 78. Structure of ZSTK474, an early potent, unselective triazine PI3K inhibitor.

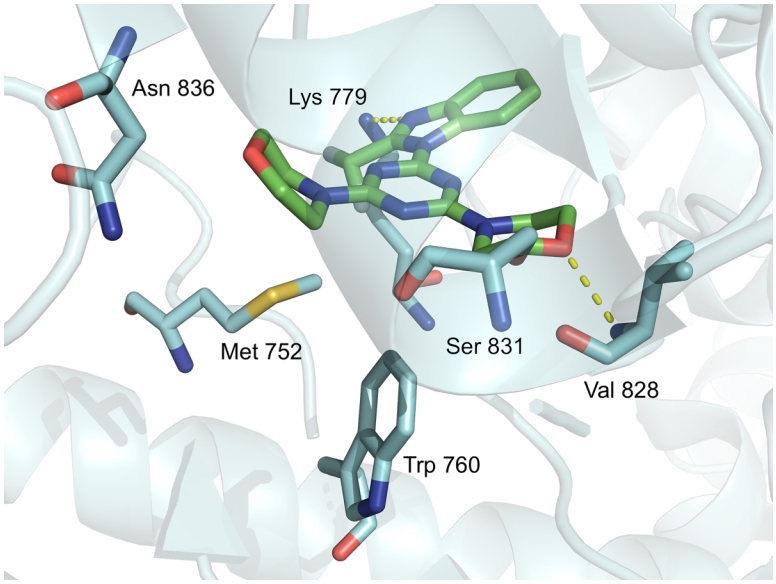


*Figure 79. ZSTK474 bound to PI3K*δ (PDB 2WXL).

In 2011, Novartis reported the identification of buparlisib (NVP-BKM120)[97], (PI3K*α* = 52 nM, PI3Kβ = 166 nM, PI3Kγ = 262 nM, PI3Kδ = 116 nM). Their original hit (Figure 80) was from a high throughput screen of a series of 2-morpholino 6-(3-hydroxyphenyl) pyrimidines identified from a solid phase combinatorial library of 2,4,6-trisubstituted pyrimidines[98][99] in the same chemical class as ZSTK474. After modification (Figure 80), these compounds had good oral bioavailability, low or sub-nanomolar biochemical potency and sub-micromolar cellular potency against PI3K*α*, but had high clearance in rat.

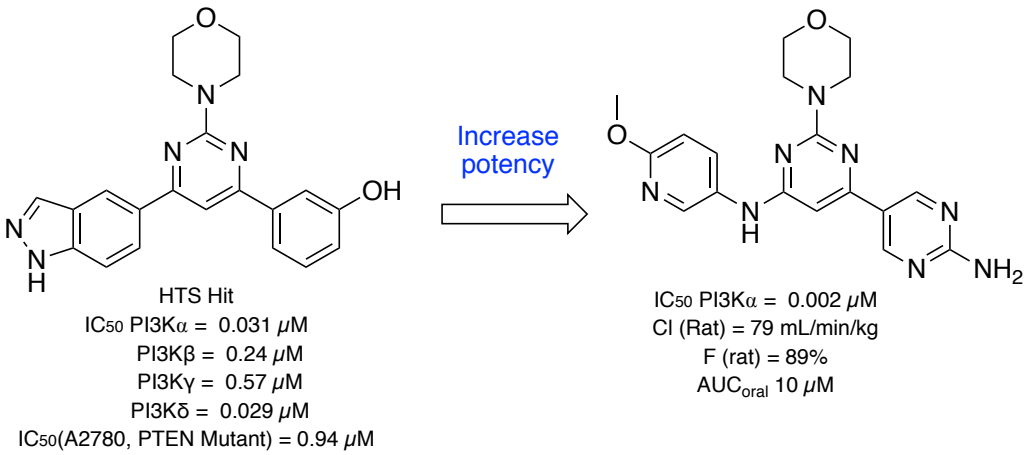


Figure 80. Modification of the HTS hit improved potency, however clearance in rat was still high, although oral bioavailability was still good.

Initially, improved clearance was achieved through substituting with an amino-quinoline in the solvent exposed region (Figure 81). Additionally, in order to increase potency they made substitutions in the activity pocket. Upon changing the pyrimidyl group to a pyridyl group they found that the biochemical potency increased upon the addition of an electron withdrawing group in the C4 position of the pyridine, also forcing the group out of plane to slightly improving aqueous solubility. Furthermore, this did not compromise the PK properties, however, the compounds still exhibited low aqueous solubility and poor Caco-2 permeability.

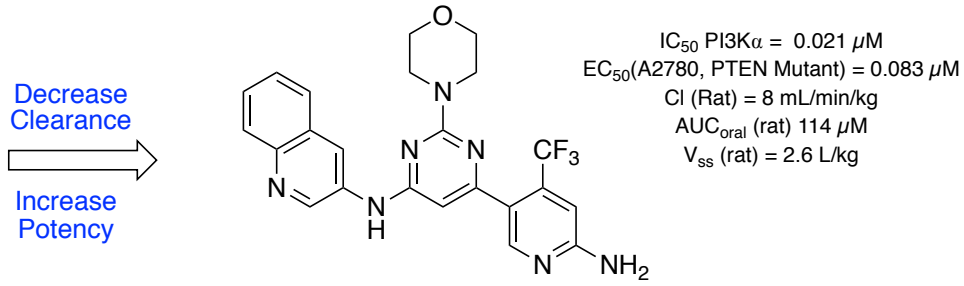


Figure 81. Modification to the solvent exposed region initially improved clearance. Subsequent modification to the activity pocket region improved potency.

From previous work it was known that substitution of the C4 position on the pyrimidine core could tolerate a wide range of moieties. Additionally, it was known that

a morpholine group at the C4 position of the core maintained reasonable potency while improving solubility relative to the aminoquinoline, and thus the aminoquinoline was substituted for a morpholine (Figure 82). The additional morpholine at the C4 position did not compromise the rat PK parameters, and solubility was improved.

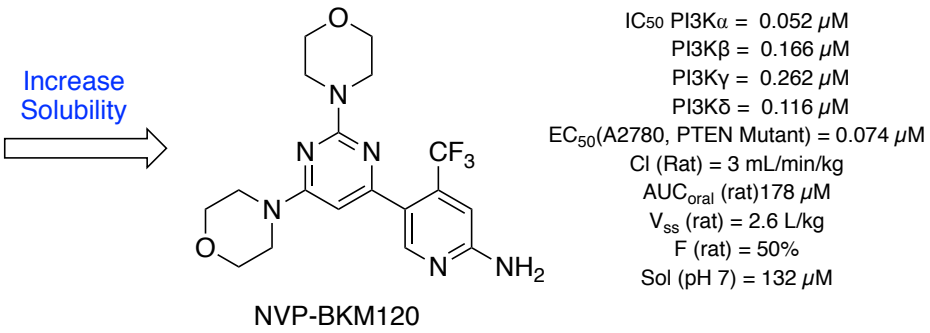


Figure 82. Structure of NVP-BKM120, buparlisib.

The biochemical activity of NVP-BKM120 was assessed across related lipid kinases, and against more than 200 protein kinases. VPS34 (2.4 μM), mTOR (4.6 μM), DNAPK (>5 μM), PIK4β (>25 μM). No significant activity was observed against the other protein kinases tested. The *in vivo* profile was characterised through PK studies conducted in several different species including mouse, rat, dog, and monkey. With the favourable cellular potency, kinase selectivity, pre-clinical pharmacology, rodent, dog, and monkey pharmacokinetics, physical properties, and preclinical safety profile, Buparlisib (NVP-BKM120) was advanced into clinical trials in 2008.

It was later reported that Buparlisib exhibits an off-target activity at high concentrations that is not related to PI3K inhibition. This off-target activity was found to be linked to mitosis, and ultimately found to be due to Buparlisib inhibition of tubulin polymerisation[100].

In order to overcome tubulin binding of Buparlisib, The University of Basel et. al. have described the discovery of Bimiralisib (PQR309)[101], Figure 83. They reported the crystal structure of Buparlisib bound to tubulin (PDB 5M7E) and reported that high affinity binding of buparlisib to tubulin occurs via the pyrimidine core C–H group which is oriented towards βMet259 of tubulin. bimiralisib was found to not bind to tubulin,

which can be explained by the core C-H being replaced with a nitrogen atom. Bimiralisib was found to be highly potent (PI3Kα = 15 nM, PI3Kβ = 11 nM, PI3Kγ = 25 nM, PI3Kδ = 25 nM), and showed a satisfactory PK profile *in vitro* showing little clearance in rat, dog, and human liver microsomes.

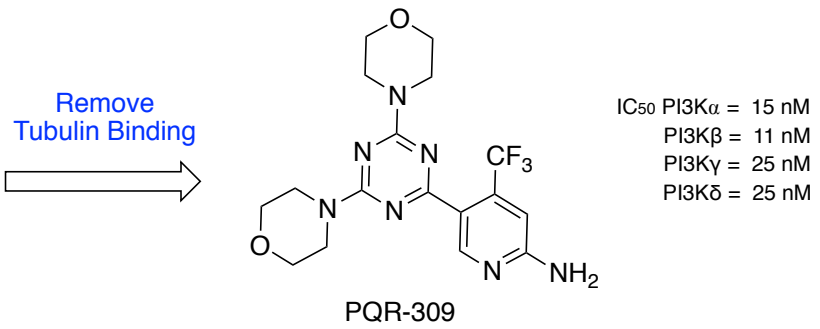


Figure 83. Structure of PQR-309, Bimiralisib. A structurally modified version of buparlisib to remove tubulin binding.

Bimiralisib was progressed to *in vivo* studies and was found to be orally bioavailable and brain penetrable. The *in vivo* profile and a PC3 xenograft model in nude rats validated Bimiralisib as a clinical candidate and thus Bimiralisib was advanced though phase I clinical trials and is currently in phase II studies in relapsed and refractory lymphoma and advanced solid tumours.

Zhang et. al., contrary to SAR studies conducted by Novartis and The University of Basel on the 4- and 6- positions, designed derivatives by replacing the C2 morpholine with various aliphatic or long-chain substituted aromatic amines. Their work led to the discovery of a series of compounds, an example shown in Figure 84, (PI3Kα = 18 nM, PI3Kβ = 2014 nM, PI3Kδ = 13 nM, PI3Kγ = 80 nM).

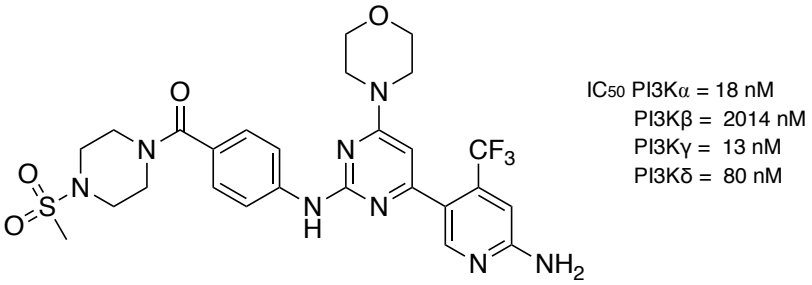


Figure 84. A representative structure from a series of molecules published by Zhang et. al.

Discovery of Gedatolisib (PKI-587 or PF05212384), Figure 88, [J. Med. Chem. 2010, 53, 2636–2645] by Wyeth (later Pfizer) was followed on from the discovery of PKI-402 (Figure 86)[102]. The initial lead compound for PKI-402 was a triazolopyrimidine that exhibited good potency against PI3Kα (83 nM), PI3Kγ (435 nM), and mTOR (250 nM); however potency, particularly against mTOR, and microsomal stability was improved by replacement of a benzylic alcohol with a urea (Figure 85). The urea containing compound was highly potent against PI3Kα (3.5 nM), PI3Kγ (24.8 nM), and mTOR (0.32 nM), unfortunately the compound exhibited very poor solubility.

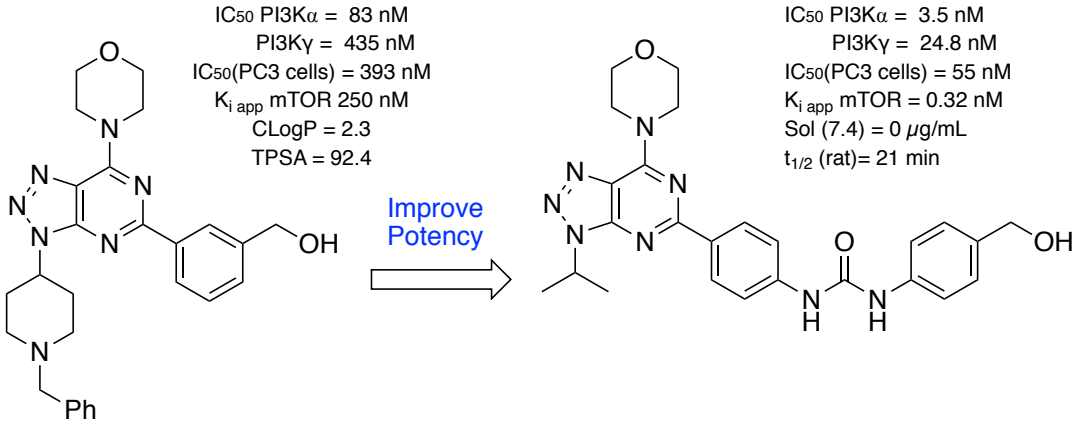


Figure 85. Introduction of urea functionality greatly improved activity, particularly against mTOR, however this introduced poor solubility.

Incorporation of basic amines onto the urea to improved upon the poor solubility. PKI-402 (Figure 86) was the result of that change, however, ultimately solubility issues still persisted, and advanced studies were halted until modifications to PKI-402 were

implemented to improve the cLogP.

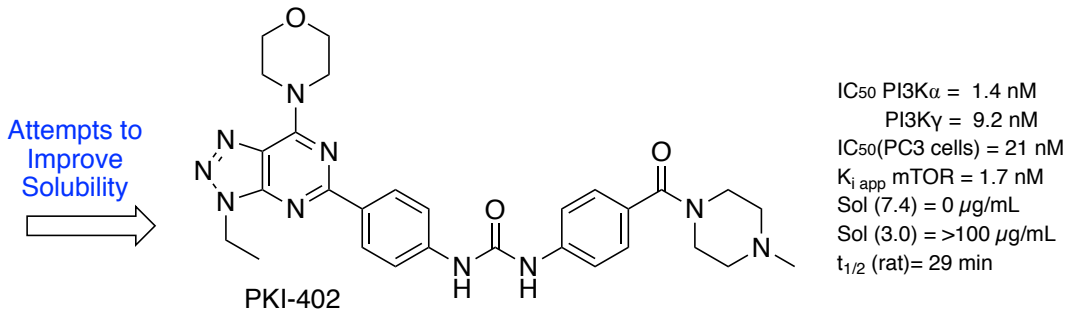


Figure 86. Introduction of basic amines onto the urea to improve solubility led to the discovery of PKI-402. Solubility issues still persisted and as such advanced studies were halted until this issue was addressed.

Initially, an additional morpholine was included to address a reported morpholine metabolic liability, via oxidation α to the morpholine ring oxygen, causing loss of potency. This morpholine modification (Figure 87) to the bismorpholino-1,3,5- triazine scaffold led to maintaining potent PI3Kα, PI3Kγ, and mTOR inhibitory activity but only moderate potency in cell proliferation assays, attributed to poor solubility and permeability.

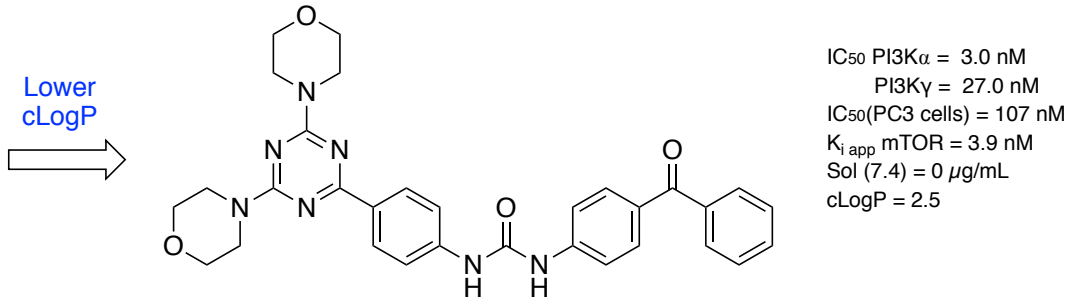


Figure 87. Introduction of a second morpholine group addressed a metabolic liability, via oxidation α to the morpholine ring oxygen.

Due to the retention of biochemical potency the SAR was probed to improve cellular potency. A drop in PI3K activity was observed when changing the phenyl groups of the urea with an alkyl group, but maintained mTOR potency, and incorporating basic amines onto the phenyl ring as in the case of Gedatolisib (Figure 88) led to excellent biochemical and cell potencies. These analogues also had good microsomal stability across species and exhibited good to moderate solubility. On the basis of enhanced po-

tency (PI3Kα = 0.4 nM, PI3Kβ = 6.0 nM, PI3Kγ = 8 nM, PI3Kδ = 6 nM, mTOR = 1.6 nM), solubility (14 μg/mL pH 7.4), microsomal stability, and lack of Cyp inhibition, Gedatolisib was chosen for further *in vivo* evaluations showing low plasma clearance (7 mL/min/kg), high volume of distribution (7.2 L/kg), and long half life (T½ = 14.4 h). Gedatolisib was also evaluated against a panel of 236 other human protein kinases at 10 μM, and it was found to be highly selective for PI3K and mTOR. Gedatolisib progressed to phase I and II clinical trials.

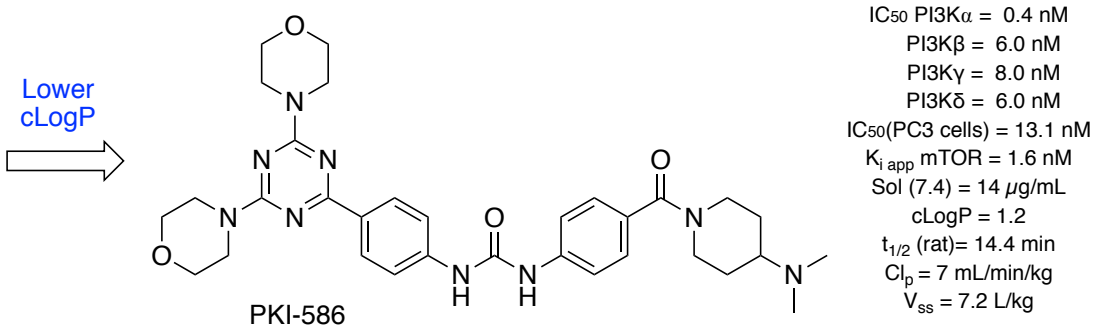


Figure 88. Further lowering of cLogP improved cellular potencies, leading to the discovery of gedatolisib (PKI-588).

Efforts from Miscellaneous Companies and Institutions

Miller et. al. [Bioorganic & Medicinal Chemistry Letters 23 (2013) 802–805] have reported a series of inhibitors in the same structural class as ZSTK474, although they were consistently less potent. Figure 73 is representative of their series (PI3Kα = 375 nM, PI3Kβ = 214 nM, PI3Kγ = >10 μM, PI3Kδ = 110 nM). Overall they found that substitution in the 5- position on the benzamidazole is consistently ~10-fold more

potent than substitution at the 6- position. Compounds were not progressed further.

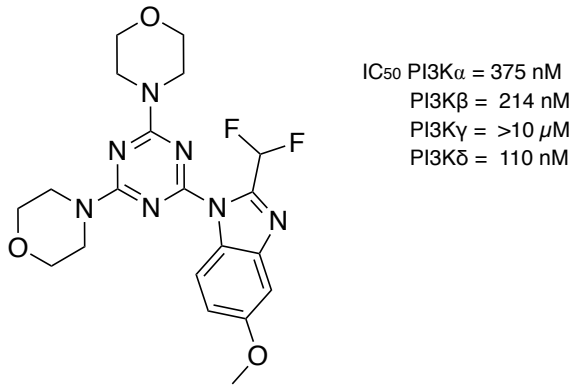


Figure 89. Miller et.al. reported a series of inhibitors in the same chemical class as ZSTK474, however they were consistently less potent.

In a subsequent paper[103] replacement of the the morpholine in the solvent exposed region with piperazine amides derived from amino acids was achieved, Figure 90 shows a representative of the series. Interactions with Asn836 of PI3Kδ were sought to gain selectivity towards PI3Kδ but it was found that thexample shown in Figure 90 was a β/δ inhibitor (PI3Kα = 2611 nM, PI3Kβ = 36 nM, PI3Kγ = 5859 nM, PI3Kδ = 12 nM).

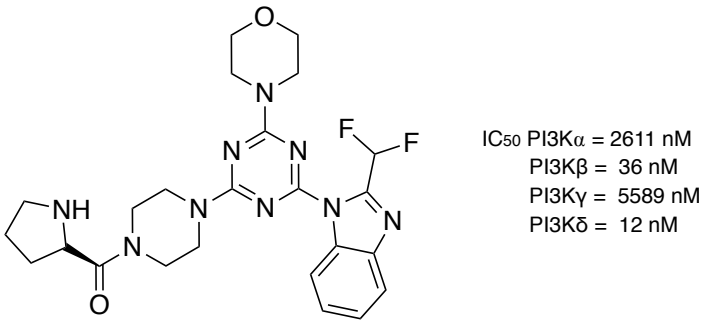


Figure 90. A represenative example of a series of inhibitors reported by Miller et. al., where they acylated the piperidine ring with amino acids in an attempt to target ASN 836 of PI3Kδ

Also in the same class are a series of inhibitors reported by Sphaera Pharma [104]. The example in Figure 91 was identified as thecandidate compound for further development, exhibiting good potency towards PI3Kα (60 nM) and good cellular potency (500 nM). The compound also showed a high level of microsomal stability, excellent oral bioavailability (AUC = 5.2 μM/h), no hERG liability, and minimal inhibition activity for CYP3A4, CYP2C19, and CYP2D6 at 10 μM concentrations.

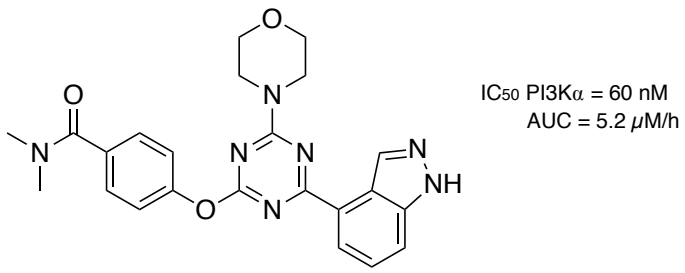


Figure 91. The candidate compound reported by Sphaera Pharma.

Gamage et. al. [105] have also produced extensive SAR on analogues of ZSTK474. Replacing one of the morpholine groups with a sulphonamide containing substituents lead to a series of PI3K inhibitors. Most compounds synthesised suffered solubility issues however the example in Figure 92 (PI3Kα = 22 nM, PI3Kβ = 116 nM, PI3Kδ = 13 nM) as the methanesulfonate salt showed suitable solubility (3.82 μg/ml) to be progressed *in vivo*. The compound was further evaluated in a mouse study using U87MG human glioblastoma tumour xenografts in Rag1-/- mice at a dose of 60 mg/kg qdx10 by ip injection effectively slowed tumour growth over the 10 day dosing period.

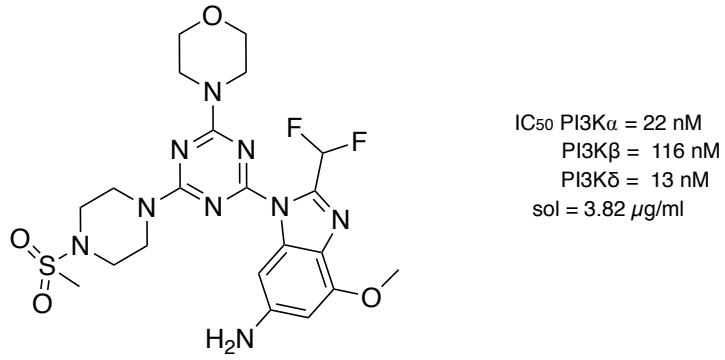


Figure 92. A represenative of a series of compounds synthesissed by Gamage et. al.

Scientists at Chugai Pharmaceutical Co[106][107] used PI-103 and LYS94002, and through superimposing them into the binding pocket with modelling tools, designed a phenolic and morpholine containing lead. Their lead compound showed excellent activity against PI3K*α*, but exhibited poor metabolic stability in human microsomes, and poor oral bioavailability in mouse mainly due to rapid glucuronidation of the phenol. The aim was to address the metabolic stability through bioisosteric replacement of the

phenol with an aminopyrimidine moiety which showed a slight reduction in PI3K*α* activity, but exhibited good antitumour activity *in vivo* in a human prostate cancer PC3 xenograft model as a result of improved metabolic stability and oral bioavailability. With room for improvement in terms of its physicochemical and ADME profile, modification of the solvent exposed region ultimately lead to the discovery CH5132799, Figure 93, a clinical candidate that showed good activity against PI3K*α* (14 nM), good oral biooavailability in mouse (F = 101%), good human liver microsomal stability, and *in vivo* antitumour activity in the PC3 xenograft model (TGI: 101% at 25 mg/kg, 11 days). CH5132799 selectively inhibits class I PI3Ks and showed less inhibition of class II PI3Ks (C2*α* = >10 μM, C2β = 5.3 μM), class III PI3K (Vps34 = >10 μM) and mTOR (1.6 μM) . Additionally, CH5132799 showed no inhibitory activity (IC_{50} >10 μM) against 26 other protein kinases.

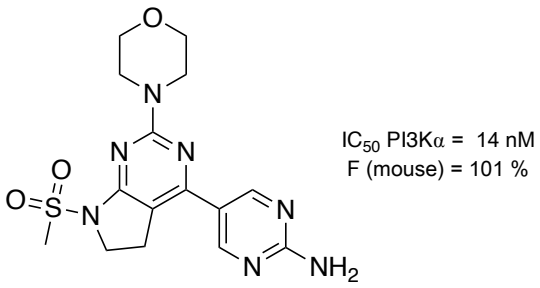


Figure 93. Structure of CH5132799

After the development of CH5132799, in 2015 Chugai Pharmaceutical Co made moddifications[108] to CH5132799 to further improve the PK profile, mainly through introducing a solubilising group in the solvent exposed region to give a series of inhibitors, an example of which is illustrated in Figure 94. Additionally, the example in Figure 94 incorporates an ortho-substituent which disrupts the molecular planarity and improves water solubility. The pharmacokinetic profile in mouse of the compound shows that the clearance (Cl = 11.1 mL/min/kg) was good and oral bioavailability (F = 86%) was greatly improved, without significant loss of inhibitory activity (PI3Kα = 42 nM).

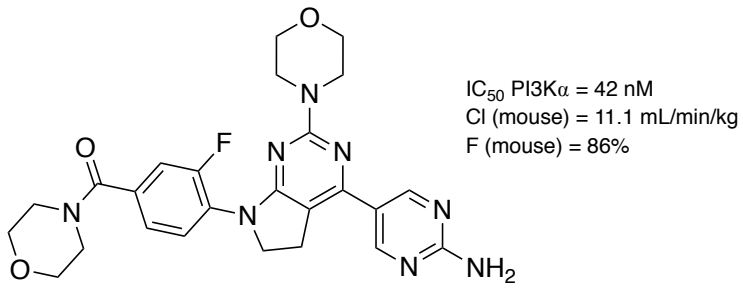


Figure 94. A representative of a series by Chugai Pharmaceutical Co. An ortho-substituent disrupts the molecular planarity and improves water solubility, improving the PK profile.

In a follow up paper from Chugai Pharmaceutical Co[109], they reported that introduction of urea functionality as in the case of the example in Figure 95 showed enhanced PI3Kα activity (42 nM). They proposed that this observation is due to the urea acting as a spacer, placing the aromatic ring close enough to the W760 to make a favourable interaction, enhancing the inhibitory activity. This change, however, introduces a solubility issue due to intermolecular hydrogen bonding between the urea and the pyrimidine core, resulting in a flat configuration that increases the crystallisation energy. Attempts to disrupt the planarity by introducing a methyl group to the ortho-position on the amino-pyrimidine led to a 8-fold reduction of potency as disrupting the planarity in this region of the inhibitor was not acceptable for keeping key interactions in the affinity pocket. Attention was shifted n back to the urea region, introducing ortho-substituents to the phenyl ring and including solubilising amines such as the ethyl piperazine. However, this was not enough to improve the solubility to a satisfactory level. Incorporating a ortho-fluoro group on the phenyl ring in which electrostatic repulsion between the fluorine atom and the urea carbonyl can be expected, results in a flat conformation, and thus poor solubility. However evaluation of the difluoro compound, showed a modest increase to the solubility, as this compound prefers a twisted conformation that avoids the electrostatic repulsion of the second fluorine atom with urea carbonyl. Liver microsomal stability was good in both mouse (Cl = 7.6 µL/min/mg) and human (Cl = 2.2 µL/min/mg), and permeability was also acceptable (1.1 x 10-6 cm/s in PAMPA).

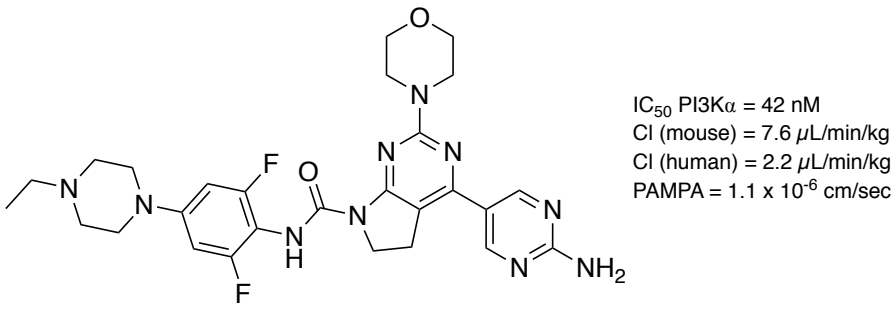


Figure 95. A representative example of of another series from Chugai Pharmaceutical Co

3.1.3 Benzoxepins

In 2011[110], after the discovery of GNE744 and GDC-0941, scientists at Genentech identified a benzopyran, in a HTS (Figure 96 A). The hi exhibited reasonable potency for PI3Kα, although in terms of physical properties it was poor (cLogP = 4.1, LE = 0.39, LipE = 2.5, MW = 356). The hit, however, was followed up upon due to the structural novelty of the scaffold. An SAR study of the aryl substituent on the aniline amide revealed the importance of the ortho-halogen. Additionally, a crystal structure (Figure 97) of Figure 96 B (PI3Kα = 0.108 μM) indicated that the N-methylaniline amide bound in a cis-fashion in the activity pocket, and that the hinge binding interaction of the pyran oxygen was suboptimal, and could be potentially be improved upon through ring expansion of the pyran. Expansion of the pyran to a 7 membered ring (Figure 96 C) led to a 4-fold increase in potency (PI3Ka = 0.024 μM), and expansion to a 8 membered ring (Figure 96 D) reduced potency drastically (>10 μM). Comparison of the crystal structures confirmed a shorter hydrogen bond and better angle for interaction with the hinge with the 7-membered ring.

Although, at this point potency had been increased, rate of clearance was consistently high across a series of analogues designed to improve the LipE with substitutions at the 8-position of the benzoxepin.

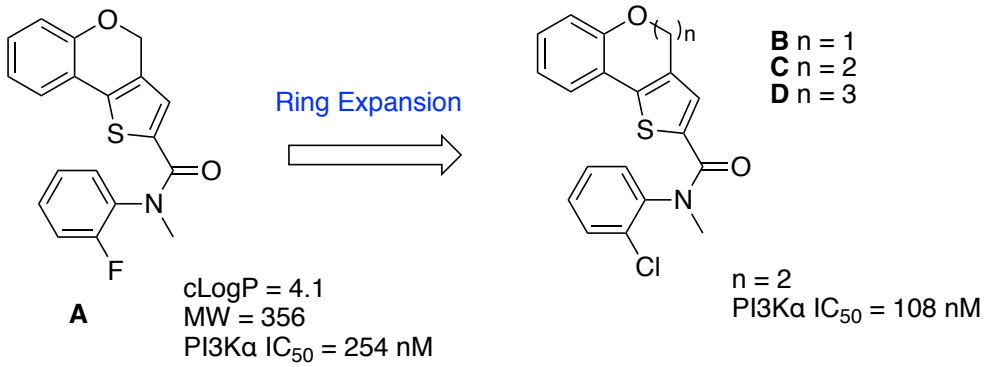


Figure 96. The benzopyran hit identified through HTS. Ring expansion to a 7-membered ring improved hinge binding interactions, whereas an 8-membered ring was less favoured.

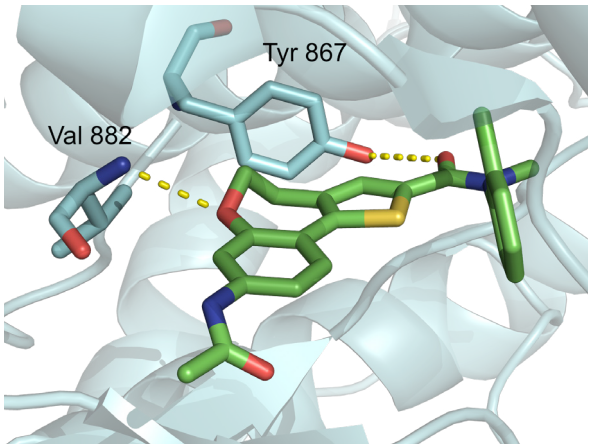


Figure 97. Crystal structure of B (3R7R) showing the hinge binding interaction of the pyran oxygen to Val882. In addition the amide bonds in a cis-fashion with the carbonyl oxygen forming a hydrogen bond with Tyr887.

A metabolite ID experiment in human hepatocytes revealed hydrolysis of the aniline amide and an oxidative metabolite resulting from de-methylation, aromatic oxidation and glucoronindation of the aniline. Para-substitution with an electron withdrawing polar amide,(GNE-614, Figure 98) reduced lipophilicity (clogP = 2.7), blocked para-oxidation, and increased clearance in rat (36 mL/min/kg). GNE-614 exhibits good potency towards the class I PI3Ks (PI3Kα = 4.6, PI3Kβ = 60 nM, PI3Kγ = 5 nM, PI3Kδ = 1.7 nM), relatively inactive against mTOR (530 nM), showed a only a moderate PK profile: rat (Cl = 36 mL/min/kg, F% = 50, AUC = 39 μM h), mouse (Cl = 15 mL/min/

kg, F% = 28, AUC = 330 µM h), and dog (Cl = 5 mL/min/kg, F% = 120, AUC = 17 µM h). GNE-614 was found to inhibit DNA-PK (6 nM), a structurally similar counter target.

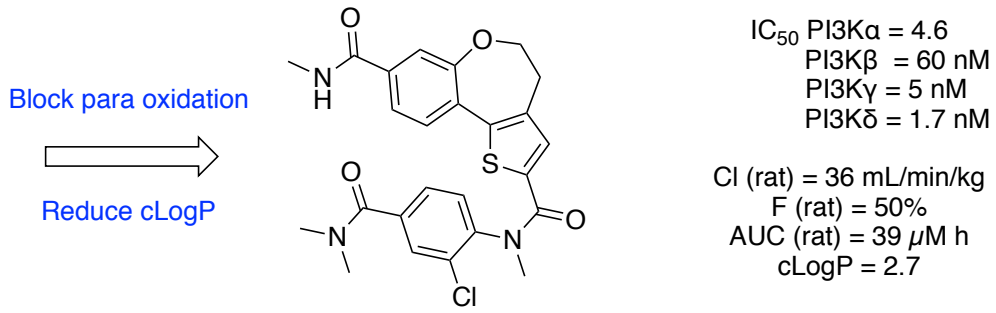


Figure 98. Substitution of the aromatic ring with a polar amide reduced lipophilicity and blocked para-oxidation, leading to GNE-614.

In a follow-up paper [111], Genentech aimed to improve the PK profile of GNE-614 by replacing the metabolically liable cis-N-methyl aniline amide with an appropriate isostere. After extensive SAR they discovered that replacing the aryl group with an alkyl group was not tolerated, however replacement with heteroaryl groups led to the discovery of a triazole (Pi3Kα = 4 nM), Figure 99, which showed improved properties for further optimisation (rat Cl = 13 mL/min/kg),.

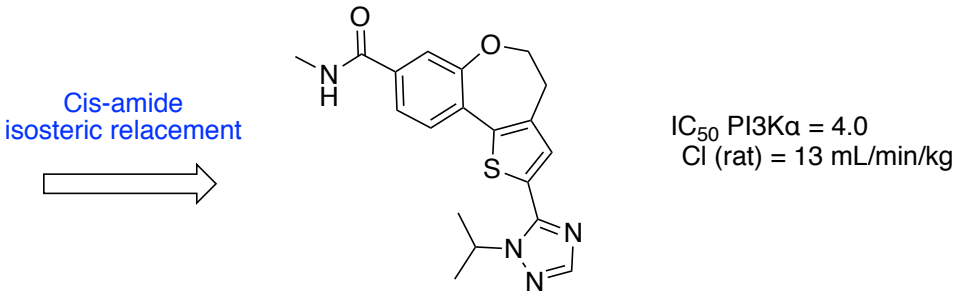


Figure 99. Bioisosteric replacement of the cis-amide with a triazole led to improved clearance in rat.

Following the discovery of the triazole (Figure 99) Genentech set out to further decrease the lipophilicity of the series by modification of the thiophene[112]. In addition, replacement of the thiophene would remove the potential metabolic liability of the thiophene, since thiophenes are known to undergo oxidative metabolism. After identifying a number of suitable heteroaryl groups, the group opted to select the thiazole, Figure 100, for further development. The thiazole was highly potent towards the class I PI3Ks

(PI3Kα = 0.27, PI3Kβ = 15 nM, PI3Kγ = 0.55 nM, PI3Kδ = 0.61 nM), although they observed that potency towards PI3Kβ was consistently lower with specific substitutions at the 8 position of the benzoxepin. They hypothesise this is due to a different conformation (in PI3Kβ) of the tryptophan residue that makes up the tryptophan shelf in the case of PI3Kδ. The thiazole showed a suitable PK profile for further advancement as it had had low clearance and high bioavailability in rodents (rat Cl = 5.4 mL/min/kg, F = 83%, mouse Cl = 9.5 mg/mL/kg, F = 110%), acceptable PK in dog (Cl = 14 mL/min/kg, F = 22) and moderate predicted clearance in human (hepatocyte Clp = 12 mL/min/kg). The thiazole showed modest tumor growth inhibition in an MCF7-neo/HER2 xenograft breast cancer model. Activity against counter targets was mTOR >4.3 μM and DNA-PK 0.34 μM.

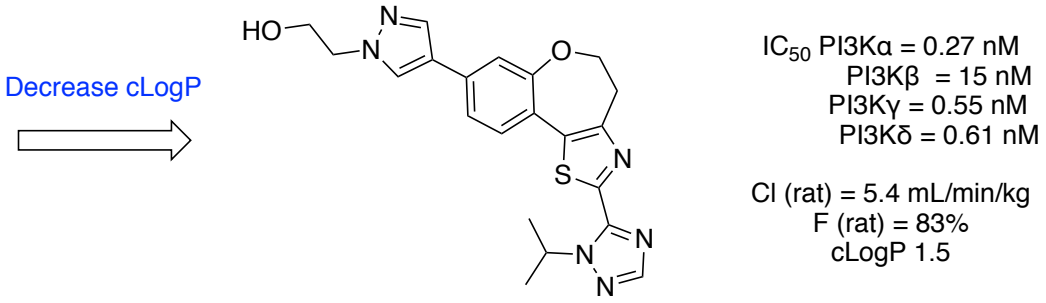
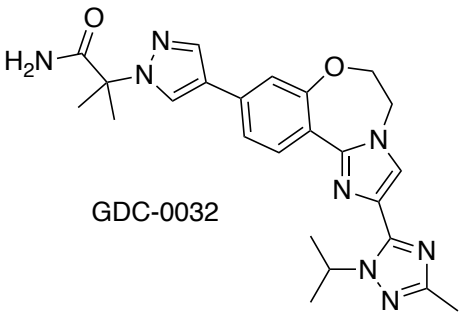


Figure 100. Structure of the thiazole

With the thiazole showing only modest tumour growth inhibition an MCF7-neo/HER2 xenograft breast cancer model despite being highly potent and exhibiting a moderate PK profile, Genetech aimed to increase the unbound exposure by aiming to reduce the lipophilicity even further. An extensive screen of heteroaryl isosteres was performed with focus on lowering the lipophilicity, leading to the discovery of Taselisib (GDC-0032), Figure 101, with a reduced clogD from 3.8 to 2.5. Taselisib showed good activity towards the class I PI3Ks, with decreased PI3Kβ activity (PI3Kα = 0.29 nM, PI3Kβ = 9.1 nM, PI3Kγ = 0.12 nM, PI3Kδ = 0.97 nM). Against a panel of 235 kinases only 2 (not including the Class I PI3Ks) inhibited greater than 50%: C2β (80.4%), and Vps34 (69.9%). Taselisib also had a good PK profile, exhibiting low *in vivo* clearance in rat (1.8 mL/min/kg), with high oral bioavailability (F = 99%). After toxicological and safe-

ty evaluation, Taselisib was progressed to clinical trials for PI3K related cancers.



GDC-0032

IC_{50} PI3Kα = 0.27 nM
PI3Kβ = 15 nM
PI3Kγ = 0.55 nM
PI3Kδ = 0.97 nM

Cl (rat) = 1.8 mL/min/kg
F (rat) = 99%
cLogP 1.1

Figure 101. Structure of Taselisib, GDC-0032

Having only reported pan or so-called β-sparing benzoxepins, in 2016 Genentech moved the focus of their program towards the development of selective PI3Kα inhibitors[113]. At the onset of their PI3Kα program, a crystal structure of one of their benzoxepin inhibitors was obtained (not shown, pdb 5DXH), revealing two residues unique to the α-isoform, Gln859 and His855. Due to the possibility to form multiple hydrogen bonds, as well as molecular modelling evidence to suggest their inhibitors had appropriate vectors, the team decided to target Gln859 in order to gain selectivity towards PI3Kα. Extensive SAR, and monitoring of torsion angle at the 8-position, focused on optimising hydrogen bonding with Gln859. This led to the discovery of GDC-0326 (Figure 102) where the primary amide makes 3 concerted hydrogen bonds with Gln859 (Figure 103, pdb 5DXT). GDC-0326 is a PI3Kα selective inhibitor (PI3Kα = 0.2 nM, α/β = 133, α/γ = 51, α/δ= 20), showed a comparable PK profile to Taselisib and was selected for further study, although it was not yet progressed into the clinic at the time of writing.

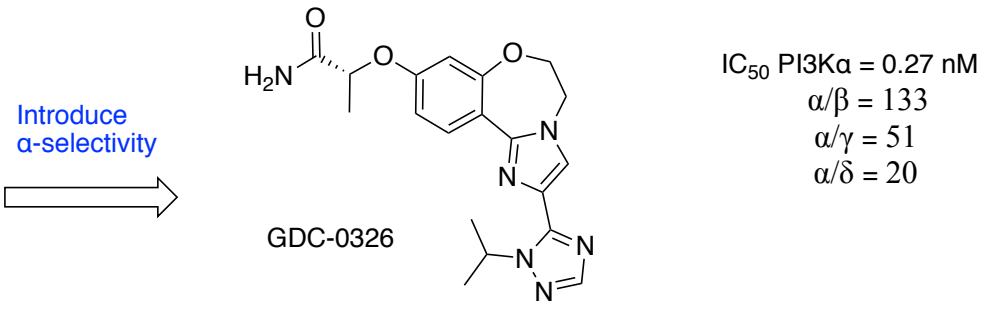


Figure 102. Structure of GDC-0326.

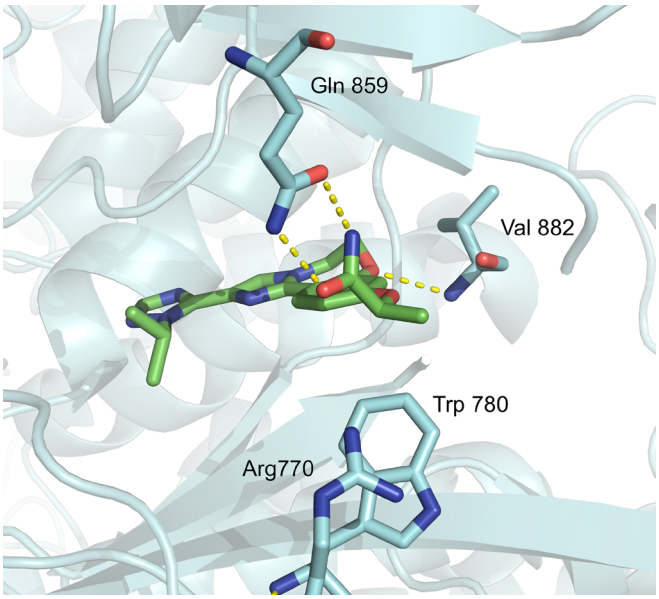


Figure 103. GDC-0326 co-crystalised with PI3Kα (pdb 5DXT). The primary amide makes 3 concerted hydrogen bonds with Gln859, unique to the PI3Kα isoform. This is thought to drive PI3Kα selectivity.

In their most recent publication[114] with regards to the benzoxepin scaffold, Genentech used their previous experience with the design of selective PI3Kδ inhibitors in order to build-in PI3Kδ selectivity into the benzoxepin core. Since the benzoxepin core was a result of ADME optimisation, and possessed favorable drug-like properties, this was an attractive endeavour. Through interaction with the tryptophan shelf, the result of this work is a δ-selective inhibitor (PI3Kδ = 1.9 nM, α/δ = 113), Figure 104. J had a low clogD (1.29), yet maintained good permeability (MDCK A to B = 10×10^{-6} cm/s).

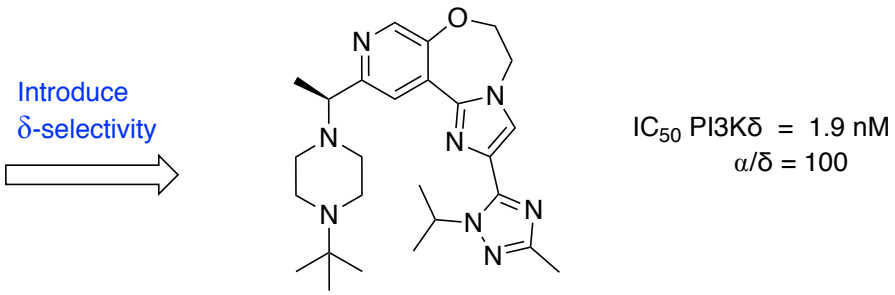


Figure 104. Genentech used their previous experience to build-in PI3Kδ selectivity into the benzoxepin core.

3.1.3.1 Benzothiazoles and derivatives

In 2012 scientists from Cellzome[115][116][117] reported HTS hits, Figure 105 A (PI3Kα < 4, PI3Kβ < 4, PI3Kγ = 5.4 , PI3Kδ = 4.5) and B (PI3Kα = 4.9, PI3Kβ = 4.7, PI3Kγ = 5.7 , PI3Kδ = 5.2) from an HTS of a kinase focused library of 16000 compounds. SARs around the core led to CZC19945, Figure 105, (PI3Kα = 5.6, PI3Kγ = 7.6 , PI3Kδ = 5.8). Further SAR on the central core led to CZC24832, PI3Kα pIC_{50} < 5, PI3Kγ pIC_{50} = 7.6 , PI3Kδ pIC_{50} = 5.1. CZC24832 showed moderate PK properties in mouse (Cl = 11.5 mL/min/kg, F = 37%), showed no inhibition of hERG up to 100 µM, no CYP inhibition, and was negative in the Ames test. In addition CZC24832 demonstrated efficacy in a chronic model of inflammation, although poor aqueous solubility (5 µg/mL) made pre-clinical development problematic. Crystallographic studies show that these compounds bind to the hinge region of PI3Kγ via the donor/acceptor motif of the triazolopyridine, with the pyridine sulphonamide interacting with the activity pocket.

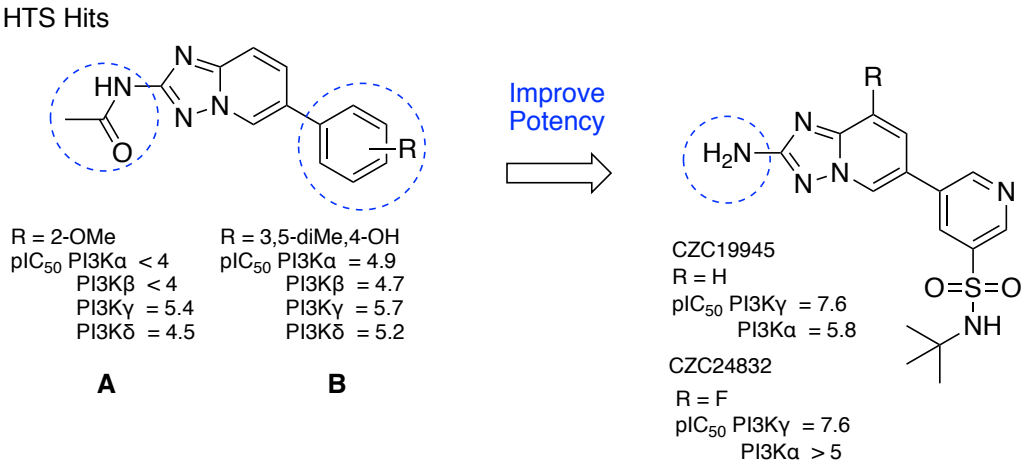


Figure 105. Cellzome took a hit from a HTS and improved upon its potency.

In a further publication Cellzome [118] detailed further SAR at the solvent exposed region, leading to γ/δ compounds such as the example in Figure 106 (PI3Kα pIC_{50} 6.4, PI3Kγ pIC_{50} = 8.4 , PI3Kδ pIC_{50} = 7.8, PI3Kβ pIC_{50} = 6.3), although poor physicochemical properties precluded them from oral absorption.

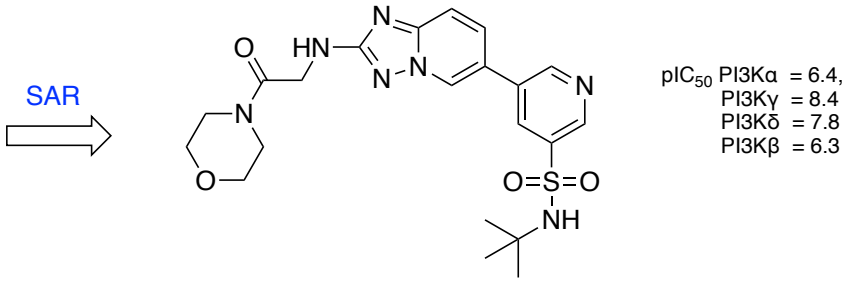


Figure 106. Further SAR lead Cellzome to γ/δ compounds.

In parallel, in 2012, scientists at Taisho Pharmaceutical Co[119] identified a hit (Figure 107) in their HTS. The hit had excellent enzymatic potency (PI3Kγ IC_{50} = 5 nM). Through structural modification and SARs, struggling initially with permeability issues, the examples in Figure 107 (PI3Kγ IC_{50} = 10 nM, α/γ = 4 and PI3Kγ IC_{50} = 3 nM, α/γ = 5) both showed low selectivity over PI3Kγ, although with improved permeability, cellular potencies were improved.

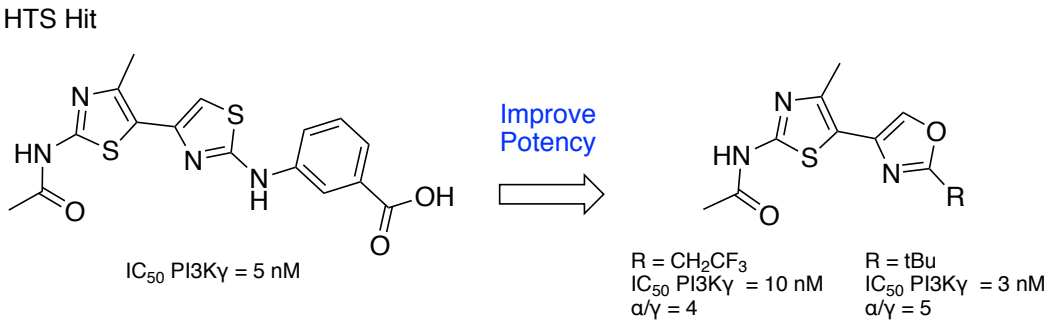


Figure 107. Taisho Pharmaceutical Co took a HTS hit and improved upon its potency

Later in 2013[120], the team reported that that the deacetylated versions of the compounds were positive in the Ames test. Although the deacetylated product was found not to be a major metabolite, they sought to mitigate mutagenic risk by replacing the oxazole ring with more pi-electron deficient heterocycles. This led the team to the 2-amino-5-oxadiazolyl thiazole (Figure 108) where both the acetylated and deacetylated analogues were negative in the Ames test. Being approximately equipotent in terms of PI3Kγ potency to the acetylated products they were able to derivatise further, leading to the discovery of TASP0415914 (PI3Kγ IC_{50} = 29 nM), Figure 108. The resulting compound exhibited a better PK profile, showed no CYP inhibition and was progressed to *in vivo* studies in a mouse collagen-induced arthritis model and was effective in a dose-dependant manner.

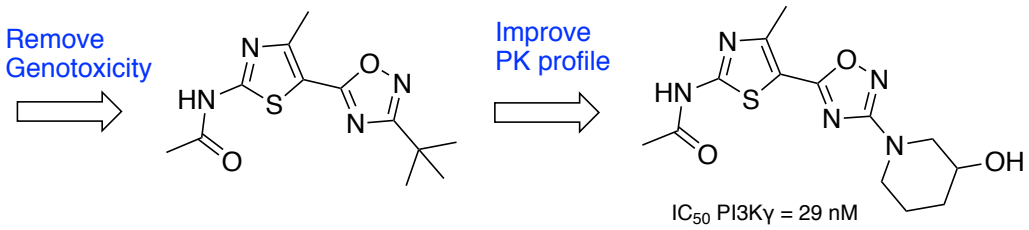


Figure 108. Replacing the oxazole ring with more pi-electron deficient 2-amino-5-oxadiazolyl thiazole, to give TASP0415914, removed genotoxicity.

Also in 2012 a paper from Novartis[121] revealed a hit (Figure 110) from a HTS targeting PI3Kγ. A docking study involving the hit showed that the the thiazole nitrogen and amide hydrogen form a bidentate donor–acceptor pair with the hinge region, and

the sulfonamide interacts with the activity pocket. They observed that residues lining the binding pocket were less conserved and hypothesised that isoform selectivity might be achievable by extending or replacing the acyl moiety with diverse substituents to exploit these differences.

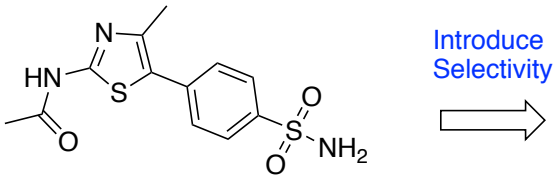


Figure 109. A HTS hit identified by Novartis. Docking studies suggested that selectivity might be achievable.

After developing a method of thiazole synthesis amenable to automation, they were able to generate approximately 400 analogues with replacements for the acyl moiety. Most of these compounds were found to be inactive, or weak pan-PI3K inhibitors, although three types of amines were identified, which led to potent isoform selective inhibitors. (S)-pyrrolidine carboxamides such as those of NVS-PI3-1 (Figure 110) (PI3Kα K_i = 0.005 μM, PI3Kβ K_i = 2.0 μM, PI3Kγ K_i = 0.53 μM, PI3Kδ K_i = 0.22 μM) and NVS-PI3-2 (Figure 110) (PI3Kα IC_{50} = 0.04 μM, PI3Kβ IC_{50} = 22.94 μM, PI3Kγ IC_{50} = 1.19 μM, PI3Kδ IC_{50} = 0.54 μM), a structurally related benzothiazole, were selective towards PI3Kα, where they suggest this is like due to the carboxamide making favourable interactions with the non-conserved Gln859 of PI3Kα.

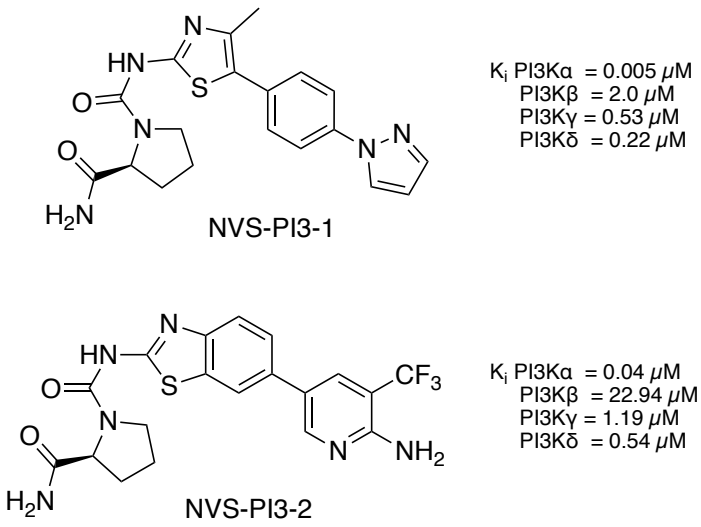


Figure 110. PI3Kα selective compounds NVS-PI3-1 and NVS-PI3-2. Selectivity is likely due to he carboxamide making favourable interactions with the non-conserved Gln859 of PI3Kα.

Aminopropionic acid derivatives such as those in NVS-PI3-3 (Figure 111) (PI3Kα Ki = 0.15 μM, PI3Kβ K_i = 0.34 μM, PI3Kγ K_i = 1.02 μM, PI3Kδ K_i = 0.004 μM), NVS-PI3-4 (Figure 113) (PI3Kα K_i = 1.89 μM, PI3Kβ K_i = 0.25 μM, PI3Kγ K_i = 0.088 μM, PI3Kδ Ki = 0.74 μM), NVS-PI3-5 (Figure 113) (PI3Kα K_i = 1.40 μM, PI3Kβ K_i = 0.32 μM, PI3Kγ K_i = 0.036 μM, PI3Kδ K_i = 0.47 μM) led to δ-selective (NVS-PI3-3) and γ-selective (NVS-PI3-4 and NVS-PI3-5). They suggest that this δ and γ selectivity is most likely derived from interactions between the terminal functional groups of the urea side chain and non-conserved amino acids at the outer edge of the binding site. Additionally, all examples in the series were much less potent towards PI3Kβ than the other isoforms. The PK properties of the series were not adequate for further progression, but this work led to some interesting observations towards selective inhibitors.

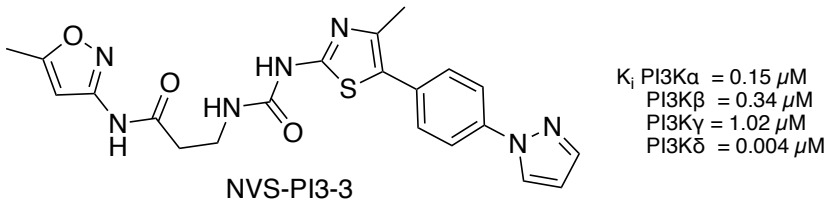


Figure 111. PI3Kδ selective aminopropionic acid derivative NVS-PI3-3.

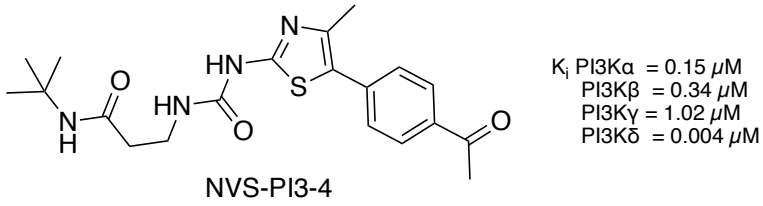


Figure 112. PI3Kγ selective aminopropionic acid derivative NVS-PI3-4.

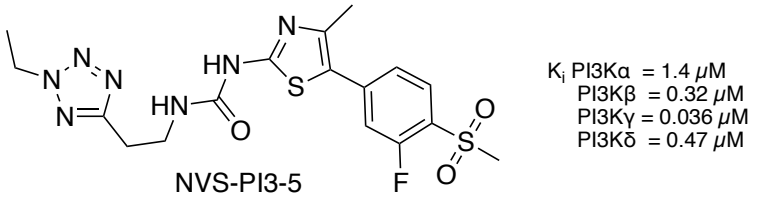


Figure 113. PI3Kγ selective aminopropionic acid derivative NVS-PI3-5.

Following this, in 2013, Novartis disclosed the discovery process of Alpelisib (NVP-BYL719)[122], Figure 114, a PI3Kα selective inhibitor (PI3Kα IC_{50} = 0.005 μM, PI3Kβ IC_{50} = 1.2 μM, PI3Kγ IC_{50} = 0.25 μM, PI3Kδ IC_{50} = 0.29 μM). Crystallograpic evidence of NVP-BYL719 in complex with PI3Kα shows that NVP-BYL719 exhibits excellent selectivity towards PI3Kα by exploiting the non-conserved Gln859 of PI3Kα (PDB 4JPS). NVP-BYL719 has a suitable PK profile. In rats, Cl = 10 mL/min/kg, Vss = 1.9 L/kg. Additionally, NVP-BYL719 showed no significant CYP inhibition, and no significant inhibition of related kinases. NVP-BYL719 was progressed to phase I clinical trials.

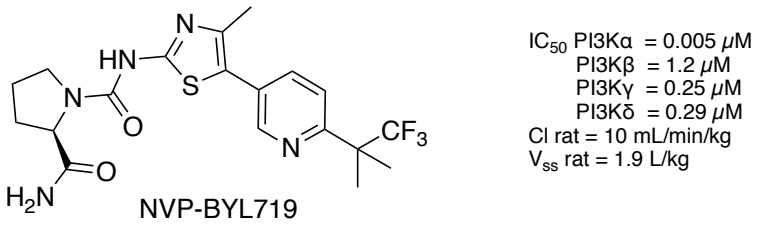


Figure 114. Structure of Alpelisip (NVP-BYL719), a selective a PI3Kα selective inhibitor.

In 2014 scientists at Vertex[123] analysed the crystal structure of PIK-93 (Figure 115) and observed that there was sufficient space in the ATP pocket to allow for a ring fusion of the thiazole into a benzothiazole, where hinge binding could be achieved through the donor-acceptor motif of the nitrogens of the aminobenzothiazole. SAR, by replacement of the activity pocket group led to the benzothiazole (PI3Kγ Ki = 0.004 μM, α/γ =1, β/γ = 10, and δ/γ = 3), Figure 115.

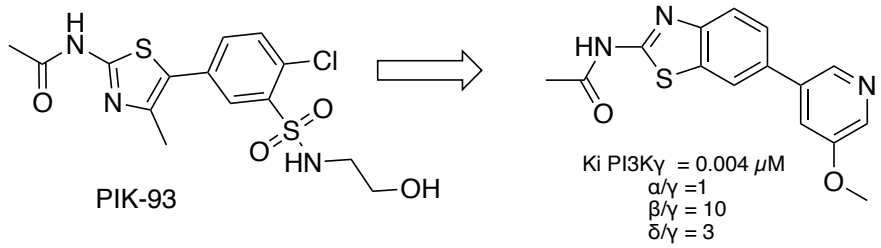


Figure 115. Structure of PIK-93. Suffiecient space in the ATP pocket allowed for ring fusion of the thiazole into a benzothiazole. Further modification of the activity pocket group led to a PI3Kγ compound.

SAR to replace the acetamide group with urea functionality gave the urea in-Figure 116 (PI3Kγ Ki = 0.002 μM, α/γ = 66, β/γ = 21, and δ/γ = 61), which exhibited isoform selectivity towards PI3Kγ.

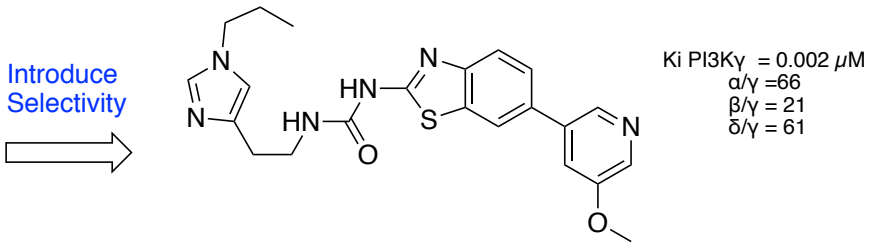


Figure 116. Replacing the acetamide group with urea functionality improved PI3Kγ selectivity.

After obtaining a crystal structure for the urea in PI3Kγ (PDB 4PS3), they hypothesise that this selectivity is a result of two non-conserved residues within the binding site. The first is Ala885, which is unique to PI3Kγ. In α, β and δ this is a serine residue where the OH of serine is involved in hydrogen bonding with the hinge valine residue. They propose that introduction of urea functionality allows for the urea carbonyl to form an additional hydrogen bond to the hinge valine, which in-turn breaks the serine-valine hydrogen bond, freeing up the OH group, introducing a steric clash with the lipophilic side chain. This steric clash is unfavourable in the anti-targets, and does not happen in the case of PI3Kγ. The second non-conserved residue is Gly829, a glutamic acid residue in PI3Kα. This aids selectivity over PI3Kα upon increasing the length of the terminal alkyl chain. These compounds were not progressed further, however they were useful in determining important residues for gaining isoform selectivity.

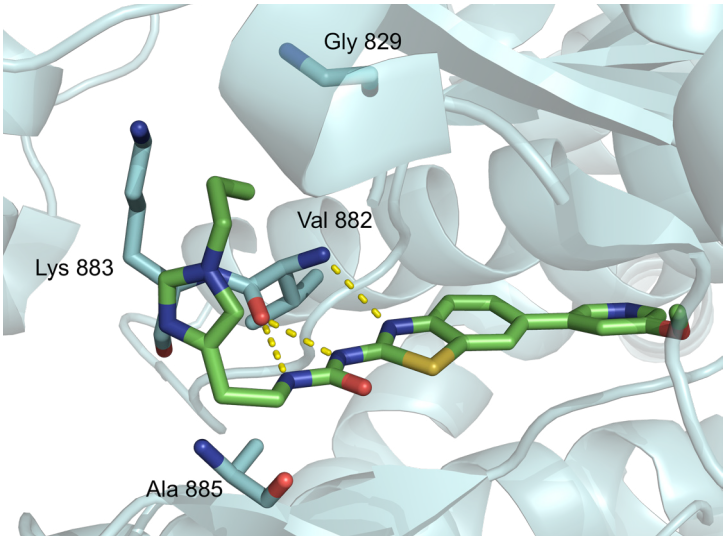


*Figure 117. Crystal structure of PI3Kγ (*PDB 4PS3) co-crystalised with the urea PI3Kγ inhibitor.

In a further publication from Vertex [124] in 2015, they aimed to improve the physicochemical properties of the urea by reducing the cLogP and increasing the FSp_3. In order to do so they replaced the central benzothiazole core with a thiazolopiperidine. Synthesis of the thiazolopiperidine analogue of the urea led to a 12-fold reduction in potency (PI3Kγ K_i = 0.048 μM), however introduction of an additional nitrogen atom 4-position of the pyrazine ring, led to an improvement in potency (PI3Kγ K_i = 0.017). Additionally, incorporating fluorine atoms onto the terminal alkyl chain brought potency back and additionally increased selectivity markedly, leading to the thiazolopiperidine (PI3Kγ K_i = 0.002 μM, α/γ = 228, β/γ = 105 and δ/γ = 395), Figure 118. They hypothesise the general increase in affinity for PI3Kγ upon addition of the fluorine atoms is due to a C−F···C=O interaction with Thr827. Additionally, they hypothesise that the drastic increase in selectivity is driven by a favorable interaction of the acidic methine proton of the fluoroethyl group with Glu814, a residue unique to PI3Kγ.

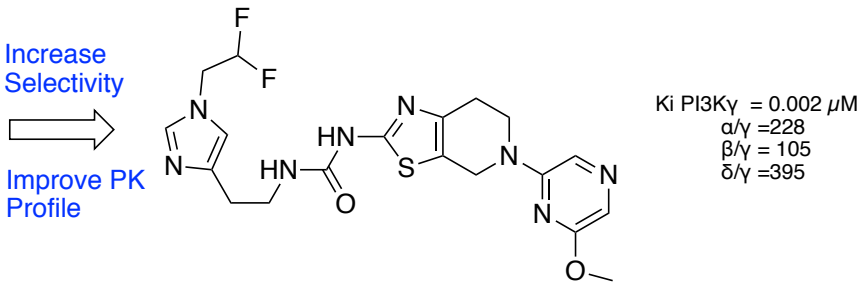


Figure 118. Replacement of the benzothiazole with a thiazolopiperidine improved selectivity and the PK profile.

Recently in 2018, AstraZeneca[125] discovered a hit (PI3Kγ pIC_{50} = 6.8) (Figure 119) in a HTS. Methylation of the acetamide nitrogen led to a large reduction in potency, suggesting that the acetamido-substituted isoxazole is the hinge binding motif. SAR to replace the isoxazole with amino heterocycles that are typical kinase hinge-binding motifs lead to replacement of the isoxazole with a thiazole, (R-enantiomer PI3Kγ pIC_{50} = 8.9), Figure 119.

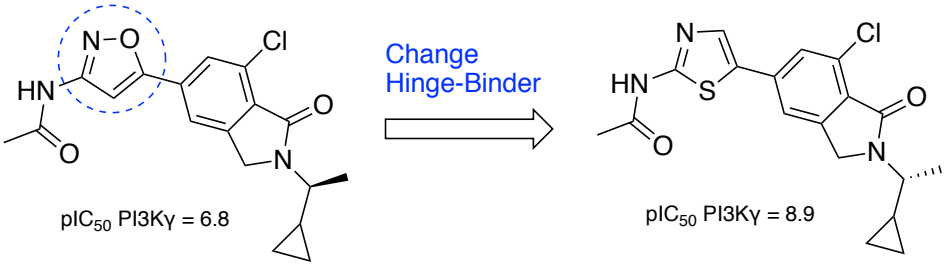


Figure 119. AstraZeneca modified their HTS hit by replacing the isoxazole hinge binder with a thiazole hinge binder, improving potency.

Failing to co-crystallise inhibitors of the series in PI3Kγ, the team looked to co-crystallise inhibitors in PI3Kδ. Successfully crystallising the thiazole (Figure 119) within PI3Kδ they confirmed the aminothiazole forms hydrogen bonds to the hinge residue Val828 and that the carbonyl of the lactam interacts with Lys779. The N-alkyl tail is oriented perpendicular to the isoindolinone core and extends deep into the ATP-binding pocket. An interesting observation was that removal of the N-alkyl group led to a 2 log decrease in PI3Kγ activity and a 1.6 log increase in PI3Kα potency suggesting that PI3Kγ selectivity seems to originate from the N-alkyl tail extending deep into the

ATP-binding pocket. The thiazoles exhibited poor properties for oral administration as they had poor solubility, high *in vitro* clearance and were very lipophilic. Introduction of a sulfone introduced excellent isoform selectivity (PI3Kα pIC_{50} < 4.5, PI3Kβ pIC_{50} < 4.5, PI3Kγ pIC_{50} = 8.1 , PI3Kδ pIC_{50} = 6.0) (Figure 120) and good bioavailability (F = 51%) and low *in vivo* clearance (Cl rat = 6.3 mL/min/kg). In a kinase screen only related kinases C2β (84%) and C2γ (71%) showed significant inhibition. In a rat LPS-induced acute inflammation model, oral administration resulted in a dose-dependent inhibition of airway neutrophilia in rats.

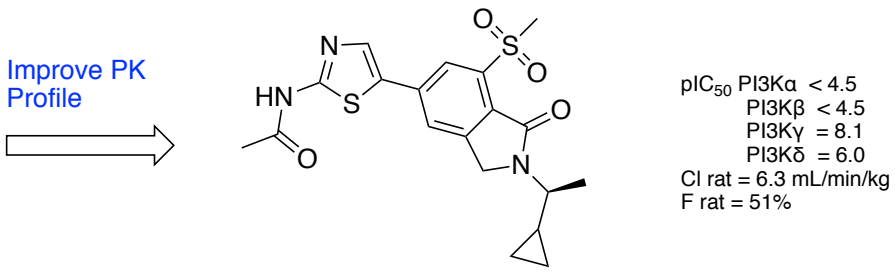


Figure 120. Introduction of a sufone improved the PK profile.

3.1.3.2 Copanlisib

Scott *et al*[126] recently reported on the identification of Copanlisib (BAY 80-6946), Figure 121, a selective PI3K α/δ inhibitor that has been granted an accelerated approval as a treatment for patients with relapsed follicular lymphoma. An X-ray crystal structure showed that the imidazoline N-1 nitrogen atom formed a critical hydrogen bond to the hinge Val882 and the 4-aminopyrimidine group interacted in the affinity pocket forming hydrogen bonds with Asp836 and Asp841 through the amino group, and with Lys833 through a pyrimidine nitrogen (PDB 5G2N). Copanlisib was shown to be a potent PI3K inhibitor (PI3Kα IC_{50} = 0.5 nM, PI3Kδ IC_{50} = 3.7 nM, PI3Kγ IC_{50} = 6.4 nM, PI3Kβ IC_{50} = 45 nM) as well as inhibiting mTOR (IC_{50} = 45 nM). The intravenous first-in-human phase I study of Copanlisib in patients with advanced solid tumors and non-Hodgkin's lymphomas showed that it exhibited dose-proportional pharmacokinetics and promising anti-tumor activity, particularly in patients with non-Hodgkin's lymphomas.

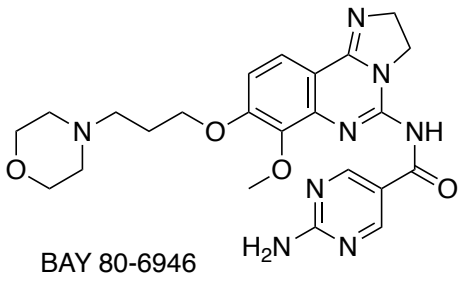


Figure 121. Structure of Copanlisib (BAY 60-6946).

3.1.4 So-called “Propellar” Inhibitors

Propellar inhibitors, which will only be breifly mentioned, are inhibitors that adopt a “propeller-shaped” conformation when bound to the enzyme leading to the stabilisation of a conformational change that opens a hydrophobic “specificity” pocket in the active site that is not present in the apo-structure of the enzyme – these are mostly PI3Kδ selective inhibitors. An example is Idelalisib[67] which was the first-in-class selective inhibitor of PI3Kδ, approved by the FDA[67] in 2014 for use with patients with chronic lymphocytic leukemia, focular lymphoma and small lymphocytic lymphoma. Idelalisib was initially discovered by Calistoga and was later advanced by Gilead and represented an important advance in the search for highly-selective PI3Kδ inhibitors. The European Medicines Agency, at the request of the European Commission, is currently reviewing[127] Idelalisib following concerns over serious adverse events in ongoing trials, mostly due to infections.

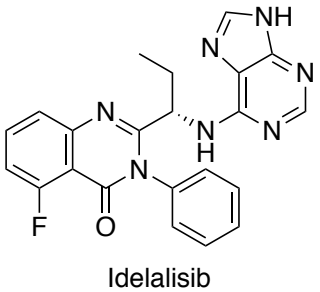


Figure 122. Structure of Idelalisib.

Unfortunately, to date there has been no journal publication detailing the dis-

covery of Idelalisib, however the ligand-bound X-ray crystal structure (PDB 4XEO) revealed the rationale for the observed high PI3Kδ selectivity. Idelalisib binds in the ATP binding site of the P110 catalytic subunit of PI3Kδ with the purine forming two hydrogen bonds with key hinge residues (Val828 and Glu826). The fluorine containing quinazolinone ring assumes a perpendicular conformation to the hinge binder and is embedded in a specificity pocket between Trp760 and Met752 that is closed in the apo structure of the enzyme. The phenyl ring adopts a binding conformation perpendicular to the quinazolinone ring and protrudes into a hydrophobic region out of the ATP-binding pocket and the improved PI3Kδ selectivity of these “propeller shaped” compounds is proposed to be a consequence of the lower energy requirement for the creation of the specificity pocket in PI3Kδ relative to the other class 1 PI3K isoforms. Further examples of “propeller” inhibitors such as duvelisib[128] (Figure 123), tenalisib (Figure 123), etc have been extensively reviewed. Duvelisib was recently approved in September 2018.

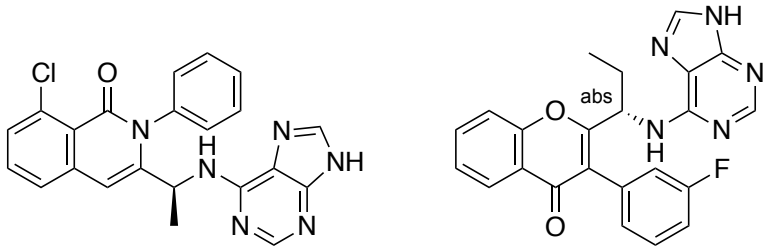


Figure 123. Structures of Duvelisib and Tenalisib.

3.2 Aims and Objectives

From the above it can be seen that a lot of effort, from both industry and academia, has been put into the development of PI3K inhibitors, however only 3 inhibitors have been approved by the FDA (Idelalisib, Copanlisib and Duvelisib), and all of these approved inibitors have side effects associated with them, due to off-target effects, as a consequence of poor selectivity profiles.

The following results and discussion section will focus on our efforts to develop isoform selective PI3K inhibitors. Additionally, since synergy with Ceritinib has been demonstrated by the pan-PI3K inhibitor, homing in on which isoform of PI3K is responsible for this observation is the next challenge. The main aim and objective of the following chapter is to develop isoform selective PI3K inhibitors and test these inhibitors with Ceritinib to asses for synergic effects.

3.3 Results and Discussion

3.3.1 PI3Kδ Inhibition

3.3.1.1 Inhibitor Design

From previous work in the field by Genentech it is evident that a thienopyrimidine core is a good central scaffold to achieve inhibition of the class I PI3Ks. Additionally, Genentech used the thienopyrimidine core to generate PI3K δ-selective compounds such as those in Figure 64 and Figure 65. In this work the thienopyrimidine core was chosen as the central scaffold with the aim of achieving δ-selectivity. Additionally, as discussed in the previous section, Genentech observed good δ-selectivity when interacting with the tryptophan shelf made up of Trp 760 and Thr 750 (δ-numbering). It is these observations that inspired the incorporation of a molecular scaffold, previously designed by the group, onto the thienopyrimidine core.

The molecular scaffold (Figure 124), reported by the group in 2014[130], is chiral and tricyclic in nature. The 3-dimentionality of the scaffold allows for the examination of the geometric isomerism (*cis*- and *trans*-ring fusion), the dihedral angle of the ring junction, and the influence of chirality on biological activity. Prior to this project, the tricyclic molecular scaffold had also been found to be biologically active when incorporated into inhibitors of dipeptidyl peptidase-4 (DPP-4) and into antagonists[131] of the C−C chemokine ceceptor type 5 (CCR5). This was published, along with this work, in 2017[132].

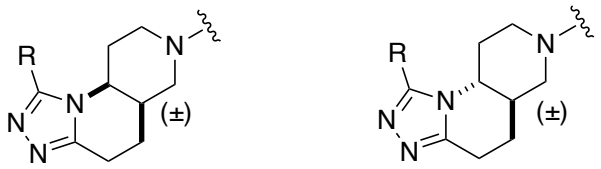


Figure 124. The cis and trans isomers of the tricyclic molecular scaffold.

The initial design was to incorporate the tricyclic molecular scaffold onto the thienopyrimidine core with the aim of interacting with the tryptophan shelf within the

solvent exposed region of PI3Kδ. An 8 x 3 array was designed (Figure 125), where for the solvent exposed region, the tricyclic scaffold and its analogues were used. The R-group on the scaffold was varied (CH_3 or CF_3) to explore the effect of changing the electronics of the triazole ring. Both the -*cis* and -*trans* versions of these compounds were considered (termed the "cyclics" for discussion purposes). We also thought to explore how the angle of the triazole could be influenced by removing the tether that keeps it locked in conformation, (termed the "acyclics" for discussion purposes). This would allow for free rotation around the carbon-nitrogen bond. Additionally, we decided to remove the triazole completely to assess what effect it has (termed the "bicyclics" for discussion purposes).

In the activity pocket, where interactions are generally formed with Asp841 (δ-numbering), we opted to select phenol, as this is generally well-known to contribute to high PI3K potency (discussed in detail in section 3.1.2). Additionally, we used 2 bioisosteres of the phenol as it is well known that the phenol group has a metabolic liability due to glucuronidation. The bioisosteres were 4-indazole and 4-indole, where these were chosen so as to explore the observed increase in δ-selectivity Genentech observed when replacing 4-indazole with 4-indole.

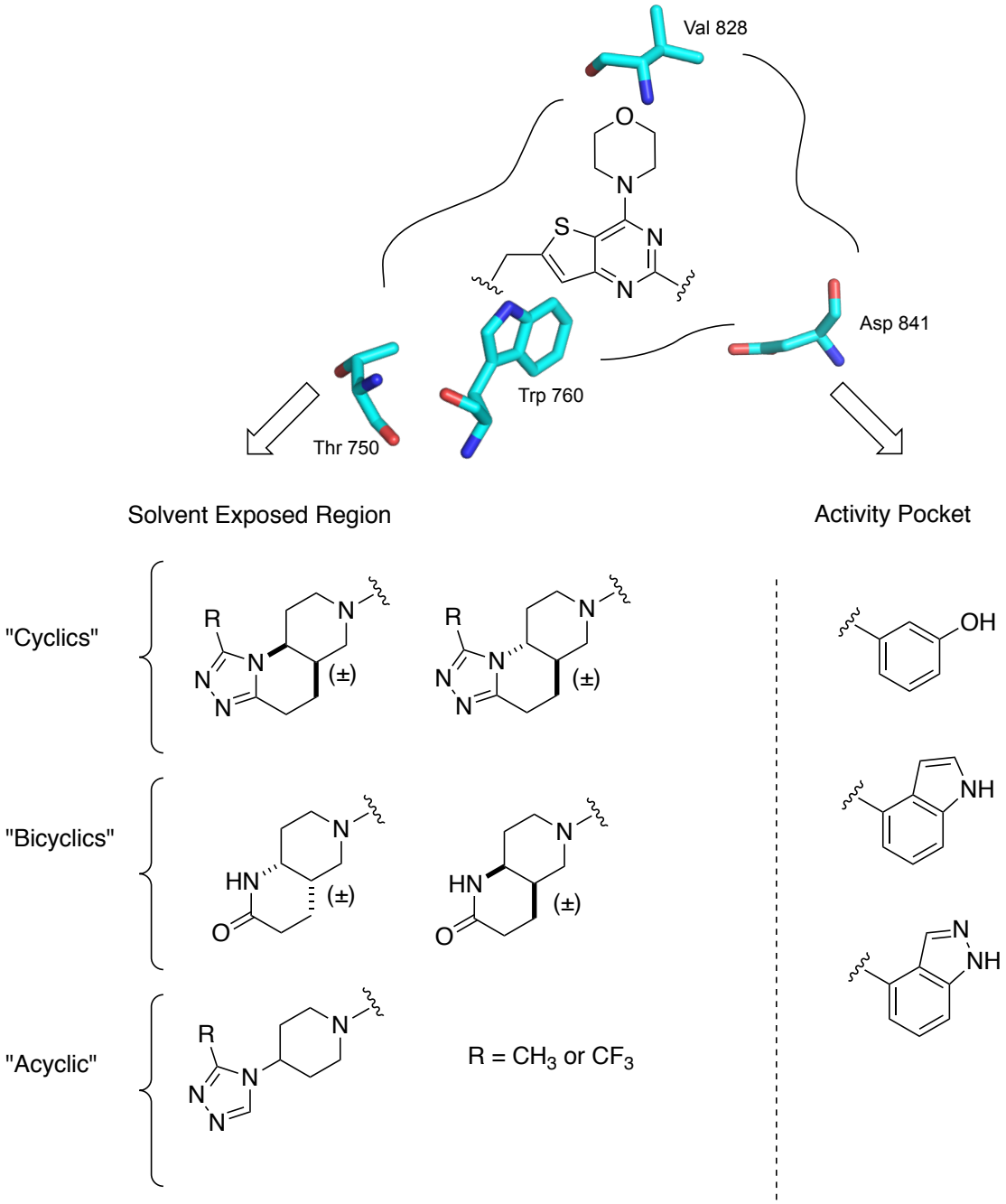


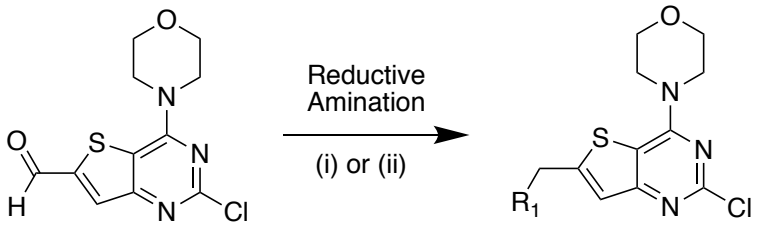
Figure 125. An 8 x 3 array of compounds to be synthesised. The solvent exposed region will comprise of the cyclics, the bicyclics, and the acyclics. The activity pocket will be comprised of the phenols, the indoles, and the indazoles.

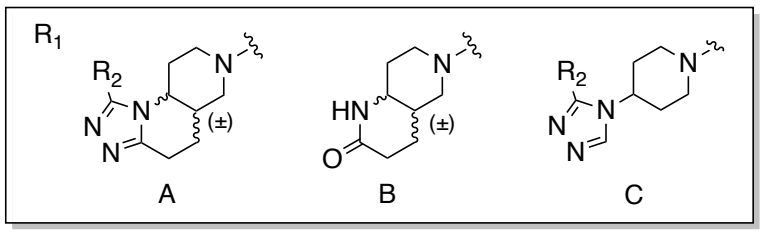
3.3.1.2 Inhibitor Synthesis

The synthesis of the PI3K inhibitors began using a chloro-thienopyrimidino morpholine scaffold, which was kindly donated to The University of Nottingham by Glax-

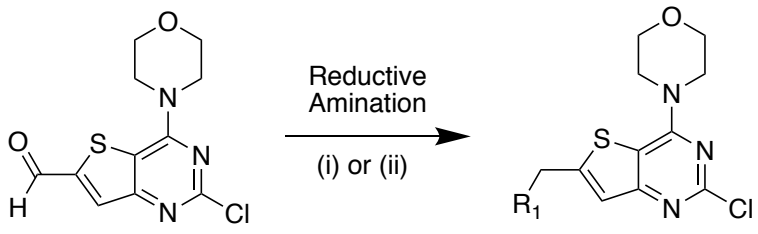
oSmithKline. The first step involves a reductive amination (Table 3) which has been optimised as follows: The aldehyde and the amine were taken up in a 10:1 mixture of dichloromethane : acetic acid mixture and sodium acetate added if the amine was in a salt form. This mixture was then heated at 45 ° C for one hour before the reducing agent, picoline borane, was added. The sodium acetate acts to free up the amine, whilst simultaneously forming sodium chloride and acetic acid, which catalyses the formation of the iminium ion. Although picoline borane is thought to selectively reduce the iminium over the aldehyde, with direct addition of the reducing agent, i.e. without time to equilibrate the iminum species, it was found that more primary alcohol was formed from reduction of the aldehyde. Alternatively, the reductive amination could be performed in acetonitrile or using sodium triacetoxyborohydride as the reducing agent. The presence of trimethylorthoformate increases yields, as this acts as a dehydrating agent, driving the formation of the iminium ion. Yields were generally good for the reaction, 30 - 90%.

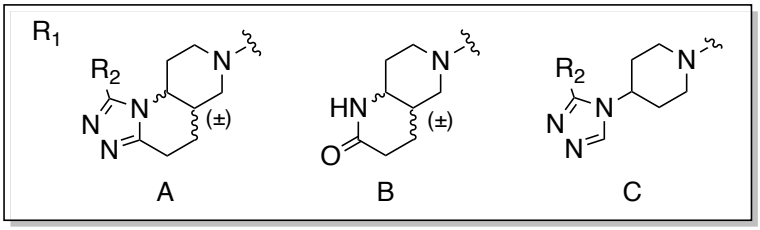
Table 3. Reductive amination to install amines. Reagents and Conditions: (i) Amine, CH2Cl2:AcOH (10:1), NaOAc, Picoline Borane, 45°C then rt.; (ii) Amine, CH3CN, Trimethylorthoformate, NaOAc, Sodium triacetoxyborohydride, 45°C then rt. Yields: 30-91%.





R_1	R_2	Ring Geometry	Yield
A	CH_3	*cis*	49%
A	CH_3	*trans*	54%
A	CF_3	*cis*	91%
A	CF_3	*trans*	62%

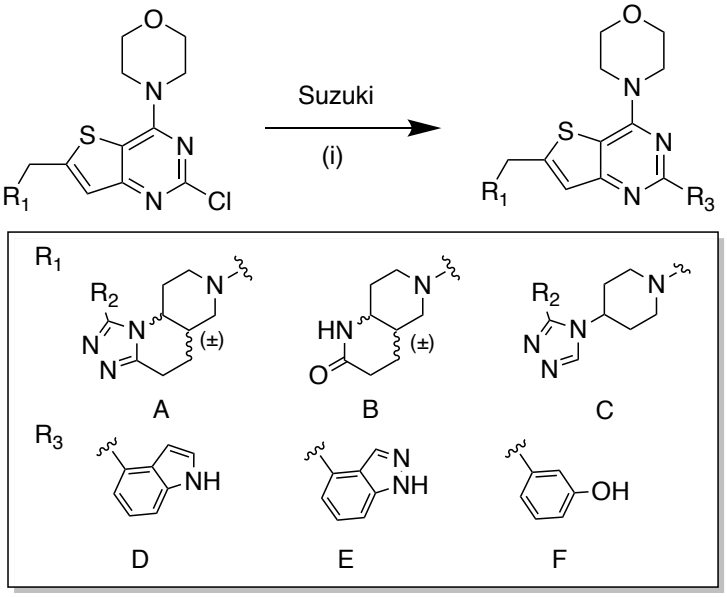




R_1	R_2	Ring Geometry	Yield
B	-	*cis*	61%
B	-	*trans*	63%
C	CH_3	-	71%
C	CF_3	-	30%

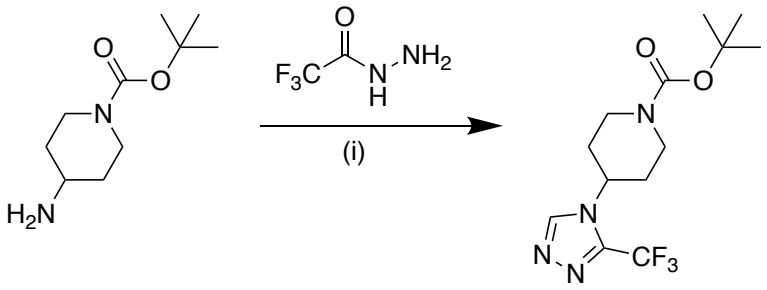
The second step is an excellent yielding Suzuki coupling[133] with the required boronic acid, where $Pd(PPh_3)_2Cl_2$ was used as the coupling catalyst and aqueous sodium carbonate was used as the base (Table 4).

Table 4. Suzuki Coupling to install aryl groups. (i) Boronic acid, $Pd_2(PPh_3)_2Cl2$, Na-2CO3, H2O:EtOH (3:1), microwave, 125 °C, 45 mins. Yields 54-97%



R_1	R_2	Ring Geometry	R_3	Yield
			D	60%
		Cis	E	62%
			F	95%
A	CH_3		D	81%
		Trans	E	58%
			F	59%
			D	65%
		Cis	E	62%
			F	72%
A	CF_3		D	81%
		Trans	E	78%
			F	81%
			D	-
		Cis	E	-
			F	-
B	-		D	94%
		Trans	E	90%
			F	80%
			D	64%
C	CH_3	-	E	54%
			F	54%
			D	97%
C	CF_3	-	E	86%
			F	89%

The amines used were previously synthesised within the group with the exception of the bicyclic trifluoromethyltriazole piperidine. This was synthesized via a triazole synthesis with DMF.DMA, trifluoromethyl hydrazide and *N*-Boc amino piperidine, with a catalytic amount of acetic acid.



Scheme 1. Reagents and conditions: Amine (1.0 eq.) DMF.DMA (1.0 eq.), AcOH (excess), CH_3CN, r.t. - 100 °C, 6 h., Yield 8%.

3.3.1.3 Assay details

The assay used by GSK to biologically evaluate the inhibitors is an HTRF® PI3 kinase assay kit provided by Millipore[134]. The assay works by firstly completing a kinase reaction. The kinase reaction involves PI3K, the substrate of PI3K (PIP2), and ATP. Since PI3K converts PIP2 to PIP3 using ATP, the products of the kinase reaction are PIP3 and ADP. After performing the kinase reaction, both without inhibitor as controls and with a range of concentrations of inhibitor, the kit provides a "stop solution" which contains biotinylated PIP3. A detection reagent is then added that contains GST-tagged pleckstrin homology domain (PH) and fluorophores streptavidin-allophycocyanin (streptavidin APC) and europium-labeled anti-GST (EU). A complex is generated between the GST-tagged PH domain and biotinylated short chain PIP3, which recruits the fluorophores to form the time-resolved fluorescence resonance energy transfer (TR-FRET) complex. Upon excitation at 330 nm, energy is transferred from Europium fluorophore to the streptavidin- allophycocyanin fluorophore, which emits at 665 nm. The TR-FRET complex can be disrupted in a competitive manner by non-biotinylated PIP3, a product formed in the kinase reaction. The Europium will then emit at its characteristic 620 nm wavelength.

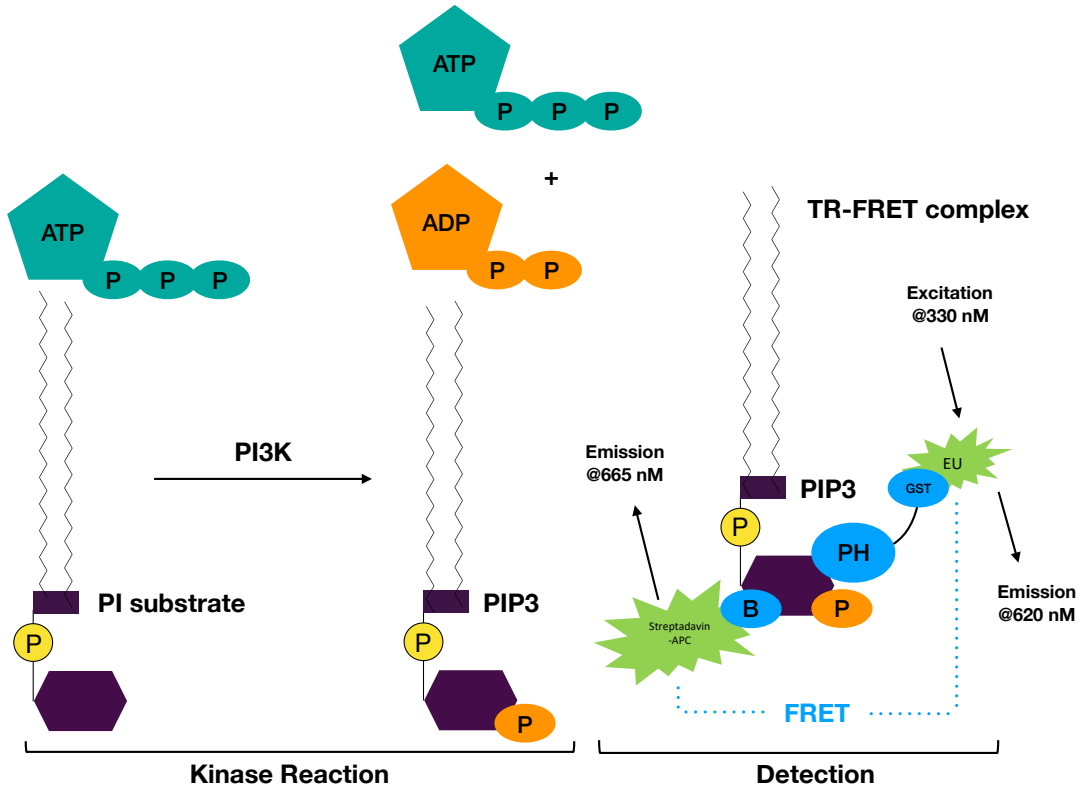
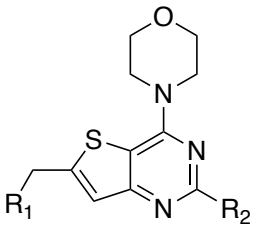


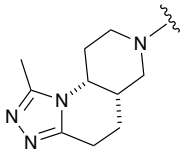
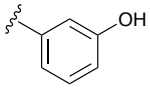
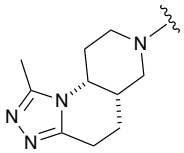
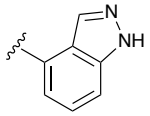
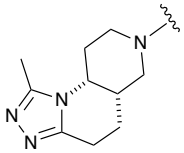
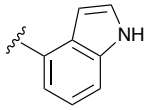
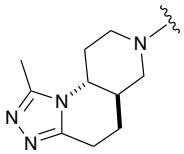
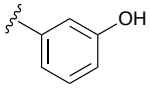
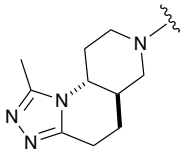
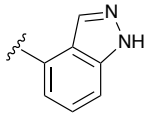
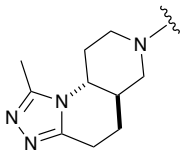
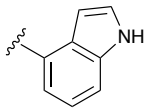
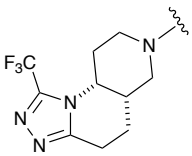
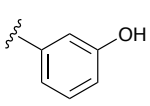
Figure 126. Principle of the HTRF® PI3 Kinase Assay. The lipid kinase reaction is performed in the presence of PIP2 and ATP. Following this, the activity of the kinase is detected: Firstly, the kinase reaction is terminated with biotinylated PIP3. Secondly, the detection reagent is then added which contains GST-tagged pleckstrin homology domain (PH) and fluorophores: Streptavidin-Allophycocyanin (Streptavidin APC) and Europium-labeled anti-GST (EU). A TR-FRET complex is generated between the GST-tagged PH domain and biotinylated short chain PIP3 which can be disrupted in a competitive manner by non-biotinylated PIP3.

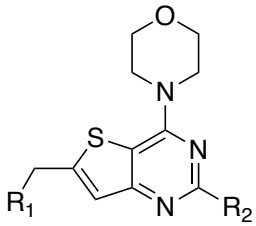
3.3.1.4 Biological Results

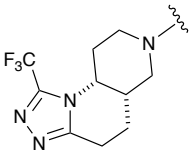
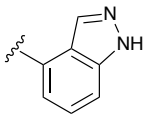
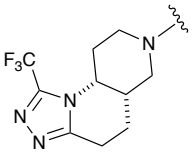
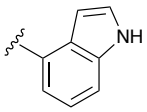
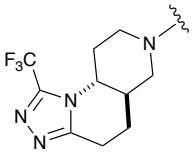
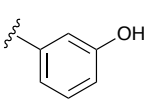
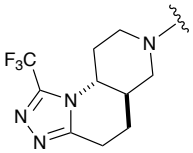
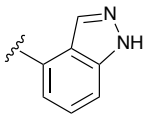
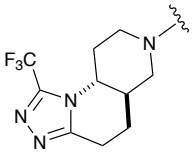
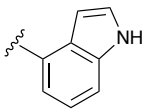
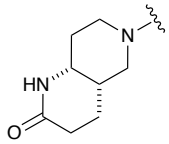
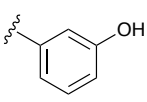
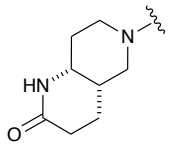
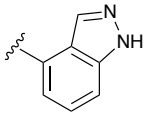
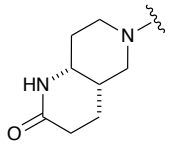
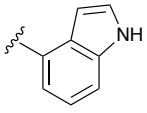
After synthesis of the array compounds, the compounds were tested by GlaxoSmithKline in Stevenage UK. The results are presented in Table 5, where the potency is expressed at the pIC_{50} (pIC_{50} = - log IC_{50}). *Compounds insoluble in buffer.

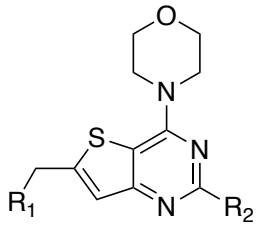
Table 5. Biological Evaluation of PI3K compounds. Potency against the different PI3K isoforms is given as pIC_{50} values (n = 2) ± the standard error of the mean. The potency threshold for the PI3K δ assay is ~ pIC_{50} = 9 due to substrate concentration.

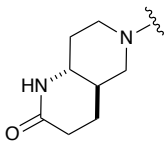
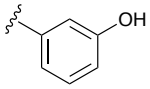
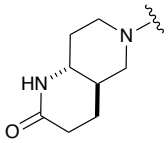
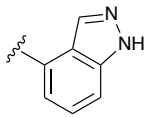
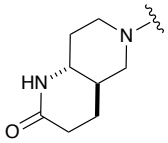
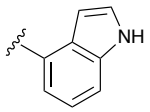
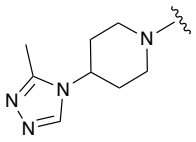
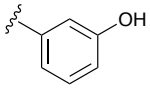
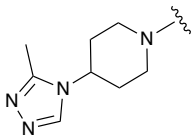
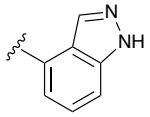
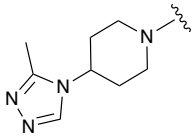
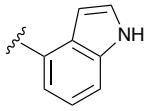
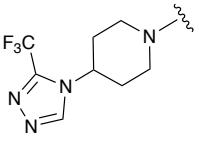
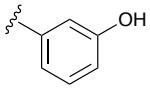
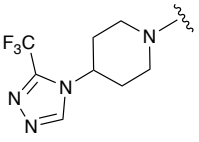
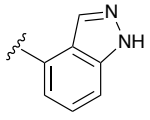
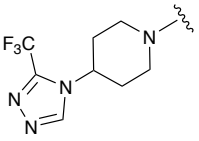
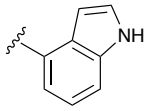


	R_1	R_2	PI3K Isoform Potency (pIC_{50})			
			δ	α	β	γ
1.			*			
2.			8.5 ± 0.4	5.8 ± 0.3	5.9 ± 0.3	5.9 ± 0.2
3.			9.1 ± 0.0	5.5 ± 0.1	6.5 ± 0.2	5.8 ± 0.0
4.			9.1 ± 0.4	7.0 ± 0.1	6.9 ± 0.1	6.3 ± 0.3
5.			8.4 ± 0.1	6.8 ± 0.2	6.3 ± 0.1	6.5 ± 0.1
6.			9.0 ± 0.0	5.7 ± 0.1	6.5 ± 0.2	6.1 ± 0.2
7.			9.2 ± 0.0	7.2 ± 0.0	7.3 ± 0.0	6.8 ± 0.0



	R_1	R_2	PI3K Isoform Potency (pIC_{50})			
			δ	α	β	γ
8.			8.6 ± 0.0	6.5 ± 0.0	6.4 ± 0.0	6.1 ± 0.0
9.			9.1 ± 0.1	5.8 ± 0.1	7.0 ± 0.1	6.2 ± 0.1
10.			9.0 ± 0.3	7.5 ± 0.1	7.3 ± 0.1	6.7 ± 0.0
11.			8.1 ± 0.0	6.8 ± 0.0	6.2 ± 0.0	6.0 ± 0.0
12.			8.8 ± 0.2	6.3 ± 0.1	6.8 ± 0.2	6.4 ± 0.2
13.			*			
14.			7.7	6.5	6.0	5.9
15.			7.9	5.6	6.1	5.7



	R_1	R_2	PI3K Isoform Potency (pIC_{50})			
			δ	α	β	γ
16.			8.6	6.7	6.7	6.3
17.			*			
18.			8.8	6.3	6.8	6.2
19.			8.4 ± 0.0	7.0 ± 0.0	6.8 ± 0.1	6.7 ± 0.1
20.			8.0 ± 0.0	6.5 ± 0.1	6.0 ± 0.2	6.0 ± 0.0
21.			8.4 ± 0.1	5.7 ± 0.2	6.4 ± 0.0	5.7 ± 0.2
22.			8.6 ± 0.2	7.2 ± 0.0	7.0 ± 0.0	6.8 ± 0.0
23.			7.7 ± 0.0	6.5 ± 0.1	5.9 ± 0.2	6.1 ± 0.0
24.			7.7 ± 0.1	5.4 ± 0.0	6.1 ± 0.2	5.5 ± 0.0

3.3.1.5 Discussion of Biological Results

From the results it is evident that the compounds are highly potent towards PI3K, particularly towards PI3Kδ. A plot of PI3K isoform activity vs Compound number, Figure 127, shows this clearly

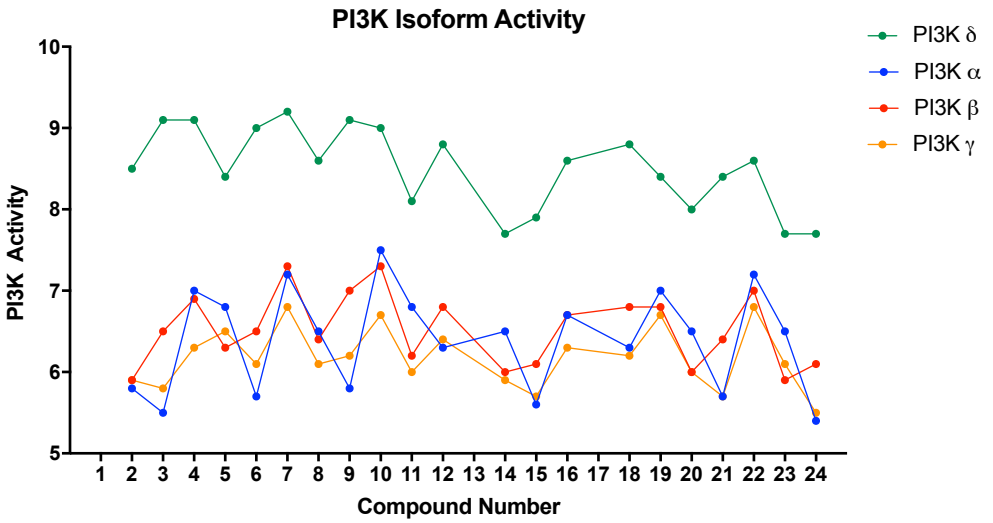


Figure 127. A plot of PI3K isoform activity for each compound. This demonstrates the high level of δ-selectivity observed for all compounds.

Effect of Headgroup

Upon examining the data, one of the aims was to determine the effect of the activity pocket group, the headgroup, on the δ-selectivity . In order to do so, plots of fold-selectivity vs PI3Kδ activity were generated. Figure 128 (A), is one of these plots, showing δ-selectivity over PI3Kα vs PI3Kδ activity. This shows that 3 compounds stand out, in terms of their PI3Kδ selectivity and high PI3Kδ activity, compounds 3,6, and 9 as highlighted on the graph. These 3 compounds are highly δ-selective over α (~4000 and 200 fold selective) and highly potent, and are all indoles, confirming Genentech's observation of enhanced δ-selectivity with indole groups. Additionally, in general, it can be seen that the indazole group shows less activity towards PI3Kδ than the phenol group, whereas the indole group shows a range of activities, but is consistently more δ-selective.

Similar plots of δ-selectvity over PI3Kβ and PI3Kγ vs PI3Kδ activity, Figure

128(B) and (C) respectively, do not illustrate such "stand-out" examples, however, generally it can be said that the indazole group shows less activity towards PI3Kδ than the phenol group.

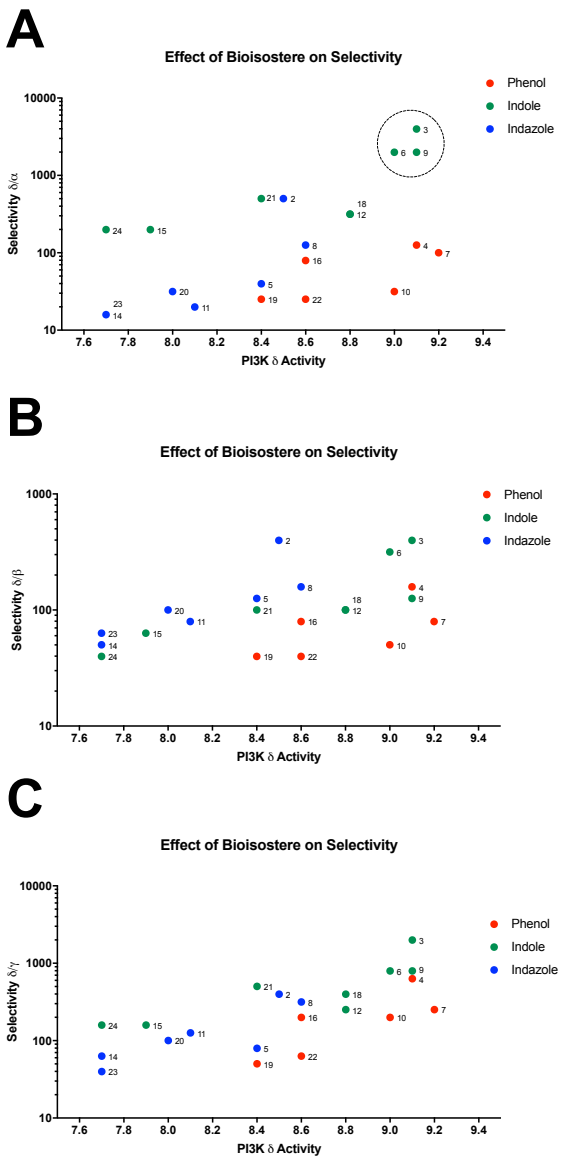


Figure 128. Plots of selectivity vs PI3Kδ activity, showing the effect of the bioisostere. (A)δ-Selectivity over PI3Kα. Compounds with the phenol group are generally more active towards PI3Kδ than the indazole compounds. Indole compounds are generally more selective towards PI3Kδ over PI3Kα. (B) δ-Selectivity over PI3Kβ. Compounds with the phenol group are generally more active towards PI3Kδ than the indazole compounds. (C) δ-Selectivity over PI3Kγ. Compounds with the phenol group are generally more active towards PI3Kδ than the indazole compounds.

The rationale behind the enhanced selectivity for indole compounds is thought to be due to a hydrogen bond between the phenol OH of Tyr813 and the carbonyl of

His909. This hydrogen bond engages Tyr813 in an HxD motif that resides in the DFG loop. This hydrogen bond is disrupted in the case of incorporating a phenol group into the inhibitor since the phenol itself can form hydrogen bonds with Tyr 813 (Figure 129 A)). Likewise, an indazole group can hydrogen bond to Tyr813 (Figure 129 B), contrary to an indole group, where there is no additional nitrogen atom to form a hydrogen bond. This lack of hydrogen bonding to the inhibitor, in the case of the indole group (Figure 129 C), allows the Tyr813 to form a hydrogen bond to His909. It is thought that in the case of an inhibitor forming hydrogen bonds with Tyr813, the conserved Tyr813-His909 hydrogen bond is broken, causing a network of hydrogen bonding to disrupt within the kinase. It is thought that the PI3Kδ isoform is more able to accommodate this shift in the hydrogen-bonding network within the affinity pocket than the other isoforms. Molecular modelling and docking of compounds 1, 2 and 3 show these proposed interactions (Figure 129).

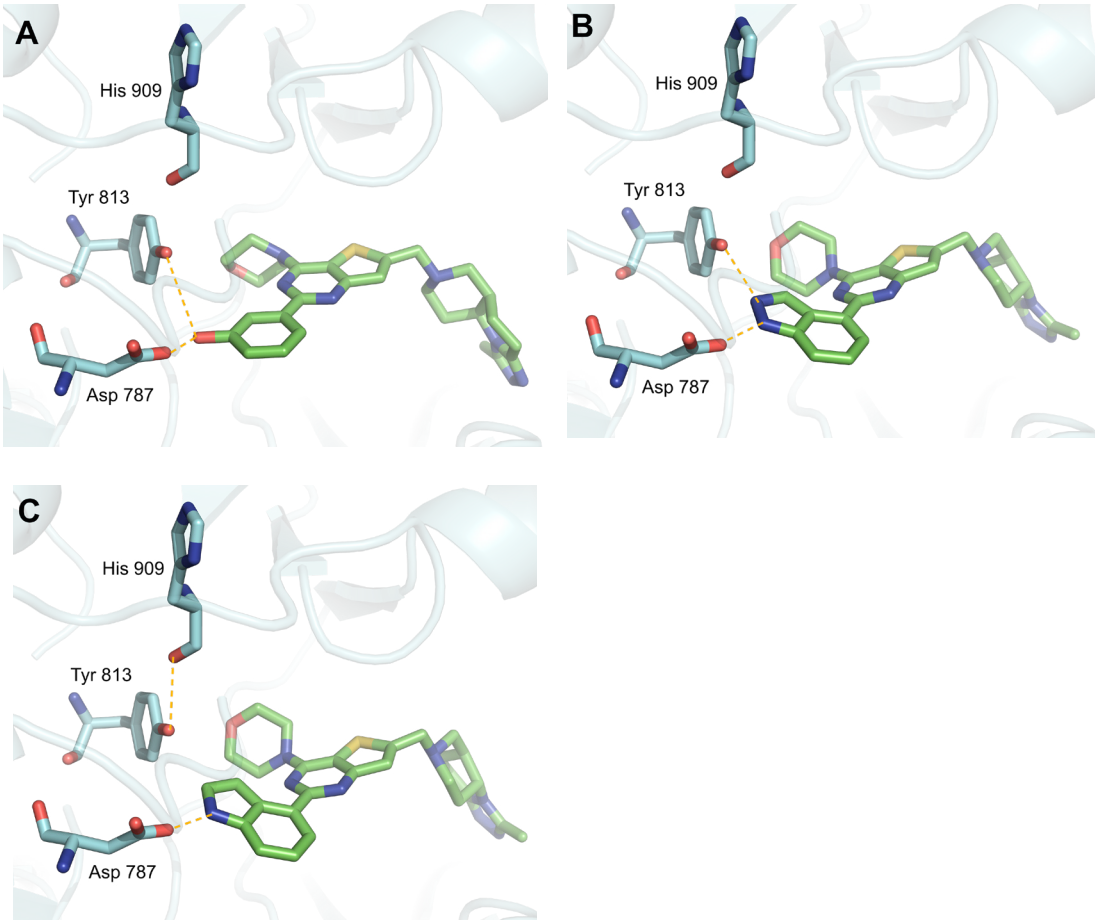


Figure 129. Molecular modelling to examine the effect of headgroup on selectivity towards PI3Kδ. Compounds 1, 2, and 3 docked in PI3Kδ (2WXP). (A) The phenol OH of compound 1 forms a 3.1 Å hydrogen bond to Tyr813 and a 3.1 Å hydrogen bond to Asp787. This disrupts the conserved hydrogen bond between Tyr813 and His909. (B) The indazole of compound 2 forms a 2.8 Å hydrogen bond to Tyr813 which disrupts the conserved hydrogen bond between Tyr813 and His909, and a 2.7 Å hydrogen bond to Asp787. (C) The indole of compound 3 forms a 2.7 Å hydrogen bond with Asp787 and cannot interact with Tyr813, leaving the Tyr813-His909 hydrogen bond intact. Disruption of the Tyr813-His909 hydrogen bond leads to disruption to a network of hydrogen bonding further away from the activity pocket. It is thought that the PI3Kδ isoform is more able to accommodate this shift in the hydrogen-bonding network than the other isoforms.

Effect of Ring junction geometry

In order to determine the effect of the *cis*/*trans* ring junction on δ-selectivity a matched-pair analysis was performed comparing *cis* analogues to their respective *trans* analogues. This was plotted in Figure 130, plots of fold-selectivity vs PI3Kδ activity. It can be seen from the resulting plots that in all cases the *cis* analogues are more potent toward PI3Kδ than their respective *trans* analogues. Additionally, the *cis* analogues are more selective than their respective *trans* analogues. This is true for selectivity over all other PI3K isoforms (Figure 130, (A),(B), and (C)).

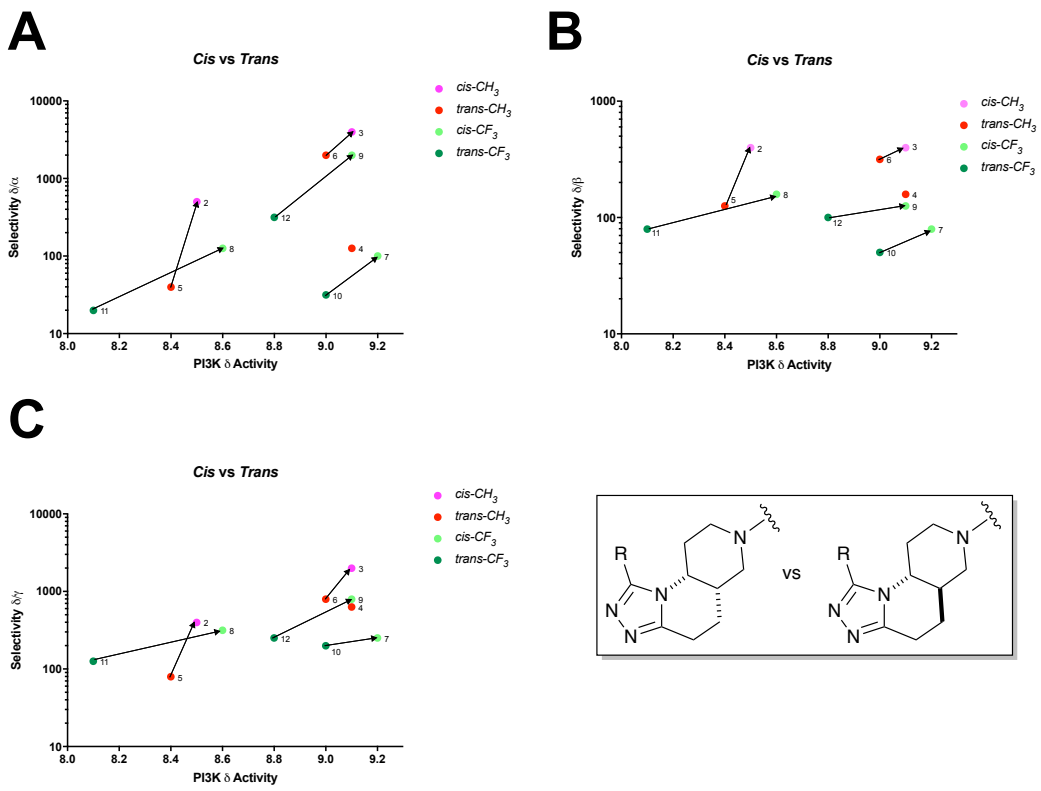


Figure 130. Plots of selectivity vs PI3Kδ activity, matched pairs showing the effect of the geometry of the ring junction (cis vs trans). In all cases the cis analogues are consistently more potent against PI3Kδ. Additionally, the cis analogues consistently show enhanced selectivity for PI3Kδ over the other isoforms. (A). δ-Selectivity over PI3Kα. (B) δ-Selectivity over PI3Kβ. (C) δ-Selectivity over PI3Kγ.

After confirming that *cis* analogues consistenly show increased activity and selectivity towards PI3Kδ, matched pair anaysis of the the *trans* analogues vs their respective "acyclic " analogues, i.e. analogues that are not tricyclic were assessed. This is plotted

in Figure 131 (A, B, and C). In all cases the *trans* analogues are consistenly more potent agains PI3Kδ than their acyclic counter parts. Additionally, they is a trend showing the *trans* analogues to be more selective to PI3Kδ over the other isoforms of PI3K.

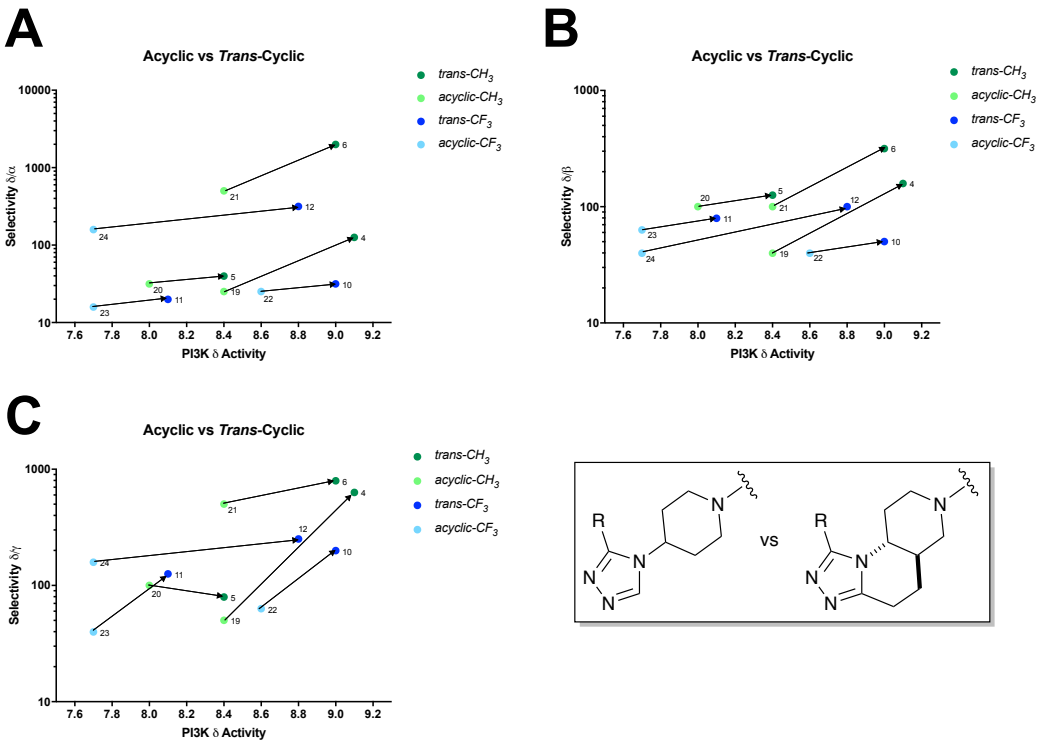


Figure 131. Plots of selectivity vs PI3Kδ activity, matched pairs showing the effect of the geometry of the ring junction (Trans vs Acyclic). In all cases the trans analogues are consistently more potent against PI3Kδ. Additionally, the trans analogues show enhanced selectivity for PI3Kδ over the other isoforms. (A). δ-Selectivity over PI3Kα. (B) δ-Selectivity over PI3Kβ. (C) δ-Selectivity over PI3Kγ.

From the above we can conclude that in terms of potency and selectivity for PI3Kδ: *cis*>*trans*>acyclic. This can be rationalised by examining potential interactions with the tryptophan shelf. Molecular docking of our inhibitors into PI3Kδ using the Shrödinger Glide Molecular Modelling Suite allowed us to visualise these interactions. Figure 132 A shows compound 3 (a *cis* analogue) docked into PI3Kδ (2WXP) with pictilisib (GDC-0941) overlayed. For comparison and viewed from the same angle, Figure 132 B shows compound 6 (a *trans* analogue). The lowest energy conformations for each isomer position the tricycle in different positions, relative to the tryptophan shelf, to form face-to-face interactions. This may provide a rational for the observed potency

and selectivity increase.

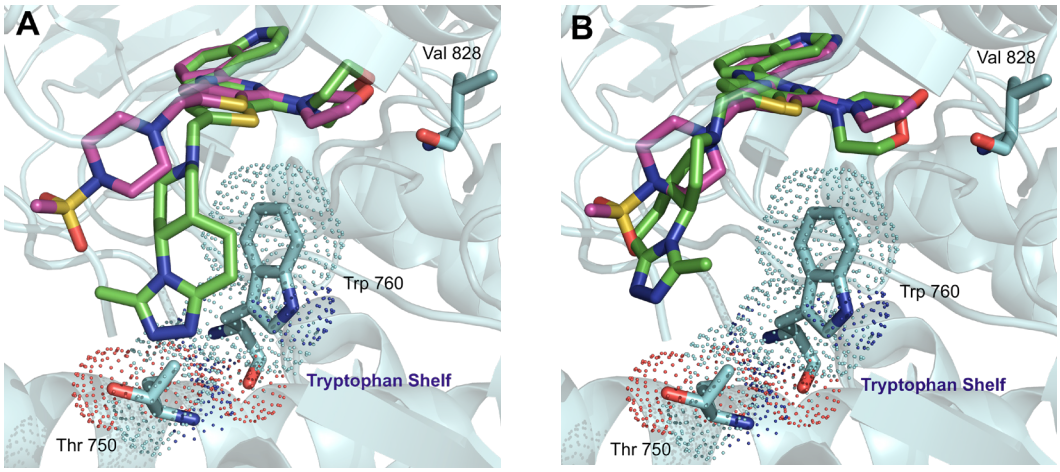


Figure 132. Cis vs Trans Molecular Modelling Images. (A) Compound 3 (green, a cis analogue), docked into PI3Kδ (2WXP). The tricycle is positioned to form a potential face-to-face interaction with Trp 760 of the Tryptophan shelf. Pictilisib (magenta), co-crystalised with PI3Kδ (2WXP) is overlayed for comparison (B) Compound 6 (trans analogue) docked into PI3Kδ (2WXP). The lowest energy conformation positions the tricycle further away from the tryptophan shelf. Pictilisib (magenta), co-crystalised with PI3Kδ (2WXP) is overlayed for comparison.

The general observed selectivity (i.e. reduced biological acivity against the anti-targets) for all analogues can be explained by the fact that Thr 750 in PI3Kδ is occuled in PI3Kα, PI3Kβ and PI3Kγ. When the amino acid sequences of PI3Kα, PI3Kβ and PI3Kγ are aligned with the amino acid sequence of PI3Kδ, the same residue is Arg 770 (α-numbering) in PI3Kα, Lys 771 PI3Kβ (β-numbering) in PI3Kβ, and Lys 802 (γ-numbering) in PI3Kγ. Figure 133 illustrates that in the cases of PI3Kα, PI3Kβ and PI3Kγ a positively charged amino acid blocks the tricycle from interacting with the tryptophan residue.

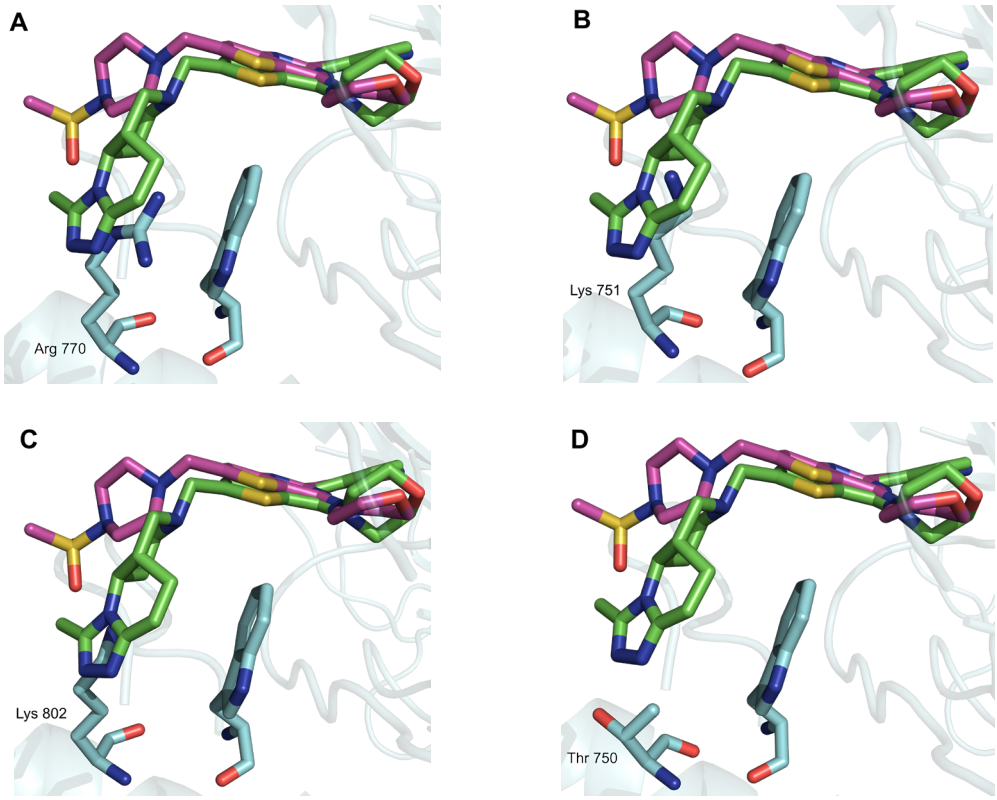


Figure 133. Molecular modelling, illustrating the tryptophan shelf region for the class I PI3Ks. Compound 3 (cyan) docked into the PI3K crystal structure (2WXP), showing pictilisib (GDC-0941, magenta) for comparison. Overlay with the crystal structure of PI3Kα (), shows the tryptophan is blocked by Arg 770 (α-numbering) in PI3Kα (A) Overlay with the crystal structure of PI3Kβ (4BFR) shows Lys771 PI3Kβ (β-numbering) in PI3Kβ (B) Overlay with the crystal structure of PI3K γ (3DBS) shows Lys802 (γ-numbering) in PI3Kγ (3DBS) (C) In PI3Kδ the tryptophan shelf is extended by Thr750 (δ-numbering), allowing inhibitors to potentially form molecular interactions with the Trp760 (δ-numbering).

Effect of Ring Substitution

The effect of the substitution on the triazole (CH_3 vs CF_3) , an electron-donating group and a strongly-electron withdrawing group, was investigated. Again, this was assessed by performing a matched pair analysis, plotted in Figure 134 (A, B, and C). For the tricyclic analogues, the CH_3 analogues are consistenly more selective over their CF_3 counterparts, although it should be noted that the CH_3 group, in general, did not greatly affect the activity towards PI3Kδ. This suggests that the selectivity is likely due to lack of activity towards the anti-targets (α,β,γ) rather than increased activity towards PI3Kδ.

In order to assess the decreased activity towards the anti-targets, matched pair analysis (CH_3 vs CF_3) was performed (Figure 134). For the *cis* and *trans* analogues, there is a general trend of decreased activity towards the antitargets (α,β,γ) for CH_3 containing compounds. i.e. CH_3 containing compounds are less potent towards the antitargets than CF_3 containing compounds. This could be due to the electon donating effect of the CH_3 group on the triazole ring. The now relatively electron rich triazole,is likely to form a less favourable interaction with the positively charged amino acids (Arg 770 (α-numbering) in PI3Kα, Lys 771 PI3Kβ (β-numbering) in PI3Kβ, and Lys 802 (γ-numbering) in PI3Kγ), in comparison to the electon deficient CF_3 triazole. On the other hand, for the acyclic analogues, the increased δ-selectivity is due to increased PI3Kδ activity for CH_3 analogues in comparison to CF_3 analogues.

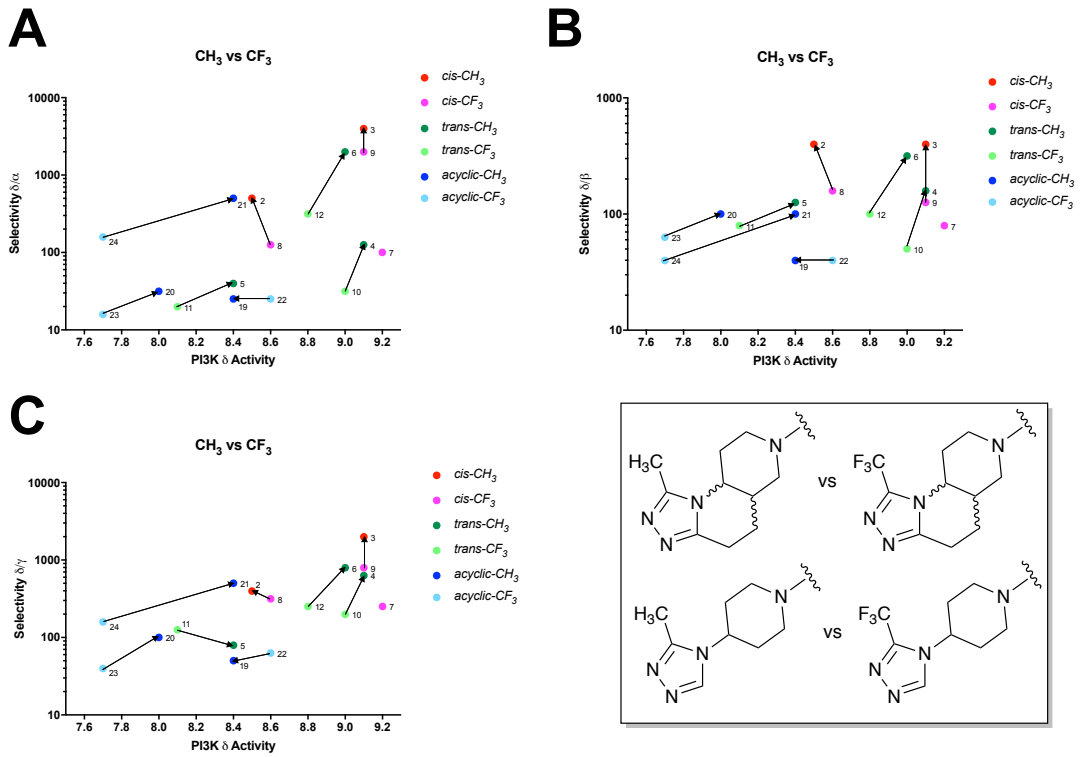


Figure 134. Plots of selectivity vs PI3Kδ activity, matched pairs showing the effect of the substitution on the triazole ring (CH3 vs CF_3). The CH3 analogues are consistently more selective to PI3Kδ. Additionally, for the tricyclic analogues the CH3 group does not . (A). δ-Selectivity over PI3Kα. (B) δ-Selectivity over PI3Kβ. (C) δ-Selectivity over PI3Kγ.

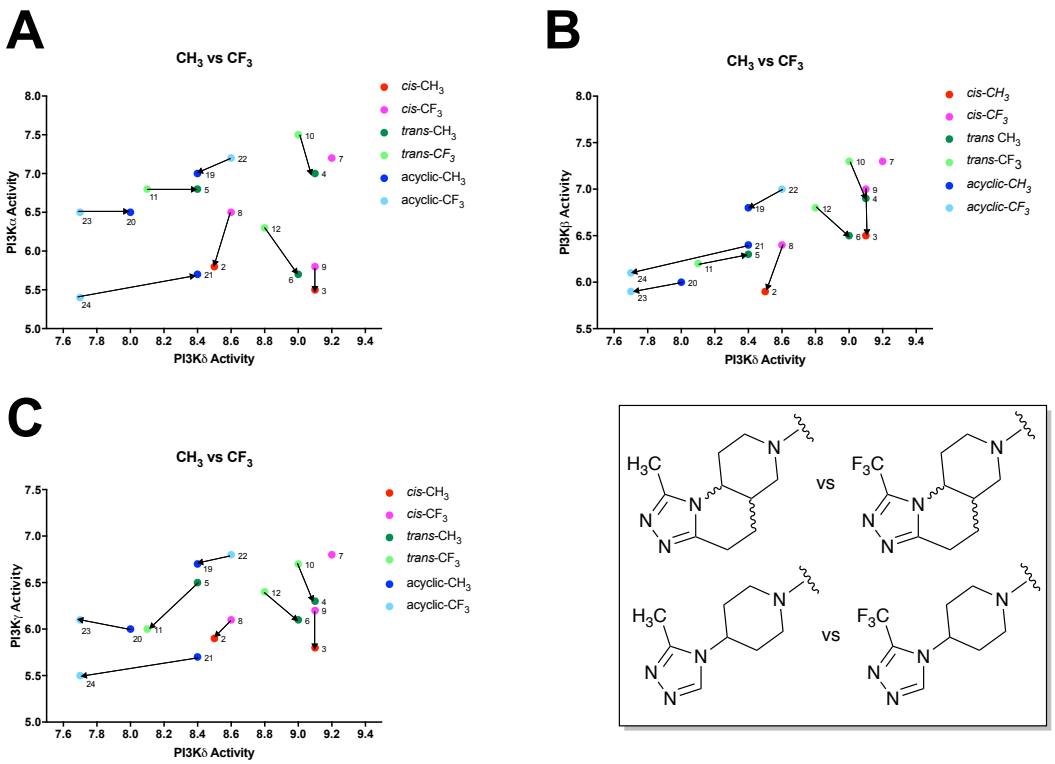


Figure 135. Plots of PI3Kx vs PI3Kδ activity, matched pairs showing the effect of the substitution on the triazole ring (CH3 vs CF_3). CH3 containing compounds are generally less potent towards the antitargets than CF_3 containing compounds for the tricyclic analogues. For the acyclic analogues, the increased δ-selectivity if likely due to increased PI3Kδ activity for CH3 analogues in comparison to CF_3 analogues. (A) PI3Kα activity vs PI3Kδ. (B) PI3Kβ activity vs PI3Kδ activity. (C) PI3Kγ activity vs PI3Kδ activity.

From the above it is evident that there are 3 effects contributing to achieve the high level of δ-Selectivity: The indole group, the *cis*-fused tricycle, and methyl substitution on the tricycle.

3.3.1.6 Discussion of Physicochemical properties

Throughout the design process the physicochemical properties were monitored and assessed. Table 6 details the measured and calculated physical properties for compounds 1-24.

Table 6. Table of Physicochemical properties for the series. MW = Molecular weight, LogD = Chrom LogD(pH 7.4), cLogP = Calculated logP, HBA = Hydrogen bond acceptors, HBD = Hydrogen bond donors, sol = Aqueous solubility (µg/mL), HSA = Human serum albumin (Plasma protein binding, % bound), and BEI = Binding efficiency or ligand efficiency (BEI = (pIC_{50}/MW) x1000), SEI = surface-binding efficiency index (SEI = pIC_{50}/ (PSA/100)), HAC = Heavy Atom Count (C, N, O, S, F, Cl, I, Br), LLE or LipE = Lipophilic Ligand Efficiency (LLE = pIC_{50} - $chromLogD_{7.4}$), LE = binding energy in kcal/mol per heavy atom) = pIC_{50} × 1.37/HAC, ARC = Aromatic ring count, PFI = Property forceast index (Chrom LogD(7.4) + ARC)).

	MW	LogD	cLogP	HBA	HBD	PSA	RB	Sol	HSA	BEI	SEI	HAC	LLE	LE	ARC	PFI
1	517.7	3.53	4.79	9	1	88.62	4	78	94.3	-	-	37	-	-	4	7.53
2	541.7	4.09	4.34	10	1	92.78	4	36	95.4	15.69	9.16	39	4.41	0.30	5	9.09
3	540.7	4.35	4.72	9	1	80.42	4	22	95.8	16.83	11.32	39	4.75	0.32	5	9.35
4	517.7	3.55	4.79	9	1	88.62	4	24	94.6	17.58	10.27	37	5.55	0.34	4	7.55
5	541.7	3.67	4.34	10	1	92.78	4	35	94.8	15.51	9.05	39	4.73	0.30	5	8.67
6	540.7	4.1	4.72	9	1	80.42	4	23	95.3	16.65	11.19	39	4.90	0.32	5	9.1
7	571.6	5.25	5.69	12	1	88.62	5	10	96.1	16.10	10.38	40	3.95	0.32	4	9.25
8	595.6	5.44	5.24	13	1	92.78	5	8	96.3	14.44	9.27	42	3.16	0.28	5	10.44
9	594.7	5.94	5.62	12	1	80.42	5	24	96.9	15.30	11.32	42	3.16	0.30	5	10.94
10	571.6	4.99	5.69	12	1	88.62	5	10	95.7	15.75	10.16	40	4.01	0.31	4	8.99
11	595.6	5.13	5.24	13	1	92.78	5	6	95.9	13.60	8.73	42	2.97	0.26	5	10.13
12	594.7	5.63	5.62	12	1	80.42	5	3	96.5	14.80	10.94	42	3.17	0.29	5	10.63
13	479.6	-	3.49	7	2	89.76	4	-	-	-	-	34	-	-	3	-
14	503.6	3.61	3.03	8	2	93.92	4	104	94.1	15.29	8.20	36	4.09	0.29	4	7.61
15	502.6	4.09	3.42	7	2	81.56	4	70	94.7	15.72	9.69	36	3.81	0.30	4	8.09
16	479.6	3.4	3.49	7	2	89.76	4	95	93.4	17.93	9.58	34	5.20	0.35	3	6.4
17	503.6	-	3.03	8	2	93.92	4	-	-	-	-	36	-	-	4	-
18	502.6	3.87	3.42	7	2	81.56	4	38	94.7	17.51	10.79	36	4.93	0.33	4	7.87
19	491.6	3.29	3.98	9	1	88.62	5	65	93.0	17.09	9.48	35	5.11	0.33	4	7.29
20	515.6	3.37	3.52	10	1	92.78	5	7	93.8	15.52	8.62	37	4.63	0.30	5	8.37
21	514.7	3.83	3.91	9	1	80.42	5	83	94.3	16.32	10.45	37	4.57	0.31	5	8.83
22	545.6	4.82	4.88	12	1	88.62	6	27	94.8	15.76	9.70	38	3.78	0.31	4	8.82
23	569.6	4.91	4.42	13	1	92.78	6	21	94.8	13.52	8.30	40	2.79	0.26	5	9.91
24	568.6	5.44	4.81	12	1	80.42	6	14	95.7	13.54	9.57	40	2.26	0.26	5	10.44

Lipinski's Rules

Lipinski's rule of 5[135][136] is often used to assess for "drug-likeness" of an inhibitor, where an inhibitor should have a molecular weight of ≤500, a logP of ≤5, ≤5 hydrogen bond donors, and ≤10 hydrogen bond acceptors. In many aspects, the physical properties of this series do not comply to these requirements. The molecular weights generally exceed 500 Daltons, and in some cases, the $chromLogD_{7.4}$ or cLogP exceeds 5, or are approaching 5. In terms of hydrogen bond donors and acceptors, all com-

pounds fulfil the hydrogen bond donor requirement, although in most cases the number of hydrogen bond acceptors exceeds or is near to exceeding the requirement. It must be noted, however, the most selective compound, compound 3 only exceeds the prescribed molecular weight by 40 Daltons, has a acceptable chromLog$D_{7.4}$, and narrowly fulfills the hydrogen bond acceptor requirements. It should be noted however, that some of the hydrogen bond acceptors counted in this are very weak hydrogen bond acceptors, such as the nitrogens in the triazole ring.

Veber's Rule

In terms of Vebers rule[137], which questions the 500 molecular weight cutoff and rather considers polar surface area (PSA) and number of rotatable bonds (RB) to predict oral bioavailablility, all compounds comply. Vebers criteria are <10 rotatable bonds and a PSA <140 Å.

Ligand Efficiency

Recently, analysis of attrition rates of clinical candidates by big pharma[138] has revealed that ligand efficiency metrics and indices are important[140][141][140]. These metrics are inherrently linked to lipophilicity[142][143]. Abbott laboratories have suggested[144] that during the optimisation process it is useful to simultaneously examine two efficiency indices, the binding efficiency index (BEI, BEI = (pIC_{50}/MW) x 1000)) and the surface-binding efficiency index (SEI, SEI = pIC_{50}/ (PSA/100)). These indices combine three crucial variables (potency, molecular weight and polar surface area), and have comparable numerical scales. They suggest that optimisation of these indices simultaneuosly allows for the monitoring of the potency per exposed PSA using the SEI, and the BEI allows monitoring of the potency per additional kDa. A plot of SEI vs BEI for a series is useful for optimisation where compounds above the diagonal show high affinity per kDa and compounds below the diagonal show high affinity per polar surface area (PSA). Abbott suggested that compounds that comply with Lipinski's rules tend to be above the diagonal, however they advise to optimise towards the diagonal.

Figure 136 shows a plot of SEI vs BEI for the series, showing that the series as

a whole is achieving high afffinity per kDa but is not achieving high affinity per PSA. However, the series is in the same region as pictilisib, but is able to provide a high level of selectivity.

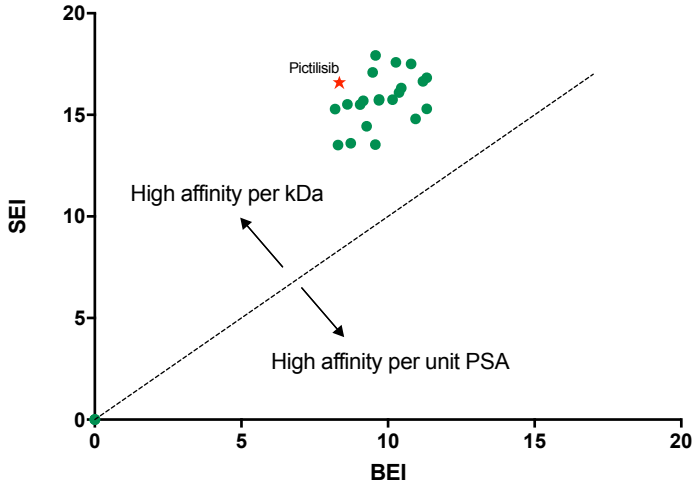


Figure 136. A plot of the surface-binding efficiency index (SEI) vs the binding efficiency index (BEI) for the series. Compounds above the diagonal show high affinity per kDa and compounds below the diagonal show high affinity per polar surface area (PSA). Optimisation of the parameters should be performed simultaneously towards the diagonal, although compounds that comply with Lipinski's rules tend to be above the diagonal. The compounds in this series (green) show high affinity per kDa, but do not show high affinity per PSA, however they are in the same region as pictilisib (red).

Another metric recently proposed is Lipophilic ligand efficiency[145][146][147] (LLE or LipE, LLE = pIC_{50} - Chrom LogD(7.4) or LLE = pIC_{50} - cLogP). LLE is a very useful parameter to consider since although optimisation of ADMET properties involves many parameters, optimisation is primarily dependant on lowering lipophilicity (with the exception of permeability). It is very difficult to optimise compounds against potency and all of the individual ADMET parameters that need to be considered simultaneously and hence LLE simplifies this process. Generally, the suggested range of LLE for compounds is between 5-7. Figure 137, shows a plot of PI3Kδ activity vs ChromLogD(7.4) indicating selected LLE values. In this series, there is a clear LLE divide between CH_3 containing compounds and CF_3 containing compounds, where CH_3 containing compounds have a LLE of appoximately 4-5, and CF_3 containing compounds have an LLE of approximately 3-4. CH_3 containing compounds are on the borderline of having ac-

ceptable LLE. This is in contrast to pictilisib (calculated from cLogP = 1.17) which has an LLE of 8.5, a very good LLE. This metric highlights that the series suffers from high lipohilicity, which negatively impacts the aqueous solubilites (Table 6) and ultimately these compounds are predicted to be poorly orally bioavailable.

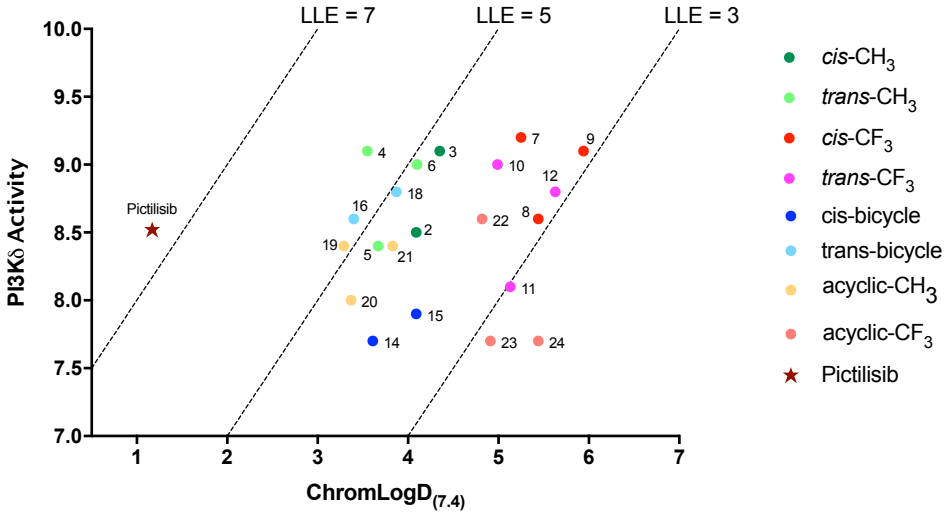


Figure 137. A plot of PI3Kδ activity vs ChromLogD(7.4) showing selected LLE values (LLE = pIC_{50} - $chromLogD_{7.4}$). There is a clear LLE divide between CH3 containing compounds and CF_3 containing compounds, where CH3 containing compounds have a LLE of appoximately 4-5, and CF_3 containing compounds have an LLE of approximately 3-4. CH3 containing compounds are on the borderline of having acceptable LLE. This is in contrast to pictilisib (calculated from cLogP = 1.17) which has an LLE of 8.5, which is a very good LLE.

Another ligand efficiency metric, simply Ligand Efficiency[148][149][150] (LE), is used in recent times to predict whether a compound will have good PK properties and ultimately good oral bioavailability. LE = binding energy in kcal/mol per heavy atom = pIC_{50} × 1.37/Heavy atom count (HAC). LE, unlike LLE considers the overall size of a molecule. This can be considered using many size metrics, but in this case HAC is used, where heavy atoms considered include C, N, O, S, F, Cl, Br, and I. Figure 138 shows a plot of LE vs LLE for the series. The LE for the series is quite low, but approaching acceptable, where a good value for LE is >0.35. This is due to the relatively high molecular weight of the series. Excellent compounds should be in the upper right quadrant

of the plot.

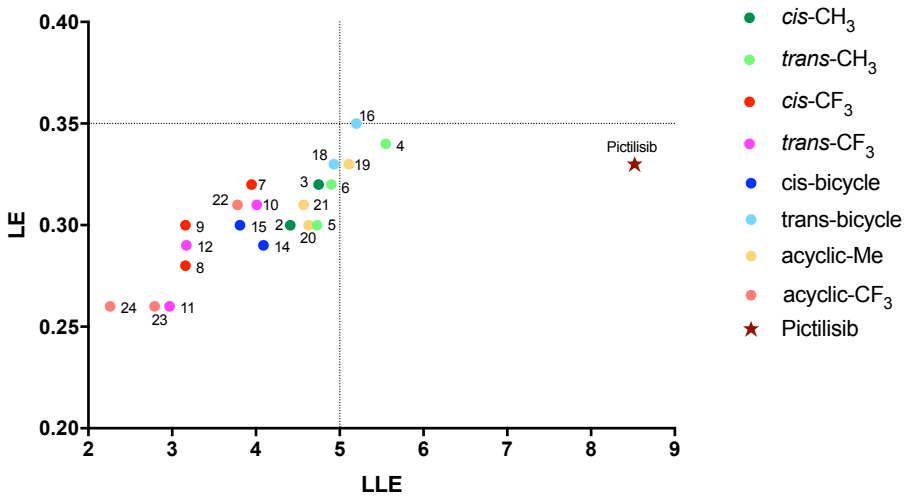


Figure 138. A plot of Ligand efficiency (LE) vs Lipophilic ligand efficiency (LLE). LLE = pIC_{50} - $ChromLogD_{7.4}$ and LE = binding energy in kcal/mol per heavy atom = pIC_{50} × 1.37/Heavy atom count (HAC). Excellent compounds would usually be found in the upper right quadrant of the plot, with an LLE >5 and an LE >0.35. Compounds in the series generally have below optimium LE and LLE due to high molecular weight and LogD.

Finally, the number of aromatic rings has been shown to have an effect on the oral bioavailability of compounds[151][152][153][154]. GSK proposed a metric, the Property Forecast Index (PFI), PFI = $chromLogD_{7.4}$ + Aromatic Ring Count (ARC), where an ideal value is <7). Figure 139 shows a plot of PI3Kδ activity vs PFI, showing that the PFI for the series is very high. This is due to the high LogD and number of aromatic rings in the molecules.

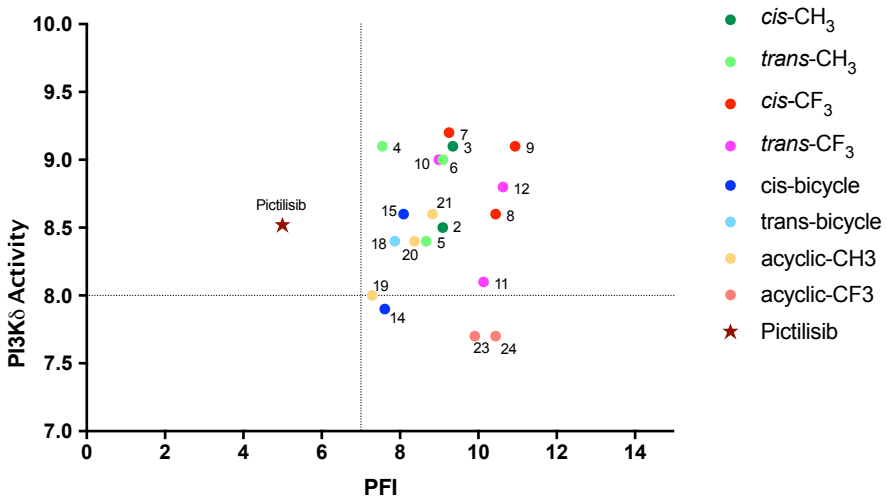
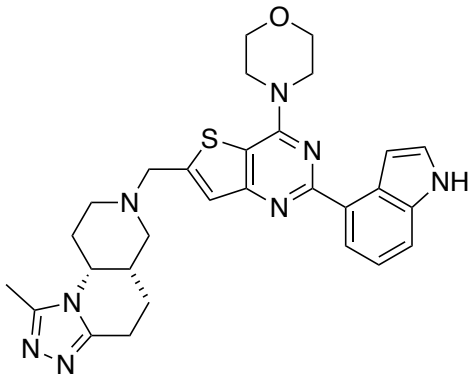


Figure 139. A plot of PI3Kδ activity vs the Property Forcast Index (PFI) for the series. PFI = chromLogD$_{7.4}$ + Aromatic Ring Count (ARC), where an ideal value is <7). The PFI for the series is very high. This is due to the high LogD and number of aromatic rings in the molecules.

3.3.1.7 Series Conclusion

Overall it can be concluded that athough there are highly potent and selective compounds such as compound 3 (Figure 140), these compounds are predicted to have poor oral bioavailability primarily due high chromLogD$_{7.4}$ leading to poor aqueous solubility. Relatively high molecular weight and a large amount of aromatic rings also contribute to a poor predicted PK profile. However, in the area of developing kinase inhibitors, where the binding pockets are extremely similar, this level of selectivity is remarkable. Compound 3 shows the desired selectivity profile to be used as a tool compound to probe synergic effects with ceritinib.



pIC50 PI3Kδ = 9.1
δ/α = 3981
δ/β = 398
δ/γ = 1995
Sol. (aq) = 22 μg/mL
chromLogD7.4 = 4.35
HSA = 95.8 %
MW = 540.7
LLE = 4.75

Figure 140. Compound 3, the best compound in the series. Compound 3 is highly potency towards PI3Kδ and exhibits high selectivity over the other isoforms of PI3K. With high chromLogD$_{7.4}$, poor aqueous solubilty, and poor ligand efficientcy metrics, compound 3 has a poor predicted PK profile for oral bioavailablity, but can be used as a tool compound to probe synergic effects with ceritinib.

3.3.1.8 Synergy with Ceritinib

In Chapter 2, the observed synergic effects between ceritinib and the pan PI3K inhibitor pictilisib were discussed. Here compound 3 was tested in combination with ceritinib.

In vitro evaluation by MTT assay of Compound 3 against the ALK- and ALK+ cell lines showed that Compound 3 had a GI_{50} of 3.3 μM ± 2.1 against the ALK- cell line and had a GI_{50} of 2.3 μM ± 0.1 against the ALK+ cell line. The dose response curves for Compound 3 and its combination with ceritinib are shown in Figure 141.

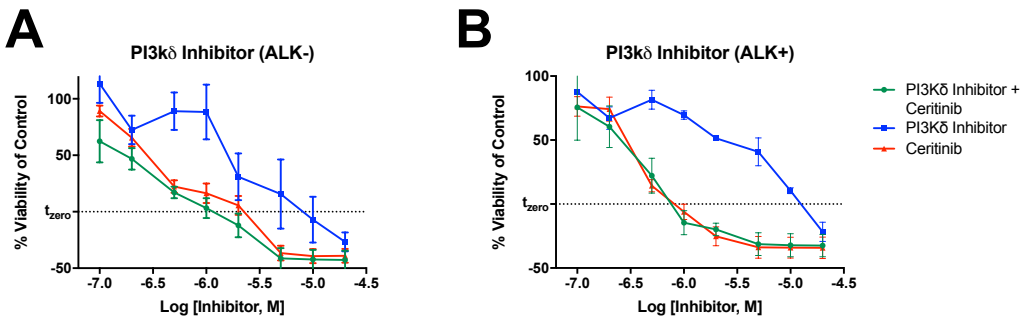


Figure 141. The Dose-response curves for ceritinib, Compound 3 and their combination against the ALK- cell line (A) and ALK+ cell line (B). Points are given as the mean ± the standard error of the mean (minimum 3 internal replicates). The dotted line shows the T_{zero} value (0% growth), and points below this line may indicate that an agent is cytotoxic. Growth is represented as percentage viability of the control, which has been normalised to 100%, where 0% is the T_{zero}.

In terms of evaluating synergy for the combination, the Webb method indicated that there was no statistical significance between the expected and observed effects at doses below 1 µM in both cell lines. However, at higher doses >1µM, there was statistical significance suggesting some synergic effects for the combination, Figure 142.

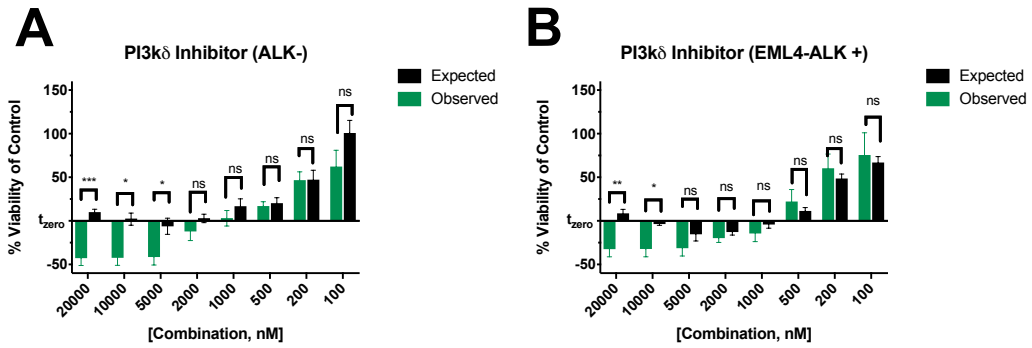


*Figure 142. Combination assay data of ceritinib and Compound 3 against the ALK- cell line (A) and ALK+ cell line (B), analysed by the Webb fractional product method, comparing the expected (additive) effect against the observed effect. Where the observed % viability is less than the expected, synergy can be assumed. Statistical significance has been determined by calculation of the p-value using t-tests where: *** $P \leq 0.001$, ** $P \leq 0.01$, * $P \leq 0.05$, ns $P > 0.05$. Error bars shown represent the standard error of the mean.*

For the Chou and Talalay method, linearisation of the dose respose curves by generation of the median effect plot gave Compound 3 Dm values of 24.2 µM ± 20.6

against the ALK- cell line and 5.57 µM ± 1.79 against the ALK+ cell line. Additionally, an m-value for Compound 3 of 0.67 ± 0.03 was obtained for the ALK- cell line, and an m-value of 0.83 ± 0.08 was obtained for the ALK+ cell line. For the combination of ceritinib and Compound 3 D_m values of 0.89 µM ± 0.68 and 0.81 µM ± 0.24 were obtained for the ALK- and ALK+ cell lines respectively. The corresponding m-values were found to be 0.93 ± 0.19 and 1.57 ± 0.50 for the ALK- and ALK+ cell lines respectively. These D_m and m-values allowed for the calculation of the combination indices across a range of doses. The combination indices at a fractional effect (Fa) of 0.5 (effectively at the IC_{50}) were found to be 0.81 and 0.91 for the ALK- and ALK+ cell lines respectively. At higher dose, at a fractional effect of 0.96, the combination indices were 1.06 against the ALK- and 0.47 ALK+ cell lines. The combination index plots for both cell lines is shown in Figure 143. Against the ALK- cell line, for the compound 3/ceritinib combination, the combination shows synergy across the whole range of fractional effects, except at really high doses. However, against the ALK+ cell line, it is only at a fractional effect requiring higher doses where the combination becomes synergic. At doses lower than this the combination can be seen to be quite antagonistic, with very high combination indices.

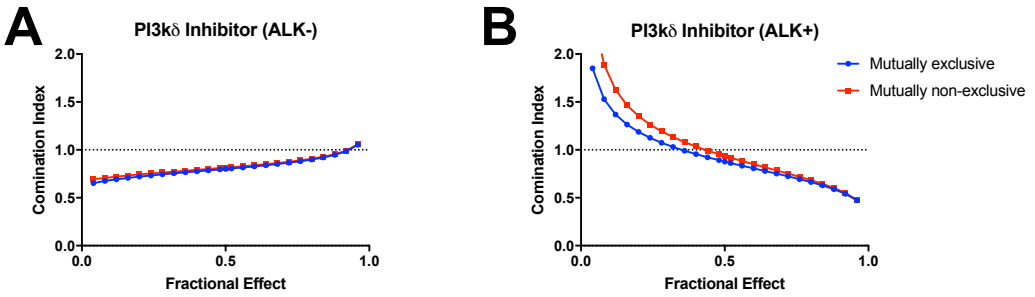


Figure 143. Combination index plots generated using the Chou and Talalay method for a 1:1 molar ratio of Compound 3 and ceritinib against the ALK- cell line (A) and the ALK+ cell line (B). A combination index at a given fractional effect of 1 is an additive effect,>1 is antagonistic and <1 is synergistic.

Comparing Compound 3's synergy to the levels of synergy observed when combining ceritinib with pictilisib it is clear that pictilisib exhibits more synergy with ceritinib than compound 3.

3.3.2 PI3Kα Inhibition

3.3.2.1 Inhibitor Design

In the previous section, in terms of physicochemical properties, the compounds were predicted to be poorly orally bioavailable. This is due to poor solubility which is inherently linked high lipohilicity and a high number of aromatic rings (a large number of Sp^2 hybridised atoms). Additionally, in the previous section, it was observed that the PI3Kα isoform has a non-conserved arginine residue in close proximity to the tryptophan residue that makes up the tryptophan shelf. In this section the aim was to redesign the central scaffold of the inhibitors in order to reduce the liphophilicity, using the previously synthesised molecular scaffold as a starting point. Additionally, the aim was to target the non-conserved arginine residue in order to achieve PI3Kα selectivity.

The first step in the design process was to utilise our existing scaffold and modify it by introducing a hinge binding atom to mimic the morpholine oxygen of previous inhibitors (Figure 144)

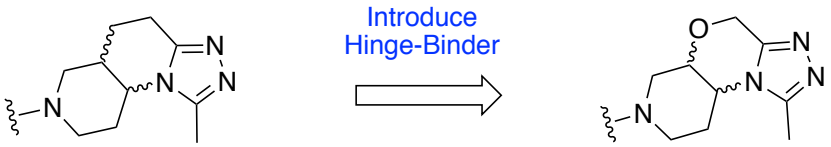


Figure 144. Introduction of an oxygen atom into the existing scaffold to act as a hinge binder, mimicking the morpholine oxgen of previous inhibitors.

With the aid of molecular modelling techniques the triazole ring was modified to an imidazole ring (Figure 145) so as to have the point of derivatisation at the correct angle in order to interact with the affinity pocket of PI3K.

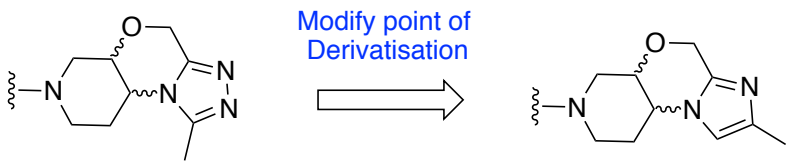


Figure 145. The triazole ring was modified to an imidazole ring so as to have the point of derivatisation at the correct angle in order to interact with the affinity pocket of PI3K.

Molecular modelling of both the *cis* and *trans* scaffolds, using methyl groups as

placeholders for points of derivatisation, shows that the *trans* scaffold is better suited due to its "flat nature". The "bent nature" of the *cis*-scaffold was unfavourable when docked into the binding site, and did not interact as expected with the hinge region. An overlay of the result with GDC-0326 shows that the newly designed *trans*-scaffold is predicted to fit into the binding pocket (Figure 146). To summarise the binding features of the tricyclic scaffold: The ether oxygen acts as the hinge binder and is predicted to form hydrogen bonds with Val 851 (α-numbering). The imidazole is predicted to pertrude into the affinity pocket and groups attached to this ring have the potential to interact with Asp 933. The piperidine ring nitrogen is a point of attachment for groups that are predicted to extend out into the solvent region and additionally interact with Arg 770 to gain α-selectivity.

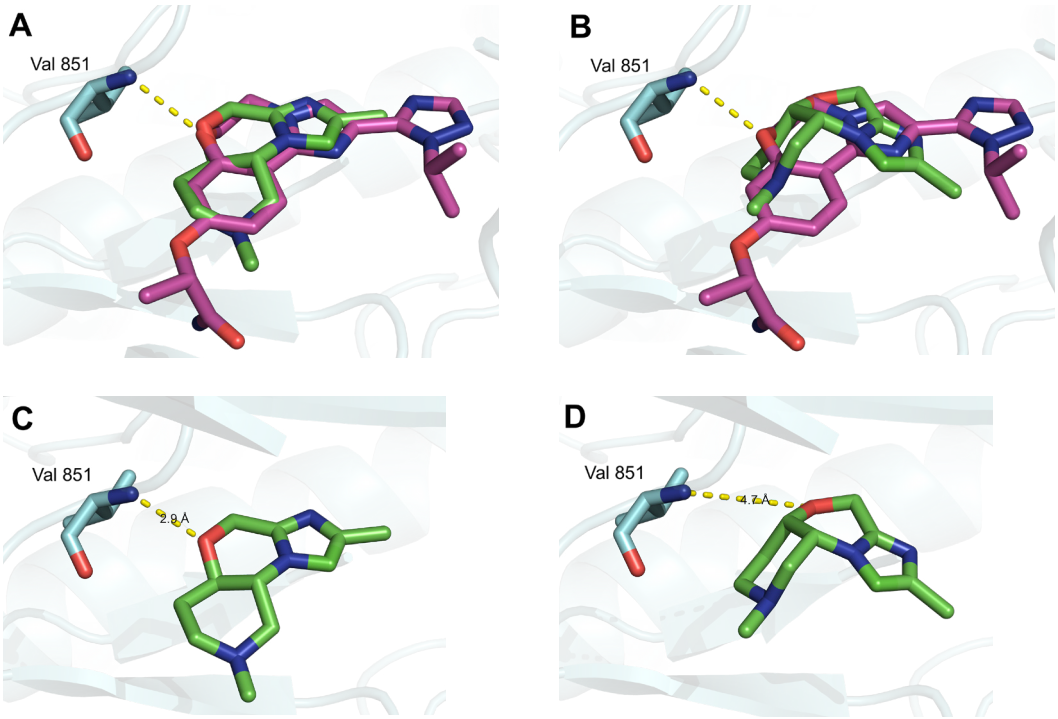


Figure 146. Molecular modelling of the cis and trans scaffolds (green). Docking performed on PI3Kδ (PDB 2WXP) and aligned and overlayed with the crystal structure of GDC-0326 (magenta) in PI3K α (PDB 5DXT). (A) The trans scaffold has a relatively flat conformation and overlays nicely with GDC-0326 forming a 2.9 Å hydrogen bond with the hinge, Val851 (α-numbering). (B) The cis scaffold has a bent conformation, and does not overlay very well with GDC-0326. Additionally, the hydrogen bond with the hinge is not as favourable at 4.7 Å. (C) The trans scaffold (D)The cis scaffold.

In terms of lipophilicity, the new molecular scaffold (Figure 147) is calculated to have approximately 750-fold reduced logP. Additionally, the number or aromatic rings has been reduced, and the number of Sp^2 carbons has been reduced by introducing Sp_3 carbons.

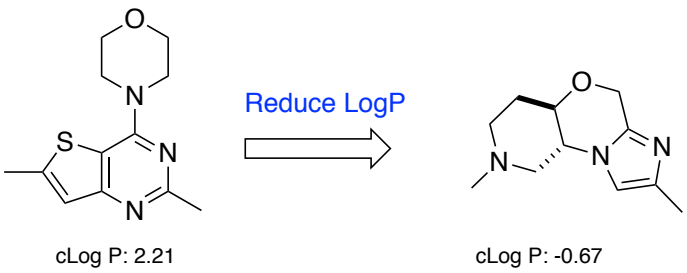


Figure 147. Comparison of the core scaffolds. The thienopyrimidine core has a cLogP of 2.21 and the tricycle has a cLogP of -0.67. Additionally the number of aromatic rings and Sp^2 carbons has been reduced.

In terms of chemical synthesis and having a common intermediate for diversification (Figure 128), a scaffold containing an iodine atom on the imidazole ring which would allow for Pd-cross coupling reactions to be performed was the target. Additionally, the aim was to keep the nitrogen atom protected, where following deprotection reactions such as amide coupling reactions or reductive amination reactions could be performed in order to produce matrices of compounds for biological evaluation.

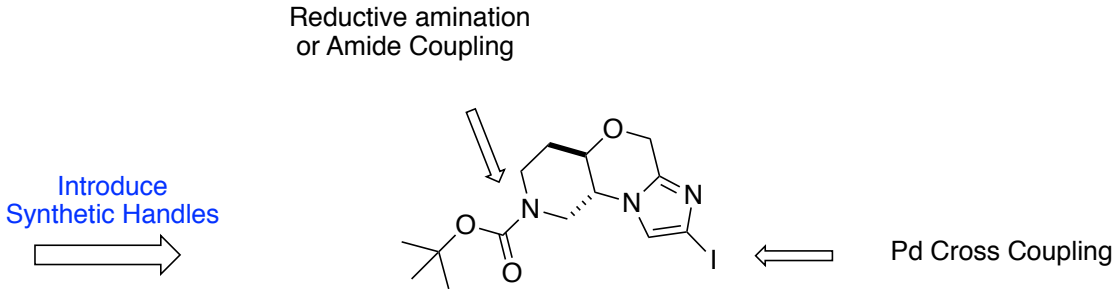


Figure 148. The synthetic target for synthesis of the core. The iodo group will allow for Pd cross coupling reactions for the introduction of activity pocket groups and the amine will allow for reductive amination and amide coupling reactions to introduce solvent exposed groups.

Figure 149 is an example structure that could be generated using the tricyclic scaffold. The compound complies with Lipinski's rules as well as Veber's rule. Most

importantly, the compound has an ideal molecular weight and low LogP, with a low number of aromatic rings.

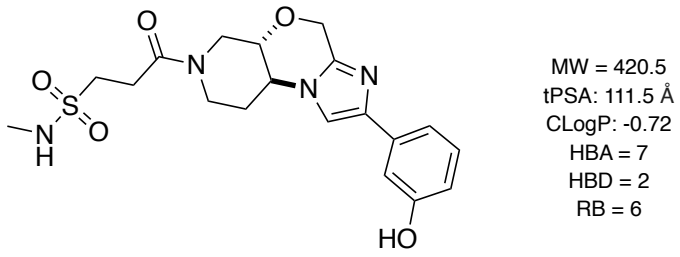
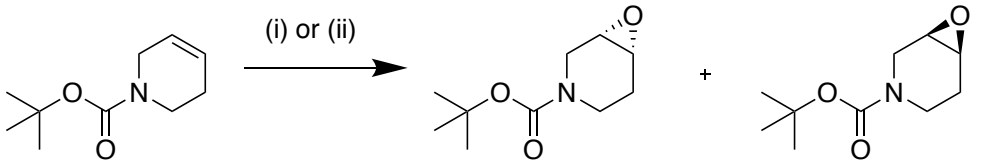


Figure 149. A potential structure that could be generated using the tricyclic scaffold. These compounds would comply with Lipinski's and Veber's rules. Additionally, the cLogP is vastly reduced, which improves the predicted PK profile considerably.

3.3.2.2 Scaffold synthesis

In terms of synthesis of the scaffold the starting point was tert-butyl 3,6-dihydropyridine-1(*2H*)-carboxylate (Scheme 2).

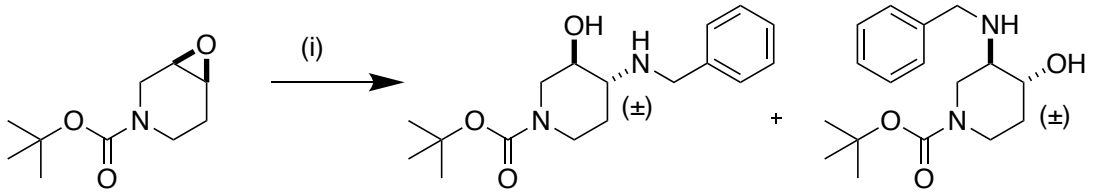


Scheme 2. Reagents and Conditions: (i) Alkene (1 eq.), mCPBA (vast excess) (ii) Alkene (1 eq.), NBS (1.2 eq.), deinoised H_2O , r.t 2 h then THF, NaOH (2M), r.t 30 min.

The first step was to generate the racemic epoxide with meta-chloroperoxybenzoic acid (mCPBA). This reaction was generally acceptable on small scale where a large excess of mCPBA could be used, however visualisation of products by TLC proved difficult due to lack of a chromophore. On larger scales, where is was unfeasible to use a large excess of mCPBA, formation of a bromohydrin with subseqent epoxidation was a more reliable method. Formation of the bromohydrin was achieved by treatment of the alkene with N-bromosuccinimide (NBS), and subsequent epoxidation was achieved by treatment of the bromohydrin with aqueous sodium hydroxide. A potential side-product (thought to be the diol or dibromo) formed if the reaction mixture was left for extended periods. At this point in the synthesis it was decided to carry though the racemic mixture, rather than perform a chiral synthesis, such as the Jacobsen epoxidation, or

separation, until it was certain that the full synthesis of the scaffold could be achieved.

Following epoxidation, the plan was to ring open the epoxide to give the *trans* product, however the epoxide can be ring-opened at both the 3- and 4- positions, and would lead to a mixture of regioisomers. A literature search of epoxide ring opening with nitrogen nucleophiles led us to perform the ring opening with benzylamine (Scheme 3) as it was reported to ring open at the desired 4- position in a 3:1 ratio[155]. Additionally, due to visualisation issues, it was with hope that introducing a benzyl group would temporarily add a chromophore and aid purification.



Scheme 3. Reagents and Conditions: (i) Epoxide (1.0 eq.), Benzylamine (neat), 115 °C, overnight.

The NMR spectrum of this mixture is complex due to the piperidine ring and mixture of products. Additionally, thin layer chromatography (TLC) visualisation issues still persisted, where the compound could not be stained properly on TLC plates using standard laboratory stains ($KMnO_4$, Ninhydrin, Iodine, Vanillin, Phosphomolybdic acid (PMA), etc), and hence purification was challenging. Attempts to distill the oil by Kugelrohr distillation were unsuccessful, and after many attempts to purify the oil via column chromatography and distillation it was decided to carry the oil forward and attempt purification at a later stage. Liquid chromatography mass spectrometry (Figure 150) was performed and the UV trace at 220 nm and 254 nm showed absorbances for the regioisomers, confirming the ring opening occured in a 3:1 ratio. Additionally, high resolution mass spectrometry confirmed that the product mass ion was present, although full characterisation by NMR could not be confirmed and thus formation of product is only assumed.

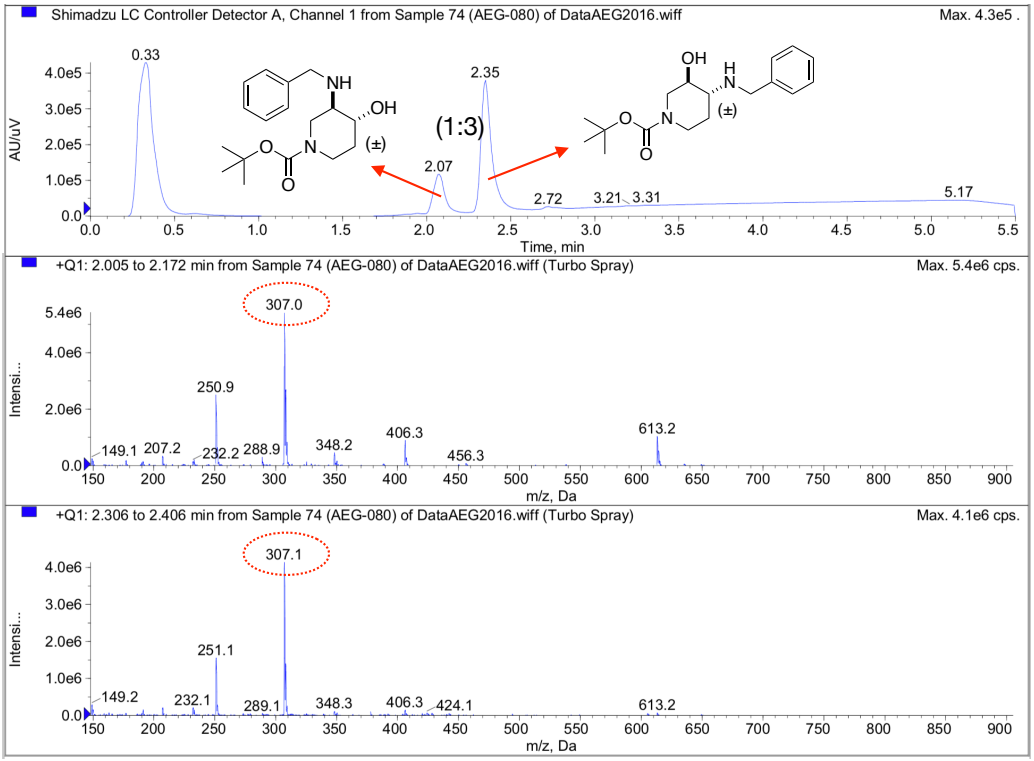
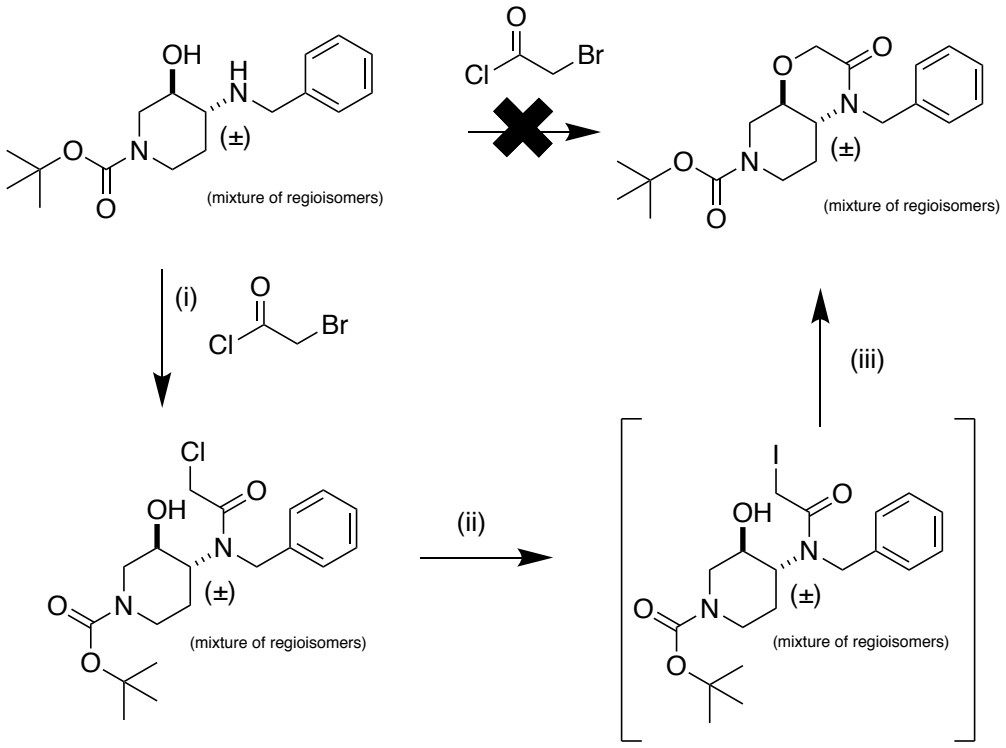


Figure 150. The LCMS trace showing the regioisomers formed in an approximate 3:1 ration, calculated from the area under the peaks. The mass ion of 307 is marked for both regioisomers.

At this point the aim was to perform a cyclisation using 2-bromoacetyl chloride (Scheme 4), however mass spectrometry (Figure 151) indicated that the cyclisation did not occur. It was postulated that following nucleophilic attack by the amine to the acid chloride and subsequent leaving of the chloride ion, the chloride ion underwent halogen exchange with the bromine, and with the C-Cl bond being stronger than the C-Br bond, the oxygen atom is not nucleophillic enough to displace the Cl. Treatment of this product with potassium iodide promoted halogen exchange to the iodide (Figure 152) then treatment with potassium tert-butoxide showed dissapearance of the uncyclised ion and appearance of the cyclised product ion by mass spectrometry (Figure 153). At this stage visualisation issues persisted, although attempted purification by column chromatography gave a white solid with the correct mass ion by LCMS. NMR spectra remained complex and impure and full characterisation was not possible.



Scheme 4. Reagents and Conditions: (i) Aminoalcohol (1.0 eq.), 2-bromoacetyl chloride (1.1 eq.), Triethylamine (3.0 eq.), CH_2Cl_2, r.t, 2 h.; (ii) Potassium iodide (1.0 eq.) MeCN, r.t., 1h; (iii) Potassium tert-butoxide (1.0 eq.).

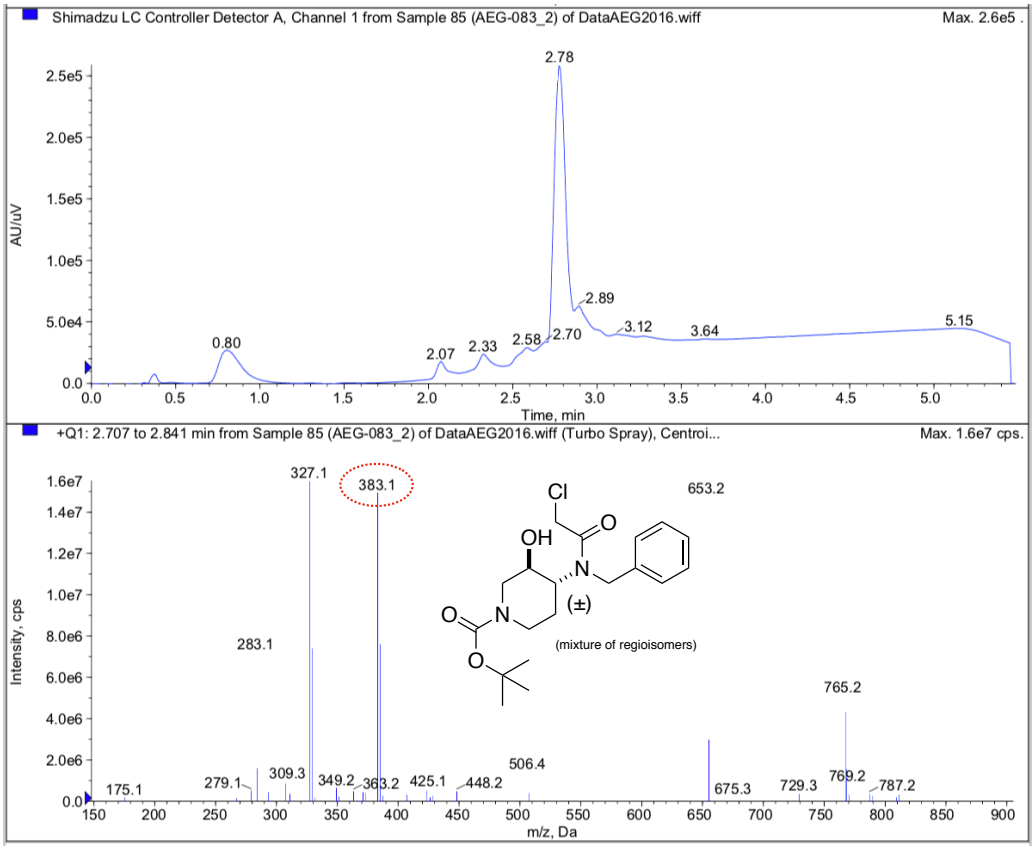


Figure 151. LCMS showing halogen exchange of the bromide to the chloride.

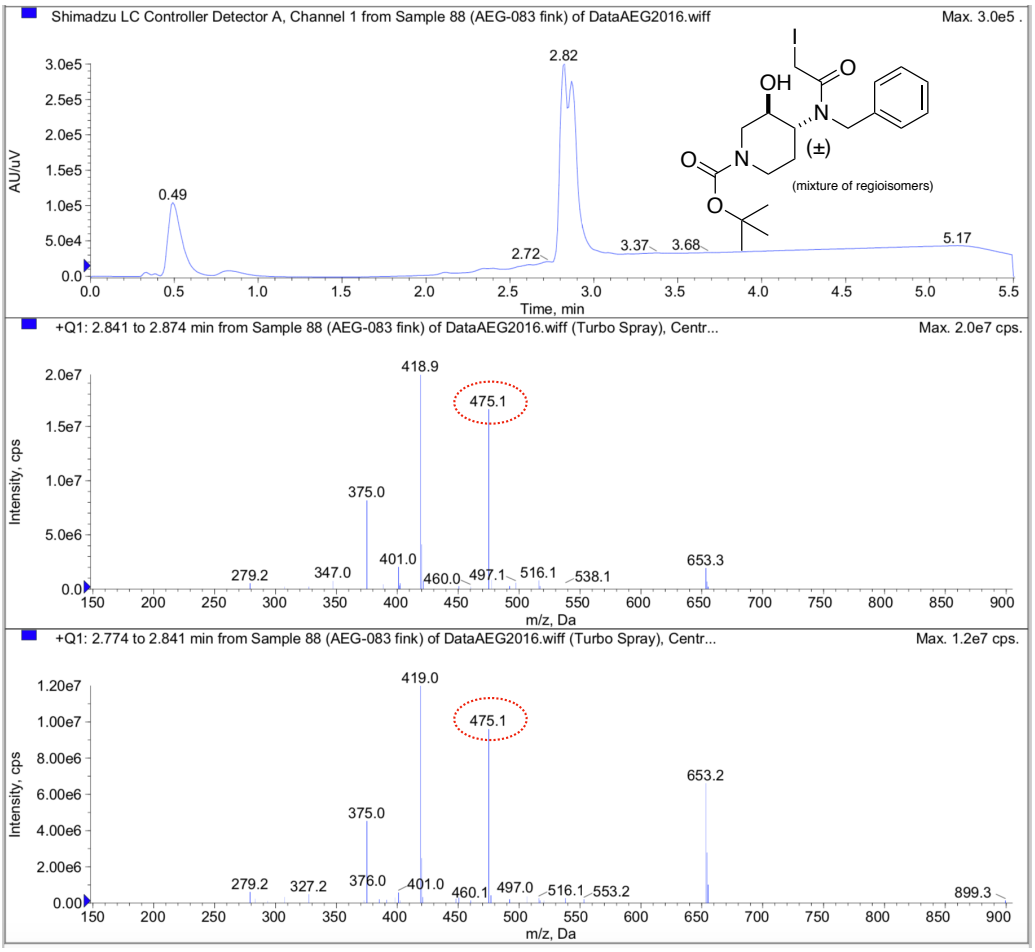


Figure 152. LCMS showing the halogen exchange of chlorine to iodine.

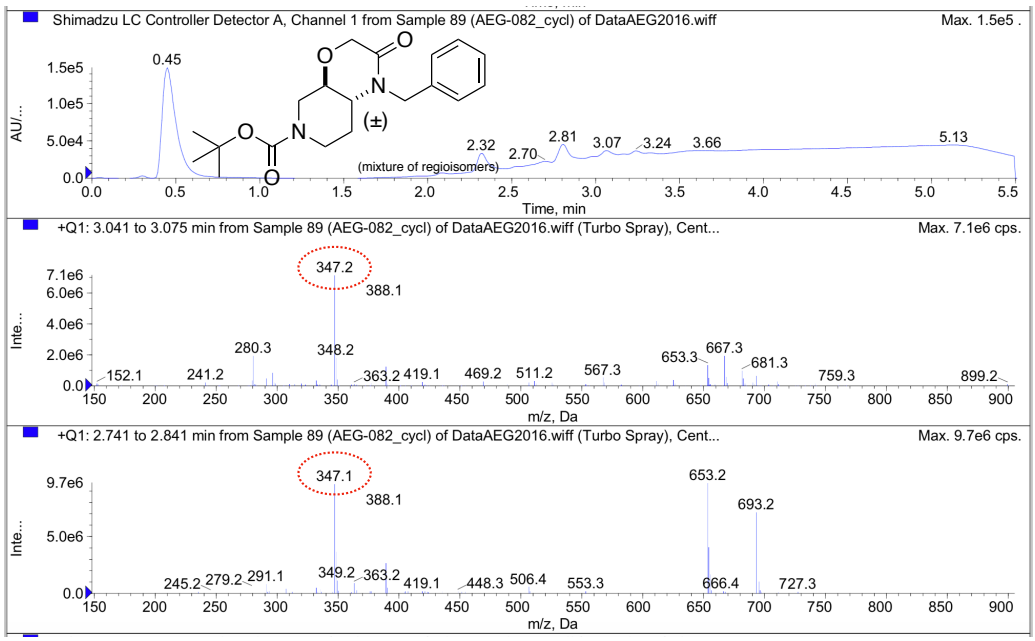
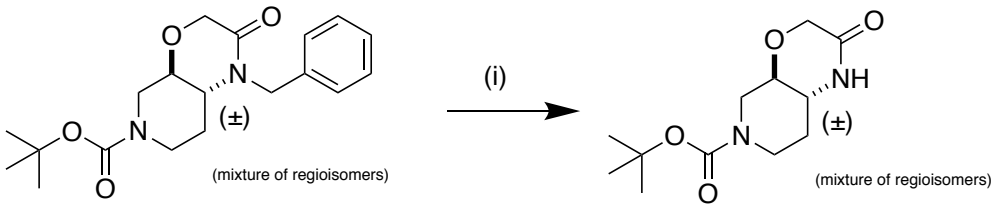


Figure 153. Mass Spectrum showing cyclisation

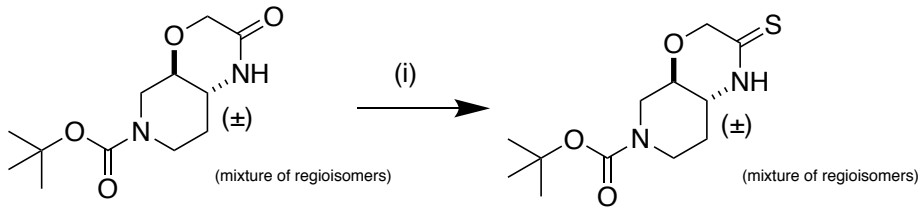
Removal of the benzyl group was achieved by hydrogenation over Pd/C in ethanol and acetic acid (Scheme 5). Purification at this stage was not possible as visualisation issues still persisted, however the plan was to form a thioamide in the next step and from previous experience with the original scaffold, the thioamide could be visualised on standard F_{254} TLC plates under UV light and could be stained using PMA. Additionally it was hoped that the regioisomers would be separable at the thioamide stage.



Scheme 5. Reagents and Conditions: Benzylated compound (1.0 eq.), H_2, Pd/C (10% w.t), EtOH, AcOH (3.0 eq.), r.t. overnight.

The reaction to potentially form a thioamide (Scheme 6) was attempted using Lawesson's reagent, and indeed as predicted, a UV active spot was seen on TLC. This spot was isolated, and an LCMS spectrum showed the correct mass, however the yield was extremely low, and like the steps before full characterisation was not possible by NMR.

Upon scaling up, the reaction did not behave in the same way. All of the starting material was lost and irrecoverable and it is assumed that it must have been consumed in the reaction. Additionally, no products were isolable. It is thought that this loss of starting material may be due to loss of the Boc protecting group under the reaction conditions or that the Lawesson's regent could be forming a thioether from the ether and then undergoing a ring opening with potential to form disulfides.



Scheme 6. Reagents and Conditions: Amide (1.0 eq.), Lawesson's reagent (0.5 eq.), toluene, r.t, overnight.

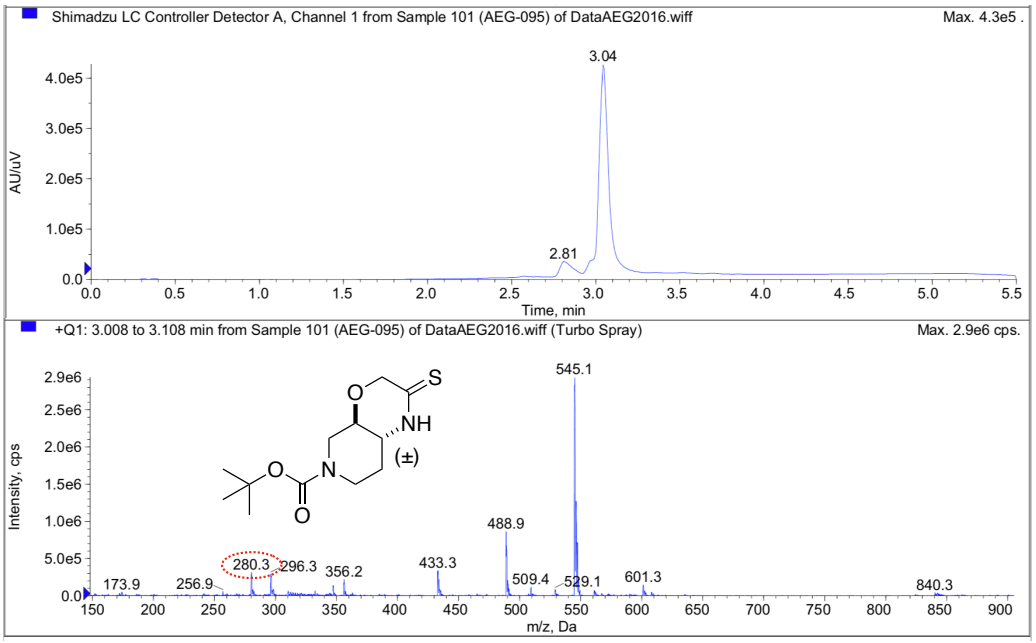
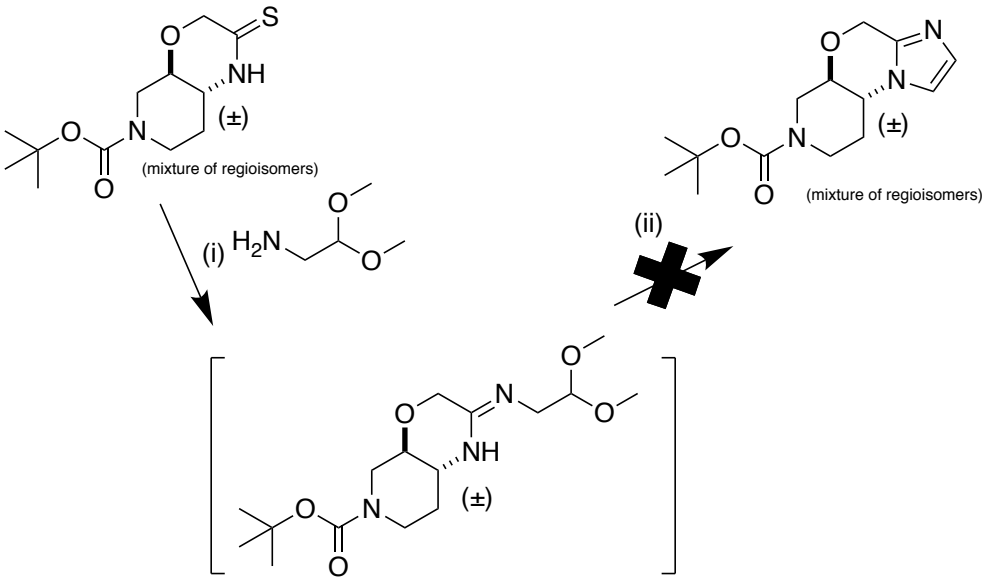


Figure 154. LCMS trace of the newly formed and isolated UV active spot, which could potentially be the thioamide. The molecular mass of the thioamide is shown, however it is unknown what the mass peak at 545.1 corresponds to.

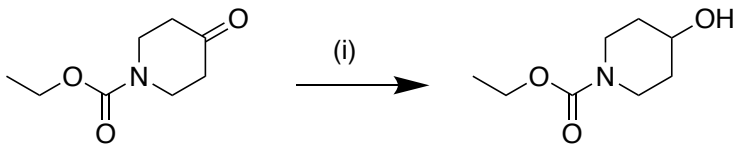
Following this, a test reaction to form the imidazole (Scheme 7), with what was presumed to be the thioamide (1.0 eq.) and 2,2-dimethoxyethan-1-amine (5.0 eq.), was attempted using diacetoxymercury (1.1 eq.) and tosic acid (4.0 eq.) in toluene, but there was no evidence to suggest that any product had formed. It was hypothesised that with mercury having a high affinity for sulfur that the diacetoxymercury would coordinate to the sulfur atom of the thioamide, allowing for nucleophillic attack by the amine of the 2,2-dimethoxyethan-1-amine into the thiocarbonyl. Indeed, this was observed in the LCMS spectrum, however it was the following step that failed to proceed. The biphasic system (H_2O:Toluene) containing tosic acid was to catalyse the hydroysis of

the actetal to allow for cyclisation by the thioamide nitrogen, however this step did not occur. These conditions were repeated using a range of acids (HCl, H_2SO_4 and AcOH), however again, the reaction paused at this stage.



Scheme 7. Reagents and Conditions: (i) Thioamide (1.0 eq.), 2,2-dimethoxyethan-1-amine (5.0 eq.), diacetoxymercury (1.1 eq.), tosic acid (4.0 eq.), toluene:H_2O (1:1), reflux, overnight.

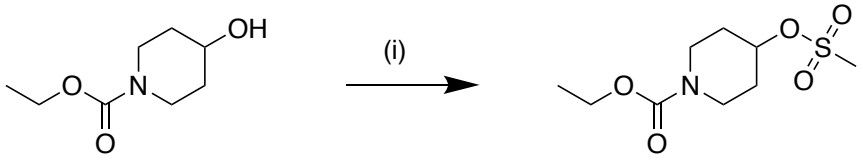
Recognising that there may be a potential issue with using a Boc protecting group, the decision was made to begin the synthesis again, using an ethyloxycarbamate (Eoc) protecting group. The first part of the synthesis was to get to ethyl 3,6-dihydropyridine-1(2H)-carboxylate, the "Eoc-alkene". The starting point was ethyl 4-oxopiperidine-1-carboxylate (1 eq.) and using sodium borohydride (2.0 eq.) in methanol, reduction of the carbonyl to the primary alcohol was achieved (Scheme 8).



Scheme 8. Reagents and Conditions: (i) Piperidone (1.0 eq.), $NaBH_4$ (2.0 eq.), MeOH, r.t., 1 h.

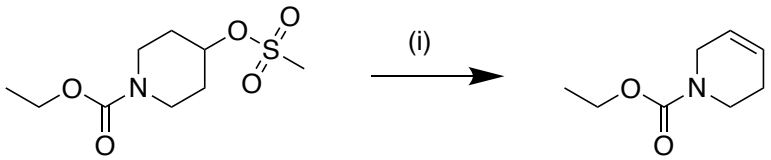
Following this, the primary alcohol (1 eq.) was activated as a leaving group by mesylation with mesyl chloride (MsCl) (1.2 eq.) and triethylamine (NEt_3) (1.2 eq.) in dichloromethane (Scheme 9). As per the previous route, the major challenge was visual-

isation by TLC, and once again purification was extremely difficult and unachievable, but a relatively pure compound was isolated and characterised.



Scheme 9. Reagents and Conditions: (i) Primary alcohol (1.0 eq.), MsCl (1.2 eq.), NEt3 (1.2 eq.), CH_2Cl_2, r.t 3h.

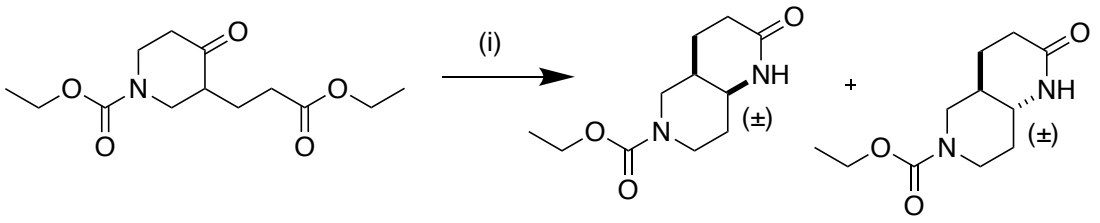
Following mesylation, elimination of the mesylate (1.0 eq.) was achieved using 1,8-Diazabicyclo(5.4.0)undec-7-ene (DBU) (3.0 eq.) in toluene at reflux (Scheme 10). Again, purification was difficult but relatively pure compound was isolated and characterised.



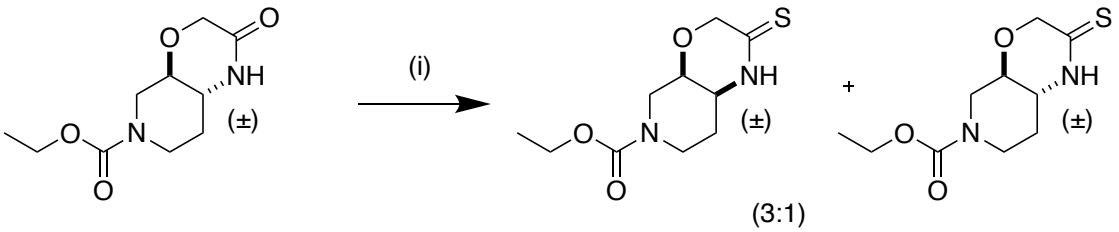
Scheme 10. Reagents and Conditions: (i) Mesylate (1.0 eq), DBU (3.0 eq.), toluene, reflux, overnight.

From this point forward, the same steps to get to the thioamide were used. However the same problems persisted. Visualisation by TLC up to the point of the amide was not possible, and hence purification and adequate characterisation was unachievable.

Following these unsucessful reactions, in order to rule out any interference from the ether oxygen, testing the chemistry without the ether oxygen began. Beginning with ethyl 3-(3-ethoxy-3-oxopropyl)-4-oxopiperidine-1-carboxylate and performing a reductive amination with ammonia using picoline borane with a subsequent cyclisation, then formation of the thioamide using Lawesson's reagent (Scheme 11 and Scheme 12).

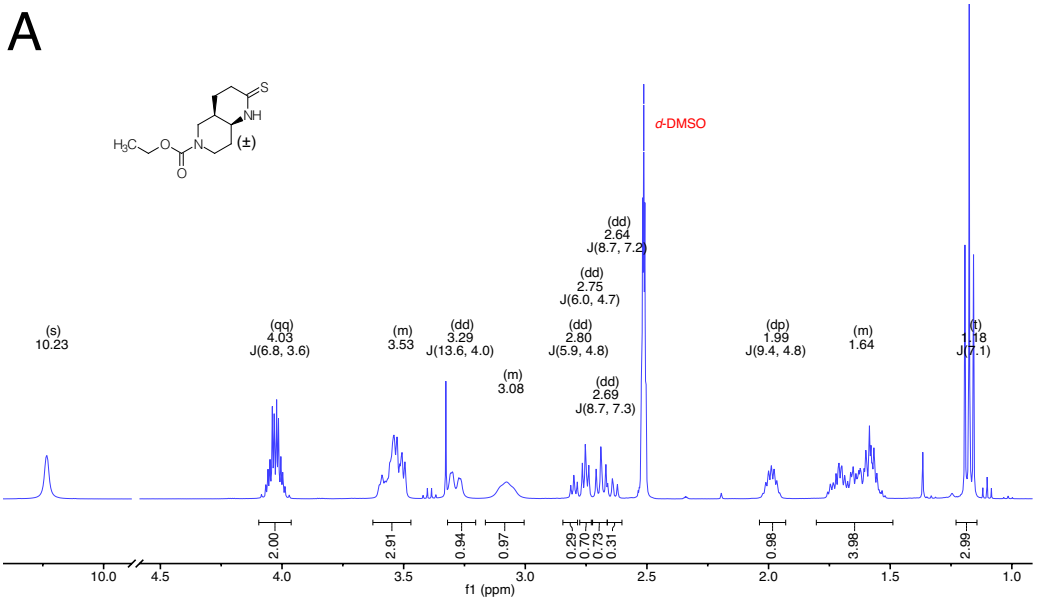


Scheme 11. Reagents and conditions (i) NH_3, 7N in MeOH (5 eq.), AcOH (10 eq.), Pic-BH_3 (1.5 eq.), 40 °C then r.t., overnight.



Scheme 12. Reagents and conditions (i) Lawesson's Reagent (0.5 eq.), CH_2Cl_2, r.t., overnight.

At the point of formation of the thioamide there were two UV active spots on the TLC, and both of these spots were isolated individually. These were the separation of the *cis* and *trans* isomers. The NMR spectra of these isolated compounds are shown in Figure 155.



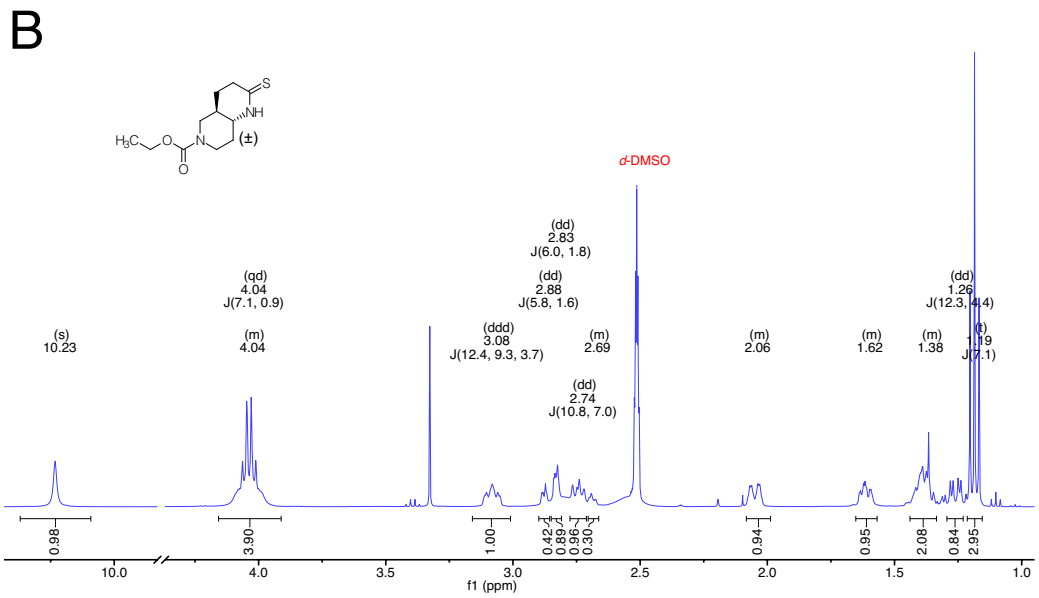


Figure 155. NMR spectra the cis (A) and trans isomers (B)

Once again the above chemistry was tested using acids (TsOH, HCl, AcOH) in an attempt to form the imazole, however these attemps were unsucessful. At this point it was postulated that due to the nucleophillic nitrogen atom of the intermediate amidine being quite basic, acids protonate the amine, removing its nucleophilicity. It was therefore decided to use oxophillic Lewis acids to catalyse the hydrolysis of the acetal. A range of conditions were tried (Figure 156), both at relux and under microwave radiation, using $TiCl_4$ and $SnCl_4$ in an attempt to form the imidazole, however all of them were unsuccessful. In addition formation of the imazole was attempted by excluding diacetoxymercury and using DIPEA, however this too was unsucessful. Lack of visualisation was also still an issue and for this reason isolation of single components from the reaction mixtures once the thioamide was consumed.

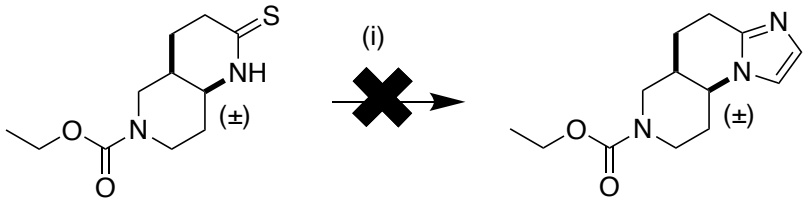
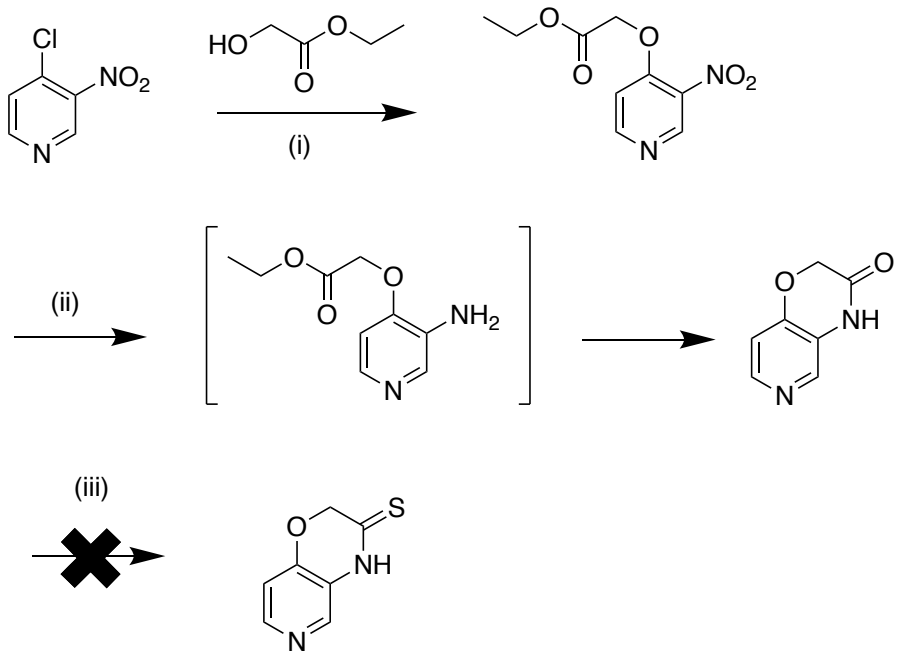


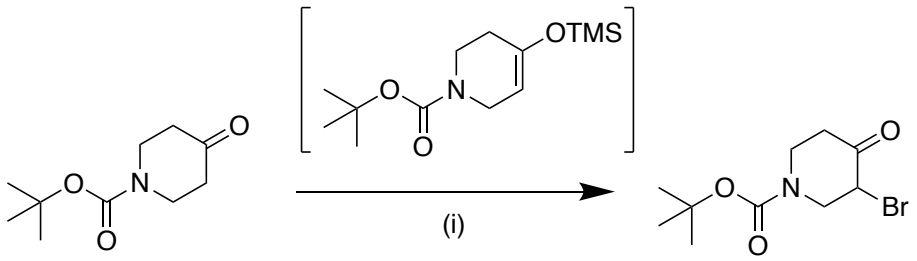
Figure 156. Reagents and conditions: (i) Thioamide (1.0 eq.), 2,2-dimethoxyethan-1-amine (2.0 eq.), diacetoxymercury (1.1 eq.), TiCl4 (0.1 eq.), xylene, reflux, overnight or MW 120 °C.; (ii) Thioamide (1.0 eq.), 2,2-dimethoxyethan-1-amine (2.0 eq.), diacetoxymercury (1.1 eq.), SnCl4 (0.25 eq.), xylene, reflux, overnight or MW 120 °C.; (iii) Thioamide (1.0 eq.), 2,2-dimethoxyethan-1-amine (2.0 eq.), TiCl4 (0.1 eq.), xylene, reflux, overnight or MW 120 °C.; (iv) Thioamide (1.0 eq.), 2,2-dimethoxyethan-1-amine (2.0 eq.), SnCl4 (0.25 eq.), xylene, reflux, overnight or MW 120 °C.; (v) Thioamide (1.0 eq.), 2,2-dimethoxyethan-1-amine (1.0 eq.), DIPEA (2.3 eq.), EtOH, reflux, overnight, then AcOH, 100 °C, 2h.

At this point simultaneous effort was underway to try to combat visualisation issues by introducing aromatics using a pyridine ring, which could later be reduced to the piperidine, which unfortunately would lead to the *cis* ring junction. The synthesis began with the chloropyridine and through nucleophillic aromatic substitution displaced the chlorine with ethyl 2-hydroxyacetate (1.2 eq.), Scheme 13. A subsequent hydrogenation of the nitro group over Pd/C in ethanol and acetic acid to the aniline was followed by an immediate cyclisation to form the amide. An attempt to convert the amide to the thioamide using Lawesson's reagent was unsuccessful, however it was decided to terminate the synthesis due to our previous unsuccessful attempts to form the imidazole.



Scheme 13. (i) 4-chloro-3-nitropyridine (1.0 eq.), NaH (1.2 eq.), ethyl hydroxyacetate (1.2 eq.); (ii) Pd/C 10%, EtOH, AcOH; (iii) Lawesson's reagent (0.5 eq.), CH_2Cl_2.

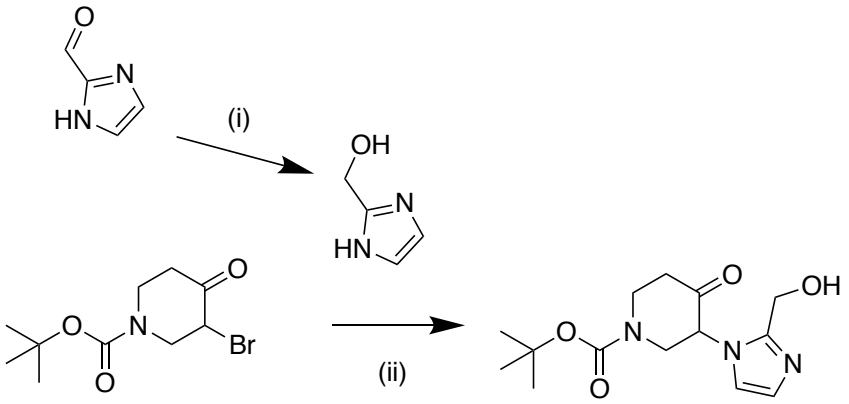
At this point the synthesis of the imidazole itself was abandoned and it was attempted to introduce the imidazole to the scaffold first. The synthesis began with tert-butyl 4-oxopiperidine-1-carboxylate and by forming an enolate with triethyl amine (2.0 eq.) and trapping with trimethyl silane (1.1 eq.) were able to form the bromoketone by quenching with N-bromosuccinamide (1.1 eq.), Scheme 14.



Scheme 14. Reagents and Conditions: (i) Tert-butyl 4-oxopiperidine-1-carboxylate (1.0 eq.), TMS-Cl (1.1 eq.), NEt_3 (2.0 eq.),0 °C, 1h then NBS (1.1 eq.), r.t., 3 h.

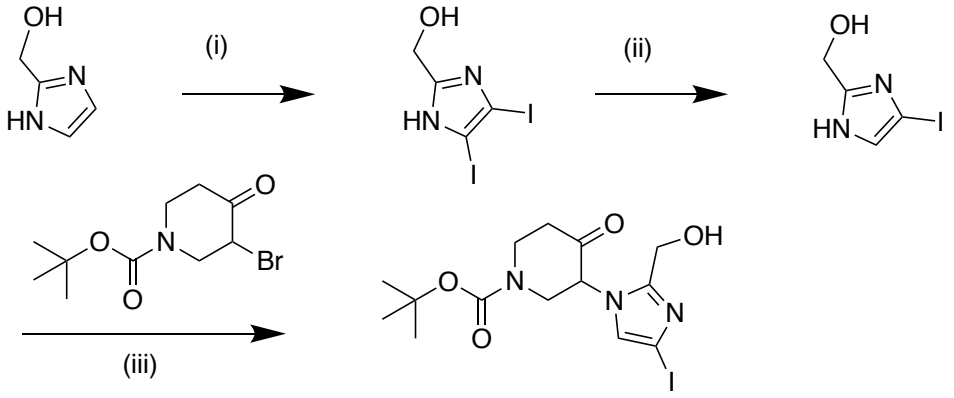
The *1H*-imidazole-2-carbaldehyde (1.0 eq.) was reduced to the primary alcohol using sodium borohydride (1.2 eq.) in isopropanol and attempted to displace the bromine of the bromoketone with the imidazole nitrogen using different bases (Cs_2CO_3, K_2CO_3, and NaH) in DMF or THF (Scheme 15). The mass ion was seen in the LCMS trace but unfortunately purification was not possible to poor visualisation. Additionally,

trifluoroacetic acid was added to the reaction mixture in an attempt to catalyse the potential cyclisation of the ketone and primary alcohol, however no mass ions were found for cyclised (including an elimination) or Boc-deprotected compounds. We were also aware at this point that this method would place the hinge binder oxygen atom in the 4-position on the ring, rather than the 3-position, however this may be tolerated and we decided to persue this route anyway.



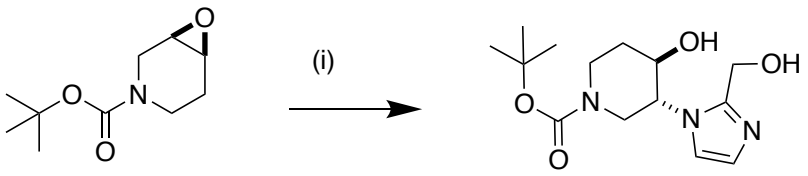
Scheme 15. Reagents and conditions: (i) 1H-imidazole-2-carbaldehyde (1.0 eq.), Sodiumborohydride (1.2 eq.), isopropanol, r.t. 1 h.; (ii) Cs_2CO_3, K_2CO_3, or NaH, (1.0 - 3.0 eq.), DMF or THF, r.t.

Due to consistent issues with visualisation, and thus purification and isolation, we decided to try to introduce iodine atoms onto the imidazole in order to aid with this issue. Iodine atoms were added onto the (1H-imidazol-2-yl)methanol (1.0 eq.) using NIS (2.0 eq.) in DMF. Following this, the labile iodine was removed from (4,5-diiodo-1H-imidazol-2-yl)methanol (1.0 eq.) using sodium thiosulphate (8.0 eq.) in ethanol:H_2O (4:6), Scheme 16. Following dispacement of the bromine of the bromoketone with the iodo-imidazole, once again a mass ion was found but purification was unsuccessful. Additionally, no evidence of cyclisation was observed. This chemistry was also attempted using the aldehyde rather than the primary alcohol and similar issues persisted.



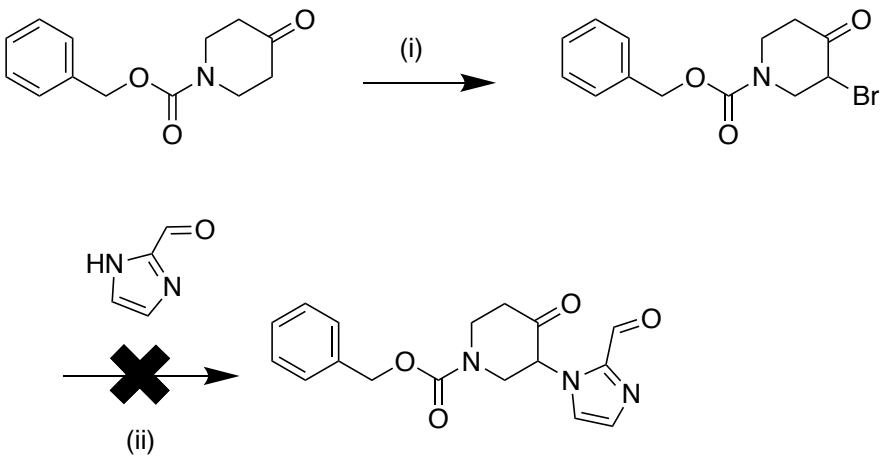
Scheme 16. Reagents and conditions: (i) (1H-imidazol-2-yl)methanol (1.0 eq.), NIS (2.0 eq.), DMF, r.t 1 h.; (ii) (4,5-diiodo-1H-imidazol-2-yl)methanol (1.0 eq.), Sodium thiosulphate (8.0 eq.), ethanol:H_2O (4:6), r.t.; (iii) Cs_2CO_3, K_2CO_3, or NaH, (1.0 - 3.0 eq.), DMF or THF, r.t.

Recogising that it was predicted that the above method would likely lead to predoninatly *cis*-product if cyclisation occurred, and we ideally needed the *trans* product, we were simultaneuosly following a similar route using the imidazole to open the epoxide (Scheme 17). Again mass ions were seen for both regioisomers, however separation, purification and isolation of single products was unsucessful.



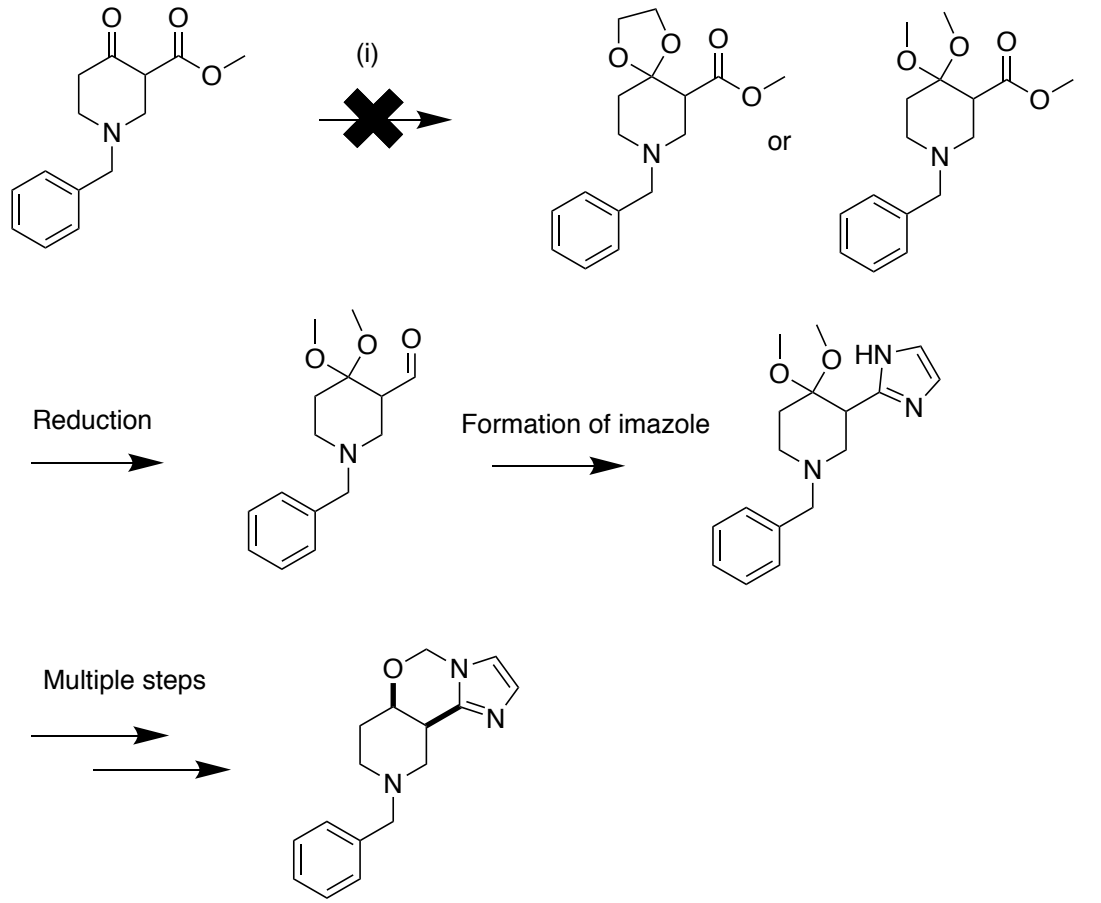
Scheme 17. Reagents and Conditions: (i) Epoxide (1.0 eq.), EtOH, 65 °C, overnight.

With persistent purification issues we decided to put one last effort into this route by trying to use a carboxybenzyl protecting group. This was attemped by starting with benzyl 4-oxopiperidine-1-carboxylate and brominating using Br_2 in ethanol to give the bromoketone (Scheme 18). Attempts to purify were once again unsuccessful and additionally, the mass ion for the desired product was not observed in the LCMS. At this point it was decided not to pursue this route due to time constraints of the project.



Scheme 18. Reagents and Conditions: (i) Piperidone (1.0 eq.), Br2 (1.1 eq.), CH_2Cl_2, r.t, 10 mins.; (ii) Bromoketone (1.0 eq.), imidazole (1.2 eq.), NaH (1.0 eq.), DMF, 0 °C then r.t. overnight.

With the timescale of the project, and not seeing any positive results, a final attempt at the scaffold was attempted. The plan was to start with methyl 1-benzyl-4-oxopiperidine-3-carboxylate and protect it by formation of an acetal (Scheme 19). Following this, we planned to reduce the ester to the aldehyde and then attempt to form the imidazole using ammonia and glyoxal. Following this, the plan was to deprotect the acetal, reduce the resulting ketone to the primary alcohol and then perform a cyclisation using dibromomethane or even produce a 7-membered ring using dibromoethane as molecular modeling suggested that a 7-membered ring could also fit in the binding pocket. This plan, however was thwarted by the fact that formation the acetals were unsuccessful despite employing methods to drive the equlibrium over to the desired product.



Scheme 19. Reagents and conditions: (i) methyl 1-benzyl-4-oxopiperidine-3-carboxylate (1.0 eq.), ethane-1,2-diol (1.0 -6.0 eq.), PTSA (0.6 eq.), mol. sieves 4 Å, reflux, overnight.

At this point in the project we were not seeing any positive results, and due to limited time, made the decision to terminate the synthesis of the scaffold and look into other alternatives in order to test the hypothesis that interaction with the arginine may lead to PI3Kα selectivity. From here we decided to look to the literature for inspiration for a new scaffold that may allow for less challenging chemistry in order to test the hypothesis.

3.3.2.3 Inhibitor design

After scientists at Amgen had used an aminobenzothiazole as a central scaffold and hinge binder to design a series of dual PI3K/mTOR inhibitors (discussed in detail in section 3.1.2) we considered using an aminobenzothiazole as our central scaffold in order to test our arginine hypothesis. The synthesis of the scaffold is generally straight-forward, and incorporation of synthetic handles was very achieveable. Unfortu-

nately, although we had initially aimed to lower the logP of the central scaffold, in opting to use the benzothiazole, we did not lower the logP, however the molecular weight was lowered significantly relative to the thienopyrimidine core (Figure 157).

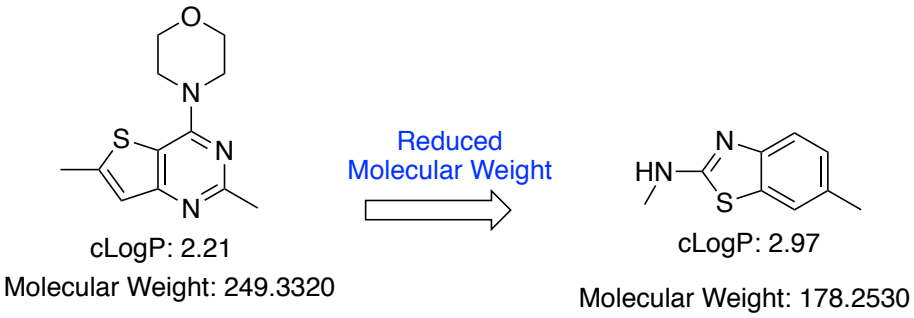


Figure 157. The thienopyrimidine core has a slightly lower lipophilicity (cLogP), although the benzothiazole scaffold has a significantly lower molecular weight.

In order to test the arginine hypothesis, a 6 x 3 array (Figure 158) using the same groups in the activity pocket that we had already used was designed. Additionally, we decided to use a simple carboxylic acid group, as this would be ionised at physiological pH and would be able to form an anion cation interaction with the arginine. In addition, we chose two well known bioisosteres of carboxylic acids, a sulfonamide and an acyl sulfonamide. These groups were placed in both the meta and para positions on the aryl ring, so as to approach the arginine residue from differing angles. Since we proposed to make carboxylic acids, we decided to include some amides in order to probe the solvent

exposed region further.

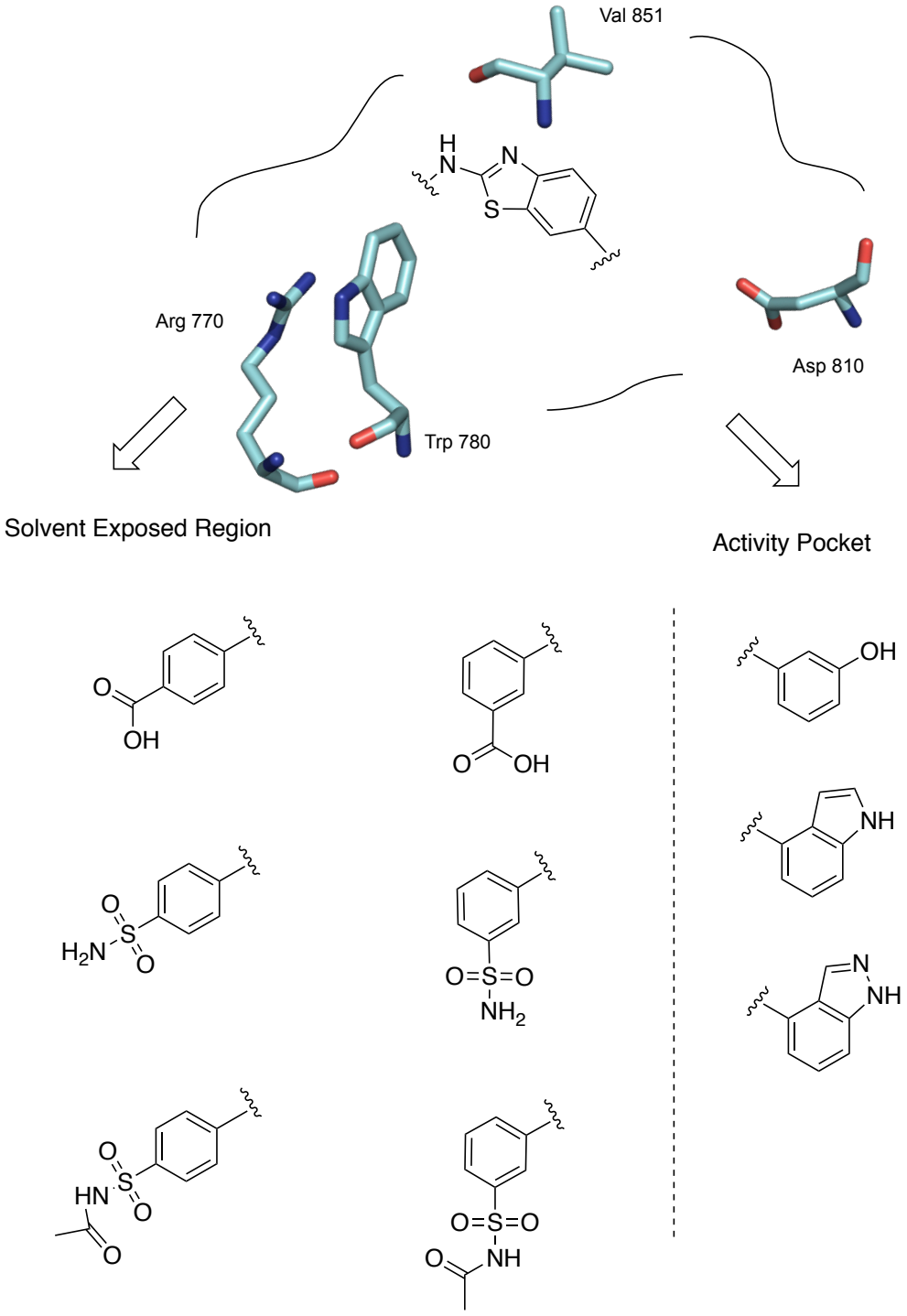


Figure 158. A 3 x 6 array.

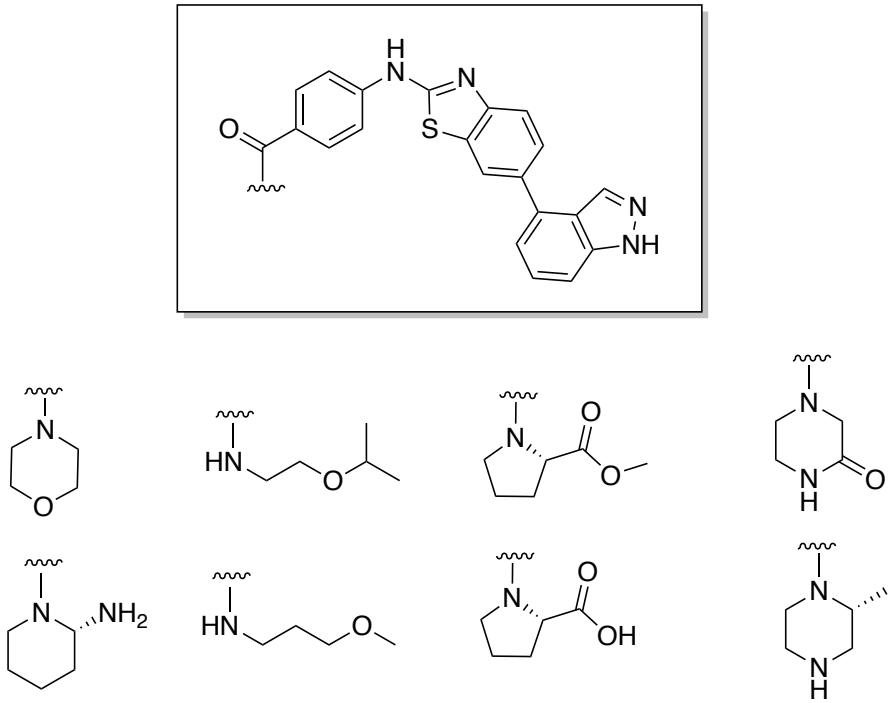
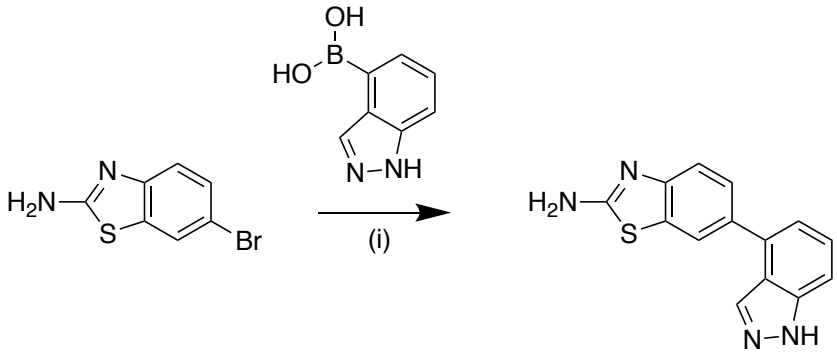


Figure 159. Additional amide compounds

3.3.2.4 Synthesis

Our synthesis began with 6-bromobenzo*[d]*thiazol-2-amine. A Suzuki Pd cross-coupling reaction with 4-indazole boronic acid using $Pd(PPh_3)_2Cl_2$ as the catalyst, Na_2CO_3 as the base, ethanol:H_2O (3:1) as the solvent, and heating at 120 °C under microwave radiation for 30 mins led to the formation of product, however, the yield was extremely poor at 12% .

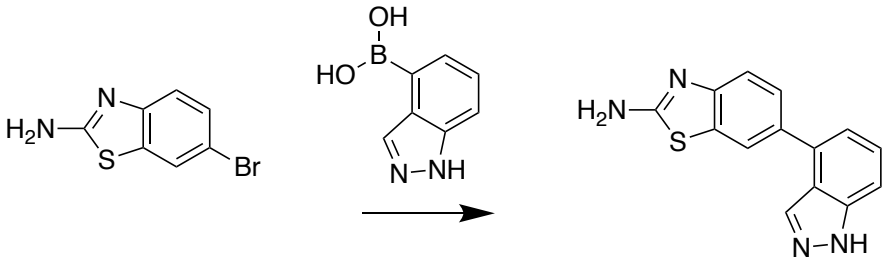


Scheme 20. Reagents and Conditions: 6-bromobenzo[d]thiazol-2-amine (1.0 eq.), $Pd(PPh_3)_2Cl_2$ (0.1 eq.), Na_2CO_3 (3.0 eq.), ethanol:H_2O (3:1), microwave 120 °C, 30 mins, yield = 12%.

With a successful, but poor yielding Suzuki reaction we tried a small range of

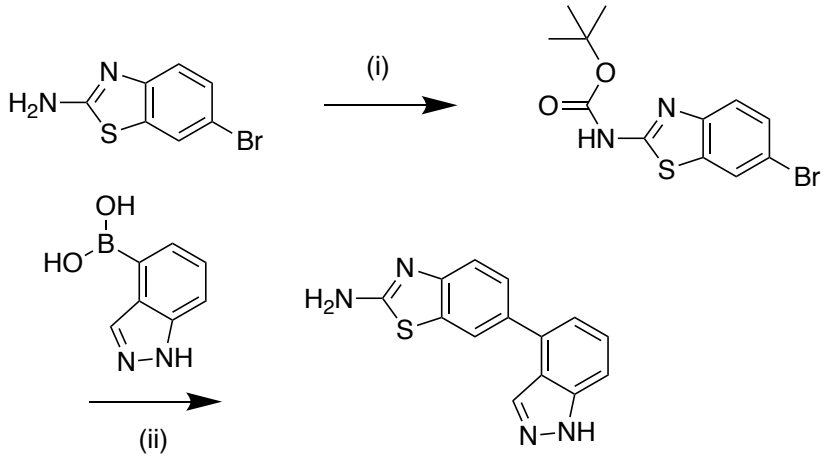
conditions in order to find approriate conditions to improve the yield. These conditions are detailed in Table 7.

Table 7. Suzuki Reaction. The catalyst was used at 0.1 eq., the base at 3.0 eq., and the boronic acid at 1.1 eq.



	Catalyst	Base	Solvent	Conditions	Yield
1.	$Pd(PPh_3)_2Cl_2$	Na_2CO_3	EtOH:H_2O (3:1)	120 °C (mw), 30 min	12 %
2	$Pd(PPh_3)_2Cl_2$	NaOH	Dioxane	120 °C (mw), 30 min	15 %
3	$Pd(dppf)_2Cl_2$	$NaHCO_3$	H_2O:Dioxane (2:1)	120 °C (mw), 30 min	16%
4	$Pd(PPh_3)_4$	K_3PO_4	H_2O:Dioxane (2:1)	120 °C (mw), 30 min	21%

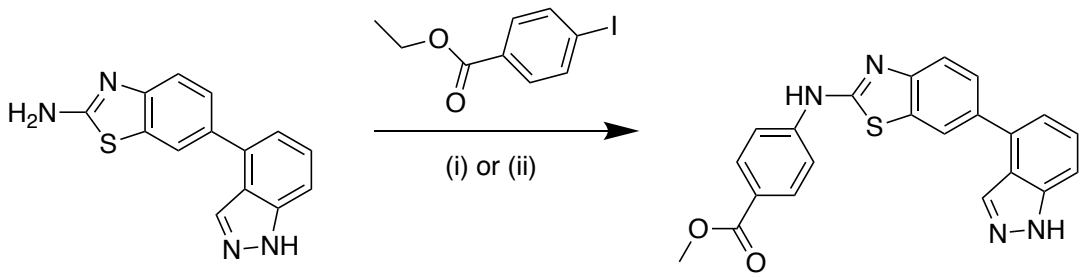
From the above table it can be seen that all of the yields from the small set of conditions were low. We hypothesised that these low yields could either be due to the indazole boronic acid, or from poisoning of the catalyst by the aniline. In order to test these hypotheses we repeated the suzuki reaction using 2-phenol boronic acid and condition set 4 in table 4. Once again low yield was obtained, 17%. We then protected the aniline nitrogen with a boc protecting group using boc anhydride in CH_2Cl_2 (Scheme 21). The reaction required a catalytic amount of DMAP in order to proceed. Following protection of the aniline , the Suzuki reaction, using condition set 4, was performed and a drastic increase in yield was observed, 82 %, with a simultaneous deprotection due to the reaction temperature. This confirmed our hypthesis that the aniline nitrogen was poisoning the catalyst and it was neccessary to protect this nitrogen or react at this position first in the synthesis.



Scheme 21. Reagents and Conditions: (i) 6-bromobenzo[d]thiazol-2-amine (1.0 eq.), Boc2O (1.2 eq.), NEt3 (1.2 eq.), DMAP (0.1 eq.), CH_2Cl_2, r.t, 10 min, yield 62 %.; (ii) tert-butyl (6-bromobenzo[d]thiazol-2-yl)carbamate (1.0 eq.), 4-Indazole boronic acid (1.1 eq.), Pd(PPh3)4 (0.1 eq.), Na_2CO_3 (3.0 eq.), dioxane:H_2O (2:1), microwave 120 °C, 30 min, yield 82%.

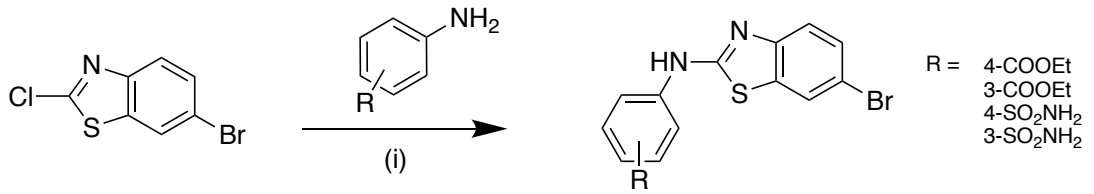
Our next aim was to identify how to introduce groups into the solvent exposed region. We began with ethyl 4-iodobenzoate and performed a Buchwald reaction[156] in dioxane in the microwave at 110 °C for 30 min using $Pd_2(dba)_3$ as a catalyst (0.05 eq.), BINAP (0.1 eq.) as the phosphine ligand, and Cs_2CO_3 as the base (Scheme 22). The reaction was successful, however only a low-moderate yield of 40% was obtained.

We then decided to try the reaction using Ullmann[158] conditions (Scheme 22) using CuI (0.5 eq.) and potassium tert-butoxide (1.0 eq.) in dioxane at 110 °C for 30 min under microwave radiation. This reaction was sucessful, however once more the yield only a low-moderate yield of 38% was obtained.



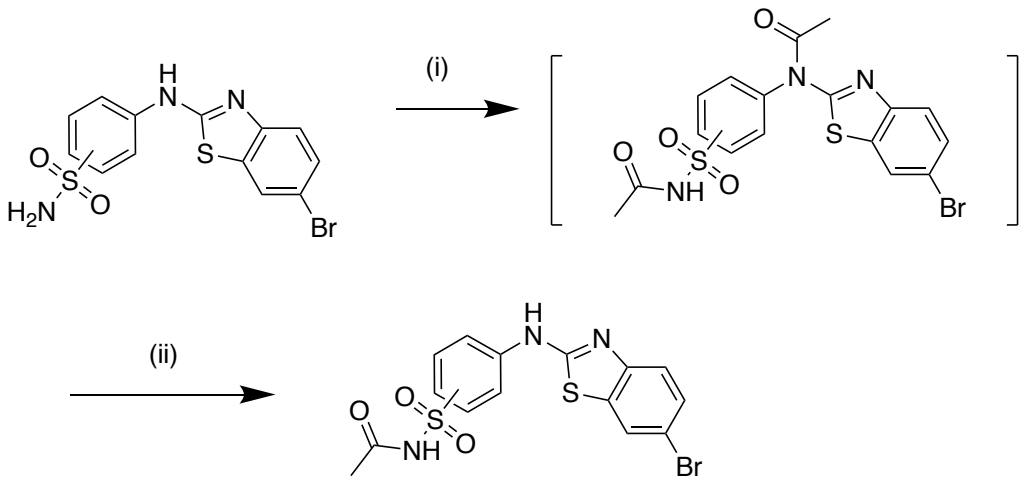
Scheme 22. Reagents and Conditions: (i) Aniline (1.0 eq.), ethyl 4-iodobenzoate (1.2 eq.), $Pd_2(dba)_3$ (0.05 eq.), BINAP (0.1 eq.), Cs_2CO_3 (2.0 eq.), dioxane, microwave 110 °C, 30 min, yield 40%; (ii) Aniline (1.0 eq.), ethyl 4-iodobenzoate (1.0), CuI (0.5 eq.), KOtBu (1.0 eq.), dioxane, microwave 110 °C, 30 min, yield 38%.

With these low yields we decided to try to switch around the nucleophile and electrophile by using 6-bromo-2-chlorobenzothiazole (1.2 eq.) and ethyl 4-aminobenzoate (1.0 eq.) and heating at 120 °C for 1 h in ethanol containing a catalytic amount of HCl in dioxane (4 M). This electrophillic aromatic substitution reaction yielded good yields (46 - 82%. With this chemistry we were able to synthesise four intermediate compounds that were to be carried on to the next step, which was to perform the suzuki reaction.



Scheme 23. Reagents and Conditions: (i) 6-bromo-2-chlorobenzothiazole (1.2 eq.),Aniline (1.0 eq.), Cat. HCl in dioxane (4 M), ethanol, 120 °C, 1 h., yields (46 - 82%).

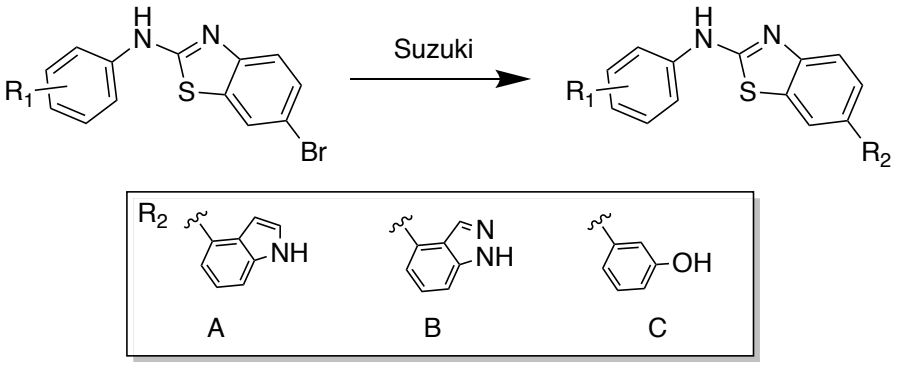
From two of the intermediates, the meta and para sulfonamides, we were able to synthesise the acyl sulfonamides (Scheme 24) using acetyl chloride (2.0 eq.) with triethylamine (2.5 eq.) in the presence of catalytic DMAP (0.05 eq.) in toluene at 55 °C for 3 h. Unfortunately the acyl chloride also reacted on the aniline nitrogen, although since it is very labile due to the good leaving group ability of the aniline, the acyl group was easily removed with lithium hydroxide in H_2O and THF. Under these conditions the acyl sulfonamide would be ionised and thus protected from hydrolysis.The compounds were isolated in excellent yields, 82 - 90%.

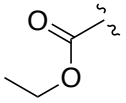
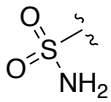
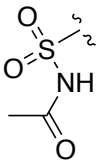


Scheme 24. Reagents and Conditions: (i) 3-Sulfonamide or 4-Sulfonamide (1.0 eq.), Acetyl chloride (2.0 eq.), NEt_3 (2.5 eq.), DMAP (0.05 eq.), toluene, 55 °C, 3 h., yields (43 - 90%).

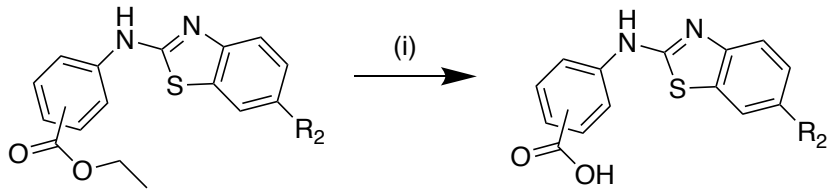
With isolation of our 6 intermediates, and the aniline nitrogen atom already reacted, we were able to easily introduce the activity pocket groups using the Suzuki reaction, Table 8. The Suzuki reaction at this point gave mostly good yields (18-90%), although reactions with phenol boronic acids were generally poorer due to the acidity of the phenol. Additionally, Suzuki reactions performed on the esters tended to have relatively poorer yields due to partial hydrolysis of the ester where the carboxyllic acid was not isolated.

Table 8. Suzuki reactions and their yields. Reagents and Conditions: Aryl bromide 1.0 eq.), $Pd(PPh_3)_2Cl2$ (0.1 eq.), $Na2CO3$ (3.0 eq.), ethanol:$H2O$ (3:1), microwave 120 °C, 30 mins



Position	R_1	R_2	Yield
-4		A	23%
		B	64%
		C	37%
-3		A	21%
		B	18%
		C	28%
-4		A	56%
		B	42%
		C	43%
-3		A	64%
		B	42%
		C	64%
-4		A	59%
		B	73%
		C	72%
-3		A	80%
		B	63%
		C	38%

Following the Suzuki reactions, esters were hydrolysed (Scheme 25) using lithium hydroxide in THF:H_2O, requiring high temperatures, particularly for esters in the 4-position.



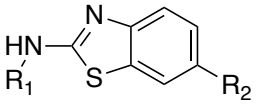
Scheme 25. Reagents and conditions: (i) Ester (1.0 eq.), LiOH (10.0 eq.), THF:H_2O, reflux, 1 h., yields 52-89%.

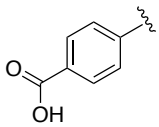
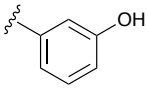
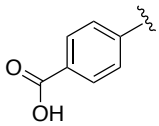
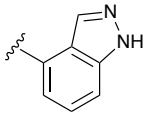
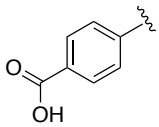
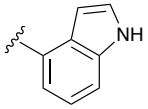
In additon, we used the para-carboxylic acid intermediate in order to generate amides. This was achieved by activation of the carboxylic acid in the presence of the amine using HATU, DIPEA as a base, and in DMF. Compounds that contained esters, were subsequently hydroysed using the conditions mentioned above. Additionally, compounds that contained the Boc protecting group were deprotected using HCl in dioxane (4 M).

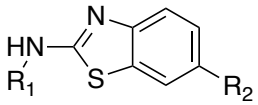
3.3.2.5 Biological Results

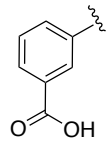
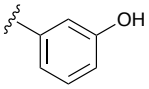
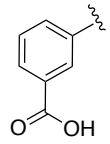
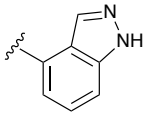
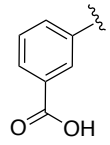
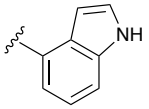
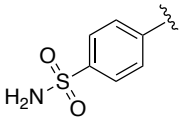
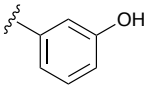
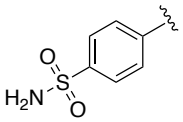
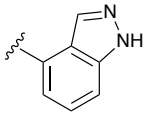
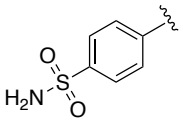
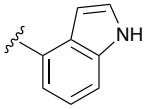
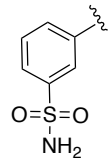
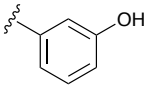
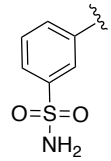
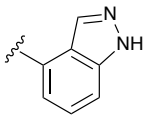
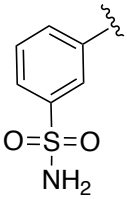
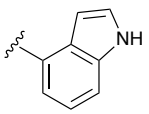
After synthesis of the array compounds, the compounds were tested by GlaxoSmithKline in Stevenage UK by the same assay as discussed above. The results are presented in Table 9, where the potency is expressed at the pIC_{50} (pIC_{50} = - log IC_{50}).

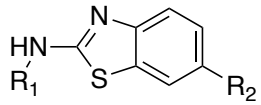
Table 9. Biological Evaluation of PI3K compounds. Potency against the different PI3K isoforms is given as pIC_{50} values (n = 1). The potency threshold for the PI3K assay is ~ pIC_{50} = 9 due to substrate concentration.

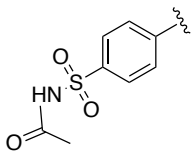
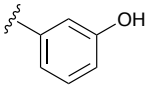
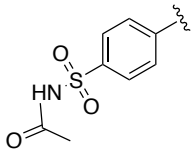
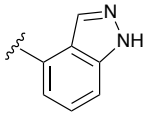
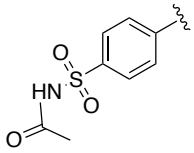
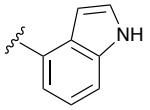
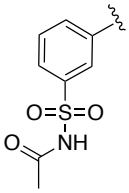
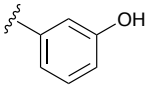
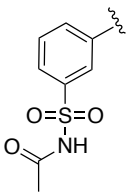
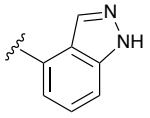
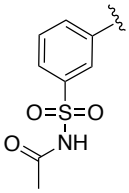
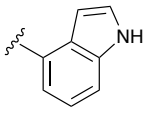
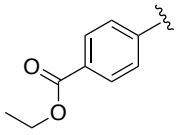
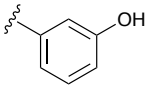
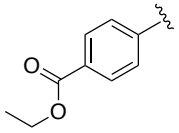
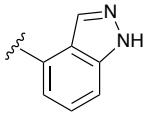


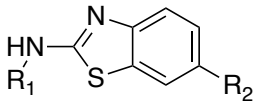
	R_1	R_2	PI3K Isoform Potency (pIC_{50})			
			γ	α	β	δ
25.			6.5	5.0	4.5	4.9
26.			6.4	4.6	4.5	5.3
27.			5.8	4.5	4.5	5.7

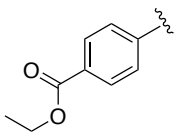
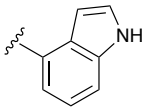
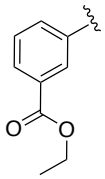
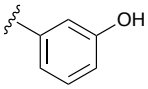
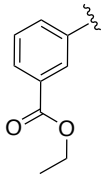
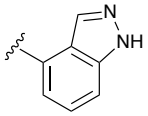
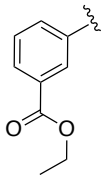
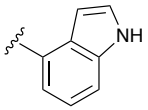


	R_1	R_2	PI3K Isoform Potency (pIC_{50})			
			γ	α	β	δ
28.			7.0	4.6	4.5	5.2
29.			5.9	4.5	4.5	4.5
30.			6.1	4.5	4.5	4.9
31.			6.2	5.4	4.5	5.4
32.			5.8	4.5	4.5	5.7
33.			5.9	4.5	4.5	4.5
34.			7.2	5.4	4.5	6.1
35.			5.5	4.5	4.5	4.6
36.			6.0	4.5	4.5	6.0



	R_1	R_2	PI3K Isoform Potency (pIC_{50})			
			γ	α	β	δ
37.			6.7	4.9	4.5	5.4
38.			6.3	4.5	4.5	5.2
39.			-	4.5	4.7	5.1
40.			7.0	5.3	4.9	5.7
41.			6.9	4.7	4.5	4.8
42.			6.8	4.5	4.6	5.3
43			5.8	4.5	5.6	5.6
44			4.5	4.5	4.5	4.9



	R_1	R_2	PI3K Isoform Potency (pIC_{50})			
			γ	α	β	δ
45			4.5	4.5	5.4	5.8
46			4.8	4.5	4.6	4.7
47			5.6	4.5	5.2	5.5
48			5.2	5.4	5.4	5.7

3.3.2.6 Discussion of Biological Results

Immediately from the table of results, it can be seen that the results were not as we predicted. Many of the compounds show little to no activity against PI3Kα (where a pIC_{50} of 4.5 is considered inactive), however the series showed potency towards PI3Kγ. Figure 160 shows a plot of isoform activity for each compound. It can immediately be observed that in addition to PI3Kγ activity, some of the compounds show weak activity against PI3Kδ. Observing that many compounds exhibited selectivity toward the PI3Kγ isoform, the following discussion will focus on examining the origin of PI3Kγ selectivity.

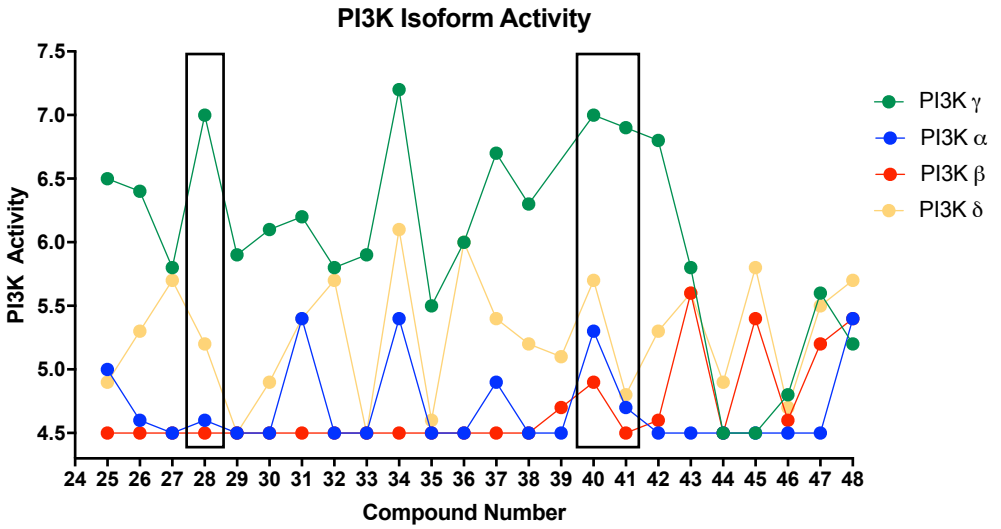


Figure 160. A plot of PI3K isoform activity for each compound. This demonstrates the observed γ-selectivity observed for a majority of the compunds.

Effect of Headgroup

We aimed to identify the effect of the head group on γ-selectivity. In order to do so, plots of fold-selectivity vs PI3Kγ selectivity were generated. Figure 161 (A-C) shows these plots showing γ-selectivity vs PI3Kγ activity. Generally, it can be seen that fold-selectivity generally increases with PI3Kγ activity. Additonally, it can be seen that the phenol containing compounds are generally more potent. On a whole however, there appears to be no trends with regards to the head group, on PI3Kγ selectivity.

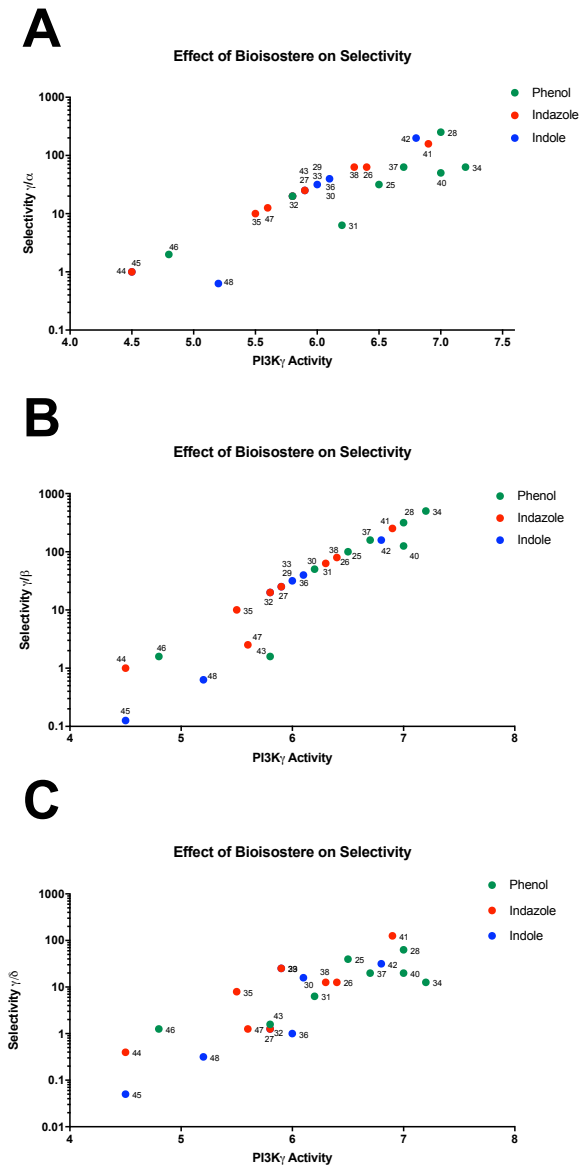


Figure 161. Plots of PI3Kγ selectivity vs PI3Kγ activity to assess the effect of the activity pocket group (phenol vs indole vs indazole) (A) γ-selectivity over PI3Kα, (B) γ-selectivity over PI3Kβ, and (C) γ-selectivity over PI3Kδ. Generally, it can be seen that the phenol containing compounds have a general trend for being slighly more potent than the other groups. Additionally,there appears to be a linear trend of increased γ -selectivity upon increased PI3Kγ activity.

Effect of Solvent Exposed Group

After seeing no trends to explain selectivity by the head group, we then looked to understand the origin of the observed PI3Kγ selectivity by looking at the effect of the solvent exposed group. Figure 162 shows plots of γ-selectivity vs PI3Kγ activity, highlighting the carboxylic acids vs the sulfonamides vs the acyl sulfonamides. From these plots it can be seen that the sulfonamides are generally less active towards PI3Kγ than the acyl sulfonamides and the carboxylic acids. In terms of selectivity there are no general trends observed when comparing the carboxylic acids vs the sulfonamides vs the acyl sulfonamides, however it should be noted that there are 3 "stand out" compounds, compounds 28, 41, and 42.

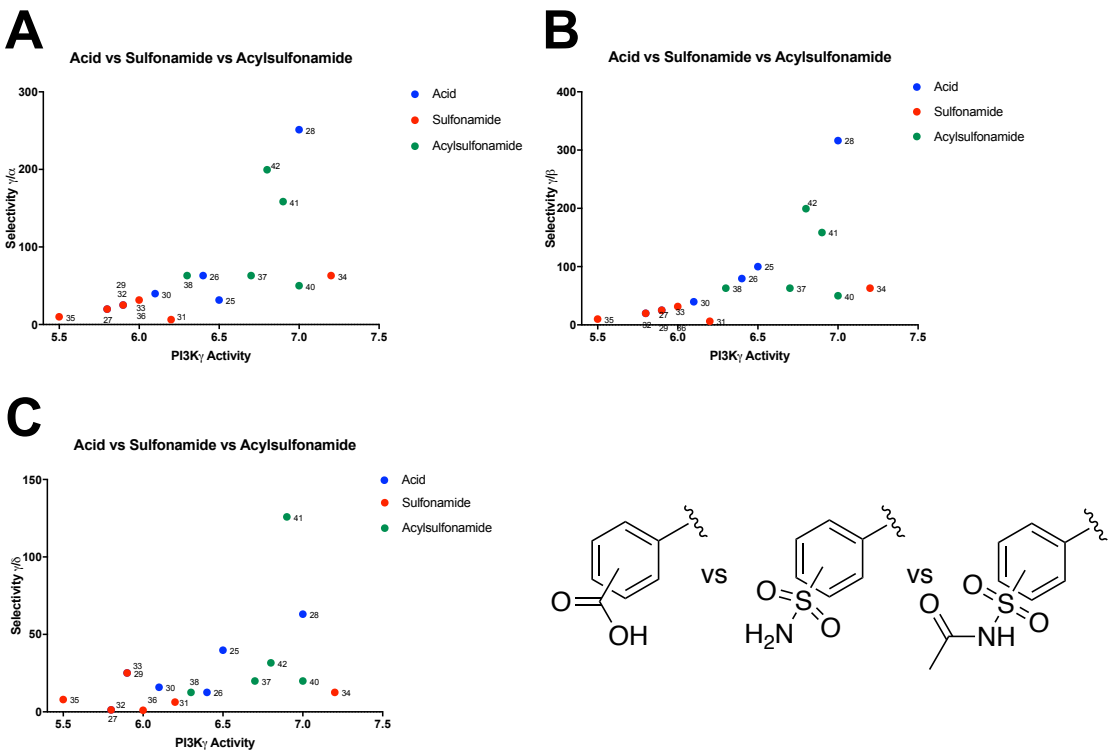


Figure 162. Plots of PI3Kγ selectivity vs PI3Kγ activity to assess the effect of the solvent exposed group (a cis vs sulfonamide vs acylsulfonamide) (A) γ-selectivity over PI3Kα, (B) γ-selectivity over PI3Kβ, and (C) γ-selectivity over PI3Kδ.

Effect of meta vs para Substitution

Plotting the same graphs as figure 113, and highlighting meta vs para substitution also shows no trends in terms of γ-selectivity. Although, it should be noted that compounds 28, 41, and 42 are all meta substituted.

Effect of the Aryl-aminobenothiazole Central Scaffold

After observing no major trends to explain the γ-selectivity when looking at the effects of the headgroup we must conclude that γ-selectivity is an inherrent property of the shared aryl-aminobenzothiazole central scaffold (Figure 163) where the selectivity is a result of lack of potency towards PI3K α, β and δ. Greater selectivity is observed upon an increase in γ-potency - this is the casse for compounds 28, 41, and 42.

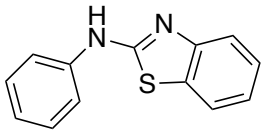


Figure 163. Aryl-aminobenothiazole central scaffold.

The γ-selectivity is a symptom of loss activity towards the α, β and δ isoforms as opposed to increased activity towards the γ-isoform.

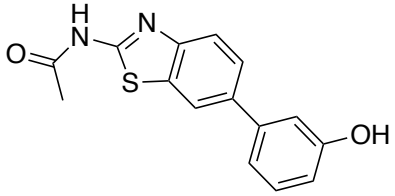
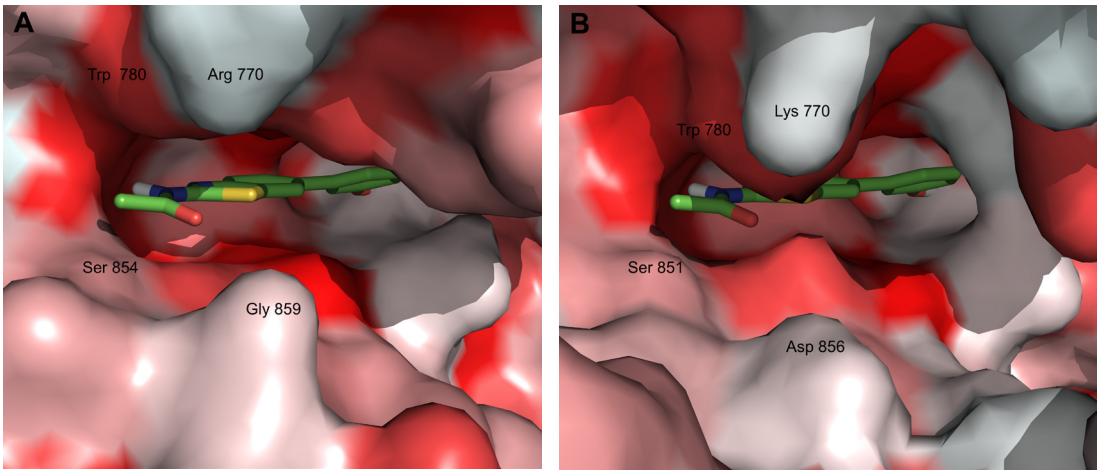


Figure 164. Simple acylated aminobenzothiazole used for molecular modelling.

Molecular modeling of a simple acyl benzothiazole (Figure 164) shows that the hydrogen bond donor/acceptor acceptor motif of the amide NH and the thiazole N makes interactions with the hinge valine. As expected, the phenol extends into the activity pocket. Additionally, we observed something similar to what was observed by Collier et.al. when replacing the acyl group (discussed in the introductory section of this chapter). Firstly Collier et. al. reported that Ala885, is unique to PI3Kγ, where in α, β, and δ this is a serine residue where the OH of serine is involved in hydrogen bonding

with the hinge valine residue. They propose that upon changing the acyl group to a urea, introduction of urea functionality allows for the urea carbonyl to form an additional hydrogen bond to the hinge valine, which in-turn breaks the serine-valine hydrogen bond, freeing up the OH group, introducing a steric clash with the lipophilic side chain. This steric clash is unfavourable in the anti-targets, and does not happen in the case of PI3Kγ. We hypothesise here that this non-conserved Ala885 residue is the root cause of the γ-selectivity where the large aryl ring clashes with the OH group of the serine residues of the α, β and δ isoforms. Additionally, Figure 165 shows the molecular modeling of the simple acylated aminobenzothiazole into PI3Kγ (PDB 3DBS), then the α (PDB 5DXT), β (PDB 4BFR) and δ (PDB 2WXP) isoforms aligned and overlayed in Pymol. Additionally, each receptor is represented as a surface, coloured by the Eisenberg hydrophobicity scale. In the γ-isoform, Ala 885 is more hydrophobic, which could potentially allow for occupation of the aryl ring. Note, this figure shows the tryptophan shelf of PI3Kδ.



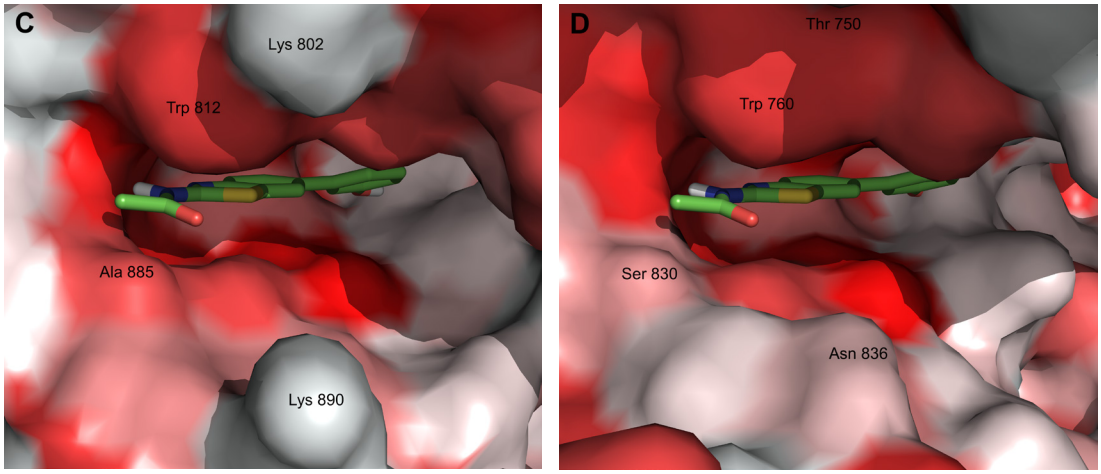


Figure 165. Molecular modeling of the simple acylated aminobenzothiazole into (A) PI3Kγ (PDB 3DBS), then (B) the α isoform (PDB 5DXT) overlayed, (C) the β isoform overlayed (PDB 4BFR) and (D) the δ isoform (PDB 2WXP) overlayed. Isoforms aligned an overlayed in Pymol. Additionally, each receptor is represented as a surface, coloured by the Eisenberg hydrophobicity scale[157]. In the γ-isoform, Ala 885 is more hydrophobic than the serine residues of the other isoforms, which could potentially allow for occupation of the aryl ring.

Additional molecular modelling showed another non-conserved residue in the binding pocket, illustrated in Figure 140. In PI3Kγ in the solvent exposed region we identified a lysine residue (Lys 890), in PI3K α, β and δ isoforms, this residue is Gly 859, Asp856 and Asn 836 respectively. The lycine residue of PI3Kγ could potentially form interactions with carboxyllic acids and their bioisosteres, would could contribute to the PI3Kγ activity.

Additional modelling of the synthesised compounds into PI3Kγ (PDB 3DBS) show that incorperation of the aryl ring forces the inhibitor out of the pocket, whereas, a small acyl group allows the inhibitor to move deeper into the hinge. Figure 141, shows that the acyl analogue makes 3.2 and 2.1 Å hydrogen bonds with the hinge, and compound 28 shows a measured distance of 3.9 Å and 4.4 Å from the hinge valine.

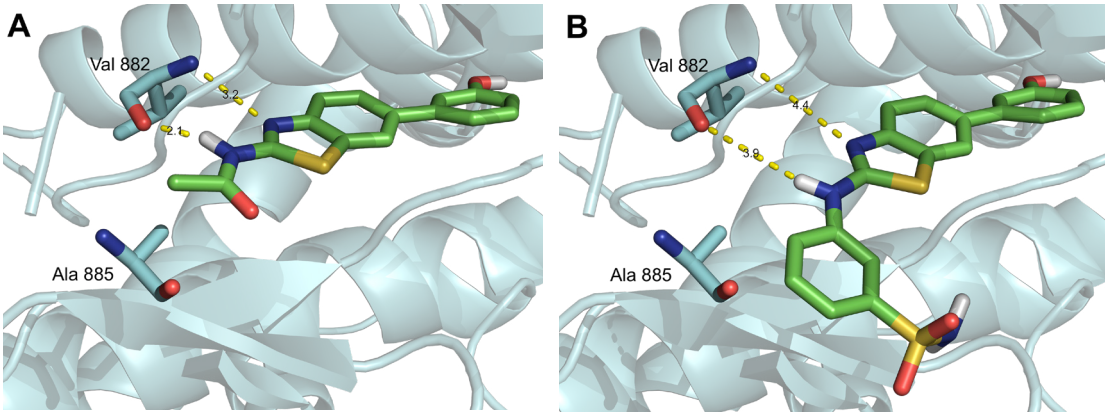


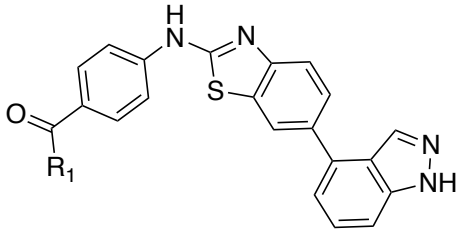
Figure 166. (A) Molecular modeling of the simple acylated aminobenzothiazole into PI3Kγ (PDB 3DBS) making 3.2 and 2.1 Å hydrogen bonds with the hinge, and (B) compound 28 shows a measured distance of 3.9 Å and 4.4 Å from the hinge valine when docked into PI3Kγ (PDB 3DBS). Incorperation of the aryl ring forces the inhibitor out of the pocket

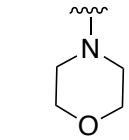
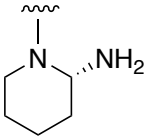
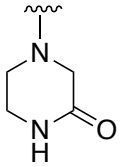
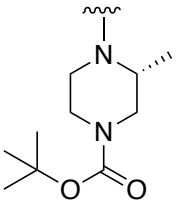
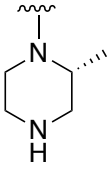
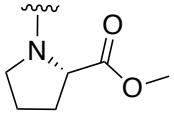
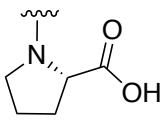
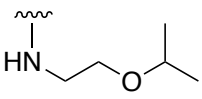
An additional observation is that the molecules are generally planar and perhaps an ortho substituent on the aryl ring could shift the aryl ring out of plane, which may alleviate some of the steric hinderance.

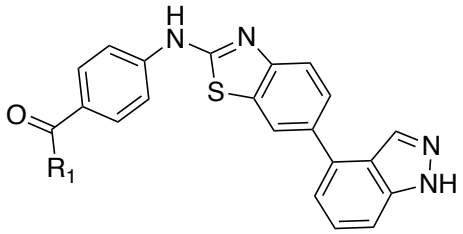
3.3.2.7 Amide compounds

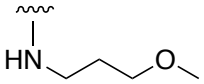
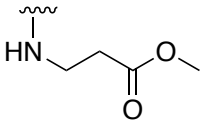
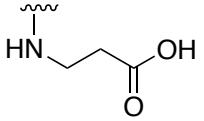
The additional amide compounds that were synthesised are listed in Table 10 with their biological results. Unfortunately, the compounds exhibited inactity or very low potecy, even towards PI3Kγ. This is likey due to them simply not fitting into the binding pocket for reasons mentioned above.

Table 10. Biological Evaluation of PI3K compounds. Potency against the different PI3K isoforms is given as pIC_{50} values (n = 1). The potency threshold for the PI3K δ assay is ~ pIC_{50} = 9 due to substrate concentration.



	R_1	PI3K Isoform Potency (pIC_{50})			
		γ	α	β	δ
49.		5.1	4.5	4.5	5.5
50.		*			
51.		4.5	4.5	4.5	4.5
52		5.3	4.5	5.5	6.0
53.		*			
54.		5.3	4.5	4.5	5.5
55.		4.9	4.5	4.5	4.7
56.		4.8	4.5	4.5	4.5



	R_1	PI3K Isoform Potency (pIC_{50})			
		γ	α	β	δ
57.		4.5	4.5	4.5	4.5
58		4.5	4.5	4.5	5.5
59		5.7	4.5	4.5	4.5

3.3.2.8 Discussion of Physicochemical properties

The physical properties of compounds 25-59 are listed in Table 11.

Table 11. Physical Properties

	MW	cLogP	HBA	HBD
25	362.4	5.54	4	3
26	386.4	5.08	5	3
27	385.4	5.47	4	3
28	362.4	5.54	4	3
29	386.4	5.08	5	3
30	385.4	5.47	4	3
31	397.5	3.15	5	3
32	421.5	3.71	6	3
33	420.5	2.74	5	3
34	397.5	4.73	5	3
35	421.5	3.71	6	3
36	420.5	3.78	5	3
37	439.5	3.40	6	3
38	463.5	3.95	7	3
39	462.5	4.03	6	3
40	439.5	3.40	6	3
41	463.5	3.95	7	3

	MW	cLogP	HBA	HBD
42	462.5	4.03	6	3
43	390.5	6.14	4	2
44	414.5	5.68	5	2
45	413.5	5.68	4	2
46	390.5	6.14	4	2
47	414.5	5.68	5	2
48	413.5	6.07	4	2
49	455.5	4.50	6	2
50	468.6	3.95	6	3
51	468.5	3.51	6	3
52	468.6	4.24	6	3
53	497.6	4.90	6	2
54	483.5	4.64	6	3
55	471.6	5.17	6	3
56	457.6	4.62	6	3
57	457.5	4.20	6	3
58	443.5	3.93	6	4
59	568.7	5.71	6	2

Lipinski's rules

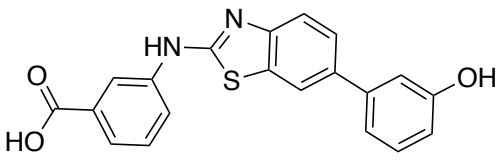
In terms of the Lipinski's rule of 5, compounds 25-59 are compliant in terms of molecular weight, and the number of hydrogen bond donors and acceptors. Lipohilicity, however is very high which will lead to high LLE and LE. Additionally, these compounds are planar due to many aromatic rings. Compounds 25-29 are not "drug-like", but instead were meant as tool compounds to test the Arginine hypothesis.

3.3.2.9 Series conclusion

The compounds were designed to be PI3Kα inhibitors able to interact with Arg770, however, upon biological evaluation, the compounds were found to be active against the PI3Kγ isoform, and generally inactive against the α, β and δ isoforms. After exploring differences in structure of head group and solvent exposed regions and finding no obvious trends that explain this PI3Kγ selectivity we looked to explain this selectivity by looking to the aryl-aminobenothiazole central scaffold that is common to all ana-

logues. The aryl ring of the aryl-aminobenothiazole central scaffold is hypothesised to have a steric clash with a serine residue of the α, β and δ isoforms, where is is occluded in PI3Kγ since this residue is an alanine residue (Ala885). This steric hinderence pushes the hinge binding motif out of the binding pocket, making the hydrgen bonding with the hinge valine residue less favourable. Thus selectivity towards PI3Kγ is hypothesised to be achieved due to lack of activity towards the α, β and δ isoforms as opposed to increased activity towards PI3Kγ.

In terms of selectivity, compound 28 (Figure 167) has the best profile, with a pIC_{50} of 7.0 and 251 fold selectivity over PI3Kα, 316-fold over PI3Kβ, and 63 fold over PI3Kδ.



pIC50 PI3Kγ = 7.0
α/γ = 251
β/γ = 316
γ//γ = 63
MW = 362.4
cLogP = 5.54
HBA = 4
HBD = 3

Figure 167. Structure and profile of compound 28, a potent and selective PI3Kγ inhibitor.

3.3.2.10 Synergy with Ceritinib

In Chapter 2, the observed synergic effects between ceritinib and the pan PI3K inhibitor pictilisib were discussed. Here compound 28 was tested in combination with ceritinib.

In vitro evaluation by MTT assasy of Compound 28 against the ALK- and ALK+ cell lines showed that Compound 28 had a GI_{50} of 556.3 μM ± 0.34 against the ALK- cell line and had a GI_{50} of 135.7 μM ± 0.13 against the ALK+ cell line. The dose response curves for Compound 28 and its combination with ceritinib are shown in Figure 168.

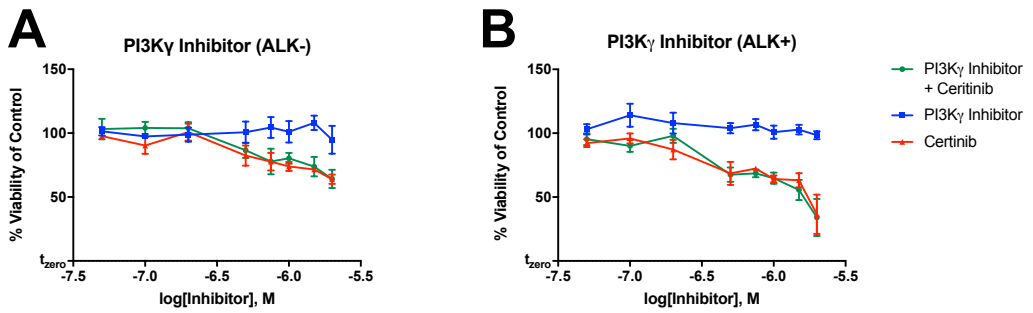


Figure 168. The Dose-response curves for ceritinib, Compound 28 and their combination against the ALK- cell line (A) and ALK+ cell line (B). Points are given as the mean ± the standard error of the mean (minimum 3 internal replicates). The dotted line shows the T_{zero} value (0% growth), and points below this line may indicate that an agent is cytotoxic. Growth is represented as percentage viability of the control, which has been normalised to 100%, where 0% is the T_{zero}.

In terms of evaluating synergy for the combination, the Webb method (Figure 169) indicated that there was no statistical significance between the expected and observed effects.

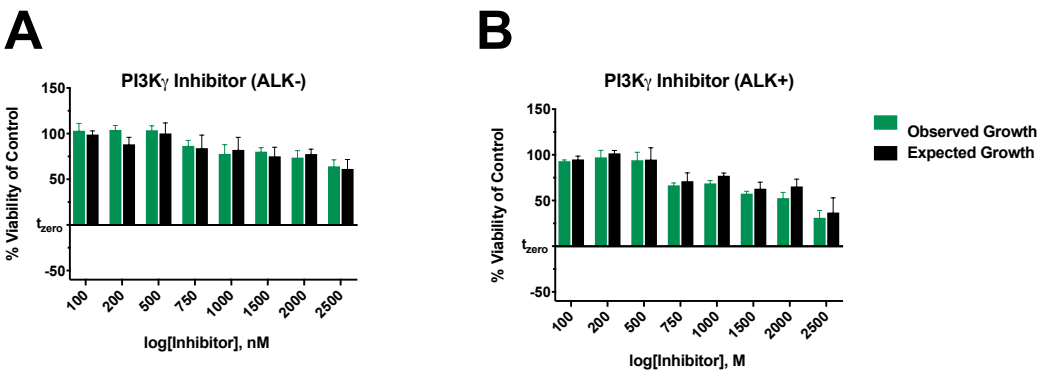


*Figure 169. Combination assay data of ceritinib and Compound 28 against the ALK- cell line (A) and ALK+ cell line (B), analysed by the Webb fractional product method, comparing the expected (additive) effect against the observed effect. Where the observed % viability is less than the expected, synergy can be assumed. Statistical significance has been determined by calculation of the p-value using t-tests where: *** $P \leq 0.001$, ** $P \leq 0.01$, * $P \leq 0.05$, ns $P > 0.05$. Error bars shown represent the standard error of the mean.*

Comparing Compound 28's synergy to the levels of synergy observed when combining ceritinib with pictilisib it is clear that pictilisib exhibits more synergy with Cer-

itinib than compound 28.

3.3.3 Iteration 2 PI3K α inhibition

3.3.3.1 Inhibitor design

From the previous section a logical path is to replace the aryl group of the aryl-aminobenothiazole central scaffold. We opted to do so with urea functionality (Figure 170). Additionally we needed to induce a conformation that directs the inhibitor away from the serine residue in PI3Kα. In oder to introduce this conformation we decided to use a proline moiety, as it is well known for introducing twists. Additionally, as opposed to targeting Arg770 for PI3Kα, we decided to target Gln859, another non-conserved residue of PI3Kα.

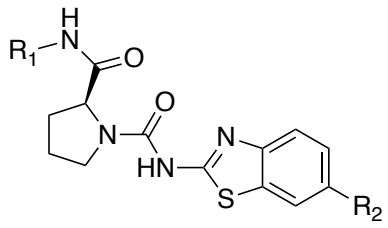
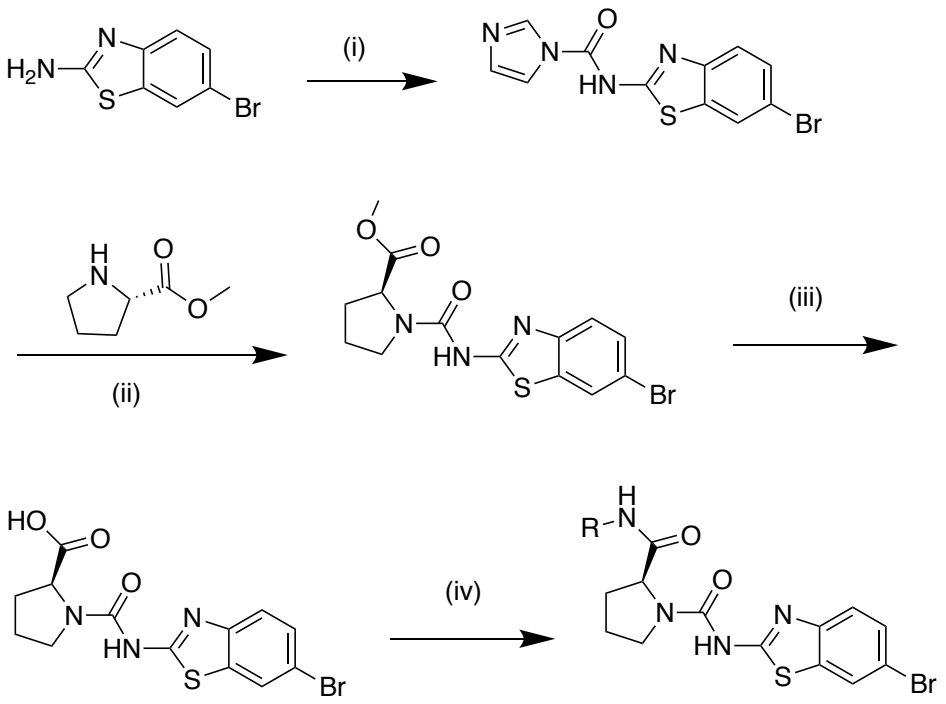


Figure 170. Proposed structures to target the non-conserved Gln859 residue of PI3Kα.

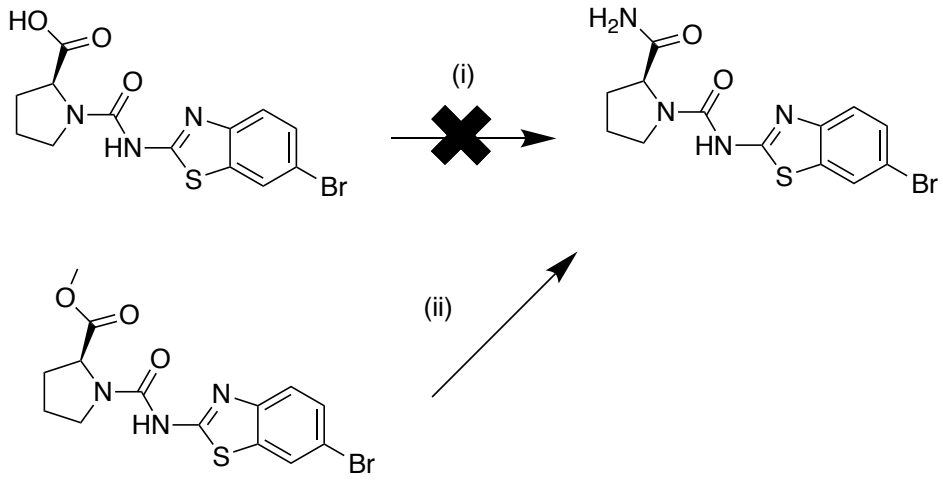
3.3.3.2 Synthesis

We began the synthesis of our inhibitors with 6-bromobenzo[d]thiazol-2-amine (Scheme 26), where formation of the urea was achieved by reacting the aniline nitrogen with carbonyldiimidazole (CDI) in DMF to form an imidazole carboxamide intermediate, which was easily isolated by filtration. The intermediate was then reacted with the methyl ester of proline, displacing imidazole. The methyl ester was then hydrolysed to the carboxylic acid using LiOH. Following hydrolysis, amide coupling with a range or amines was achieved using HATU in DMF, using DIPEA as the base.



Scheme 26. Reagents and Conditions: (i) 6-bromobenzo[d]thiazol-2-amine (1.0 eq.), CDI (4.0 eq.),, DMF r.t., 1 h, Yield 95%; (ii) Carboxamide intermediate (1.0 eq.), Proline methyl ester (1.0 eq.), NEt3 (3.0 eq.), DMF, r.t. overnight, Yield 93%; (iii) Ester (1.0 eq.), LiOH (3.0 eq.), THF:H_2O 1:1, r.t., overnight, Yield 96%; (iv) Carboxylic acid (1.0 eq.), Amines (3.0 -10.0 eq.), HATU (1.2 eq.), DIPEA (3.0 eq.), DMF, r.t. overnight, Yields 72 - 83%.

Alernatively, as opposed to forming amides from the carboxyllic acid, we formed the carboxamide, by performing an aminolysis reaction from the methyl ester (Scheme 27). This method was chosen to form the carboxamide since we were unable to form the caboxamide through amide coupling with various sources of ammonia.

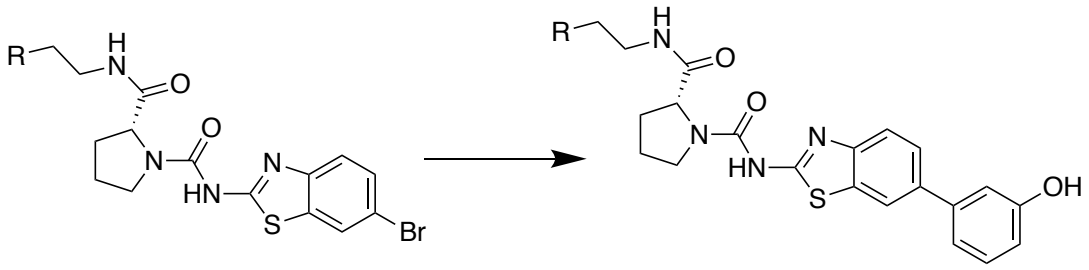


Scheme 27. Reagents and conditions: (i) Methanolic Ammonia (7N, 10.0 eq.) or ammonium hydroxide (excess), HATU (1.2 eq.), DIPEA (3.0 eq.), DMF, r.t. overnight.; (ii) ammonium hydroxide:THF (1:1), 3 h. Yield 83%.

Following purification of the amides or carboxamide, we intended to introduce the activity pocket group using a Suzuki reaction, with the same conditions that we had previously employed in the previous section ($Pd(PPh_3)_2Cl_2$ as the catalyst, Na_2CO_3 as the base, ethanol:H_2O (3:1) as the solvent, and heating at 120 °C under microwave radiation for 30 mins). Unfortunately, these conditions (Table 12, condition set 1) led to decomposition of the urea, potentially by formation of ethoxide, then nucleophilic attack by the ethoxide into the urea. The reaction was repeated replacing the ethanol with THF (Table 12, condition set 2), however we still observed decomposition of the urea, but we were able to isolate product, although in a low yield, 15%. Hypothesising that carbonate base may be the issue in generating anions that can attack the urea, we decided to use potassium acetate as a replacement, using standard Suzuki reaction conditions (Table 12, condition set 3) using $Pd(dppf)_2Cl_2$. Unfortunately we still saw decomposition of the urea and were unable to isolate any product.

At this point we had a suspicion that the urea may be undergoing a thermal decompostion and decided to attempt literature conditions for room temperature Suzuki reactions (Table 12, conditions 4 and 5). Unfortunately these were unsuccesful and no product was isolated.

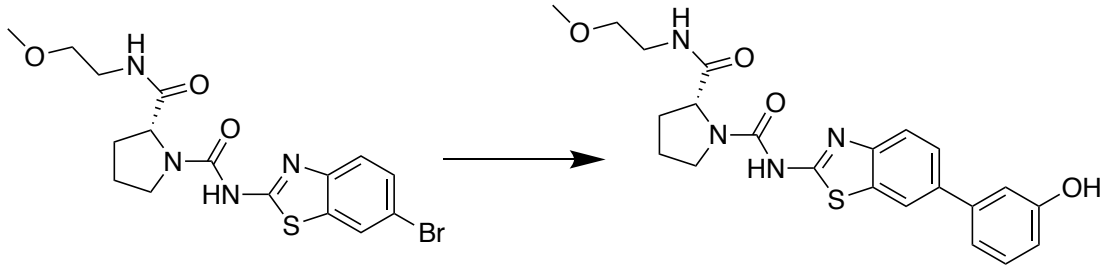
Table 12. Suzuki Reaction. The catalyst was used at 0.1 eq., the base at 3.0 eq., and the boronic acid at 1.5 eq.



	Catalyst	Base	R	Solvent	Conditions	Yield
1.	$Pd(PPh_3)_2Cl_2$	Na_2CO_3	OMe	EtOH:H_2O (3:1)	120 °C (mw), 30 min	-
2	$Pd(PPh_3)_2Cl_2$	Na_2CO_3	$N(Me)_2$	THF:H_2O (3:1)	120 °C (mw), 30 min	15 %
3	$Pd(dppf)_2Cl_2$	KOAc	$N(Me)_2$	H_2O:Dioxane (2:1)	120 °C (mw), 15 min	-
4	$Pd(OAc)_2$	Urea, K_2CO_3	$N(Me)_2$	^{i}PrOH:H_2O (1:1)	r.t., overnight	-
5	Pd/C	Na_2CO_3	$N(Me)_2$	EtOH:H_2O (1:1)	r.t., overnight	-

With another suspicion that the Pd catalysts may be chelating to the urea and proline carbonyls we decided to attempt Suzuki reactions in the presence of phosphine ligands. We tried a range of phosphine ligands in parallel, Table 13, however unfortunately, none of the conditions yielded any product.

Table 13. Suzuki Reaction. The catalyst was used at 0.1 eq., the base at 3.0 eq., and the boronic acid at 1.1 eq. Ligands shown in figure 145.



	Catalyst	Base	Ligands	Solvent	Conditions	Yield
6	Pd(OAc)2	Na_2CO_3	CyJohnPhos	H_2O:Dioxane (1:1)	120 °C (mw), 15 min	-
7	Pd(OAc)2	Na_2CO_3	JohnPhos	H_2O:Dioxane (1:1)	120 °C (mw), 15 min	-
8	$Pd(OAc)_2$	Na_2CO_3	XantPhos	H_2O:Dioxane (1:1)	120 °C (mw), 15 min	-
9	$Pd(OAc)_2$	Na_2CO_3	Tri-o-tol-Phos	H_2O:Dioxane (1:1)	120 °C (mw), 15 min	-
10	$Pd(OAc)_2$	Na_2CO_3	DavePhos	H_2O:Dioxane (1:1)	120 °C (mw), 15 min	-
11	$Pd(OAc)_2$	Na_2CO_3	XPhos	H_2O:Dioxane (1:1)	120 °C (mw), 15 min	-
12	$Pd(OAc)_2$	Na_2CO_3	S-Phos	H_2O:Dioxane (1:1)	120 °C (mw), 15 min	-

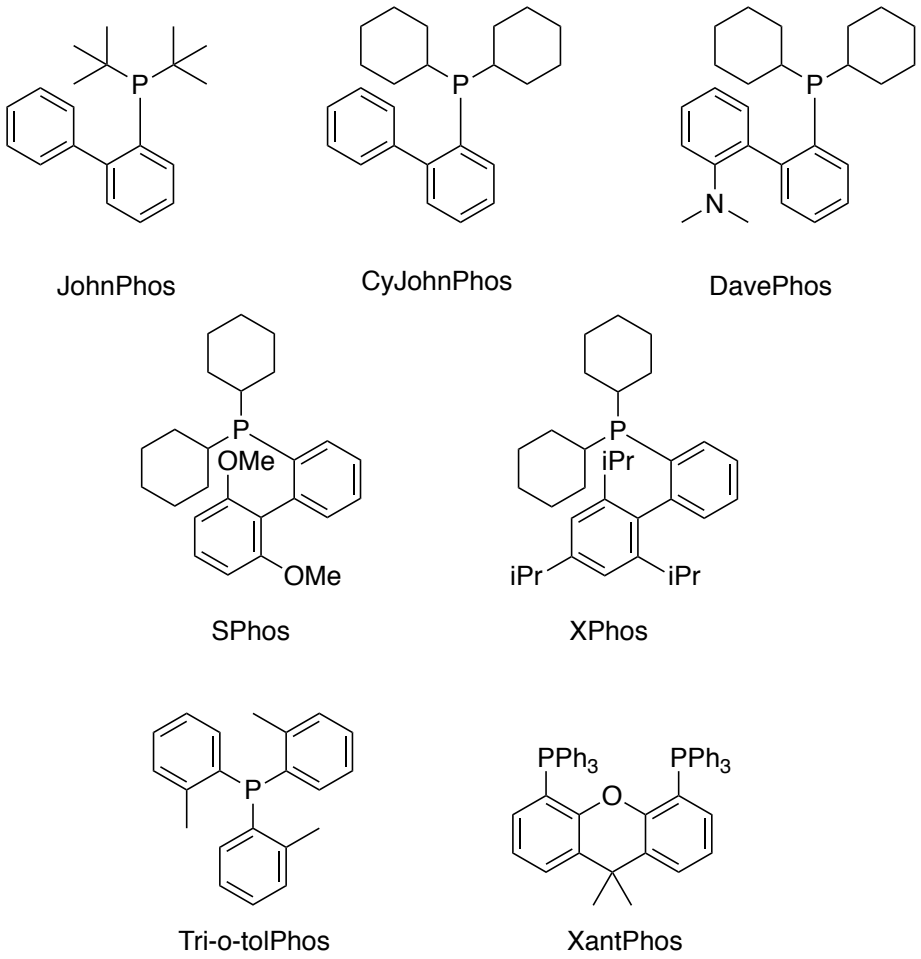
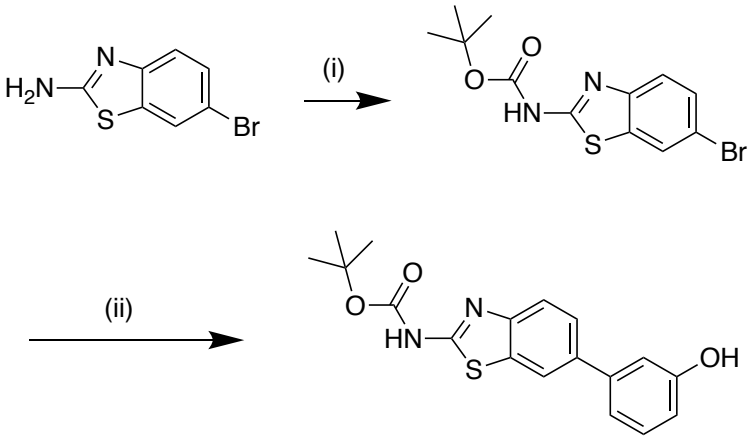


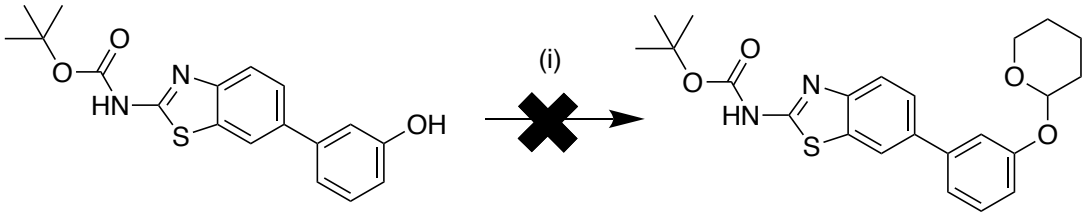
Figure 171. Phosphine ligands used for Suzuki screen, Table 13.

With the poor yield and lack of success with the Suzuki reaction we decided to rearrange the order of the steps of the synthesis starting with the Suzuki reaction first, so as to not have to do the Suzuki reaction in the presence of the chelating urea. This was achieved by starting with 6-bromobenzo[d]thiazol-2-amine and protecting the nitrogen with a Boc protecting group (Scheme 28). The Suzuki reaction was then performed, using $Pd(PPh_3)_2Cl_2$ as the catalyst, Na_2CO_3 as the base, THF:H_2O (3:1) as the solvent at reflux so as to allow for scale up. Additionally, we used the phenol boronic acid due to it being significantly less expensive than the pyridine boronic acid.



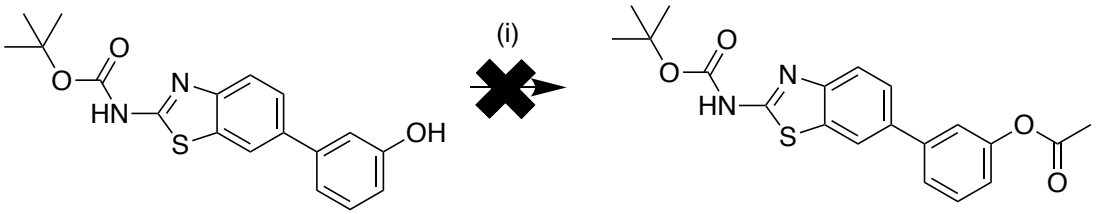
Scheme 28. Reagents and Conditions: (i) 6-bromobenzo[d]thiazol-2-amine (1.0 eq.), Boc_2O (1.2 eq.), NEt_3 (3.0 eq.), DMAP (0.1 eq.), CH_2Cl_2, r.t., 1 h, Yield 62%; (ii) 6-bromobenzo[d]thiazol-2-yl)carbamate (1.0 eq.), (3-hydroxyphenyl)boronic acid (2.0 eq.), Na_2CO_3 (3.0 eq.), $Pd(PPh_3)_2Cl_2$ (0.05 eq.), reflux, overnight, Yield 67%.

Following the Suzuki reaction, we set out to protect the phenol group as we suspected that during formation of the urea, due to the acidity of the phenol group, a carbonate could be formed. We first attempted protection of the phenol with a tetrahydropyran (THP) protecting group (Scheme 29), although, even with vast excess of 3,4-dihydropyran, we could not get the reaction to proceed.



Scheme 29. Reagents and conditions: (i) Phenol (1.0 eq.), 3,4-Dihydropyran (1.0 - 10 eq.), HCl in dioxane (cat.), CH_2Cl_2, r.t. and reflux overnight.

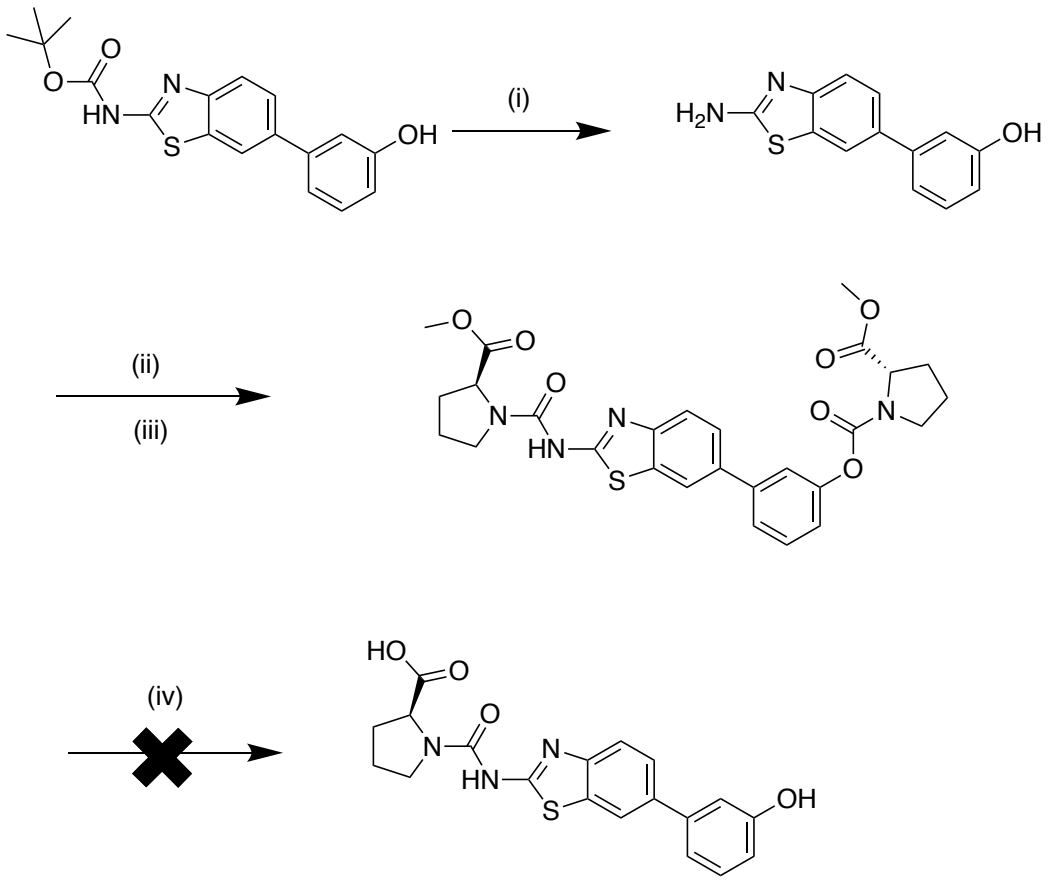
Failing protection with a THP group, we decided to try to protect the phenol group with the more reactive acetyl chloride, to protect the phenol with an acyl group (Scheme 30). However, again protection of the phenol was unsuccessful.



Scheme 30. Reagents and conditions: Phenol (1.0 eq.), Acetyl chloride (1.2 - 5.0 eq), K_2CO_3 (1.1 eq.), CH_3CN, r.t. then reflux overnight.

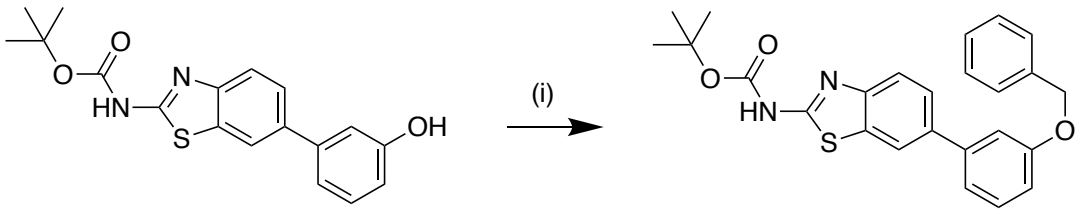
Following two unsuccessful protections of the phenol, we decided to try to form the urea (Scheme 31) since it appeared that the phenol group was not as reactive as we had predicted. This was done by first deprotecting the nitrogen Boc group using HCl, then obtaining the free base by washing with staturated sodium bicarbonate, and extracting the product in organic solvent. The amine was then reacted with CDI as before, and after the formation of the imidazole carboxamide intermediate, and excess CDI removed, proline methyl ester was added to the reaction mixture. Unfortunately, as we predicted originally, the phenol group reacted with the CDI, thus activating the phenol for carbamate formation with the proline methyl ester.

Suspecting that the urea is much more stable than a carbamate, and that a carbamate could be hydrolysed using LiOH and a urea could not, we set out to hydrolyse the carbamate. Unfortunately, the carbamate did not hydrolyse, even at high temperatures and we were therefore unable to obtain the desired product.



Scheme 31. Reagents and Condidtions: (i) Boc Amine (1.0 eq.), TFA:CH_2Cl_2 (1:1) then $NaHCO_3$ (aq); (ii) Aminobenzothiazole (1.0 eq.), CDI (4.0 eq.), DMF r.t., 1 h, then Proline methyl ester (1.0 eq.), $NaHCO_3$ (3.0 eq.), DMF, r.t. overnight; (iii) Ester (1.0 eq.), LiOH (10.0 eq.), THF:H_2O 1:1, r.t., overnight then reflux overnight.

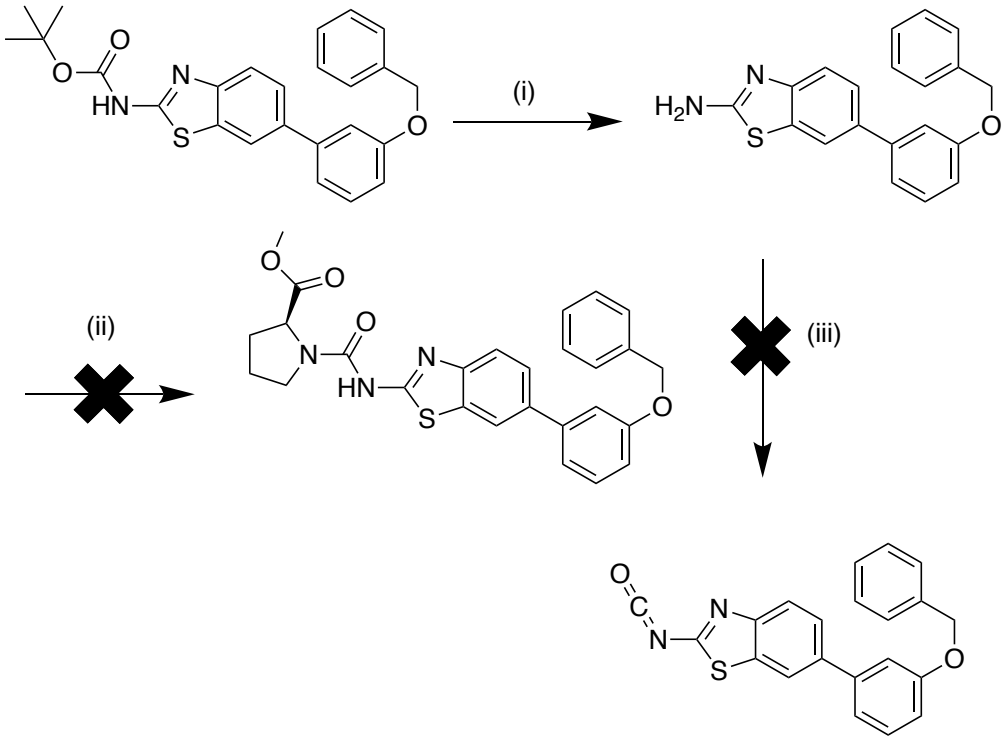
Due to the formation of the carbamate, we decided to try once again to protect the phenol group. At this point we decided to attempt to protect the phenol with a benzyl group. This reaction was sucessful, the product formed in excellent yield, and was achieved by reacting the phenol with benzyl bromide (Scheme 32).



Scheme 32. Reagents and Conditions: Phenol (1.0 eq.), Benzylbromide (1.2 eq.), $Cs2CO_3$ (1.0 eq), N_2, DMF, r.t. 1 h. Yield 92%.

Following the protection of the phenol, we then deprotected the boc group to expose the amine, using TFA (Scheme 33). Then, following the same procedure as before

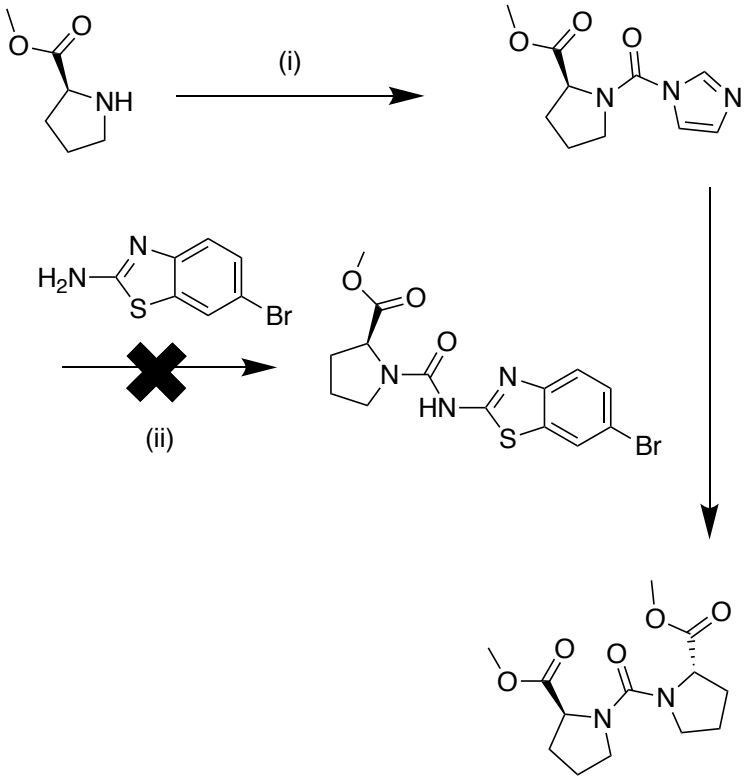
we attempted to form the urea. Unfortunately, after following the same procedure we were unable to detect or isolate any product, or even the imidazole carboxamide intermediate (or potentially, the isocyanate). We suspect that introduction of the protected phenol altered the electronics of the aminobenzothiazole ring, reducing the nucleophilicity of the amine. With reduced nucleophilicity we thought to use a more reactive reagent, such as triphosgene, which forms phosgene *in situ*, to form the urea. Unfortunately, even after trying with an excess of triphosgene we were unable to obtain the product or the isocyanate. Although we did observe dimerisation of the aminobenzothiazole, suggesting that the isocyanate forms slowly and since it is very electrophillic, is rapidly attacked by other molecules of the aminobenzothiazole is the reaction mixture.



Scheme 33. Reagents and conditions(i) Boc Amine (1.0 eq.), TFA:CH_2Cl_2 (1:1) then $NaHCO_3$ (aq); (ii) Aminobenzothiazole (1.0 eq.), CDI (4.0 eq.), DMF r.t., 1 h, then Proline methyl ester (1.0 eq.), $NaHCO_3$ (3.0 eq.), DMF, r.t. overnight; (iii) Aminobenzothiazole (1.0 eq.), triphosgene (0.3 - 1 eq.) $NaHCO_3$ (sat aq):CH_2Cl_2 (1:1), N_2, r.t., overnight.

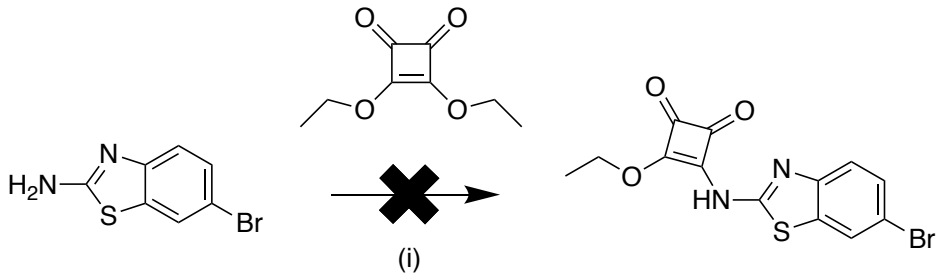
We then tried to form the urea by forming the imidazole carboxamide intermediate on the proline first (Scheme 34). By following the same procedure as before we were unable to isolate any product. We believe that this is due to the reactivity of the

proline nitrogen. The nitrogen of the proline is much more reactive than the nitrogen of the aminobenzothiazole, which allows for the proline nitrogen to attack the imidazole carboxamide intermediate forming the dimer. This occured even when using a vast excess of CDI.



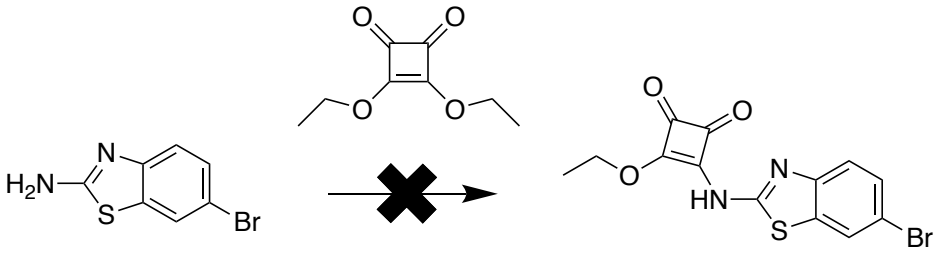
Scheme 34. Reagents and Conditions: (i) Proline methyl ester (1.0 eq.), CDI (1.0 - 4.0 eq.), DMF r.t., 1 h, ; (ii) Carboxamide intermediate (1.0 eq.), 6-bromobenzo[d]thiazol-2-amine (1.0 eq.), NEt3 (3.0 eq.), DMF, r.t. overnight.

Due to issues forming the urea, we decided to try to replace the urea moiety with a urea bioisostere, a squaramide (Scheme 35). Unfortunately, even after trying various condition sets (Table 14) we were unable to displace the ethoxy group with the amino benzothiazole nitrogen, due to its poor nucleophilicity.



Scheme 35. Reagents and Conditions: Table 14

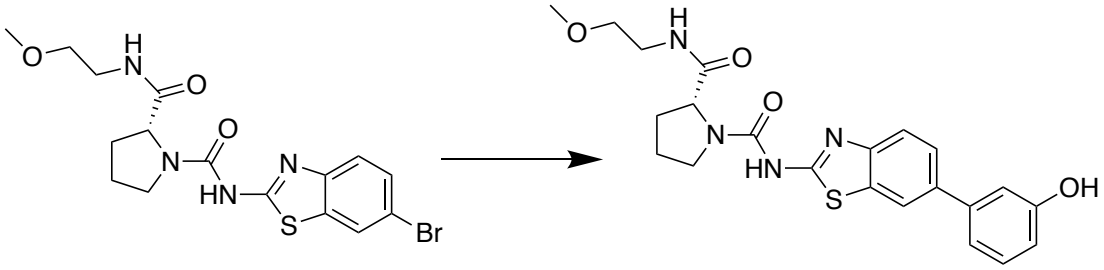
Table 14. Suzuki Reaction. The catalyst was used at 0.1 eq., the base at 3.0 eq., and the boronic acid at 1.5 eq.



	Acid/Base	Squaric ester	Solvent	Conditions	Yield
1.	DIPEA, 3.0 eq.	1.3 - 2.6 eq.	MeOH	Room Temperature	-
2	DIPEA, 3.0 eq.	1.3 - 2.6 eq.	MeOH	Reflux	-
3	DIPEA, 3.0 eq.	1.3 - 2.6 eq.	EtOH	Room Temperature	-
4	DIPEA, 3.0 eq.	1.3 - 2.6 eq.	EtOH	Reflux	-
5	-	1.1 eq.	^{i}PrOH	120 °C (mw), 30 min	-
6	DIPEA, 3.0 eq.	1.1 eq.	^{i}PrOH	120 °C (mw), 30 min	-
7	-	1.1 eq.	EtOH	120 °C (mw), 30 min	-
8	DIPEA, 3.0 eq.	1.1 eq.	EtOH	120 °C (mw), 30 min	-
9	HCl in Dioxane cat.	1.1 eq.	EtOH	120 °C (mw), 30 min	-
10	-	1.1 eq.	MeOH	120 °C (mw), 30 min	-
11	DIPEA, 3.0 eq.	1.1 eq.	MeOH	120 °C (mw), 30 min	-
12	-	1.0	neat	120 °C (mw), 30 min	-

Due to time restrictions on the project we were forced to return to the Suzuki reaction and accept poor yields. We once again ran a Suzuki reaction screen to determine which catalyst was most effective, however this time yields are approximate and were determined solely by LCMS, Table 15. Unfortunately, although yields looked high by LCMS, isolated yields of final compounds for biological evaluation were still very low (6 -22%). This is likely due to the difficulties purifying highly polar compounds by normal phase chromatography, or due to the poor solubility of the ureas.

Table 15. Suzuki Conditions: Boronic acid at 1.2 eq.

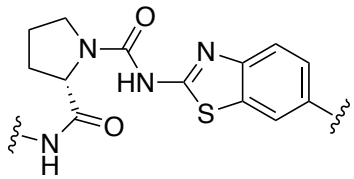


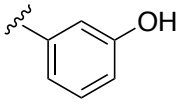
	Catalyst	Base	Solvent	Conditions	% Conv.
1.	Pd(PPh3)4	Na_2CO_3	THF:H_2O (3:1)	120 °C (mw), 15 min	21%
2	Pd2(dba)3	Na_2CO_3	THF:H_2O (3:1)	120 °C (mw), 15 min	5%
3	Pd(dppf)2Cl_2	Na_2CO_3	THF:H_2O (3:1)	120 °C (mw), 15 min	57%
4	Pd(OAc)2	Na_2CO_3	THF:H_2O (3:1)	120 °C (mw), 15 min	18%
5	Pd(PPh3)2Cl_2	Na_2CO_3	THF:H_2O (3:1)	120 °C (mw), 15 min	75%

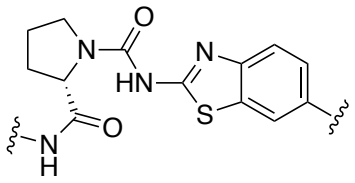
3.3.3.3 Biological Results

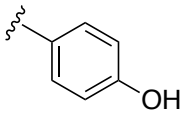
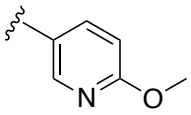
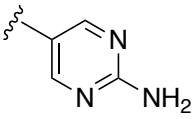
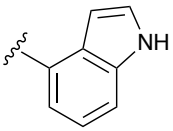
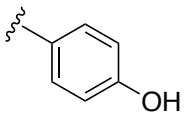
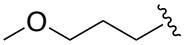
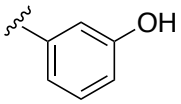
After synthesis of the compounds, they were tested by GlaxoSmithKline in Stevenage UK by the same assay as discussed above. The results are presented in Table 16, where the potency is expressed at the pIC_{50} (pIC_{50} = - log IC_{50}).

Table 16. Biological Evaluation of PI3K compounds. Potency against the different PI3K isoforms is given as pIC_{50} values (n = 1). The potency threshold for the PI3K assay is ~ pIC_{50} = 9 due to substrate concentration.



	R_1	R_2	PI3K Isoform Potency (pIC_{50})			
			γ	α	β	δ
60.			5.1	4.5	4.5	4.5



	R_1	R_2	PI3K Isoform Potency (pIC_{50})			
			γ	α	β	δ
61.			5.0	4.5	4.5	4.5
62.			5.8	4.9	4.5	4.5
63.			4.9	4.5	4.5	4.6
64			4.5	4.5	4.5	4.5
65.			5.4	6.0	4.5	4.6
66.			4.7	4.5	4.5	5.1

From the results above it can be seen that the compounds do not exhibit the same level of activity as previously synthesised analogues. Compounds 60- 63 show low selectivity over PI3Kγ similar to the previous analogues. Compound 64 is effectively inactive since 4.5 is the cut-off of the assay. Compound 65, in addition to showing low activity towards PI3Kγ, shows modest activity towards PI3Kα. The activity towards PI3Kα is likely due to an interaction of the carboxamide with Gln859. Compound 66, in addition to showing low activity towards PI3Kγ, shows modest activity towards PI3Kδ. These results are consistent with the observations made by Novartis on their benzothazole series (page 96).

3.3.3.4 Synergy with Ceritinib

In Chapter 2, the observed synergic effects between ceritinib and the pan PI3K inhibitor pictilisib were discussed. At the time of writing we did not have a selective PI3Kα inhibitor from our laboratory to test, however for completion, we purchased alpelisib, a selective PI3Kα inhibitor for *in vitro* evaluation in combination with ceritinib. alpelisib: PI3Kα IC_{50} = 0.005 µM, PI3Kβ IC_{50} = 1.2 µM, PI3Kγ IC_{50} = 0.25 µM, PI3Kδ IC_{50} = 0.29 µM

In vitro evaluation by MTT assay of alpelisib against the ALK- and ALK+ cell lines showed that alpelisib had a GI_{50} of 36.7 µM ± 0.06 against the ALK- cell line and had a GI_{50} of 10.7 µM ± 0.27 against the ALK+ cell line. The dose response curves for alpelisib and its combination with ceritinib are shown in Figure 172.

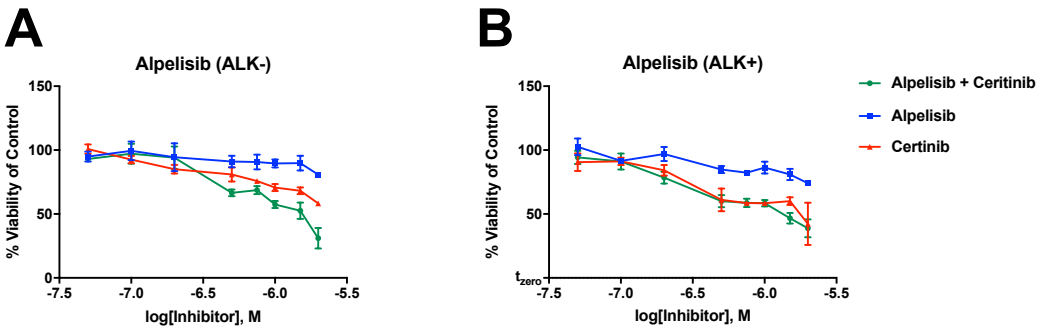


Figure 172. The Dose-response curves for ceritinib, alpelisib and their combination against the ALK- cell line (A) and ALK+ cell line (B). Points are given as the mean ± the standard error of the mean. Points are given as the mean ± the standard error of the mean (minimum 3 internal replicates). The dotted line shows the T_{zero} value (0% growth), and points below this line may indicate that an agent is cytotoxic. Growth is represented as percentage viability of the control, which has been normalised to 100%, where 0% is the T_{zero}.

In terms of evaluating synergy for the combination (Figure 173), the Webb method indicated that there was no statistical significance between the expected and ob-

served effects.

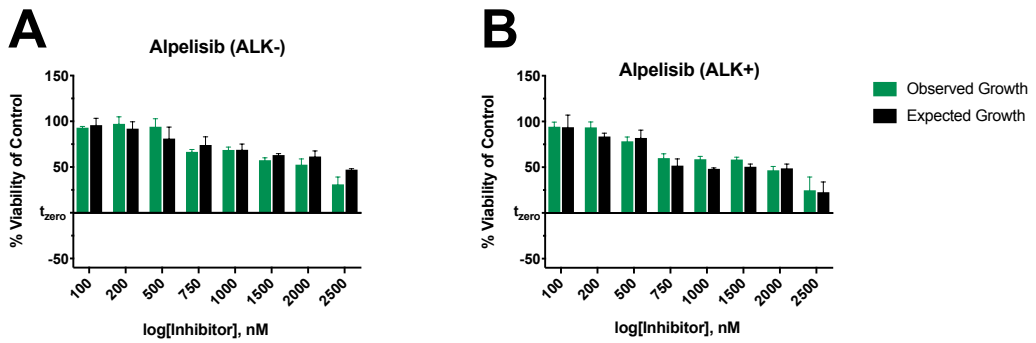


*Figure 173. Combination assay data of ceritinib and alpelisib against the ALK- cell line (A) and ALK+ cell line (B), analysed by the Webb fractional product method, comparing the expected (additive) effect against the observed effect. Where the observed % viability is less than the expected, synergy can be assumed. Statistical significance has been determined by calculation of the p-value using t-tests where: *** $P \leq 0.001$, ** $P \leq 0.01$, * $P \leq 0.05$, ns $P > 0.05$. Error bars shown represent the standard error of the mean.*

From this, we can see that a selective PI3K inhibitor does not lead to synergy with ceritinib.

3.4 Chapter Conclusion

In this chapter we have focused on PI3K inhibition. Initially, we used a tricyclic scaffold previously synthesised by the group and incorporated it into the solvent exposed region using pictilisib's thienopyrimidine core. The synthetic chemistry for these inhibitors was relatively straightforward and we were able to synthesise all compounds sucessfully. These compounds were then biologically evaluated at GSK and the series was found to be highly potent and selective towards PI3Kδ. The high level of PI3Kδ activity and selectivity is attributed to favourable interactions with the tryptophan shelf, comprised of Thr 750 and Trp 760, where the threonine is unique to PI3Kδ. Comparing the different features of the molecules revealed that there are 3 effects contributing to achieve the high level of δ-Selectivity: The indole group, the *cis*-fused tricycle, and methyl substitution on the tricycle. The PI3Kδ inhibitors generally complied with Lipinski's rules, although in general, they suffered high lipohilicity, which leads to a poor pridicted PK profile. Compound 3 proved useful as a tool for evaluating synergy with ceritinib, which showed only modest synergy at doses below 500 nM.

After developing the series of PI3Kδ inhibitors we then moved our focus towards the development of PI3Kα inhibitors. Developing a hypothesis that interacting with Arg 770, unique to PI3Kα, and identifying that the PI3Kδ series suffered from high lipophilicity, we set out to modify the tricyclic scaffold to act as the central scaffold, namely by introduction of a hinge binding oxygen and morphing of the triazole to an imidazole so as to position the synthetic handle at the correct angle to access the activity pocket. Reduction of the number of aromatic rings and Sp^2 carbons would have reduced the lipohilicity considerably. Additionally, molecular modelling showed that the *trans* fused scaffold, being more "flat" made the most favourable interaction with the hinge valine. Unfortunately, the synthetic chemistry prooved too challenging for the time frame and as such we moved our focus to a benzothiazole scaffold.

The benzothiazole scaffold proved easier to synthesise, and therefore we were able to readily synthesise an array of compounds that were designed to target Arg 770

through introduction of carboxylic acids and bioisosteres of carboxylic acids. The compounds were biologically evaluated at GSK and the results unexpectedly revealed that the series was very potent and selective towards PI3Kγ. Comparing features of the scaffold showed no general trends. However molecular modelling revealed that the aryl group of the aryl-aminobenzothiazole scaffold could be undergoing a steric clash with serine residues in the α, β, and δ isoforms. This steric clash does not occur in PI3Kγ since the serine residue is an alanine residue in PI3Kγ, Ala885. The physical properties of these compounds generally complied with Lipinski's rules, although they suffered terribly from high lipophilicy. Compound 28 proved a useful tool when evaluating synergy with ceritinib, revealing no synergic effects in combination with ceritinib.

Still on the hunt for a selective PI3Kα inhibitor, we looked to replace the aryl ring on the aminobenzothiazole with urea functionality. Additionally, intoduction of a proline, would introduce a twist, potentially allowing for interaction with Gln859, another PI3Kα non-conserved residue. Synthetically, installing activity pocket groups was challenging due to issues with the Suzuki reaction where the urea was undergoing decomposition and the catalyst was potentially chelating to the urea and proline carbonyls. 7 analogues were synthesised and ae currently being screened. In terms of assesing synergy with a slective PI3Kα inhibitor, we purchased alpelisib and tested this *in vitro* in combination with ceritinib, revealing no synergic effects.

At this point we have tested ceritinib in combination with selective inhibitors of the α, δ, and γ isoforms and have not observed the same level of synergy as we observed in combination with Pictilisb. Here we hypothesise two reasons why we think it may be that we have not seen increased synergic effects with a selective compound. Firstly, we have not tested a selective PI3Kβ inhibitor, and cannot rule this out as the isoform that may be giving rise to the synergy seen with pictilisib. Secondly, pictilisib is also weakly active against mTOR (IC_{50} = 580 nM). Both pictilisib and Compound 3 both share the same thienopyrimidine core. Addtionally, gedatolisib , a dual PI3K/mTOR inhibitor, also shares this core. These compounds all showwed a level of synergy in combination with pictilisib, suggesting that it may be possible that the observed synergy is from in-

hibition of mTOR.

Having identified that pictilisib is the best compound for combination with ceritinib, in the next chapter our focus will be to generate bifunctional prodrugs comprising of ceritinib and pictilisib.

4. Bifunctional Ligands.

4.1 Introduction

Most drugs are designed to act on a single target and with prolonged use, in the areas of cancer and infectious disease, resistance[17] occurs inevitably, reducing the efficacy of the drug. Most drugs target a single node ,which encourages resistance to rapidly develop in the form of single mutations or by transfer of resistant genes. Drug combinations have been shown to slow down this evolution of resistance as the drugs in combination simultaneously operate with different mechanisms of action thus reducing the probability of resistance mutations. It has also been shown that drug combinations exhibiting synergistic drug interactions, or drugs that increase sensitivity to another drug in the combination slow down resistance further.

Combining drugs into a single molecule has the potential to simultaneously deliver them to the target area as well as alter the pharmacokinetic and pharmacodynamics, potentially reducing toxicity effects, improving uptake, or even improving drug retention.

Bifunctional inhibitors can be split into two categories[160],[161]: (a) molecules with two or more drug molecules joined together by a linker that is either cleavable or non-cleavable or (b) molecules that contain the pharmacophores of different drugs. The advantage of these approaches comes from any observed synergistic effects from the pharmacologically active components. Additionally, as regulatory approval of combination becomes increasingly complex, one solution is to combine therapies into a single drug molecule.

Bivalent or bifunctional ligands can be used as prodrugs: A prodrug is defined as a compound that is pharmacologically inactive upon administration and after administration is metabolised or converted in the body into a pharmacologically active drug. Prodrugs are often used to improve the bioavailability of a drug, or even to improve how a drug selectively interacts with cells. This is particularly important for cancer therapy as the desire is to destroy cancer cells whilst ensuring healthy cells are not targeted. Additionally, prodrugs can be used as a slow-release drug delivery method.

Although bifunctional ligands are a relatively new field of study, there are many examples of bifunctional ligands in the literature. Below are some examples of bifunctional ligands developed for numerous diseases and conditions.

4.1.1 Linked Bifunctional Compounds

The following describes some linked bifunctional compounds currently being developed:

Jorg *et al* [162] have designed a dual action ligand incorporating ropinirole, a dopamine D_2 receptor agonist, as well as ZM 241385 an adenosine A_{2A} receptor antagonist (Figure 174). Additionally, they designed a series of integrated dual acting molecules that showed promising results for improved penetration of the blood brain barrier. These bifunctional drugs can potentially slow down the degeneration of dopaminergic neurons, delaying the progress of Parkinsons disease.

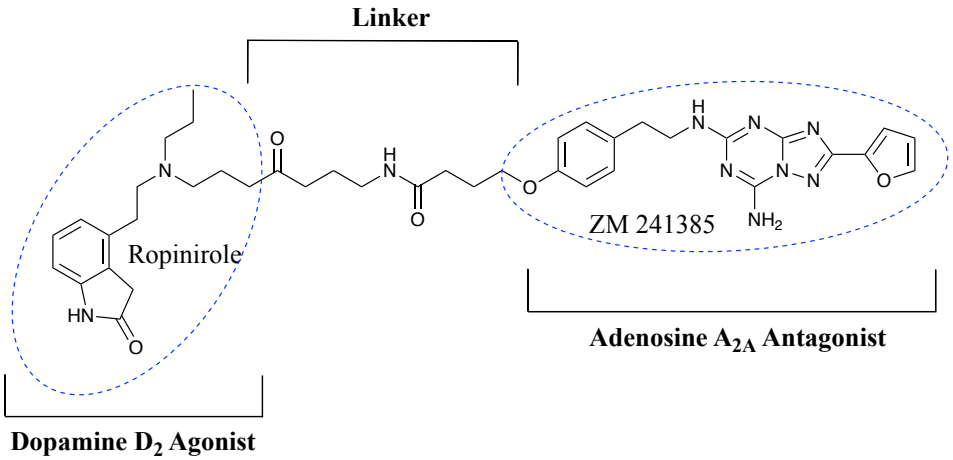


Figure 174. Comprised of ropinirole, a dopamine D_2 receptor agonist, as well as ZM 241385 an adenosine A_{2A} receptor antagonist.

Wang *et al* [163] have designed a bifunctional hybrid drug (Figure 175) that limits resistance by evading the action of the multiple antibiotic resistance pathways. They found that bacteria which evolved in the presence of the hybrid gained less resistance mutations than bacteria populations in eqimolar mixtures of the hybrid components.

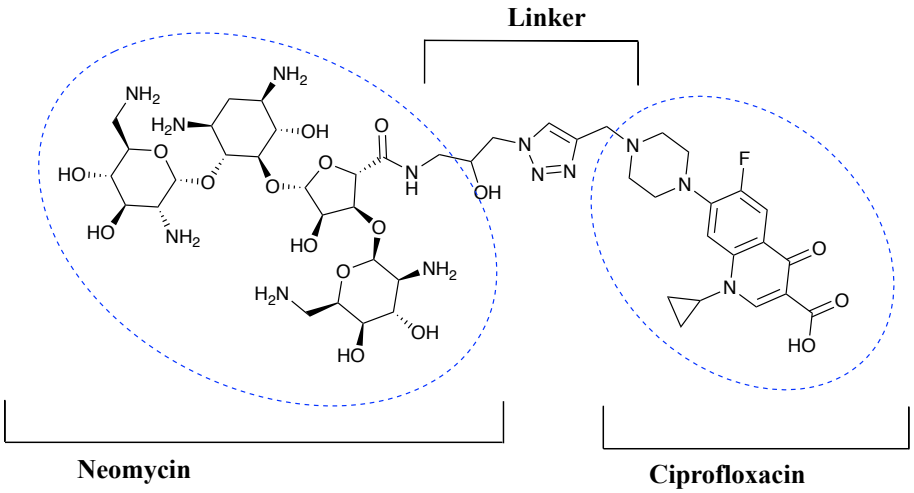


Figure 175. A bifunctional ligand comprised of ciprofloxacin and Neomycin B, antibacterial agents.

Batefenterol (Figure 176), is a muscarinic receptor antagonist, β2-receptor agonist possessing both muscarinic antagonist and β2-adrenoceptor agonist properties (MABA)[164],[165]. Clinical studies have shown that a combination of these two types of drugs provide enhanced efficacy over the individual components. This allows for lower dosing and thus fewer side effects.

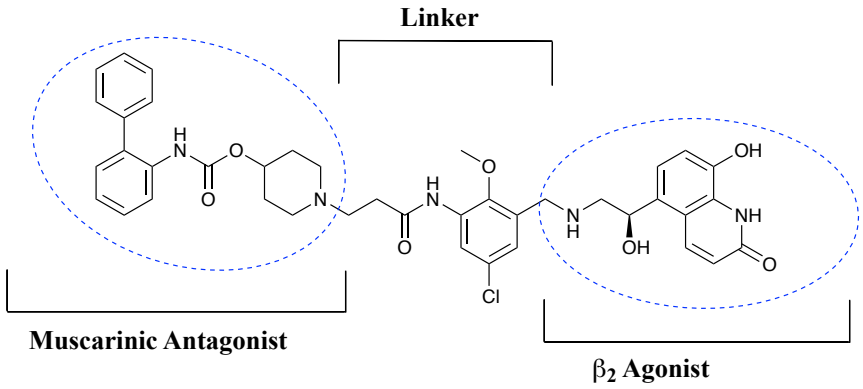


Figure 176. A bifunctional ligand comprised of a muscarinic antagonist and β2-adrenoceptor agonist, designed for the treatment of asthma or constructive obstructive pulmonary disease.

Chojnacki *et al* [166] have designed a bifunctional compound (Figure 177) as a potential neuroprotectant for Alzheimers disease. The compounds are comprised of curcumin as the "war-head", with the steroid, diosgenin, acting as a lipid membrane anchor.

The group found that these compounds revealed antioxidative and anti-oligomerization ability, which may be responsible for their protective activity. Additionally, they noticed that the linker length was related to the increase and decrease of protective activity.

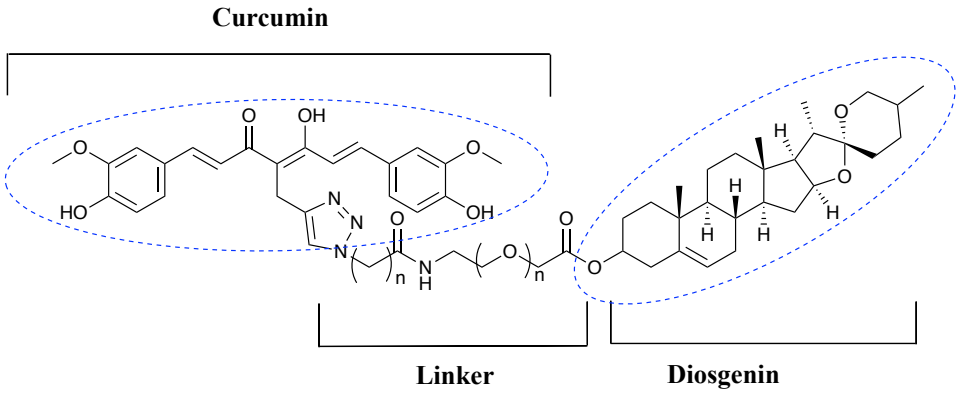


Figure 177. A bifunctional ligand comprised of curcumin and diosgenin for the treatment of Alzheimers.

All of the above compounds are linked together *via* a covalent linker. To date there have been no reports of a bifunctional ligand that is cleaved to release active payloads, although single drug prodrugs have made use of pH dependant release mechanisms. pH sensitive moieties are primarily found in the field of drug delivery or release, where common pH labile functional groups (Figure 178) that trigger the degradation or cleavage of biomaterials include: carbamates[167], guanidine[168], dialkyl and diaryldialkoxysilanes[169], orthoesters[170], acetals[171], aconityls[172], hydrazones[173], b-thiopropionates[174], phosphoramidates[175], imines[176],[177], trityls[178], vinyl ethers[179], and polyketals[180],[181].

With cleavable bifunctional ligands not having been explored before, this presented the opportunity to explore the possibility of linking drugs with appropriate synthetic handles. This will be the focus of this chapter.

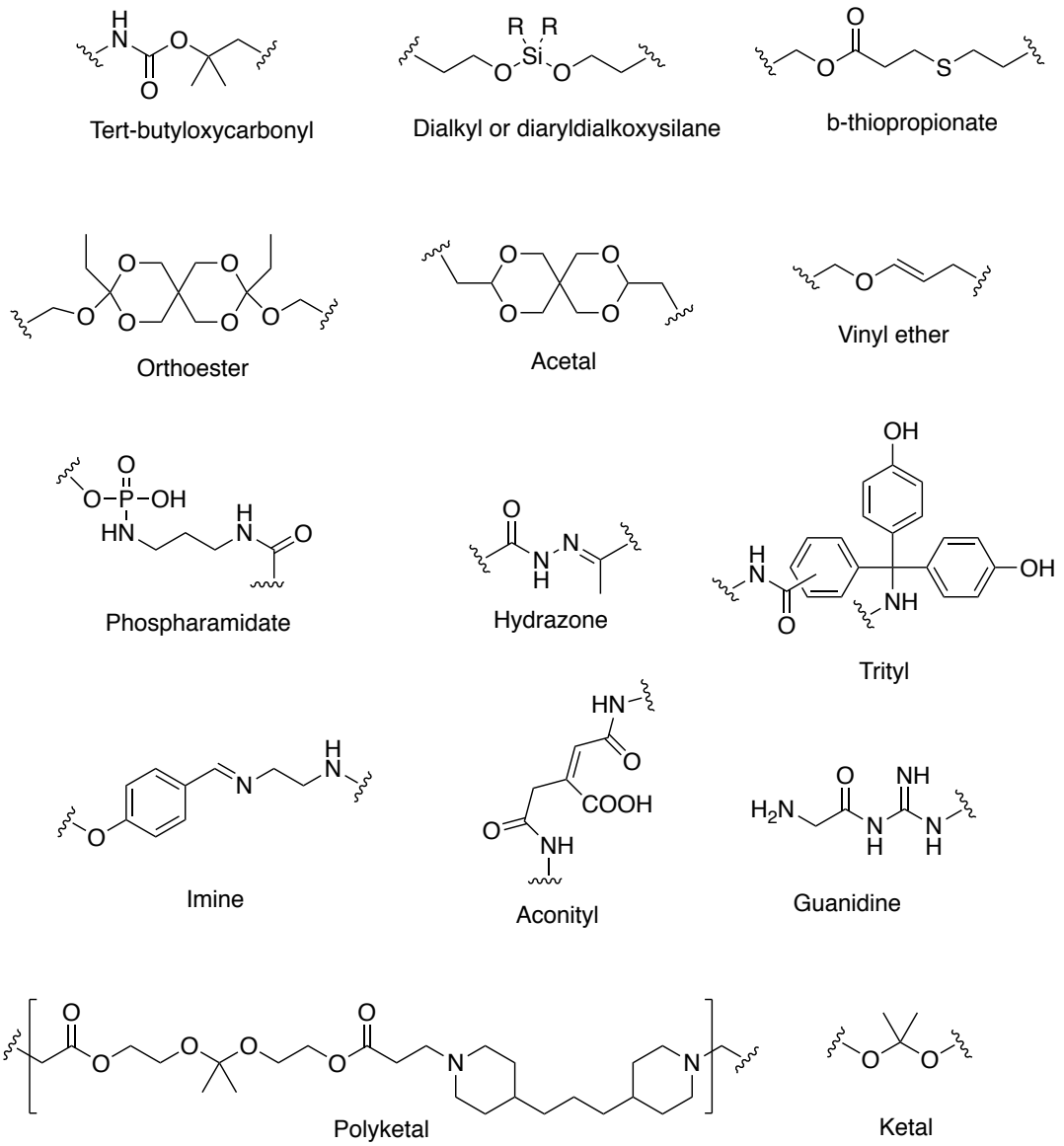


Figure 178. Examples of pH sensitive moieties.

4.2 Aims and Objectives

In Chapter I it was discussed that pictilisib and ceritinib exhibit severe side effects, and reduction of dose is highly desirable. Chapter II showed that pictilisib exhibits excellent synergy with ceritinib, where drug combination is a means of reducing dosage. Another strategy for lowering dosage is through drug delivery to the site of action, via controlled release i.e. in the form of a prodrug, thus the aim of the work in this chapter was to link these two inhibitors together to form a prodrug.

From the introduction to this chapter it can be seen that there are quite a range of bifunctional ligands that are joined by a linker, however in all cases this linker is covalent. At the time of writing there are no reported examples of a bifunctional compound, combining two inhibitors via a non-covalent, cleavable linker. A cleavable linker would function as a prodrug; a slow-release drug delivery system Additionally if a bifunctional ligand sporting a pH dependent cleavable linker was synthesised, this would introduce a tunable method for controlled release since it is well-known that cancer cells can have a range of pH states (5.7 - 7.8), mainly due to hypoxia[182][183].

In the next section the results of this endeavour will be discussed.

4.3 Results and Discussion

4.3.1 Prodrug Model Systems

4.3.1.1 Model Prodrug Design

The piperidine ring on ceritinib and the indazole of pictilisib were identified as appropriate synthetic handles (Figure 179).

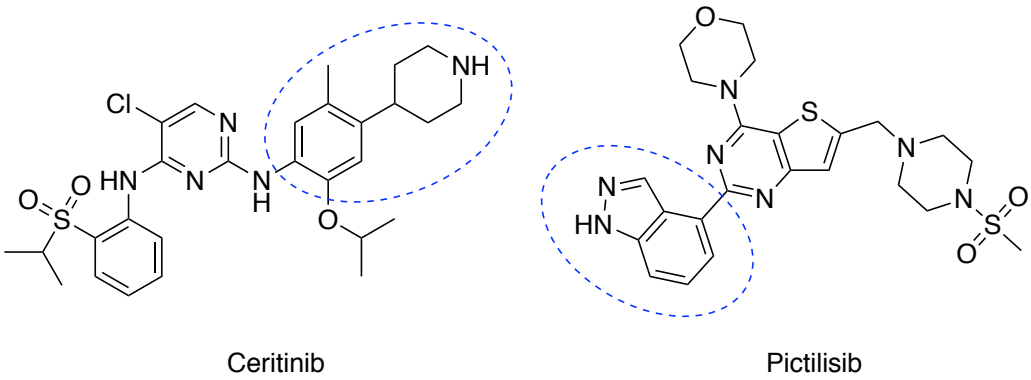


Figure 179. Ceritinib and pictilisib. The piperidine nitrogen of ceritinib was chosen as the synthetic handle for ceritinib and the indazole nitrogen of pictilisib was chosen as the synthetic handle of pictilisib.

A model system was designed in order to test the designed linker (Figure 180). Phenyl piperidine and bromo indazole were used as drug mimetics.

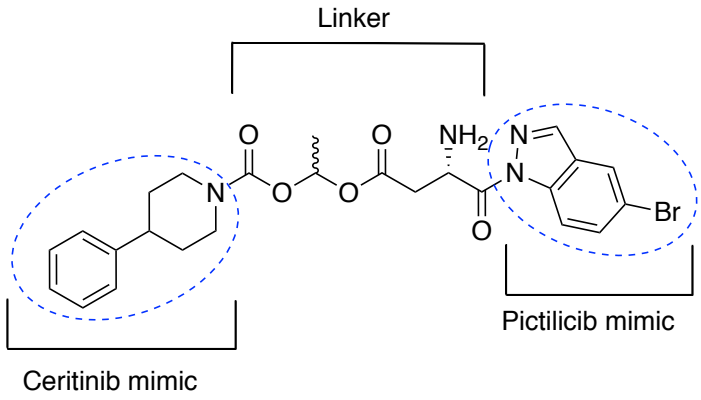


Figure 180. Model prodrug system using 4-phenyl piperidine as the ceritinib mimetic and 6-bromoindazole as the pictilisib mimetic. The linker comprises of an alpha amino amide formed from aspartic acid, and a carbonate pseudo acetal.

With the indazole as a superior leaving group than the piperidine, this was used to form an α-amino amide. The α-amino amide[184] was chosen with the hypothesis that

the amino group will either aid hydrolysis through anchimeric assistance via hydrogen bonding of the non-protected amine to water, or protect the amide from hydrolysis through protonation of the amine (pK_a ~ 7.08 - calculated in MarvinSketch[185]). This hypothesis forms the basis of the pH dependant linker (Figure 180). An aspartic acid analogue was chosen to form part of the linker due to the well-known cyclisation mechanism of amino acid cleavage, which would present itself following hydrolysis of the alpha amino amide, releasing pictilisib. If this cyclisation were to proceed after pictilisib release, it was hypothesised that there would be subsequent release of acetaldehyde and CO_2, with successive release of ceritinib. The proposed mechanism of release is illustrated in Figure 181.

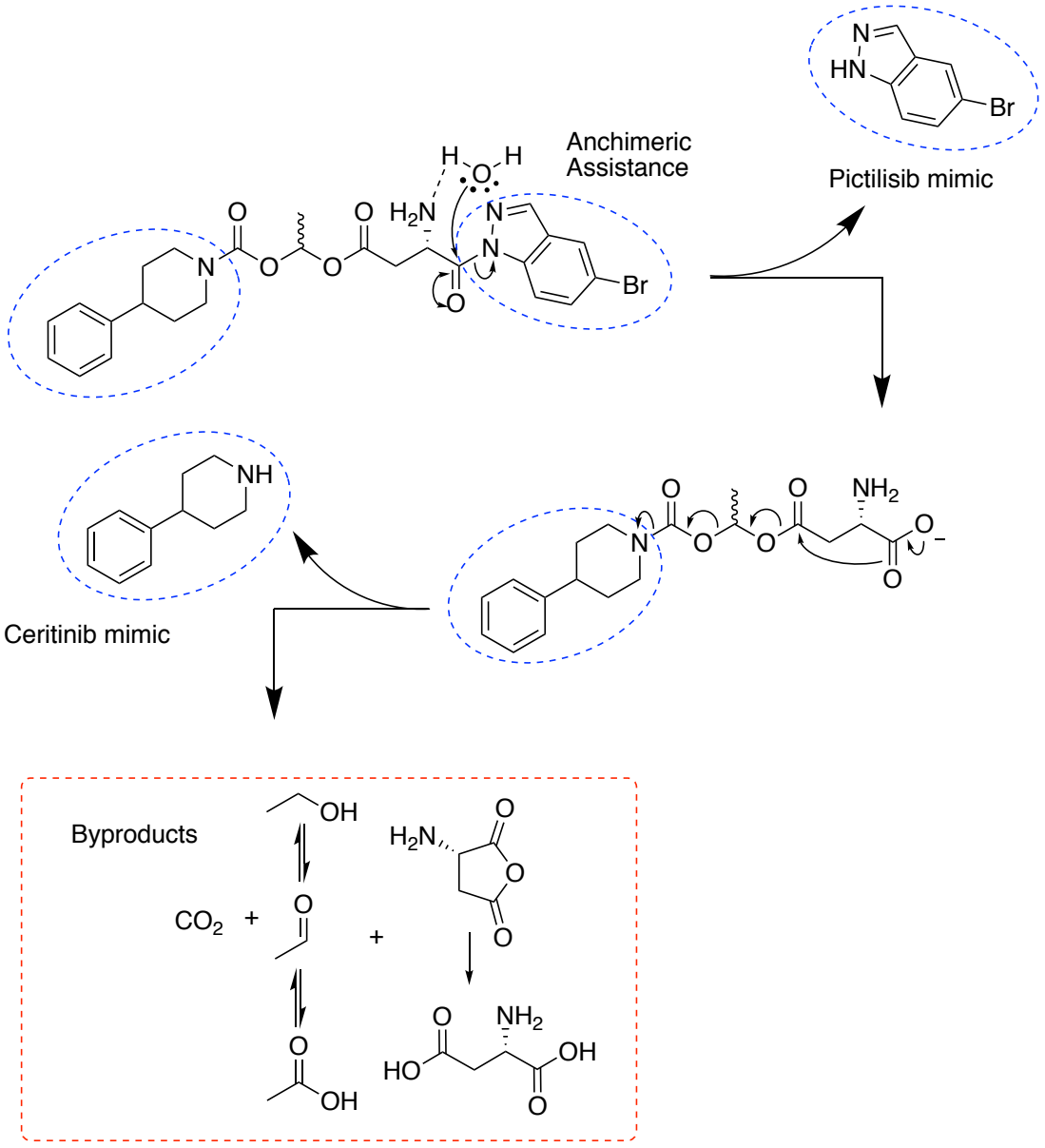
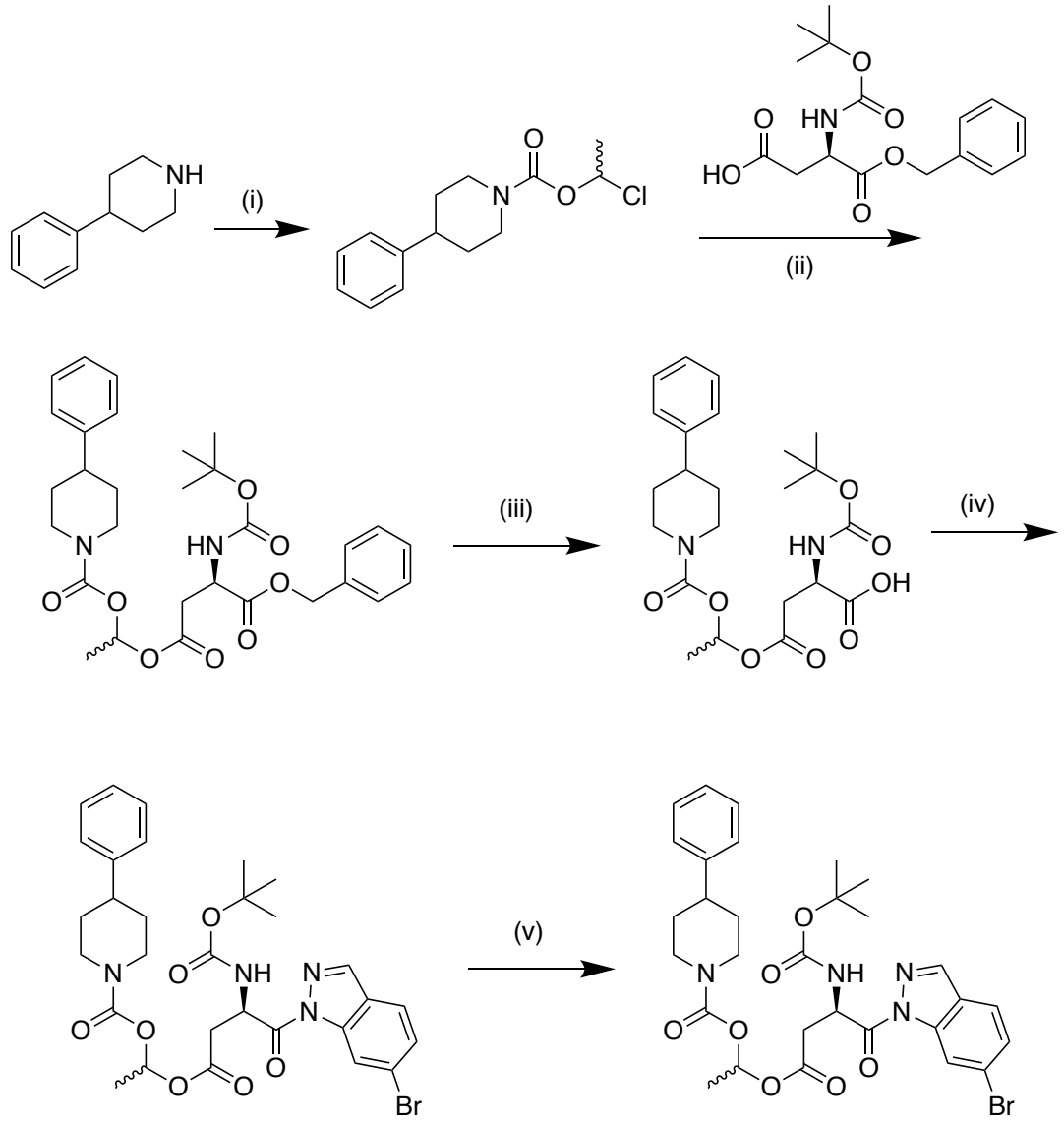


Figure 181. The hypothesised cleavage mechanism of the prodrug. The α-amino group delivers water to the site of hydrolysis by anchimeric assistance through hydrogen bonding. This achimeric assistance can either be hindered or assisted, depending on the pH, as the amino group will have a different percentage ionisation at differing pH. Following the delivery of water and release of pictilisib, the prodrug has been designed to degrade via a well known cyclisation mechanism, yielding the anhydride (which is subsequently hydrolysed to the amino acid). This is followed by collapse, eliminating acetaldehyde (which disproportionates- as seen by NMR), carbon dioxide, and ultimately ceritinib.

4.3.1.2 Model Prodrug Synthesis

Synthesis of the prodrug model systems, Scheme 36, began with substitution 1-chloroethyl chloroformate (ACE-Cl) with phenyl piperidine in the presence of N-methyl morpholine (NMM). The product of this reaction was carried forward as the crude material, as it was not possible to purify on silica gel due to its reactivity. Coupling of the amino acid partner was achieved using silver oxide, which inserts into the C-Cl bond, allowing the carboxylic acid to displace the chloride in a reduction elimination process. This is carried out in a catalytic amount of *tert*-butyl ammonium bromide and heated in toluene to 60 °C. Following deprotection of the benzyl group to yield the acid, a classic amide coupling was performed using HATU along with DIPEA as the base. An aqueous work-up was avoided so as not to initiate the cleavage mechanism and thus the reaction mixture was simply absorbed onto silica gel. At this point the primary amine is still protected with the boc protecting group, and the model systems are significantly more stable in this state, provided they are stored correctly. Once required, the boc-group is removed with TFA to give the TFA salt of the desired model system.



Scheme 36. Regents and Conditions: (i) Phenylpiperidine (1.0 eq.), Chloroethyl chloroformate (1.1 eq.), NMM (2.0 eq.), CH_2Cl_2, -10 °C, 45 mins; (ii) N-boc-Cbz-protected amino acid (0.8 eq.), Ag_2O, NBu_4Br (0.16 eq.) , Toluene, 60 °C, overnight, Yield 37-55%; (iii) Pd/C, H_2, EtOAc, rt, overnight, Yield 76-99%; (iv), 5-bromoindazole (1.0 eq.), HATU (1.1 eq.), DIPEA (3.0 eq.), CH_2Cl_2, rt, 6 hr, Yield 68-88%; (v) TFA, CH_2Cl_2, rt, 1 hr, 100%.

4.3.1.3 Prodrug Model Kinetic Study

Following synthesis of the model system a kinetic study was performed of the release of the drug mimetics in buffered solutions. Initially, use of use LCMS or HPLC to monitor the reactions was attempted, however there were issues visualising phenyl piperidine with the UV detectors of the LC systems. Time-course NMR studies were thus investigated. Unfortunately, the model system was insoluble in buffer alone, and it was

necessary to add 50% DMSO in order to get the model system into solution although at relatively low concentration. At these low concentrations, our 400 MHz system was not sensitive enough for the experiment and it was therefore necessary to use a higher field 800 MHz system, which has good resolution at low concentrations up to 10 μM. The NMR experiments performed were at a concetration of approximately >1 mM, based on the internal standard 4,4-dimethyl-4-silapentane-1-sulfonic acid (DSS). Additionally, since pH is dependent on hydrogen ion concentration, H_2O buffer was used, rather than D_2O buffer, adding deuterated DMSO as a deuterated solvent for the spectrometer to lock to. Since water was used, water suppression was applied to the experiment, which causes "baseline wobble" and difficulty phasing the spectrum around 3.5 ppm. This was not a major issue since the peaks of interest were in the aromatic and aliphatic regions of the spectrum.

Since it was anticipated that the rate of release would be slower at lower pH, the study began by performing the time course experiment at the lowest pH of pH 6.4. The spectra of the time course are shown in Figure 182, where the key peaks are illustrated. For monitoring the release of the pictilisib mimetic (6-bromo indazole), the integrations of peaks at 8.02 ppm and 7.41 ppm were followed. For release of the ceritinib mimetic (4-phenyl-piperidine), the integrations of peaks 1.73 ppm and 1.41 ppm were followed. For disappearance of the prodrug, integration of peaks 1.31 ppm, 6.51 ppm , and 7.92 ppm were followed. The experiments was run at 21 °C for approximately 14 h, obtaining 512 spectra over the period. Note that upon setting up the experiment a blank containing the solvent system was used in order to lock and shim the spectrometer. There was still a dead time, however, where the sample was prepared as quickly as possible, filtered, and inserted into the spectrometer. This dead-time also contains the time it takes the spectrometer to perform a 32 scan proton NMR spectrum. It is estimated the total dead time to be approximately 8 mins.

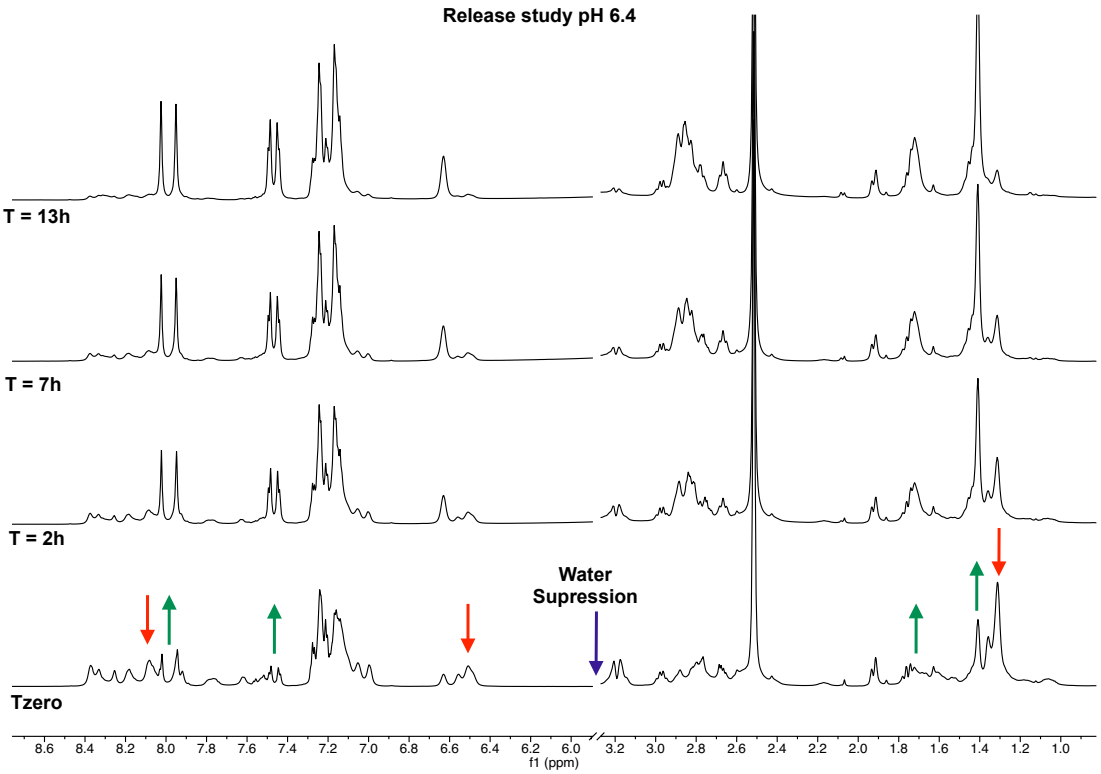


Figure 182. Spectra at 0 h, 2 h, 7 h, and 13 h showing selected slices of a time course experiment (512 slices) of the β-amino prodrug model system performed at 21 °C in pH 6.4 phosphate buffer and d_6- DMSO (1:1). Peaks showing the appearance of drug mimetics are shown by green arrows, and peaks showing the disappearance of prodrug are shown by green arrows. Note that water suppression was applied, causing "baseline wobble" at approximately 3.5 ppm.

Following the integration of these peaks over time produced the graphs in Figure 183. All of these graphs fit a one phase dissociative exponential decay function, and the mean of their half-lives are illustrated on the plots. This shows that the overall half life

of the release is $t_{1/2}$ = 4.64 ± 0.5 h.

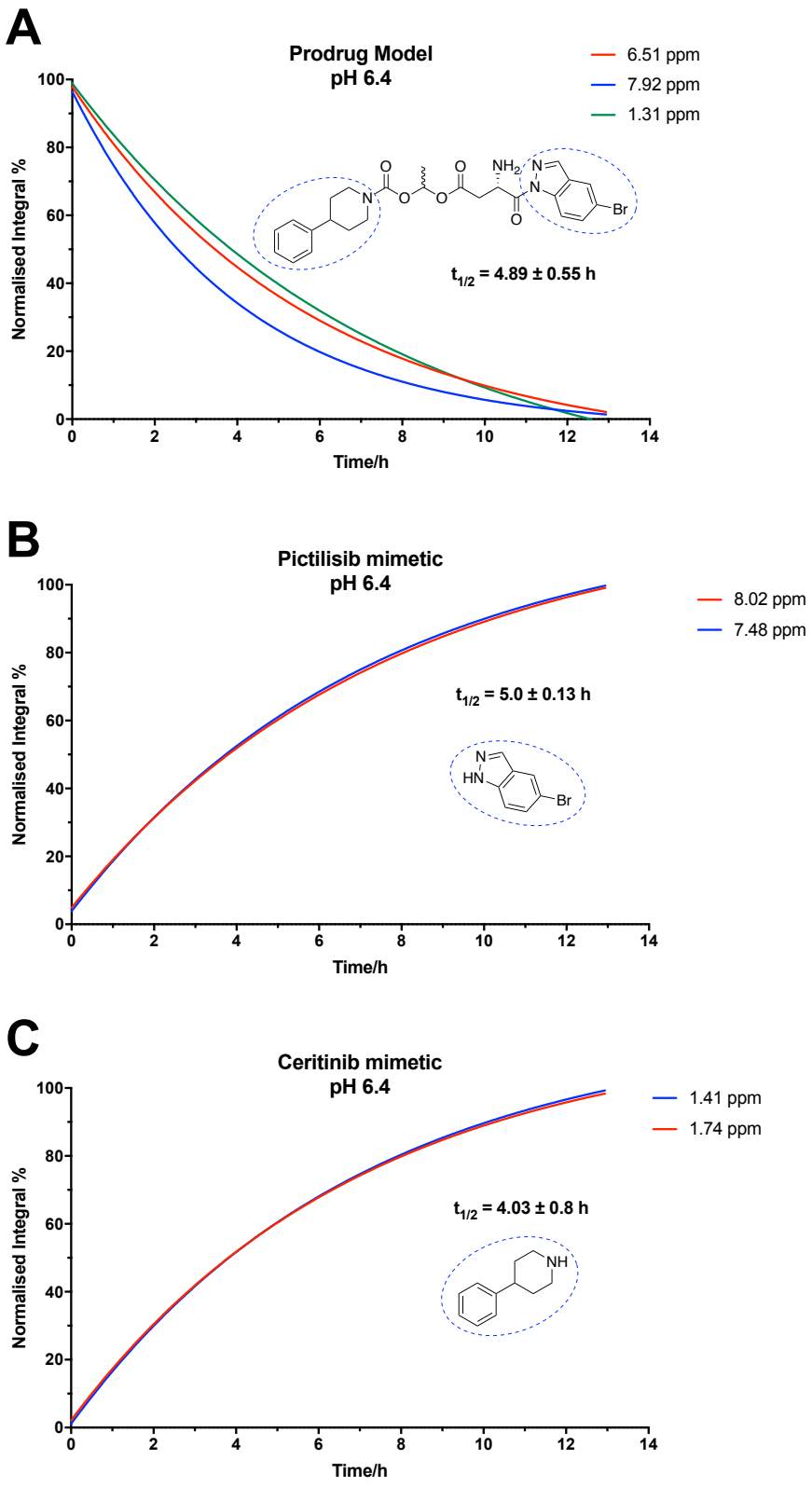


Figure 183. Graphs showing the integration of NMR spectra peaks over time. (A) Shows degradation of the prodrug looking at peaks from each component of the prodrug. The peak at 1.31 ppm shows disappearance of a peak from the pictilisib mimetic region, and

the peak at 7.92 ppm shows disappearance of a peak in the ceritinib mimetic region of the prodrug. Additionally, the peak at 6.51 ppm shows disappearance of a peak from the linker region of the prodrug. These peaks fit a one phase exponential decay function with r^2 = >99. (B) Shows the release of the pictilisib mimetic using the disappearance of peaks at 8.02 ppm and 7.41 ppm. (C) Shows the release of the ceritinib mimetic using the disappearance of peaks at 1.73 ppm and 1.41 ppm.

The kinetics of the reaction mechanism proposed in Figure 181 can be examined by considering the consecutive irreversible reaction:

$$Prodrug \overset{k_1}{\rightarrow} Prodrug\ Carboxylic\ Acid \overset{k_2}{\rightarrow} Ceritinib\ Mimetic$$

Where k_1 is the rate constant for the release of the pictilisib mimetic and k_2 is the rate constant for the release of the ceritinib release.

The rate equations for the concentration of the prodrug, the prodrug carboxylic acid intermediate and the ceritinib mimetic are:

(1) $$\frac{d[Prodrug]}{dt} = -k_1[Prodrug]$$

(2) $$\frac{d[Prodrug\ Carboxylic\ Acid]}{dt} = -k_1[Prodrug\ ] - k_2[Prodrug$$

(3) $$\frac{d[Ceritinib\ Mimetic]}{dt} = -k_2[Prodrug\ Carboxylic\ Acid]$$

Integrating the rate equation (1) for the prodrug gives:

$$[Prodrug] = [Prodrug]_0\, e^{(-k_1 t)}$$

Substituting this into (2) gives a differential equation with the solution:

$$[Prodrug\ Carboxylic\ Acid] = \frac{k_1}{k_2 - k_1}\left\{e^{(-k_1 t)} - e^{(-k_2 t)}\right\}[A]_0$$

Since:

$$[Ceritinib\ Mimetic] = [Prodrug]_0 - [Prodrug\ Carboxylic\ Acid] - [Prodrug]$$

Then:

$$[Ceritinib\ Mimetic] = \left(1 + \frac{k_1 e^{(-k_2 t)} - k_2 e^{(-k_1 t)}}{k_2 - k_1}\right)[Prodrug]_0$$

There are two likely scenarios when considering the reaction:

$$k_1 \gg k_2 \text{ or } k_1 \ll k_2$$

In the first case where $k_1 >> k_2$ it is expected to observe the prodrug rapidly converted into the prodrug carboxylic acid, then the prodrug carboxylic acid would be slowly consumed and converted into the ceritinib mimetic. This would mean that the second step would be the rate determining step. In this case it is expected to observe graphs where the concentration of the prodrug rapidly appears but the formation of ceritinib would appear at a much slower rate. However, this is not the case, and it is expected that the ceritinib mimetic appears as fast as the prodrug is formed. This is since case 2 is in operation where $k_1 << k_2$. Since k_2 is much greater than k_1, k_1 becomes negligible.

Thus:

$$[Ceritinib\ Mimetic] = \{1 - e^{-k_1 t}\}[Prodrug]_0$$

Taking the natural logarithm of this equation and rearranging gives:

$$Ln\left(\frac{[Ceritinib\ Mimetic]}{[Prodrug]_0}\right) = -k_1 t$$

The reaction is therefore *pseudo* first order since the overall rate is dependant only on the first, rate determining step, the hydrolysis of the ester. Plotting Ln([Prodrug]$_0$/[Prodrug]) *vs* time gives a linear graph (Figure 184) with an r^2 value of >0.99, where the rate constant k_1 can be obtained from the slope. At pH 6.4, the rate constant for this reaction is $k = 0.22 \pm 0.003\ s^{-1}$.

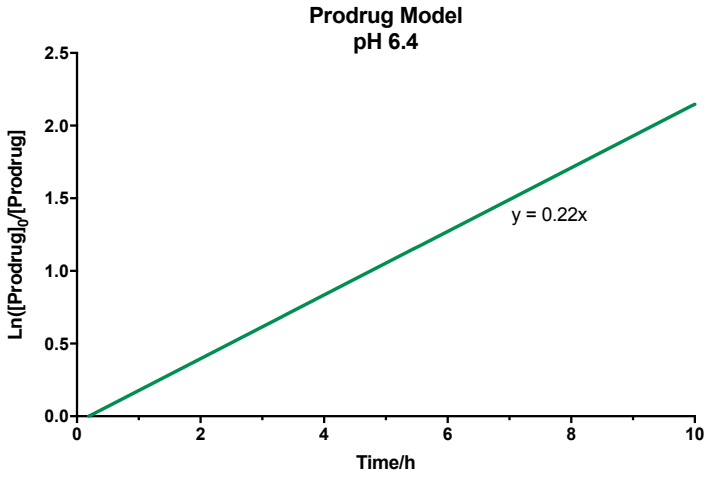


Figure 184. A plot of Ln([Prodrug]0/[Prodrug]) vs time for the prodrug model system at pH 6.4.

The experiment was repeated on the same model system at both pH 6.8 and pH 7.4 with $k = 0.84 \pm 0.06\ s^{-1}$ at pH 6.8 and $k = 1.37 \pm 0.17\ s^{-1}$ at pH 7.4 (Figure 185).

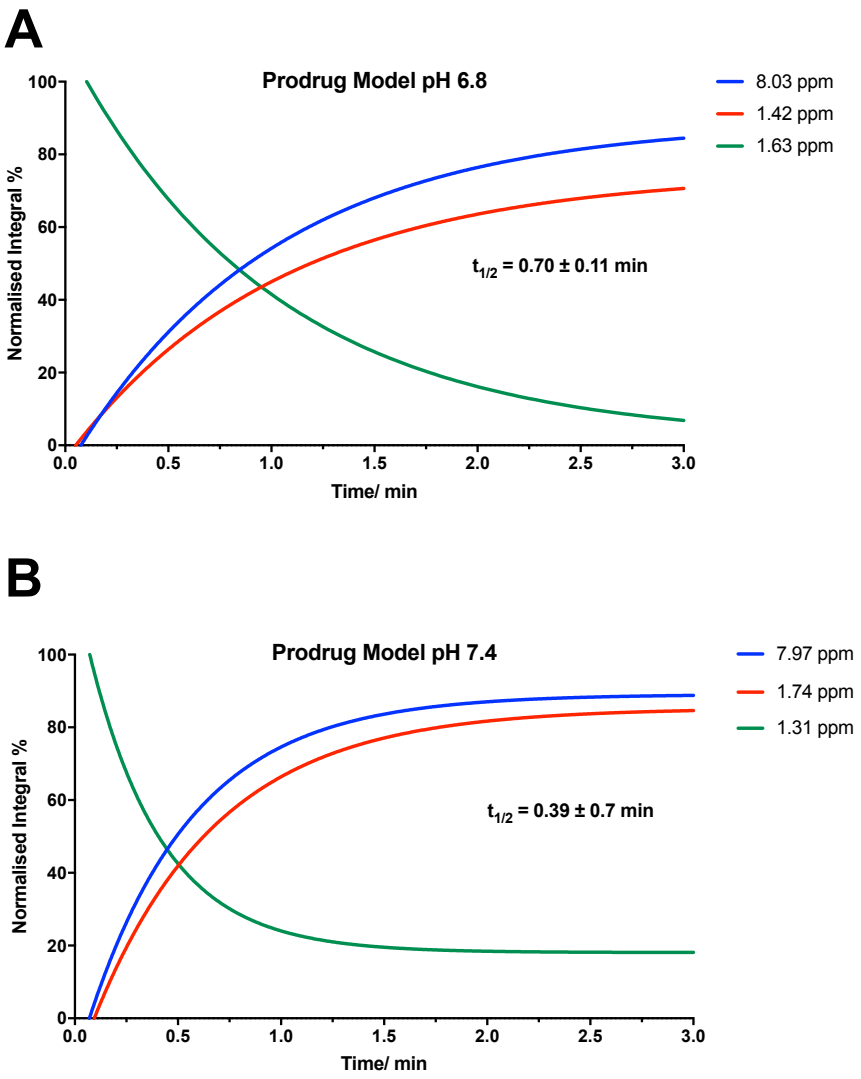


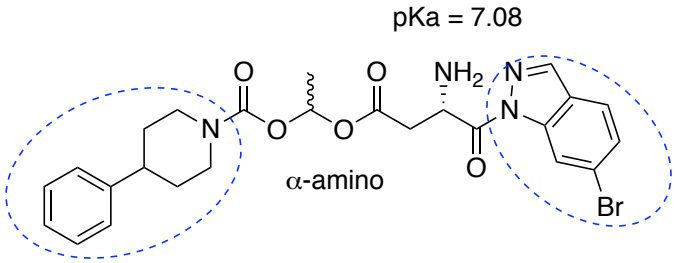
Figure 185. Graphs showing the rate of disappearance of the prodrug (green) and release of the drug mimetics for pictilisib (blue) and ceritinib (red) at (A) pH 6.8 and (B) 7.4.

Immediately it could see that at these pH level the prodrug was releasing quicker with half-lives in the order of minutes rather than in the order of hours as in the case at pH 6.4. Considering the pK_a of the protonated α-amino group was calculated to be 7.08, the percentage ionisation can be calculated and thus the percentage unionised at these pH levels using the equation:

$$pH = pKa + log\left(\frac{[H^+]}{[B]}\right)$$

The calculated percentage unionised at pH 6.4, 6.8, and 7.4 are 17.3%, 34.4%, and 67.6% respectively. A mechanism was previously hypothesised where the α-amino group delivers water to the amide carbonyl through anchimeric assistance *via* hydrogen bonding. The fact that the rate of reaction increases with the percentage unionised is evidence is favour of this hypothesis. Conversely, the rate decreased upon percentage ionised, suggesting that through protonation, the lone pair of electrons on the nitrogen is no longer available for hydrogen bonding, thus not providing anchimeric assistance.

Table 17. Half-lives and rate constants for the release of drugs from the prodrug model system at a range of pH levels.



pH	$t_{1/2}$	k_1	% Unionised
6.4	4.64 ± 0.5 h	0.22 ± 0.003 s^{-1}	17.3%
6.8	0.70 ± 0.11 min	0.84 ± 0.06 s^{-1}	34.4%
7.4	0.39 ± 0.7 min	1.37 ± 0.17 s^{-1}	67.6%

Since the first step is a hydrolysis and relies on the formation of hydroxide ions through the equilibrium with water, in theory the first step in itself is pseudo first order since at the pHs that these experiments were conducted there is a large excess of hydroxide ions relative to the concentration of the prodrug.

The fact that the overall rate of the reaction is dependent on the hydrolysis of the ester means that we can control the rate of the reaction by altering the rate of the ester hydrolysis. In order to test this we synthesised two further analogues (Figure 186) of our

prodrug model systems using the same procedure detailed in Scheme 36.

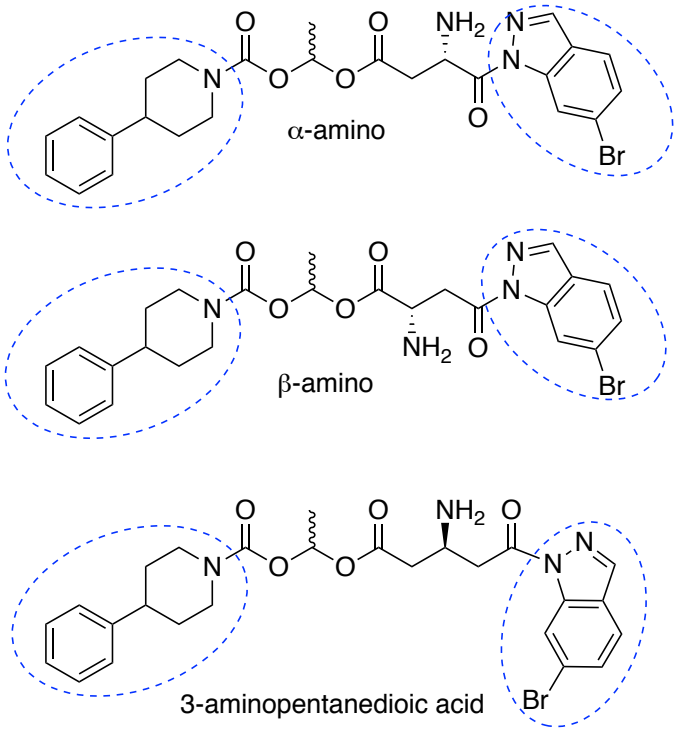
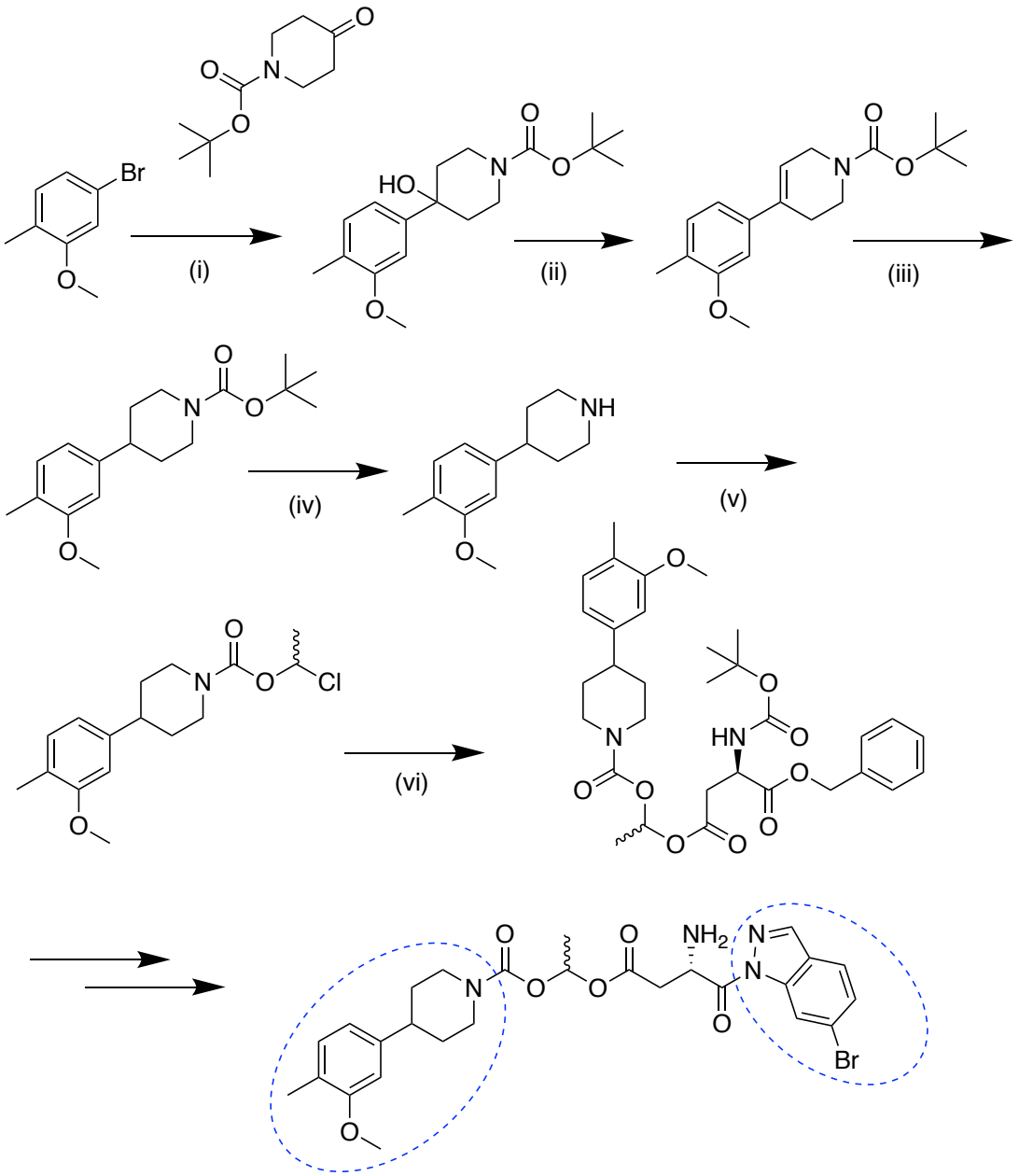


Figure 186. Synthesised prodrug model systems. The a-amino model system, the b-amino model system, and the 3-aminopentanedioic acid model system.

The systems were synthesised so as to assess the effect of the α-amino group on the rate of hydrolysis of the ester. It was hypothesised that the β-amino group may direct water to the other carbonyl group resulting in a different method of release (figure 177), however, we were unable to perform the same NMR experiments as before because instability of the prodrug was observed and decomposition before instrument time could be obtained, which was difficult due to the level of demand of a high end 800 MHz instrument. Similarly, this was also observed this for the 3-aminopentanedioic acid analogue and thus it was decided to try to synthesise a model system that could be analysed by HPLC or LCMS.

This was achieved by synthesising a 4-(3-methoxy-4-methylphenyl)piperidine analogue of the α-amino model system (Scheme 37). During the synthesis it was observed that the more electron rich aromatic ring changed the UV absorption and allowed visualisation with UV detectors on the LC systems. Synthesis began with the formation

of the aryl Grignard from the commercially available arylbromide, followed by addition of the Grignard reagent to 4-boc amino piperidone. The elimination of the resulting primary alcohol was achieved using TFA in CH_2Cl_2, where the compound was reprotected using boc anhydride. The subsequent hydrogenation of the resulting alkene was reduced over Pd/C, followed by a boc-deprotection using TFA. The rest of the synthesis is as per the previous analogues.



Scheme 37. Reagents and conditions: (i) 4-bromo-2-methoxy-1-methylbenzene (1.0 eq.), Mg (1.2 eq), THF (anhydrous), 3h, r.t then tert-butyl 4-oxopiperidine-1-carboxylate (0.8 eq.); (ii) TFA:CH_2Cl_2 (1:1), 0 °C - r.t., 30 mins then Boc_2O (1.2 eq.), NEt_3 (excess), r.t., overnight, Yield 58%; (iii) Alkene (1.0 eq.), EtOH, Pd/C (10%), H_2, 90 min, Yield 91%; (iv) TFA:DCM (v) Chloroethyl chloroformate (1.1 eq.), NMM (2.0 eq.), CH_2Cl_2, -10 °C, 45 mins; (vi) N-boc-Cbz-protected aspartic acid (0.8 eq.), Ag_2O, NBu_4Br (0.16 eq.) , Toluene, 60 °C, overnight, Yield 79%.

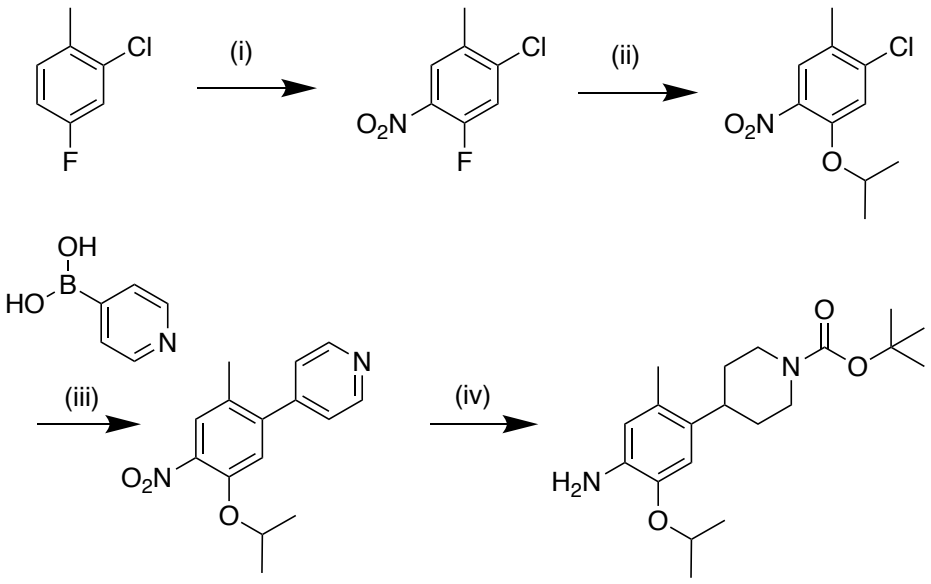
Following the synthesis kinetic experiments were attempted, however once again solubility issues in phosphate buffer persisted. In fact, the solubility was so poor that it was decided to move on from the model systems and progress to the development of the real prodrug since the half-life of approximately 5 h at pH 6.4 in the absence of

biological interference from enzymes, proteins, etc was acceptable.

4.3.2 Ceritinib/Pictilisib Prodrug, AEG-118

4.3.2.1 Synthesis of AEG-118

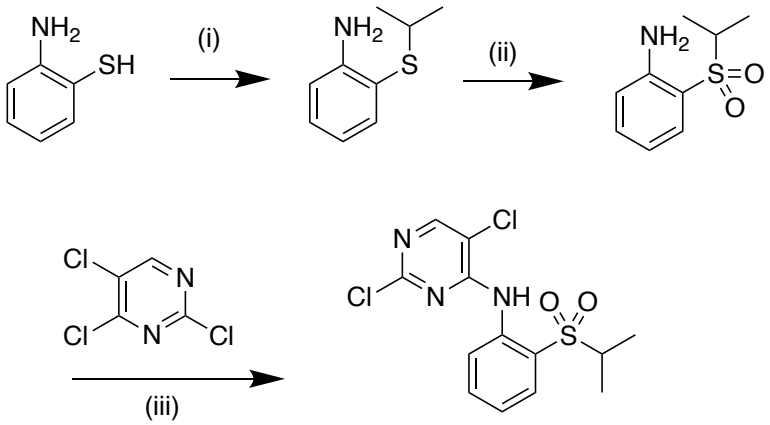
For the preparation of ceritinib (Scheme 38), the synthetic route used by Marsilje *et al* [186] was used with modification. The first fragment of the molecule was synthesized by nitration of 2-chloro-4-fluoromethylbenzene with concentrated sulfuric acid and potassium nitrate at room temperature. This was performed on large scale, ~20 g, and achieved quantitative yield, where the nitro group was installed exclusively in the desired position as seen by NMR. Subsequently, the fluoro group was then displaced by isopropoxide in a classic nucleophilic aromatic substitution, also on large scale, giving good yield. This was followed by Suzuki coupling with pyridine-4-boronic acid on a smaller scale, using $Pd_2(dba)_3$ as the coupling catalyst and sodium carbonate as the base. The yield obtained for the Suzuki reaction was slightly higher than reported. The pyridine ring was reduced to the piperidine by hydrogenation over platinum oxide, followed by boc-protection of the secondary amine with boc-anhydride.



Scheme 38. Reagents and Conditions: (i) Conc. H_2SO_4, KNO_3, rt, overnight, Yield 54%; (ii) IPA, $CsCO_3$, 60 ° C, overnight, Yield 100% (ii) $Pd_2(dba)_3$, S-Phos, $NaCO_3$ (2 M), EtOH:H_2O, mw 150 °C 20 mins, Yield 72%; (iv) Pt_2O, H_2, TFA, AcOH, rt, overnight, Yield 100%; (v) CH_2Cl_2, Boc_2O, 40 mins, Yield 86%.

The second fragment of the molecule was synthesised (Scheme 39) by first alky-

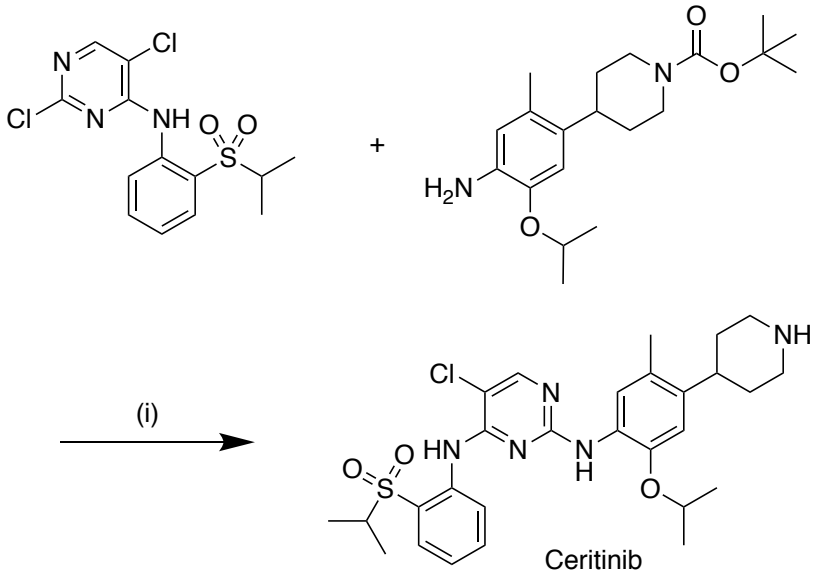
lating 2-aminothiophenol using potassium *tert*-butoxide to deprotonate the thiophenol then substitution on isopropyl iodide in anhydrous THF. This reaction was very high yielding, contrary to previous attempts where potassium carbonate was used as a base and isopropyl chloride were used. In these attempts the disulfide was isolated as the major product. *In situ* reduction with sodium borohydride was attempted to reform the thiol, although this proved unsuccessful. Following the alkylation, oxidation to the sulfone was accomplished using oxone in methanol and water. Smaller scale test reactions showed that oxone was superior to *m*-CPBA as, even in vast excess of *m*-CPBA, the oxidation was difficult to drive to the sulfone from the sulfoxide intermediate. Coupling of this product to 2,4,5-trichloropyrimidine was performed by deprotonation of the aniline with sodium hydride then addition of the 2,4,5-trichloropyrimidine. The reaction gave moderate yield, despite using excess sodium hydride as the product itself has an acid proton. Substitution occurred exclusively at the chloride in the 4-position due that position being more electrophilic due to the resonance that can be drawn for 2,4,5-trichloropyrimidine.



Scheme 39. (i) Aminothiophenol (1.0 eq.), KOtBu (1.0 eq.), THF (anhydrous), 0 °C, 20 mins, Isopropyliodide (1.0 eq.), overnight, Yield 92%; (ii) Thioether (1.0 eq.), Oxone (3.0 eq.), MeOH:H_2O, overnight, Yield 67% ; (iii) Sulfoxide (1.0 eq.), NaH (>1.0 eq.), pyrimidine (1.1 eq.), DMF, overnight, Yield 59%.

The two fragments were prepared to be joined together (Scheme 40) *via* a Buchwald-Hartwig reaction; however reported yields were low and thus a nucleophilic substitution was attempted. Initially, the fragments were taken up in IPA and heated under microwave radiation for 15 mins, however very little product was formed. Upon addi-

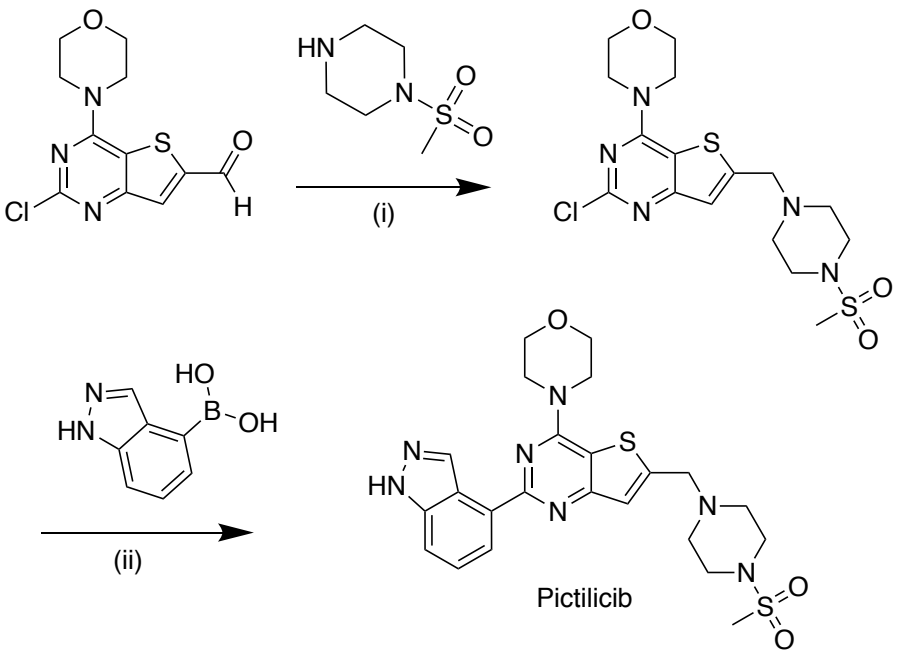
tion of a catalytic amount of hydrochloric acid in dioxane and further heating, the reaction proceeded to the final product in good yield, with simultaneous deprotection of the boc-group. The free-base was isolated on an SCX2 ion exchange resin.



Scheme 40. (i) Pyrimidine (1.0 eq.), Aniline (1.0 eq.), HCl (2 M), IPA, mw 150° C 15 mins, Yield 98%.

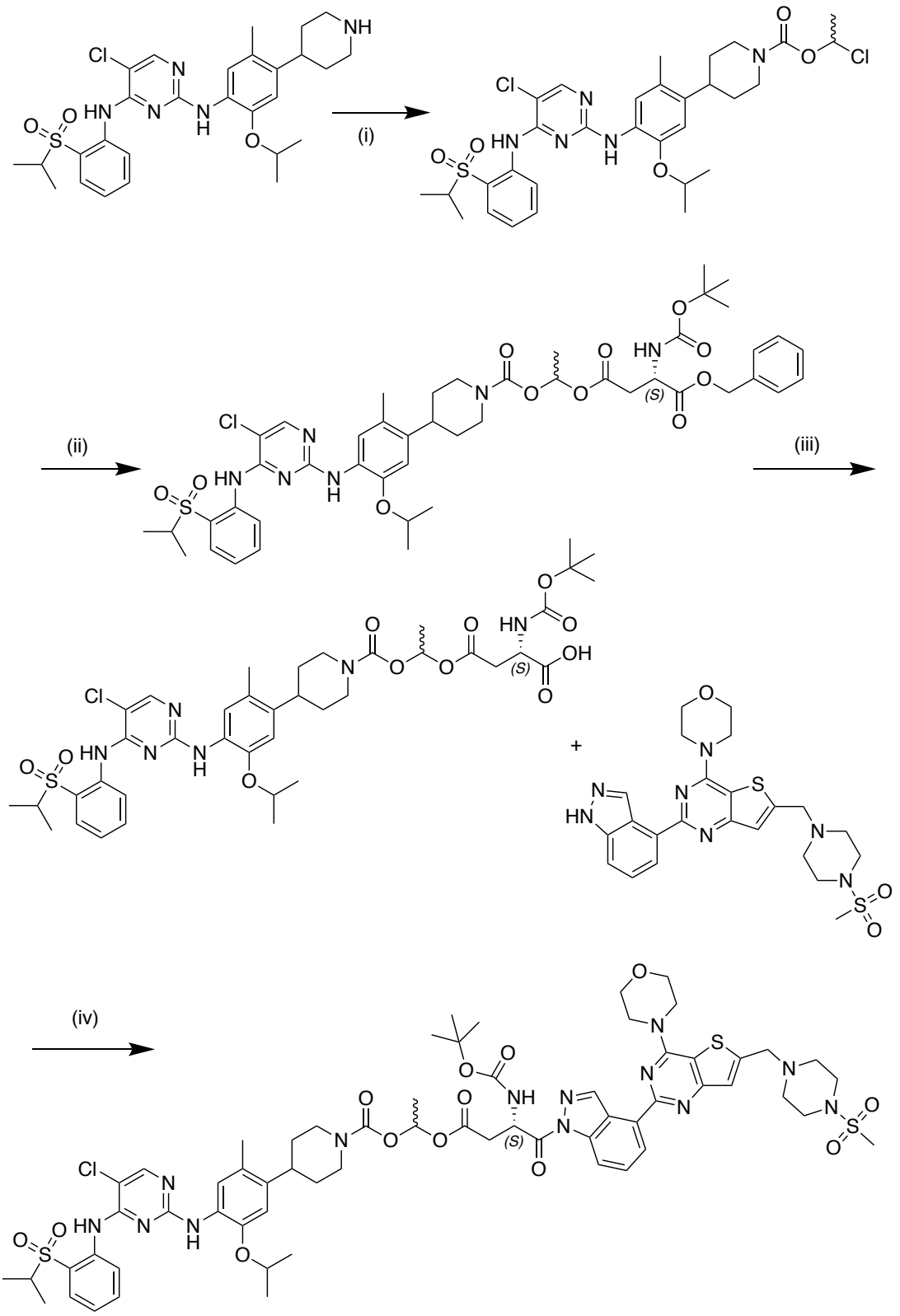
To synthesise pictilisib (Scheme 41), the first step involves a reductive amination which has been optimised as follows. The aldehyde and the amine were taken up in a 10:1 mixture of dichloromethane : acetic acid mixture and sodium acetate added if the amine was in a salt form. This mixture was then heated at 45 °C for one hour before the reducing agent, picoline borane, was added. The sodium acetate acts to free up the amine, whilst simultaneously forming sodium chloride and acetic acid, which catalyses the formation of the iminium ion. Although picoline borane is thought to selectively reduce to the iminium over the aldehyde, with direct addition of the reducing agent, i.e. without time to equilibrate the iminum species, it was found that more primary alcohol was formed from reduction of the aldehyde. Alternatively, the reductive amination could be performed in acetonitrile or using sodium triacetoxyborohydride as the reducing agent. The presence of trimethylorthoformate increases yields as this acts as a dehydrating agent, driving the formation of the iminium ion. The second step is a excellent yielding Suzuki coupling with the required boronic acid, where $Pd(PPh_3)_2Cl_2$ was used

as the coupling catalyst and sodium carbonate was used as the base.



Scheme 41. (i) Pyrimidine (1.0 eq.), methylsulfonylpiperizine (1.2 eq.), CH_2Cl_2:AcOH (10:1), NaOAc, Picoline Borane (1.2 eq.), 45°C then rt, Yield 76%; (ii) Boronic acid, $Pd_2(PPh_3)_2Cl_2$, $NaCO_3$, H_2O:EtOH (3:1), microwave, 125 °C, 45 mins, Yield 80%.

After the synthesis of the drugs, ceritinib and pictilisib, the same chemistry as in the case of the model systems was used to link them together, Scheme 42.



Scheme 42. (i) Ceritinib (1.0 eq.), Chloroethyl chloroformate (1.1 eq.), NMM (2.0 eq.), CH_2Cl_2, -10 °C, 45 mins; (ii) N-Boc-Cbz-protected amino acid (0.8 eq.), Ag_2O, NBu_4Br (0.16 eq.) , Toluene, 60 °C, overnight, Yield 77%; (iii) Pd/C, H_2, EtOAc, rt, overnight, Yield 100%; (iv), 5-bromoindazole (1.0 eq.), HATU (1.1 eq.), DIPEA (3.0 eq.), CH_2Cl_2, rt, 6 hrs, Yield 3%; (v) TFA, CH_2Cl_2, rt, 1 hr, 100%.

The protected prodrug, which in total was 14 steps to synthesise, was purified by preparative HPLC and freeze-dried giving a white solid which was stable in air at room temperature. Even up to a year after synthesis no decomposition was observed by LCMS. This stability was anticipated since the α-amino group is unable to deliver water to the amide carbonyl for hydrolysis. The prodrug was stored as the protected form until required for biological evaluation or stability studies. Once needed the protected prodrug was accurately weighed and deprotected using TFA in the desired quantity to give the *bis* TFA salt of the deprotected prodrug (AEG-118, Figure 187). Excess TFA was removed by additions of diethyl ether which was removed under a flow of nitrogen gas. This procedure was repeated until a white solid remained, which was then dried under high vacuum until the assay was performed.

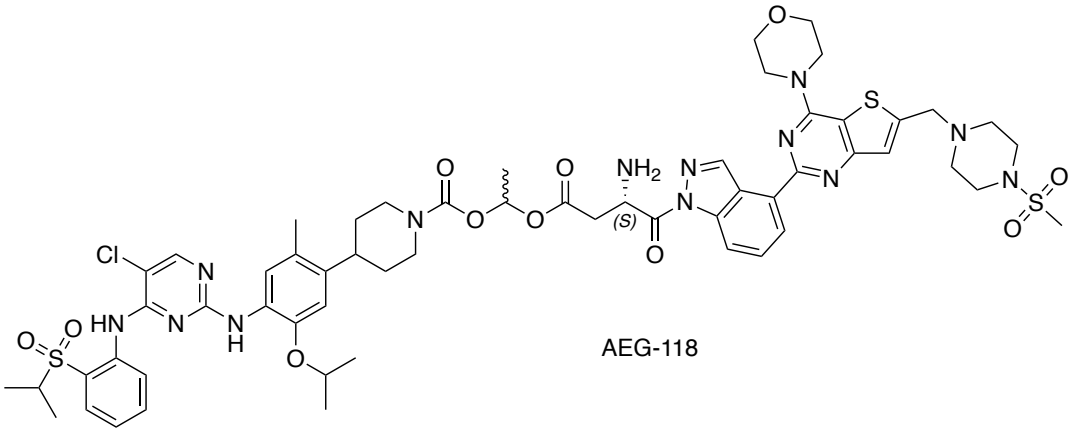


Figure 187. Structure of AEG-118, the alpha amino prodrug.

4.3.2.2 In vitro Stability studies of AEG-118

After synthesis of AEG-118 the stability was investigated in buffered solutions supplemented with bovine serum albumin (BSA), 4% by HPLC methods. Initially the experiment was attempted in phosphate buffer and DMSO without the supplemented BSA, although solubility issues did not allow for the experiment to be performed. The release study was performed by taking aliquots of the reaction and acidifiying to pH 1 to quench the reaction for HPLC analysis. The results of this experiment at both pH 6.5 and pH 7.4 is shown in Figure 188.

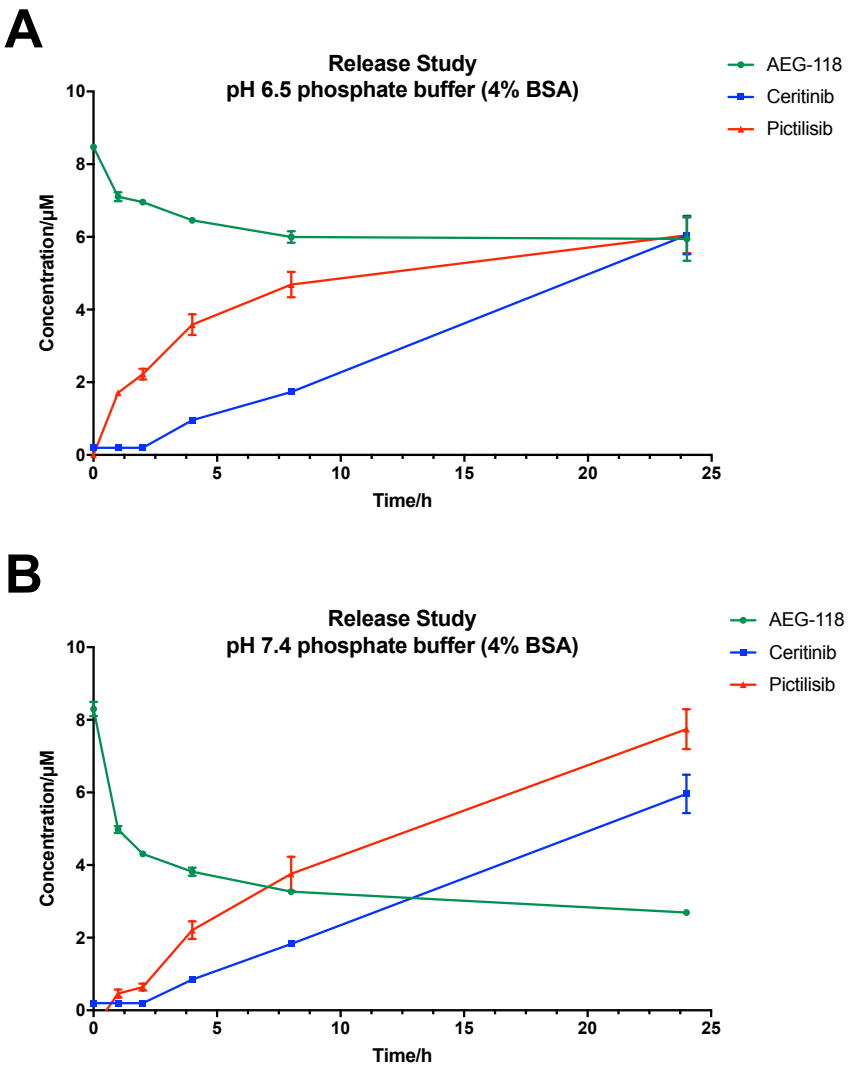


Figure 188. Release study of AEG-118 at (A) pH 6.5 and (B) in pH 7.4 phosphate buffer containing 4% bovine serum albumin showing degradation of the prodrug with release of pictilisib followed by the subsequent release of ceritinib.

The kinetics of this experiment is very complex due to the addition of BSA. Since in addition to the equilibrium of H^+ and OH^- due to the pH, there is also an equilibrium between the unbound and protein bound prodrug since the prodrug is both highly lipohillic (cLogP = 4.98) and ionised:

$$[Prodrug] + [BSA] \rightleftharpoons [Prodrug.BSA\ complex]$$

The formation of the Prodrug.BSA complex is quite rapid and therefore we can consider this as the starting point of the reaction since when bound the prodrug will

unlikely be able to hydroyse. In addition, any free prodrug molecule that hydrolyses to release pictilisib will form the carboxylic acid intermediate, which itself has a high likelyhood of binding to BSA to form its own complex. This will also form an equilibrium that is likely to lie far over to the side of highly protein bound, where only unbound prodrug carboxylic acid will be able to undergo the cyclisation to release ceritinib. This can be shown simplistically as:

$$[Prodrug.BSA\ complex\ ] \underset{}{\overset{k_1}{\rightleftharpoons}} [Prodrug] + [BSA]$$

$$[Prodrug] \overset{k_2}{\rightarrow} [Prodrug\ Carboxylic\ Acid] + [Pictilicib]$$

$$[Prodrug\ Carboxylic\ Acid.BSA\ complex\ ] \underset{}{\overset{k_3}{\rightleftharpoons}} [Prodrug\ Carboxylic\ acid] + [BSA]$$

$$[Prodrug\ Carboxylic\ acid] \overset{k_4}{\rightarrow} [Ceritinib]$$

The overall rate of release will be dependent on a rate determining step therefore an observed rate constant k_{obs} can be calculated from the slope of a plot of Ln([Prodrug]$_0$/[Prodrug]) vs time. k_{obs} = 0.036 ± 0.01 at pH 6.5 and k_{obs}= 0.094 ± 0.04 at pH 7.4. Additionally, both one-phase and two phase decay functions don't fit the data, therefore the half-life was calculated from the *pseudo* first-order rate law:

$$t_{1/2} = \frac{Ln\ 2}{k_1}$$

The half lives for AEG-118 were calculated to be 19.2 h and 7.4 h at pH 6.5 and pH 7.4 respectively.

In terms of the mixture of diastereomers, the separation was observed on the analytical HPLC system and it was observed that there was no difference in the rates of release.

Performing the same experiment on the protected compound (Figure 189) showed no release of the drugs, however disappearance of prodrug is observed, likely due to the prodrug binding to BSA and precipitating out of the solution. More importantly, this experiment shows the importance of the α-amino group lone pair and its ability to provide anchimeric assistance.

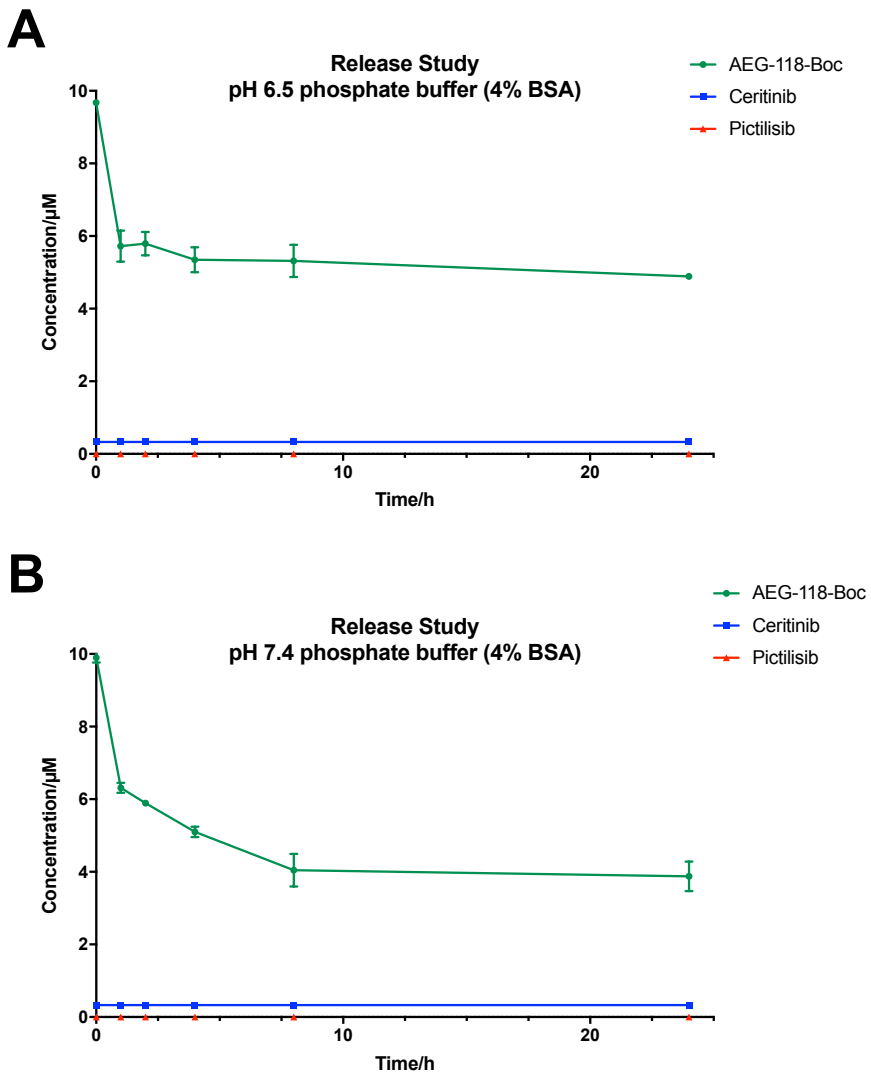


Figure 189. Release study of the Boc protected AEG-118 at (A) pH 6.5 and (B) in pH 7.4 phosphate buffer containing 4% bovine serum albumin showing potential binding of the protected prodrug to BSA, with no release of the drugs. This shows the importance of the α-amino group for the release of the drugs.

4.3.2.3 Plasma Stability of AEG-118

The stability of the prodrug was tested in rat plasma (Figure 190) shows the result of this experiment, a plot of [Prodrug] *vs* time which shows a linear relationship. The kinetics of this reaction is zero order and can be expressed as the rate law:

$$k = -\frac{d[Prodrug]}{dt}$$

Integrated this gives:

$$[Prodrug] = -kt + [Prodrug]_0$$

Where the rate constant is obtained from the slope of a plot of [Prodrug] vs time and the half life can be calculated from:

$$t_{1/2} = \frac{[Prodrug]_0}{2k}$$

The rate constant for the prodrug stability in rat plasma is calculated to be 0.06 ± 0.003 μM s^{-1} and the half life is 58 mins.

The stability of protected AEG-118 was assessed and it was seen that after 1 h incubation in rat plasma no release of the drugs was observed. This shows the importance of the α-amino group.

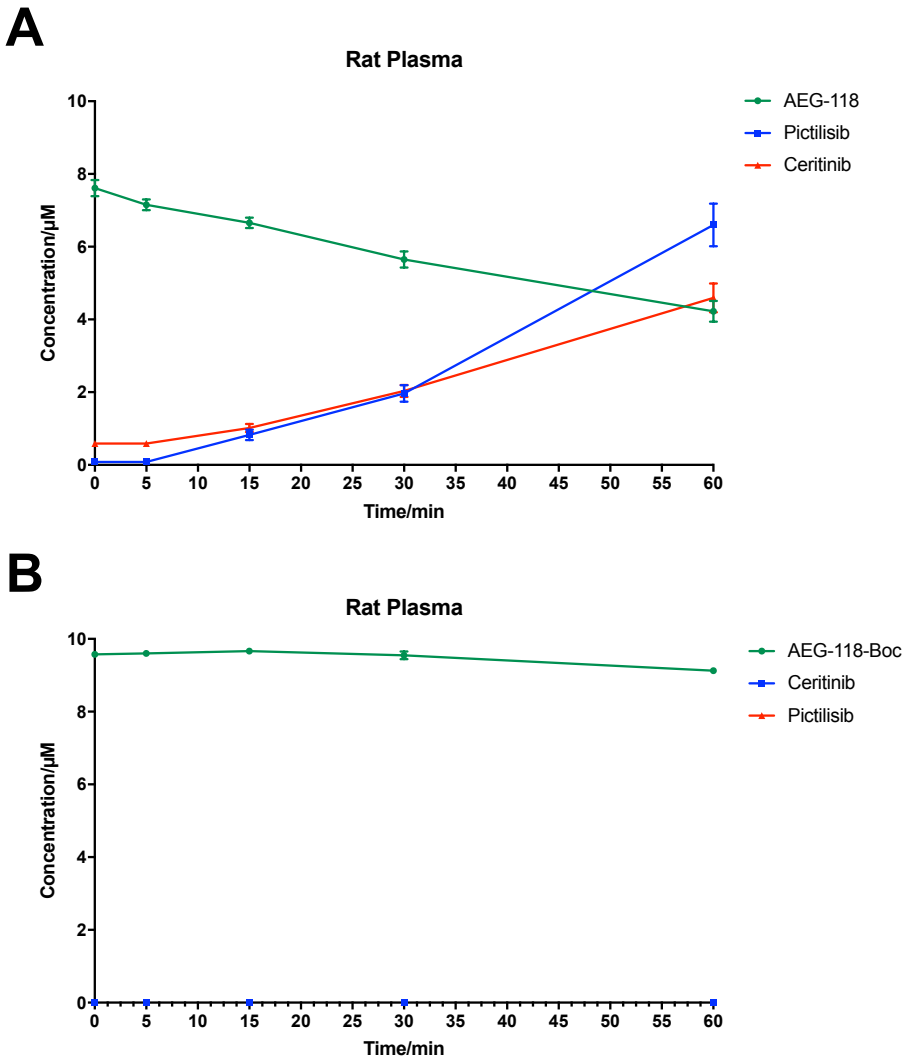
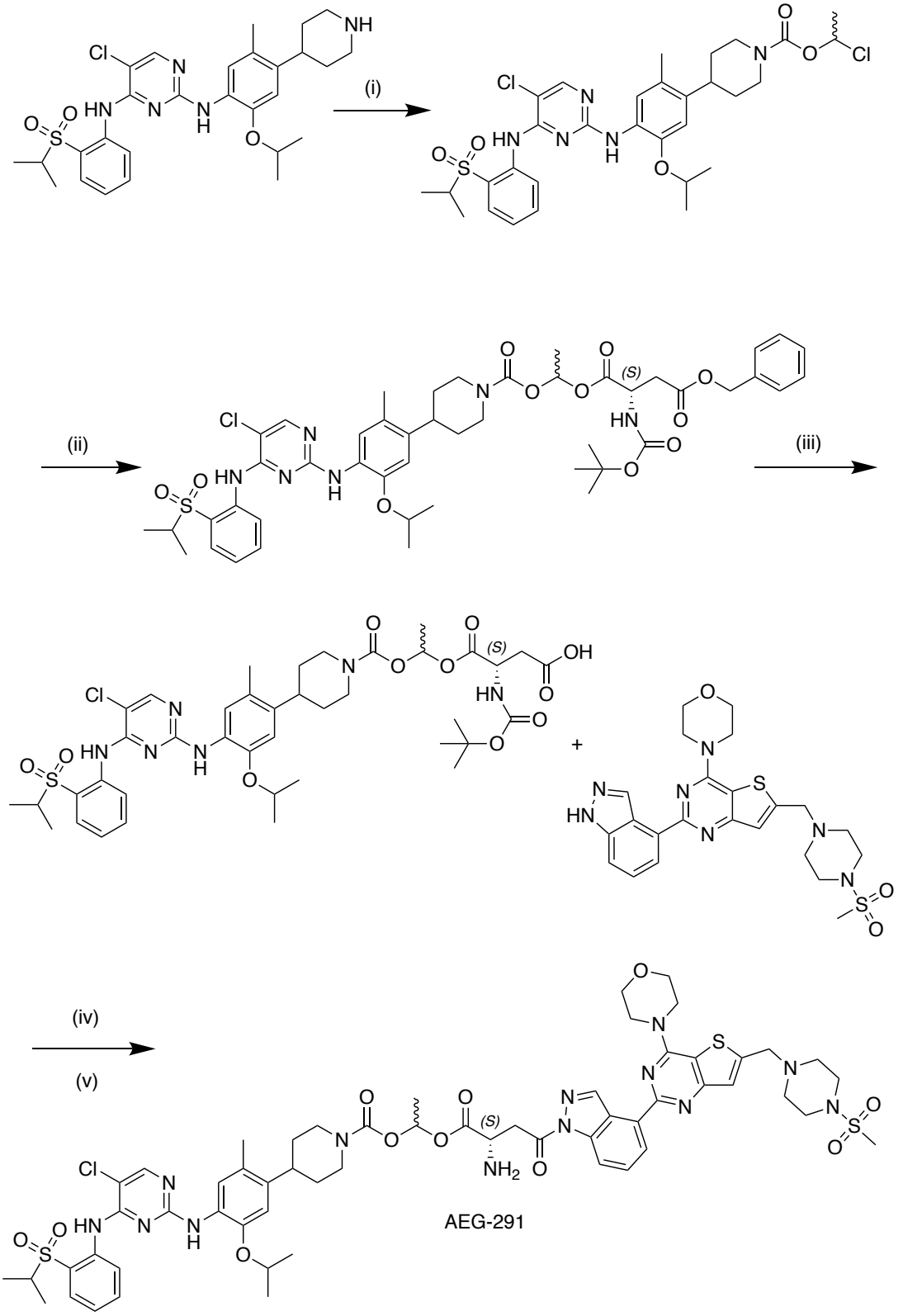


Figure 190. Stability study of (A) AEG-118 and (B) protected AEG-118 in rat plasma. The half-life of AEG-118 in rat plasma was found to be 58 mins and protected AEG-118 was found to be stable in rat plasma, seeing no release of the drugs after 1 h.

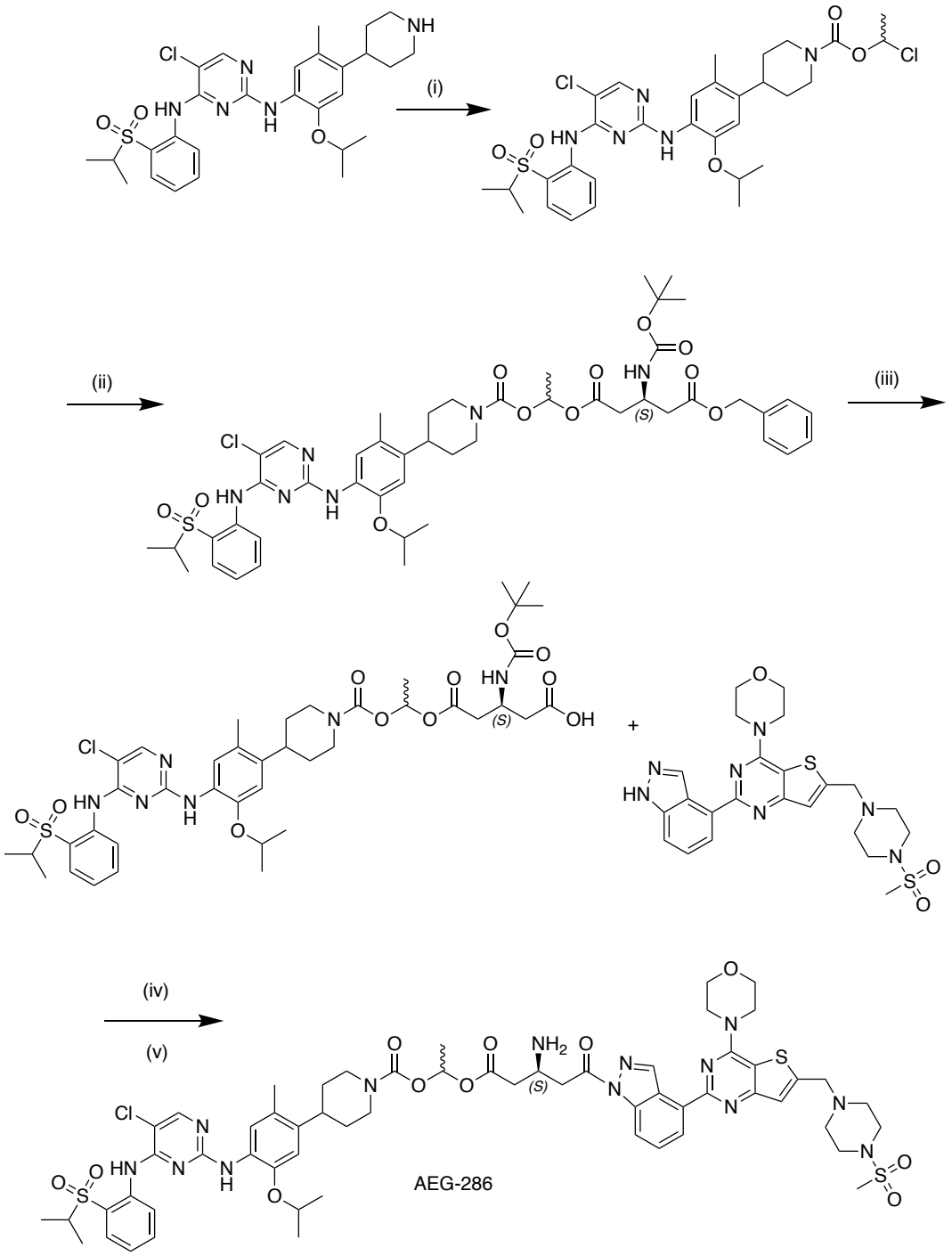
4.3.3 Analogues of AEG-118

4.3.3.1 Synthesis of Analogues of AEG-118

In addition to the synthesis and stability evaluation of AEG-118, the analogous systems, that were synthesised as model systems, were also synthesised. These are the β-amino and 3-aminopentanedioic acid prodrug systems, AEG-291 and AEG-286 respectively (Scheme 43 and Scheme 44), taking 14 chemical steps to synthesise each prodrug.



Scheme 43. (i) Ceritinib (1.0 eq.), Chloroethyl chloroformate (1.1 eq.), NMM (2.0 eq.), CH_2Cl_2, -10 °C, 45 mins; (ii) N-Boc-Cbz-protected amino acid (0.8 eq.), Ag_2O, NBu_4Br (0.16 eq.) , Toluene, 60 °C, overnight, Yield 34%; (iii) Pd/C, H_2, EtOAc, rt, overnight, Yield 100%; (iv), 5-bromoindazole (1.0 eq.), HATU (1.1 eq.), DIPEA (3.0 eq.), CH_2Cl_2, rt, 6 hrs, Yield 11%; (v) TFA, CH_2Cl_2, rt, 1 hr, 100%.



Scheme 44. (i) Ceritinib (1.0 eq.), Chloroethyl chloroformate (1.1 eq.), NMM (2.0 eq.), CH_2Cl_2, -10 °C, 45 mins; (ii) N-Boc-Cbz-protected amino acid (0.8 eq.), Ag2O, NBu4Br (0.16 eq.) , Toluene, 60 °C, overnight, Yield 26%; (iii) Pd/C, H_2, EtOAc, rt, overnight, Yield 83%; (iv), 5-bromoindazole (1.0 eq.), HATU (1.1 eq.), DIPEA (3.0 eq.), CH_2Cl_2, rt, 6 hrs, Yield 5%; (v) TFA, CH_2Cl_2, rt, 1 hr, 100%.

In Addition, a further two prodrugs were synthesised adding substituents to the *α*-amino group in order to affect its pKa. These were AEG-171, the n-butyl analogue

and AEG-165, the benzyl analogue (Figure 191).

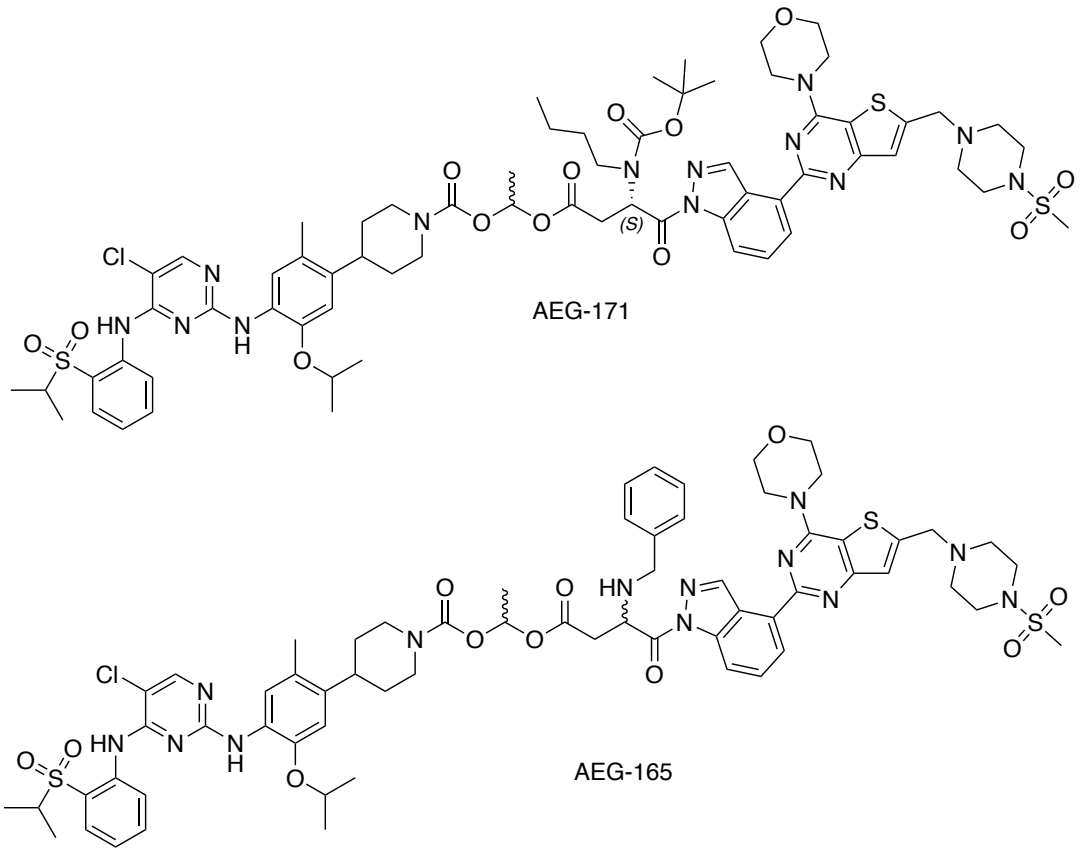
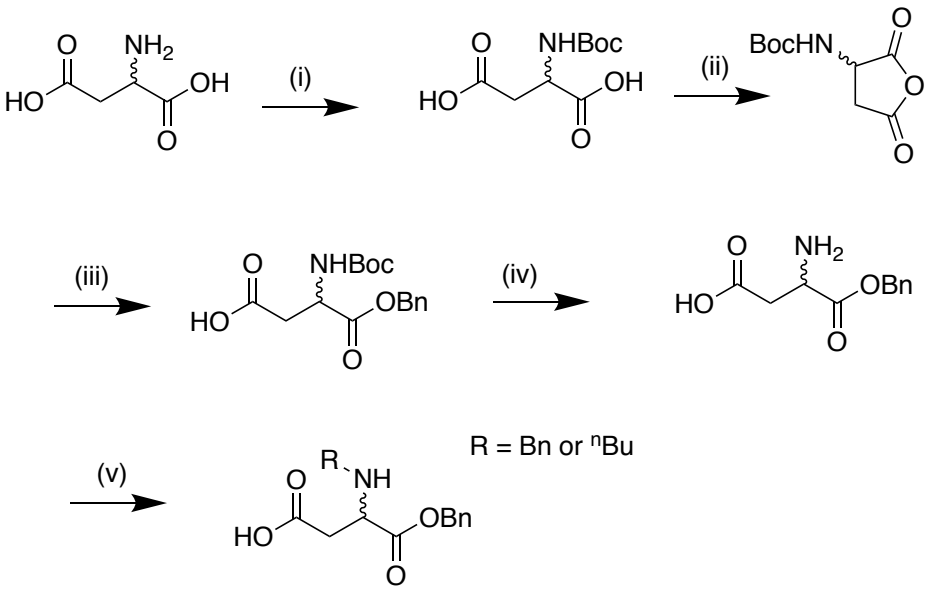


Figure 191. Structures of AEG-171 and AEG-165.

These prodrug systems took and additional 5 steps to synthesise since the amino acids were not commercially available. Scheme 45 shows the synthesis of the required amino acids, bringing the total number of steps to 19.



Scheme 45. Synthesis of substituted alpha-amino acids. Reagents and Conditions: (i) D/L Aspartic acid (1.0 eq.), NaOH (1.0 eq.), Boc2O (1.0 eq.), CH_2Cl_2:H_2O (1:1), 0 °C - r.t., overnight. (ii) Boc-Asp (1.0 eq.), Acetic anhydride, r.t., overnight, 100%; (iii) Anhydride (1.0 eq.), benzyl alcohol (1.2 eq.), dioxane, 75 °C, overnight, Yield 73%, (iv) TFA:CH_2Cl_2 (1:4), 1 h, 100%;, (v) Cbz-Asp (1.0 eq.), Aldehyde (1.1 eq.), CH_2Cl_2:AcOH (10:1), NaOAc, Picoline Borane (1.2 eq.), 45°C then r.t. Yield 32 - 42%.

AEG-291 and AEG-286 were synthesised without any issues. However, AEG-171 and AEG-165 presented a challenge. For AEG-171, synthesis up to the point of the boc-protected prodrug was achieved without any major issues, however at the point of deprotection the synthesis failed. Rather than observing the usual deprotection two new peaks were observed in the LCMS. One of these peaks corresponded to the release of pictilisib, and the other peak corresponded to something new. Further analysis revealed that this was due to a cyclisation where the t-butyl group of the boc protecting group was eliminated by TFA, leaving the carbamate oxygen to attack the amide, releasing pictilisib and forming a oxazolidine-dione (Figure 192). This is likely due to the large lipophillic n-butyl group causing the prodrug to wrap around itself through the hydrophobic effect positioning the carbamate oxygen in an optimum position to form the tetrahedral intermediate from the amide carbonyl. This unfortunately excluded AEG-171 from further study, although we did perform stability studies on the boc protected compound and observed decomposition unknown compounds, not the desired pictilisib

and ceritinib.

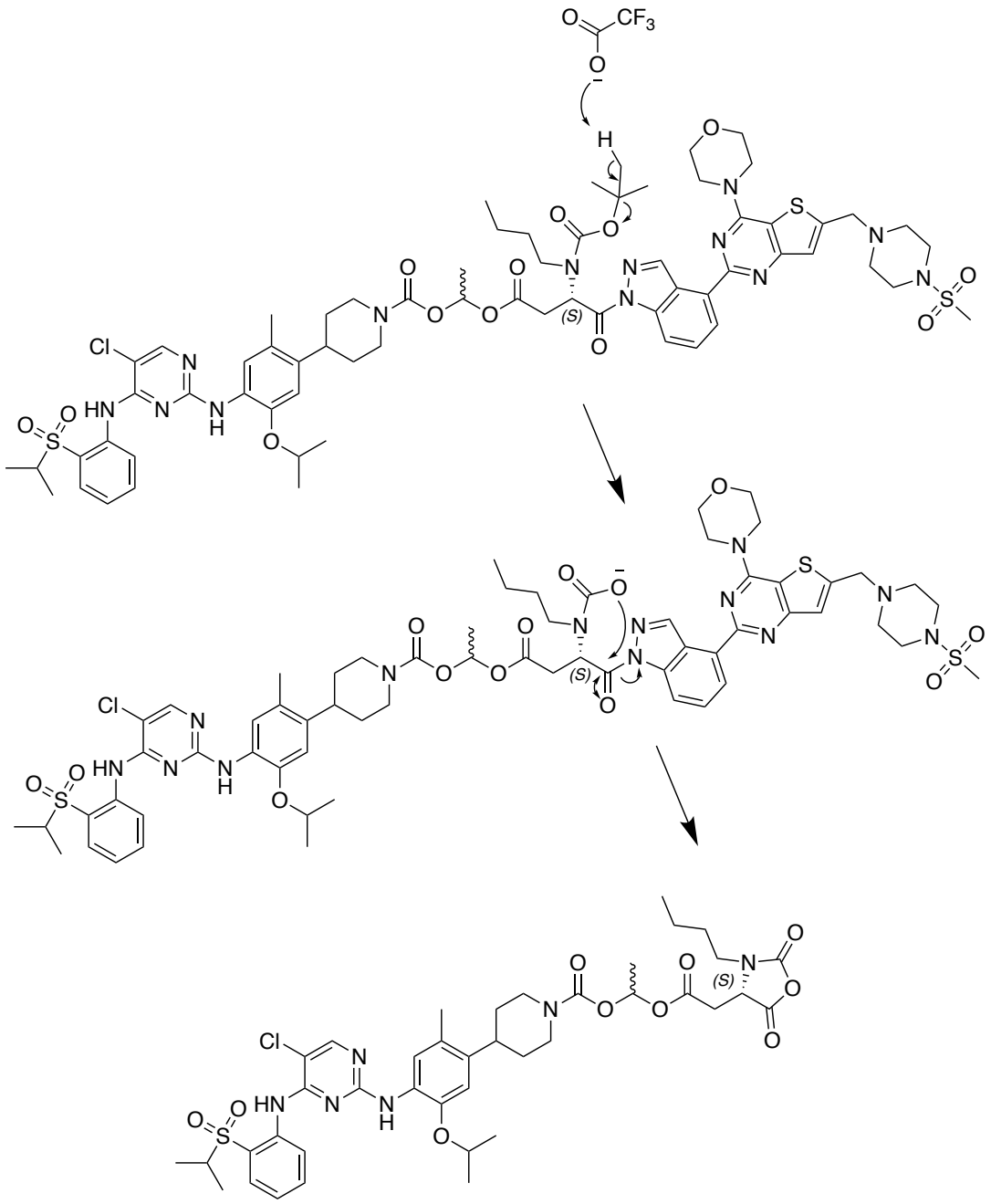


Figure 192. Decomposition of protected AEG-171 upon deprotection.

AEG-165 was unstable in the final amide coupling reaction where pictilisib was introduced. Product peak was identified and the reaction mixture was stored in the freezer in a well-sealed vial until the following day when instrument time on the preparative HPLC system was obtained, however upon injection we observed that the prodrug had cleaved to the desired pictilisb and ceritinib, suggesting that the prodrug cleaved as

desired however, release was rapid. Since the release was likely to be too rapid for the purpose, AEG-165 was excluded from further study.

4.3.3.2 In vitro Stability of Analogues of AEG-118

Stability Studies of AEG-291

The Stability of AEG-291 was analysed by the same procedure as AEG-118. The result of this experiment is shown in Figure 193.

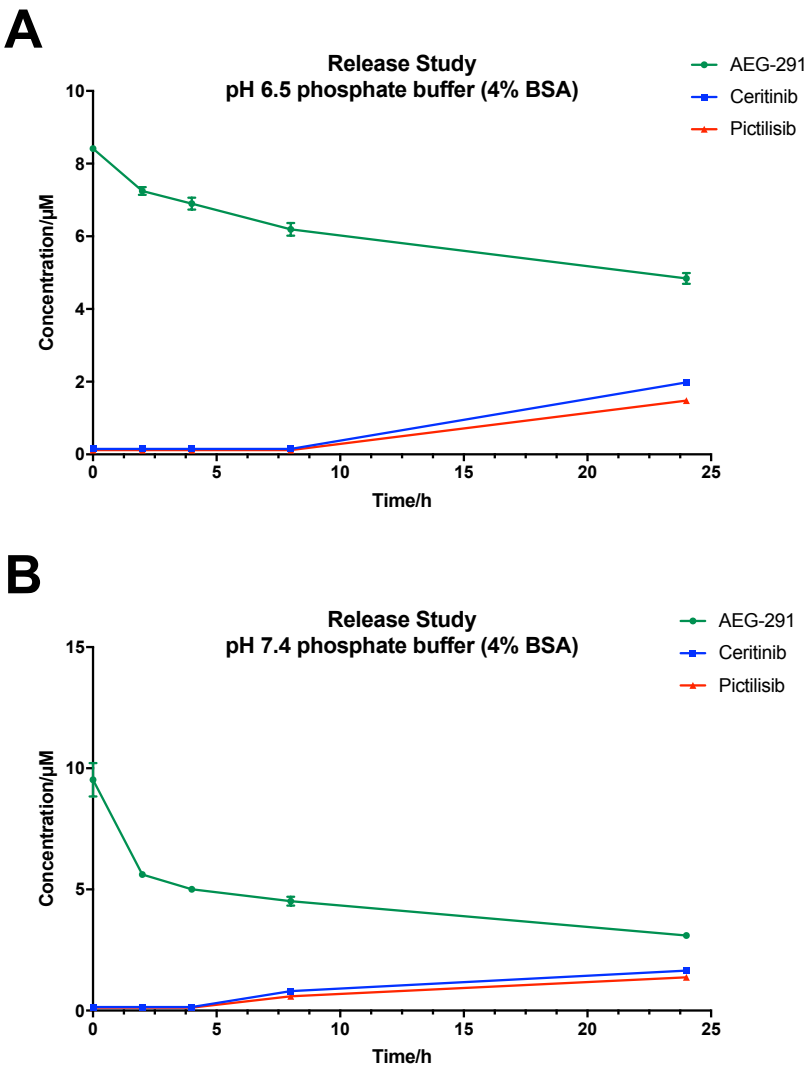


Figure 193. Release study of AEG-291 at (A) pH 6.5 and (B) in phosphate buffer containing 4% bovine serum albumin showing degradation of the prodrug with release of pictilisib followed by the subsequent release of ceritinib.

Immediately, by comparison to the result of AEG-118, it can be seen that there is a slower release of the drugs from the system. Calculation of the observed rate constants

from the slope of a Ln([Prodrug]$_0$/[Prodrug]) *vs* time plot at pH 6.6 and pH 7.4 gave k_{obs} = 0.02 ± 0.003 s^{-1} and k_{obs} = 0.036 ± 0.01 s^{-1} respectively. Additionally, the half-lives at pH 6.5 and pH 7.4 were calculated to be 34.7 h and 19.3 h respectively. The boc protected compounds were evaluated and showed stability after 2 h.

In rat plasma, the degradation of the prodrug is different to that of AEG-118, which showed a zero order degradation (a linear plot of [Prodrug] *vs* time). AEG-291 shows a first order degradation profile, with a linear plot of Ln[Prodrug] *vs* time (Figure 194 A). This suggests a different mechanism of degradation, although it should be noted that the experiment for AEG-118 was for 60 mins and the experiment for AEG-291 was for 120 mins. Additionally, the boc protected compound was assessed for its stability in rat plasma, showing no degradation after 120 mins (graph not shown).

The kinetics of this reaction is first order and can be expressed as the rate law:

$$k[Prodrug] = -\frac{d[Prodrug]}{dt}$$

Integrated this gives:

$$[Prodrug] = [Prodrug]_0 e^{-kt}$$

Taking the natural logarithm gives:

$$Ln[Prodrug] = ln[Prodrug]_0 - kt$$

The rate constant can be calculated from the slope of the Ln[Prodrug] vs time graph (Figure 194 B) and was found to be 0.018 ± 0.001 s^{-1}. The half life can be calculated from the first order rate law and was calculated to be 38 mins.

$$t_{1/2} = \frac{Ln\ 2}{k}$$

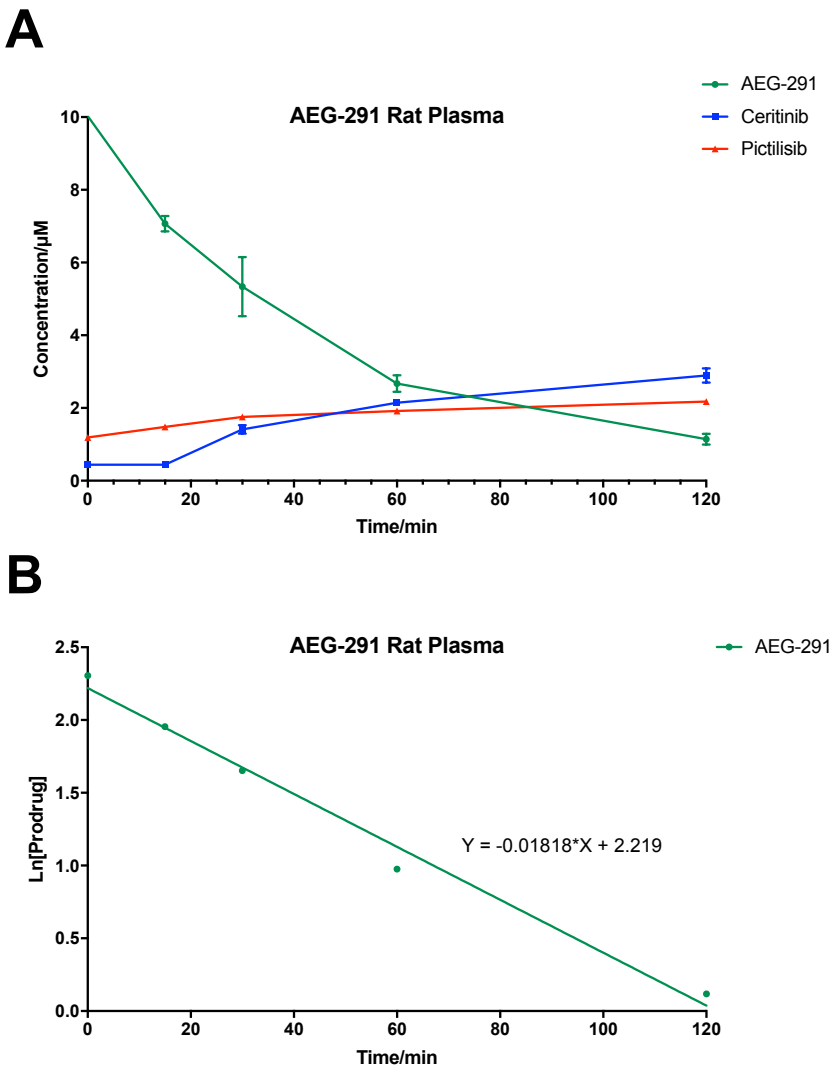


Figure 194. (A) Stability study of AEG-291 in rat plasma. The half-life of AEG-291 in rat plasma was found to be 38 mins. (B) A plot of Ln concentration vs time shows a linear and thus first order degradation.

Stability Studies of AEG-286

The stability of AEG-286 was analysed by the same procedure as AEG-118. The results of this experiment are shown in Figure 195.

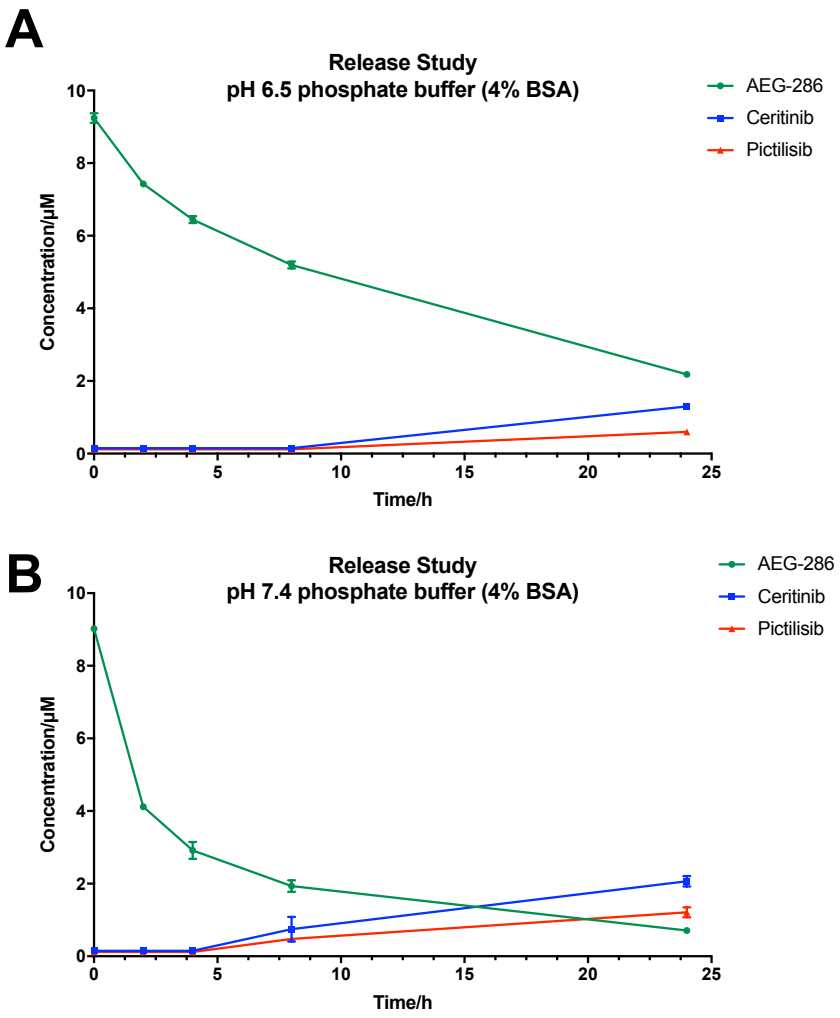


Figure 195. Release study of AEG-291 at (A) pH 6.5 and (B) in phosphate buffer containing 4% bovine serum albumin showing degradation of the prodrug with release of pictilisib followed by the subsequent release of ceritinib.

Calculation of the observed rate constants from the slope of a Ln([Prodrug]$_0$/[Prodrug]) vs time plot at pH 6.6 and pH 7.4 gave k_{obs} = 0.058 ± 0.003 s^{-1} and k_{obs} = 0.091 ± 0.02 s^{-1} respectively. Additionally, the half-lives at pH 6.5 and pH 7.4 were calculated to be 12.0 h and 7.6 h respectively. The boc protected compounds were evaluated and showed stability after 24 h.

In rat plasma, like in the case of AEG-291, the degradation follows a first order

degradation. The results of this experiment are shown in Figure 196 A, where k = 0.01 ± 0.001 and the half-life is 69 mins.

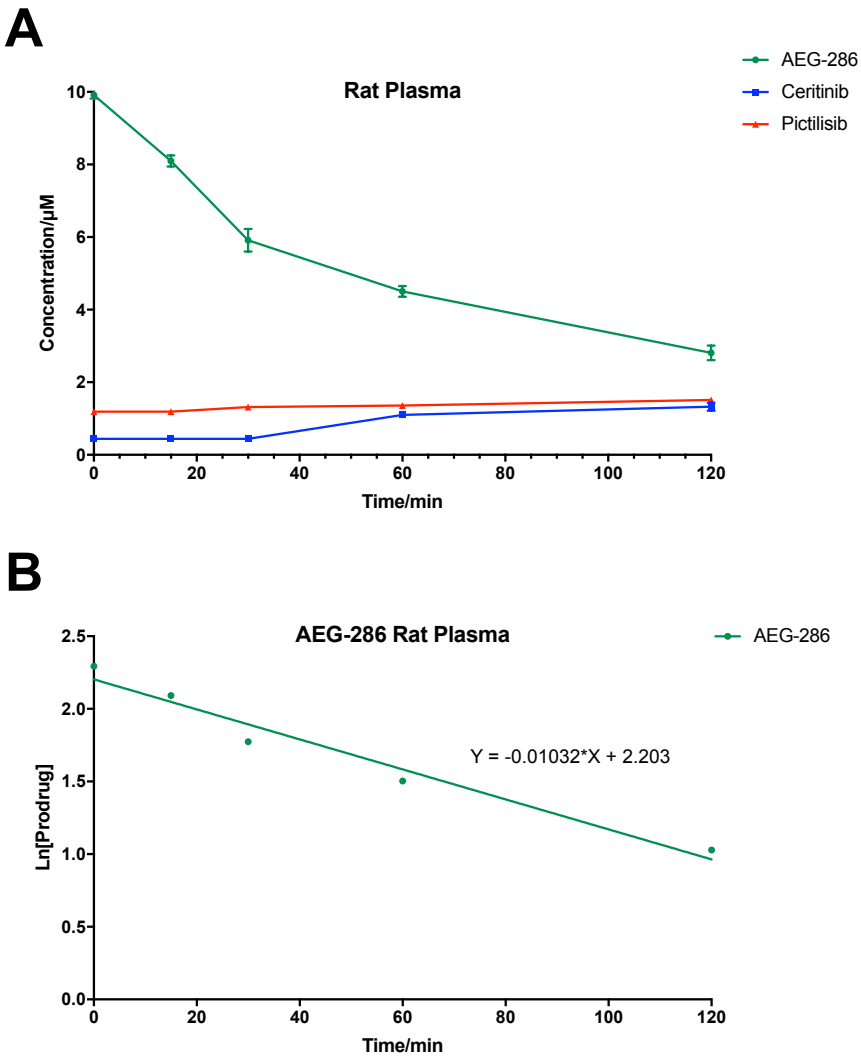


Figure 196. A) Stability study of AEG-286 in rat plasma. The half-life of AEG-291 in rat plasma was found to be 69 mins. (B) A plot of Ln concentration vs time shows a linear and thus first order degradation.

4.3.4 Summary of Pharmacokinetics

The summary of half-lives and rate constants for the prodrug systems is given in Table 18.

Table 18. Summary of half-lives and rate constants for the prodrug systems.

Prodrug	pH	k/ s^{-1}	$t_{1/2}$/ h	r^2
AEG-118	6.5	0.036 ± 0.01	19.3	0.79
	7.4	0.094 ± 0.04	7.4	0.70
AEG-291	6.5	0.02 ± 0.003	34.7	0.93
	7.4	0.036 ± 0.01	19.3	0.74
AEG-286	6.5	0.058 ± 0.003	12.0	0.99
	7.4	0.091 ± 0.02	7.6	0.87

From the table above it can be seen that the half-lives of the prodrugs at pH 6.5 are longer than the half-lives at pH 7.4. It is likely that this effect is due to protonation of the amino group, however it is not clear whether this affects the rate of hydrolysis or whether it affects the percentage protein binding. In the case of AEG-118 release of ceritinib and pictilisb are observed, however in the cases of AEG-291 and AEG-286 significantly less “drug release” was observed, however we observe disappearance of the prodrug. Disappearance of the prodrug is likely due to it being protein bound.

It is hypothesised that for the cases of AEG-291 and AEG-286, where there is no alpha amino amide, hydrolysis of the free fraction is slow due to lack of anchimeric assistance. Conversely, in the case of AEG-118, where there is an alpha amino amide to provide anchimeric assistance, even with a low % free fraction hydrolysis can occur through anchimeric assistance.

The summary of the rate constant and half-lives in plasma is given in Table 19. Firstly, the degradation of AEG-118 was observed to be zero order and the degradation of AEG-291 and AEG-286 was observed to be first order. Examining the graphical data for these systems it can be seen that in the case of AEG-291 and AEG-286 there is significantly less release of ceritinib and pictilisib compared to that of AEG-118. This suggests that once again the alpha amino amide is important.

Table 19. Summary of rate constants and half-lives for the prodrug systems

Prodrug	k	$t_{1/2}$/min	r^2
AEG-118	0.069 ± 0.02 μM s^{-1}	58 min	0.85
AEG-291	0.018 ± 0.001 s^{-1}	38 min	0.99
AEG-286	0.01 ± 0.001 s^{-1}	69 min	0.97

Although the kinetics of the system is complex and not fully understood, AEG-118 was selected for further study over AEG-286 and AEG-291 due to the fact that in the pharmacokinetic experiments there was a much higher percentage release of ceritinib and pictilisib for AEG-118.

4.3.5 Biological evaluation of AEG-118

The biological evaluation of AEG-118 was studied by MTT assay, where the results were compared to the MTT assay results of the ceritinib/pictilisib combination study discussed in chapter 2. The result of this experiment is shown in Figure 197.

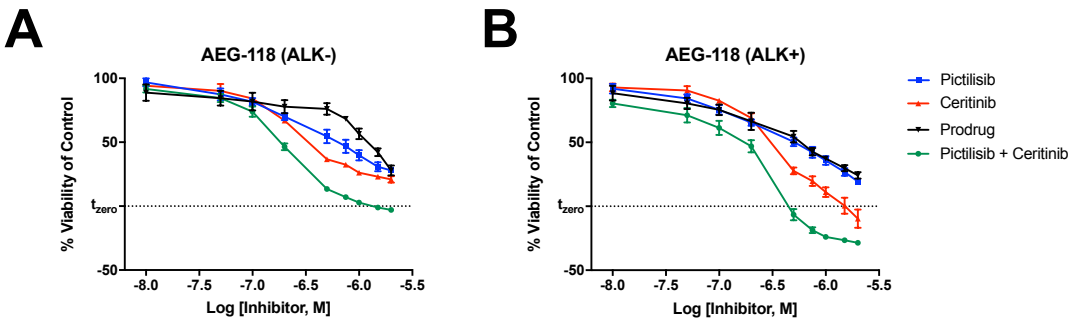


Figure 197. The Dose-response curves for AEG-118, ceritinib, pictilisib and their combination against the ALK- cell line (A) and ALK+ cell line (B). Points are given as the mean ± the standard error of the mean (minimum 3 internal replicates). The dotted line shows the T_{zero} value (0% growth), and points below this line may indicate that an agent is cytotoxic. Growth is represented as percentage viability of the control, which has been normalised to 100%, where 0% is the T_{zero}.

Immediately from the graphs it can be seen that the prodrug does not have the same effect in the assay as the combination of drugs. Against the ALK- cell line the prodrug appears to have an approximate 10-fold shift to the right, resulting in a 10-fold decrease in activity and in the ALK+ cell line the prodrug has either undergone a log unit shift, or is following the same activity as pictilisib.

Since the dose-response curve in the ALK+ cell line appears to mirror the activity

of pictilisib, this suggests that only pictilisib is released and ceritinib remains bound to the linker where the cyclisation mechanism cannot occur. In the ALK- cell line, it could be speculated that pictilisib has been released, however the prodrug has not fully cleaved to provide the drugs in the desired concentration. These observations could be due to four reasons: Firstly, protein binding; the cells are cultured in RPMI medium supplemented with 10% foetal bovine serum. This serum contains albumin and other proteins that the prodrug could be highly bound to. Secondly, during the incubation period the cells are metabolising, releasing CO_2, and forming carbonic acid in the culture medium. This leads to an decrease in pH, which from the previous section was shown to decrease the rate of release of the drugs due to the percentage ionised of the α-amino amide. The culture medium contains an indicator (phenol red), and visually, the ALK+ cell line, being more active, led to more acidic culture medium. These pH shifts are quite subtle (~ pH 6.5 - pH 7.5) since the cells are sensitive to pH changes and growth would be affected at drastic pH shifts. Thirdly, the assay is for a duration of 72 hours. This may not be sufficient time for the prodrug to release the active payloads. Fourthly, the culture medium contains a high level of salts of magnesium and calcium. These ions are not in the phosphate buffers used in previous experiments and could potentially interfere with the hydrolysis, through salt formation of the amine.

In order to test if the percentage of FBS had an effect, the experiment was repeated using 4% FBS, 10% FBS and 20% FBS. The results of this experiment are shown in Figure 198. The GI_{50} values were calculated for each curve and are shown in table 17. Statistical analysis using a one-way ANOVA (Dunnett's multiple comparisons test) to compare the GI_{50} of the 4% and 20% to the 10% GI_{50} showed that for the ALK- cell line there was no statistical significance. However, in the ALK+ cell line there is statistical significance when comparing 4% with 10% ($p = 0.017$), and statistical significance when comparing 20% to 10% ($p = <0.0001$).

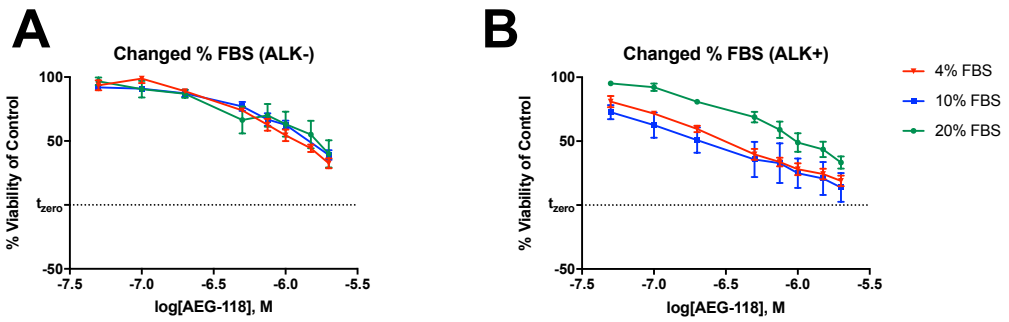


Figure 198. The Dose-response curves for AEG-118 against the ALK- cell line (A) and ALK+ cell line (B) with varied % foetal Bovine serum (FBS). Points are given as the mean ± the standard error of the mean (minimum 3 internal replicates). The dotted line shows the T_{zero} value (0% growth), and points below this line may indicate that an agent is cytotoxic. Growth is represented as percentage viability of the control, which has been normalised to 100%, where 0% is the T_{zero}.

Table 20. GI_{50} values of AEG-118 upon varied % FBS.

	GI50 /µM	
FBS	**ALK-**	**ALK+**
4%	1.17 ± 0.03	0.21 ± 0.10
10%	1.47 ± 0.04	0.21 ± 0.10
20%	1.60 ± 0.09	1.05 ± 0.03

In order to test if time had an effect the incubation period of the assay was increased from 72 h to 120 h. The results of this experiment are shown in Figure 199. The GI_{50} values were calculated for each curve and are shown in Table 18. Statistical analysis using a one-way ANOVA (Dunnett's multiple comparisons test) to compare 120 h exposure to 72 h exposure showed statistical significance in the ALK- cell line ($p = 0.0031$), although a greater difference was seen in the ALK+ cell line ($p = <0.0001$).

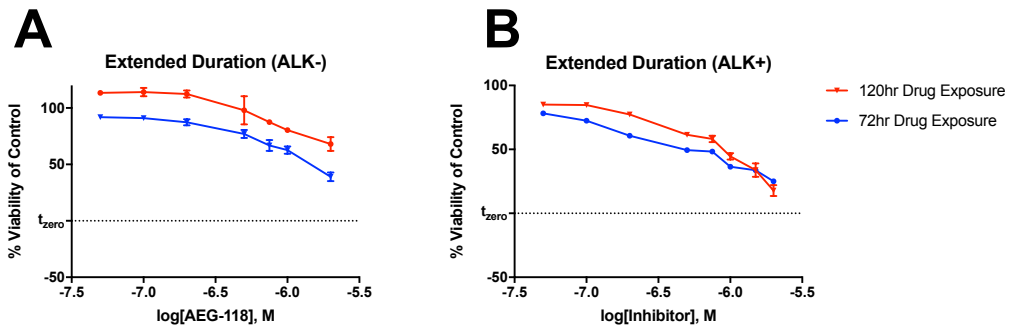


Figure 199. The Dose-response curves for AEG-118 against the ALK- cell line (A) and ALK+ cell line (B) with extended exposure . Points are given as the mean ± the standard error of the mean (minimum 3 internal replicates). The dotted line shows the T_{zero} value (0% growth), and points below this line may indicate that an agent is cytotoxic. Growth is represented as percentage viability of the control, which has been normalised to 100%, where 0% is the T_{zero}.

Table 21. GI_{50} values of AEG-118 upon extended duration.

	GI_{50} /µM	
Duration	**ALK-**	**ALK+**
72 h	1.47 ± 0.04	0.21 ± 0.10
120 h	2.95 ± 0.15	0.74 ± 0.04

In order to test both time and exposure to cells, AEG-118 was pre-incubated in cell culture medium for 48 h prior to the experiment. The results of this experiment are shown in Figure 200. The GI_{50} values were calculated for each curve and are shown in Table 19. Statistical analysis using a one-way ANOVA (Dunnett's multiple comparisons test) to compare the 48 h pre-incubated to the non pre-incubated showed that in the ALK- cell line there was statistical significance ($p = 0.0004$), and for the ALK+ cell line there was also statistical significance ($p = 0.0028$) but this showed that non pre-incubated was more efficacious.

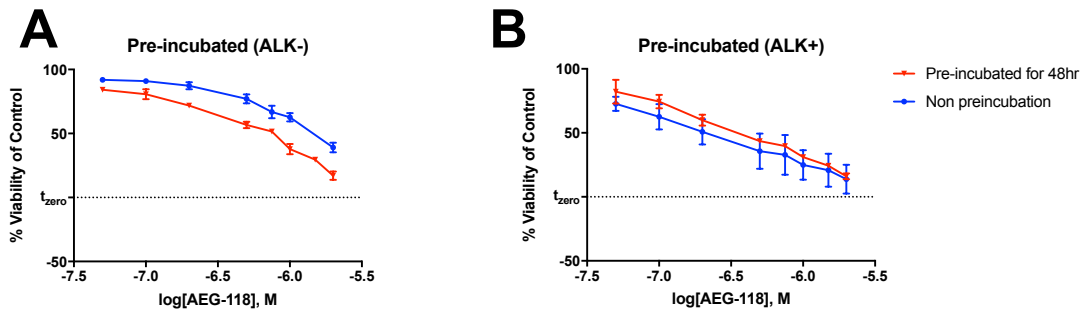


Figure 200. The Dose-response curves for AEG-118 against the ALK- cell line (A) and ALK+ cell line (B) with pre-incubation . Points are given as the mean ± the standard error of the mean (minimum 3 internal replicates). The dotted line shows the T_{zero} value (0% growth), and points below this line may indicate that an agent is cytotoxic. Growth is represented as percentage viability of the control, which has been normalised to 100%, where 0% is the T_{zero}.

Table 22. GI_{50} values of AEG-118 upon pre-incubation.

	GI_{50} /µM	
Pre-incubation	**ALK-**	**ALK+**
-	1.47 ± 0.04	0.21 ± 0.10
48 h	0.58 ± 0.03	0.36 ± 0.03

Since there was accumulating evidence that the FBS may have an effect AEG-118 was incubated in RPMI medium containing 10 % FBS in cell culture conditions without cells. The release of the drugs was followed by HPLC. The result of this experiment is shown in Figure 201. It can be seen from this experiment that even after 72 h the prod-rug has not released its active payloads. This is highly likely due to protein binding.

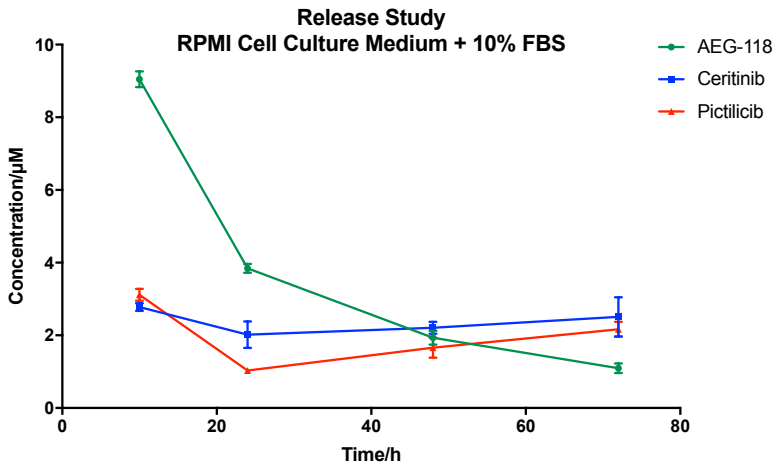


Figure 201. Release study of AEG-118 in RPMI cell culture medium containing 10% foetal bovine serum at 37 C, showing potential binding of the protected prodrug to proteins, with minimal release of the drugs after 72 h.

4.4 Chapter Conclusion

In this chapter, the aim was to develop a bifunctional compound comprised of pictilisib and ceritinib joined together with a cleavable linker. The study began by looking at model systems and performing time course NMR experiments. This showed that the alpha amino amide provides some control over the rate of hydrolysis and additionally provides strong support for the hypothesised mechanism of release which involves hydrolysis of the alpha amino amide releasing pictilisib, followed by a cyclisation, release of CO_2 and acetaldehyde, with subsequent release of ceritinib.

Following work on the model system, the real prodrug systems were synthesised, requiring up to 19 synthetic steps each. The *in vitro* stability of these compounds showed that AEG-118 showed good release of the active payloads, pictilisib and ceritinib, although protein binding was identified as an issue. AEG-118 was progressed to *in vitro* biological evaluation by MTT assay where it was found to be less efficacious than the combination of ceritinib and pictilisib. Further study points towards protein binding as being problematic for the release of pictilisib and ceritinib.

5. Conclusions and Future Work

5.1 Conclusion

There are four FDA approved drugs (crizotinib, ceritinib, alectinib, and brigatinib Figure 3 on page 6) for the treatment of EML4-ALK positive non-small cell lung cancer, and although efficacious, resistance rapidly develops and patients inevitably relapse. This work seeked to identify a suitable combination therapy that could be employed to target multiple signalling nodes to potentially suppress the survival and emergence of resistant tumour cells. This was the focus of chapter II, where multiple drug combinations with ceritinib were explored. It was identified that pictilisib (Figure 22 on page 27), a pan-PI3K inhibitor, exhibited good synergy with ceritinib, as calculated by both the Webb method and Chou & Talalay method (Figure 24 on page 29 and Figure 25 on page 30).

From this discovery, it was decided to explore isoform selective PI3K inhibitors in combination with ceritinib. In chapter III selective PI3Kδ inhibitors were designed and synthesised using a thienopyrimidine core. Compound 3 (Figure 140 on page 139) is highly potent with a pIC_{50} of 9.1 against PI3Kδ, and is highly selective over the other PI3K isoforms, particularly over PI3Kα (δ/α =3981). On the quest for PI3Kα selective compounds with a benzothiazole core PI3Kγ inhibitors were synthesised. Compound 28 (Figure 167 on page 185) was potent with a pIC_{50} of 7.0 and selective over the other isoforms of PI3K, particularly PI3Kβ (δ/β 316 fold). These compounds and a commercial PI3Kα inhibitor (alpelisib, Figure 114 on page 102) were tested in combination with ceritinib and it was found that these combinations did not exhibit the same level of synergy as the combination with ceritinib.

Having identified that pictilisib is the best compound for combination with ceritinib the project focus on this combination. These therapies are known to exhibit severe side effects, and reduction of dose is highly desirable. One strategy for lowering dosage is through drug delivery to the site of action, via controlled release i.e. in the form of a prodrug. In this work, a successful combination was brought together into a bifunctional ligand (AEG-118, Figure 187 on page 235), where the inhibitors are linked via a pH

dependent cleavable linker, introducing a tunable method for controlled release since it is well-known that cancer cells can have a range of pH states (5.7 - 7.8), mainly due to hypoxia. The *in vitro* stability of AEG-118 ($t_{1/2}$ = 58 min) showed good release of the active payloads, pictilisib and ceritinib, although protein binding was identified as an issue. AEG-118 was progressed to *in vitro* biological evaluation by MTT assay where it was found to be less efficacious than the combination of ceritinib and pictilisib. Further study pointed towards protein binding as being problematic for the release of pictilisib and ceritinib.

5.2 Future Work

In terms of combination studies it is recommended that an mTOR inhibitor be tested in combination with Ceritinib. This is due to pictilisib exhibiting good synergy with Ceritinib and the selective PI3K inhibitors not showing synergy. This could be due to pictilisib's weak off-target mTOR activity (mTOR = 0.58 μM), and the synergy may be due to synergic effects from mTOR inhibition. An mTOR inhibitor such as AZD8055 (0.8 nM in MDA-MB-468 cells with excellent selectivity (~1,000-fold) against PI3K isoforms) should be testing in combination with Ceritinib.

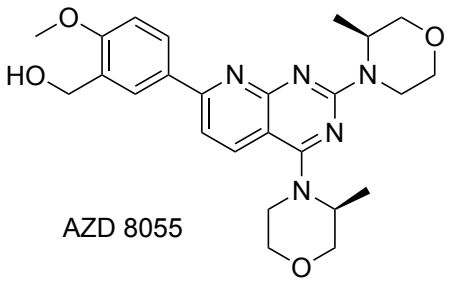


Figure 202. Structure of AZD8055.

If the combination is synergistic the combination could be combined into a bi-functional compound with ceritinib.

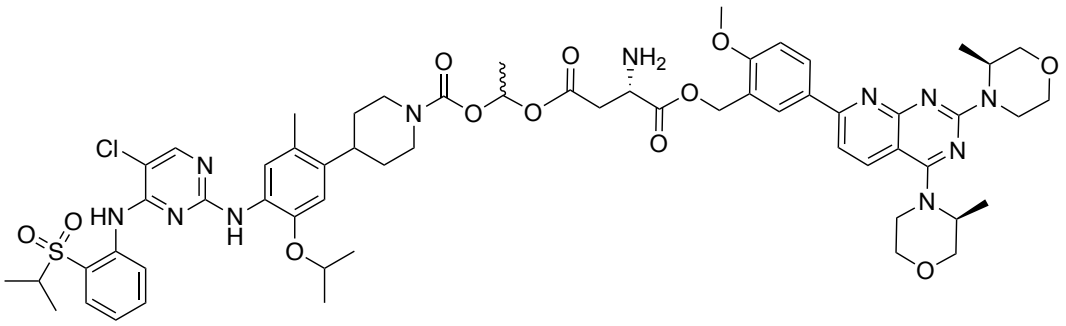


Figure 203. Proposed bifunctional compound comprised of Ceritinib and AZD8055.

6. Experimental

6.1 Pharmacological Protocols

6.1.1 Protocols for Chapter II

6.1.1.1 Mammalian Cell Tissue Culture and Equipment

A549 and ATCC® CCL-185IG™ (A549 EML4-ALK+), H226 and H460 cell lines were obtained from American Type Culture Collection (ATTC). Cell lines were incubated at 37 °C under 5% CO_2 and cultured in RPMI 1640 culture medium supplemented with 10% heat deactivated foetal bovine serum (FBS). All cell culture procedures were performed in a class II laminar flow hood using sterile techniques.

Cell lines were passaged in the growth phase before reaching confluence. To passage, RPMI medium was aspirated and the cells washed with warm phosphate buffered saline (PBS), (~3 mL). The PBS was aspirated and the cells incubated with trypsin/EDTA (1 mL) until the cells detached from the flask. Once detached, the trypsin was deactivated with RPMI medium (6 mL), and an aliquot (500 µL for A549 and H460, 1.5 mL for H226) dispensed into flasks containing culture medium (13 mL).

Stock cell lines were preserved cryogenically in a liquid nitrogen cell bank. To generate stocks of cells, the procedure for trypsinisation above was followed, however following deactivation of the trypsin the cells were pelleted using a centrifuge. The supernatant was aspirated and the pellet was dispersed in 1 mL of freezing medium (5% DMSO in FBS), which was dispensed into a cryovial. The cells were then stored overnight in the standard lab freezer (~ -20 °C) and then next day placed in a -80 °C freezer. After 24 h the cells were moved to the liquid nitrogen cell bank (-196 °C). When required, cells were thawed by placing the cryovial in a water bath set to 37°C. Once thawed the cell suspension was transferred into a flask containing RPMI medium supplemented with 10% FBS. After 24 h the medium was aspirated and replaced. Cells were passaged at least twice before they were used for assays. Passage numbers did not exceed 30.

Standard equipment used for mammalian cell culture included a Beckham-Coulter allegro centrifuge, a Perkin Elmer Envsion plate reader, and a FC-500 Beckham-Coul-

ter flow cytometer.

6.1.1.2 MTT Assay

Inhibition of Cell Growth and Metabolic Activity Assay

3-(4, 5-Dimethylthiazol-2-yl)-2,5-diphenyltetrazolium bromide (MTT; AlfaAesar) was used to quantify an inhibitor's ability to inhibit growth and metabolic activity of human-derived lung cancer cell lines. Cells were plated in 96-well microtiter plates at a density of 3 x 10^3 (A549, ATCC® CCL-185IG™, H460) and 1 x 10^4 (H226) cells per well in 180 µL for single agents and 160 µL for combination assays. Cells were allowed to attach for 24 h before test agent was introduced. Serial dilutions from a 10 mM top stock solution in DMSO were prepared in RPMI medium before each assay and were introduced to the assay in 20 µL aliquots, in a minimum of 3 wells per concentration (n = 3 - 6). Measurements representative of viable cells were performed at the time of test agent addition (T_{zero}) and after 72 h treatment by adding 50 µL of MTT to each well followed by 2.5 h incubation at 37 °C, allowing time for MTT reduction by viable cell dehydrogenases to violet formazan. The supernatant of each well was then aspirated followed by addition of 150 µL 100 % DMSO (Sigma Aldrich) for formazan solubilisation. Optical density values were retrieved at 570 nm. There were a minimum of three replicates per assay (n = 3).

6.1.1.3 Clonogenic Assay

Cells were seeded at 400 cells per well in 6- well plates with RPMI medium (2 mL) and allowed to attach for 24 h, after which time cells in control wells were treated with vehicle (RPMI medium) alone, and cells in treatment wells were treated with inhibitor. Following 24 h or 72 h exposure, RPMI medium containing inhibitor was aspirated, and the cells carefully washed with of PBS (1 mL) and fresh RPMI medium (2 mL) was added to each well. Plates incubated in the CO_2 incubator at 37 °C and inspected under microscope daily until cells in control wells formed colonies of ~50 cells (approx. 5 - 7 days). The RPMI medium was aspirated and the cells carefully washed with PBS (1 mL) before fixation with 100% methanol (0.5 ml) for 15 min and then stained

with 0.5% methylene blue in 1:1 water:methanol (700 µL) for an additional 10 min. The stained cells were washed with tap water and colonies counted by eye. 2 internal repeats were performed per repeat. 3 repeats wwere performed for each experiment, n = 3.

6.1.1.4 Cell Cycle Analysis Assay

Cells were seeded at 1×10^5 cells per well in 6-well plates with RPMI medium (2 mL) for 24 h exposure and at the lower seeding density of $5x10^4$ cells for 72 h exposure. Cells were allowed to attach for 24 h, after which time cells in control wells were treated with vehicle (medium) alone, and cells in treatment wells were treated with inhibitor using the GI50 values obtained from the MTT assays i.e. 1 x GI50 and 2 x GI50. Following treatment (24 h or 72 h), RPMI medium containing floating cells was collected from each well into FACS (fluorescence activated cell sorting) tubes on ice (4 °C). Attached cells were trypsinised and once detached, the RPMI medium containing the floating cells was reintroduced into the corresponding well, mixed and the pooled cells transferred back into the corresponding FACs tube and stored on ice. Collated samples were pelleted at 1200 rpm for 5 min at 4 °C. The supernatants were discarded and the pellets were disturbed by gently flicking the tubes. The pelleted cells were re-suspended in cold (4 °C) fluorochrome solution (400 µL, PI 50 µg/ml, RNase 100µg/ml, 0.1% sodium citrate and 0.1% (v/v) triton X-100 in PBS) and stored overnight in the dark at 4 °C. After storing samples at 4 °C overnight the cell suspensions were gently syringed into 23G needle to obtain single cell suspension and immediately before analysis, the samples vortexed. A minimum of 10 000 events were recorded on 2 internal repeats , where experiments were repeated 3 times (n = 3). Data was analysed using the flow cytometry software Weasel, where gates were applied on dot plots and histograms for treated samples relative to the vehicle treated control.

6.1.1.5 Apoptosis Annexin V (FIT-C/PI) Assay

Annexin V-FITC Apoptosis detection kit was purchased from Invitrogen™. Cells were seeded at 1×10^5 cells per well in 6-well plates with RPMI medium (2 mL) for 24 h exposure and at the lower seeding density of $5x10^4$ cells for 72 h exposure. Cells

were allowed to attach for 24 h, after which time cells in control wells were treated with vehicle (medium) alone, and cells in treatment wells were treated with inhibitor using the GI_{50} values obtained from the MTT assays i.e. 1 x GI_{50} and 2 x GI_{50}. Following treatment (24 h or 72 h), RPMI medium containing floating cells was collected from each well into FACS (fluorescence activated cell sorting) tubes on ice (4 °C). Attached cells were trypsinised and once detached, the RPMI medium containing the floating cells was reintroduced into the corresponding well, mixed and the pooled cells transferred back into the corresponding FACs tube and stored on ice using a syringe and 23G needle to obtain single cell suspension. Collated samples were pelleted at 1200 rpm for 5 min at 4 °C. The supernatants were discarded and the pellets were disturbed by gently flicking the tubes. The pelleted cells were re-suspended in annexin binding buffer (100 µL) and Annexin V-FITC (5 µl). Tubes were briefly vortexed and left at room temperature in the dark for approximately 15 min after which time annexin binding buffer (400 µL) and Propidium Iodide solution (10 µL, 20 µg/mL) were added to each tube. Tubes were vortexed and kept on ice in the dark for 10 min prior to analysis on the flow cytometer. Samples were analysed within 1 h of completion of the above protocol to avoid deterioration of cells. Gates were set up on a dual colour plot for vehicle treated samples and the percentages of early apoptotic cells (annexin V – FITC positive, PI negative) or late apoptotic/ necrotic cells (annexin V – FITC positive, PI positive) recorded.

6.1.1.6 Pharmacological Data Analysis

The concentration required to inhibit cell proliferation by 50 % (GI_{50}) was calculated by equation 6 and is expressed as the mean value ± the standard error of the mean (SEM). The D_m value and m-value were calculated from the median effect plot using linear regression and are expressed as the mean value ± SEM. The combination index is calculated from the means of the D_m and m-values. A detailed method for determining the combination index is given in section 1.3. In brief, both the Webb fractional product and the Chou and Talalay combination index methods were used. Graphs and statistacal analyses were generated and performed using GraphPad Prism. Statistical significance was determined using t-tests, one-way analysis of variance (ANOVA) or

two-way ANOVA.

6.1.2 Protocols for Chapter III

6.1.2.1 HTRF PI3K assay.

Potency (IC_{50}), inhibition of PI3K enzymatic activity was tested at GlaxoSmith-Kline (GSK) Stevenage, by Dr. James Rowedder using a homogeneous time-resolved fluorescence (HTRF) technique, a kit provided by Millipore. Reactions were performed in assay buffer containing 50 mM HEPES, pH 7.0, 150 mM NaCl, 10 mM MgCl2, <1% cholate (w/v), <1% CHAPS (w/v), 0.05% sodium azide (w/v), and 1 mM DTT. Enzymes were preincubated with compound, serially diluted 4-fold in 100% DMSO, for 15 min prior to reaction initiation upon addition of substrate solution containing ATP at Km for the specific isoform tested (α at 250 μM, β at 400 μM, δ at 80 μM, and γ at 15 μM), PIP2 at either 5 μM (PI3Kδ) or 8 μM (PI3Kα, -β, and -γ) and 10 nM biotin-PIP3. Assays were quenched after 60 min by addition of a quench/detection solution prepared in 50 mM HEPES, pH 7.0, 150 mM NaCl, <1% cholate, <1% Tween 20, 30 mM EDTA, 40 mM potassium fluoride, and 1 mM DTT containing 16.5 nM GRP- 1 PH domain, 8.3 nM streptavidin-APC, and 2 nM europium-anti- GST and were left for a further 60 min in the dark to equilibrate prior to reading using a BMG RubyStar plate reader. Ratio data were normalized to high (no compound) and low (no enzyme) controls prior to fitting using a logistical four-parameter equation to determine IC_{50}.

6.1.2.2 Lipophilicty determination ($mLogD_{7.4}$)

$mLogD_{7.4}$ was measured using reverse phase HPLC techniques at GSK Stevenage by Dr. James Rowedder.

6.1.2.3 Aqueous solubility determination.

Aqueous solubility was measured at GSK Stevenage by Dr. James Roewedder using a precipitative method. GSK in-house kinetic solubility assay involved the following: 5 mL of 10 mM DMSO stock solution diluted to 100 μL with pH 7.4 phosphate buffered saline, equilibrated for 1 h at room temperature, filtered through Millipore Multiscreen HTS-PCF filter plates (MSSL BPC). The filtrate was quantified by suitably

calibrated flow injection chemiluminescent nitrogen detection (CLND).The standard error of the CLND solubility determination was ±30 μM, and the upper limit of the solubility is 500 μM when working from 10 mM DMSO stock solution.

6.2 Molecular Modelling

6.2.1 Modelling for Chapter III

For PI3K δ compounds: The three-dimensional coordinates of the cocrystal structure of PI3K δ in complex with pictilisib (pdb code 2WXP) was retrieved from the Protein Data Bank (PDB). All non-protein atoms, including water and sugar molecules were removed from the model. Using MAKE RECEPTOR 3.0.0 software (OpenEye Scientific Software) an active site model was prepared for the active site. No constraints were used during this preparation of the receptor model. A database composed of suggested compounds for docking and the reference ligand (pictilisib PI3K δ) and the newly designed compounds were processed with the Omega 2.5.1.4 software (OpenEye Scientific Software Inc.) to generate the 200 lowest energy conformations for each compound. Finally, the compounds were docked into the active site models using the FRED 3.0.1 software and the Chemgauss4 scoring function (OpenEye Scientific Software Inc.). The docking was visually analyzed for the top 5 best scored poses for the conformation of the designed compounds using VIDA 4.3.0 and outputs visualized using PyMOL (The PyMOL Molecular Graphics System, Version 1.8 Schrödinger, LLC). The poses were visually compared with the co-crystallized reference ligand and the best overlaying docking pose was used.

For PI3Kα compounds: The three-dimensional coordinates of the cocrystal structures of PI3K (pdb codes 2WXP, 4BFR, 3DBS, 5DXT) were retrieved from the Protein Data Bank. The Schrödinger software suite Maestro was used to prepared the protein and ligand files as above. Schrödinger's Glide softweare was used to perform the docking, where no constraints were employed. Docking poses were visualised in Maestro and Pymol as above.

6.3 Pharmacokinetic Protocols

6.3.1 Pharmacokinetics for Chapter IV

6.3.1.1 NMR Kinetic Studies

The a-amino model system was deprotected and dried under vacuum on the same day as the kinetic study. Prior to the experiment a blank ample containing the solvent system (10mM phosphate buffer: *d*-6 DMSO, 1:1) was inserted into the Bruker AV(I-II)800 spectrometer and a pre lock and shim were performed. Samples were prepared by adding d-6 DMSO (300 µL) to approximately 1 mg of sample, solublising the sample. Phosphate buffer (10 mM, 300µL) was then added, and solids removed by filtration taking care to be as quick as possible to perform the procedure to reduce "dead-time". The sample was quickly inserted directly into the spectrometer, bypassing the autosampler, and measurements were performed as rapidly as possible. Total dead time is approximately 7-8 mins for each sample. This time includes all steps from addition of the DMSO until the first spectrum was acquired. 512 spectra were then obtained for each sample with ~91 s between each time point for pH 6.4, and ~3.6 s between each time point for pH 6.8 and 7.4. Since the experiment was performed in buffer made up in H_2O, water suppression was applied to the experiment.

The 2D dataset was analysed using TopSpin 4.0.5 using T1/T2 dynamics, performing manual integration to a slice of the dataset and applying these integrals to the whole dataset. The integrals were exported to a text file and the data analysed in graph pad prism, normalising the integrals where zero was set as the lowest integral value, and 100% set as the highest integral value. The normalised integrals, now as a percentage, were plotted against time and a single phase exponential function was fitted to the data to obtain the half life. The rate constants were obtained from the slope of a plot of Ln([Ceritinib Mimetic]/$[Prodrug]_0$) vs time.

6.3.1.2 HPLC Kinetic studies

The prodrugs were deprotected and dried under vacuum on the same day as the stability study. The deprotected prodrugs were then tested for their stability and conversion into their parent drugs, Pictilisib and Ceritinib. Potassium phosphate buffer (10 mM) supplemented with 4% BSA (w/v) at pH 6.5 and 7.4 was used for chemical conversion of the prodrug. Rat plasma was used to investigate contribution of enzymatic reaction to the conversion. A stock solution of the prodrug was spiked into each test medium at 10 μM of starting concentration and the reaction mixtures were incubated at 37°C at 200 rpm using a shaking incubator (Thermo Scientific MaxQ4000, Waltham, MA, USA). Samples (50 μL) were withdrawn at pre-determined time points and the reaction was quenched with addition of acetonitrile with 0.1 M HCl (150 μL). The samples were briefly vortex-mixed and centrifuged at 1700 g for 5 min. The supernatant was collected and 10 μL was injected to the HPLC-UV system. All experiments were conducted in triplicate.

6.4 Chemical Synthesis

6.4.1 General

Reagents were purchased from commercial sources (typically, Sigma Aldrich, Alpha Aesar, Fisher Scientific, Fluorochem or Activate Scientific), and were used without further purification. Anhydrous solvents were purchased from Fisher scientific and were used without further distillation. All reactions with air- and moisture-sensitive reagents were carried out under an atmosphere of nitrogen. The flasks were flushed with nitrogen. The liquids were added using plastic syringes.

6.4.2 Nuclear Magnetic Resonance

Routine ^{1}H and ^{13}C, experiments were attained on a Bruker AV400, spectrometer operating at 400 MHz, where coupling constants (J) are reported to the nearest 0.1 Hz. Additionally, a Bruker AV(III)500 operating at 500 MHz was used for lower concentration samples, and a Bruker AV(III)800 operating at 800 MHz, was used for kinetic experiments and exceptionally low concentration samples. Measurements were recorded at 21 °C unless otherwise stated. All ^{13}C NMR are ^{1}H- broadband-decoupled. The chemical shifts δ are given in [ppm] and all coupling constants J are given in [Hz] and are reported to the nearest 0.1 Hz. The spectra are referenced to the signal of the deuterated solvent. The following abbreviations were used to describe signal shapes and multiplicity: s (singlet), s. br (broad singlet), d (doublet), dd (doublet of doublet), ddd (doublet of a doublet of a doublet), dddd (doublet of a doublet of a doublet of a doublet), t (triplet), dt (doublet of a triplet), q (quartet), dq (doublet of a quartet) and m (multiplet). The processing of the NMR data was carried out using the NMR software Mestrenova (Mnova).

6.4.3 Mass Spectrometry

Liquid chromatography mass spectrometry (LCMS) data was recorded on a Shimadzu UFLCXR (High performance liquid chromatography (HPLC) system coupled to an Applied Biosystems API2000 electrospray ionization mass spectrometer (ESI-MS). The column used was a Phenomenex Gemini-NX 3µm 110 Å C-18, 50 x 2 mm thermo-

stated at 40 °C. The flow rate was 0.5 mL / min of a solvent system of increasing gradient of acetonitrile (5-95%) in water, each containing 0.1% formic acid. UV detection was at 220 nm and 254 nm. m/z values are reported in Daltons to one decimal place and retention times (r.t.) are provided in minutes to two decimal places.

All high resolution mass spectra (HRMS) time of flight electrospray were recorded on a Bruker Daltonics micrOTOF Electrospray ionisation- time of flight mass spectrometer (ESI-TOF MS). Measured (m/z) is withing 6 ppm of the theoretical (m/z).

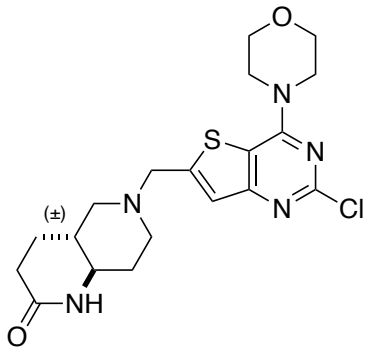
6.4.4 Chromatography

Where thin-layer chromatography (TLC) was performed, UV light and standard TLC stains were used to visualise the Merck Silica gel 60 Å F_{254} plates. Compounds were purified via column chromatography using either a Thompson pump and normal phase Interchim Puriflash pre-packed cartridges consisting of 50 μM silica, or a glass column using Merck Geduran silica gel 60 Å (230-240 μm) Column size selected was generally 40-60 times the loading amount. STX cartridges

6.4.5 Synthesis

6.4.5.1 Synthesis for Chapter III

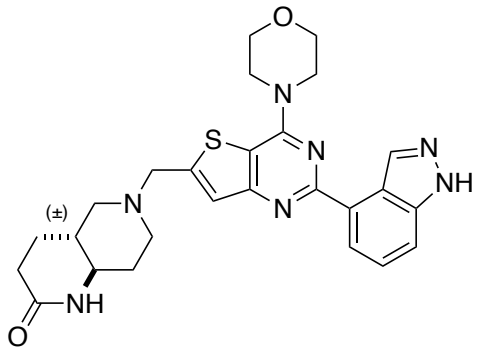
±(4aRS,8aRS)-6-((2-chloro-4-morpholinothieno[3,2-d]pyrimidin-6-yl)methyl) octahydro-1,6-naphthyridin-2(1H)-one



Tert-butyl trans-2-oxooctahydro-1,6-naphthyridine-6(2H)-carboxylate (300 mg, 1.18 mmol) was stirred in HCl in dioxane (2 mL, 4 M) overnight, after which time excess HCl in dioxane was removed *in vacuo* and the resulting white solid, the deprotected amine, was triturated with diethyl ether and dried *in vacuo*. The solid was taken up in MeCN (3mL) to form a white suspension to which 2-chloro-4-morpholinothieno[3,2-d]

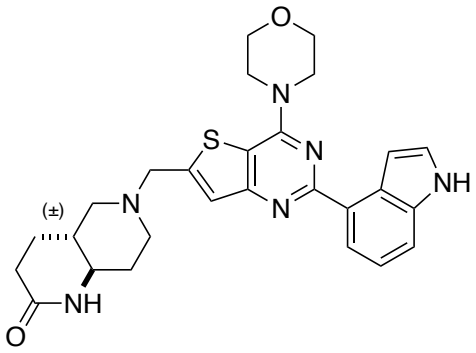
pyrimidine-6-carbaldehyde (335 mg, 1.18 mmol), trimethylorthoformate (0.65 mL, 5.9 mmol) and sodium acetate (194 mg, 2.36 mmol) were added. The reaction mixture was heated to 45 °C and stirred for 2 hours before leaving to cool to room temperature. After stirring at room temperature for 1 h, sodium triacetoxyborohydride (750 mg, 3.54 mmol) was added and the reaction mixture was stirrred for a further 6 hours. Deionised water (20 mL) was poured onto the reaction mixture, which was then extracted with dichloromethane (3 x 20 mL). The combined organic extracts were dried ($MgSO_4$), filtered, and solvent removed *in vacuo* to give a pale yellow oil. Purification by flash column chromatograhy (silica gel), eluting with 0-6% MeOH containing NH_3 (0.7 N) in CH_2Cl_2 gave the product as an off-white solid (316 mg, 63%). ^{1}H NMR (400 MHz, DMSO) δ 7.59 (s, 1H), 7.29 (s, 1H), 3.93 – 3.85 (m, 4H), 3.89 – 3.83 (m, 2H), 3.80 – 3.72 (m, 4H), 2.97 – 2.84 (m, 2H), 2.83 (td, *J* = 11.4, 10.0, 2.5 Hz, 1H), 2.28 – 2.18 (m, 1H), 2.14 (td, *J* = 12.0, 11.4, 2.5 Hz, 1H), 1.88 (t, *J* = 10.8 Hz, 1H), 1.82 (dd, *J* = 12.6, 3.6 Hz, 1H), 1.65 – 1.52 (m, 2H), 1.56 – 1.43 (m, 1H), 1.45 – 1.29 (m, 2H). ^{13}C NMR (101 MHz, DMSO) δ 170.7, 163.1, 158.3, 156.2, 153.6, 122.0, 112.7, 66.3, 57.1, 56.7, 55.8, 51.8, 46.4, 38.8, 32.1, 31.5, 25.1. LCMS (m/z): calc'd for $C_{19}H_{24}ClN_5O_2S$ $[M + H]^+$ 422.9, found 422.3, r.t. 1.94.

±(4aRS,8aRS)-6-((2-(1H-indazol-4-yl)-4-morpholinothieno[3,2-d]pyrimidin-6-yl) methyl)octahydro-1,6-naphthyridin-2(1H)-one (Compound 17)



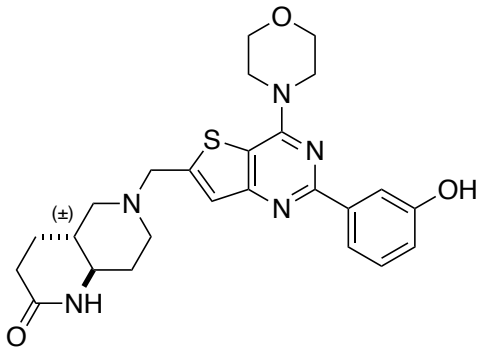
A mixture of ±(4aRS,8aRS)-6-((2-chloro-4-morpholinothieno[3,2-d]pyrimidin-6-yl)methyl)octahydro-1,6-naphthyridin-2(1H)-one (70 mg, 0.17 mmol), (1H-indazol-4-yl)boronic acid (40 mg, 0.25 mmol), aqueous Na_2CO_3 (225 µL, 0.51 mmol, 2 M) and bis(triphenylphosphine)palladium chloride (12 mg, 0.017 mmol) in EtOH: deionised water, (3 mL, 3:1) was irradiated under microwave radiation for 45 mins at 125 °C. After concentration the residue was purified by flash column chromatography (silica gel), eluting with 0-10% MeOH in CH_2Cl_2 containing NH_3 (0.7 N) to give the product as a white solid (77 mg, 90%). ^{1}H NMR (400 MHz, DMSO) δ 13.21 (s, 1H), 8.90 (s, 1H), 8.24 (d, *J* = 7.2 Hz, 1H), 7.68 (d, *J* = 8.2 Hz, 1H), 7.60 (s, 1H), 7.53 – 7.44 (m, 2H), 4.06 – 3.98 (m, 4H), 3.97 – 3.89 (m, 2H), 3.89 – 3.79 (m, 4H), 3.02 – 2.89 (m, 2H), 2.84 (td, *J* = 11.5, 3.5 Hz, 1H), 2.28 – 2.11 (m, 3H), 1.90 (t, *J* = 11.0 Hz, 1H), 1.89 – 1.81 (m, 1H), 1.68 – 1.49 (m, 2H), 1.46 – 1.34 (m, 2H). ^{13}C NMR (101 MHz, DMSO) δ 170.7, 162.7, 160.1, 158.1, 151.6, 141.2, 135.6, 131.6, 126.1, 123.6, 121.6, 121.4, 112.8, 112.5, 66.5, 57.1, 56.9, 55.8, 51.8, 46.6, 38.9, 32.2, 31.5, 25.1. LCMS (m/z): calc'd for $C_{26}H_{29}N_7O_2S$ $[M + H]^+$ 504.3 found 504.6, r.t. 2.01, purity 95%.

±(4aRS,8aRS)-6-((2-(1H-indol-4-yl)-4-morpholinothieno[3,2-d]pyrimidin-6-yl) methyl)octahydro-1,6-naphthyridin-2(1H)-one (Compound 18)



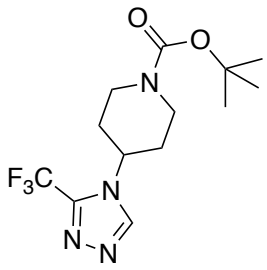
A mixture of ±(4aRS,8aRS)-6-((2-chloro-4-morpholinothieno[3,2-d]pyrimidin-6-yl)methyl)octahydro-1,6-naphthyridin-2(1H)-one (70 mg, 0.17 mmol), (1H-indol-4-yl) boronic acid (40 mg, 0.25 mmol), aqueous Na_2CO_3 (225 µL, 0.51 mmol, 2 M) and bis(triphenylphosphine)palladium chloride (12 mg, 0.017 mmol) in EtOH: deionised water, (3 mL, 3:1) was irradiated under microwave radiation for 45 mins at 125 °C. After concentration the residue was purified by flash column chromatography (silica gel), eluting with 0-10% MeOH in CH_2Cl_2 containing 1% NH_3 to give the product as a grey white solid (80 mg, 94%). ^{1}H NMR (400 MHz, DMSO) δ 11.24 (s, 1H), 8.14 (d, J = 7.5 Hz, 1H), 7.60 (s, 1H), 7.53 (d, J = 7.9 Hz, 1H), 7.49 – 7.40 (m, 3H), 7.21 (t, J = 7.7 Hz, 1H), 4.04 – 3.96 (m, 4H), 3.91 – 3.87 (m, 2H), 3.86 – 3.80 (m, 4H), 3.01 – 2.89 (m, 2H), 2.83 (td, J = 11.2, 10.8, 3.8 Hz, 1H), 2.29 – 2.10 (m, 3H), 1.93 – 1.80 (m, 2H), 1.65 – 1.46 (m, 2H), 1.47 – 1.30 (m, 2H). ^{13}C NMR (101 MHz, DMSO) δ 170.7, 162.8, 161.7, 158.0, 151.1, 137.5, 130.2, 126.8, 126.4, 123.6, 120.9, 120.9, 113.8, 112.1, 103.9, 66.5, 57.1, 56.9, 55.9, 51.8, 46.5, 38.9, 32.2, 31.5, 25.1. LCMS (m/z): calc'd for $C_{27}H_{30}N_6O_2S$ $[M + H]^+$ 503.6, found 503.6, r.t. 1.95, purity 98%.

±(4aRS,8aRS)-6-((2-(3-hydroxyphenyl)-4-morpholinothieno[3,2-d]pyrimidin-6-yl)methyl)octahydro-1,6-naphthyridin-2(1H)-one (Compound 16)



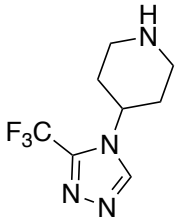
A mixture of ±(4aRS,8aRS)-6-((2-chloro-4-morpholinothieno[3,2-d]pyrimidin-6-yl)methyl)octahydro-1,6-naphthyridin-2(1H)-one (70 mg, 0.17 mmol), (3-hydroxyphenyl) boronic acid (35 mg, 0.25 mmol), aqueous Na_2CO_3 (225 µL, 0.51 mmol, 2 M) and bis(triphenylphosphine)palladium chloride (12 mg, 0.017 mmol) in EtOH: deionised water, (3 mL, 3:1) was irradiated under microwave radiation for 45 mins at 125 °C. After concentration the residue was purified by flash column chromatography (silica gel), eluting with 0-10% MeOH in CH_2Cl_2 containing 1% NH_3 to give the product as a grey white solid (65 mg, 80%). ^{1}H NMR (400 MHz, DMSO) δ 9.50 (s, 1H), 7.89 – 7.82 (m, 2H), 7.59 (s, 1H), 7.37 (s, 1H), 7.28 (t, *J* = 7.9 Hz, 1H), 6.87 (dd, *J* = 8.6, 2.1 Hz, 1H), 4.01 – 3.94 (m, 4H), 3.89 – 3.84 (m, 2H), 3.84 – 3.78 (m, 4H), 2.99 – 2.86 (m, 2H), 2.83 (ddd, *J* = 13.4, 10.3, 3.7 Hz, 1H), 2.27 – 2.08 (m, 3H), 1.93 – 1.79 (m, 2H), 1.65 – 1.45 (m, 2H), 1.46 – 1.29 (m, 2H). ^{13}C NMR (101 MHz, DMSO) δ 170.7, 162.8, 159.5, 157.9, 157.9, 151.5, 139.9, 129.7, 123.3, 119.0, 117.5, 114.9, 112.6, 66.5, 57.1, 56.9, 55.8, 51.8, 46.3, 38.9, 32.2, 31.5, 25.1. LCMS (m/z): calc'd for $C_{25}H_{29}N_5O_3S$ $[M + H]^+$ 480.6, found 480.3, r.t. 1.98, purity 98%.

Tert-butyl 4-(3-(trifluoromethyl)-4H-1,2,4-triazol-4-yl)piperidine-1-carboxylate



To a stirred solution of trifluoroacetic hydrazide (704 mg, 5.5 mmol) in anhydrous MeCN (5 mL) was added DMF.DMA (733 μL, 5.5 mmol). The reaction mixture was heated to 50 °C and after 30 mins 4-aminopiperidine-N-boc (1.0 g, 5.0 mmol) was added along with AcOH (1mL) and the reaction temperature was increased to 100 °C. After a further 6 hours the reraction mixture was concentrated and absorbed onto silica. Purification by flash column chromatography (silica gel), eluting with CH_2Cl_2: MeOH (0-2%) gave the product as a white foam (140 mg, 8%). ^{1}H NMR (400 MHz, $CDCl_3$) δ 8.37 (s, 1H), 4.46 – 4.34 (m, 2H), 4.33 (tt, *J* = 12.2, 4.0 Hz, 1H), 2.94 – 2.82 (m, 2H), 2.22 – 2.08 (m, 2H), 1.87 (qd, *J* = 12.4, 4.5 Hz, 2H), 1.51 (s, 9H). ^{13}C NMR (101 MHz, DMSO) δ 145.8, 142.66 (q, *J* = 37.9 Hz), 119.23 (q, *J* = 269.9 Hz), 55.8, 55.8, 45.5, 34.4, 34.4.

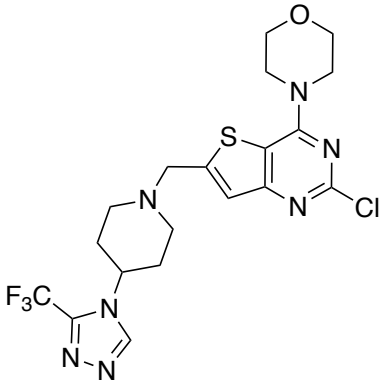
4-(3-(trifluoromethyl)-4H-1,2,4-triazol-4-yl)piperidine



Tert-butyl 4-(3-(trifluoromethyl)-4H-1,2,4-triazol-4-yl)piperidine-1-carboxylate (258 mg, 0.49 mmol) was stirred in TFA (2 mL) for 1 hr, after which time excess TFA was removed *in vacuo* and the resulting white solid, the deprotected amine, was triturated with diethyl ether and dried *in vacuo*. The product (177 mg, 100%), a white solid, as the free base was obtained by flushing the TFA salt through an STX cartridge, eluting with MeOH then MeOH containing NH_3 (0.7 N). ^{1}H NMR (400 MHz, DMSO) δ 9.17

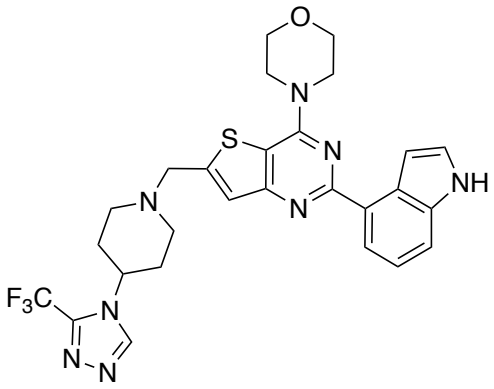
(s, 1H), 4.19 (tt, *J* = 11.7, 4.3 Hz, 1H), 3.06 (dt, *J* = 13.4, 2.8 Hz, 2H), 2.60 (td, *J* = 12.5, 2.7 Hz, 2H), 1.98 – 1.91 (m, 2H), 1.85 (qd, *J* = 12.0, 4.1 Hz, 2H). ^{13}C NMR (101 MHz, DMSO) δ 145.8, 142.7 (q, *J* = 37.9 Hz), 119.2 (q, *J* = 269.9 Hz) 55.8, 45.5, 34.4.

4-(2-chloro-6-((4-(3-(trifluoromethyl)-4H-1,2,4-triazol-4-yl)piperidin-1-yl)methyl) thieno[3,2-d]pyrimidin-4-yl)morpholine



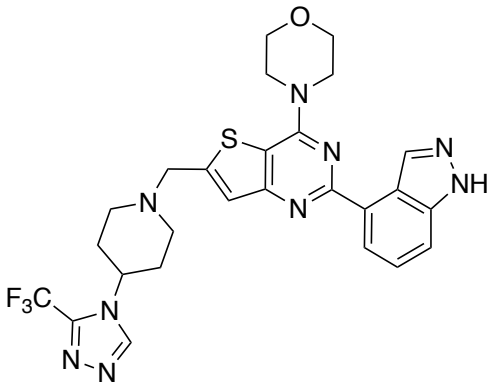
To a stirred solution of 4-(3-(trifluoromethyl)-4H-1,2,4-triazol-4-yl)piperidine (177 mg, 0.81 mmol) in CH_2Cl_2: AcOH (10:1)v (4 mL) was added 2-chloro-4-morpholinothieno[3,2-d]pyrimidine-6-carbaldehyde (229 mg, 0.81 mmol). The reaction mixture was heated at 45 °C for 1 hr then cooled to room temperature and picoline borane (95 mg, 0.89 mmol) added. The reaction was stirred for a further 2 hours after which time the reaction mixture was concentrated and absorbed onto silica gel. Purification by flash column chromatography (silica gel), eluting with EtOAc (100%), then CH_2Cl_2: MeOH, containing 0.7 N NH_3 (5-10%), gave the product as a off-white solid (118 mg, 30%). ^{1}H NMR (400 MHz, DMSO) δ 9.26 (s, 1H), 7.32 (s, 1H), 4.19 (ddt, *J* = 11.4, 8.5, 4.7 Hz, 1H), 3.95 – 3.92 (m, 2H), 3.92 – 3.87 (m, 4H), 3.81 – 3.74 (m, 4H), 3.08 – 3.00 (m, 2H), 2.31 (td, *J* = 11.8, 2.5 Hz, 2H), 2.17 – 1.95 (m, 4H). ^{13}C NMR (101 MHz, DMSO) δ 163.0, 158.4, 156.3, 152.9, 145.8, 142.8 (q, *J* = 38.2 Hz), 122.4, 119.2 (q, *J* = 241.2 Hz), 112.7, 66.3, 56.4, 54.9, 52.2, 46.4, 32.8. LCMS (m/z): calc'd for $C_{19}H_{21}ClF_3N_7OS$ $[M + H]^+$ 488.9, found 488.3, r.t 2.27.

4-(2-(1H-indol-4-yl)-6-((4-(3-(trifluoromethyl)-4H-1,2,4-triazol-4-yl)piperidin-1-yl)methyl)thieno[3,2-d]pyrimidin-4-yl)morpholine (Compound 24)



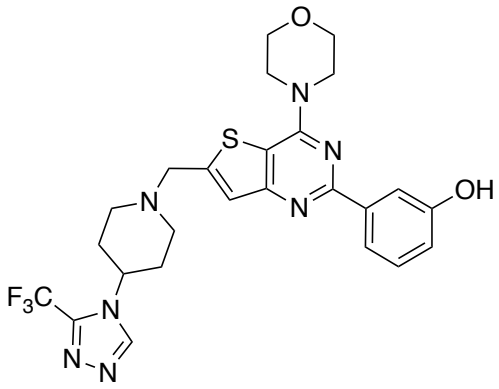
A mixture of 4-(2-chloro-6-((4-(3-(trifluoromethyl)-4H-1,2,4-triazol-4-yl)piperidin-1-yl)methyl)thieno[3,2-d]pyrimidin-4-yl)morpholine (30 mg, 0.061 mmol), (1H-indol-4-yl) boronic acid (14 mg, 0.087 mmol), aqueous Na_2CO_3 (90 µL, 0.18 mmol, 2 M) and bis(triphenylphosphine)palladium chloride (4 mg, 0.006 mmol) in EtOH: deionised water, (3 mL, 3:1) was irradiated under microwave radiation for 45 mins at 125 °C. After concentration the residue was purified by flash column chromatography (silica gel), eluting with 0 - 10% MeOH containing NH_3 (0.7 N) in CH_2Cl_2 to give the product as an off-white solid (33 mg, 97%). ^{1}H NMR (400 MHz, DMSO) δ 11.24 (s, 1H), 9.28 (s, 1H), 8.14 (d, *J* = 7.5 Hz, 1H), 7.53 (d, *J* = 8.0 Hz, 1H), 7.49 – 7.43 (m, 3H), 7.21 (t, *J* = 7.7 Hz, 1H), 4.26 – 4.15 (m, 1H), 4.05 – 3.99 (m, 4H), 3.98 – 3.93 (m, 2H), 3.88 – 3.81 (m, 4H), 3.16 – 3.05 (m, 2H), 2.32 (t, *J* = 11.5 Hz, 2H), 2.19 – 2.05 (m, 2H), 2.06 – 2.01 (m, 2H). ^{13}C NMR (101 MHz, DMSO) δ 162.8, 161.8, 158.0, 157.9, 150.6, 145.8, 145.7, 142.9 (q, *J* = 33.8 Hz), 137.5, 130.2, 126.8, 126.4, 123.9, 119.3 (q, *J* = 195.0 Hz), 113.8, 112.1, 103.9, 66.5, 56.6, 55.0, 52.2, 46.5, 32.9. LCMS (m/z): calc'd for $C_{27}H_{27}F_3N_8OS$ $[M + H]^+$ 569.6, found 569.4, r.t. 2.19, purity 97%.

4-(2-(1H-indazol-7-yl)-6-((4-(3-(trifluoromethyl)-4H-1,2,4-triazol-4-yl)piperidin-1-yl)methyl)thieno[3,2-d]pyrimidin-4-yl)morpholine (Compound 23)



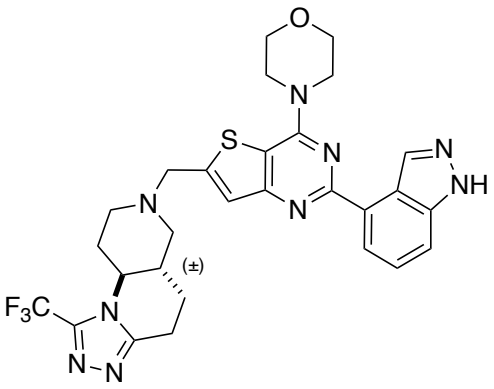
A mixture of 4-(2-chloro-6-((4-(3-(trifluoromethyl)-4H-1,2,4-triazol-4-yl)piperidin-1-yl)methyl)thieno[3,2-d]pyrimidin-4-yl)morpholine (30 mg, 0.061 mmol), (1H-indazol-4-yl) boronic acid (15 mg, 0.093 mmol), aqueous Na_2CO_3 (90 µL, 0.18 mmol, 2 M) and bis(triphenylphosphine)palladium chloride (4 mg, 0.006 mmol) in EtOH: deionised water, (3 mL, 3:1) was irradiated under microwave radiation for 45 mins at 125 °C. After concentration the residue was purified by flash column chromatography (silica gel), eluting with 0-10% MeOH containing NH_3 (0.7 N) in CH_2Cl_2 to give the product as a off-white solid (30 mg, 86%). ^{1}H NMR (400 MHz, DMSO) δ 13.21 (s, 1H), 9.28 (s, 1H), 8.90 (s, 1H), 8.24 (d, *J* = 7.3 Hz, 1H), 7.68 (d, *J* = 8.3 Hz, 1H), 7.53 (s, 1H), 7.48 (t, *J* = 7.8 Hz, 1H), 4.27 – 4.19 (m, 1H), 4.03 (t, *J* = 4.7 Hz, 4H), 3.99 – 3.94 (m, 2H), 3.90 – 3.82 (m, 4H), 3.10 (d, *J* = 11.4 Hz, 2H), 2.33 (t, *J* = 11.5 Hz, 2H), 2.17 – 2.09 (m, 2H), 2.07 – 2.02 (m, 2H). LCMS (m/z): calc'd for $C_{27}H_{27}F_3N_8OS$ $[M + H]^+$ 570.6, found 570.5, r.t 2.25, purity 97%.

3-(4-morpholino-6-((4-(3-(trifluoromethyl)-4H-1,2,4-triazol-4-yl)piperidin-1-yl) methyl)thieno[3,2-d]pyrimidin-2-yl)phenol (Compound 22)



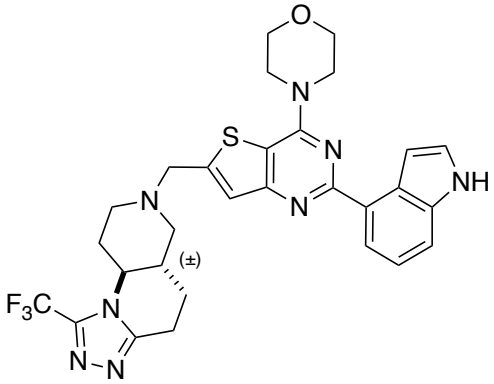
A mixture of 4-(2-chloro-6-((4-(3-(trifluoromethyl)-4H-1,2,4-triazol-4-yl)piperidin-1-yl)methyl)thieno[3,2-d]pyrimidin-4-yl)morpholine (38 mg, 0.078 mmol), (3-hydroxyphenyl)boronic acid (17 mg, 0.12 mmol), aqueous Na_2CO_3 (90 µL, 0.18 mmol, 2 M) and bis(triphenylphosphine)palladium chloride (6 mg, 0.008 mmol) in EtOH: deionised water, (3 mL, 3:1) was irradiated under microwave radiation for 45 mins at 125 °C. After concentration the residue was purified by flash column chromatography (silica gel), eluting with 0-10% MeOH containing NH_3 (0.7 N) in CH_2Cl_2 to give the product as a off-white solid (38 mg, 89%). ^{1}H NMR (400 MHz, DMSO) δ 9.50 (s, 1H), 9.27 (s, 1H), 7.85 (d, *J* = 7.1 Hz, 2H), 7.41 (s, 1H), 7.28 (t, *J* = 8.0 Hz, 1H), 6.90 – 6.83 (m, 1H), 4.23 – 4.18 (m, 1H), 4.02 – 3.97 (m, 4H), 3.96 – 3.92 (m, 2H), 3.86 – 3.79 (m, 4H), 3.11 – 3.03 (m, 2H), 2.31 (t, *J* = 11.6 Hz, 2H), 2.12 (dt, *J* = 12.4, 6.7 Hz, 2H), 2.05 – 2.00 (m, 2H)^{13}C NMR (101 MHz, DMSO) δ 162.7, 159.6, 157.9, 157.8, 150.9, 145.8, 139.9, 129.7, 123.6, 119.0 (q, *J* = 161.0 Hz), 117.5, 114.9, 112.6, 110.0, 66.5, 65.4, 56.6, 52.2, 46.3, 32.8 (quaternaty carbon adjacent to Quaternaty carbon adjacent to CF_3 not visable, usually ~ 142 ppm). LCMS (m/z): calc'd for $C_{25}H_{26}F_3N_7O_2S$ $[M + H]^+$ 546.6, found 546.4, r.t. 2.18, purity 98%.

4-(2-(1H-indazol-4-yl)-6-(((5aS,9aS)-1-(trifluoromethyl)-4,5,5a,8,9,9a-hexahydro-[1,2,4]triazolo[4,3-a][1,6]naphthyridin-7(6H)-yl)methyl)thieno[3,2-d]pyrimidin-4-yl)morpholine (Compound 11)



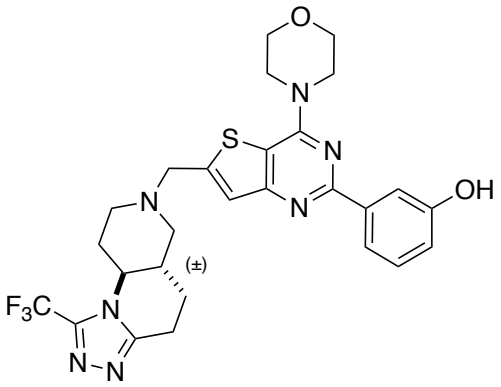
A mixture of Trans-4-(2-chloro-6-((1-(trifluoromethyl)-4,5,5a,8,9,9a-hexahydro-[1,2,4]triazolo[4,3-a][1,6]naphthyridin-7(6H)-yl)methyl)thieno[3,2-d]pyrimidin-4-yl)morpholine (80 mg, 0.16 mmol), (1H-indazol-4-yl) boronic acid (38 mg, 0.23 mmol), aqueous Na_2CO_3 (234 µL, 0.47 mmol, 2 M) and bis(triphenylphosphine)palladium chloride (11 mg, 0.016 mmol) in EtOH: deionised water, (3 mL, 3:1) was irradiated under microwave radiation for 45 mins at 125 °C. After concentration the residue was purified by flash column chromatography (silica gel), eluting with 0-10% MeOH containing NH_3 (0.7 N) in CH_2Cl_2 to give the product as an off-white solid (72 mg, 78%). ^{1}H NMR (400 MHz, DMSO) δ 11.24 (s, 1H), 8.14 (d, *J* = 7.4 Hz, 1H), 7.53 (d, *J* = 8.0 Hz, 1H), 7.48 – 7.43 (m, 3H), 7.21 (t, *J* = 7.8 Hz, 1H), 5.77 (s, 1H), 4.03 – 3.96 (m, 4H), 3.97 – 3.91 (m, 2H), 3.87 – 3.79 (m, 4H), 3.19 – 3.06 (m, 2H), 3.08 – 2.91 (m, 2H), 2.35 (t, *J* = 12.2 Hz, 2H), 2.10 (p, *J* = 11.1 Hz, 2H), 1.83 (ddt, *J* = 27.0, 13.8, 7.3 Hz, 2H), 1.59 (tt, *J* = 13.5, 6.7 Hz, 1H). ^{13}C NMR (101 MHz, DMSO) δ 162.8, 161.7, 158.0, 156.1, 150.4, 137.5, 130.2, 126.8, 126.4, 123.9, 120.9, 113.8, 112.1, 110.0, 103.9, 66.5, 60.5, 57.0, 56.4, 55.4, 51.9, 46.5, 30.5, 23.4, 22.7. LCMS (m/z): calc'd for $C_{27}H_{28}F_3N_7O_2S$ $[M + H]^+$ 572.6 found 572.4, r.t 2.28, purity 98%.

4-(2-(1H-indol-4-yl)-6-(((5aS,9aS)-1-(trifluoromethyl)-4,5,5a,8,9,9a-hexahydro-[1,2,4]triazolo[4,3-a][1,6]naphthyridin-7(6H)-yl)methyl)thieno[3,2-d]pyrimidin-4-yl)morpholine (Compound 12)



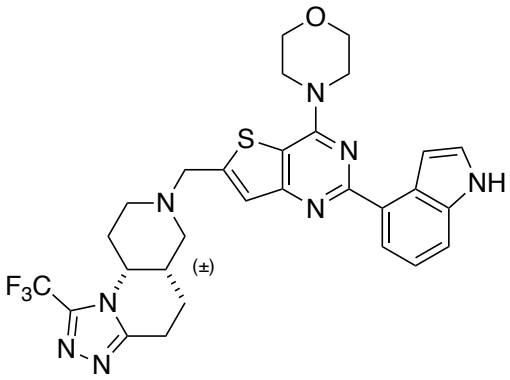
A mixture of 4-(2-chloro-6-((1-(trifluoromethyl)-4,5,5a,8,9,9a-hexahydro-[1,2,4]triazolo[4,3-a][1,6]naphthyridin-7(6H)-yl)methyl)thieno[3,2-d]pyrimidin-4-yl)morpholine (80 mg, 0.16 mmol), (1H-indol-4-yl) boronic acid (37 mg, 0.23 mmol), aqueous Na_2CO_3 (240 µL, 0.48 mmol, 2 M) and bis(triphenylphosphine)palladium chloride (11 mg, 0.016 mmol) in EtOH: deionised water, (3 mL, 3:1) was irradiated under microwave radiation for 45 mins at 125 °C. After concentration the residue was purified by flash column chromatography (silica gel), eluting with 0-10% MeOH containing NH_3 (0.7 N) in CH_2Cl_2 to give the product as an off-white solid (77 mg, 81%). ^{1}H NMR (400 MHz, DMSO) δ 11.24 (s, 1H), 8.14 (d, *J* = 7.4 Hz, 1H), 7.53 (d, *J* = 8.0 Hz, 1H), 7.46 (s, 3H), 7.21 (t, *J* = 7.8 Hz, 1H), 5.77 (s, 1H), 4.03 – 3.96 (m, 4H), 3.87 – 3.79 (m, 4H), 3.34 (s, 1H), 3.19 – 3.02 (m, 3H), 2.95 (ddd, *J* = 17.3, 11.4, 6.2 Hz, 1H), 2.41 – 2.29 (m, 2H), 2.18 – 2.02 (m, 2H), 1.92 – 1.74 (m, 2H), 1.59 (tt, *J* = 13.5, 6.7 Hz, 1H).^{13}C NMR (101 MHz, DMSO) δ 162.8, 161.7, 158.0, 156.1, 150.4, 137.5, 130.2, 126.8, 126.4, 123.9, 120.9, 113.8, 112.1, 110.0, 103.9, 66.5, 60.5, 57.0, 56.4, 55.4, 51.9, 46.5, 30.5, 30.4, 23.4, 22.7 (Quaternaty carbon adjacent to CF_3 not visable, usually ~ 142 ppm). LCMS (m/z): calc'd for $C_{29}H_{29}F_3N_8OS$ $[M + H]^+$ 595.7, found 595.5, r.t 2.22, purity 98%.

3-(4-morpholino-6-((1-(trifluoromethyl)-4,5,5a,8,9,9a-hexahydro-[1,2,4]triazolo[4,3-a][1,6]naphthyridin-7(6H)-yl)methyl)thieno[3,2-d]pyrimidin-2-yl) phenol (Compound 10)



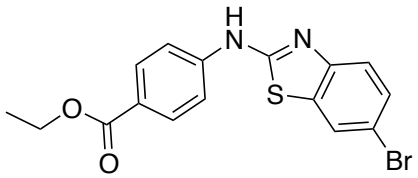
A mixture of 4-(2-chloro-6-((1-(trifluoromethyl)-4,5,5a,8,9,9a-hexahydro-[1,2,4] triazolo[4,3-a][1,6]naphthyridin-7(6H)-yl)methyl)thieno[3,2-d]pyrimidin-4-yl)morpholine (80 mg, 0.16 mmol), (3-hydroxyphenyl) boronic acid (32 mg, 0.23 mmol), aqueous Na_2CO_3 (240 µL, 0.48 mmol, 2 M) and bis(triphenylphosphine)palladium chloride (11 mg, 0.016 mmol) in EtOH: deionised water, (3 mL, 3:1) was irradiated under microwave radiation for 45 mins at 125 °C. After concentration the residue was purified by flash column chromatography (silica gel), eluting with 0-10% MeOH containing NH_3 (0.7 N) in CH_2Cl_2 to give the product as an off-white solid (74 mg, 81%). ^{1}H NMR (400 MHz, DMSO) δ 9.50 (s, 1H), 7.89 – 7.82 (m, 2H), 7.40 (s, 1H), 7.28 (t, *J* = 8.0 Hz, 1H), 6.91 – 6.83 (m, 1H), 4.01 – 3.95 (m, 5H), 3.93 (s, 2H), 3.81 (t, *J* = 4.7 Hz, 4H), 3.18 – 3.02 (m, 3H), 3.02 – 2.88 (m, 1H), 2.37 (d, *J* = 12.1 Hz, 2H), 2.19 – 2.02 (m, 2H), 1.81 (ddd, *J* = 24.5, 12.3, 4.6 Hz, 2H), 1.60 (tt, *J* = 13.6, 6.5 Hz, 1H). ^{13}C NMR (101 MHz, DMSO) δ 162.7, 159.5, 157.9, 157.9, 156.1, 150.8, 139.9, 129.7, 123.6, 119.0, 117.5, 114.9, 112.7, 66.5, 60.5, 57.0, 56.4, 51.9, 46.3, 30.5, 23.4, 22.7 (Quaternaty carbon adjacent to CF_3 not visable, usually ~ 142 ppm, CF_3 also not viable, usually ~ 120 ppm). LCMS (m/z): calc'd for $C_{27}H_{28}F_3N_7O_2S$ $[M + H]^+$ 572.6, found 572.4 , r.t. 2.23, purity 99%.

4-(2-(1H-indol-4-yl)-6-((cis-1-(trifluoromethyl)-4,5,5a,8,9,9a-hexahydro-[1,2,4] triazolo[4,3-a][1,6]naphthyridin-7(6H)-yl)methyl)thieno[3,2-d]pyrimidin-4-yl) morpholine (Compound 9)



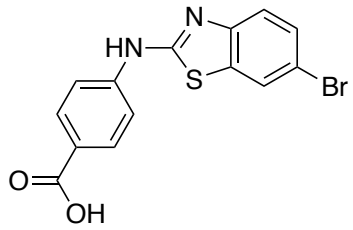
A mixture of 4-(2-chloro-6-((cis-1-(trifluoromethyl)-4,5,5a,8,9,9a-hexahydro-[1,2,4]triazolo[4,3-a][1,6]naphthyridin-7(6H)-yl)methyl)thieno[3,2-d]pyrimidin-4-yl)morpholine (90 mg, 0.18 mmol), (1H-indol-4-yl) boronic acid (42 mg, 0.26 mmol), aqueous Na_2CO_3 (263 µL, 0.52 mmol, 2 M) and bis(triphenylphosphine)palladium chloride (12 mg, 0.018 mmol) in EtOH: deionised water, (3 mL, 3:1) was irradiated under microwave radiation for 45 mins at 125 °C. After concentration the residue was purified by flash column chromatography (silica gel), eluting with 0-10% MeOH containing NH_3 (0.7 N) in CH_2Cl_2 to give the product as an off-white solid (64 mg, 62%). ^{1}H NMR (400 MHz, DMSO) δ 11.27 – 11.21 (m, 1H), 8.13 (dd, *J* = 7.5, 1.0 Hz, 1H), 7.53 (d, *J* = 7.9 Hz, 1H), 7.49 – 7.41 (m, 3H), 7.21 (t, *J* = 7.7 Hz, 1H), 4.48 (dt, *J* = 11.1, 5.1 Hz, 1H), 4.08 – 3.95 (m, 4H), 3.94 (s, 1H), 3.88 – 3.79 (m, 4H), 3.34 (s, 1H), 3.22 – 3.12 (m, 1H), 3.04 – 2.97 (m, 2H), 2.96 – 2.82 (m, 1H), 2.46 (td, *J* = 11.0, 9.6, 5.3 Hz, 2H), 2.29 (dd, *J* = 13.6, 5.9 Hz, 2H), 2.00 (pd, *J* = 12.0, 11.4, 3.6 Hz, 1H), 1.96 (s, 1H), 1.87 – 1.77 (m, 1H). ^{13}C NMR (101 MHz, DMSO) δ 162.9, 161.7, 158.0, 154.2, 150.8, 137.5, 130.2, 126.8, 126.4, 123.6, 120.9, 118.2, 113.8, 112.1, 103.8, 66.5, 65.4, 56.9, 56.6, 54.2, 52.1, 46.6, 33.6, 29.6, 21.3, 20.1, 15.7. LCMS (m/z): calc'd for $C_{29}H_{29}F_3N_8OS$ $[M + H]^+$ 596.7, found 596.5, r.t. 2.33, purity 99%.

Ethyl 4-((6-bromobenzo[d]thiazol-2-yl)amino)benzoate



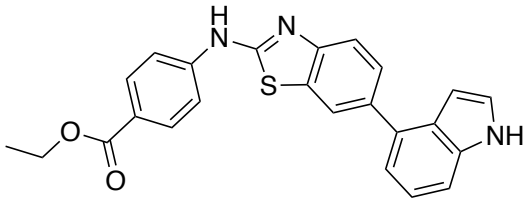
To a mixture of 6-bromo-2-chlorobenzo[d]thiazole (2.0 g, 8.06 mmol) and ethyl 4-aminobenzoate (1.21 g, 7.33 mmol) in EtOH (5 mL) was added HCl as a solution in dioxane (2 mL, 4 M) and the reaction mixure irradiated with microwave radiation for 1 h at 120 °C. After cooling to room temperature and concentrating, the residue was purified by flash colum chromatography (silica gel), eluting with 0-30% EtOAc in petroleum ether gave the product as a white solid (1.86 g, 67 %). LCMS (m/z) calc'd for $C_{16}H_{13}BrN_2O_2S$ $[M + H]^+$ 380.3 found 380.2, r.t. 3.20, 98% purity.

4-((6-bromobenzo[d]thiazol-2-yl)amino)benzoic acid



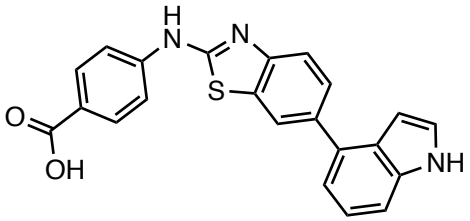
To a stirred solution of Ethyl 4-((6-bromobenzo[d]thiazol-2-yl)amino)benzoate (45 mg, 0.11 mmol) in THF (1 mL) was added LiOH (14 mg, 1.57 mmol) as a solution in deionised H_2O (1 mL). The reaction was heated to 60 °C for 1 hr after which time the reaction was cooled to room temperature and THF removed *in vacuo*. HCl (2 M, 10 mL) was added and the precipitate collected by filtration and washed with deionised water. The product, obtained as a white solid (45 mg, 83%) was dried in a vacuum dessicator containing Ca_2CO_3 as a dessicant. ^{1}H NMR (400 MHz, DMSO) δ 12.65 (s, 1H), 11.14 (s, 1H), 8.11 (d, J = 2.0 Hz, 1H), 7.96 (d, J = 8.9 Hz, 2H), 7.91 (d, J = 8.9 Hz, 2H), 7.60 (d, J = 8.6 Hz, 1H), 7.49 (dd, J = 8.6, 2.1 Hz, 1H), ^{13}C NMR (101 MHz, DMSO) δ 167.4, 162.2, 151.4, 144.7, 132.9, 131.2, 129.4, 124.4, 124.2, 121.5, 117.5, 114.8. (m/z) calc'd for $C_{14}H_9BrN_2O_2S$ $[M + H]^+$ 351.2 found 351.2, r.t. 2.88, 98% purity.

Ethyl 4-((6-(1H-indol-4-yl)benzo[d]thiazol-2-yl)amino)benzoate (Compound 45)



To a suspension, purged with N_2 gas, of Ethyl 4-((6-bromobenzo[d]thiazol-2-yl) amino)benzoate (200 mg, 0.52 mmol), 1H-indol-4-yl boronic acid pinacol ester (156 mg, 0.64 mmol) and Na_2CO_3 (2 M, 780 µL) in THF was added bis(triphenylphosphine) palladium chloride (40 mg, 0.052 mmol). The reaction mixture was irradiated under microwave radiation for 45 mins at 125 °C. After concentration, the residue was purified by flash column chromatography (silica gel), eluting with 20 - 30 % EtOAc in petroleum ether with 2% AcOH to give a white solid (48 mg, 23%). ^{1}H NMR (400 MHz, DMSO) δ 11.27 (s, 1H), 10.94 (s, 1H), 8.18 - 8.13 (m, 1H), 8.04 - 7.92 (m, 4H), 7.82 - 7.75 (m, 1H), 7.72 - 7.64 (m, 1H), 7.46 - 7.38 (m, 2H), 7.20 (t, J = 7.6 Hz, 1H), 7.13 (d, J = 7.2 Hz, 1H), 6.62 (t, J = 2.4 Hz, 1H), 4.31 (q, J = 7.1 Hz, 2H), 1.34 (t, J = 7.1 Hz, 3H). ^{13}C NMR (101 MHz, DMSO) δ 165.9, 161.6, 151.2, 145.2, 136.9, 136.4, 133.2, 131.3, 131.1, 127.0, 126.3, 126.1, 123.2, 121.9, 121.1, 120.1, 119.0, 117.4, 111.1, 100.8, 25.4, 14.8. (m/z) calc'd for $C_{24}H_{19}N_3O_2S$ $[M + H]^+$ 414.5 found 414.0, r.t. 3.10, 99% purity.

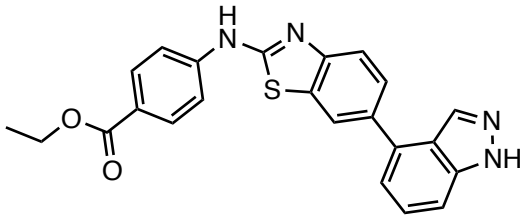
4-((6-(1H-indol-4-yl)benzo[d]thiazol-2-yl)amino)benzoic acid (Compound 27)



To a stirred solution of Ethyl 4-((6-(1H-indol-4-yl)benzo[d]thiazol-2-yl)amino) benzoate (57 mg, 0.14 mmol) in THF (1 mL) was added LiOH (34 mg, 1.4 mmol) as a solution in deionised H_2O (1 mL). The reaction was heated to 60 °C for 1 hr after which time the reaction was cooled to room temperature and THF removed *in vacuo*. HCl (2 M, 10 mL) was added and the precipitate collected by filtration and washed with deionised water. The product, obtained as a white solid (45 mg, 83%) was dried in a vacuum

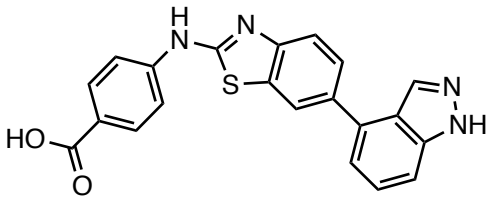
dessicator containing Ca_2CO_3 as a dessicant. ^{1}H NMR (400 MHz, DMSO) δ 11.00 (s, 1H), 8.43 - 8.37 (m, 1H), 8.29 - 8.22 (m, 2H), 8.14 (dd, *J* = 7.9, 2.2 Hz, 1H), 7.79 - 7.68 (m, 2H), 7.66 - 7.60 (m, 1H), 7.61 - 7.48 (m, 2H), 7.45 (t, *J* = 7.7 Hz, 1H), 7.28 (d, *J* = 7.0 Hz, 1H). ^{13}C NMR (101 MHz, DMSO) δ 167.7, 162.7, 151.7, 141.2, 141.1, 134.3, 133.2, 132.1, 131.3, 129.8, 126.9, 126.7, 123.5, 122.5, 121.4, 121.2, 119.9, 119.8, 119.1, 109.6 (m/z) calc'd for $C_{22}H_{15}N_3O_2S$ $[M + H]^+$ 386.4 found 386.3, r.t. 2.83, 93% purity.

Ethyl 4-((6-(1H-indazol-4-yl)benzo[d]thiazol-2-yl)amino)benzoate (Compound 44)



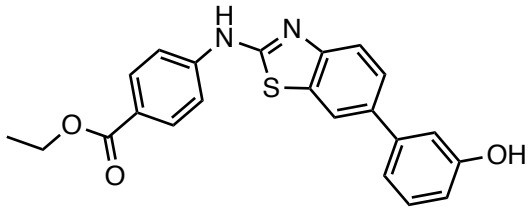
To a suspension, purged with N_2 gas, of ethyl 4-((6-bromobenzo[d]thiazol-2-yl) amino)benzoate (200 mg, 0.52 mmol), 1H-indazol-4-yl boronic acid (156 mg, 0.64 mmol) and Na_2CO_3 (2 M, 780 μL) in THF was added bis(triphenylphosphine)palladium chloride (40 mg, 0.052 mmol). The reaction mixture was irradiated under microwave radiation for 45 mins at 125 °C. After concentration, the residue was purified by flash column chromatography (silica gel), eluting with eluting with 20 - 30 % EtOAc in petroleum ether with 2% AcOH to give a white solid (138 mg, 64%). ^{1}H NMR (400 MHz, DMSO) δ 13.24 (s, 1H), 10.98 (s, 1H), 8.31 - 8.22 (m, 2H), 8.06 - 7.91 (m, 4H), 7.85 - 7.70 (m, 2H), 7.58 - 7.51 (m, 1H), 7.49 - 7.41 (m, 1H), 7.32 - 7.26 (m, 1H), 4.31 (q, *J* = 7.1 Hz, 2H), 1.34 (t, *J* = 7.1 Hz, 3H). ^{13}C NMR (101 MHz, DMSO) δ 165.8, 162.1, 151.9, 145.1, 141.0, 134.6, 134.2, 133.3, 131.6, 131.1, 129.2, 126.8, 123.3, 121.5, 121.3, 120.4, 119.8, 117.5, 109.5, 60.8, 14.7. (m/z) calc'd for $C_{23}H_{18}N_4O_2S$ $[M + H]^+$ 414.5 found 414.9, r.t. 3.01, 100% purity.

4-((6-(1H-indazol-4-yl)benzo[d]thiazol-2-yl)amino)benzoic acid (Compound 26)



To a stirred solution of ethyl 4-((6-(1H-indol-4-yl)benzo[d]thiazol-2-yl)amino) benzoate (50 mg, 0.12 mmol) in THF (1 mL) was added LiOH (29 mg, 1.2 mmol) as a solution in deionised H_2O (1 mL). The reaction was heated to 60 °C for 1 hr after which time the reaction was cooled to room temperature and THF removed *in vacuo*. HCl (2 M, 10 mL) was added and the precipitate collected by filtration and washed with deionised water. The product, obtained as a white solid (34 mg, 73%) was dried in a vacuum dessicator containing Ca_2CO_3 as a dessicant. ^{1}H NMR (400 MHz, DMSO) δ 13.23 (s, 1H), 10.96 (s, 1H), 8.27 (d, *J* = 3.5 Hz, 2H), 7.96 (q, *J* = 8.5 Hz, 4H), 7.81 (d, *J* = 8.3 Hz, 1H), 7.74 (d, *J* = 8.5 Hz, 1H), 7.55 (d, *J* = 8.3 Hz, 1H), 7.45 (t, *J* = 7.8 Hz, 1H), 7.28 (d, *J* = 7.1 Hz, 1H). ^{13}C NMR (101 MHz, DMSO) δ 167.4, 162.1, 151.9, 144.8, 141.1, 134.6, 134.2, 131.6, 131.2, 126.8, 124.2, 121.5, 121.2, 120.3, 119.8, 117.4 (some quaternary carbons indistinguisable from the baseline). (m/z) calc'd for $C_{21}H_{14}N_4O_2S$ $[M + H]^+$ 387.4 found 387.0, r.t. 2.72, 100% purity.

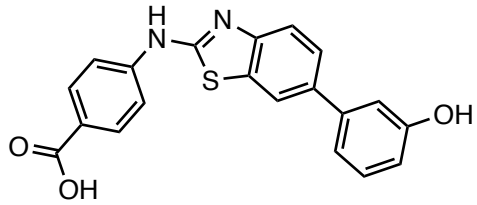
Ethyl 4-((6-(3-hydroxyphenyl)benzo[d]thiazol-2-yl)amino)benzoate (Compound 43)



To a suspension, purged with N_2 gas, of ethyl 4-((6-bromobenzo[d]thiazol-2-yl) amino)benzoate (200 mg, 0.52 mmol), 3-hydroxyphenyl boronic acid (88 mg, 0.64 mmol) and Na_2CO_3 (2 M, 780 µL) in THF was added bis(triphenylphosphine)palladium chloride (40 mg, 0.052 mmol). The reaction mixture was irradiated under microwave radiation for 45 mins at 125 °C. After concentration, the residue was purified by flash column chromatography (silica gel), eluting with eluting with 20 - 30 % EtOAc in pe-

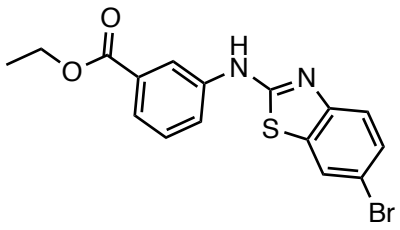
troleum ether with 2% AcOH to give a white solid (80 mg, 37%). ^{1}H NMR (400 MHz, DMSO) δ 10.94 (s, 1H), 9.52 (s, 1H), 8.12 (d, *J* = 1.9 Hz, 1H), 8.03 - 7.90 (m, 4H), 7.72 (d, *J* = 8.4 Hz, 1H), 7.60 (dd, *J* = 1.9, 8.4 Hz, 1H), 7.26 (t, *J* = 7.9 Hz, 1H), 7.11 (d, *J* = 7.8 Hz, 1H), 7.06 (t, *J* = 2.0 Hz, 1H), 6.77 (dd, *J* = 2.2, 8.1 Hz, 1H), 4.31 (q, *J* = 7.1 Hz, 2H), 1.33 (t, *J* = 7.1 Hz, 3H). ^{13}C NMR (101 MHz, DMSO) δ 165.8, 161.8, 158.3, 151.7, 145.1, 141.8, 135.7, 131.6, 131.1, 130.4, 125.3, 123.3, 120.3, 119.7, 117.9, 117.5, 114.6, 113.9, 60.8, 14.7. (m/z) calc'd for $C_{22}H_{18}N_2O_3S$ $[M + H]^+$ 390.5 found 390.9, r.t. 2.98, 100% purity.

4-((6-(3-hydroxyphenyl)benzo[d]thiazol-2-yl)amino)benzoic acid (Compound 25))



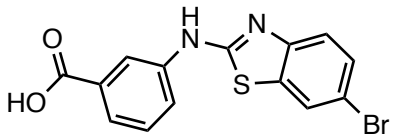
To a stirred solution of ethyl 4-((6-(3-hydroxyphenyl)benzo[d]thiazol-2-yl)amino)benzoate (47 mg, 0.12 mmol) in THF (1 mL) was added LiOH (29 mg, 1.2 mmol) as a solution in deionised H_2O (1 mL). The reaction was heated to 60 °C for 1 hr after which time the reaction was cooled to room temperature and THF removed *in vacuo*. HCl (2 M, 10 mL) was added and the precipitate collected by filtration and washed with deionised water. The product, obtained as a white solid (39 mg, 89%) was dried in a vacuum dessicator containing Ca_2CO_3 as a dessicant. ^{1}H NMR (400 MHz, DMSO) δ 12.65 (s, 1H), 10.91 (s, 1H), 9.52 (s, 1H), 8.12 (d, *J* = 1.9 Hz, 1H), 7.94 (dd, 4H), 7.72 (d, *J* = 8.4 Hz, 1H), 7.59 (dd, *J* = 1.9, 8.4 Hz, 1H), 7.26 (t, *J* = 7.9 Hz, 1H), 7.12 (d, *J* = 7.8 Hz, 1H), 7.06 (t, *J* = 2.1 Hz, 1H), 6.77 (dd, *J* = 2.3, 8.0 Hz, 1H). ^{13}C NMR (101 MHz, DMSO) δ 167.4, 161.8, 158.3, 151.7, 144.8, 141.8, 135.6, 131.5, 131.2, 130.4, 125.3, 124.2, 120.2, 119.7, 117.9, 117.4, 114.6, 113.9. (m/z) calc'd for $C_{20}H_{14}N_2O_3S$ $[M + H]^+$ 363.4 found 363.2, r.t. 2.70, 99% purity.

Ethyl 3-((6-bromobenzo[d]thiazol-2-yl)amino)benzoate



To a mixture of 6-bromo-2-chlorobenzo[d]thiazole (2.0 g, 8.06 mmol) and ethyl 3-aminobenzoate (1.21 g, 7.33 mmol) in EtOH (5 mL) was added HCl as a solution in dioxane (2 mL, 4 M) and the reaction mixure irradiated with microwave radiation for 1 h at 120 °C. After cooling to room temperature and concentrating, the residue was purified by flash colum chromatography (silica gel), eluting with 0-30% EtOAc in petroleum ether gave the product as a white solid (1.81 g, 60 %). ^{1}H NMR (400 MHz, DMSO) δ 10.80 (s, 1H), 8.38 (t, *J* = 1.9 Hz, 1H), 8.17 - 8.07 (m, 2H), 7.66 - 7.59 (m, 1H), 7.63 - 7.45 (m, 3H), 4.34 (q, *J* = 7.1 Hz, 2H), 1.36 (t, *J* = 7.1 Hz, 3H). ^{13}C NMR (101 MHz, DMSO) δ 166.0, 162.5, 151.6, 141.1, 132.7, 131.1, 130.0, 129.4, 124.1, 123.2, 122.6, 121.3, 118.7, 114.6, 61.3, 14.6. (m/z) calc'd for $C_{16}H_{13}BrN_2O_2S$ $[M + H]^+$ 379.3 found 379.2, r.t. 3.18, 92% purity.

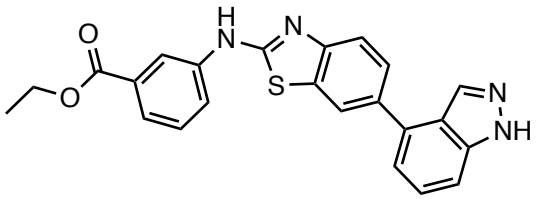
3-((6-bromobenzo[d]thiazol-2-yl)amino)benzoic acid



To a stirred solution of ethyl 4-((6-(3-hydroxyphenyl)benzo[d]thiazol-2-yl)amino)benzoate (21 mg, 0.06 mmol) in THF (1 mL) was added LiOH (13 mg, 0.6 mmol) as a solution in deionised H_2O (1 mL). The reaction was heated to 60 °C for 1 hr after which time the reaction was cooled to room temperature and THF removed *in vacuo*. HCl (2 M, 10 mL) was added and the precipitate collected by filtration and washed with deionised water. The pro duct, obtained as a white solid (11 mg, 52%) was dried in a vacuum dessicator containing Ca_2CO_3 as a dessicant. ^{1}H NMR (400 MHz, DMSO) δ 13.02 (s, 1H), 11.00 (s, 1H), 8.36 (t, *J* = 1.9 Hz, 1H), 8.10 (dd, *J* = 2.1, 6.8 Hz, 2H), 7.65 - 7.43 (m, 4H). ^{13}C NMR (126 MHz, DMSO) δ 167.6, 162.6, 151.6, 141.1, 132.8, 132.0,

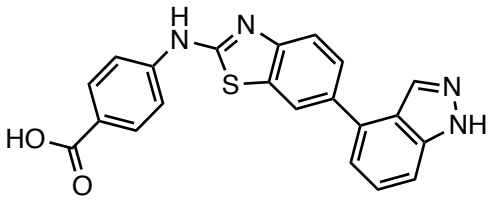
129.8, 129.3, 124.1, 123.5, 122.4, 121.3, 118.9, 114.5. (m/z) calc'd for $C_{14}H_9BrN_2O_2S$ $[M + H]^+$ 350.2 found 350.1, r.t. 2.89, 97% purity.

Ethyl 3-((6-(1H-indazol-4-yl)benzo[d]thiazol-2-yl)amino)benzoate (Compound 47)



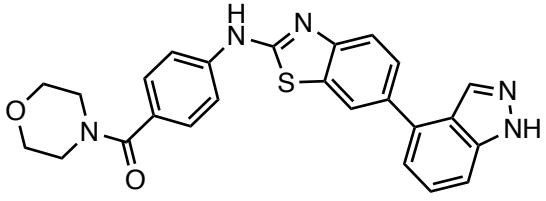
To a suspension, purged with N_2 gas, of ethyl 3-((6-bromobenzo[d]thiazol-2-yl) amino)benzoate (200 mg, 0.52 mmol), 1H-indazol-4-yl boronic acid pinacol ester (156 mg, 0.64 mmol) and Na_2CO_3 (2 M, 780 µL) in THF was added bis(triphenylphosphine) palladium chloride (40 mg, 0.052 mmol). The reaction mixture was irradiated under microwave radiation for 45 mins at 125 °C. After concentration, the residue was purified by flash column chromatography (silica gel), eluting with 20 - 30 % EtOAc in petroleum ether with 2% AcOH to give a white solid (41 mg, 18%). ^{1}H NMR (400 MHz, DMSO) δ 13.23 (s, 1H), 10.80 (s, 1H), 8.44 (t, *J* = 1.9 Hz, 1H), 8.28 - 8.22 (m, 2H), 8.17 (dd, *J* = 2.3, 7.8 Hz, 1H), 7.80 - 7.69 (m, 2H), 7.67 - 7.60 (m, 1H), 7.60 - 7.49 (m, 2H), 7.45 (t, *J* = 7.7 Hz, 1H), 7.28 (d, *J* = 7.1 Hz, 1H), 4.36 (q, *J* = 7.1 Hz, 2H), 1.37 (t, *J* = 7.1 Hz, 3H). ^{13}C NMR (101 MHz, DMSO) δ 166.1, 162.5, 152.1, 141.3, 141.0, 134.3, 134.2, 133.3, 131.5, 131.2, 130.0, 126.8, 126.8, 123.0, 122.6, 121.5, 121.2, 120.1, 119.8, 118.7, 109.5, 61.3, 14.7. (m/z) calc'd for $C_{23}H_{18}N_4O_2S$ $[M + H]^+$ 414.5 found 414.9, r.t. 2.99, 100% purity.

3-((6-(1H-indazol-4-yl)benzo[d]thiazol-2-yl)amino)benzoic acid (Compound 26)



To a stirred solution of ethyl 3-((6-(1H-indazol-4-yl)benzo[d]thiazol-2-yl)amino) benzoate (29 mg, 0.07 mmol) in THF (1 mL) was added LiOH (17 mg, 1.2 mmol) as a solution in deionised H_2O (1 mL). The reaction was heated to 60 °C for 1 hr after which time the reaction was cooled to room temperature and THF removed *in vacuo*. HCl (2 M, 10 mL) was added and the precipitate collected by filtration and washed with deionised water. The product, obtained as a white solid (19 mg, 70%) was dried in a vacuum dessicator containing Ca_2CO_3 as a dessicant. ^{1}H NMR (400 MHz, DMSO) δ 11.29 (s, 1H), 10.82 (s, 1H), 8.39 (t, *J* = 1.9 Hz, 1H), 8.17 - 8.05 (m, 2H), 7.76 - 7.68 (m, 1H), 7.68 - 7.58 (m, 2H), 7.52 (t, *J* = 7.9 Hz, 1H), 7.46 - 7.38 (m, 2H), 7.19 (t, *J* = 7.6 Hz, 1H), 7.13 (d, *J* = 7.2 Hz, 1H), 6.64 - 6.59 (m, 1H). ^{13}C NMR (101 MHz, DMSO) δ 167.7, 162.1, 151.2, 141.3, 136.9, 136.1, 133.2, 132.1, 131.1, 129.8, 126.9, 126.2, 126.1, 123.3, 122.3, 121.8, 121.1, 119.7, 119.0, 118.9, 111.1, 100.8. (m/z) calc'd for $C_{22}H_{15}N_3O_2S$ $[M + H]^+$ 386.4 found 386.2, r.t. 2.82, 99% purity.

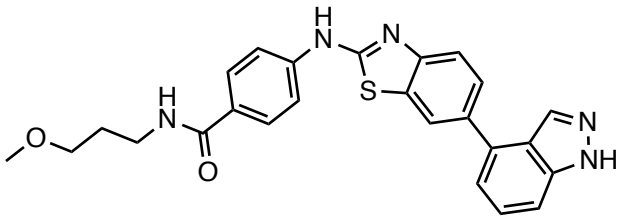
(4-((6-(1H-indazol-4-yl)benzo[d]thiazol-2-yl)amino)phenyl)(morpholino)methanone (Compound 49)



To a stirred solution of 3-((6-(1H-indazol-4-yl)benzo[d]thiazol-2-yl)amino)benzoic acid (50 mg, 0.13 mmol) in DMF (5 mL) was added NMM (43 µl, 0.39 mmol) then morpholine (17 µL, 0.20 mmol). HATU (61 mg, 0.16 mmol) was added in one portion and the reaction was stirred under N_2 for 45 mins after which time the solvent was removed *in vacuo* and purified by flash column chromatography eluting with 1-3 % MeOH containing 0.7 N ammonia in CH_2Cl_2. The product was obtained as a white solid

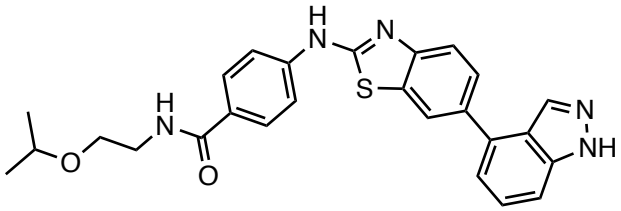
(53 mg, 89%). ^{1}H NMR (400 MHz, DMSO) δ 13.24 (s, 1H), 10.81 (s, 1H), 8.28 - 8.22 (m, 2H), 7.94 - 7.87 (m, 2H), 7.82 - 7.68 (m, 2H), 7.59 - 7.41 (m, 4H), 7.28 (d, *J* = 7.0 Hz, 1H), 3.62 (d, *J* = 4.6 Hz, 4H), 3.53 (s, 4H). ^{13}C NMR (101 MHz, DMSO) δ 169.5, 162.3, 152.1, 142.2, 141.0, 134.4, 134.2, 133.3, 131.5, 129.1, 129.0, 126.8, 126.7, 125.3, 121.5, 121.2, 120.1, 119.8, 117.6, 66.7, 66.6. (m/z) calc'd for $C_{25}H_{21}N_5O_2S$ $[M + H]^+$ 456.5 found 456.2, r.t. 2.72, 99% purity.

4-((6-(1H-indazol-4-yl)benzo[d]thiazol-2-yl)amino)-N-(3-methoxypropyl)benzamide (Compound 57)



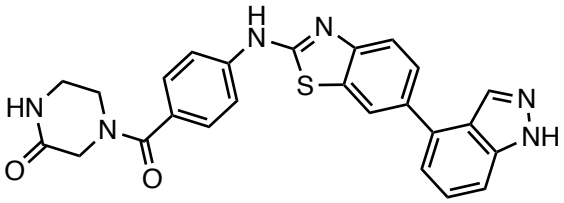
To a stirred solution of 3-((6-(1H-indazol-4-yl)benzo[d]thiazol-2-yl)amino)benzoic acid (50 mg, 0.13 mmol) in DMF (5 mL) was added DIPEA (43 µl, 0.39 mmol) then 3-methoxypropan-1-amine (17 µL, 0.16 mmol). HATU (61 mg, 0.16 mmol) was added in one portion and the reaction was stirred under N_2 for 45 mins after which time the solvent was removed *in vacuo* and purified by flash column chromatography eluting with EtOAc,petroleum ether, and MeOH containing 0.7 N ammonia (5:5:1) The product was obtained as a white solid (55 mg, 92%). ^{1}H NMR (400 MHz, DMSO) δ 13.27 (s, 1H), 8.28 – 8.23 (m, 1H), 8.05 – 7.97 (m, 3H), 7.89 (s, 2H), 7.83 – 7.69 (m, 1H), 7.65 – 7.59 (m, 1H), 7.58 – 7.44 (m, 2H), 7.40 (d, *J* = 7.0 Hz, 1H), 3.43 – 3.29 (m, 4H), 3.22 (s, 3H), 3.16 – 3.07 (m, 2H), 1.34 – 1.17 (m, 2H). ^{13}C NMR (126 MHz, DMSO) δ 166.2, 165.0, 162.3, 161.5, 152.1, 143.3, 141.0, 134.2, 133.3, 132.7, 131.6, 128.8, 128.4, 126.8, 121.9, 120.9, 119.8, 117.3, 110.1, 69.9, 58.4, 34.8, 29.6. (m/z) calc'd for $C_{25}H_{23}N_5O_2S$ $[M + H]^+$ 458.6 found 458.5, r.t. 2.74, 87% purity

4-((6-(1H-indazol-4-yl)benzo[d]thiazol-2-yl)amino)-N-(2-isopropoxyethyl)benzamide (Compound 56)



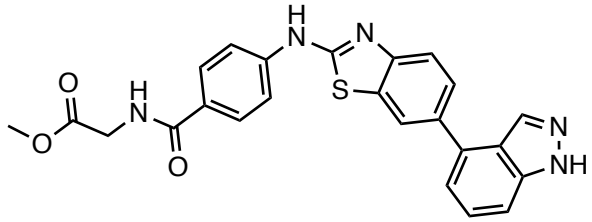
To a stirred solution of 3-((6-(1H-indazol-4-yl)benzo[d]thiazol-2-yl)amino)benzoic acid (50 mg, 0.13 mmol) in DMF (5 mL) was added DIPEA (43 µl, 0.39 mmol) then 2-isopropoxyethan-1-amine (17 µL, 0.16 mmol). HATU (61 mg, 0.16 mmol) was added in one portion and the reaction was stirred under N_2 for 45 mins after which time the solvent was removed *in vacuo* and purified by flash column chromatography eluting with 3 % MeOH containing 0.7 N ammonia in DCM. The product was obtained as a white solid (53 mg, 87%). ^{1}H NMR (400 MHz, DMSO) δ 13.25 (d, *J* = 15.9 Hz, 1H), 10.83 (s, 1H), 8.38 (t, *J* = 5.6 Hz, 1H), 8.26 (d, *J* = 1.6 Hz, 2H), 7.91 - 7.87 (m, 3H), 7.80 (d, *J* = 8.4 Hz, 1H), 7.73 (dd, *J* = 1.9, 8.3 Hz, 1H), 7.64 - 7.36 (m, 3H), 7.28 (d, *J* = 7.0 Hz, 1H), 3.59 (p, *J* = 6.1 Hz, 1H), 3.50 (t, *J* = 6.2 Hz, 2H), 3.40 (t, *J* = 5.9 Hz, 2H), 1.11 (d, *J* = 6.1 Hz, 6H). ^{13}C NMR (126 MHz, DMSO) δ 166.2, 162.3, 152.1, 143.4, 141.0, 134.4, 134.2, 133.3, 131.6, 128.8, 128.2, 126.8, 126.8, 121.5, 121.2, 120.2, 119.8, 117.3, 110.1, 71.3, 66.5, 40.6, 22.6. LCMS (m/z) calc'd for $C_{26}H_{25}N_5O_2S$ $[M + H]^+$ 472.6 found 472.4, r.t. 2.83, 100% purity.

4-(4-((6-(1H-indazol-4-yl)benzo[d]thiazol-2-yl)amino)benzoyl)piperazin-2-one (Compound 51)



To a stirred solution of 3-((6-(1H-indazol-4-yl)benzo[d]thiazol-2-yl)amino)benzoic acid (50 mg, 0.13 mmol) in DMF (5 mL) was added DIPEA (43 µl, 0.39 mmol) then piperazin-2-one (16 mg, 0.16 mmol). HATU (61 mg, 0.16 mmol) was added in one portion and the reaction was stirred under N_2 for 45 mins after which time the solvent was removed *in vacuo* and purified by flash column chromatography eluting with 3 -10 % MeOH containing 0.7 N ammonia in DCM. The product was obtained as a white solid (40 mg, 67%). ^{1}H NMR (400 MHz, DMSO) δ 13.24 (s, 1H), 10.83 (s, 1H), 8.26 (s, 2H), 8.13 (s, 1H), 7.95 - 7.88 (m, 2H), 7.82 - 7.76 (m, 1H), 7.76 - 7.70 (m, 1H), 7.58 - 7.49 (m, 3H), 7.49 - 7.40 (m, 1H), 7.31 - 7.25 (m, 1H), 4.09 - 4.04 (m, 2H), 3.69 - 3.64 (m, 2H), 3.31 - 3.22 (m, 2H). ^{13}C NMR (126 MHz, DMSO) δ 169.4, 162.3, 152.1, 142.5, 141.0, 134.4, 134.2, 133.3, 132.0, 131.5, 129.1, 128.7, 126.8, 126.8, 121.5, 121.2, 120.2, 119.8, 117.6, 109.5, 55.4, 49.1, 28.0. LCMS (m/z) calc'd for $C_{25}H_{20}N_6O_2S$ $[M + H]^+$ 469.5 found 469.3, r.t. 2.53, 95% purity.

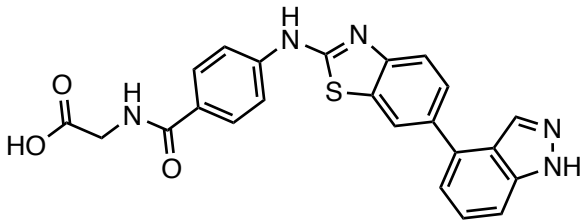
Methyl (4-((6-(1H-indazol-4-yl)benzo[d]thiazol-2-yl)amino)benzoyl)glycinate (Compound 58)



To a stirred solution of 3-((6-(1H-indazol-4-yl)benzo[d]thiazol-2-yl)amino)benzoic acid (50 mg, 0.13 mmol) in DMF (5 mL) was added DIPEA (43 µl, 0.39 mmol) then methyl glycinate (15 mg, 0.16 mmol). HATU (61 mg, 0.16 mmol) was added in one portion and the reaction was stirred under N_2 for 45 mins after which time the solvent was removed *in vacuo* and purified by flash column chromatography eluting with 3

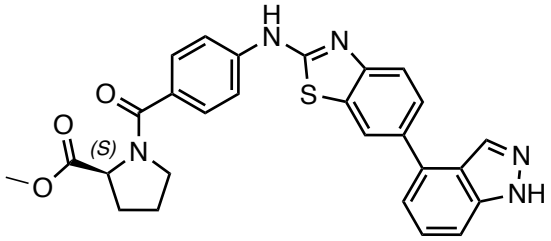
-10 % MeOH containing 0.7 N ammonia in DCM. The product was obtained as a white solid (32 mg, 54%). ^{1}H NMR (400 MHz, DMSO) δ 13.24 (s, 1H), 10.87 (s, 1H), 8.85 (t, *J* = 5.8 Hz, 1H), 8.29 - 8.24 (m, 2H), 7.92 (s, 4H), 7.81 (d, *J* = 8.3 Hz, 1H), 7.74 (dd, *J* = 1.9, 8.3 Hz, 1H), 7.55 (d, *J* = 8.3 Hz, 1H), 7.45 (t, *J* = 7.7 Hz, 1H), 7.29 (d, *J* = 7.0 Hz, 1H), 4.09 - 3.98 (m, 2H), 3.68 (s, 3H). ^{13}C NMR (101 MHz, DMSO) δ 171.0, 166.5, 162.2, 152.0, 143.7, 141.0, 134.5, 134.2, 133.3, 131.6, 129.0, 127.3, 126.8, 126.8, 121.5, 121.2, 120.3, 119.8, 117.4, 109.5, 52.2, 41.7. (m/z) calc'd for $C_{24}H_{19}N_5O_3S$ $[M + H]^+$ 458.5 found 458.2, r.t. 2.68, 100% purity.

(4-((6-(1H-indazol-4-yl)benzo[d]thiazol-2-yl)amino)benzoyl)glycine (Compound 59)



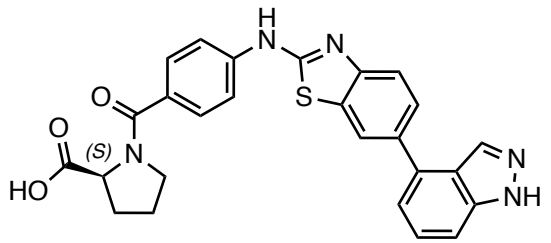
To a stirred solution of methyl (4-((6-(1H-indazol-4-yl)benzo[d]thiazol-2-yl)amino)benzoyl)glycinate (10 mg, 0.02 mmol) in THF (1 mL) was added LiOH (5 mg, 0.20 mmol) as a solution in deionised H_2O (1 mL). The reaction was stirred for 1 hr after which time the THF removed *in vacuo*. HCl (2 M, 3 mL) was added and the precipitate collected by filtration and washed with deionised water. The product, obtained as a white solid (8 mg, 90%) was dried in a vacuum dessicator containing Ca_2CO_3 as a dessicant. ^{1}H NMR (400 MHz, DMSO) δ 11.25 (s br., 1H), 8.81 (t, *J* = 6.0 Hz, 1H), 8.28 - 8.23 (m, 2H), 7.95 (d, *J* = 1.9 Hz, 4H), 7.80 (d, *J* = 8.3 Hz, 1H), 7.73 (dd, *J* = 8.3, 1.9 Hz, 1H), 7.55 (d, *J* = 8.3 Hz, 1H), 7.45 (t, *J* = 7.7 Hz, 1H), 7.28 (d, *J* = 7.0 Hz, 1H), 3.93 (d, *J* = 5.4 Hz, 2H). ^{13}C NMR (126 MHz, DMSO) δ 172.0, 166.4, 162.4, 151.9, 143.7, 141.1, 134.4, 134.2, 133.2, 131.6, 128.9, 127.5, 126.9, 126.7, 121.4, 121.2, 120.1, 119.8, 117.4, 109.6, 41.7. LCMS (m/z) calc'd for $C_{23}H_{17}N_5O_3S$ $[M + H]^+$ 444.5 found 444.3+, r.t. 2.62, purity 92%.

Ethyl (4-((6-(1H-indazol-4-yl)benzo[d]thiazol-2-yl)amino)benzoyl)-L-prolinate (Compound 54)



To a stirred solution of 3-((6-(1H-indazol-4-yl)benzo[d]thiazol-2-yl)amino)benzoic acid (50 mg, 0.13 mmol) in DMF (5 mL) was added NMM (43 µl, 0.39 mmol) then methyl L-prolinate (19 mg, 0.15 mmol). HATU (61 mg, 0.16 mmol) was added in one portion and the reaction was stirred under N_2 for 45 mins after which time the solvent was removed *in vacuo* and purified by flash column chromatography eluting with 0.5 -1 % MeOH containing 0.7 N ammonia in DCM. The product was obtained as a white gum (48 mg, 74%). ^{1}H NMR (400 MHz, DMSO-d_6) δ 13.23 (s, 1H), 10.83 (s, 1H), 8.26 (d, J = 1.6 Hz, 2H), 7.90 (d, J = 8.3 Hz, 2H), 7.79 (d, J = 8.4 Hz, 1H), 7.73 (dd, J = 1.8, 8.3 Hz, 1H), 7.64 (d, J = 8.4 Hz, 2H), 7.55 (d, J = 8.4 Hz, 1H), 7.45 (t, J = 7.7 Hz, 1H), 7.28 (d, J = 7.0 Hz, 1H), 4.53 - 4.46 (m, 1H), 3.68 (s, 3H), 3.64 (s, 2H), 2.04 - 1.76 (m, 4H). (m/z) calc'd for $C_{27}H_{23}N_5O_3S$ $[M + H]^+$ 498.6 found 498.2, r.t. 2.77, 97% purity.

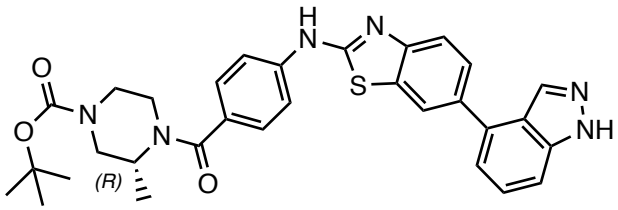
(4-((6-(1H-indazol-4-yl)benzo[d]thiazol-2-yl)amino)benzoyl)-L-proline (Compound 55)



To a stirred solution of ethyl (4-((6-(1H-indazol-4-yl)benzo[d]thiazol-2-yl)amino)benzoyl)-L-prolinate (10 mg, 0.02 mmol) in THF (1 mL) was added LiOH (5 mg, 0.20 mmol) as a solution in deionised H_2O (1 mL). The reaction was stirred for 1 hr after which time the THF removed *in vacuo*. HCl (2 M, 3 mL) was added and the precipitate collected by filtration and washed with deionised water. The product, obtained as a white solid (7 mg, 72%) was dried in a vacuum dessicator containing Ca_2CO_3 as

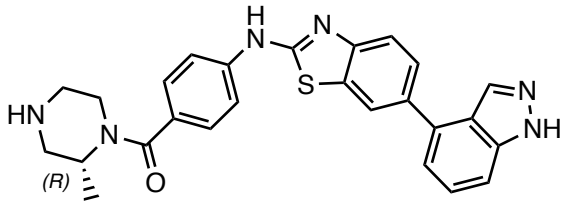
a dessicant. ^{1}H NMR (400 MHz, DMSO) δ 13.42 (s, 1H), 12.19 (s, 1H), 11.45 (s, 1H), 8.23 (s, 2H), 8.01 - 7.95 (m, 2H), 7.79 - 7.67 (m, 2H), 7.63 - 7.52 (m, 2H), 7.48 - 7.39 (m, 2H), 7.30 - 7.23 (m, 1H), 4.43 - 4.39 (m, 1H), 3.62 - 3.58 (m, 2H), 1.99 - 1.78 (m, 4H). (m/z) calc'd for $C_{26}H_{21}N_5O_3S$ $[M + H]^+$ 484.5 found 484.4, r.t. 2.66, 97% purity.

tert-butyl (R)-4-(4-((6-(1H-indazol-4-yl)benzo[d]thiazol-2-yl)amino)benzo-yl)-3-methylpiperazine-1-carboxylate (Compound 52)



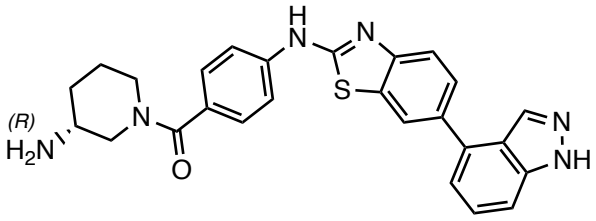
To a stirred solution of 3-((6-(1H-indazol-4-yl)benzo[d]thiazol-2-yl)amino)benzoic acid (50 mg, 0.13 mmol) in DMF (5 mL) was added NMM (43 µl, 0.39 mmol) then tert-butyl (R)-3-methylpiperazine-1-carboxylate (34 mg, 0.16 mmol). HATU (61 mg, 0.16 mmol) was added in one portion and the reaction was stirred under N_2 for 45 mins after which time the solvent was removed *in vacuo* and purified by flash column chromatography eluting with 1 -3 % MeOH containing 0.7 N ammonia in DCM. The product was obtained as a white gum (50 mg, 68%). ^{1}H NMR (400 MHz, DMSO) δ 13.26 - 13.21 (m, 1H), 10.82 - 10.76 (m, 1H), 8.28 - 8.23 (m, 2H), 7.94 - 7.86 (m, 2H), 7.81 - 7.69 (m, 2H), 7.57 - 7.51 (m, 1H), 7.48 - 7.42 (m, 3H), 7.32 - 7.24 (m, 1H), 4.34 (s, 1H), 3.81 - 3.73 (m, 1H), 3.27 - 2.96 (m, 5H), 1.42 (d, J = 3.3 Hz, 9H), 1.19 - 1.09 (m, 3H). ^{13}C NMR (101 MHz, DMSO) δ 169.8, 162.4, 154.7, 152.1, 142.1, 141.0, 134.4, 134.2, 133.3, 132.7, 131.9, 131.5, 129.7, 129.2, 128.7, 126.8, 126.8, 126.8, 121.9, 121.5, 121.2, 120.9, 120.1, 119.8, 117.7, 110.1, 109.5, 79.5, 28.5. (m/z) calc'd for $C_{31}H_{32}N_6O_3S$ $[M + H]^+$ 569.7 found 569.3, r.t. 2.97, 98% purity.

(R)-(4-((6-(1H-indazol-4-yl)benzo[d]thiazol-2-yl)amino)phenyl)(2-methylpiperazin-1-yl)methanone (COmpound 53)



Tert-butyl (R)-4-(4-((6-(1H-indazol-4-yl)benzo[d]thiazol-2-yl)amino)benzoyl)-3-methylpiperazine-1-carboxylate (14 mg, 0.02 mmol) was taken up in dioxane (1 mL) conatining HCl (4 M). The reaction was stirred for 1 h, after which time the solvent was removed *in vacuo* and the residue trituated with diethy ether to give the HCl salt of the product as a white solid (8 mg, 86%). ^{1}H NMR (400 MHz, DMSO) δ 10.92 (s, 1H), 9.46 (s, 1H), 8.98 (s, 1H), 8.29 - 8.23 (m, 2H), 7.93 (d, *J* = 8.4 Hz, 2H), 7.81 - 7.68 (m, 2H), 7.58 - 7.51 (m, 1H), 7.54 - 7.41 (m, 3H), 7.28 (d, *J* = 7.0 Hz, 1H), 4.56 - 4.51 (m, 1H), 4.11 - 4.00 (m, 1H), 3.73 - 3.68 (m, 1H), 3.28 - 3.17 (m, 3H), 3.07 - 2.99 (m, 1H), 1.35 (d, *J* = 7.1 Hz, 3H). ^{13}C NMR (126 MHz, DMSO) δ 169.4, 161.9, 151.6, 142.0, 141.6, 140.6, 134.0, 133.8, 131.1, 128.4, 128.2, 126.4, 126.3, 121.0, 120.8, 119.6, 119.4, 117.2, 109.1, 62.8, 46.1, 42.6, 40.7 , 15.2. (m/z) calc'd for $C_{26}H_{24}N_6OS$ $[M + H]^+$ 469.6 found 469.5, r.t. 2.24, 98% purity.

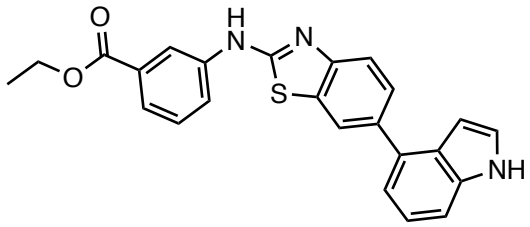
(R)-(4-((6-(1H-indazol-4-yl)benzo[d]thiazol-2-yl)amino)phenyl)(3-aminopiperidin-1-yl)methanone (Compound 50)



To a stirred solution of 3-((6-(1H-indazol-4-yl)benzo[d]thiazol-2-yl)amino)benzoic acid (50 mg, 0.13 mmol) in DMF (5 mL) was added NMM (43 µl, 0.39 mmol) then (R)-piperidin-3-amine (34 mg, 0.32 mmol). HATU (61 mg, 0.16 mmol) was added in one portion and the reaction was stirred under N_2 for 45 mins after which time the solvent was removed *in vacuo* and purified by flash column chromatography eluting with 3 -7 % MeOH containing 0.7 N ammonia in DCM. The product was obtained as

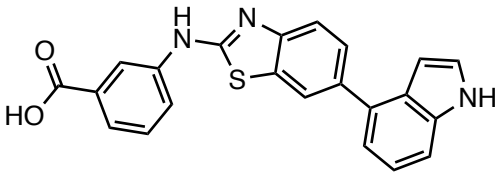
a colourless gum (6 mg, 10%). ^{1}H NMR (400 MHz, DMSO) δ 10.92 (s, 1H), 9.46 (s, 1H), 8.98 (s, 1H), 8.29 – 8.23 (m, 2H), 7.93 (d, *J* = 8.4 Hz, 2H), 7.81 – 7.68 (m, 2H), 7.58 – 7.51 (m, 1H), 7.54 – 7.41 (m, 3H), 7.28 (d, *J* = 7.0 Hz, 1H), 4.56 – 4.51 (m, 1H), 4.11 – 4.00 (m, 1H), 3.73 – 3.68 (m, 1H), 3.28 – 3.17 (m, 3H), 3.07 – 2.99 (m, 1H), 1.35 (d, *J* = 7.1 Hz, 3H). (m/z) calc'd for $C_{26}H_{24}N_6OS$ $[M + H]^+$ 469.6 found 469.2, r.t. 2.24, 94% purity.

Ethyl 3-((6-(1H-indol-4-yl)benzo[d]thiazol-2-yl)amino)benzoate (Compound 48)



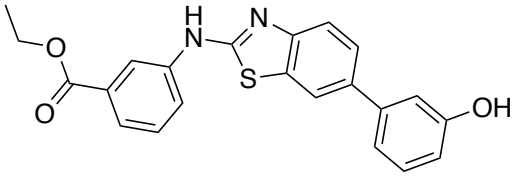
To a suspension, purged with N_2 gas, of ethyl 3-((6-bromobenzo[d]thiazol-2-yl) amino)benzoate (200 mg, 0.52 mmol), 1H-indol-4-yl boronic acid pinacol ester (156 mg, 0.64 mmol) and Na_2CO_3 (2 M, 780 μL) in THF was added bis(triphenylphosphine) palladium chloride (40 mg, 0.052 mmol). The reaction mixture was irradiated under microwave radiation for 45 mins at 125 °C. After concentration, the residue was purified by flash column chromatography (silica gel), eluting with eluting with 20 - 30 % EtOAc in petroleum ether with 2% AcOH to give a white solid (48 mg, 21%). ^{1}H NMR (400 MHz, DMSO) δ 11.27 (s, 1H), 10.76 (s, 1H), 8.47 - 8.40 (m, 1H), 8.20 - 8.14 (m, 1H), 8.13 (s, 1H), 7.77 - 7.70 (m, 1H), 7.70 - 7.59 (m, 2H), 7.59 - 7.50 (m, 1H), 7.46 - 7.37 (m, 2H), 7.23 - 7.16 (m, 1H), 7.16 - 7.10 (m, 1H), 6.62 (t, *J* = 2.4 Hz, 1H), 4.36 (q, *J* = 7.0 Hz, 2H), 1.37 (t, *J* = 7.1 Hz, 3H). ^{13}C NMR (101 MHz, DMSO) δ 166.1, 162.0, 151.4, 141.4, 136.9, 136.1, 133.3, 131.2, 131.1, 130.0, 126.9, 126.2, 126.1, 122.9, 122.5, 121.8, 121.1, 119.8, 119.0, 118.6, 111.1, 100.8, 61.3, 14.7. (m/z) calc'd for $C_{24}H_{19}N_3O_2S$ $[M + H]^+$ 413.5 found 413.8, r.t. 3.09, 99% purity.

3-((6-(1H-indol-4-yl)benzo[d]thiazol-2-yl)amino)benzoic acid (Compound 30)



To a stirred solution of ethyl 3-((6-(1H-indol-4-yl)benzo[d]thiazol-2-yl)amino) benzoate (32 mg, 0.08 mmol) in THF (1 mL) was added LiOH (19 mg, 0.80 mmol) as a solution in deionised H_2O (1 mL). The reaction was heated to 60 °C for 1 hr after which time the reaction was cooled to room temperature and THF removed *in vacuo*. HCl (2 M, 10 mL) was added and the precipitate collected by filtration and washed with deionised water. The product, obtained as a white solid (25 mg, 81%) was dried in a vacuum dessicator containing Ca_2CO_3 as a dessicant. ^{1}H NMR (400 MHz, DMSO) δ 11.00 (s, 1H), 8.43 - 8.37 (m, 1H), 8.29 - 8.22 (m, 2H), 8.14 (dd, *J* = 7.9, 2.2 Hz, 1H), 7.79 - 7.68 (m, 2H), 7.66 - 7.60 (m, 1H), 7.61 - 7.48 (m, 2H), 7.45 (t, *J* = 7.7 Hz, 1H), 7.28 (d, *J* = 7.0 Hz, 1H). ^{13}C NMR (101 MHz, DMSO) δ 167.7, 162.1, 151.2, 141.3, 136.9, 136.1, 133.2, 132.1, 131.1, 129.8, 126.9, 126.2, 126.1, 123.3, 122.3, 121.8, 121.1, 119.7, 119.0, 118.9, 111.1, 100.8. (m/z) calc'd for $C_{22}H_{15}N_3O_2S$ $[M + H]^+$ 386.4 found 386.3, r.t. 2.83, 93% purity.

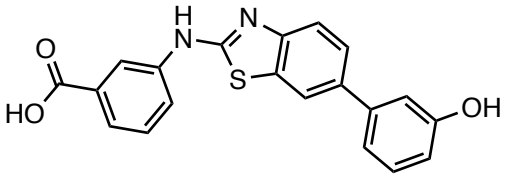
Ethyl 3-((6-(3-hydroxyphenyl)benzo[d]thiazol-2-yl)amino)benzoate (Compound 46)



To a suspension, purged with N_2 gas, of ethyl 4-((6-bromobenzo[d]thiazol-2-yl) amino)benzoate (200 mg, 0.52 mmol), 3-hydroxyphenyl boronic acid (88 mg, 0.64 mmol) and Na_2CO_3 (2 M, 780 µL) in THF was added bis(triphenylphosphine)palladium chloride (40 mg, 0.052 mmol). The reaction mixture was irradiated under microwave radiation for 45 mins at 125 °C. After concentration, the residue was purified by flash column chromatography (silica gel), eluting with eluting with 20 - 30 % EtOAc

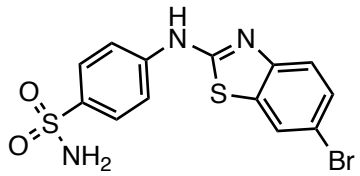
in petroleum ether with 2% AcOH to give a white solid (56 mg, 28%). ^{1}H NMR (400 MHz, DMSO) δ 10.76 (s, 1H), 9.52 (s, 1H), 8.45 - 8.39 (m, 1H), 8.18 - 8.12 (m, 1H), 8.10 (s, 1H), 7.71 - 7.49 (m, 4H), 7.31 - 7.19 (m, 1H), 7.11 (d, *J* = 7.8 Hz, 1H), 7.06 (s, 1H), 6.76 (dd, *J* = 2.4, 8.0 Hz, 1H), 4.36 (q, *J* = 7.1 Hz, 2H), 1.37 (t, *J* = 7.1 Hz, 3H). ^{13}C NMR (101 MHz, DMSO) δ 166.1, 162.2, 158.3, 151.9, 141.9, 141.3, 135.4, 131.4, 131.1, 130.4, 130.0, 125.3, 123.0, 122.5, 120.0, 119.6, 118.6, 117.9, 113.9, 106.6, 61.3, 14.7. (m/z) calc'd for $C_{22}H_{18}N_2O_3S$ $[M + H]^+$ 391.5 found 390.9, r.t. 2.98, 86% purity.

3-((6-(3-hydroxyphenyl)benzo[d]thiazol-2-yl)amino)benzoic acid (Compound 28)



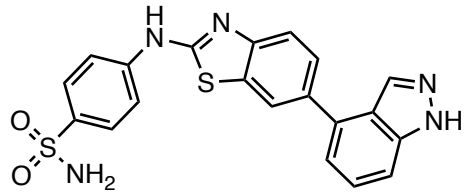
To a stirred solution of ethyl 3-((6-(3-hydroxyphenyl)benzo[d]thiazol-2-yl)amino)benzoate (30 mg, 0.08 mmol) in THF (1 mL) was added LiOH (19 mg, 0.80 mmol) as a solution in deionised H_2O (1 mL). The reaction was heated to 60 °C for 1 hr after which time the reaction was cooled to room temperature and THF removed *in vacuo*. HCl (2 M, 10 mL) was added and the precipitate collected by filtration and washed with deionised water. The product, obtained as a white solid (25 mg, 81%) was dried in a vacuum dessicator containing Ca_2CO_3 as a dessicant. ^{1}H NMR (400 MHz, DMSO) δ 10.84 (s, 1H), 8.37 (s, 1H), 8.16 - 8.07 (m, 2H), 7.70 - 7.63 (m, 1H), 7.65 - 7.53 (m, 2H), 7.56 - 7.47 (m, 1H), 7.26 (t, *J* = 7.9 Hz, 1H), 7.11 (d, *J* = 7.8 Hz, 1H), 7.06 (t, *J* = 2.1 Hz, 1H), 6.76 (dd, *J* = 2.3, 8.1 Hz, 1H). ^{13}C NMR (101 MHz, DMSO) δ 167.7, 162.3, 158.3, 151.7, 141.9, 141.2, 135.4, 132.0, 131.4, 130.4, 129.8, 125.2, 123.3, 122.4, 119.9, 119.6, 118.9, 117.8, 114.6, 113.9. (m/z) calc'd for $C_{20}H_{14}N_2O_3S$ $[M + H]^+$ 362.4 found 362.9, r.t. 2.76, 96% purity.

4-((6-bromobenzo[d]thiazol-2-yl)amino)benzenesulfonamide



To a mixture of 6-bromo-2-chlorobenzo[d]thiazole (500 mg, 2.0 mmol) and 4-aminobenzenesulfonamide (316 mg, 1.83 mmol) in EtOH (5 mL) was added HCl as a solution in dioxane (2 mL, 4 M) and the reaction mixure irradiated with microwave radiation for 1 h at 120 °C. After cooling to room temperature and concentrating, the residue was purified by flash colum chromatography (silica gel), eluting with 3 - 5% MeOH containing 7 N ammonia in CH_2Cl_2 gave the product as a white solid (352 mg, 46 %). ^{1}H NMR (400 MHz, DMSO) δ 10.95 (s, 1H), 8.13 (d, *J* = 2.0 Hz, 1H), 7.93 (d, *J* = 8.6 Hz, 2H), 7.82 (d, *J* = 8.8 Hz, 2H), 7.60 (d, *J* = 8.6 Hz, 1H), 7.51 (dd, *J* = 2.1, 8.6 Hz, 1H), 7.26 (s, 2H). ^{13}C NMR (101 MHz, DMSO) δ 162.3, 151.4, 143.5, 137.7, 132.8, 129.5, 127.5, 124.2, 121.6, 117.7, 114.9. (m/z) calc'd for $C_{13}H_{10}BrN_3O_2S_2$ $[M + H]^+$ 385.3 found 385.8, r.t. 2.78, 100% purity.

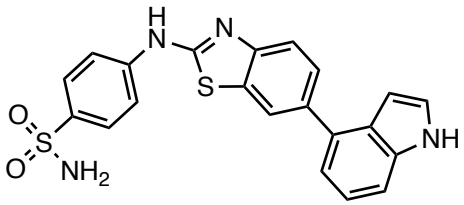
4-((6-(1H-indazol-4-yl)benzo[d]thiazol-2-yl)amino)benzenesulfonamide (Compound 32)



To a suspension, purged with N_2 gas, of 4-((6-bromobenzo[d]thiazol-2-yl)amino) benzenesulfonamide (70 mg, 0.18 mmol), 1H-indazoll-4-yl boronic acid (36 mg, 0.22 mmol) and Na_2CO_3 (2 M, 270 µL) in EtOH:H_2O (3:1) was added bis(triphenylphosphine)palladium chloride (12 mg, 0.018 mmol). The reaction mixture was irradiated under microwave radiation for 45 mins at 125 °C. After concentration, the residue was purified by flash column chromatography (silica gel), eluting with 20 - 30 % EtOAc in petroleum ether with 2% AcOH to give a white solid (32 mg, 42%). ^{1}H NMR (400 MHz, DMSO) δ 13.26 (d, *J* = 14.5 Hz, 1H), 10.96 (s, 1H), 8.30 - 8.23 (m, 1H), 8.09 - 7.91 (m,

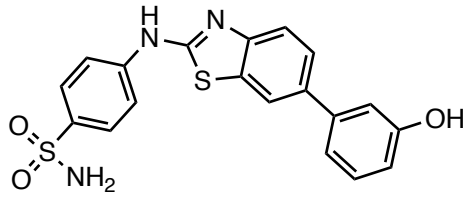
2H), 7.90 - 7.78 (m, 2H), 7.80 - 7.71 (m, 1H), 7.72 - 7.56 (m, 1H), 7.60 - 7.30 (m, 3H), 7.32 - 7.17 (m, 2H). ^{13}C NMR (101 MHz, DMSO) δ 162.2, 151.9, 143.7, 141.0, 137.5, 134.2, 133.3, 132.0, 131.6, 127.5, 126.8, 121.5, 121.3, 120.9, 120.4, 119.8, 117.6, 110.1. (m/z) calc'd for $C_{20}H_{15}N_5O_2S_2$ $[M + H]^+$ 422.5 found 422.0, r.t. 2.64, 90% purity.

4-((6-(1H-indol-4-yl)benzo[d]thiazol-2-yl)amino)benzenesulfonamide (Compound 33)



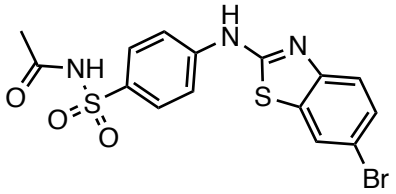
To a suspension, purged with N_2 gas, of 4-((6-bromobenzo[d]thiazol-2-yl)amino) benzenesulfonamide (100 mg, 0.26 mmol), 1H-indol-4-yl boronic acid pinacol ester 75 mg, 0.31 mmol) and Na_2CO_3 (2 M, 390 μL) in EtOH:H_2O (3:1) was added bis(triphenylphosphine)palladium chloride (17 mg, 0.026 mmol). The reaction mixture was irradiated under microwave radiation for 45 mins at 125 °C. After concentration, the residue was purified by flash column chromatography (silica gel), eluting with 20 - 30 % EtOAc in petroleum ether with 2% AcOH to give a white solid (62 mg, 56%). ^{1}H NMR (400 MHz, DMSO) δ 11.27 (s, 1H), 10.91 (s, 1H), 8.15 (d, *J* = 1.8 Hz, 1H), 7.97 (d, *J* = 8.5 Hz, 2H), 7.84 (d, *J* = 8.8 Hz, 2H), 7.78 (d, *J* = 8.3 Hz, 1H), 7.68 (dd, *J* = 1.9, 8.3 Hz, 1H), 7.46 - 7.38 (m, 2H), 7.26 (s, 2H), 7.20 (t, *J* = 7.6 Hz, 1H), 7.17 - 7.10 (m, 1H), 6.62 (t, *J* = 2.4 Hz, 1H). ^{13}C NMR (101 MHz, DMSO) δ 161.7, 151.2, 143.8, 137.4, 136.9, 136.37, 133.2, 131.3, 127.5, 126.9, 126.3, 126.1, 121.85, 121.1, 120.1, 119.0, 117.6, 111.1, 100.8. (m/z) calc'd for $C_{21}H_{16}N_4O_2S_2$ $[M + H]^+$ 421.5 found 421.2, r.t. 2.75, 97% purity.

4-((6-(3-hydroxyphenyl)benzo[d]thiazol-2-yl)amino)benzenesulfonamide (Compound 31)



To a suspension, purged with N_2 gas, of 4-((6-bromobenzo[d]thiazol-2-yl)amino) benzenesulfonamide (100 mg, 0.26 mmol), 3-hydroxyphenyl boronic acid (43 mg, 0.31 mmol) and Na_2CO_3 (2 M, 390 µL) in EtOH:H_2O (3:1) was added bis(triphenylphosphine)palladium chloride (17 mg, 0.026 mmol). The reaction mixture was irradiated under microwave radiation for 45 mins at 125 °C. After concentration, the residue was purified by flash column chromatography (silica gel), eluting with 2 - 3% MeOH in CH_2Cl_2 to give a white solid (44 mg, 43%). ^{1}H NMR (400 MHz, DMSO) δ 10.91 (s, 1H), 9.52 (s, 1H), 8.15 - 8.10 (m, 1H), 7.99 - 7.87 (m, 2H), 7.83 (d, *J* = 8.7 Hz, 2H), 7.76 - 7.67 (m, 1H), 7.64 - 7.56 (m, 1H), 7.31 - 7.15 (m, 3H), 7.15 - 7.03 (m, 2H), 6.77 (dd, *J* = 2.2, 8.0 Hz, 1H). ^{13}C NMR (101 MHz, DMSO) δ 161.9, 158.3, 151.7, 143.7, 141.8, 137.4, 135.7, 131.5, 130.4, 127.5, 125.3, 120.3, 119.7, 117.9, 117.6, 114.6, 113.9. (m/z) calc'd for $C_{19}H_{15}N_3O_3S_2$ $[M + H]^+$ 398.5 found 398.2, r.t. 2.63, 96% purity.

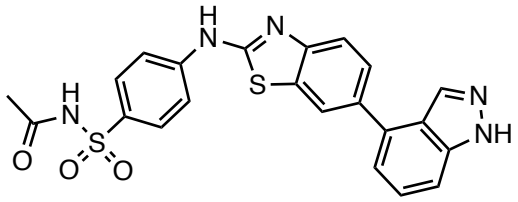
N-((4-((6-bromobenzo[d]thiazol-2-yl)amino)phenyl)sulfonyl)acetamide



To a stirred solution of 4-((6-bromobenzo[d]thiazol-2-yl)amino)benzenesulfonamide (50 mg, 0.13 mmol), DMAP (1 mg, 5.5 µmol)and NEt_3 (38 µL, 0.28 mmol) at 55 °C in toluene (5 mL) was added dropwise aceytl chloride (19 µL, 0.26 mmol) as a solution in toluene (1 mL) . The reaction was heated at 55 °C for 3 h, after which time the reaction mixture was cooled to room temperature and EtOAc (10 mL) and H_2O (10 mL) added. The aqueous was exteracted with EtOAc (2 x 10 mL) and the combined organics

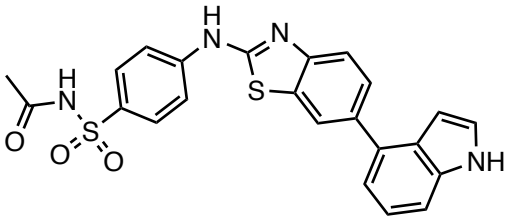
concentrated *in vacuo*. The residue was taken up in THF (3 mL) and LiOH (10 mg, 0.42 mmol) added as a solution in H_2O (3 mL) and stirred. After 30 min the reaction mixture was concentrated *in vacuo* and HCl (2 M, 10 mL) added to give the product as a white precipitate. The product (49 mg, 90%) was collected by filtration, and washed with deionised water and dried in a vacuum dessicator containing Ca_2CO_3 as a dessicant. ^{1}H NMR (400 MHz, DMSO) δ 12.22 (s, 1H), 8.30 (d, *J* = 2.0 Hz, 1H), 8.12 (d, 2H), 7.86 (d, *J* = 8.5 Hz, 2H), 7.74 (d, *J* = 1.4 Hz, 1H), 7.58 (d, *J* = 8.7 Hz, 1H), 7.51 (dd, *J* = 2.1, 8.6 Hz, 1H), 2.02 (s, 3H). ^{13}C NMR (101 MHz, DMSO) δ 170.7, 169.6, 161.0, 147.2, 144.5, 140.6, 134.8, 130.7, 129.6, 127.1, 124.6, 123.2, 118.8, 116.5, 24.6. (m/z) calc'd for $C_{15}H_{12}BrN_3O_3S_2$ $[M + H]^+$ 428.3 found 428.1, r.t. 2.78, 99% purity.

N-((4-((6-(1H-indazol-4-yl)benzo[d]thiazol-2-yl)amino)phenyl)sulfonyl)acetamide (Compound 38)



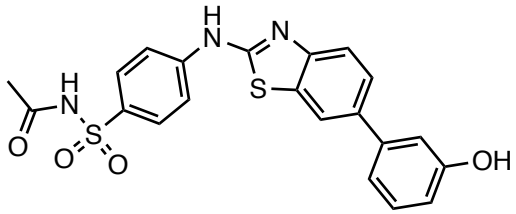
To a suspension, purged with N_2 gas, of N-((4-((6-bromobenzo[d]thiazol-2-yl) amino)phenyl)sulfonyl)acetamide (100 mg, 0.21 mmol), 1H-indazol-4-yl boronic acid (41 mg, 0.25 mmol) and Na_2CO_3 (2 M, 315 µL) in EtOH:H_2O (3:1) was added bis(t-riphenylphosphine)palladium chloride (15 mg, 0.021 mmol). The reaction mixture was irradiated under microwave radiation for 45 mins at 125 °C. After concentration, the residue was purified by flash column chromatography (silica gel), eluting with 70 - 90 % EtOAc in petroleum ether with 1% AcOH to give a white solid (32 mg, 42%) ^{1}H NMR (400 MHz, DMSO) δ 13.24 (s, 1H), 11.97 (s, 1H), 11.04 (s, 1H), 8.27 (d, *J* = 5.7 Hz, 2H), 7.98 (d, *J* = 8.4 Hz, 2H), 7.89 (d, *J* = 8.6 Hz, 2H), 7.81 (d, *J* = 8.1 Hz, 1H), 7.75 (d, *J* = 8.1 Hz, 1H), 7.55 (d, *J* = 8.2 Hz, 1H), 7.49 - 7.41 (m, 1H), 7.32 - 7.24 (m, 1H), 1.88 (s, 3H), ^{13}C NMR (126 MHz, DMSO) δ 172.5, 162.1, 151.8, 144.6, 141.0, 134.7, 134.2, 133.3, 131.7, 129.5, 127.5, 127.1, 126.8, 121.5, 121.3, 121.3, 120.4, 119.9, 117.4, 24.4. (m/z) calc'd for $C_{22}H_{17}N_5O_3S_2$ $[M + H]^+$ 464.5 found 464.1, r.t. 2.70, 99% purity.

N-((4-((6-(1H-indol-4-yl)benzo[d]thiazol-2-yl)amino)phenyl)sulfonyl)acetamide (Compound 39)



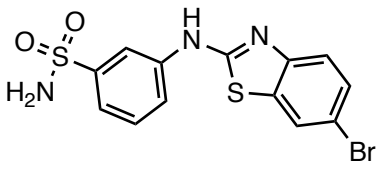
To a suspension, purged with N_2 gas, of N-((4-((6-bromobenzo[d]thiazol-2-yl) amino)phenyl)sulfonyl)acetamide (100 mg, 0.21 mmol), 1H-indol-4-yl boronic acid pinacol ester (61 mg, 0.25 mmol) and Na_2CO_3 (2 M, 315 μL) in EtOH:H_2O (3:1) was added bis(triphenylphosphine)palladium chloride (15 mg, 0.021 mmol). The reaction mixture was irradiated under microwave radiation for 45 mins at 125 °C. After concentration, the residue was purified by flash column chromatography (silica gel), eluting with 70 - 90 % EtOAc in petroleum ether with 2% AcOH to give a white solid (62 mg, 64%). ^{1}H NMR (400 MHz, DMSO) δ 11.65 (s, 1H), 11.28 (s, 1H), 11.07 (s, 1H), 8.16 (d, *J* = 1.7 Hz, 1H), 8.01 (d, *J* = 8.8 Hz, 2H), 7.91 (d, *J* = 8.7 Hz, 2H), 7.87 - 7.75 (m, 1H), 7.69 (dd, *J* = 1.8, 8.3 Hz, 1H), 7.46 - 7.38 (m, 2H), 7.20 (t, *J* = 7.6 Hz, 1H), 7.17 - 7.10 (m, 1H), 6.62 (t, *J* = 2.5 Hz, 1H), 1.91 (s, 3H). ^{13}C NMR (101 MHz, DMSO) δ 169.6, 161.6, 151.1, 145.1, 136.9, 136.5, 133.2, 132.5, 131.4, 129.6, 127.0, 126.3, 126.1, 121.8, 121.2, 120.2, 119.1, 117.4, 111.1, 100.7, 24.0. (m/z) calc'd for $C_{23}H_{18}N_4O_3S_2$ $[M + H]^+$ 463.5 found 463.2, r.t. 2.79, 98% purity.

N-((4-((6-(3-hydroxyphenyl)benzo[d]thiazol-2-yl)amino)phenyl)sulfonyl)acetamide (Comnpound 37)



To a suspension, purged with N_2 gas, of N-((4-((6-bromobenzo[d]thiazol-2-yl) amino)phenyl)sulfonyl)acetamide (100 mg, 0.21 mmol), 3-hydroxyphenyl boronic acid 35 mg, 0.25 mmol) and Na_2CO_3 (2 M, 351 μL) in EtOH:H_2O (3:1) was added bis(triphenylphosphine)palladium chloride (15 mg, 0.021 mmol). The reaction mixture was irradiated under microwave radiation for 45 mins at 125 °C. After concentration, the residue was purified by flash column chromatography (silica gel), eluting with 70 - 90 % EtOAc in petroleum ether with 2% AcOH to give a white solid (67 mg, 64%). ^{1}H NMR (400 MHz, DMSO) δ 11.98 (s, 1H), 11.05 (s, 1H), 9.53 (s, 1H), 8.14 (d, *J* = 1.8 Hz, 1H), 8.00 (d, *J* = 8.7 Hz, 2H), 7.91 (d, *J* = 8.9 Hz, 2H), 7.73 (d, *J* = 8.4 Hz, 1H), 7.61 (dd, *J* = 1.9, 8.4 Hz, 1H), 7.27 (t, *J* = 7.8 Hz, 1H), 7.12 (d, *J* = 7.8 Hz, 1H), 7.06 (s, 1H), 6.77 (dd, *J* = 2.2, 8.1 Hz, 1H), 1.92 (s, 3H). ^{13}C NMR (101 MHz, DMSO) δ 169.3, 161.7, 158.3, 151.9, 151.6, 145.1, 141.8, 135.8, 131.6, 130.4, 129.7, 125.4, 120.4, 119.7, 117.9, 117.5, 114.7, 113.9, 23.8. (m/z) calc'd for $C_{21}H_{17}N_3O_4S_2$ $[M + H]^+$ 440.1found 440.2, r.t. 2.68, 99% purity.

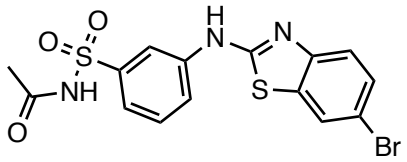
3-((6-bromobenzo[d]thiazol-2-yl)amino)benzenesulfonamide



To a mixture of 6-bromo-2-chlorobenzo[d]thiazole (500 mg, 2.0 mmol) and 3-aminobenzenesulfonamide (316 mg, 1.83 mmol) in EtOH (5 mL) was added HCl as a solution in dioxane (2 mL, 4 M) and the reaction mixure irradiated with microwave radiation for 1 h at 120 °C. After cooling to room temperature and concentrating, the residue was purified by flash colum chromatography (silica gel), eluting with 0-30% EtOAc in

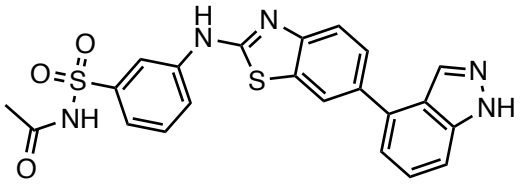
petroleum ether gave the product as a white solid (490 mg, 64 %). ^{1}H NMR (400 MHz, DMSO) δ 10.89 (s, 1H), 8.31 - 8.25 (m, 1H), 8.11 (d, *J* = 2.0 Hz, 1H), 8.01 (dd, *J* = 2.2, 7.9 Hz, 1H), 7.62 - 7.53 (m, 2H), 7.54 - 7.46 (m, 2H), 7.42 (s, 2H). ^{13}C NMR (101 MHz, DMSO) δ 162.4, 151.5, 145.4, 141.1, 132.7, 130.3, 129.4, 124.2, 121.4, 121.1, 119.7, 115.2, 114.7. (m/z) calc'd for $C_{13}H_{10}BrN_3O_2S_2$ 384.3 found 384.1, r.t. 2.78, 99% purity.

N-((3-((6-bromobenzo[d]thiazol-2-yl)amino)phenyl)sulfonyl)acetamide



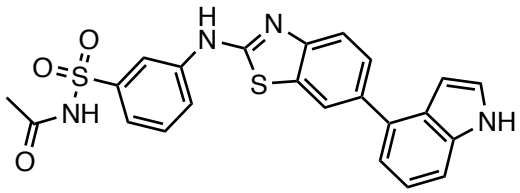
To a stirred solution of 3-((6-bromobenzo[d]thiazol-2-yl)amino)benzenesulfonamide (100 mg, 0.26 mmol), DMAP (2 mg, 11 µmol), and NEt_3 (74 µL, 0.56 mmol) at 55 °C in toluene (7 mL) was added dropwise aceytl chloride (38 µL, 0.56 mmol) as a solution in toluene (2 mL) . The reaction was heated at 55 °C for 3 h, after which time the reaction mixture was cooled to room temperature and EtOAc (15 mL) and H_2O (15 mL) added. The aqueous was extracted with EtOAc (2 x 10 mL) and the combined organics concentrated *in vacuo*. The residue was taken up in THF (5 mL) and LiOH (10 mg, 0.42 mmol) added as a solution in H_2O (3 mL) and stirred. After 30 min the reaction mixture was concentrated *in vacuo* and HCl (2 M, 20 mL) added to give the product as a white precipitate. The product (91 mg, 82%) was collected by filtration, and washed with deionised water and dried in a vacuum dessicator containing Ca_2CO_3 as a dessicant. ^{1}H NMR (400 MHz, DMSO) δ 12.18 (s, 1H), 11.10 (s, 1H), 8.42 (t, *J* = 2.0 Hz, 1H), 8.11 (dd, *J* = 2.1, 7.7 Hz, 2H), 7.62 (t, *J* = 8.0 Hz, 1H), 7.62 - 7.53 (m, 3H), 1.96 (s, 3H). ^{13}C NMR (101 MHz, DMSO) δ 173.1, 169.3, 162.4, 141.2, 140.6, 132.8, 130.4, 129.4, 124.2, 124.2, 122.7, 121.4, 121.1, 114.8, 23.7. (m/z) calc'd for $C_{15}H_{12}BrN_3O_3S_2$ $[M + H]^+$ 427.3 found 427.2, r.t. 2.84, 95% purity.

N-((3-((6-(1H-indazol-4-yl)benzo[d]thiazol-2-yl)amino)phenyl)sulfonyl)acetamide (Compiund 41)



To a suspension, purged with N_2 gas, of N-((3-((6-bromobenzo[d]thiazol-2-yl) amino)phenyl)sulfonyl)acetamide (100 mg, 0.21 mmol), 1H-indazoll-4-yl boronic acid (41 mg, 0.25 mmol) and Na_2CO_3 (2 M, 315 µL) in EtOH:H_2O (3:1) was added bis(t-riphenylphosphine)palladium chloride (15 mg, 0.021 mmol). The reaction mixture was irradiated under microwave radiation for 45 mins at 125 °C. After concentration, the residue was purified by flash column chromatography (silica gel), eluting with 70-90% EtOAc in petroleum ether to give a white solid (71 mg, 73%). ^{1}H NMR (400 MHz, DMSO) δ 13.24 (s, 1H), 11.97 (s, 1H), 11.04 (s, 1H), 8.27 (d, *J* = 5.7 Hz, 2H), 7.98 (d, *J* = 8.4 Hz, 2H), 7.89 (d, *J* = 8.6 Hz, 2H), 7.81 (d, *J* = 8.1 Hz, 1H), 7.75 (d, *J* = 8.1 Hz, 1H), 7.55 (d, *J* = 8.2 Hz, 1H), 7.49 - 7.41 (m, 1H), 7.32 - 7.24 (m, 1H), 1.88 (s, 3H). ^{13}C NMR (126 MHz, DMSO) δ 172.5, 162.1, 151.9, 151.8, 144.6, 141.0, 134.7, 134.2, 133.3, 131.7, 129.5, 127.5, 127.1, 126.8, 124.3, 121.5, 121.3, 121.3, 120.4, 119.9, 117.4, 24.4. (m/z) calc'd for $C_{22}H_{17}N_5O_3S_2$ $[M + H]^+$ 464.5 found 464.1, r.t. 2.70, 99% purity.

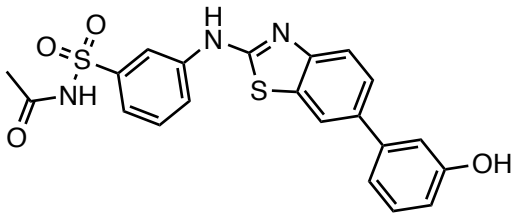
N-((3-((6-(1H-indol-4-yl)benzo[d]thiazol-2-yl)amino)phenyl)sulfonyl)acetamide (Compound 42)



To a suspension, purged with N_2 gas, of N-((3-((6-bromobenzo[d]thiazol-2-yl) amino)phenyl)sulfonyl)acetamide (100 mg, 0.21 mmol), 1H-indol-4-yl boronic acid pinacol ester (61 mg, 0.25 mmol) and Na_2CO_3 (2 M, 315 µL) in EtOH:H_2O (3:1) was added bis(triphenylphosphine)palladium chloride (15 mg, 0.021 mmol). The reaction mixture was irradiated under microwave radiation for 45 mins at 125 °C. After concen-

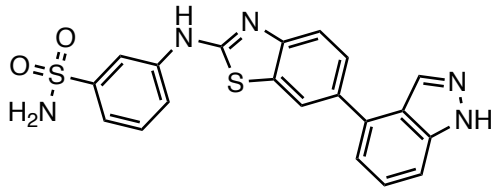
tration, the residue was purified by flash column chromatography (silica gel), eluting with 70 - 90 % EtOAc in petroleum ether with 2% AcOH to give a white solid (57 mg, 59%). ^{1}H NMR (400 MHz, DMSO) δ 11.65 (s, 1H), 11.28 (s, 1H), 11.07 (s, 1H), 8.16 (d, *J* = 1.7 Hz, 1H), 8.01 (d, *J* = 8.8 Hz, 2H), 7.91 (d, *J* = 8.7 Hz, 2H), 7.87 - 7.75 (m, 1H), 7.69 (dd, *J* = 1.8, 8.3 Hz, 1H), 7.46 - 7.38 (m, 2H), 7.20 (t, *J* = 7.6 Hz, 1H), 7.17 - 7.10 (m, 1H), 6.62 (t, *J* = 2.5 Hz, 1H), 1.91 (s, 3H). ^{13}C NMR (101 MHz, DMSO) δ 172.5, 169.7, 161.8, 151.2, 141.4, 141.1, 136.9, 136.3, 133.2, 131.2, 130.3, 127.0, 126.3, 126.1, 122.3, 121.9, 121.1, 120.8, 119.9, 119.0, 116.4, 111.1, 100.8, 24.0. (m/z) calc'd for $C_{23}H_{18}N_4O_3S_2$ $[M + H]^+$ 463.5 found 463.2, r.t. 2.79, 98% purity.

N-((4-((6-(3-hydroxyphenyl)benzo[d]thiazol-2-yl)amino)phenyl)sulfonyl)acetamide (Compound 40)



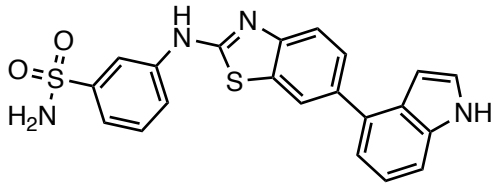
To a suspension, purged with N_2 gas, of 3-((6-bromobenzo[d]thiazol-2-yl)amino) benzenesulfonamide (100 mg, 0.21 mmol), 3-hydroxyphenyl boronic acid 35 mg, 0.25 mmol) and Na_2CO_3 (2 M, 351 μL) in EtOH:H_2O (3:1) was added bis(triphenylphosphine)palladium chloride (15 mg, 0.021 mmol). The reaction mixture was irradiated under microwave radiation for 45 mins at 125 °C. After concentration, the residue was purified by flash column chromatography (silica gel), eluting with 70 - 90 % EtOAc in petroleum ether with 2% AcOH to give a white solid (67 mg, 72%). ^{1}H NMR (400 MHz, DMSO) δ 11.98 (s, 1H), 11.05 (s, 1H), 9.53 (s, 1H), 8.14 (d, *J* = 1.8 Hz, 1H), 8.00 (d, *J* = 8.7 Hz, 2H), 7.91 (d, *J* = 8.9 Hz, 2H), 7.73 (d, *J* = 8.4 Hz, 1H), 7.61 (dd, *J* = 1.9, 8.4 Hz, 1H), 7.27 (t, *J* = 7.8 Hz, 1H), 7.12 (d, *J* = 7.8 Hz, 1H), 7.06 (s, 1H), 6.77 (dd, *J* = 2.2, 8.1 Hz, 1H), 1.92 (s, 3H). ^{13}C NMR (101 MHz, DMSO) δ 169.6, 162.0, 158.3, 151.7, 141.8, 141.3, 141.0, 135.6, 131.5, 130.4, 130.3, 125.3, 122.4, 120.9, 120.1, 119.7, 117.9, 116.5, 114.6, 113.9, 23.9. (m/z) calc'd for $C_{21}H_{17}N_3O_4S_2$ 429.5 found 440.2, r.t. 2.68, 99% purity.

3-((6-(1H-indazol-4-yl)benzo[d]thiazol-2-yl)amino)benzenesulfonamide (Compound 35)



To a suspension, purged with N_2 gas, of 3-((6-bromobenzo[d]thiazol-2-yl)amino) benzenesulfonamide (100 mg, 0.26 mmol), 1H-indazoll-4-yl boronic acid (51 mg, 0.31 mmol) and Na_2CO_3 (2 M, 390 µL) in EtOH:H_2O (3:1) was added bis(triphenylphosphine)palladium chloride (18 mg, 0.026 mmol). The reaction mixture was irradiated under microwave radiation for 45 mins at 125 °C. After concentration, the residue was purified by flash column chromatography (silica gel), eluting with 2 - 3% MeOH in CH_2Cl_2 to give a white solid (69 mg, 63%). ^{1}H NMR (400 MHz, DMSO) δ 13.30 - 13.21 (m, 1H), 10.88 (s, 1H), 8.33 (s, 1H), 8.26 (s, 2H), 8.07 (d, *J* = 8.2 Hz, 1H), 7.81 - 7.70 (m, 2H), 7.71 - 7.37 (m, 6H), 7.28 (d, *J* = 7.1 Hz, 1H). ^{13}C NMR (101 MHz, DMSO) δ 162.4, 152.0, 145.4, 141.3, 141.0, 134.4, 134.2, 133.3, 132.0, 131.9, 131.5, 130.3, 126.8, 126.8, 121.2, 121.0, 120.2, 119.8, 118.0, 115.1, 109.5. (m/z) calc'd for $C_{20}H_{15}N_5O_2S_2$ 421.5 found 422.2, r.t. 2.65, 90% purity. (m/z) calc'd for $C_{21}H_{17}N_3O_4S_2$ $[M + H]^+$ 440.5 found 440.2, r.t. 2.68, 99% purity.

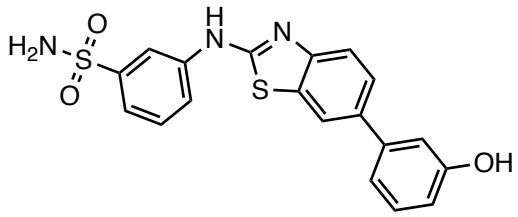
3-((6-(1H-indol-4-yl)benzo[d]thiazol-2-yl)amino)benzenesulfonamide (Compound 36)



To a suspension, purged with N_2 gas, of 3-((6-bromobenzo[d]thiazol-2-yl)amino) benzenesulfonamide (100 mg, 0.26 mmol), 1H-indol-4-yl boronic acid pinacol ester 75 mg, 0.31 mmol) and Na_2CO_3 (2 M, 390 µL) in EtOH:H_2O (3:1) was added bis(triphenylphosphine)palladium chloride (17 mg, 0.026 mmol). The reaction mixture was irradiated under microwave radiation for 45 mins at 125 °C. After concentration, the residue was purified by flash column chromatography (silica gel), eluting with 2 - 3%

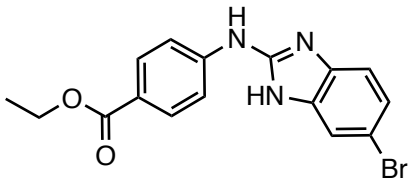
MeOH in CH_2Cl_2 to give a white solid (88 mg, 80%). ^{1}H NMR (400 MHz, DMSO) δ 11.27 (s, 1H), 10.84 (s, 1H), 8.32 (t, *J* = 2.0 Hz, 1H), 8.14 (d, *J* = 1.7 Hz, 1H), 8.07 (dd, *J* = 2.2, 8.2 Hz, 1H), 7.75 (d, *J* = 8.3 Hz, 1H), 7.71 - 7.64 (m, 1H), 7.61 - 7.56 (m, 1H), 7.53 - 7.45 (m, 1H), 7.44 - 7.41 (m, 3H), 7.20 (t, *J* = 7.6 Hz, 1H), 7.16 - 7.10 (m, 1H), 6.62 (t, *J* = 2.5 Hz, 1H). ^{13}C NMR (126 MHz, DMSO) δ 161.4, 150.9, 144.9, 140.9, 136.4, 135.8, 132.8, 130.8, 129.8, 126.5, 125.8, 125.6, 121.4, 120.6, 120.5, 119.5, 119.0, 118.6, 114.6, 110.6, 100.3. (m/z) calc'd for $C_{21}H_{16}N_4O_2S_2$ $[M + H]^+$ 421.5 found 421.3, r.t. 2.75, 96% purity.

3-((6-(3-hydroxyphenyl)benzo[d]thiazol-2-yl)amino)benzenesulfonamide (Compound 34)



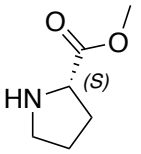
To a suspension, purged with N_2 gas, of 3-((6-bromobenzo[d]thiazol-2-yl)amino) benzenesulfonamide (100 mg, 0.26 mmol), 3-hydroxyphenyl boronic acid (43 mg, 0.31 mmol) and Na_2CO_3 (2 M, 390 μL) in EtOH:H_2O (3:1) was added bis(triphenylphosphine)palladium chloride (17 mg, 0.026 mmol). The reaction mixture was irradiated under microwave radiation for 45 mins at 125 °C. After concentration, the residue was purified by flash column chromatography (silica gel), eluting with 2 - 3% MeOH in CH_2Cl_2 to give a white solid (39 mg, 38%). ^{1}H NMR (400 MHz, DMSO) δ 10.84 (s, 1H), 9.52 (s, 1H), 8.31 (t, *J* = 2.0 Hz, 1H), 8.11 (d, *J* = 1.9 Hz, 1H), 8.04 (dd, *J* = 2.2, 8.1 Hz, 1H), 7.69 (d, *J* = 8.4 Hz, 1H), 7.63 - 7.54 (m, 2H), 7.49 (d, *J* = 7.8 Hz, 1H), 7.42 (s, 2H), 7.26 (t, *J* = 7.9 Hz, 1H), 7.11 (d, *J* = 7.8 Hz, 1H), 7.06 (t, *J* = 2.0 Hz, 1H), 6.76 (dd, *J* = 2.3, 8.1 Hz, 1H). ^{13}C NMR (101 MHz, DMSO) δ 162.06, 158.28, 151.78, 145.38, 141.86, 141.26, 135.51, 131.47, 130.39, 130.25, 125.27, 120.97, 120.09, 119.64, 119.49, 117.87, 115.06, 114.59, 113.89. (m/z) calc'd for $C_{19}H_{15}N_3O_3S_2$ $[M + H]^+$ 398.5 found 398.2, r.t. 2.65, 98% purity.

ethyl 4-((6-bromo-1H-benzo[d]imidazol-2-yl)amino)benzoate



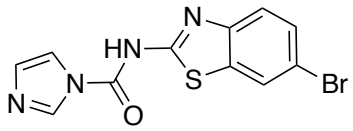
To a stirred solution of 4-bromobenzene-1,2-diamine (1.35 g, 7.24 mmol) in MeCN (25 mL) was added ethyl 4-isothiocyanatobenzoate (1.50 g, 7.24 mmol), BOP (4.8 g, 10.9 mmol), DBU (2.2 mL, 14.5 mmol). The reaction mixture was stirred for 2 hours after which time the reaction mixture was concentrated and purified by column chromatography (silica gel) 50 - 100% EtOAc in petroleum ether containing 1 % NEt_3. The product was isolated as a white solid (1.42 g, 54%). ^{1}H NMR (400 MHz, DMSO) δ 11.06 (s, 1H), 9.77 (s, 1H), 7.93 (d, *J* = 8.5 Hz, 2H), 7.84 (d, *J* = 8.6 Hz, 2H), 7.53 (s, 1H), 7.32 (d, *J* = 8.3 Hz, 1H), 7.17 (dd, *J* = 8.4, 1.9 Hz, 1H), 4.31 (q, *J* = 7.1 Hz, 2H), 1.34 (t, *J* = 7.1 Hz, 3H). LCMS (m/z) calc'd for $C_{16}H_{14}BrN_3O_2$ $[M + H]^+$ 362.2 found 362.2, r.t. 2.53, 96% purity.

Methyl L-prolinate



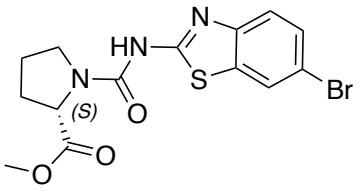
To a stirred solution of L-Proline (300 mg, 2.61 mmol) in MeOH (5 mL) at 0 °C was slowly added thionyl chloride (189 µL, 2.61 mmol). The reaction was allowed to warm to room temperature and stirred for a further 6 h after which time the volatiles were removed *in vacuo* to give the product as a pale yellow oil (330 mg, 98%). ^{1}H NMR (400 MHz, DMSO) δ 9.98 (s, 1H), 4.33 (dd, *J* = 8.5, 7.4 Hz, 1H), 3.72 (s, 3H), 3.28 – 3.09 (m, 2H), 2.23 (ddt, *J* = 11.8, 7.7, 6.2 Hz, 1H), 2.04 – 1.91 (m, 1H), 1.95 – 1.84 (m, 2H). ^{13}C NMR (101 MHz, DMSO) δ 169.5, 58.8, 53.4, 45.5, 28.1, 23.5. HRMS (m/z): calc'd for $C_6H_{11}NO_2$ 129.0863 $[M + H]^+$ and 152.0688 [M + Na] found 130.0877 and 152.0682.

N-(6-bromobenzo[d]thiazol-2-yl)-1H-imidazole-1-carboxamide



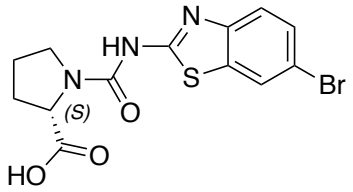
To a stirred solution of 2,6-dibromobenzo[d]thiazole (5.0 g, 21.8 mmol) in DMF (30 mL) was added CDI (14.2 g, 87.3 mmol). After 1 hr the reaction mixture contained a large amount of white precipitate. The reaction mixture was diluted with CH_2Cl_2 (100 mL) and the product as a white solid (6.7 g, 95%) collected by filtration and washed with CH_2Cl_2 (2 x 50 mL). The compound was extremely insoluble and was carried forward without further purification.

Methyl ((6-bromobenzo[d]thiazol-2-yl)carbamoyl)-L-prolinate



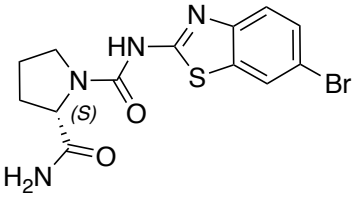
To a stirred suspention of N-(6-bromobenzo[d]thiazol-2-yl)-1H-imidazole-1-carboxamide (6.7 g, 20.7 mmol) in DMF (30 mL) was added NEt_3 (9.1 mL, 65.4 mmol) and methyl L-prolinate (4.4 g, 26.2 mmol). The reaction was left overnight after which time the reaction mixture had become homogeneous. The DMF was concentrated *in vacuo* and EtOAc (100 mL) was added. Deionised H_2O (100 mL) was added and the organic layer separated. The organic layer was washed with deionised H_2O (3 x 50 mL) and brine (50 mL), then dried ($MgSO_4$), filtered, and solvent removed *in vacuo* to give a white solid (7.37 g, 93%). ^{1}H NMR (400 MHz, DMSO) δ 8.11 (s, 1H), 7.57 – 7.46 (m, 2H), 4.44 – 4.39 (m, 1H), 3.66 (s, 3H), 2.27 – 2.14 (m, 2H), 1.95 – 1.90 (m, 4H). LCMS (m/z) calc'd for $C_{14}H_{14}BrN_3O_3S$ $[M + H]^+$ 386.2 found 386.1, r.t. 2.79.

((6-bromobenzo[d]thiazol-2-yl)carbamoyl)-L-proline



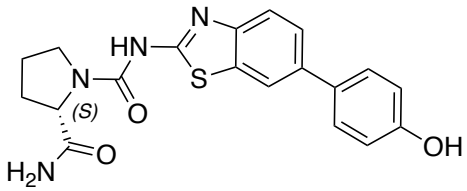
To a stirred solution of Methyl ((6-bromobenzo[d]thiazol-2-yl)carbamoyl)-L-prolinate (5.0 g, 13.1 mmol) in THF (25 mL) was added LiOH (1.25 g, 52.4 mmol) as a solution in deionised H_2O (25 mL). The reaction was stirred overnight, after which time the THF was removed *in vacuo* and HCl (2 M, 50 mL) was added and the reaction mixture rapidly stirred. The product, a white solid (4.7 g, 96%), was collected by filtration and washed with deionised water (3 x 25 mL) and dried in a vacuum dessicator containing $CaCO_3$. ^{1}H NMR (400 MHz, DMSO, 70 °C) δ 11.53 (s, 2H), 8.07 (s, 1H), 7.55 – 7.46 (m, 2H), 4.48 (s, 1H), 3.65 – 3.56 (m, 2H), 2.30 – 2.17 (m, 1H), 2.03 – 1.89 (m, 3H). LCMS (m/z) calc'd for $C_{13}H_{12}BrN_3O_3S$ $[M + H]^+$ 372.2 found 372.2 , r.t. 2.60.

(S)-N1-(6-bromobenzo[d]thiazol-2-yl)pyrrolidine-1,2-dicarboxamide



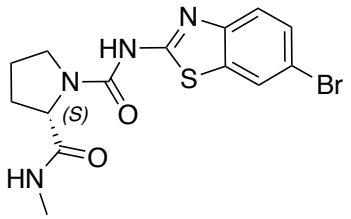
Methyl ((6-bromobenzo[d]thiazol-2-yl)carbamoyl)-L-prolinate (2.23 g, 5.8 mmol) was taken up in THF (10 mL) and NH_4OH (aq) (5 mL) added. The reaction mixture was stirred for 3 h after which time the reaction mixture was acidified to pH 2 with conc. HCl and extracted with EtOAc (3 x 50 mL). The combined organics were washed with brine (50 mL), dried ($MgSO_4$), filtered, and solvent removed *in vacuo* to give a white solid (1.76 g, 83%). ^{1}H NMR (400 MHz, DMSO) δ 11.41 (s, 2H), 8.16 – 8.11 (m, 1H), 7.57 – 7.47 (m, 2H), 7.43 (s, 1H), 4.32 (s, 1H), 3.69 – 3.60 (m, 1H), 3.56 – 3.45 (m, 1H), 2.25 – 2.04 (m, 1H), 1.91 – 1.85 (m, 3H). LCMS (m/z) calc'd for $C_{13}H_{13}BrN_4O_2S$ $[M + H]^+$ 371.2 found 371.2 , r.t. 2.47.

(S)-N1-(6-(4-hydroxyphenyl)benzo[d]thiazol-2-yl)pyrrolidine-1,2-dicarboxamide (Compound 65)



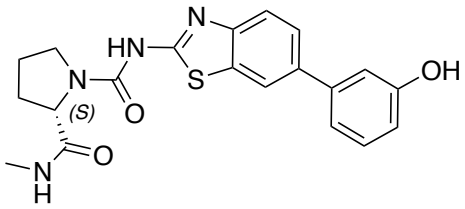
A suspension of (S)-N_1-(6-bromobenzo[d]thiazol-2-yl)pyrrolidine-1,2-dicarboxamide (200 mg, 0.54 mmol) and (3-hydroxyphenyl)boronic acid (150 mg, 1.08 mmol) in THF (2 mL) containing Na_2CO_3 (2 M, 810 µL) was purged with N_2 gas and bis(triphenylphosphine)palladium chloride (38 mg, 0.054 mmol) added. The reaction mixture was heated at 120 °C under microwave radiation for 15 mins then cooled to room temperature. The reaction mixture was diluted with EtOAc (25 mL) and NaOH (2 M, 25 mL) added. MeOH (~ 10 mL) was added until solids at the interface dissolved. The aqueous layer was extracted with EtOAc (2 x 25 mL) and the combined organics were washed with brine (25 mL), dried ($MgSO_4$), filtered, and solvent removed *in vacuo*. The residue was purified by flash column chromatography (silica gel), eluting with 2.5 - 5% 10% MeOH in CH_2Cl_2 to give the compound as a white solid (17 mg, 8%). ^{1}H NMR (400 MHz, DMSO) δ 11.01 (s, 1H), 9.51 (s, 1H), 8.07 (s, 1H), 7.63 (s, 1H), 7.61 – 7.55 (m, 1H), 7.55 – 7.45 (m, 2H), 7.42 (s, 1H), 6.98 (s, 1H), 6.88 – 6.82 (m, 2H), 4.34 – 4.30 (m, 1H), 3.67 – 3.63 (m, 1H), 3.55 – 3.48 (m, 1H), 2.15 – 2.07 (m, 1H), 1.91 – 1.87 (m, 3H). LCMS (m/z) calc'd for $C_{19}H_{18}N_4O_3S$ $[M + H]^+$ 383.4 found 383.2, r.t. 2.37, purity 98%.

(S)-N1-(6-bromobenzo[d]thiazol-2-yl)-N2-methylpyrrolidine-1,2-dicarboxamide



To a stirred solution of ((6-bromobenzo[d]thiazol-2-yl)carbamoyl)-L-proline (540 mg, 1.46 mmol) in DMF (15 mL) was added DIPEA (3 mL, 4.86 mmol), methylamine hydrochloride (520 mg, 8.10 mmol), and HATU (739 mg, 1.94 mmol). The reaction was stirred overnight under an atmosphere of N_2 after which time saturated $NaHCO_3$ (20 mL) and EtOAc (20 mL) was added and the organic layer separated. The organic layer was washed with deionised H_2O (3 x 20 mL) and brine (20 mL), dried ($MgSO_4$), filtered, and solvent removed *in vacuo* and the residue purified by flash column chromatography, eluting with 5% MeOH in CH_2Cl_2 to give a colourless gum (462 mg, 83%). ^{1}H NMR (400 MHz, DMSO) δ 8.16 – 8.12 (m, 1H), 7.55 – 7.51 (m, 2H), 7.40 – 7.36 (m, 1H), 4.33 (s, 1H), 3.64 (s, 1H), 3.57 – 3.51 (m, 1H), 2.62 (s, 3H), 2.23 – 2.06 (m, 1H), 1.93 – 1.87 (m, 3H). LCMS (m/z) calc'd for $C_{14}H_{15}BrN_4O_2S$ $[M + H]^+$ 385.3 found 385.2, r.t. 2.54.

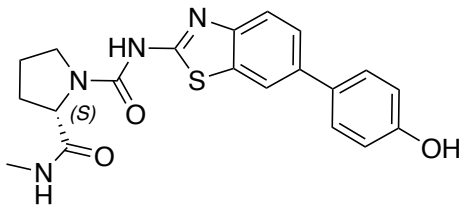
(S)-N1-(6-(3-hydroxyphenyl)benzo[d]thiazol-2-yl)-N2-methylpyrrolidine-1,2-dicarboxamide (Compound 60)



A suspension of (S)-N_1-(6-bromobenzo[d]thiazol-2-yl)-N_2-methylpyrrolidine-1,2-dicarboxamide (186 mg, 0.49 mmol) and (3-hydroxyphenyl)boronic acid (134 mg, 0.97 mmol) in THF (2 mL) containing Na_2CO_3 (2 M, 735 µL) was purged with N_2 gas and bis(triphenylphosphine)palladium chloride (35 mg, 0.049 mmol) added. The reaction mixture was heated at 120 °C under microwave radiation for 15 mins then cooled to room temperature. The reaction mixture was diluted with EtOAc (25 mL) and NaOH

(2 M, 25 mL) added. MeOH (~ 10 mL) was added until solids at the interface dissolved. The aqueous layer was extracted with EtOAc (2 x 25 mL) and the combined organics were washed with brine (25 mL), dried ($MgSO_4$), filtered, and solvent removed *in vacuo*. The residue was purified by flash column chromatography (silica gel), eluting with 2.5 - 10% MeOH in CH_2Cl_2 to give the compound as a yellow solid (23 mg, 12%). ^{1}H NMR (400 MHz, DMSO) δ 11.10 (s, 1H), 9.52 (s, 1H), 8.11 (s, 1H), 7.91 (s, 1H), 7.65 (s, 1H), 7.63 – 7.53 (m, 1H), 7.26 (t, *J* = 7.8 Hz, 1H), 7.22 – 7.04 (m, 2H), 6.82 – 6.72 (m, 1H), 4.36 – 4.32 (m, 1H), 3.69 – 3.64 (m, 1H), 3.56 – 3.49 (m, 1H), 2.60 (d, *J* = 4.5 Hz, 3H), 2.13 – 2.03 (m, 1H), 1.88 (s, 3H). ^{13}C NMR (101 MHz, DMSO) δ 174.5, 172.6, 158.3, 157.0, 142.0, 135.6, 130.4, 128.8, 125.2, 121.3, 119.8, 118.0, 117.4, 114.6, 114.0, 60.8, 49.1, 47.1, 29.5, 26.1. LCMS (m/z) calc'd for $C_{20}H_{20}N_4O_3S$ $[M + H]^+$ 397.5 found 397.2 $[M + H]^+$, r.t. 2.47, purity 99%.

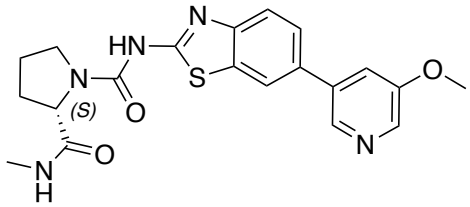
(S)-N1-(6-(4-hydroxyphenyl)benzo[d]thiazol-2-yl)-N2-methylpyrrolidine-1,2-dicarboxamide (Compound 61)



A suspension of (S)-N_1-(6-bromobenzo[d]thiazol-2-yl)-N_2-methylpyrrolidine-1,2-dicarboxamide (287 mg, 0.75 mmol) and (4-hydroxyphenyl)boronic acid (207 mg, 0.97 mmol) in THF (2 mL) containing Na_2CO_3 (2 M, 1.1 mL) was purged with N_2 gas and bis(triphenylphosphine)palladium chloride (53 mg, 0.075 mmol) added. The reaction mixture was heated at 120 °C under microwave radiation for 15 mins then cooled to room temperature. The reaction mixture was diluted with EtOAc (25 mL) and NaOH (2 M, 25 mL) added. MeOH (~ 10 mL) was added until solids at the interface dissolved. The aqueous layer was extracted with EtOAc (2 x 25 mL) and the combined organics were washed with brine (25 mL), dried ($MgSO_4$), filtered, and solvent removed *in vacuo*. The residue was purified by flash column chromatography (silica gel), eluting with 2.5 - 10% MeOH in CH_2Cl_2 to give the compound as a brown solid (43 mg, 14%).

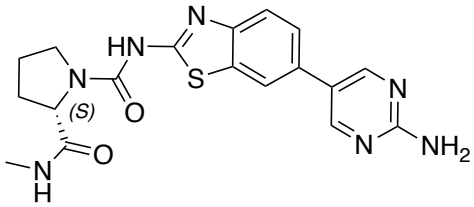
^{1}H NMR (400 MHz, DMSO) δ 11.04 (s, 1H), 9.51 (s, 1H), 8.10 – 8.05 (m, 1H), 7.91 – 7.87 (m, 1H), 7.66 – 7.62 (m, 1H), 7.61 – 7.55 (m, 1H), 7.52 (d, *J* = 8.1 Hz, 2H), 6.85 (d, *J* = 8.4 Hz, 2H), 4.36 – 4.31 (m, 1H), 3.69 – 3.64 (m, 1H), 3.54 – 3.50 (m, 1H), 2.60 (d, *J* = 4.5 Hz, 3H), 2.13 – 2.07 (m, 1H), 1.90 – 1.86 (m, 3H). LCMS (m/z) calc'd for $C_{20}H_{20}N_4O_3S$ $[M + H]^+$ 397.5 found 397.2 , r.t. 2.44, purity 98%.

(S)-N1-(6-(5-methoxypyridin-3-yl)benzo[d]thiazol-2-yl)-N2-methylpyrrolidine-1,2-dicarboxamide (Compound 62)



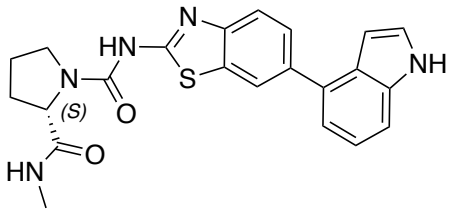
A suspension of (S)-N_1-(6-bromobenzo[d]thiazol-2-yl)-N_2-methylpyrrolidine-1,2-dicarboxamide (287 mg, 0.75 mmol) and (5-methoxypyridin-3-yl)boronic acid (230 mg, 1.49 mmol) in THF (2 mL) containing Na_2CO_3 (2 M, 1.1 mL) was purged with N_2 gas and bis(triphenylphosphine)palladium chloride (53 mg, 0.075 mmol) added. The reaction mixture was heated at 120 °C under microwave radiation for 15 mins then cooled to room temperature. The reaction mixture was diluted with EtOAc (25 mL) and NaOH (2 M, 25 mL) added. MeOH (~ 10 mL) was added until solids at the interface dissolved. The aqueous layer was extracted with EtOAc (2 x 25 mL) and the combined organics were washed with brine (25 mL), dried ($MgSO_4$), filtered, and solvent removed *in vacuo*. The residue was purified by flash column chromatography (silica gel), eluting with 2.5 - 10% MeOH in CH_2Cl_2 to give the compound as a beige solid (34 mg, 11%). ^{1}H NMR (400 MHz, DMSO) δ 11.19 (s, 1H), 8.54 (d, *J* = 1.9 Hz, 1H), 8.31 (s, 1H), 8.27 (d, *J* = 2.7 Hz, 1H), 7.90 (d, *J* = 5.7 Hz, 1H), 7.77 (dd, *J* = 8.4, 1.9 Hz, 1H), 7.71 (s, 1H), 7.68 (t, *J* = 2.4 Hz, 1H), 4.35 (s, 1H), 3.93 (s, 3H), 3.69 – 3.65 (m, 1H), 3.56 – 3.49 (m, 1H), 2.60 (d, *J* = 4.6 Hz, 3H), 2.15 – 2.05 (m, 1H), 1.91 – 1.86 (m, 3H). ^{13}C NMR (101 MHz, DMSO) δ 172.6, 156.1, 140.3, 136.8, 136.6, 132.0, 125.5, 120.5, 118.6, 60.8, 56.1, 47.1, 40.6, 40.4, 40.2, 40.0, 39.8, 39.6, 39.4, 26.1. LCMS (m/z) calc'd for $C_{20}H_{21}N_5O_3S$ $[M + H]^+$ 412.5 found 412.2, r.t. 2.25, purity 99%.

(S)-N1-(6-(2-aminopyrimidin-5-yl)benzo[d]thiazol-2-yl)-N2-methylpyrrolidine-1,2-dicarboxamide (Compound 63)



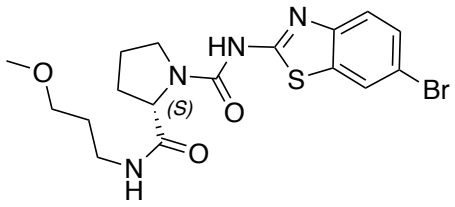
A suspension of (S)-N_1-(6-bromobenzo[d]thiazol-2-yl)-N_2-methylpyrrolidine-1,2-dicarboxamide (200 mg, 0.52 mmol) and (2-aminopyrimidin-5-yl)boronic acid (145 mg, 1.04 mmol) in THF (2 mL) containing Na_2CO_3 (2 M, 783 µL) was purged with N_2 gas and bis(triphenylphosphine)palladium chloride (37 mg, 0.052 mmol) added. The reaction mixture was heated at 120 °C under microwave radiation for 15 mins then cooled to room temperature. The reaction mixture was diluted with EtOAc (25 mL) and NaOH (2 M, 25 mL) added. MeOH (~ 10 mL) was added until solids at the interface dissolved. The aqueous layer was extracted with EtOAc (2 x 25 mL) and the combined organics were washed with brine (25 mL), dried ($MgSO_4$), filtered, and solvent removed *in vacuo*. The residue was purified by flash column chromatography (silica gel), eluting with 2.5 - 20% MeOH in CH_2Cl_2 to give the compound as a yellow solid (18 mg, 9%). ^{1}H NMR (400 MHz, DMSO) δ 11.15 (s, 1H), 8.62 (s, 2H), 8.14 (s, 1H), 7.89 (s, 1H), 7.65 – 7.58 (m, 2H), 6.75 (s, 2H), 4.36 – 4.32 (m, 1H), 3.68 – 3.64 (m, 1H), 3.55 – 3.49 (m, 1H), 2.60 (d, *J* = 4.6 Hz, 3H), 2.09 (s, 1H), 1.88 (s, 3H). LCMS (m/z) calc'd for $C_{18}H_{19}N_7O_2S$ $[M + H]^+$ 398.5 found 398.2 $[M + H]^+$, r.t. 2.13, purity 95%.

(S)-N1-(6-(1H-indol-4-yl)benzo[d]thiazol-2-yl)-N2-methylpyrrolidine-1,2-dicarboxamide (Compound 64)



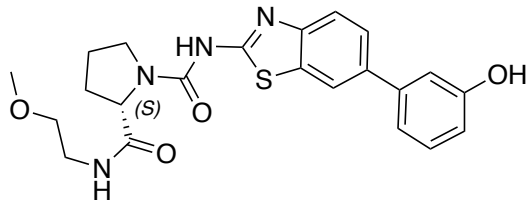
A suspension of (S)-N_1-(6-bromobenzo[d]thiazol-2-yl)-N_2-methylpyrrolidine-1,2-dicarboxamide (287 mg, 0.75 mmol) and 4-(4,4,5,5-tetramethyl-1,3,2-dioxaborolan-2-yl)-1H-indole (365 mg, 1.5 mmol) in THF (2 mL) containing Na_2CO_3 (2 M, 1.1 mL) was purged with N_2 gas and bis(triphenylphosphine)palladium chloride (53 mg, 0.075 mmol) added. The reaction mixture was heated at 120 °C under microwave radiation for 15 mins then cooled to room temperature. The reaction mixture was diluted with EtOAc (25 mL) and NaOH (2 M, 25 mL) added. MeOH (~ 10 mL) was added until solids at the interface dissolved. The aqueous layer was extracted with EtOAc (2 x 25 mL) and the combined organics were washed with brine (25 mL), dried ($MgSO_4$), filtered, and solvent removed *in vacuo*. The residue was purified by flash column chromatography (silica gel), eluting with 5% MeOH in CH_2Cl_2 to give the compound as a yellow solid (19 mg, 6%). ^{1}H NMR (400 MHz, DMSO) δ 11.26 (s, 1H), 11.08 (s, 1H), 8.14 (s, 1H), 7.91 – 7.81 (m, 2H), 7.72 – 7.65 (m, 1H), 7.45 – 7.33 (m, 2H), 7.19 (t, J = 7.6 Hz, 1H), 7.13 (dd, J = 7.3, 1.1 Hz, 1H), 6.62 – 6.58 (m, 1H), 4.35 (s, 1H), 3.67 (s, 1H), 3.57 – 3.50 (m, 1H), 2.61 (d, J = 4.5 Hz, 3H), 2.15 – 2.05 (m, 1H), 1.88 (s, 3H). LCMS (m/z) calc'd for $C_{22}H_{21}N_5O_2S$ $[M + H]^+$ 420.5 found 420.2, r.t. 2.59, purity 88%.

(S)-N1-(6-bromobenzo[d]thiazol-2-yl)-N2-(3-methoxypropyl)pyrrolidine-1,2-dicarboxamide



To a stirred solution of ((6-bromobenzo[d]thiazol-2-yl)carbamoyl)-L-proline (300 mg, 0.68 mmol) in DMF (2 mL) was added DIPEA (350 µL, 2.0 mmol), 3-methoxypropan-1-amine (84 µL , 0.82 mmol), and HATU (312 mg, 0.82 mmol). The reaction was stirred overnight under an atmosphere of N_2 after which time saturated $NaHCO_3$ (20 mL) and EtOAc (20 mL) was added and the organic layer separated. The organic layer was washed with deionised H_2O (3 x 20 mL) and brine (20 mL), dried ($MgSO_4$), filtered, and solvent removed *in vacuo*. The residue was purified by column chromatography (silica gel), eluting with 2% MeOH in CH_2Cl_2 to give a colourless gum (227 mg, 76%). ^{1}H NMR (400 MHz, DMSO-d_6) δ 11.14 (s, 1H), 8.15 (s, 1H), 8.01 (s, 1H), 7.55 – 7.47 (m, 2H), 4.37 (s, 1H), 3.67 – 3.58 (m, 1H), 3.57 – 3.48 (m, 1H), 3.47 – 3.42 (m, 1H), 3.32 – 3.18 (m, 2H), 3.19 – 3.09 (m, 1H), 2.90 (s, 3H), 2.19 – 1.99 (m, 1H), 1.99 – 1.75 (m, 3H). LCMS (m/z) calc'd for $C_{16}H_{19}BrN_4O_3S$ $[M + H]^+$ 429.3 found 429.1, r.t. 2.59.

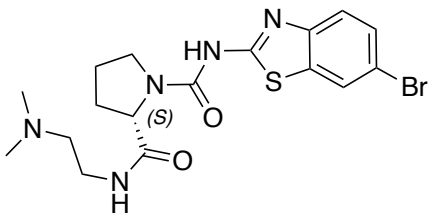
(S)-N1-(6-(3-hydroxyphenyl)benzo[d]thiazol-2-yl)-N2-(2-methoxyethyl)pyrrolidine-1,2-dicarboxamide (Compound 66)



A suspension of (S)-N_1-(6-bromobenzo[d]thiazol-2-yl)-N_2-(3-methoxypropyl) pyrrolidine-1,2-dicarboxamide (200 mg, 0.47 mmol) and (3-hydroxyphenyl)boronic acid (129 mg, 0.94 mmol) in THF (2 mL) containing Na_2CO_3 (2 M, 705 µL) was purged with N_2 gas and bis(triphenylphosphine)palladium chloride (33 mg, 0.047 mmol) added. The reaction mixture was heated at 120 °C under microwave radiation for 15 mins

then cooled to room temperature. The reaction mixture was diluted with EtOAc (25 mL) and NaOH (2 M, 25 mL) added. MeOH (~ 10 mL) was added until solids at the interface dissolved. The aqueous layer was extracted with EtOAc (2 x 25 mL) and the combined organics were washed with brine (25 mL), dried ($MgSO_4$), filtered, and solvent removed *in vacuo*. The residue was purified by flash column chromatography (silica gel), eluting with 2.5 - 20% MeOH in CH_2Cl_2 to give the compound as an orange solid (45 mg, 22%). ^{1}H NMR (400 MHz, DMSO) δ 11.06 (s, 1H), 9.50 (s, 1H), 8.12 (s, 1H), 8.01 (s, 1H), 7.67 (s, 1H), 7.60 (d, *J* = 8.0 Hz, 1H), 7.30 – 7.15 (m, 1H), 7.11 (d, *J* = 7.6 Hz, 1H), 7.06 (t, *J* = 2.1 Hz, 1H), 6.81 – 6.72 (m, 1H), 4.38 (s, 1H), 3.66 (s, 1H), 3.55 – 3.51 (m, 1H), 3.40 – 3.28 (m, 2H), 3.33 (s, 3H), 3.26 – 3.16 (m, 2H), 2.15 – 2.04 (m, 1H), 1.92 – 1.85 (m, 3H). LCMS (m/z) calc'd for $C_{22}H_{24}N_4O_4S$ $[M + H]^+$ 441.5 found 441.2, r.t. 2.50, purity 96%.

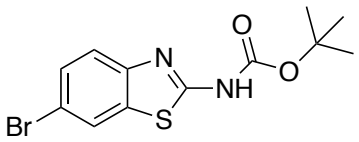
(S)-N1-(6-bromobenzo[d]thiazol-2-yl)-N2-(2-(dimethylamino)ethyl)pyrrolidine-1,2-dicarboxamide



To a stirred solution of ((6-bromobenzo[d]thiazol-2-yl)carbamoyl)-L-proline (700 mg, 1.89 mmol) in DMF (5 mL) was added DIPEA (986 µL, 5.67 mmol), N_1,N_1-dimethylethane-1,2-diamine (309 µL , 2.83 mmol), and HATU (863 mg, 2.27 mmol). The reaction was stirred overnight under an atmosphere of N_2 after which time saturated $NaHCO_3$ (20 mL) and EtOAc (20 mL) was added and the organic layer separated. The organic layer was washed with deionised H_2O (3 x 20 mL) and brine (20 mL), dried ($MgSO_4$), filtered, and solvent removed *in vacuo*. The residue was purified by column chromatography (silica gel), eluting with 5 - 10 % MeOH containing ammonia (7 N) in CH_2Cl_2 to give a colourless gum (598 mg, 72%). ^{1}H NMR (400 MHz, DMSO) δ 8.26 – 8.19 (m, 1H), 8.17 – 8.11 (m, 1H), 7.59 – 7.46 (m, 2H), 7.12 (s, 1H), 4.35 – 4.31 (m, 1H), 3.69 – 3.59 (m, 1H), 3.59 – 3.49 (m, 1H), 3.41 – 3.35 (m, 1H), 3.27 – 3.20 (m, 1H),

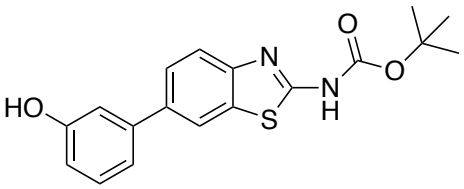
3.16 – 3.05 (m, 1H), 3.06 – 2.96 (m, 1H), 2.70 (s, 6H), 2.18 – 2.06 (m, 1H), 1.93 – 1.88 (m, 3H). LCMS (m/z) calc'd for $C_{17}H_{22}BrN_5O_2S$ $[M + H]^+$ 442.4 found 442.1, r.t. 2.08.

6-bromobenzo[d]thiazol-2-yl)carbamate



To a stirred suspension of 6-bromobenzo[d]thiazol-2-amine (500 mg, 2.18 mmol) in CH_2Cl_2 (10 mL) was added NEt_3 (365 µL) and Boc2O (572 mg, 2.62 mmol). After stirring for 1 hr, no product had formed. DMAP (24 mg, 0.22 mmol) was added and after 10 mins the reaction was complete. The reaction mixture was concentrated *in vacuo* and was purified by flash column chromatography (silica gel) eluting with 30-70% EtOAc in petroleum ether to give the product as a beige solid (2.35 g, 62%). ^{1}H NMR (400 MHz, DMSO-d_6) δ 11.88 (s, 1H), 8.21 (d, J = 2.0 Hz, 1H), 7.62 (d, J = 8.5 Hz, 1H), 7.54 (dd, J = 8.6, 2.0 Hz, 1H), 1.53 (s, 9H). LCMS (m/z) calc'd for $C_{12}H_{13}BrN_2O_2S$ $[M + H]^+$ 331.2 found 331.3, r.t 3.06.

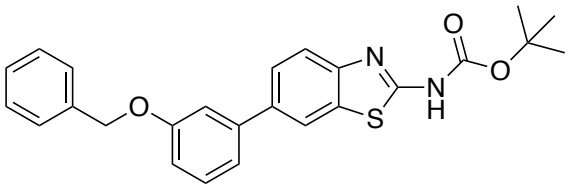
Tert-butyl (6-(3-hydroxyphenyl)benzo[d]thiazol-2-yl)carbamate



A suspension of 6-bromobenzo[d]thiazol-2-yl)carbamate (2.33 g, 7.08 mmol) and (3-hydroxyphenyl)boronic acid (1.05 g, 14.2 mmol) in THF (10 mL) containing Na_2CO_3 (2 M, 10.6 mL) was purged with N_2 gas and bis(triphenylphosphine)palladium chloride (250 mg, 0.36 mmol) added. The reaction mixture was heated at refux overnight then cooled to room temperature. The reaction mixture was diluted with EtOAc (100 mL) and NaOH (2 M, 75 mL) added. MeOH (~ 25 mL) was added until solids at the interface dissolved. The aqueous layer was extracted with EtOAc (2 x 100 mL) and the combined organics were washed with brine (75 mL), dried ($MgSO_4$), filtered, and solvent removed *in vacuo*. The residue was purified by flash column chromatography

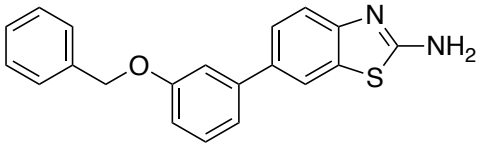
(silica gel), eluting with 30-50% EtOAc in petroleum ether to give the product as a beige solid (1.63 g, 67%). LCMS (m/z) calc'd for $C_{18}H_{18}N_2O_3S$ $[M + H]^+$ 343.4 found 343.1, r.t. 2.87.

Tert-butyl (6-(3-(benzyloxy)phenyl)benzo[d]thiazol-2-yl)carbamate



To a stirred solution of Tert-butyl (6-(3-hydroxyphenyl)benzo[d]thiazol-2-yl)carbamate (500 mg, 1.46 mmol) in DMF (5 mL) was added $Cs2CO_3$ (475 mg, 1.46 mmol) then Benzylbromide (208 μL, 1.75 mmol). The reaction was stirred under an atmosphere of N_2 for 1 h, after which time deionised H_2O (20 mL) and EtOAc (20 mL) was added. The aqueous was extracted with EtOAc (2 x 20 mL), and the combined organics washed with brine (20 mL), dried ($MgSO_4$), filtered, and solvent removed *in vacuo*. The compound was purified by flash column chromatography, eluting with 85-90% EtOAc in petroleum ether to give a beige solid (685 mg, 92%). ^{1}H NMR (400 MHz, DMSO) δ 9.54 (s, 1H), 8.21 (d, *J* = 1.8 Hz, 1H), 7.79 (d, *J* = 8.4 Hz, 1H), 7.64 (dd, *J* = 8.4, 1.9 Hz, 1H), 7.36 – 7.30 (m, 4H), 7.30 – 7.24 (m, 2H), 7.15 – 7.10 (m, 1H), 7.10 – 7.07 (m, 1H), 6.78 (ddd, *J* = 8.1, 2.4, 1.0 Hz, 1H), 5.40 (s, 2H), 1.46 (s, 9H). ^{13}C NMR (101 MHz, DMSO) δ 172.5, 167.2, 161.5, 158.3, 153.0, 148.4, 141.8, 138.0, 136.5, 134.3, 130.4, 128.9, 127.7, 127.4, 125.4, 121.4, 119.7, 118.1, 114.8, 114.1, 84.3, 50.4, 28.0. LCMS (m/z) calc'd for $C_{25}H_{24}N_2O_3S$ $[M + H]^+$ 433.5 found 433.1, r.t. 3.26.

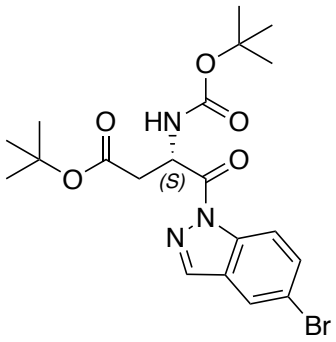
6-(3-(benzyloxy)phenyl)benzo[d]thiazol-2-amine



To a stirred solution of Tert-butyl (6-(3-(benzyloxy)phenyl)benzo[d]thiazol-2-yl) carbamate (650 mg, 1.50 mmol) in CH_2Cl_2 (5 mL) was added TFA (5 mL). The reaction mixture was stirred for 1 hr after which time volatiles were removed *in vacuo* and EtOAc (25 mL) and aqueous saturated sodium bicarbonate (25 ml) added to the residue. The aqueous was extracted with EtOAc (2 x 25 ml), and the combined organics washed with brine (25 mL), dried ($MgSO_4$), filtered, and solvent removed *in vacuo* to give the product as a pink solid (464 mg, 93%). ^{1}H NMR (400 MHz, DMSO) δ 9.58 (s, 1H), 8.58 (t, *J* = 5.8 Hz, 1H), 7.92 (d, *J* = 1.7 Hz, 1H), 7.46 – 7.43 (m, 2H), 7.42 – 7.31 (m, 4H), 7.30 – 7.20 (m, 2H), 7.09 – 7.03 (m, 1H), 7.02 – 6.99 (m, 1H), 6.72 (dd, *J* = 8.0, 2.3 Hz, 1H), 4.61 (d, *J* = 5.6 Hz, 2H). ^{13}C NMR (101 MHz, DMSO) δ 167.2, 158.2, 152.4, 142.1, 139.3, 133.9, 131.7, 130.4, 128.9, 127.8, 127.6, 124.9, 119.4, 118.6, 117.7, 114.3, 113.7, 47.7. LCMS (m/z) calc'd for $C_{20}H_{16}N_2OS$ $[M + H]^+$ 333.4 found 333.0, r.t. 2.79.

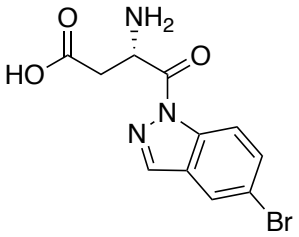
6.4.5.2 Synthesis for Chapter IV

Tert-butyl (S)-4-(5-bromo-1H-indazol-1-yl)-3-((tert-butoxycarbonyl)amino)-4-oxobutanoate



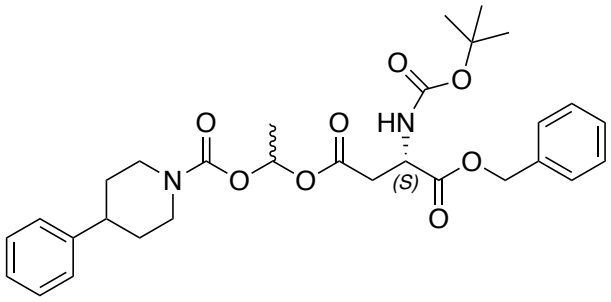
To a stirred solution of (S)-4-(tert-butoxy)-2-((tert-butoxycarbonyl)amino)-4-oxobutanoic acid (300 mg, 1.04 mmol), 5-bromo-H-indazole (205 mg, 1.04 mmol) and HATU (435 mg, 1.14 mmol) in DMF (10 mL) was added NMM (0.34 mL, 3.1 mmol) under an atmosphere of N_2 at room temperature. Upon addition of the NMM the colourless reaction mixture became pale yellow in colour. After stirring overnight, sodium bicarbonate (25 mL) and EtOAc (25 mL) were added to the reaction mixture and the aqueous layer separated and extracted with EtOAc (3 x 20 mL). The combined organic extracts were washed with brine (4 x 25 mL), dried ($MgSO_4$) and solvent removed *in vacuo* to give a pale orange oil. The title compound (294 mg, 60 %) was obtained as a white solid by purification by flash column chromatography, eluting with 0 - 10% EtOAc in petroleum ether (40-60). ^{1}H NMR (400 MHz, $CDCl_3$) δ 8.35 – 8.28 (m, 1H), 8.14 – 8.09 (m, 1H), 7.91 – 7.88 (m, 1H), 7.66 (dd, *J* = 8.8, 1.8 Hz, 1H), 5.79 – 5.62 (m, 2H), 2.98 (d, *J* = 5.2 Hz, 1H), 1.45 (s, 9H), 1.37 (s, 9H). LCMS (m/z): calc'd for $C_{20}H_{26}BrN_3O_5$ $[M + H]^+$ 470.4, found 470.4, r.t .3.30.

(S)-4-(5-bromo-1H-indazol-1-yl)-3-(carboxyamino)-4-oxobutanoic acid



A solution of tert-butyl (S)-4-(5-bromo-1H-indazol-1-yl)-3-((tert-butoxycarbonyl)amino)-4-oxobutanoate (175 mg, 0.57 mmol) in TFA (3 mL) was stirred overnight after which time MeOH (10 mL) was added then removed *in vacuo*. A further two volumes of MeOH were added and subsequently removed *in vacuo* to remove excess TFA. The product (145 mg, 47% was obtained as a white solid by triturating with Et_2O. ^1H NMR (400 MHz, DMSO) δ 13.30 (s, 1H), 8.07 (d, *J* = 1.0 Hz, 1H), 8.02 (dd, *J* = 1.8, 0.7 Hz, 1H), 7.55 (dt, *J* = 8.8, 0.9 Hz, 1H), 7.46 (dd, *J* = 8.8, 1.8 Hz, 1H), 3.94 (dd, *J* = 8.4, 4.4 Hz, 1H), 2.92 – 2.74 (m, 1H), 2.61 (dd, *J* = 16.6, 4.4 Hz, 1H).

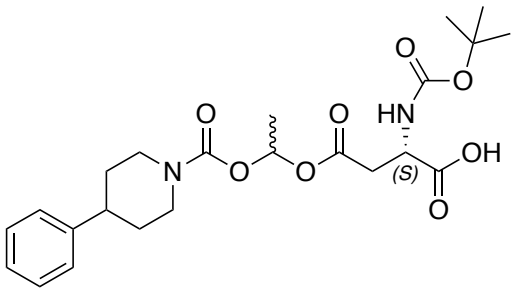
1-benzyl 4-(1-((4-phenylpiperidine-1-carbonyl)oxy)ethyl) (tert-butoxycarbonyl) aspartate



To a precooled (-10 °C) solution of 4-phenylpiperidine (1.0 g, 6.20 mmol) in CH_2Cl_2 (~100 mL) was added NMM (1.5 mL, 13.6 mmol) then ACE-Cl (0.73 mL, 6.8 mmol). The reaction was allowed to warm to room temperature and stirred for a further 1.5 h after which time the reaction mixture was poured onto HCl (2 M, 30 mL) and extracted with dichloromethane (3 x 30 mL). The combined organics were dried ($MgSO_4$), filtered, and solvent removed *in vacuo* to give a orange oil which was taken up in toluene (~100 mL). 4-(benzyloxy)-3-((tert-butoxycarbonyl)amino)-4-oxobutanoic acid (1.34 g, 5.02 mmol), Ag_2O (1.40 g, 6.02 mmol) and tertbutylammoniumbromide (0.32 g, 1.00 mmol) were added, and the reaction stirred at room temperature for 1 h before

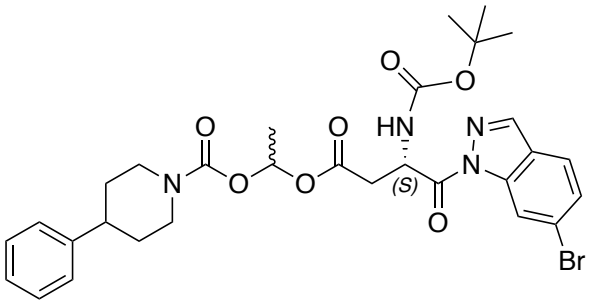
heating at 65 °C overnight. The reaction mixture was then absorbed onto silica gel and purified by flash column chromatography, eluting with 10 - 50% EtOAc in petroleum ether to give a yellow oil (1.59 g, 48%), NMR (400 MHz, MeOD) δ 7.43 – 7.14 (m, 10H), 6.90 – 6.74 (m, 1H), 5.23 – 5.08 (m, 2H), 4.77 – 4.72 (m, 1H), 4.68 – 4.57 (m, 1H), 4.21 (s, 2H), 3.02 – 2.77 (m, 4H), 2.75 – 2.61 (m, 1H), 2.01 (s, 3H), 1.82 – 1.71 (m, 2H), 1.67 – 1.52 (m, 1H), 1.49 – 1.36 (m, 9H); LCMS (m/z): calc'd for $C_{30}H_{38}N_2O_8$ $[M + H]^+$ 555.3 found 555.6, r.t. 3.29.

2-((tert-butoxycarbonyl)amino)-4-oxo-4-(1-((4-phenylpiperidine-1-carbonyl)oxy) ethoxy)butanoic acid



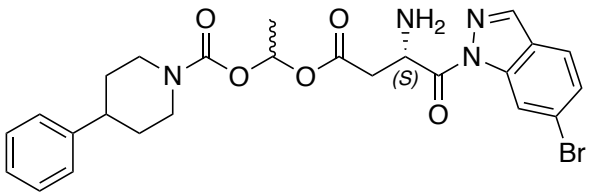
To a solution of 1-benzyl 4-(1-((4-phenylpiperidine-1-carbonyl)oxy)ethyl) (tert-butoxycarbonyl)aspartate (1.39 g, 2.51 mmol) in EtOAc (25 mL) was added Pd/C (139 mg, 10% wt) as a suspension in EtOAc. The reaction was stirred under an atmosphere of hydrogen for 3 h after which time the reaction was filtered and solvent removed *in vacuo* to give a white foam (1.06 g, 76%). The compound was used without further purification. NMR (400 MHz, MeOD) δ 7.26 (ddd, *J* = 25.5, 16.3, 7.3 Hz, 5H), 6.83 – 6.78 (m, 1H), 4.57 – 4.47 (m, 1H), 4.29 – 4.21 (m, 2H), 3.06 – 2.83 (m, 5H), 2.76 (tt, *J* = 12.1, 3.7 Hz), 1.89 – 1.84 (m, 1H), 1.66 (tt, *J* = 12.6, 6.4 Hz, 1H), 1.52 (d, *J* = 5.4, 3H), 1.50 – 1.42 (m, 10H). LCMS (m/z): calc'd for $C_{23}H_{32}N_2O_8$ $[M + H]^+$ 465.5, found 465.4, r.t. 2.97.

1-((4-(6-bromo-1H-indazol-1-yl)-3-((tert-butoxycarbonyl)amino)-4-oxobutanoyl) oxy)ethyl 4-phenylpiperidine-1-carboxylate



To a stirred solution of 2-((tert-butoxycarbonyl)amino)-4-oxo-4-(1-((4-phenylpiperidine-1-carbonyl)oxy)ethoxy)butanoic acid (0.97 g, 1.75 mmol) in CH_2Cl_2 (50 mL) was added HATU (730 mg, 1.92 mmol), 5-bromoindazole (344 mg, 1.75 mmol),and DIPEA (0.91 mL, 5.24 mmol). After 2.5 h the reaction mixture was absorbed onto slica and purified by flash column chromatography, eluting with 0-15% EtOAc in petroleum ether to give a colourless gum (989 mg, 88%). ^{1}H NMR (400 MHz, $CDCl_3$) δ 8.37 – 8.30 (m, 1H), 8.14 – 8.10 (m, 1H), 7.93 – 7.88 (m, 1H), 7.70 – 7.65 (m, 1H), 7.38 – 7.29 (m, 2H), 7.29 – 7.18 (m, 3H), 6.82 (q, *J* = 5.4, 1H), 5.97 – 5.92 (m, 1H), 5.82 – 5.74 (m, 1H), 5.32 (1H, s), 4.38 – 4.25 (1H, m), 4.22 – 4.09 (1H, m), 3.30 – 3.21 (m, 1H), 3.17 – 3.07 (m, 1H), 2.94 – 2.85 (m, 2H), 2.75 – 2.62 (m, 1H), 1.86 (d, *J* = 11.4, 3H), 1.79 – 1.57 (m, 2H), 1.47 (d, *J* = 6.3, 9H) LCMS (m/z): calc'd for $C_{30}H_{35}BrN_4O_7$ $[M + H]^+$ 643.5, found 643.5, r.t. 3.42.

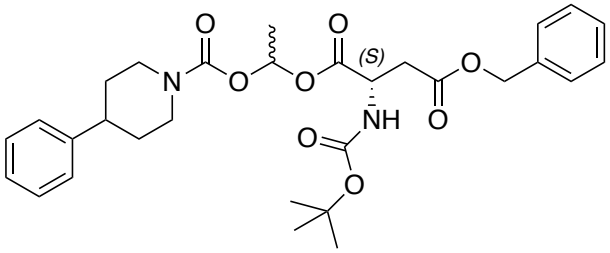
1-((3-amino-4-(6-bromo-1H-indazol-1-yl)-4-oxobutanoyl)oxy)ethyl 4-phenylpiperidine-1-carboxylate



To a stirred solution of 4-benzyl 1-(1-((4-phenylpiperidine-1-carbonyl)oxy)ethyl) (tert-butoxycarbonyl)-L-aspartate (1.28 g, 0.21 mmol) in CH_2Cl_2 (1 mL) was added TFA (1 mL). After 1 h, the solvent and TFA were removed *in vacuo* and the residual solid was triturated with diethyl ether to give a white solid. ^{1}H NMR (400 MHz, DMSO) δ 8.63 – 8.58 (m, 1H), 8.28 – 8.24 (m, 3H), 7.36 – 7.27 (m, 2H), 7.27 – 7.20 (m, 5H), 6.68

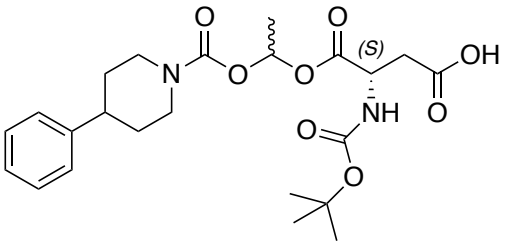
(dq, *J* = 11.0, 5.4 Hz, 1H), 5.33 – 5.26 (m, 1H), 4.02 – 3.98 (m, 3H), 3.25 – 2.60 (m, 2H), 1.78 – 1.73 (m, 3H), 1.51 – 1.46 (m, 3H), 1.43 (t, *J* = 5.1 Hz, 3H), LCMS (m/z): calc'd for $C_{25}H_{27}BrN_4O_5$ $[M + H]^+$ 543.4, found 543.3 , r.t. 2.51.

4-benzyl 1-(1-((4-phenylpiperidine-1-carbonyl)oxy)ethyl) (tert-butoxycarbonyl)-L-aspartate



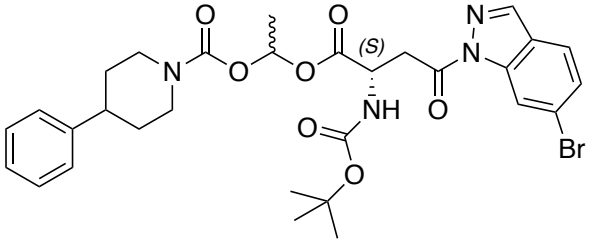
To a precooled (-10 °C) solution of 4-phenylpiperidine (1.0 g, 6.20 mmol) in dichloromethane (~50 mL) was added NMM (1.73 mL, 6.80 mmol) then ACE-Cl (0.73 mL, 6.8 mmol). The reaction was allowed to warm to room temperature and stirred for a further 1.5 h after which time the reaction mixture was poured onto HCl (2 M, 50 mL) and extracted with dichloromethane (3 x 25 mL). The combined organics were dried ($MgSO_4$), filtered, and solvent removed *in vacuo* to give a orange oil which was taken up in toluene (~100 mL). (S)-4-(benzyloxy)-2-((tert-butoxycarbonyl)amino)-4-oxobutanoic acid (2.20 g, 6.81 mmol), Ag_2O (1.89 g, 8.80 mmol) and tertbutylammoniumbromide (0.44 g, 1.36 mmol) were added, and the reaction stirred at room temperature for 30 min before heating at 65 °C for 2 h. The reaction mixture was then absorbed onto silica gel and purified by flash column chromatography, eluting with 10 - 30% ethyl acetate in petroleum ether to give a yellow oil (1.28 g, 37%). LRMS (m/z): calc'd for $C_{30}H_{38}N_2O_8$ $[M + H]^+$ 555.3 found 555.6, r.t. 2.87.

(3S)-3-((tert-butoxycarbonyl)amino)-4-oxo-4-(1-((4-phenylpiperidine-1-carbonyl) oxy)ethoxy)butanoic acid



To a solution of 1-benzyl 4-(1-((4-phenylpiperidine-1-carbonyl)oxy)ethyl) (tert-butoxycarbonyl)aspartate (1.28 g, 2.31 mmol) in ethyl acetate (25 mL) was added Pd/C (128 mg, 10% wt) as a suspension in ethyl acetate. The reaction was stirred under an atmosphere of hydrogen for 3 h after which time the reaction was filtered and solvent removed *in vacuo* to give a white foam (0.88 g, 82%). The compound was used without further purification. ^{1}H NMR (400 MHz, DMSO) δ 7.39 – 7.26 (m, 2H), 7.24 (dtd, *J* = 7.1, 3.3, 1.5 Hz, 3H), 6.32 (d, *J* = 6.6 Hz, 1H), 3.90 (d, *J* = 10.0 Hz, 1H), 3.36 (dt, *J* = 13.0, 2.8 Hz, 2H), 2.98 (td, *J* = 12.8, 3.0 Hz, 2H), 2.83 (tt, *J* = 12.1, 3.7 Hz, 1H), 2.61 – 2.44 (m, 6H), 2.36 (dd, *J* = 15.8, 2.9 Hz, 1H), 1.97 – 1.87 (m, 2H), 1.78 (qd, *J* = 13.0, 4.0 Hz, 2H), 1.38 (s, 9H). LCMS (m/z): calc'd $C_{23}H_{32}N_2O_8$ $[M + H]^+$ 465.2 found 465.3, r.t. 2.90.

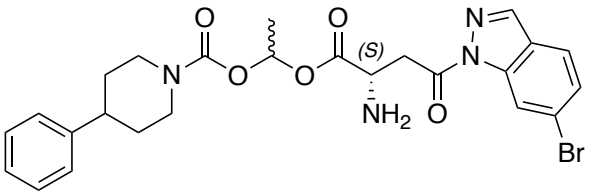
1-(((S)-4-(6-bromo-1H-indazol-1-yl)-2-((tert-butoxycarbonyl)amino)-4-oxobutanoyl)oxy)ethyl 4-phenylpiperidine-1-carboxylate



To a stirred solution of (3S)-3-((tert-butoxycarbonyl)amino)-4-oxo-4-(1-((4-phenylpiperidine-1-carbonyl)oxy)ethoxy)butanoic acid (362 mg, 0.78 mmol) in dichloromethane (20 mL) was added HATU (326 mg, 0.86 mmol), 5-bromoindazole (155 mg, 0.78 mmol),and DIPEA (4071 µL, 2.34 mmol). After 2.5 h the reaction mixture was absorbed onto slica and purified by flash column chromatography, eluting with 0-15% ethyl acetate in petroleum ether to give a colourless gum (340 mg, 68%). ^{1}H NMR (400

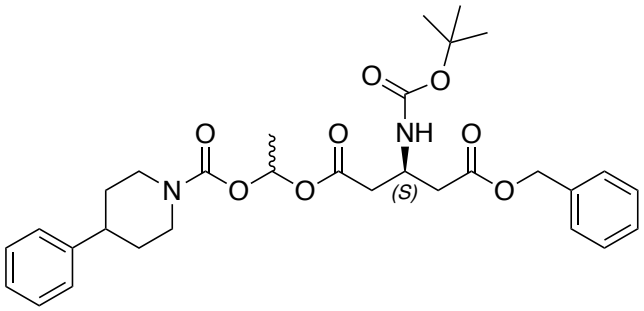
MHz, DMSO) δ 8.51 – 8.47 (m, 1H), 8.30 – 8.23 (m, 1H), 8.22 – 8.17 (m, 1H), 7.82 – 7.78 (m, 1H), 7.58 – 7.49 (m, 1H), 7.35 – 7.08 (m, 4H), 6.72 – 6.68 (m, 1H), 4.64 – 4.59 (m, 1H), 4.14 – 3.89 (m, 2H), 3.75 – 3.71 (m, 1H), 3.55 – 3.50 (m, 1H), 2.85 – 2.81 (m, 1H), 2.76 – 2.63 (m, 6H), 1.76 – 1.72 (m, 2H), 1.59 – 1.32 (m, 11H). LCMS (m/z): calc'd $C_{30}H_{35}BrN_4O_7$ $[M + H]^+$ 645.5 found 645.3, r.t. 3.39.

1-(((S)-2-amino-4-(6-bromo-1H-indazol-1-yl)-4-oxobutanoyl)oxy)ethyl 4-phenylpiperidine-1-carboxylate



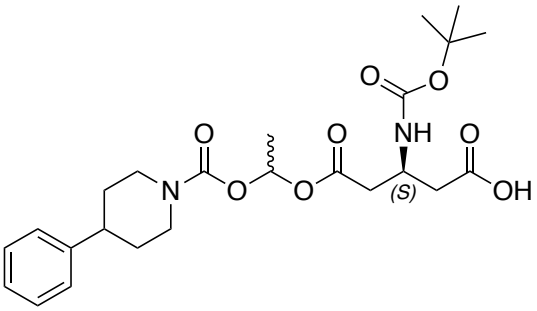
To a stirred solution of 4-benzyl 1-(1-((4-phenylpiperidine-1-carbonyl)oxy)ethyl) (tert-butoxycarbonyl)-L-aspartate (200 mg, 0.31 mmol) in CH_2Cl_2 (1 mL) was added TFA (1 mL). After 1 h, the solvent and TFA were removed *in vacuo* and the residual solid was triturated with diethyl ether to give a white solid (168 mg, 100%). ^{1}H NMR (400 MHz, DMSO) δ 8.54 (s, 2H), 8.30 – 8.20 (m, 4H), 8.25 – 8.21 (m, 1H), 7.84 (dd, *J* = 8.8, 1.9 Hz, 2H), 7.42 – 7.18 (m, 2H), 4.48 – 4.41 (m, 2H), 3.88 (dd, *J* = 18.0, 5.1 Hz, 2H), 3.72 (dd, *J* = 18.0, 6.3 Hz, 2H), 3.51 – 3.12 (m, 4H), 3.02 (t, *J* = 12.9 Hz, 1H), 2.92 – 2.74 (m, 1H), 2.04 – 1.20 (m, 4H). LCMS (m/z): calc'd $C_{25}H_{27}BrN_4O_5$ $[M + H]^+$ 543.4 found 543.3, r.t. 2.46.

1-benzyl 5-(1-((4-phenylpiperidine-1-carbonyl)oxy)ethyl) (3S)-3-((tert-butoxycarbonyl)amino)pentanedioate



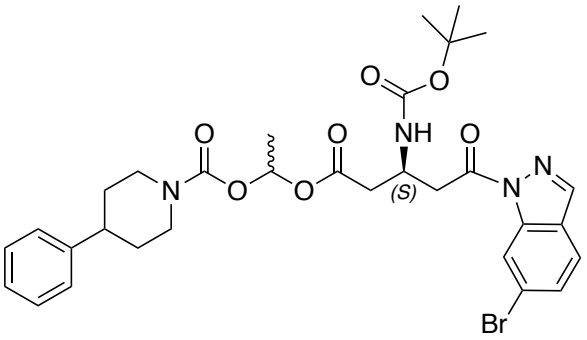
To a precooled (-10 °C) solution of 4-phenylpiperidine (250 mg, 1.55 mmol) in dichloromethane (10 mL) was added NMM (375 µL, 3.41 mmol) then ACE-Cl (185 µL, 1.71 mmol). The reaction was allowed to warm to room temperature and stirred for a further 1.5 h after which time the reaction mixture was poured onto HCl (2 M, 15 mL) and extracted with CH_2Cl_2 (3 x 30 mL). The combined organics were dried ($MgSO_4$), filtered, and solvent removed *in vacuo* to give a orange oil which was taken up in toluene (~10 mL). (R)-5-(benzyloxy)-3-((tert-butoxycarbonyl)amino)-5-oxopentanoic acid (523 g, 1.55 mmol), Ag_2O (431 g, 1.86 mmol) and tertbutylammoniumbromide (100 mg, 0.31 mmol) were added, and the reaction stirred at room temperature for 1 h before heating at 65 °C overnight. The reaction mixture was then absorbed onto silica gel and purified by flash column chromatography, eluting with 10 - 50% ethyl acetate in petroleum ether to give a yellow oil (483 mg, 55%). ^{1}H NMR (400 MHz, DMSO-d_6) δ 7.52 – 7.09 (m, 10H), 6.95 (dd, J = 8.6, 6.4 Hz, 1H), 6.70 (q, J = 5.3 Hz, 1H), 5.08 (s, 2H), 4.20 (dq, J = 13.5, 6.7 Hz, 1H), 4.12 – 4.01 (m, 2H), 3.05 – 2.75 (m, 2H), 2.77 – 2.65 (m, 1H), 2.64 – 2.48 (m, 4H), 1.80 – 1.72 (m, 2H), 1.61 – 1.47 (m, 2H), 1.44 (d, J = 5.4 Hz, 3H), 1.37 (s, 9H). ^{13}C NMR (101 MHz, DMSO) δ 170.8, 169.4, 169.2, 155.1, 152.8, 146.0, 136.6, 128.9, 128.8, 128.4, 128.3, 127.2, 126.7, 90.0, 78.4, 66.1, 45.2, 44.4, 41.9, 39.1, 33.1, 28.6, 20.1, 20.0.

(3S)-3-((tert-butoxycarbonyl)amino)-5-oxo-5-(1-((4-phenylpiperidine-1-carbonyl) oxy)ethoxy)pentanoic acid



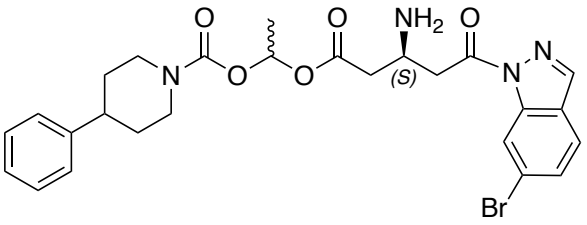
To a solution of 1-benzyl 5-(1-((4-phenylpiperidine-1-carbonyl)oxy)ethyl) (3S)-3-((tert-butoxycarbonyl)amino)pentanedioate (483 mg, 0.85 mmol) in EtOAc (20 mL) was added Pd/C (48 mg, 10% wt) as a suspension in EtOAc. The reaction was stirred under an atmosphere of hydrogen for 3 h after which time the reaction was filtered and solvent removed *in vacuo* to give a white foam (401 mg, 99%). The compound was used without further purification. ^{1}H NMR (400 MHz, DMSO) δ 12.24 (s, 1H), 7.35 – 7.28 (m, 2H), 7.28 – 7.22 (m, 2H), 7.25 – 7.16 (m, 1H), 6.85 (t, *J* = 7.8 Hz, 1H), 6.69 (q, *J* = 5.4 Hz, 1H), 4.17 – 4.07 (m, 2H), 4.07 (s, 1H), 3.02 – 2.85 (m, 2H), 2.72 (dd, *J* = 13.9, 10.4 Hz, 1H), 2.52 – 2.45 (m, 2H), 2.45 – 2.38 (m, 2H), 1.81 – 1.74 (m, 2H), 1.63 – 1.52 (m, 2H), 1.44 (d, *J* = 5.4 Hz, 3H), 1.38 (s, 9H). ^{13}C NMR (101 MHz, DMSO) δ 172.0, 168.8, 154.6, 152.3, 145.6, 128.4, 126.7, 126.2, 89.5, 77.8, 44.7, 43.9, 39.1, 38.8, 32.4, 28.2, 20.7, 19.5.

1-(((S)-5-(6-bromo-1H-indazol-1-yl)-3-((tert-butoxycarbonyl)amino)-5-oxopentanoyl)oxy)ethyl 4-phenylpiperidine-1-carboxylate



To a stirred solution of (3S)-3-((tert-butoxycarbonyl)amino)-5-oxo-5-(1-((4-phenylpiperidine-1-carbonyl)oxy)ethoxy)pentanoic acid (400 mg, 0.70 mmol) in CH_2Cl_2 (10 mL) was added HATU (294 mg, 0.77 mmol), 5-bromoindazole (138 mg, 0.70mmol),and DIPEA (365 µL, 2.1 mmol). After 2.5 h the reaction mixture was absorbed onto slica gel and purified by flash column chromatography, eluting with 0-15% ethyl acetate in petroleum ether to give a colourless gum (371 mg, 81%). ^{1}H NMR (400 MHz, DMSO) δ 8.48 – 8.43 (m, 1H), 8.29 – 8.22 (m, 1H), 8.17 (s, 1H), 7.81 – 7.74 (m, 1H), 7.30 (t, *J* = 7.5 Hz, 2H), 7.21 (q, *J* = 7.3, 6.0 Hz, 3H), 7.01 (dd, *J* = 8.4, 5.3 Hz, 1H), 6.70 (t, *J* = 5.3 Hz, 1H), 4.45 – 4.38 (m, 1H), 4.13 – 3.97 (m, 2H), 3.49 – 3.24 (m, 4H), 3.04 – 2.73 (m, 1H), 2.69 – 2.64 (m, 2H), 1.77 – 1.69 (m, 2H), 1.53 – 1.48 (m, 2H), 1.45 (t, *J* = 5.6 Hz, 3H), 1.34 – 1.29 (m, 9H). ^{13}C NMR (101 MHz, DMSO) δ 171.1, 169.4, 155.2, 152.8, 146.0, 139.9, 137.7, 132.7, 128.9, 128.3, 127.1, 126.7, 124.7, 123.3, 117.1, 90.1, 78.3, 65.4, 60.2, 56.3, 45.0, 41.9, 32.6, 30.1, 28.6. LCMS (m/z) calc'd for $C_{31}H_{37}BrN_4O_7$ $[M + H]^+$ 659.6 found 659.4, r.t 3.32.

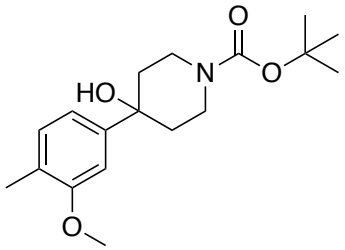
1-(((S)-3-amino-5-(6-bromo-1H-indazol-1-yl)-5-oxopentanoyl)oxy)ethyl 4-phenylpiperidine-1-carboxylate



To a stirred solution of 41-(((S)-5-(6-bromo-1H-indazol-1-yl)-3-((tert-butoxy-

carbonyl)amino)-5-oxopentanoyl)oxy)ethyl 4-phenylpiperidine-1-carboxylate (10 mg, 15.2 μmol) in CH_2Cl_2 (1 mL) was added TFA (1 mL). After 10 min, the solvent and TFA were removed *in vacuo* and the residual solid was triturated with diethyl ether to give a white solid (8 mg, 100%). ^{1}H NMR (400 MHz, DMSO) δ 8.53 – 8.42 (m, 1H), 8.28 – 8.24 (m, 1H), 8.21 – 8.17 (m, 1H), 8.16 – 8.10 (m, 2H), 7.83 – 7.79 (m, 1H), 7.36 – 7.08 (m, 5H), 6.76 – 6.71 (m, 1H), 4.48 – 4.32 (m, 1H), 4.09 – 4.01 (m, 3H), 3.71 – 3.48 (m, 1H), 3.51 – 3.22 (m, 1H), 2.95 – 2.86 (m, 2H), 2.74 – 2.61 (m, 2H), 1.75 – 1.71 (m, 2H), 1.51 – 1.40 (m, 2H), 1.32 – 1.28 (m, 3H). HRMS (m/z): calc'd for $C_{26}H_{29}BrN_4O_5$ 557.1394 $[M + H]^+$ and 579.1219 [M + Na] and found 557.1414 and 579.1232.

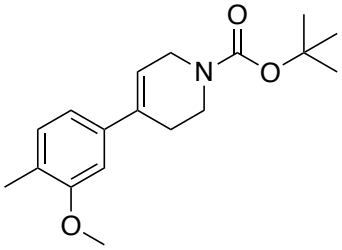
Tert-butyl 4-hydroxy-4-(3-methoxy-4-methylphenyl)piperidine-1-carboxylate



Under an atmosphere of N_2, a crystal of iodine was added to magnesium turnings (750 mg, 31.2 mmol) and warmed until iodine vapour was seen. Anhydrous THF (100 mL) was slowly added after which a portion of 4-bromo-2-methoxy-1-methylbenzene (5.0 g, 24.9 mmol) was slowly added dropwise to the reaction mixture in a solution of anhydrous THF (25 mL). After warming with a heat gun, the reaction did not initiate and thus 1,2 dichloroethane (0.2 mL) was added and the reaction mixture gently warmed. The reaction still did not initiate and thus EtMgBr (0.05 mL) was added and the reaction mixture gently warmed, initiating the reaction. The reaction mixture was stirred for 3 h after which time the reaction mixture was trasferred dropwise via cannula into a precooled (0 °C) solution of tert-butyl 4-oxopiperidine-1-carboxylate (4.14 g, 20.8 mmol). The reaction was allowed to slowly warm to room temperature and left to stir overnight. H_2O (50 mL) was added and the volatiles concentated *in vacuo*. The compound was extracted from the aqueous with EtOAc (3 x 50 mL) and the combined organics washed with brine (50 mL), dried ($MgSO_4$), filtered and solvent removed in-

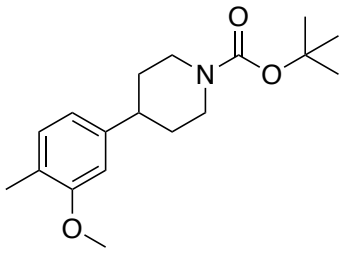
vacuo to give a yellow oil, which was carried forward without purification. LCMS (m/z): calc'd for $C_{18}H_{27}NO_4$ $[M + H]^+$ 322.2 found 322.4, r.t. 3.04.

Tert-butyl 4-(3-methoxy-4-methylphenyl)-3,6-dihydropyridine-1(2H)-carboxylate



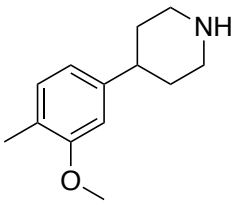
Tert-butyl-4-hydroxy-4-(3-methoxy-4-methylphenyl)piperidine-1-carboxylate (carried forward from the previous step) was taken up in CH_2Cl_2 (70 mL) and cooled to 0 °C. TFA (10 mL) was added and the reaction mixture warmed to room temperature andd stirred for 30 mins. Volatiles were removed *in vacuo* and the reaction mixture azeotroped with toluene (3 x 50 mL) to remove excess TFA. The residue was taken up in CH_2Cl_2 (60 mL) and triethyl amine (10 mL) added folowed by di-tert-butyl dicarbonate (7.0 g, 32.1 mmol). The reaction was stirred at room temperature overnight after which time the reaction mixture was concentrated *in vacuo* and purified by flash column chromatography (silica gel), eluting with 0 - 30% EtOAc in petroleum ether to give a pale straw coloured oil (5.48 g, 58%). ^{1}H NMR (400 MHz, $CDCl_3$) δ 7.30 – 7.24 (m, 2H), 7.12 (dd, J = 7.8, 1.7 Hz, 1H), 5.27 – 5.14 (m, 1H), 4.01 (s, 3H), 3.74 – 3.10 (m, 4H), 2.34 (s, 3H), 2.21 (s, 2H), 1.64 (s, 9H). LCMS (m/z): calc'd for $C_{18}H_{25}NO_3$ 304.2 $[M + H]^+$ found 304.4, r.t. 3.19.

Tert-butyl 4-(3-methoxy-4-methylphenyl)piperidine-1-carboxylate



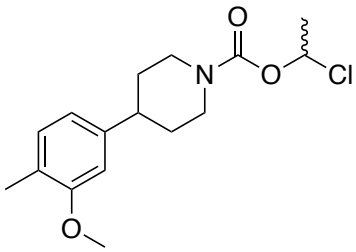
To a solution of tert-butyl 4-(3-methoxy-4-methylphenyl)-3,6-dihydropyridine-1(2H)-carboxylate (500 mg, 1.66 mmol) in ethanol (8 mL) was added Pd/C (50 mg) as a suspension in EtOAc. The reaction was stirred under an atmosphere of hydrogen for 1.5 h after which time the reaction was filtered and solvent removed *in vacuo* to give a straw coloured oil (460 mg, 91%). LCMS (m/z): calc'd for $C_{18}H_{27}NO_3$ $[M + H]^+$ 306.2 found 306.3 $[M + H]^+$, r.t. 3.18.

4-(3-methoxy-4-methylphenyl)piperidine



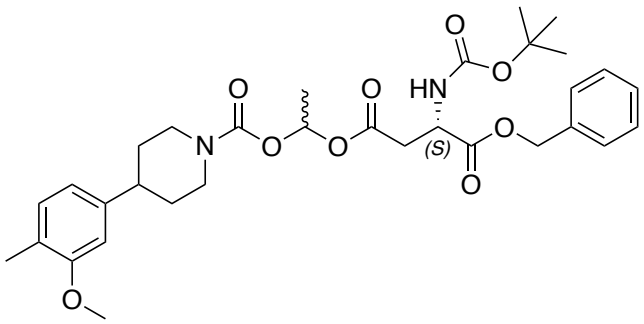
Tert-butyl 4-(3-methoxy-4-methylphenyl)piperidine-1-carboxylate (460 mg, 1.51 mmol) was taken up in CH_2Cl_2 (8 mL) and TFA (1.5 mL) added. The reaction mixture was stirred at room temperature for 1 h after which time volatiles were removed *in vacuo* and the reaction mixture azeotroped with toluene to remove excess TFA affording the product as a straw coloured gum (270 mg, 88%). LCMS (m/z): calc'd for $C_{13}H_{19}NO$ $[M + H]^+$ 206.2 found 206.2, r.t. 2.95.

1-chloroethyl 4-(3-methoxy-4-methylphenyl)piperidine-1-carboxylate



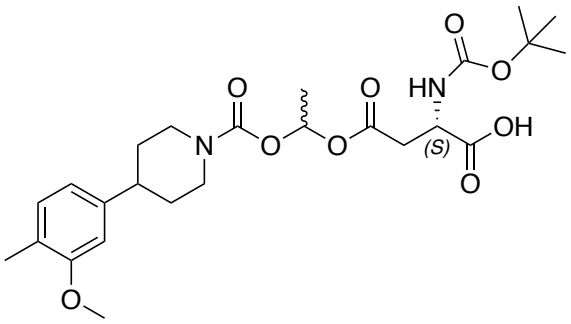
To a precooled (- 10 °C) solution of 4-(3-methoxy-4-methylphenyl)piperidine (270 mg, 1.32 mmol) in CH_2Cl_2 (5 mL) was added NMM (410 µL, 3.7 mmol) followed by ACE-Cl (146 µL, 1.35 mmol). The reaction mixture was allowed to warm to room temperature and stirred for 1 h, after which time HCl (2M, 10 mL) was added. The aqueous was extracted with CH_2Cl_2 (2 x 15 mL) and the combined organics washed with brine (15 mL), dried ($MgSO_4$), filtered, and solvent removed *in vacuo* to give an orange solid (349 mg, 1.12 mmol) which was carried forward without further purification. LCMS (m/z): calc'd for $C_{16}H_{22}ClNO_3$ $[M + H]^+$ 312.1 found 312.5, r.t. 2.80.

1-benzyl 4-(1-((4-(3-methoxy-4-methylphenyl)piperidine-1-carbonyl)oxy)ethyl) (tert-butoxycarbonyl)-L-aspartate



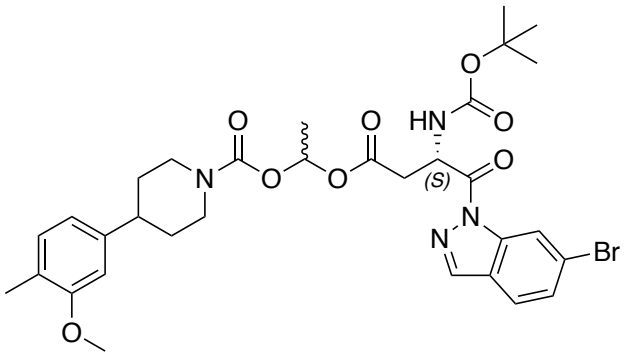
To a stirred solution of 1-chloroethyl 4-(3-methoxy-4-methylphenyl)piperidine-1-carboxylate (349 mg, 1.12 mmol) was added (S)-4-(benzyloxy)-3-((tert-butoxycarbonyl)amino)-4-oxobutanoic acid (437 mg, 1.35 mmol) followed by Ag2O (313 mg, 1.35 mmol) and tertbutylammonium bromide (71 mg, 0.22 mmol). The reaction was stirred at room temperature for 1 h before heating at 65 °C overnight. The reaction mixture was then absorbed onto silica gel and purified by flash column chromatography, eluting with 10 - 30% ethyl acetate in petroleum ether to give the product as a beige oil (526 mg, 79%).

(2S)-2-((tert-butoxycarbonyl)amino)-4-(1-((4-(3-methoxy-4-methylphenyl)piperidine-1-carbonyl)oxy)ethoxy)-4-oxobutanoic acid



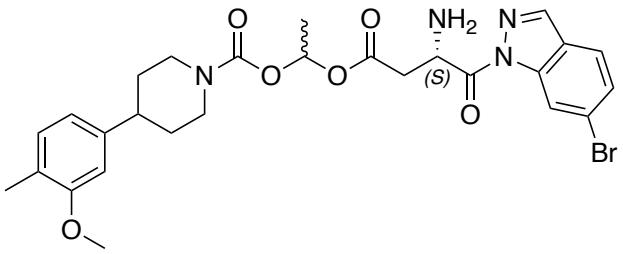
To a solution of 1-benzyl 4-(1-((4-(3-methoxy-4-methylphenyl)piperidine-1-carbonyl)oxy)ethyl) (tert-butoxycarbonyl)-L-aspartate (526 mg, 0.88 mmol) in EtOAc (15 mL) was added Pd/C (100 mg) as a suspension in EtOAc. The reaction was stirred under an atmosphere of hydrogen for 1.5 h after which time the reaction was filtered and solvent removed *in vacuo* to give a straw coloured oil (450 mg, 0.88 mmol). LCMS (m/z): calc'd for $C_{25}H_{36}N_2O_9$ $[M + H]^+$ 509.2 found 509.3, r.t. 2.99.

1-(((S)-4-(6-bromo-1H-indazol-1-yl)-3-((tert-butoxycarbonyl)amino)-4-oxobutanoyl)oxy)ethyl 4-(3-methoxy-4-methylphenyl)piperidine-1-carboxylate



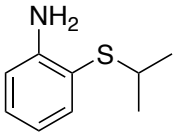
To a stirred solution of (2S)-2-((tert-butoxycarbonyl)amino)-4-(1-((4-(3-methoxy-4-methylphenyl)piperidine-1-carbonyl)oxy)ethoxy)-4-oxobutanoic acid (450 mg, 0.88 mmol) in CH_2Cl_2 (20 mL) was added HATU (401 mg, 1.06 mmol), 5-bromoindazole (94 mg, 0.97 mmol),and DIPEA (460 µL, 2.64 mmol). After 2.5 h the reaction mixture was absorbed onto slica and purified by flash column chromatography, eluting with 0-15% ethyl acetate in petroleum ether to give a straw coloured gum (404 mg, 67%). LCMS (m/z): calc'd for $C_{32}H_{39}BrN_4O_8$ $[M + H]^+$ 689.2 found 689.3, r.t. 3.37.

1-(((S)-3-amino-4-(6-bromo-1H-indazol-1-yl)-4-oxobutanoyl)oxy)ethyl 4-(3-methoxy-4-methylphenyl)piperidine-1-carboxylate



To a stirred solution of 1-(((S)-4-(6-bromo-1H-indazol-1-yl)-3-((tert-butoxycarbonyl)amino)-4-oxobutanoyl)oxy)ethyl 4-(3-methoxy-4-methylphenyl)piperidine-1-carboxylate (5 mg, 7.3 μmol) in CH_2Cl_2 (800 μL) was added TFA (200 μL). After sonication for 5 mins volatiles were removed *in vacuo* and the residue trituated with diethyl ether to give a wwhite solid (4.3 mg, 100%) ^{1}H NMR (400 MHz, DMSO) δ 8.70 (s, 2H), 8.63 – 8.52 (m, 1H), 8.28 – 8.23 (m, 2H), 8.09 – 7.98 (m, 1H), 7.94 – 7.82 (m, 1H), 7.57 – 7.41 (m, 1H), 7.06 – 6.98 (m, 1H), 6.78 (s, 1H), 6.68 (dq, *J* = 16.2, 5.3 Hz, 1H), 5.40 – 5.36 (m, 1H), 4.18 – 3.81 (m, 2H), 3.77 (s, 3H), 3.27 – 3.21 (m, 1H), 3.02 – 2.56 (m, 3H), 2.13 – 2.07 (m, 3H), 1.76 – 1.71 (m, 2H), 1.56 – 1.45 (m, 2H), 1.42 (t, *J* = 4.8 Hz, 3H).

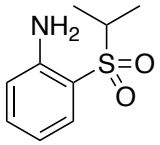
2-(isopropylthio)aniline



To a stirred solution of 2-aminothiophenol (20 mL, 187 mmol) in anhydrous THF (300 mL) at 0 °C was added, as a solid, portionwise over a period of 20 mins, potassium tert-butoxide (21.0 g, 187 mmol). After 30 min, isopropyl iodide (18.65 mL, 187 mmol) was slowly added and the reaction mixture was allowed to warm to room temperature and stirred overnight. The reaction mixture was diluted with CH_2Cl_2 (100 mL), filtered, and the filtrate concentrated *in vacuo*. The residue was taken up in EtOAc (100 mL) and washed with sodium bicarbonate (150 mL). The aqueous layer was extracted with EtOAc (2 x 75 mL), the combined organics dried ($MgSO_4$), filtered, and solvent removed *in vacuo* to give the product as red oil (28.8 g, 92 %) which was used without

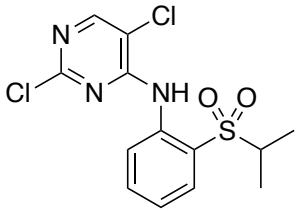
further purification. ^{1}H NMR (400 MHz, $CDCl_3$) δ 7.37 (dd, *J* = 7.6, 1.6 Hz, 1H), 7.20 – 7.08 (m, 1H), 6.78 – 6.63 (m, 2H), 4.38 (s, 2H), 3.20 (hept, *J* = 6.7 Hz, 1H), 1.25 (d, *J* = 6.7 Hz, 6H). ^{13}C NMR (101 MHz, $CDCl_3$) δ 137.2, 129.9, 118.3, 114.8, 95.8, 38.7, 23.3 (quaternary carbons not visable). LCMS (m/z): calc'd for $C_9H_{13}NS$ $[M + H]^+$ 167.1, found 167.7, r.t 2.91.

2-(isopropylsulfonyl)aniline



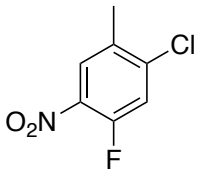
To a stirred solution of 2-(isopropylthio)aniline (15.45 g, 0.09 mol) in MeOH (250 mL) at 0 °C was slowly added oxone (85.27 g, 0.28 mol) as a solution in deionised water (250 mL). The reaction mixture was allowed to warm to room temperature and stirred overnight. The reaction mixture was concentrated to remove MeOH *in vacuo* and EtOAc (300 mL) added. The aqueous layer was extracted with EtOAc (2 x 100 mL), and the combined organics were dried *in vacuo* to give a dark red oil. Purification by flash column chromatography (silica gel), eluting with 3% EtOAc in petroleum ether gave the product as an orange solid (2.05 g, 67%). ^{1}H NMR (400 MHz, $CDCl_3$) δ 7.66 (ddd, *J* = 7.9, 1.6, 0.4 Hz, 1H), 7.37 (ddd, *J* = 8.2, 7.2, 1.6 Hz, 1H), 6.82 (ddd, *J* = 8.2, 7.2, 1.1 Hz, 1H), 6.74 (ddd, *J* = 8.2, 1.1, 0.4 Hz, 1H), 5.10 (s, 2H), 3.35 (hept, *J* = 6.9 Hz, 1H), 1.33 (d, *J* = 6.9 Hz, 7H). ^{13}C NMR (101 MHz, $CDCl_3$) δ 147.2, 135.0, 134.0, 131.3, 118.2, 117.5, 54.2, 15.3. LCMS (m/z): calc'd for $C_9H_{13}NSO_2$ $[M + H]^+$ 200.1, found 200.0 $[M + H]^+$, r.t. 2.54.

2,5-dichloro-N-(2-(isopropylsulfonyl)phenyl)pyrimidin-4-amine



To a stirred solution of 2-(isopropylsulfonyl)aniline (10.0 g, 50.2 mmol) in DMF (100 mL) at 0 °C was slowly added NaH (4.42 g) as a dispersion in 60% mineral oil. After 40 mins 2,4,5-trichloropyrimidine (6.33 mL, 55.3 mmol) was slowly added and the reaction mixture was left to warm to room temperature. After 1.5 days, EtOAc (150 mL) and saturated ammonium chloride (100 mL) was added to the reaction mixture. The aqueous layer was extracted with EtOAc (2 x 150 mL) and the combined organics dried ($MgSO_4$) and solvent removed *in vacuo* to give a dark oil. Purification by flash column chromatography (silica gel), eluting with 0 - 20% EtOAc in petroleum ether, gave the product as a yellow solid (10.27 g, 59%). ^{1}H NMR (400 MHz, DMSO) δ 9.83 (s, 1H), 8.57 (s, 1H), 8.34 (dd, *J* = 8.3, 1.2 Hz, 1H), 7.91 (dd, *J* = 7.9, 1.5 Hz, 1H), 7.87 (ddd, *J* = 8.3, 7.5, 1.6 Hz, 1H), 7.49 (td, *J* = 7.7, 1.2 Hz, 1H), 3.55 (hept, *J* = 6.8 Hz, 1H), 1.18 (d, *J* = 6.9 Hz, 6H). ^{13}C NMR (101 MHz, DMSO) δ 157.2, 156.4, 137.1, 135.7, 131.6, 126.8, 125.7, 125.0, 115.3, 55.1, 15.3 (quaternary carbon not visable). LCMS (m/z): calc'd for $C_{13}H_{15}ClN_4SO_2$ $[M + H]^+$ 326.0, found 326.1 , r.t 2.99.

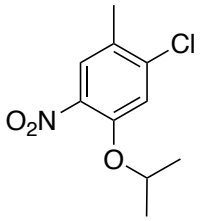
1-chloro-5-fluoro-2-methyl-4-nitrobenzene



To a stirred solution of 2-chloro-4-fluoro-1-methylbenzene (20 mL, 117.2 mmol) in conc. H_2SO_4 at 0 °C was slowly added, portionwise as a solid, KNO_3 (14.8 g, 146.5 mmol). The reaction was allowed to warm to room temperature and left overnight. The reaction mixture was poured onto ice and extracted with EtOAc (3 x 150 mL). The combined organics were concentrated *in vacuo* and the residue flushed through a large plug of silica with 0 -3% EtOAc in petroleum ether to give the product as a pale yellow

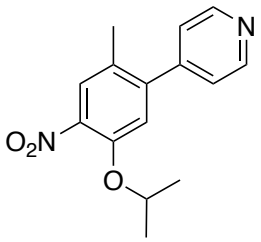
solid (12.0 g, 54%). ^{1}H NMR (400 MHz, $CDCl_3$) δ 7.99 (d, *J* = 7.7 Hz, 1H), 7.35 (d, *J* = 10.3 Hz, 1H), 2.45 (t, *J* = 1.0 Hz, 3H), 1.27 (s, 1H). ^{13}C NMR (101 MHz, $CDCl_3$) δ 154.9, 152.2, 141.3, 133.4, 127.4, 119.2, 19.4.

1-chloro-5-isopropoxy-2-methyl-4-nitrobenzene



To a stirred solution of 1-chloro-5-fluoro-2-methyl-4-nitrobenzene (11.47 g, 60.5 mmol) in IPA (500 mL) was added $CsCO_3$ (98.56 g, 302 mmol). Upon addition the pale yellow solution turned orange. The reaction was heated to 60 °C and stirred overnight. The reaction mixture was concentrated *in vacuo* and EtOAc (300 mL) and H_2O (200 mL) added. The aqueous layer was extracted with EtOAc (2 x 100 mL), and the combined organics dried ($MgSO_4$), filtered, and solvent removed *in vacuo* to give a yellow solid which was flushed through a large plug of silica with 0-3% EtOAc in petroleum ether to give the product as a pale yellow solid (13.85 g, 100%). ^{1}H NMR (400 MHz, $CDCl_3$) δ 7.72 – 7.67 (m, 1H), 7.10 – 7.05 (m, 1H), 4.60 (hept, *J* = 6.0 Hz, 1H), 2.34 (s, 3H), 1.39 (d, *J* = 6.1 Hz, 6H). ^{13}C NMR (101 MHz, $CDCl_3$) δ 150.0, 139.6, 139.1, 128.3, 127.1, 117.1, 73.4, 21.8, 19.0.

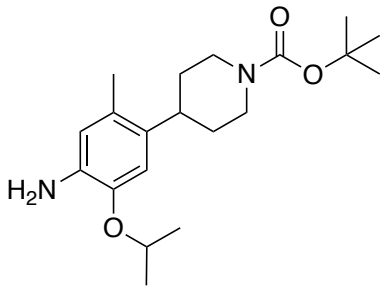
4-(5-isopropoxy-2-methyl-4-nitrophenyl)pyridine



1-chloro-5-isopropoxy-2-methyl-4-nitrobenzene (2.25 g, 9.83 mmol), pyridin-4-ylboronic acid (2.21 g, 10.8 mmol), SPhos (1.01 g, 2.46 mmol), Pd2(dba)3 (0.9 g, 0.98 mmol) and Na_2CO_3 (2.08 g, 19.66 mmol) were suspended in dioxane:H_2O (2:1) (20 mL) and irradiated with microwave radiation for 20 mins at 150 °C. The reaction mixture was filtered, EtOAc (150 mL) added, and washed with NaOH (2 M, 3 x 100 mL).

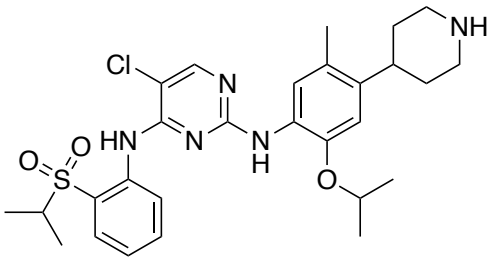
The combined organics were dried ($MgSO_4$), filtered, and solvent removed *in vacuo* to give a brown oil. Purification by flash column chromatography (silica gel), eluting with 10-30% EtOAc in petroleum ether gave the product as a pale brown solid (1.93 g, 72%). ^{1}H NMR (400 MHz, $CDCl_3$) δ 8.77 – 8.71 (m, 2H), 7.74 (s, 1H), 7.29 – 7.23 (m, 2H), 6.92 (s, 1H), 4.66 (p, *J* = 6.1 Hz, 1H), 2.24 (s, 3H), 1.41 (d, *J* = 6.1 Hz, 6H). ^{13}C NMR (101 MHz, $CDCl_3$) δ 150.1, 149.3, 147.9, 144.4, 140.5, 127.5, 127.2, 123.6, 117.4, 73.1, 21.9, 19.2. (m/z): calc'd for $C_{15}H_{16}N_2O_3$ $[M + H]^+$+ 273.3, found 273.1, r.t 2.58.

Tert-butyl 4-(4-amino-5-isopropoxy-2-methylphenyl)piperidine-1-carboxylate



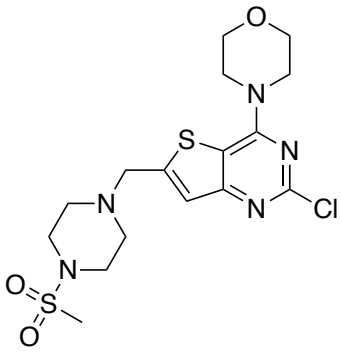
To a stirred solution of 4-(5-isopropoxy-2-methyl-4-nitrophenyl)pyridine (1.50 g, 5.51 mmol) in AcOH (100 mL) was added TFA (0.84 mL, 11.0 mmol). The reaction mixture was stirred under an atmosphere of H_2 gas. After 1.5 days the reaction mixture was filtered, and the filtrate concentrated *in vacuo* to give a red residue which was taken up in CH_2Cl_2 (50 mL) and di-tert-butyl dicarbonate (0.97 g, 4.43 mmol) added as a solution in CH_2Cl_2 (2 mL). After stirring at room temperature for 40 mins, the reaction mixture was concentrated *in vacuo* to give a dark red residue. Purification by flash column chromatography (silica gel), eluting with 0-15% EtOAc in petroleum ether to give the product (1.65 g, 86%) as a red oil that solidified upon standing. ^{1}H NMR (400 MHz, $CDCl_3$) δ 6.61 (1H, s), 6.56 – 6.50 (m, 1H), 4.44 (hept, *J* = 6.1, 1H), 4.33 – 4.17 (m, 2H), 2.84 – 2.76 (m, 2H), 2.73 (tt, *J* = 12.0 and 3.5, 1H), 2.20 (s, 3H), 1.78 – 1.66 (m, 2H), 1.49 (s, 9H), 1.46 – 1.43 (m, 2H), 1.32 (d, *J* = 6.1, 6H). LCMS (m/z): calc'd for $C_{20}H_{30}N_2O_3$ $[M + H]^+$ 349.5, found 349.2, r.t. 3.63.

5-chloro-N2-(2-isopropoxy-5-methyl-4-(piperidin-4-yl)phenyl)-N4-(2-(isopropylsulfonyl)phenyl)pyrimidine-2,4-diamine (Ceritinib)



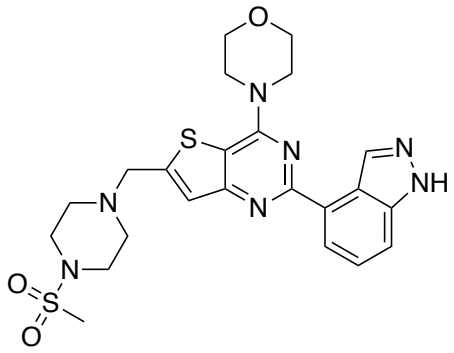
To a stirred solution of Tert-butyl 4-(4-amino-5-isopropoxy-2-methylphenyl)piperidine-1-carboxylate (629 mg, 1.82 mmol) in IPA (5 mL) was added 2,5-dichloro-N-(2-(isopropylsulfonyl)phenyl)pyrimidin-4-amine (634 mg, 1.82 mmol). HCl as a solution in dioxane (2 mL, 4 M) was added and the reaction mixure irradiated with microwave radiation for 15 mins at 150 °C. After cooling to room temperature and concentrating, the residue was purified by flash colum chromatography, eluting with 0-30% EtOAc in petroleum ether gave the product as the HCl salt, an orange solid (1.0 g, 1.72 mmol, 98%). The free base was obtained by flushing the salt through an STX cartridge. ^{1}H NMR (400 MHz, $CDCl_3$) δ 9.49 (s, 1H), 8.58 (dd, *J* = 8.4, 1.1 Hz, 1H), 8.15 (s, 1H), 8.00 (s, 1H), 7.93 (dd, *J* = 7.9, 1.6 Hz, 1H), 7.62 (ddd, *J* = 8.4, 7.3, 1.7 Hz, 1H), 7.54 (s, 1H), 7.25 (ddd, *J* = 8.3, 7.4, 1.1 Hz, 1H), 6.80 (s, 1H), 5.30 (s, 3H), 4.55 (hept, *J* = 6.1 Hz, 1H), 3.32 – 3.20 (m, 3H), 2.79 (td, *J* = 12.1, 2.5 Hz, 3H), 2.16 (s, 3H), 1.82 – 1.74 (m, 2H), 1.67 (qd, *J* = 13.0, 12.5, 3.9 Hz, 2H), 1.36 (d, *J* = 6.1 Hz, 7H), 1.32 (d, *J* = 6.9 Hz, 7H). LCMS (m/z): calc'd for $C_{28}H_{36}ClN_5O_3S$ 557.2, found 558.5 $[M + H]^+$, r.t. 2.43 purity 99%. HRMS (m/z): calc'd for $C_{28}H_{36}ClN_5O_3S$ $[M + H]^+$ 558.2300 and $[M + Na]^+$ 580.2125 found 558.2313 and 580.2120.

4-(2-chloro-6-((4-(methylsulfonyl)piperazin-1-yl)methyl)thieno[3,2-d]pyrimidin-4-yl)morpholine.



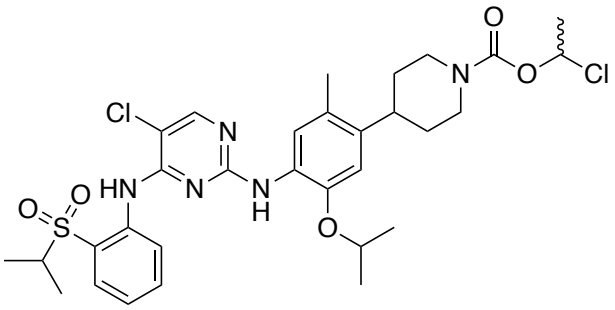
To a stirred suspension of 2-chloro-4-morpholinothieno[3,2-d]pyrimidine-6-carbaldehyde (1.0 g, 3.53 mmol) in MeOH: AcOH (10:1) (4 mL) was added 1-(methylsulfonyl)piperizine (0.69 g, 4.2 mmol). The reaction mixture was heated at 45 °C for 1 hr then cooled to room temperature and picoline borane (0.41 g, 3.85 mmol) added. The reaction was stirred for a further 2 hours after which time the reaction mixture was concentrated and absorbed onto silica gel. Purification by flash column chromatography (silica gel), eluting with CH_2Cl_2: MeOH, containing 0.7 N NH_3 (1 - 5%), gave the product as an off- white solid (1.22 g, 80%). ^{1}H NMR (400 MHz, DMSO) δ 7.34 – 7.30 (m, 1H), 3.93 – 3.91 (m, 2H), 3.91 – 3.85 (m, 4H), 3.80 – 3.72 (m, 4H), 3.15 (t, J = 4.9 Hz, 4H), 2.91 (s, 3H), 2.59 (t, J = 4.9 Hz, 4H); ^{13}C NMR (101 MHz, DMSO) δ 163.0, 158.3, 156.3, 152.6, 122.5, 112.8, 66.3, 56.5, 52.3, 46.3, 45.8, 34.3.; LCMS (m/z): calc'd for $C_{16}H_{22}ClN_5O_3S_2$ $[M + H]^+$ 432.9, found 432.3.

4-(2-(1H-indazol-4-yl)-6-((4-(methylsulfonyl)piperazin-1-yl)methyl)thieno[3,2-d] pyrimidin-4-yl)morpholine (Pictilisib)



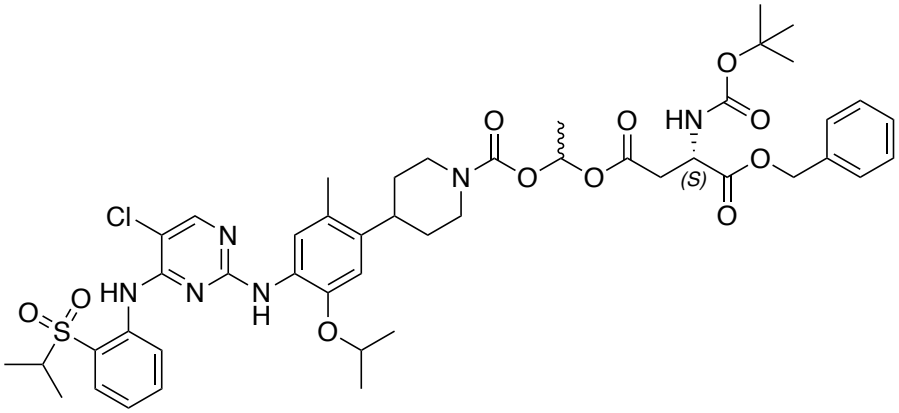
A mixture of 4-(2-chloro-6-((4-(3-(trfluoromethyl)-4H-1,2,4-triazol-4-yl)piperidin- 1-yl) methyl)thieno[3,2-d]pyrimidin-4-yl)morpholine (1 g, 2.3 mmol), (1H-indazol-4-yl) boronic acid (0.56 g, 3.47 mmol), aqueous Na_2CO_3 (3.5 mL, 6.94 mmol, 2 M) and bis(triphenylphosphine) palladium (II) chloride (162 mg, 0.006 mmol) in EtOH: deionised water, (12 mL, 3:1) was irradiated under microwave radiation for 45 mins at 125 °C. After concentration the residue was purified by flash column chromatography (silica gel), eluting with 0 - 10% MeOH containing NH_3 (0.7 N) in CH_2Cl_2 to give the product as an off-white solid (1.0 g, 83%). ^{1}H NMR (400 MHz, DMSO) δ 13.21 (s, 1H), 8.90 (t, *J* = 1.3 Hz, 1H), 8.24 (dd, *J* = 0.9, 7.2 Hz, 1H), 7.68 (dt, *J* = 0.9, 8.2 Hz, 1H), 7.56 – 7.44 (m, 2H), 4.05 – 3.99 (m, 4H), 3.99 – 3.96 (m, 2H), 3.88 – 3.83 (m, 4H), 3.21 – 3.14 (m, 4H), 2.92 (s, 3H), 2.66 – 2.61 (m, 4H). ^{13}C NMR (101 MHz, DMSO) δ 162.7, 160.2, 158.1, 150.7, 141.2, 135.6, 135.5, 131.5, 126.1, 124.0, 121.7, 121.4, 112.8, 66.5, 56.7, 52.3, 46.5, 45.9, 34.3. LCMS (m/z): calc'd for $C_{23}H_{27}N_7O_3S_2$ 513.2 found 513.9 $[M + H]^+$, r.t. 2.23, purity 99%. HRMS (m/z): calc'd for $C_{23}H_{27}N_7O_3S_2$ $[M + H]^+$ 514.1690 found 514.1690.

1-chloroethyl 4-(4-((5-chloro-4-((2-(isopropylsulfonyl)phenyl)amino)pyrimidin-2-yl)amino)-5-isopropoxy-2-methylphenyl)piperidine-1-carboxylate



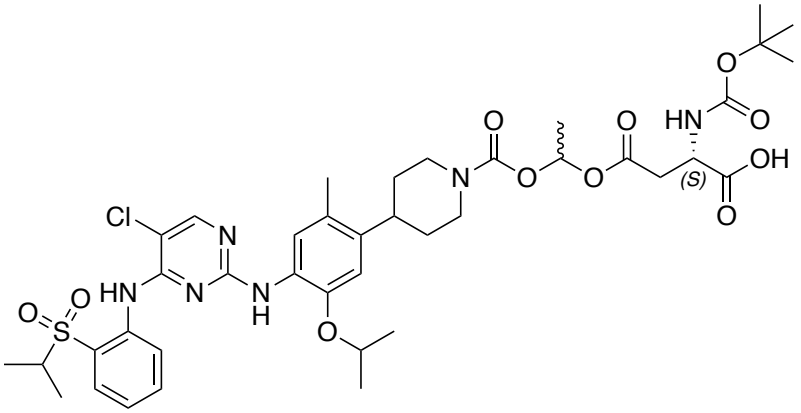
To a precooled (-10 °C) solution of 5- chloro-N_2-(2-isopropoxy-5-methyl-4-(piperidin-4-yl)phenyl)-N_4-(2- (isopropylsulfonyl) phenyl)pyrimidine-2,4-diamine (170 mg , 0.30 mmol) in CH_2Cl_2 (4 mL) was added NMM (134 µL, 1.22 mmol) then ACE-Cl (40 µL, 0.37 mmol). The reaction was allowed to warm to room temperature and stirred for a further 1.5 h after which time the reaction mixture was poured onto HCl (2 M, 30 mL) and extracted with CH_2Cl_2 (3 x 30 mL). The combined organics were dried ($MgSO_4$), filtered, and solvent removed *in vacuo* to give a pale yellow solid (197 mg, 100%) which was used without further purification. (m/z): calc'd for $C_{31}H_{39}Cl_2N_5O_5S$ $[M + H]^+$ 664.2 found 664.0, r.t 3.43.

1-benzyl 4-(1-((4-(4-((5-chloro-4-((2-(isopropylsulfonyl)phenyl)amino)pyrimidin-2-yl)amino)-5-isopropoxy-2-methylphenyl)piperidine-1-carbonyl)oxy)ethyl) (tert-butoxycarbonyl)-L-aspartate



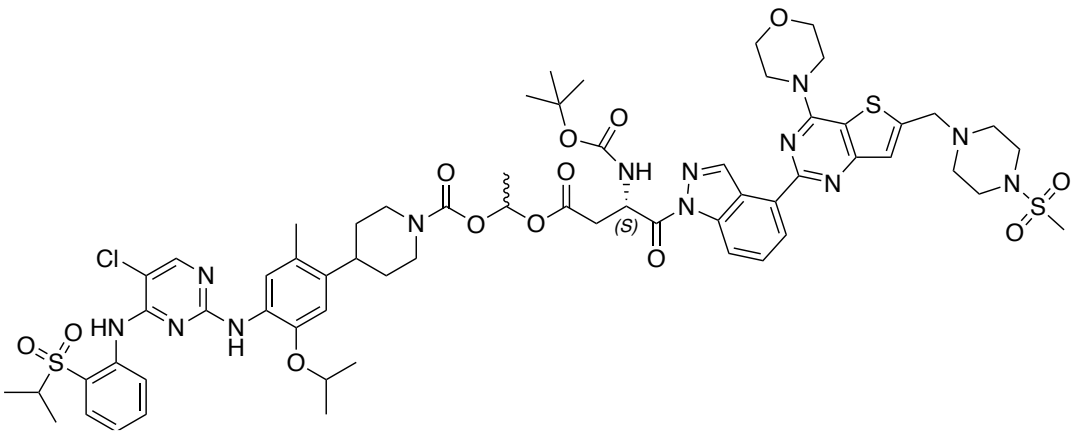
To a stirred solution of 1-chloroethyl 4-(4-((5-chloro-4-((2-(isopropylsulfonyl) phenyl)amino)pyrimidin-2-yl)amino)-5-isopropoxy-2-methyl-phenyl)piperidine-1-carboxylate (100 mg, 0.15 mmol) was added 4- (benzyloxy)-3-((tert-butoxycarbonyl) amino)-4-oxobutanoic acid (58 mg, 0.18 mmol), Ag2O (42 mg, 0.18 mmol) and tert-butylammonium- bromide (10 mg, 0.03 mmol) were added, and the reaction stirred at room temperature for 1 h before heating at 65 °C overnight. The reaction mixture was then absorbed onto silica gel and purified by flash column chromatography, eluting with 10 - 50% ethyl acetate in petroleum ether to give a yellow oil (110 mg, 77 %). ^{1}H NMR (400 MHz, DMSO) δ 9.47 (s, 1H), 8.47 (d, J = 8.4 Hz, 1H), 8.26 (s, 1H), 8.05 (s, 1H), 7.85 (dd, J = 7.9, 1.7 Hz, 1H), 7.63 (t, J = 7.6 Hz, 1H), 7.54 (s, 1H), 7.41 – 7.30 (m, 6H), 6.70 (s, 1H), 5.13 (s, 2H), 4.69 – 4.51 (m, 1H), 4.49 – 4.39 (m, 1H), 4.19 – 4.01 (m, 3H), 3.45 (p, J = 6.7 Hz, 1H), 3.07 – 2.63 (m, 3H), 2.15 (s, 3H), 1.70 – 1.65 (m, 2H), 1.62 – 1.55 (m, 2H), 1.46 – 1.40 (m, 2H), 1.40 – 1.35 (m, 9H), 1.32 – 1.23 (m, 4H), 1.23 – 1.14 (m, 12H). LCMS (m/z): calc'd for $C_{47}H_{59}ClN_6O_{11}S$ $[M + H]^+$ 951.4 found 951.1, rt 3.56.

(2S)-2-((tert-butoxycarbonyl)amino)-4-(1-((4-(4-((5-chloro-4-((2-(isopropylsulfonyl)phenyl)amino)pyrimidin-2-yl)amino)-5-isopropoxy-2-methylphenyl)piperidine-1-carbonyl)oxy)ethoxy)-4-oxobutanoic acid



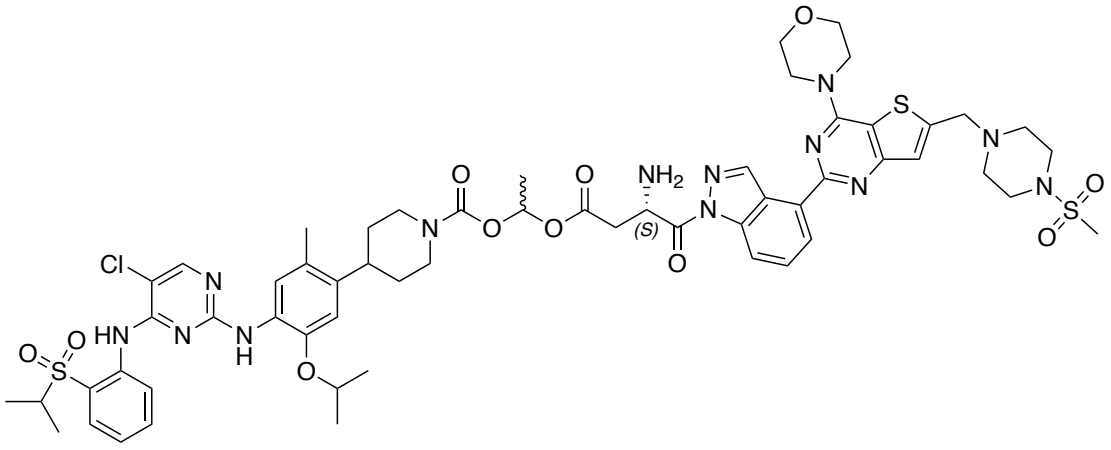
To a solution of 1-benzyl 4-(1-((4-(4-((5-chloro-4-((2-(isopropylsulfonyl) phenyl) amino)pyrimidin-2-yl)amino)-5-isopropoxy-2- methylphenyl) piperidine-1-carbonyl)oxy)ethyl) (tert- butoxycarbonyl)aspartate. (110 mg, 0.12 mmol) in ethyl acetate (3 mL) was added Pd/C (22 mg, 20% wt) as a suspension in EtOAc. The reaction was stirred under an atmosphere of hydrogen for 3 h after which time the reaction was filtered and solvent removed *in vacuo* to give a white foam (104 mg, 100%). The compound was used without further purification. (m/z): calc'd for $C_{40}H_{53}ClN_6O_{11}S$ $[M + H]^+$ 861.3 found 861.0, r.t. 3.29.

1-(((S)-3-((tert-butoxycarbonyl)amino)-4-(4-(6-((4-(methylsulfonyl)piperazin-1-yl)methyl)-4-morpholinothieno[3,2-d]pyrimidin-2-yl)-1H-indazol-1-yl)-4-oxobutanoyl)oxy)ethyl 4-(4-((5-chloro-4-((2-(isopropylsulfonyl)phenyl)amino) pyrimidin-2-yl)amino)-5-isopropoxy-2-methylphenyl)piperidine-1-carboxylate (AEG-118)



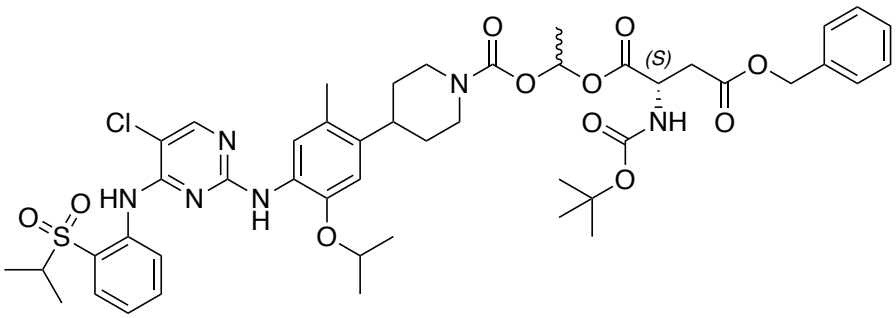
To a stirred solution of 2-((tert-butoxycarbonyl)amino)-4-(1-((4-(4-((5-chloro-4-((2-(isopropylsulfonyl)phenyl)amino)pyrimidin-2-yl)amino)-5-isopropoxy-2-methylphenyl)piperidine-1- carbonyl)oxy)ethoxy)-4-oxobutanoic acid (104 mg, 0.12 mmol) inDMF (4 mL) was added HATU (50 mg, 0.13 mmol), 4-(2-(1H-indazol-4-yl)-6-((4-(methylsulfonyl)piperazin-1-yl)methyl)thieno[3,2- d]pyrimidin-4-yl) morpholine (62 mg, 0.12 mmol), and DIPEA (63 µL, 0.36 mmol). After 2.5 h the reaction mixture was directly purified by preperative HPLC, method A, and was freeze dried to give a white solid (2.5 mg, 3%). ^{1}H NMR (800 MHz, $CDCl_3$) δ 9.51 (s, 1H), 9.20 (s, 1H), 8.58 (d, *J* = 8.3 Hz, 1H), 8.55 – 8.48 (m, 1H), 8.42 (d, *J* = 7.5 Hz, 1H), 8.16 – 8.14 (m, 1H), 8.03 – 7.96 (m, 1H), 7.93 (dd, *J* = 7.9, 1.5 Hz, 1H), 7.66 (s, 1H), 7.62 (dd, *J* = 8.6, 1.4 Hz, 2H), 7.53 (s, 1H), 6.82 (d, *J* = 5.7 Hz, 1H), 6.73 – 6.67 (m, 1H), 5.98 – 5.84 (m, 2H), 4.54 (s, 1H), 4.33 (s, 1H), 4.16 (s, 1H), 4.07 (s, 4H), 3.93 – 3.90 (m, 5H), 3.32 – 3.29 (m, 4H), 3.26 (p, *J* = 6.8 Hz, 1H), 3.13 – 3.10 (m, 1H), 2.91 – 2.78 (m, 3H), 2.82 (s, 3H), 2.71 – 2.69 (m, 4H), 2.15 (s, 3H), 1.75 – 1.73 (m, 2H), 1.70 – 1.38 (m, 24H), 1.32 (d, *J* = 6.7 Hz, 6H). LCMS (m/z): calc'd for $C_{63}H_{78}ClN_{13}O_{13}S_3$ 1355.5 found 1356.3 $[M + H]^+$, r.t. 3.52, 99% purity. HRMS (m/z): calc'd for $C_{63}H_{78}ClN_{13}O_{13}S_3$ $[M + H]^+$ 1355.4687 found 1356. 4712.

1-(((S)-3-amino-4-(4-(6-((4-(methylsulfonyl)piperazin-1-yl)methyl)-4-morpholinothieno[3,2-d]pyrimidin-2-yl)-1H-indazol-1-yl)-4-oxobutanoyl)oxy)ethyl 4-(4-((5-chloro-4-((2-(isopropylsulfonyl)phenyl)amino)pyrimidin-2-yl)amino)-5-isopropoxy-2-methylphenyl)piperidine-1-carboxylate (AEG-118_deprotected)



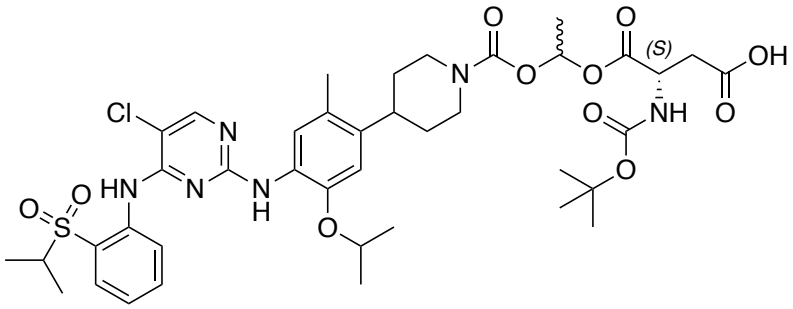
1-(((S)-3-((tert-butoxycarbonyl)amino)-4-(4-(6-((4-(methylsulfonyl)piperazin-1-yl)methyl)-4-morpholinothieno[3,2-d]pyrimidin-2-yl)-1H-indazol-1-yl)-4-oxobutanoyl)oxy)ethyl 4-(4-((5-chloro-4-((2-(isopropylsulfonyl)phenyl)amino)pyrimidin-2-yl)amino)-5-isopropoxy-2-methylphenyl)piperidine-1-carboxylate (1 mg, 0.74 μmol) was taken up in TFA (20 μL, 20% v:v in CH_2Cl_2) and sonicated. After 5 mins, the solvent and TFA were removed *in vacuo* and the residual solid was triturated with diethyl ether to give a white solid (93 μg, 100%). LCMS (m/z): calc'd for $C_{58}H_{70}ClN_{13}O_{11}S_3$ 1255.4 found 1256.6 , r.t. 2.68, 100% purity. HRMS (m/z): calc'd for $C_{58}H_{70}ClN_{13}O_{11}S_3$ $[M + H]^+$ 1255.4163 found 1255.4456.

4-benzyl 1-(1-((4-(4-((5-chloro-4-((2-(isopropylsulfonyl)phenyl)amino)pyrimidin-2-yl)amino)-5-isopropoxy-2-methylphenyl)piperidine-1-carbonyl)oxy)ethyl) (tert-butoxycarbonyl)-L-aspartate



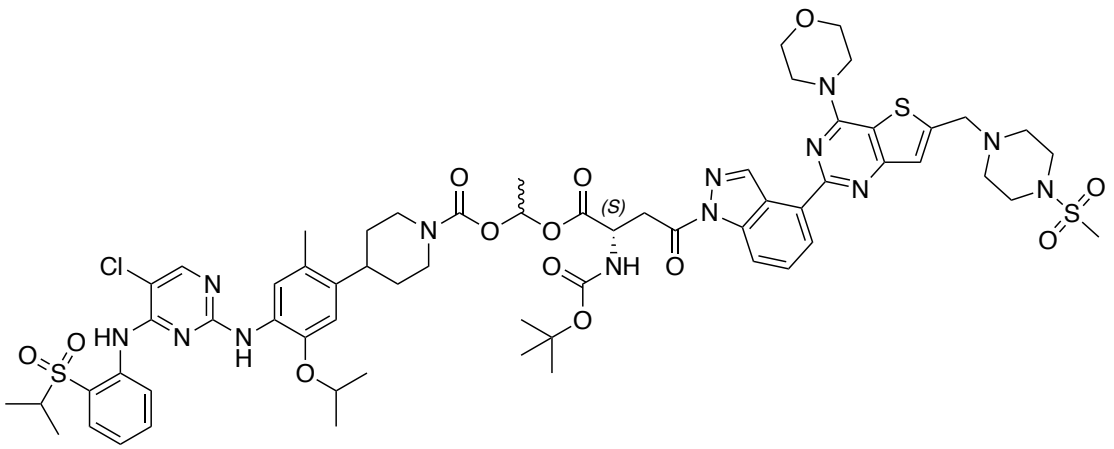
To a precooled (-10 °C) solution of 5-chloro-N_2-(2-isopropoxy-5-methyl-4-(piperidin-4-yl)phenyl)-N_4-(2-(isopropylsulfonyl)phenyl)pyrimidine-2,4-diamine (150 mg , 0.27 mmol) in CH_2Cl_2 (4 mL) was added NMM (67 µL, 0.60 mmol) then ACE-Cl (32 µL, 0.30 mmol). The reaction was allowed to warm to room temperature and stirred for a further 1.5 h after which time the reaction mixture was poured onto HCl (2 M, 30 mL) and extracted with CH_2Cl_2 (3 x 30 mL). The combined organics were dried ($MgSO_4$), filtered, and solvent removed *in vacuo* to give an orange residue which was taken up in toluene. (S)-4-(benzyloxy)-3-((tert-butoxycarbonyl)amino)-4-oxobutanoic acid (105 mg, 0.32 mmol), Ag2O (75 mg, 0.32 mmol) and tertbutylammonium- bromide (18 mg, 0.05 mmol) were added, and the reaction stirred at room temperature for 1 h before heating at 65 °C overnight. The reaction mixture was then absorbed onto silica gel and purified by flash column chromatography, eluting with 10 - 50% ethyl acetate in petroleum ether to give the product as a beige oil (88 mg, 34%). LCMS (m/z): calc'd for $C_{47}H_{59}ClN_6O_{11}S$ $[M + H]^+$ 951.4 found 951.7, rt 3.50.

(3S)-3-((tert-butoxycarbonyl)amino)-4-(1-((4-(4-((5-chloro-4-((2-(isopropylsulfonyl)phenyl)amino)pyrimidin-2-yl)amino)-5-isopropoxy-2-methylphenyl)piperidine-1-carbonyl)oxy)ethoxy)-4-oxobutanoic acid



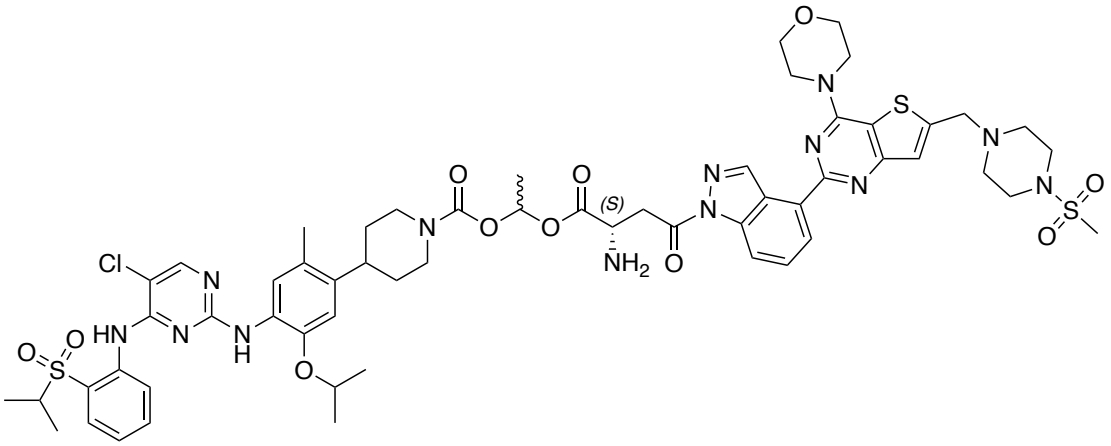
To a solution of 4-benzyl 1-(1-((4-(4-((5-chloro-4-((2-(isopropylsulfonyl)phenyl)amino)pyrimidin-2-yl)amino)-5-isopropoxy-2-methylphenyl)piperidine-1-carbonyl)oxy)ethyl) (tert-butoxycarbonyl)-L-aspartate (88 mg, 93 μmol) in ethyl acetate (3 mL) was added Pd/C (17 mg, 20% wt) as a suspension in ethyl acetate. The reaction was stirred under an atmosphere of hydrogen for 3 h after which time the reaction was filtered and solvent removed *in vacuo* to give a white foam (80 mg, 100%). The compound was used without further purification.

1-(((S)-2-((tert-butoxycarbonyl)amino)-4-(4-(6-((4-(methylsulfonyl)piperazin-1-yl)methyl)-4-morpholinothieno[3,2-d]pyrimidin-2-yl)-1H-indazol-1-yl)-4-oxobutanoyl)oxy)ethyl 4-(4-((5-chloro-4-((2-(isopropylsulfonyl)phenyl)amino)pyrimidin-2-yl)amino)-5-isopropoxy-2-methylphenyl)piperidine-1-carboxylate (AEG-291)



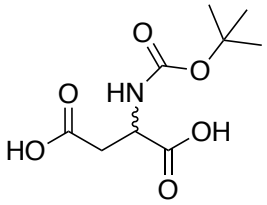
To a stirred solution of (3S)-3-((tert-butoxycarbonyl)amino)-4-(1-((4-(4-((5-chloro-4-((2-(isopropylsulfonyl)phenyl)amino)pyrimidin-2-yl)amino)-5-isopropoxy-2-methylphenyl)piperidine-1-carbonyl)oxy)ethoxy)-4-oxobutanoic acid (80 mg, 93 μmol) in DMF (3 mL) was added HATU (39 mg, 102 μmol), 4-(2-(1H-indazol-4-yl)-6-((4-(methylsulfonyl)piperazin-1-yl)methyl)thieno[3,2- d]pyrimidin-4-yl) morpholine (48 mg, 93 μmol), and DIPEA (49 μL, 0.28 mmol). After 2.5 h the reaction mixture was directly purified by preperative HPLC, method A, and was freeze dried to give a white solid (14 mg, 11%). ^{1}H NMR (800 MHz, $CDCl_3$) δ 9.55 – 9.46 (m, 1H), 9.24 – 9.16 (m, 1H), 8.61 (d, *J* = 8.3 Hz, 1H), 8.58 – 8.50 (m, 1H), 8.51 – 8.35 (m, 2H), 8.19 (s, 1H), 8.07 – 7.99 (m, 1H), 7.96 (dd, *J* = 7.5, 1.4 Hz, 1H), 7.65 (dd, *J* = 8.6, 1.2 Hz, 1H), 7.64 – 7.48 (m, 2H), 6.97 – 6.95 (m, 1H), 6.81 – 6.60 (m, 1H), 5.76 – 5.67 (m, 1H), 4.91 – 4.88 (m, 1H), 4.82 – 4.55 (m, 2H), 4.38 – 4.34 (m, 1H), 4.25 (s, 1H), 4.08 (d, *J* = 33.7 Hz, 4H), 3.93 (s, 5H), 3.78 (s, 1H), 3.35 – 3.33 (m, 4H), 3.32 – 3.27 (m, 1H), 2.85 (s, 3H), 2.74 – 2.72 (m, 5H), 2.22 – 2.02 (m, 3H), 1.88 – 1.16 (m, 32H). LCMS (m/z): calc'd for $C_{63}H_{78}ClN_{13}O_{13}S_3$ 1355.5 found 1356.5 $[M + H]^+$, r.t. 3.46, 100% purity. HRMS (m/z): calc'd for $C_{63}H_{78}ClN_{13}O_{13}S_3$ $[M + H]^+$ 1356.4687 found 1356.4679.

1-(((S)-2-amino-4-(4-(6-((4-(methylsulfonyl)piperazin-1-yl)methyl)-4-morpholinothieno[3,2-d]pyrimidin-2-yl)-1H-indazol-1-yl)-4-oxobutanoyl)oxy)ethyl 4-(4-((5-chloro-4-((2-(isopropylsulfonyl)phenyl)amino)pyrimidin-2-yl)amino)-5-isopropoxy-2-methylphenyl)piperidine-1-carboxylate (AEG-291_deprotected)



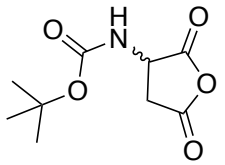
1-(((S)-2-((tert-butoxycarbonyl)amino)-4-(4-(6-((4-(methylsulfonyl)piperazin-1-yl)methyl)-4-morpholinothieno[3,2-d]pyrimidin-2-yl)-1H-indazol-1-yl)-4-oxobutanoyl)oxy)ethyl 4-(4-((5-chloro-4-((2-(isopropylsulfonyl)phenyl)amino)pyrimidin-2-yl)amino)-5-isopropoxy-2-methylphenyl)piperidine-1-carboxylate (250 µg, 0.18 µmol) was taken up in TFA (20 µL, 20% v:v in CH_2Cl_2) and sonicated. After 5 mins, the solvent and TFA were removed *in vacuo* and the residual solid was triturated with diethyl ether to give a white solid (213 µg, 100%). LCMS (m/z): calc'd for $C_{58}H_{70}ClN_{13}O_{11}S_3$ 1255.4 found 1256.5 [M +H], r.t. 2.55, 100% purity. HRMS (m/z): calc'd for $C_{58}H_{70}ClN_{13}O_{11}S_3$ $[M + H]^+$ 1256.4163 found 1256.4339.

(tert-butoxycarbonyl)aspartic acid



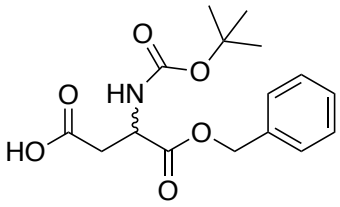
To a suspension of D/L Aspartic acid (10 g, 75.1 mmol) in CH_2Cl_2 (75 mL) was added NaOH (6.0 g, 150.2 mmol) as a solution in deionised H_2O (75 mL). The reaction mixture was rapidly stirred at room temperature for 15 mins then cooled to 0 °C and di-tert-butyl dicarbonate (16.4 g, 75.1 mmol) slowly added as a solution in CH_2Cl_2 (20 mL). After stirring overnight volatiles were removed *in vacuo* and the aqueous was acidified to pH 1 with conc. HCl. EtOAc (200 mL) was added and the aqueous separated . The aqueous was extracted with EtOAc (2 x 100 mL) and the combined organics washed with brine (100 mL), dried ($MgSO_4$), filtered, and solvent removed *in vacuo* to give a white solid (8.62 g, 80%). ^{1}H NMR (400 MHz, D_2O) δ 4.50 – 4.31 (m, 1H), 2.91 – 2.78 (m, 2H), 1.35 (s, 9H). ^{13}C NMR (101 MHz, D_2O) δ 174.9, 174.5, 157.4, 81.7, 50.2, 36.1, 27.5. HRMS (m/z): calc'd for $C_9H_{15}N_1O_6$ 234.0972 $[M + H]^+$ and 256.0797 [M + Na] found 234.0962 and 256.0789.

Tert-butyl (2,5-dioxotetrahydrofuran-3-yl)carbamate



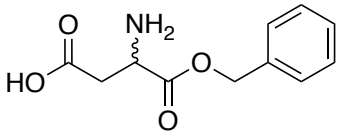
A suspension of (tert-butoxycarbonyl)aspartic acid (8.6 g, 35.4 mmol) in acetic anhydride (50 mL) and was stirred at room temperature overnight yielding a colourless solution. The reaction mixture was evaporated to dryness and azeotroped with toluene (3 x 50 mL) to remove excess actetic anhydride, yielding a white solid (7.97 g, 100%). ^{1}H NMR (400 MHz, DMSO) δ 7.04 (d, J = 8.4 Hz, 1H), 4.26 (td, J = 8.1, 5.5 Hz, 1H), 2.67 (dd, J = 16.4, 5.6 Hz, 1H), 2.58 – 2.49 (m, 1H), 1.38 (s, 9H). ^{13}C NMR (101 MHz, DMSO) δ 173.4, 172.3, 155.7, 78.6, 50.5, 40.6, 40.4, 40.2, 40.0, 39.8, 39.6, 39.3, 36.5, 28.6.

4-(benzyloxy)-3-((tert-butoxycarbonyl)amino)-4-oxobutanoic acid



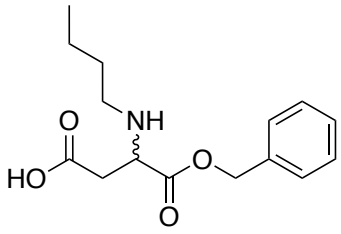
To a stirred solution of 4-(benzyloxy)-3-((tert-butoxycarbonyl)amino)-4-oxobutanoic acid (7.9 g, 35 mmol) in dioxane (50 mL) was added benzyl alcohol (4.35 mL, 42 mmol). The reaction mixture was heated at 75 °C overnight. After cooling to room temperature the resulting white precipitate was filtered and washed with diethyl ether to give the product as a white solid (8.25 g, 73%). ^{1}H NMR (400 MHz, DMSO) δ 12.51 (s, 1H), 7.39 – 7.34 (m, 6H), 5.12 (s, 2H), 4.40 (td, *J* = 8.0, 5.6 Hz, 1H), 2.74 (dd, *J* = 16.5, 5.7 Hz, 1H), 2.59 (dd, *J* = 16.5, 7.8 Hz, 1H), 1.37 (s, 9H). ^{13}C NMR (101 MHz, DMSO) δ 172.0, 171.8, 155.7, 136.4, 128.8, 128.5, 128.1, 78.9, 66.5, 50.8, 40.6, 36.3, 28.6. HRMS (m/z): calc'd for $C_{16}H_{21}N_1O_6$ $[M + H]^+$ 324.1442, $[M + Na]^+$ 346.1267 and $[M + NH_4]^+$ 341.1713 found 324.1439, 346.1260 and 341.1719.

3-amino-4-(benzyloxy)-4-oxobutanoic acid



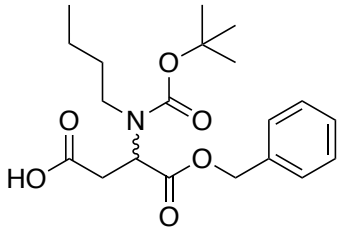
To a stirred suspension of 4-(benzyloxy)-3-((tert-butoxycarbonyl)amino)-4-oxobutanoic acid (6.0 g, 18.6 mmol)in CH_2Cl_2 (20 mL) was slowly added TFA (5 mL). After 1 h the reaction mixture was concentrated and trituated with diethyl ether to give a white solid (5.7 g, 100%). ^{1}H NMR (400 MHz, $CDCl_3$) δ 7.91 (s, 2H), 7.40 – 7.37 (m, 1H), 7.36 – 7.20 (m, 5H), 5.13 (s, 2H), 4.29 – 4.22 (m, 1H), 3.11 – 3.02 (m, 2H). HRMS (m/z): calc'd for $C_{11}H_{13}N_1O_4$ $[M + H]^+$ 224.084 and $[M + Na]^+$ 246.0742 found 224.092 and 246.0737.

4-(benzyloxy)-3-(butylamino)-4-oxobutanoic acid



To a stirred solution of 3-amino-4-(benzyloxy)-4-oxobutanoic acid (1.0 g, 4.48 mmol) in MeOH:AcOH (10:1) (10 mL) was added butyric aldehyde (485 μL, 5.38 mmol). The reaction was heated to 40 °C for 30 mins after which time picoline borane (0.53 g, 4.93 mmol) was added. After stirring overnight the reaction mixture was concentrated and purified by flash colmn chromatography (silica gel), eluting with 5% MeOH in CH_2Cl_2 to afford the product as a white foam (524 mg, 42%). ^{1}H NMR (400 MHz, DMSO) δ 7.45 – 7.39 (m, 7H), 5.25 (s, 2H), 4.43 (t, J = 5.4 Hz, 1H), 3.08 – 2.95 (m, 4H), 1.67 – 1.50 (m, 2H), 1.40 – 1.20 (m, 2H), 0.94 – 0.80 (m, 3H). ^{13}C NMR (101 MHz, DMSO) δ 171.2, 168.4, 146.9, 128.9, 128.8, 128.5, 67.9, 55.6, 46.8, 34.1, 27.8, 19.7, 13.9. HRMS (m/z): calc'd for $C_{18}H_{19}NO_4$ $[M + H]^+$ 314.1387 and $[M + Na]^+$ 336.1212 found 314.1387 and 336.1191.

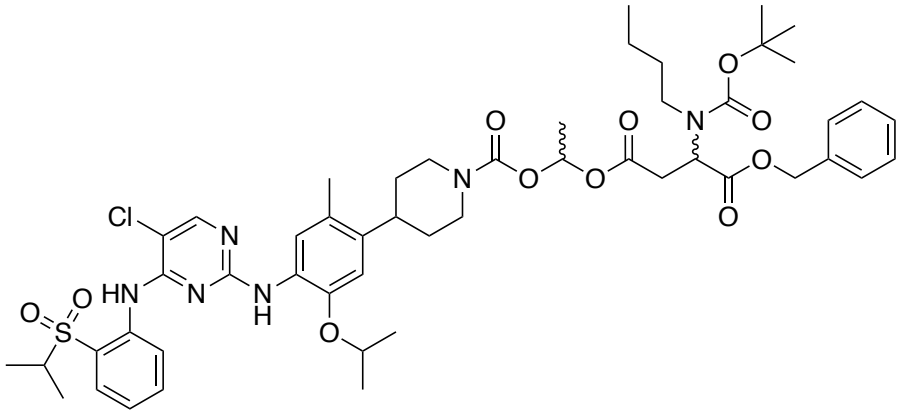
4-(benzyloxy)-3-((tert-butoxycarbonyl)(butyl)amino)-4-oxobutanoic acid



To a stirred solution of 4-(benzyloxy)-3-(butylamino)-4-oxobutanoic acid (488 mg, 1.68 mmol) in CH_2Cl_2 (5 mL) was added triethylamine (393 μL, 1.68 mmol) and di-tert-butyl dicarbonate (366 mg, 1.68 mmol). The reaction mixture was stirred for 2 h after which time the reaction mixture was concentrated and purified by flash column chromatography (silica gel) eluting with 3-7% MeOH in CH_2Cl_2 to give a colourlesss gum (394 mg, 62%). ^{1}H NMR (400 MHz, $CDCl_3$) δ 7.42 – 7.32 (m, 5H), 5.27 – 5.09 (m, 1H), 4.35 – 4.24 (m, 1H), 3.77 – 2.22 (m, 5H), 1.55 (s, 9H), 1.44 – 1.39 (m, 2H),

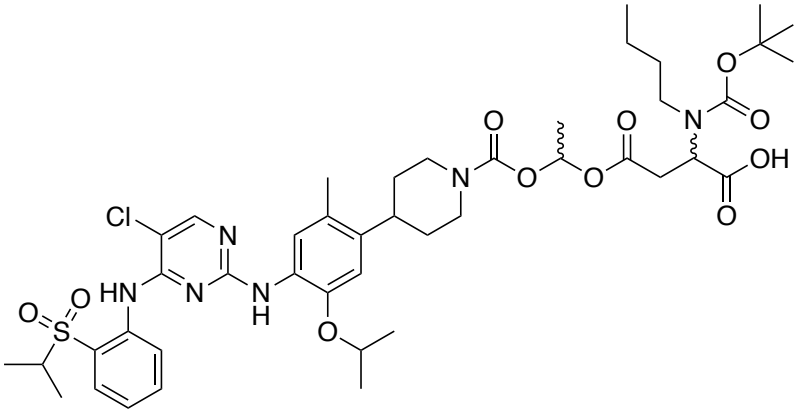
1.39 – 1.35 (m, 2H), 0.90 – 0.86 (m, 4H). HRMS (m/z): calc'd for $C_{20}H_{29}N_1O_6$ $[M + H]^+$ 380.2068 and $[M + Na]^+$ 402.1893 found 380.2081 and 402.1894.

1-benzyl 4-(1-((4-(4-((5-chloro-4-((2-(isopropylsulfonyl)phenyl)amino)pyrimidin-2-yl)amino)-5-isopropoxy-2-methylphenyl)piperidine-1-carbonyl)oxy)ethyl) N-(tert-butoxycarbonyl)-N-butylaspartate



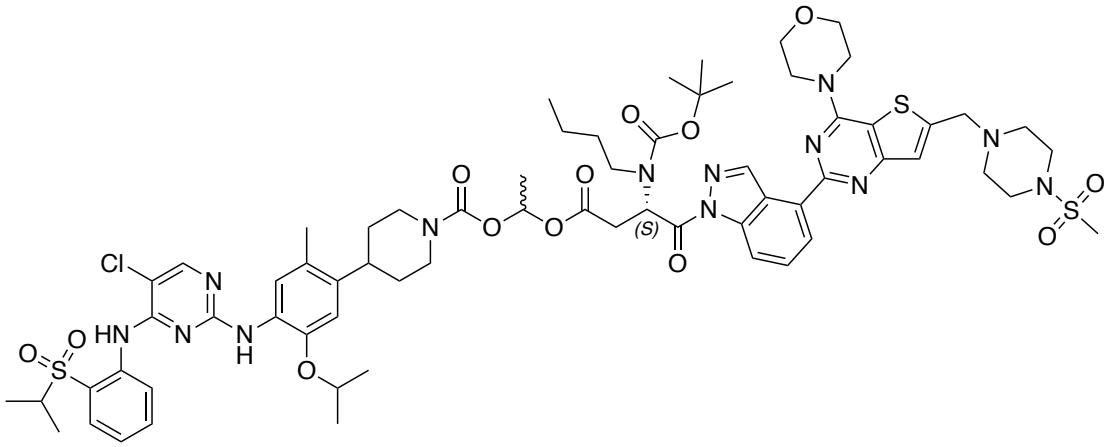
To a stirred solution of 1-chloroethyl 4-(4-((5-chloro-4-((2-(isopropylsulfonyl) phenyl)amino)pyrimidin-2-yl)amino)-5-isopropoxy-2-methylphenyl)piperidine-1-carboxylate (50 mg, 75µmol) in toluene (10 mL) was added 4-(benzyloxy)-3-((tert-butoxycarbonyl)(butyl)amino)-4-oxobutanoic acid (24 mg, 90 µmol), Ag2O (21 mg, 90 µmol) and tertbutylammonium- bromide (5 mg, 15 µmol). The reaction was stirred at room temperature for 1 h before heating at 65 °C overnight. The reaction mixture was then absorbed onto silica gel and purified by flash column chromatography, eluting with 10 - 50% ethyl acetate in petroleum ether to give the product as a beige oil (28 mg, 31%). LCMS (m/z): calc'd for $C_{51}H_{67}ClN_6O_{11}S$ $[M + H]^+$ 1007.4 found 1007.3, r.t 3.94.

2-((tert-butoxycarbonyl)(butyl)amino)-4-(1-((4-(4-((5-chloro-4-((2-(isopropylsulfonyl)phenyl)amino)pyrimidin-2-yl)amino)-5-isopropoxy-2-methylphenyl)piperidine-1-carbonyl)oxy)ethoxy)-4-oxobutanoic acid



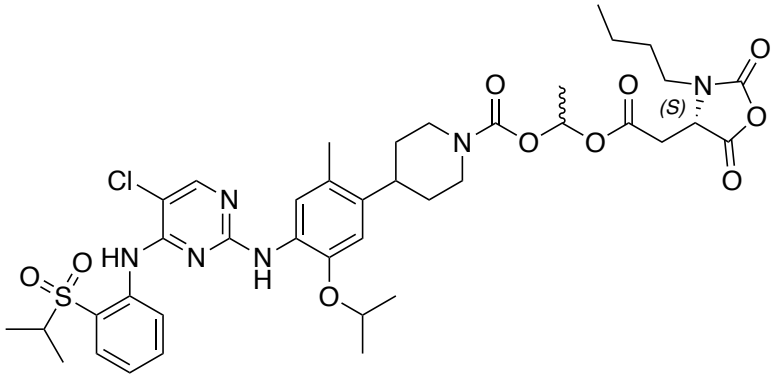
To a solution of 1-benzyl 4-(1-((4-(4-((5-chloro-4-((2-(isopropylsulfonyl)phenyl)amino)pyrimidin-2-yl)amino)-5-isopropoxy-2-methylphenyl)piperidine-1-carbonyl)oxy)ethyl) N-(tert-butoxycarbonyl)-N-butylaspartate (28 mg, 28 μmol) in ethyl acetate (3 mL) was added Pd/C (10 mg) as a suspension in ethyl acetate. The reaction was stirred under an atmosphere of hydrogen for 3 h after which time the reaction was filtered and solvent removed *in vacuo* to give a white foam (14 mg, 56%). The compound was used without further purification. LCMS (m/z): calc'd for $C_{44}H_{61}ClN_6O_{11}S$ $[M + H]^+$ 917.4 found 917.4 , r.t. 3.46.

1-(((S)-3-((tert-butoxycarbonyl)(butyl)amino)-4-(4-(6-((4-(methylsulfonyl)piperazin-1-yl)methyl)-4-morpholinothieno[3,2-d]pyrimidin-2-yl)-1H-indazol-1-yl)-4-oxobutanoyl)oxy)ethyl 4-(4-((5-chloro-4-((2-(isopropylsulfonyl)phenyl)amino)pyrimidin-2-yl)amino)-5-isopropoxy-2-methylphenyl)piperidine-1-carboxylate (AEG-171)



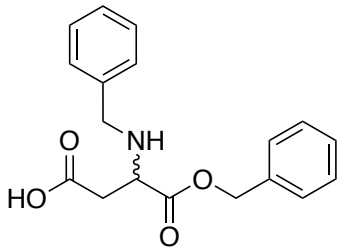
To a stirred solution of 2-((tert-butoxycarbonyl)(butyl)amino)-4-(1-((4-(4-((5-chloro-4-((2-(isopropylsulfonyl)phenyl)amino)pyrimidin-2-yl)amino)-5-isopropoxy-2-methylphenyl)piperidine-1-carbonyl)oxy)ethoxy)-4-oxobutanoic acid (14 mg, 15 µmol) in DMF (2 mL) was added HATU (7 mg, 18 µmol), 4-(2-(1H-in- dazol-4-yl)-6-((4-(methylsulfonyl)piperazin-1-yl)methyl)thieno[3,2- d]pyrimidin-4-yl)morpholine (8 mg, 19 µmol), and DIPEA (8 µL, 46 mmol). After 2.5 h the reaction mixture was directly purified by preperative HPLC, method A, and was freeze dried to give a white solid (6 mg, 28 %). ^{1}H NMR (800 MHz, $CDCl_3$) δ 9.54 (s, 1H), 9.19 (s, 1H), 8.61 (d, *J* = 8.4 Hz, 1H), 8.53 (s, 1H), 8.45 – 8.43 (m, 1H), 8.19 (s, 1H), 8.07 – 8.05 (m, 1H), 7.96 (d, *J* = 7.9 Hz, 1H), 7.70 – 7.63 (m, 2H), 7.57 (s, 1H), 7.41 (s, 1H), 7.00 – 6.90 (m, 1H), 6.82 – 6.65 (m, 1H), 6.03 (s, 0.5H), 5.54 (s, 0.5H), 4.58 (s, 1H), 4.37 – 4.17 (m, 3H), 4.10 (s, 4H), 3.97 – 3.93 (m, 6H), 3.66 – 3.54 (m, 1H), 3.47 – 3.45 (m, 1H), 3.35 (s, 4H), 3.30 (dt, *J* = 13.7, 6.8 Hz, 1H), 2.88 (d, *J* = 97.3 Hz, 1H), 2.85 (s, 3H), 2.74 (s, 4H), 2.20 (s, 3H), 1.89 – 1.12 (m, 33H), 1.01 – 0.81 (m, 6H). LCMS (m/z): calc'd for $C_{67}H_{86}ClN_{13}O_{13}S_3$ 1411.5 found 1412.4 $[M + H]^+$, r.t. 3.88, 100% purity. HRMS (m/z): calc'd for $C_{67}H_{86}ClN_{13}O_{13}S_3$ $[M + H]^+$ 1412.5391 and $[M + Na]^+$ 1434.5216 found 1412.5313 and 1434.5136.

1-(2-((S)-3-butyl-2,5-dioxooxazolidin-4-yl)acetoxy)ethyl 4-(4-((5-chloro-4-((2-(isopropylsulfonyl)phenyl)amino)pyrimidin-2-yl)amino)-5-isopropoxy-2-methylphenyl)piperidine-1-carboxylate



1-(((S)-3-((tert-butoxycarbonyl)(butyl)amino)-4-(4-(6-((4-(methylsulfonyl)piperazin-1-yl)methyl)-4-morpholinothieno[3,2-d]pyrimidin-2-yl)-1H-indazol-1-yl)-4-oxobutanoyl)oxy)ethyl 4-(4-((5-chloro-4-((2-(isopropylsulfonyl)phenyl)amino)pyrimidin-2-yl)amino)-5-isopropoxy-2-methylphenyl)piperidine-1-carboxylate (200 µg, 0.14 µmol) was taken up in TFA (20 µL, 20% v:v in CH_2Cl_2) and sonicated. After 5 mins, the solvent and TFA were removed *in vacuo* and the residual solid was triturated with diethyl ether to give a white solid (120 µg, 100%). LCMS (m/z): calc'd for $C_{40}H_{51}ClN_6O_{10}S$ 842.3 found 843.4 $[M + H]^+$, r.t 7.96, method B. HRMS (m/z): calc'd for $C_{40}H_{51}ClN_6O_{10}S$ $[M + H]^+$ 843.3076 found 843.3158 .

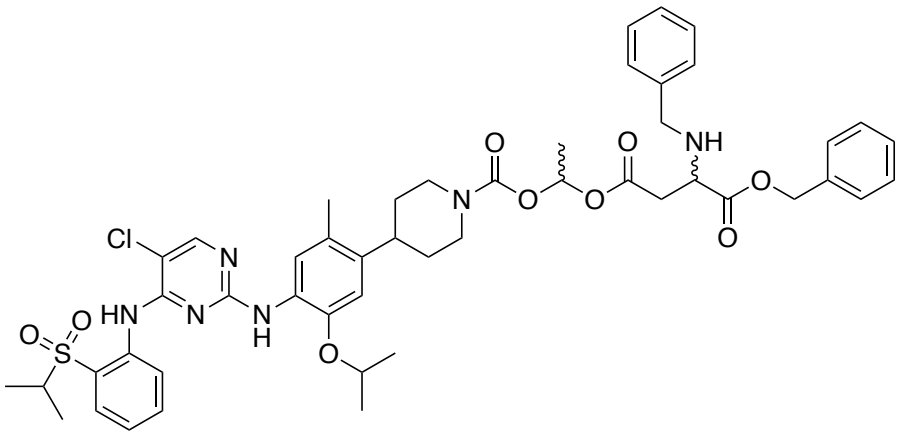
3-(benzylamino)-4-(benzyloxy)-4-oxobutanoic acid



To a stirred solution of 3-amino-4-(benzyloxy)-4-oxobutanoic acid (1.0 g, 4.48 mmol) in MeOH:AcOH (10:1) (10 mL) was added benzaldehyde (546 µL, 5.38 mmol). The reaction was heated to 40 °C for 30 mins after which time picoline borane (0.53 g, 4.93 mmol) was added. After stirring overnight the reaction mixture was concentrated and purified by flash colmn chromatography (silica gel), eluting with 5% MeOH in CH_2Cl_2 to afford the product as a white gum (475 mg, 34%). ^1H NMR (400 MHz,

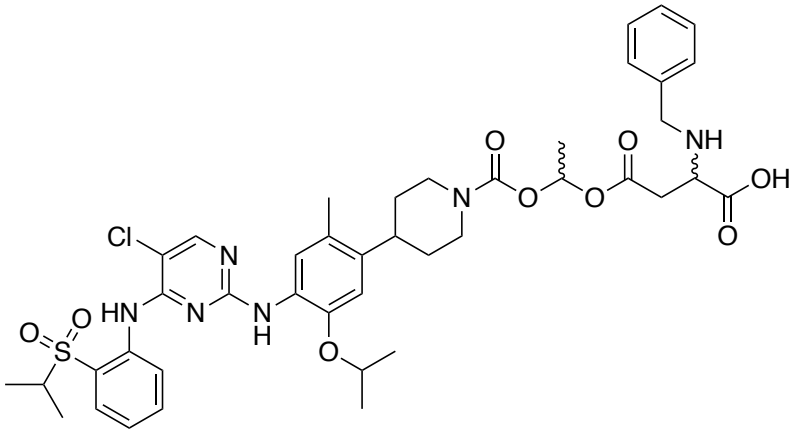
DMSO) δ 7.93 (s, 2H), 7.44 – 7.15 (m, 10H), 5.15 (td, *J* = 14.1, 13.0, 1.9 Hz, 2H), 3.83 (d, *J* = 13.5 Hz, 1H), 3.68 (d, *J* = 13.5 Hz, 1H), 3.64 (t, *J* = 6.7 Hz, 1H), 2.73 – 2.54 (m, 2H). ^{13}C NMR (101 MHz, DMSO) δ 173.1, 172.4, 149.4, 136.5, 128.9, 128.6, 128.5, 128.5, 128.4, 127.4, 66.3, 56.9, 51.0, 37.6. HRMS (m/z): calc'd for $C_{18}H_{19}N_1O_4$ $[M + H]^+$ 314.1387 and $[M + Na]^+$ 336.1212 found 314.1387 and 336.1191.

1-benzyl 4-(1-((4-(4-((5-chloro-4-((2-(isopropylsulfonyl)phenyl)amino)pyrimidin-2-yl)amino)-5-isopropoxy-2-methylphenyl)piperidine-1-carbonyl)oxy)ethyl) benzylaspartate



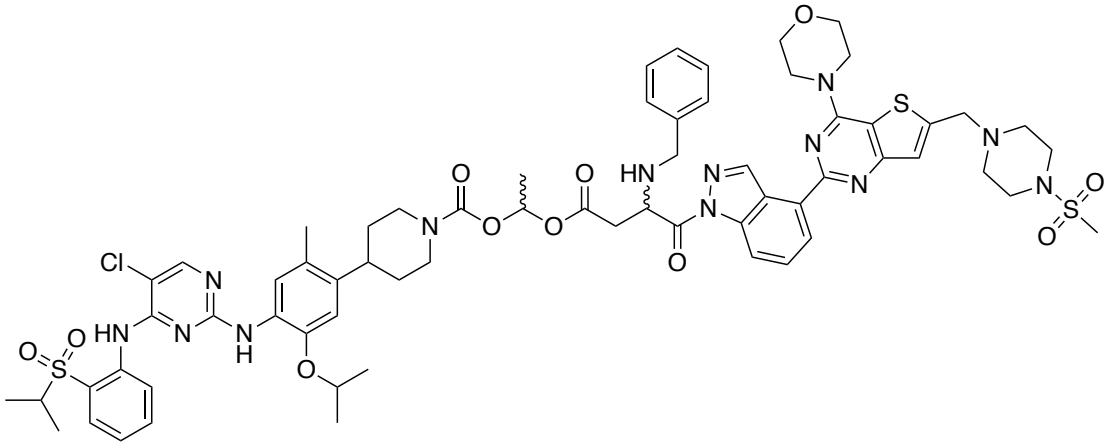
To a stirred solution of 1-chloroethyl 4-(4-((5-chloro-4-((2-(isopropylsulfonyl) phenyl)amino)pyrimidin-2-yl)amino)-5-isopropoxy-2-methylphenyl)piperidine-1-carboxylate (50 mg, 75µmol) in toluene (10 mL) was added 3-(benzylamino)-4-(benzyloxy)-4-oxobutanoic acid (21 mg, 90 µmol), Ag2O (21 mg, 90 µmol) and tertbutylammonium bromide (5 mg, 15 µmol). The reaction was stirred at room temperature for 1 h before heating at 65 °C overnight. The reaction mixture was then absorbed onto silica gel and purified by flash column chromatography, eluting with 10 - 50% ethyl acetate in petroleum ether to give the product as a beige oil (55 mg, 78%). ^{1}H NMR (400 MHz, $CDCl_3$) δ 9.53 (s, 1H), 8.60 (d, *J* = 8.3 Hz, 1H), 8.18 (s, 1H), 8.05 (s, 1H), 7.96 (dd, *J* = 8.0, 1.7 Hz, 1H), 7.78 – 7.71 (m, 2H), 7.64 (t, 1H), 7.60 – 7.51 (m, 2H), 7.40 – 7.36 (m, 4H), 7.33 – 7.22 (m, 4H), 6.91 – 6.84 (m, 1H), 6.72 (s, 1H), 5.22 – 5.17 (m, 2H), 4.57 (p, *J* = 6.1 Hz, 1H), 4.46 – 4.04 (m, 4H), 3.93 – 3.84 (m, 1H), 3.81 – 3.69 (m, 2H), 3.29 (p, *J* = 6.8 Hz, 1H), 3.02 – 2.69 (m, 2H), 2.19 (s, 3H), 1.90 – 1.63 (m, 6H), 1.44 – 1.13 (m, 15H). LCMS (m/z): calc'd for $C_{49}H_{57}ClN_6O_9S$ $[M + H]^+$ 941.4 found 941.5, r.t. 2.96.

2-(benzylamino)-4-(1-((4-(4-((5-chloro-4-((2-(isopropylsulfonyl)phenyl)amino) pyrimidin-2-yl)amino)-5-isopropoxy-2-methylphenyl)piperidine-1-carbonyl)oxy) ethoxy)-4-oxobutanoic acid



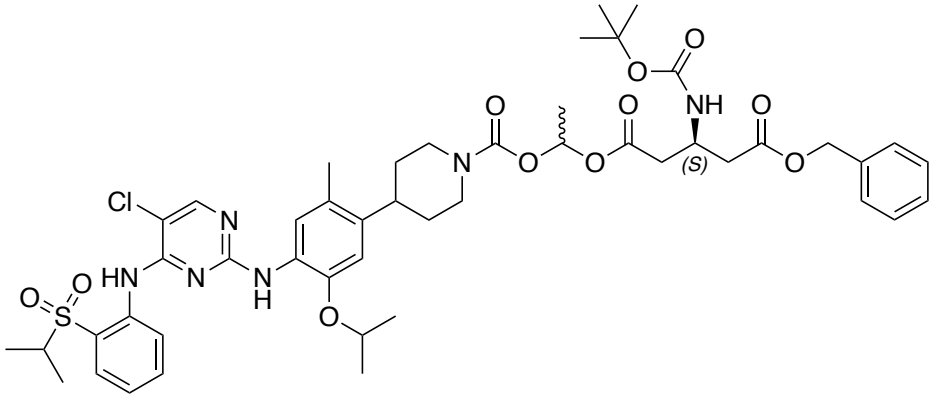
To a solution of 1-benzyl 4-(1-((4-(4-((5-chloro-4-((2-(isopropylsulfonyl)phenyl) amino)pyrimidin-2-yl)amino)-5-isopropoxy-2-methylphenyl)piperidine-1-carbonyl) oxy)ethyl) benzylaspartate (55 mg, 59 μmol) in ethyl acetate (3 mL) was added Pd/C (10 mg) as a suspension in ethyl acetate. The reaction was stirred under an atmosphere of hydrogen for 3 h after which time the reaction was filtered and solvent removed *in vacuo* to give a white foam (50 mg, 90%). The compound was used without further purification. LCMS (m/z): calc'd for $C_{42}H_{51}ClN_6O_9S$ $[M + H]^+$ 851.3 found 851.2, r.t. 3.20.

1-((3-(benzylamino)-4-(4-(6-((4-(methylsulfonyl)piperazin-1-yl)methyl)-4-morpholinothieno[3,2-d]pyrimidin-2-yl)-1H-indazol-1-yl)-4-oxobutanoyl)oxy)ethyl 4-(4-((5-chloro-4-((2-(isopropylsulfonyl)phenyl)amino)pyrimidin-2-yl)amino)-5-isopropoxy-2-methylphenyl)piperidine-1-carboxylate (AEG-165)



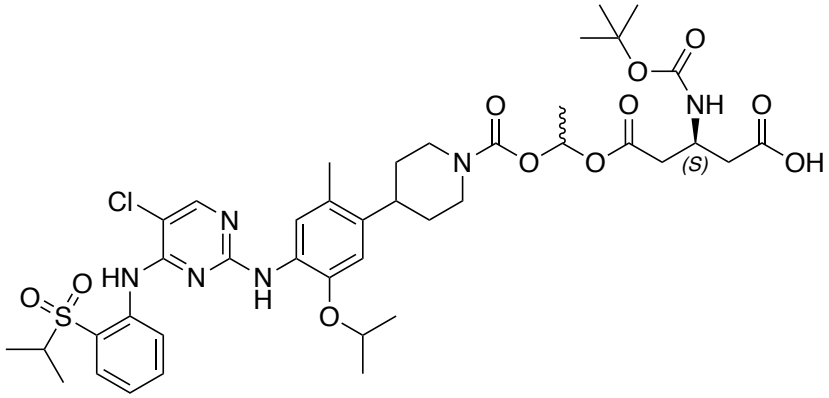
To a stirred solution of 2-(benzylamino)-4-(1-((4-(4-((5-chloro-4-((2-(isopropylsulfonyl)phenyl)amino)pyrimidin-2-yl)amino)-5-isopropoxy-2-methylphenyl)piperidine-1-carbonyl)oxy)ethoxy)-4-oxobutanoic acid (50 mg, 53 μmol) in DMF (2 mL) was added HATU (23 mg, 58 μmol), 4-(2-(1H-in- dazol-4-yl)-6-((4-(methylsulfonyl) piperazin-1-yl)methyl)thieno[3,2- d]pyrimidin-4-yl)morpholine (27 mg, 53 μmol), and DIPEA (27 μL, 159 mmol). After 2.5 h the reaction mixture showed formation of the product however purification by prep HPLC was not achieved due to release of 4-(2-(1H-in- dazol-4-yl)-6-((4-(methylsulfonyl)piperazin-1-yl)methyl)thieno[3,2- d]pyrimidin-4-yl)morpholine during isolation. LCMS (m/z): calc'd for $C_{65}H_{76}ClN_{13}O_{11}S_3$ $[M + H]^+$ 1346.5 found 1346.2 $[M + H]^+$, r.t. 3.54.

1-benzyl 5-(1-((4-(4-((5-chloro-4-((2-(isopropylsulfonyl)phenyl)amino)pyrimidin-2-yl)amino)-5-isopropoxy-2-methylphenyl)piperidine-1-carbonyl)oxy)ethyl) (3S)-3-((tert-butoxycarbonyl)amino)pentanedioate



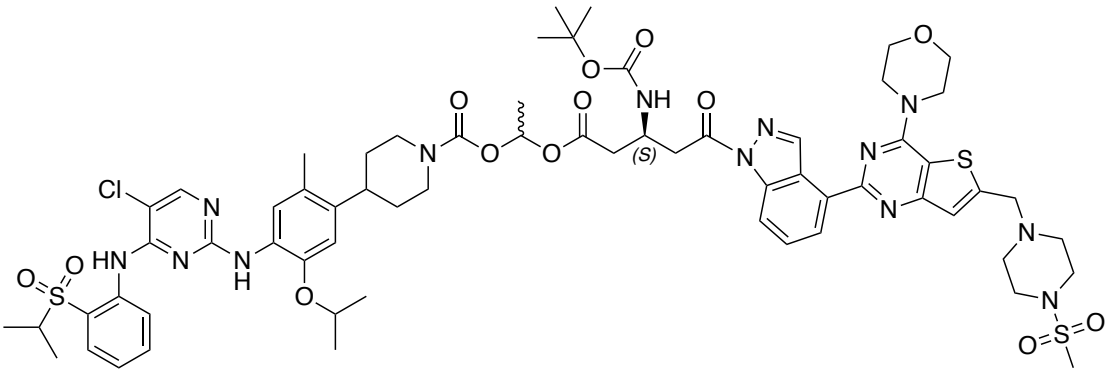
To a precooled (-10 °C) solution of 5-chloro-N_2-(2-isopropoxy-5-methyl-4-(piperidin-4-yl)phenyl)-N_4-(2-(isopropylsulfonyl)phenyl)pyrimidine-2,4-diamine (150 mg , 0.27 mmol) in CH_2Cl_2 (4 mL) was added NMM (67 µL, 0.60 mmol) then ACE-Cl (32 µL, 0.30 mmol). The reaction was allowed to warm to room temperature and stirred for a further 1.5 h after which time the reaction mixture was poured onto HCl (2 M, 30 mL) and extracted with CH_2Cl_2 (3 x 30 mL). The combined organics were dried ($MgSO_4$), filtered, and solvent removed *in vacuo* to give an orange residue which was taken up in toluene. (R)-5-(benzyloxy)-3-((tert-butoxycarbonyl)amino)-5-oxopentanoic acid (109 mg, 0.32 mmol), Ag_2O (75 mg, 0.32 mmol) and tertbutylammonium bromide (18 mg, 0.05 mmol) were added, and the reaction stirred at room temperature for 1 h before heating at 65 °C overnight. The reaction mixture was then absorbed onto silica gel and purified by flash column chromatography, eluting with 10 - 50% ethyl acetate in petroleum ether to give the product as a beige oil (67 mg, 26%). ^{1}H NMR (400 MHz, $CDCl_3$) δ 9.53 (s, 1H), 8.60 (d, *J* = 8.5 Hz, 1H), 8.18 (s, 1H), 8.05 (s, 1H), 7.96 (d, *J* = 8.1 Hz, 1H), 7.65 (t, *J* = 7.8 Hz, 1H), 7.59 – 7.54 (m, 1H), 7.37 (s, 6H), 6.89 – 6.84 (m, 1H), 6.75 – 6.70 (m, 1H), 5.32 (s, 1H), 5.15 (s, 2H), 4.60 – 4.55 (m, 1H), 4.44 – 4.16 (m, 3H), 3.68 – 3.64 (m, 1H), 3.49 – 3.45 (m, 1H), 3.29 (p, *J* = 7.0 Hz, 1H), 2.86 – 2.81 (m, 6H), 2.80 – 2.67 (m, 4H), 2.19 (s, 3H), 1.79 – 1.75 (m, 3H), 1.68 – 1.02 (m, 20H). LCMS (m/z): calc'd for $C_{48}H_{61}ClN_6O_{11}S$ $[M + H]^+$ 965.4 found 965.8, r.t. 3.50.

(3S)-3-((tert-butoxycarbonyl)amino)-5-(1-((4-(4-((5-chloro-4-((2-(isopropylsulfonyl)phenyl)amino)pyrimidin-2-yl)amino)-5-isopropoxy-2-methylphenyl)piperidine-1-carbonyl)oxy)ethoxy)-5-oxopentanoic acid



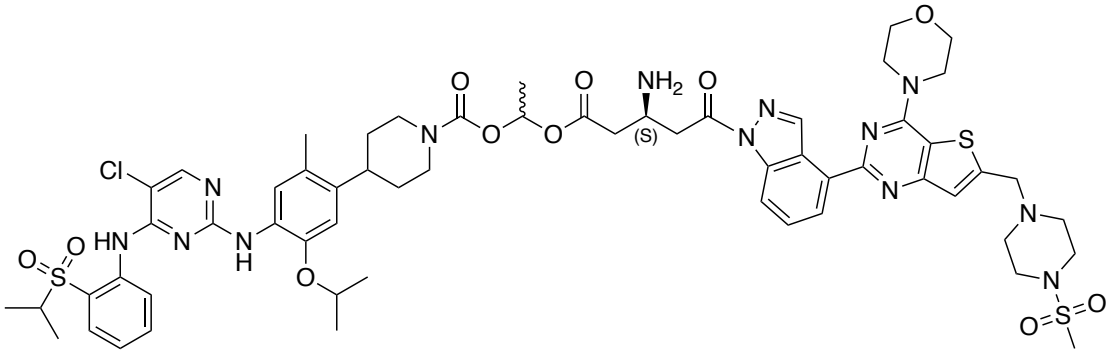
To a solution of 1-benzyl 5-(1-((4-(4-((5-chloro-4-((2-(isopropylsulfonyl)phenyl)amino)pyrimidin-2-yl)amino)-5-isopropoxy-2-methylphenyl)piperidine-1-carbonyl)oxy)ethyl) (3S)-3-((tert-butoxycarbonyl)amino)pentanedioate (67 mg, 69 μmol) in ethyl acetate (3 mL) was added Pd/C (15 mg) as a suspension in ethyl acetate. The reaction was stirred under an atmosphere of hydrogen for 3 h after which time the reaction was filtered and solvent removed *in vacuo* to give a white foam (50 mg, 83%). The compound was used without further purification. LCMS (m/z): calc'd for $C_{41}H_{55}ClN_6O_{11}S$ $[M + H]^+$ 875.3 found 875.5 , r.t. 3.50.

1-(((S)-3-((tert-butoxycarbonyl)amino)-5-(4-(6-((4-(methylsulfonyl)piperazin-1-yl)methyl)-4-morpholinothieno[3,2-d]pyrimidin-2-yl)-1H-indazol-1-yl)-5-oxopentanoyl)oxy)ethyl 4-(4-((5-chloro-4-((2-(isopropylsulfonyl)phenyl)amino)pyrimidin-2-yl)amino)-5-isopropoxy-2-methylphenyl)piperidine-1-carboxylate (AEG-286)



To a stirred solution of 2(3S)-3-((tert-butoxycarbonyl)amino)-5-(1-((4-(4-((5-chloro-4-((2-(isopropylsulfonyl)phenyl)amino)pyrimidin-2-yl)amino)-5-isopropoxy-2-methylphenyl)piperidine-1-carbonyl)oxy)ethoxy)-5-oxopentanoic acid (50 mg, 57 μmol) in DMF (2 mL) was added HATU (24 mg, 63 μmol), 4-(2-(1H-in- dazol-4-yl)-6-((4-(methylsulfonyl)piperazin-1-yl)methyl)thieno[3,2-d]pyrimidin-4-yl) morpholine (30 mg, 57 μmol), and DIPEA (30 μL, 171 mmol). After 2.5 h the reaction mixture was directly purified by preperative HPLC, method A, and was freeze dried to give a white solid (4.5 mg, 5%). ^{1}H NMR (800 MHz, $CDCl_3$) δ 9.54 (s, 1H), 9.21 – 9.19 (m, 1H), 8.62 – 8.58 (m, 1H), 8.58 – 8.56 (m, 1H), 8.45 – 8.43 (m, 1H), 8.18 (s, 1H), 8.05 – 8.02 (m, 1H), 7.96 (d, J = 7.7 Hz, 1H), 7.69 – 7.67 (m, 1H), 7.66 – 7.61 (m, 1H), 7.58 – 7.56 (m, 1H), 6.92 – 6.89 (m, 1H), 6.78 – 6.70 (m, 1H), 5.67 – 5.51 (m, 1H), 4.66 – 4.63 (m, 1H), 4.58 – 4.56 (m, 1H), 4.34 – 4.31 (m, 1H), 4.27 – 4.25 (m, 1H), 4.12 – 4.08 (m, 3H), 3.97 – 3.92 (m, 6H), 3.74 – 3.72 (m, 1H), 3.60 – 3.58 (m, 1H), 3.35 – 3.33 (m, 4H), 3.29 (p, J = 6.9 Hz, 1H), 2.94 – 2.92 (m, 2H), 2.85 (s, 3H), 2.74 – 2.71 (m, 4H), 2.18 (d, J = 6.0 Hz, 3H), 1.78 – 1.75 (m, 2H), 1.71 – 1.12 (m, 32H). LCMS (m/z): calc'd for $C_{64}H_{80}ClN_{13}O_{13}S_3$ $[M + H]^+$ 1370.5 found 1370.5 , r.t. 3.44. HRMS (m/z): calc'd for $C_{64}H_{80}ClN_{13}O_{13}S_3$ $[M - H]^-$. 1368.4849 found 1368.4768.

1-(((S)-3-amino-5-(4-(6-((4-(methylsulfonyl)piperazin-1-yl)methyl)-4-morpholinothieno[3,2-d]pyrimidin-2-yl)-1H-indazol-1-yl)-5-oxopentanoyl)oxy)ethyl 4-(4-((5-chloro-4-((2-(isopropylsulfonyl)phenyl)amino)pyrimidin-2-yl)amino)-5-isopropoxy-2-methylphenyl)piperidine-1-carboxylate (AEG-286_deprotected)



1-(((S)-3-((tert-butoxycarbonyl)amino)-5-(4-(6-((4-(methylsulfonyl)piperazin-1-yl)methyl)-4-morpholinothieno[3,2-d]pyrimidin-2-yl)-1H-indazol-1-yl)-5-oxopentanoyl)oxy)ethyl 4-(4-((5-chloro-4-((2-(isopropylsulfonyl)phenyl)amino)pyrimidin-2-yl)amino)-5-isopropoxy-2-methylphenyl)piperidine-1-carboxylate (250 µg, 0.18 µmol) was taken up in TFA (20 µL, 20% v:v in CH_2Cl_2) and sonicated. After 5 mins, the solvent and TFA were removed *in vacuo* and the residual solid was triturated with diethyl ether to give a white solid (232 µg, 100%). LCMS (m/z): calc'd for $C_{59}H_{72}ClN_{13}O_{13}S_3$ 1270.5 $[M + H]^+$ found 1270.6 , r.t. 2.58, 100% purity. HRMS (m/z): calc'd for $C_{59}H_{72}ClN_{13}O_{13}S_3$ $[M + H]^+$ 1270.4325 found 1270.4363 .

7. References

7.1 Bibliography

1 *Cancer Rese*arch UK: http://www.cancerresearchuk.org (accessed August, 2018).

2 American Cancer Society http://www.cancer.org. (accessed June, 2016).

3 NHS Choices http://www.nhs.uk/Conditions/Cancer-of-the-lung/Pages/Introduction.aspx (accessed June, 2016).

4 National Cancer Institute: http://www.cancer.gov/about-cancer/treatment/drugs/lung#1 (accessed June, 2016).

5 Pao, W.; Hutchinson, K. E. Chipping Away at the *Lung Cancer* Genome. *Nat. Med.* **2012**, 18 (3), 349–351.

6 Chiarle, R.; Voena, C.; Ambrogio, C.; Piva, R.; Inghirami, G. The Anaplastic Lymphoma Kinase in the Pathogenesis of Cancer. *Nat. Rev. Cancer* **2008**, 8 (1), 11–23.

7 Hallberg, B.; Palmer, R. H. Mechanistic Insight into ALK Receptor Tyrosine Kinase in Human Cancer Biology. *Nat. Rev. Cancer* **2013**, 13 (10), 685–700.

8 Tabbò, F.; Pizzi, M.; Kyriakides, P. W.; Ruggeri, B. Oncogenic Kinase Fusions : An Evolving Arena with Innovative Clinical Opportunities. *Oncotarget* **2015**, 7 (18), 25064–25086.

9 Soda, M.; Choi, Y. L.; Enomoto, M.; Takada, S.; Yamashita, Y.; Ishikawa, S.; Fujiwara, S.; Watanabe, H.; Kurashina, K.; Hatanaka, H.; et al. Identification of the Transforming EML4–ALK Fusion Gene in Non-Small-Cell *Lung Cancer*. *Nature* **2007**, 448 (7153), 561–566.

10 Li, C.; Fang, R.; Sun, Y.; Han, X.; Li, F.; Gao, B.; Iafrate, A. J.; Liu, X. Y.; Pao, W.; Chen, H.; et al. Spectrum of Oncogenic Driver Mutations in Lung Adenocarcinomas from East Asian Never Smokers. *PLoS One* **2011**, 6 (11), 2–7.

11 Bayliss, R.; Choi, J.; Fennell, D. A.; Fry, A. M.; Richards, M. W. Molecular Mechanisms That Underpin EML4-ALK Driven Cancers and Their Response to Targeted Drugs. *Cell*. Mol. Life Sci. **2016**, 73 (6), 1209–1224.

12 Roskoski, R. Anaplastic Lymphoma Kinase (ALK): Structure, Oncogenic Activation, and Pharmacological Inhibition. *Pharmacol. Res*. **2013**, 68 (1), 68–94.

13 Palmer, R. H.; Vernersson, E.; Grabbe, C.; Hallberg, B. Anaplastic Lymphoma Kinase: Signalling in Development and Disease. *Biochem. J*. **2009**, 420 (3), 345–361.

14 Rothschild, S. I.; Gautschi, O. Crizotinib in the Treatment of Non Small-Cell *Lung Cancer*. Clin. *Lung Cancer* **2013**, 14 (5), 473–480.

15 Awad, M. M.; Shaw, A. T. ALK Inhibitors in Non-Small *Cell Lung Cancer*: Crizotinib and Beyond. *Clin. Adv. Hematol. Oncol.* **2014**, 12 (7), 429–439.

16 FDA : http://www.fda.gov/Drugs/InformationOnDrugs/ApprovedDrugs/ucm376058.htm (accessed June 2016).

17 Holohan, C.; Van Schaeybroeck, S.; Longley, D. B.; Johnston, P. G. Cancer Drug Resistance: An Evolving Paradigm. *Nat. Rev. Cancer* **2013**, 13 (10), 714–726.

18 Marsilje, T. H.; Pei, W.; Chen, B.; Lu, W.; Uno, T.; Jin, Y.; Jiang, T.; Kim, S.; Li, N.; Warmuth, M.; et al. Synthesis, Structure–Activity Relationships, and in Vivo Efficacy of the Novel Potent and Selective Anaplastic Lymphoma Kinase (ALK) Inhibitor 5-Chloro- N 2-(2-Isopropoxy-5-Methyl-4-(Piperidin-4-Yl)Phenyl)- N 4-(2-(Isopropylsulfonyl)Phenyl)Pyrimidine-2,4-. *J. Med. Chem.* **2013**, 56 (14), 5675–5690.

19 Friboulet, L.; Li, N.; Katayama, R.; Lee, C. C.; Gainor, J. F.; Crystal, A. S.; Michellys, P.-Y.; Awad, M. M.; Yanagitani, N.; Kim, S.; et al. The ALK Inhibitor Ceritinib Overcomes Crizotinib Resistance in Non-Small-Cell-Lung-Cancer. *Cancer Discov.* **2014**, 4 (6), 662–673.

20 Shaw, A. T.; Kim, D.-W.; Mehra, R.; Tan, D. S. W.; Felip, E.; Chow, L. Q. M.; Camidge, D. R.; Vansteenkiste, J.; Sharma, S.; De Pas, T.; et al. Ceritinib in ALK -Rearranged Non–Small-Cell-Lung-Cancer. *N. Engl. J. Med.* **2014**, 370 (13), 1189–1197.

21 Kim, E.; Burns, M. Profile of Ceritinib in the Treatment of ALK+ Metastatic Non-Small-Cell-Lung-Cancer. *Lung Cancer Targets Ther*. **2015**, 35.

22 FDA: http://www.fda.gov/drugs/informationondrugs/approveddrugs/ucm395386.htm (accessed June 2016).

23 Santarpia, M.; Altavilla, G.; Rosell, R. Alectinib: A Selective, next-Generation ALK Inhibitor for Treatment of ALK-Rearranged Non-Small-Cell-Lung-Cancer. *Expert Rev. Respir. Med.* **2015**, 9 (3), 255–268.

24 FDA: http://www.fda.gov/NewsEvents/Newsroom/PressAnnouncements/ucm476926.htm (accessed June 2016).

25 Johnson, T. W.; Richardson, P. F.; Bailey, S.; Brooun, A.; Burke, B. J.; Collins, M. R.; Cui, J. J.; Deal, J. G.; Deng, Y.; Dinh, D.; et al. Discovery of (10 R)-7-Amino-12-Fluoro-2,10,16-Trimethyl-15-Oxo-10,15,16,17-Tetrahydro- 2H -8,4-(Metheno)Pyrazolo[4,3- h][2,5,11]-Benzoxadiazacyclotetradecine-3-Carbonitrile (PF-06463922), a Macrocyclic Inhibitor of Anaplastic Lymphoma Kinase (ALK) and C. *J. Med. Chem.* **2014**, 57 (11), 4720–4744.

26 Huang, W.-S.; Liu, S.; Zou, D.; Thomas, M.; Wang, Y.; Zhou, T.; Romero, J.; Kohlmann, A.; Li, F.; Qi, J.; et al. Discovery of Brigatinib (AP26113), a Phosphine Oxide-Containing, Potent, Orally Active Inhibitor of Anaplastic Lymphoma Kinase. *J. Med. Chem.* **2016**, 59 (10), 4948–4964.

27 Dong, X.; Fernandez-Salas, E.; Li, E.; Wang, S. Elucidation of Resistance Mechanisms to Second-Generation ALK Inhibitors Alectinib and Ceritinib in Non–Small-Cell-Lung-Cancer-Cells. *Neoplasia* **2016**, 18 (3), 162–171.

28 Doebele, R. C.; Pilling, A. B.; Aisner, D. L.; Kutateladze, T. G.; Le, A. T.; Weickhardt, A. J.; Kondo, K. L.; Linderman, D. J.; Heasley, L. E.; Franklin, W. A.; et al. Mechanisms of Resistance to Crizotinib in Patients with ALK Gene Rearranged Non–Small-Cell-Lung-Cancer. *Clin. Cancer Res.* **2012**, 18 (5), 1472–1482.

29 Camidge, D. R.; Doebele, R. C. Treating ALK-Positive *Lung Cancer*—Early Successes and Future Challenges. *Nat. Rev. Clin. Oncol.* **2012**, 9 (5), 268–277.

30 Crystal, A. S.; Shaw, A. T.; Sequist, L. V; Friboulet, L.; Niederst, M. J.; Lockerman, E. L.; Frias, R. L.; Gainor, J. F.; Amzallag, A.; Greninger, P.; et al. Patient-Derived Models of Acquired Resistance Can Identify Effective Drug Combinations for Cancer. *Science* **2014**, 346 (6216), 1480–1486.

31 Santarpia, M.; Gil, N.; Rosell, R. Strategies to Overcome Resistance to Tyrosine Kinase Inhibitors in Non-Small-Cell-Lung-Cancer. *Expert Rev. Clin. Pharmacol.* **2015**, 8 (4), 461–477.

32 Zhou, B.; Cox, A. D. Up-Front Polytherapy for ALK-Positive-Lung-Cancer. *Nat. Med.* **2015**, 21 (9), 974–975.

33 Lovly, C. M.; Shaw, A. T. Molecular Pathways: Resistance to Kinase Inhibitors and Implications for Therapeutic Strategies. *Clin. Cancer Res.* **2014**, 20 (9), 2249–2256.

34 Kuwano, M.; Sonoda, K.; Murakami, Y.; Watari, K.; Ono, M. Overcoming Drug Resistance to Receptor Tyrosine Kinase Inhibitors: Learning from *Lung Cancer*. Pharmacol. Ther. **2016**, 161, 97–110.

35 Knight, Z. A.; Lin, H.; Shokat, K. M. Targeting the Cancer Kinome through Polypharmacology. *Nat. Rev. Cancer* **2010**, 10 (2), 130–137.

36 Hopkins, A. L. Network Pharmacology: The next Paradigm in Drug Discovery. *Nat. Chem. Biol.* **2008**, 4 (11), 682–690.

37 Webb, J. L. Effect of More than One Inhibitor, Antagonism. Summation, and Synergism. In Enzyme and Metabolic Inhibitors.; Academic Press: New York, 1963; pp 488–512.

38 Chou, T.; Talalay, P. Quantitative Dose-Effect Relationships : The Combined Effects of Multiple Drug or Enzyme Inhibitors. *Adv. Enzym. Regul*. **1984**, 22, 27–55.

39 Chou, T.; Kurin, E.; Mučaji, P.; Nagy, M.; Hidalgo, M.; Sánchez-Moreno, C.; de Pascual-Teresa, S.; Iacopini, P.; Baldi, M.; Storchi, P.; et al. Theoretical Basis, Experimental Design, and Computerized Simulation of Synergism and Antagonism in Drug Combination Studies. *J. Food Compos. Anal.* **2010**, 67 (3), 621–681.

40 Chou, T.-C. Drug Combination Studies and Their *Synergy* Quantification Using the Chou-Talalay Method. *Cancer Res.* **2010**, 70 (2), 440–446.

41 Chou, T.-C. Frequently Asked Questions in Drug Combinations and the Mass-Action Law-Based Answers. *Synergy* **2014**, 1 (1), 3–21.

42 Yang, L.; Li, G.; Zhao, L.; Pan, F.; Qiang, J.; Han, S. Blocking the PI3K Pathway Enhances the Efficacy of ALK-Targeted Therapy in EML4-ALK-Positive Nonsmall-Cell-Lung-Cancer. *Tumor Biol.* **2014**, 35 (10), 9759–9767.

43 Garrett, J. T.; Chakrabarty, A.; Arteaga, C. L. Will PI3K Pathway Inhibitors Be Effective as Single Agents in Patients with Cancer? *Oncotarget* **2011**, 2 (12), 1314–1321.

44 Tanizaki, J.; Okamoto, I.; Takezawa, K.; Sakai, K.; Azuma, K.; Kuwata, K.; Yamaguchi, H.; Hatashita, E.; Nishio, K.; Janne, P. a; et al. Combined Effect of ALK and MEK Inhibitors in EML4–ALK-Positive Non-Small-Cell-Lung-Cancer-Cells. *Br. J. Cancer* **2012**, 106 (4), 763–767.

45 Hrustanovic, G.; Bivona, T. G. RAS Signaling in ALK Fusion *Lung Cancer*. *Small GTPases* **2016**, 7 (1), 32–33.

46 Zhou, B.; Cox, A. D. Up-Front Polytherapy for ALK-Positive *Lung Cancer*. *Nat. Med.* **2015**, 21 (9), 974–975.

47 Wilson, F. H.; Johannessen, C. M.; Piccioni, F.; Tamayo, P.; Kim, J. W.; Van Allen, E. M.; Corsello, S. M.; Capelletti, M.; Calles, A.; Butaney, M.; et al. A Functional Landscape of Resistance to ALK Inhibition in Lung-Cancer. *Cancer Cell* **2015**, 27 (3), 397–408.

48 Gower, A.; Hsu, W. H.; Hsu, S. T.; Wang, Y.; Giaccone, G. EMT Is Associated with, but Does Not Drive Resistance to ALK Inhibitors among EML4-ALK Non-Small *Cell Lung Cancer*. Mol. Oncol. **2016**, 10 (4), 601–609.

49 Wang, M.; Shen, A.; Zhang, C.; Song, Z.; Ai, J.; Liu, H.; Sun, L.; Ding, J.; Geng, M.; Zhang, A. Development of Heat Shock Protein (Hsp90) Inhibitors To Combat Resistance to Tyrosine Kinase Inhibitors through Hsp90–Kinase Interactions. *J. Med. Chem.* **2016**, 59 (12), 5563–5586.

50 Kindon, N.; Davis, A.; Dougall, I.; Dixon, J.; Johnson, T.; Walters, I.; Thom, S.; McKechnie, K.; Meghani, P.; Stocks, M. J. From UTP to AR-C11**8925**, the Discovery of a Potent Non Nucleotide Antagonist of the P2Y2receptor. *Bioorg. Med. Chem. Lett.* **2017**, 27 (21), 4849–4853.

51 Dehnhardt, C. M.; Venkatesan, A. M.; Delos Santos, E.; Chen, Z.; Santos, O.; Ayral-Kaloustian, S.; Brooijmans, N.; Mallon, R.; Hollander, I.; Feldberg, L.; et al. Lead Optimization of N-3-Substituted 7-Morpholinotriazolopyrimidines as Dual Phosphoinositide 3-Kinase/Mammalian Target of Rapamycin Inhibitors: Discovery of PKI-402. *J. Med. Chem.* **2010**, 53 (2), 798–810.

52 Folkes, A. J.; Ahmadi, K.; Alderton, W. K.; Alix, S.; Baker, S. J.; Box, G.; Chuckowree, I. S.; Clarke, P. A.; Depledge, P.; Eccles, S. A.; et al. The Identification of 2-(1 H -Indazol-4-Yl)-6-(4-Methanesulfonyl-Piperazin-1-Ylmethyl)-4-Morpholin-4-Yl-Thieno[3,2- d]Pyrimidine (GDC-0941) as a Potent, Selective, Orally Bioavailable Inhibitor of Class I PI3 Kinase for the Treatment of Can. *J. Med. Chem.* **2008**, 51 (18), 5522–5532.

53 Chuckowree, I.; Folkes, A.; Hancox, T.; Shuttleworth, S. Pharmaceutical Compounds, WO2007129161A2, 24 April 2006.

54 Seefeld M. A.; Rouse M. B.; Heerding D. A.; Peace S.; Yamashita D. S.; McNulty K. C. Invented are novel heterocyclic carboxamide compounds, the use of such compounds as inhibitors of protein kinase B activity and in the treatment of cancer and arthritis. WO2008098104 (A1), 18 November 2009.

55 Amzel, L. M.; Huang, C.-H.; Mandelker, D.; Lengauer, C.; Gabelli, S. B.; Vogelstein, B. Structural Comparisons of Class I Phosphoinositide 3-Kinases. *Nat. Rev. Cancer* **2008**, 8 (9), 665–669.

56 Leevers, S. J.; Vanhaesebroeck, B.; Waterfield, M. D. Signalling through Phosphoinositide 3-Kinases: The Lipids Take Centre Stage. Curr. Opin. *Cell Biol.* **1999**, 11 (2), 219–225.

57 Whitman, M.; Downes, C. P.; Keeler, M.; Keller, T.; Cantley, L. Type I Phosphatidylinositol Kinase Makes a Novel Inositol Phospholipid, Phosphatidylinositol-3-Phosphate. *Nature* **1988**, 332, 644.

58 Auger, K. R.; Serunian, L. A.; Soltoff, S. P.; Libby, P.; Cantley, L. C. PDGF-Dependent Tyrosine Phosphorylation Stimulates Production of Novel Polyphosphoinositides in Intact *Cells*. *Cell* **1989**, 57 (1), 167–175.

59 Ito, K.; Caramori, G.; Adcock, I. M. Therapeutic Potential of Phosphatidylinositol 3-Kinase Inhibitors in Inflammatory Respiratory Disease. *J. Pharmacol. Exp. Ther.* **2007**, 321 (1), 1–8.

60 Walker, E. H.; Perisic, O.; Ried, C.; Stephens, L.; Williams, R. L. Structural Insights into Phosphoinositide 3-Kinase Catalysis and Signalling. *Nature* **1999**, 402 (6759), 313–320.

61 Li, H.; Wu, X.; Hou, S.; Malek, M.; Kielkowska, A.; Noh, E.; Makondo, K. J.; Du, Q.; Wilkins, J. A.; Johnston, J. B.; et al. Phosphatidylinositol-3,4-Bisphosphate and Its Binding Protein Lamellipodin Regulate Chemotaxis of Malignant B Lymphocytes. *J. Immunol.* **2016**, 196 (2), 586 LP-595.

62 Backer, J. The Regulation and Function of Class III PI3Ks: Novel Roles for Vps34. *Biochem. J.* **2008**, 410 (1), 1–17.

63 Savitsky, K.; Bar-Shira, A.; Gilad, S.; Rotman, G.; Ziv, Y.; Vanagaite, L.; Tagle, D. A.; Smith, S.; Uziel, T.; Sfez, S.; et al. A Single Ataxia Telangiectasia Gene with a Product Similar to PI-3 Kinase. *Science* (80). **1995**, 268 (5218), 1749–1753.

64 Ito, K.; Caramori, G.; Adcock, I. M. Therapeutic Potential of Phosphatidylinositol 3-Kinase Inhibitors in Inflammatory Respiratory Disease. *J. Pharmacol. Exp. Ther.* **2007**, 321 (1), 1–8.

65 Walker, E. H.; Perisic, O.; Ried, C.; Stephens, L.; Williams, R. L. Structural Insights into Phosphoinositide 3-Kinase Catalysis and Signalling. *Nature* **1999**, 402 (6759), 313–320.

66 FDA: http://www.fda.gov/Drugs/InformationOnDrugs/ApprovedDrugs/ucm406410.htm (accessed June 2016)

67 Fowler, K.; Huang, D.; Kesicki, E.; Ooi, H. C.; Oliver, A. R.; Fuqiang, R.; Treiberg, J. Quinazolinones as inhibitors of human phosphatidylinositol 3-kinase delta, WO2005113556A1, 12 May 2005.

68 Winkler, D. G.; Faia, K. L.; Dinitto, J. P.; Ali, J. A.; White, K. F.; Brophy, E. E.; Pink, M. M.; Proctor, J. L.; Lussier, J.; Martin, C. M.; et al. Article PI3Kd and PI3Kg Inhibition by IPI-145 Abrogates Immune Responses and Suppresses Activity in Autoimmune and Inflammatory Disease Models. *Chem. Biol.* **2013**, 20 (11), 1364–1374.

69 Yap, T. A.; Bjerke, L.; Clarke, P. A.; Workman, P. Drugging PI3K in Cancer: Refining Targets and Therapeutic Strategies. *Curr. Opin. Pharmacol.* **2015**, 23, 98–107.

70 Wee, S.; Wiederschain, D.; Maira, S.-M.; Loo, A.; Miller, C.; deBeaumont, R.; Stegmeier, F.; Yao, Y.-M.; Lengauer, C. PTEN-Deficient Cancers Depend on PIK3CB. *Proc. Natl. Acad. Sci.* **2008**, 105 (35), 13057 LP-13062.

71 Certal, V.; Halley, F.; Virone-oddos, A.; Karlsson, A.; Rak, A.; Abecassis, P.; Lejeune, P.; Vincent, L.; Nicolas, J.; Bertrand, T.; et al. Discovery and Optimization of New Benzimidazole- and Benzoxazole-Pyrimidone Selective PI3K β Inhibitors for the Treatment of Phosphatase and TENsin Homologue (PTEN)-Deficient Cancers. *J. Med. Chem.* **2012**, 55, 4788–4805.

72 Traxler, P.; Furet, P. Strategies toward the Design of Novel and Selective Protein Tyrosine Kinase Inhibitors. *Pharmacol. Ther.* **1999**, 82 (98), 195–206.

73 Vlahos, C. J.; Matter, W. F.; Hui, K. Y.; Brown, R. F. A Specific Inhibitor of Phosphatidylinositol 3-Kinase, 2-(4-Morpholinyl)-8-Phenyl-4H-1-Benzopyran-4-One (LY294002). J. Biol. Chem. **1994**, 269 (7), 5241–5248.

74 Arcaro, A.; Wymann, M. P. Wortmannin Is a Potent Phosphatidylinositol 3-Kinase Inhibitor: The Role of Phosphatidylinositol 3,4,5-Trisphosphate in Neutrophil Responses. *Biochem. J.* **1993**, 296 (Pt 2) (Pt 2), 297–301.

75 Folkes, A. J.; Ahmadi, K.; Alderton, W. K.; Alix, S.; Baker, S. J.; Box, G.; Chuckowree, I. S.; Clarke, P. A.; Depledge, P.; Eccles, S. A.; et al. The Identification of 2-(1 H -Indazol-4-Yl)-6-(4-Methanesulfonyl-Piperazin-1-Ylmethyl)-4-Morpholin-4-Yl-Thieno[3,2- d]Pyrimidine (GDC-0941) as a Potent, Selective, Orally Bioavailable Inhibitor of Class I PI3 Kinase for the Treatment of Cancer. *J. Med. Chem.* **2008**, 51 (18), 5522–5532.

76 Hayakawa, M.; Kaizawa, H.; Moritomo, H.; Koizumi, T.; Ohishi, T.; Okada, M.; Ohta, M.; Tsukamoto, S.; Parker, P.; Workman, P.; et al. Synthesis and Biological Evaluation of 4-Morpholino-2-Phenylquinazolines and Related Derivatives as Novel PI3 Kinase P110α Inhibitors. *Bioorg. Med. Chem.* **2006**, 14 (20), 6847–6858.

77 Sutherlin, D. P.; Sampath, D.; Berry, M.; Castanedo, G.; Chang, Z.; Chuckowree, I.; Dotson, J.; Folkes, A.; Friedman, L.; Goldsmith, R.; et al. Discovery of (Thienopyrimidin-2-Yl)Aminopyrimidines as Potent, Selective, and Orally Available Pan-PI3-Kinase and Dual Pan-PI3-Kinase/MTOR Inhibitors for the Treatment of Cancer. *J. Med. Chem.* **2010**, 53 (3), 1086–1097.

78 Heffron, T. P.; Berry, M.; Castanedo, G.; Chang, C.; Chuckowree, I.; Dotson, J.; Folkes, A.; Gunzner, J.; Lesnick, J. D.; Lewis, C.; et al. Identification of GNE-477, a Potent and Efficacious Dual PI3K/MTOR Inhibitor. Bioorganic Med. Chem. Lett. **2010**, 20 (8), 2408–2411.

79 Safina, B. S.; Baker, S.; Baumgardner, M.; Blaney, P. M.; Chan, B. K.; Chen, Y. H.; Cartwright, M. W.; Castanedo, G.; Chabot, C.; Cheguillaume, A. J.; et al. Discovery of Novel PI3-Kinase δ Specific Inhibitors for the Treatment of Rheumatoid Arthritis: Taming CYP3A4 Time-Dependent Inhibition. *J. Med. Chem.* **2012**, 55 (12), 5887–5900.

80 Heffron, T. P.; Salphati, L.; Alicke, B.; Cheong, J.; Dotson, J.; Edgar, K.; Goldsmith, R.; Gould, S. E.; Lee, L. B.; Lesnick, J. D.; et al. The Design and Identification of Brain Penetrant Inhibitors of Phosphoinositide 3-Kinase α. *J. Med. Chem.* **2012**, 55 (18), 8007–8020.

81 Sutherlin, D. P.; Baker, S.; Bisconte, A.; Blaney, P. M.; Brown, A.; Chan, B. K.; Chantry, D.; Castanedo, G.; Depledge, P.; Goldsmith, P.; et al. Potent and Selective Inhibitors of PI3Kδ: Obtaining Isoform Selectivity from the Affinity Pocket and Tryptophan Shelf. *Bioorg. Med. Chem. Lett.* **2012**, 22 (13), 4296–4302.

82 Murray, J. M.; Sweeney, Z. K.; Chan, B. K.; Balazs, M.; Bradley, E.; Castanedo, G.; Chabot, C.; Chantry, D.; Flagella, M.; Goldstein, D. M.; et al. Potent and Highly Selective Benzimidazole Inhibitors of PI3-Kinase Delta. *J. Med. Chem.* **2012**, 55 (17), 7686–7695.

83 Safina, B. S.; Sweeney, Z. K.; Li, J.; Chan, B. K.; Bisconte, A.; Carrera, D.; Castanedo, G.; Flagella, M.; Heald, R.; Lewis, C.; et al. Identification of GNE-293, a Potent and Selective PI3Kδ Inhibitor: Navigating in Vitro Genotoxicity While Improving Potency and Selectivity. *Bioorg. Med. Chem. Lett.* **2013**, 23 (17), 4953–4959.

84 Heffron, T. P.; Ndubaku, C. O.; Salphati, L.; Alicke, B.; Cheong, J.; Drobnick, J.; Edgar, K.; Gould, S. E.; Lee, L. B.; Lesnick, J. D.; et al. Discovery of Clinical Development Candidate GDC-**0084**, a Brain Penetrant Inhibitor of PI3K and MTOR. *ACS Med. Chem. Lett.* **2016**, 7 (4), 351–356.

85 Qian, C.; Lai, C.-J.; Bao, R.; Wang, D.-G.; Wang, J.; Xu, G.-X.; Atoyan, R.; Qu, H.; Yin, L.; Samson, M.; et al. Cancer Network Disruption by a Single Molecule Inhibitor Targeting Both Histone Deacetylase Activity and Phosphatidylinositol 3-Kinase Signaling. *Clin. Cancer Res.* **2012**, 18 (15), 4104–4113.

86 Wang, J.; Wang, X.; Chen, Y.; Chen, S.; Chen, G.; Tong, L.; Meng, L.; Xie, Y.; Ding, J.; Yang, C. Discovery and Bioactivity of 4-(2-Arylpyrido[3',2':3,4] Pyrrolo[1,2-f][1,2,4]Triazin-4-Yl) Morpholine Derivatives as Novel PI3K Inhibitors. *Bioorg. Med. Chem. Lett.* **2012**, 22 (1), 339–342.

87 Martinez Gonzalez, S.; Rodriguez-Aristegui, S.; Hernandez, A. I.; Varela, C.; Gonzalez Cantalapiedra, E.; Alvarez, R. M.; Rodriguez Hergueta, A.; Bischoff, J. R.; Albarran, M. I.; Cebria, A.; et al. Generation of Tricyclic Imidazo[1,2-a]Pyrazines as Novel PI3K Inhibitors by Application of a Conformational Restriction Strategy. *Bioorg. Med. Chem. Lett.* **2017**, 27 (11), 2536–2543.

88 Martínez González, S.; Hernández, A. I.; Álvarez, R. M.; Rodríguez, A.; Ramos-Lima, F.; Bischoff, J. R.; Albarrán, M. I.; Cebriá, A.; Hernández-Encinas, E.; García-Arocha, J.; et al. Identification of Novel PI3K Inhibitors through a Scaffold Hopping Strategy. *Bioorg. Med. Chem. Lett.* **2017**, 27 (21), 4794–4799.

89 Hart, S.; Novotny-Diermayr, V.; Goh, K. C.; Williams, M.; Tan, Y. C.; Ong, L. C.; Cheong, A.; Ng, B. K.; Amalini, C.; Madan, B.; et al. VS-**5584**, a Novel and Highly Selective PI3K/MTOR Kinase Inhibitor for the Treatment of Cancer. *Mol. Cancer Ther.* **2013**, 12 (2), 151–161.

90 Nacht, M.; Qiao, L.; Sheets, M. P.; St. Martin, T.; Labenski, M.; Mazdiyasni, H.; Karp, R.; Zhu, Z.; Chaturvedi, P.; Bhavsar, D.; et al. Discovery of a Potent and Isoform-Selective Targeted Covalent Inhibitor of the Lipid Kinase PI3Kα. *J. Med. Chem.* **2013**, 56 (3), 712–721.

91 Saurat, T.; Buron, F.; Rodrigues, N.; de Tauzia, M.-L.; Colliandre, L.; Bourg, S.; Bonnet, P.; Guillaumet, G.; Akssira, M.; Corlu, A.; et al. Design, Synthesis, and Biological Activity of Pyridopyrimidine Scaffolds as Novel PI3K/MTOR Dual Inhibitors. *J. Med. Chem.* **2014**, 57 (3), 613–631.

92 Dugar, S.; Hollinger, F. P.; Kuila, B.; Arora, R.; Sen, S.; Mahajan, D. Synthesis and Evaluation of Pyrrolotriazine Based Molecules as PI3 Kinase Inhibitors. *Bioorg. Med. Chem. Lett.* **2015**, 25 (16), 3142–3146.

93 Wang, X.-M.; Xin, M.-H.; Xu, J.; Kang, B.-R.; Li, Y.; Lu, S.-M.; Zhang, S.-Q. Synthesis and Antitumor Activities Evaluation of M-(4-Morpholinoquinazolin-2-Yl)Benzamides in Vitro and in Vivo. Eur. *J. Med. Chem.* **2015**, 96, 382–395.

94 Xu, S.; Sun, C.; Chen, C.; Zheng, P.; Zhou, Y.; Zhou, H.; Zhu, W. Synthesis and Biological Evaluation of Novel 8-Morpholinoimidazo[1,2-a]Pyrazine Derivatives Bearing Phenylpyridine/Phenylpyrimidine-Carboxamides. *Molecules* **2017**, 22 (2), 310.

95 Yaguchi, S.; Fukui, Y.; Koshimizu, I.; Yoshimi, H.; Matsuno, T.; Gouda, H.; Hirono, S.; Yamazaki, K.; Yamori, T. Antitumor Activity of ZSTK474, a New Phosphatidylinositol 3-Kinase Inhibitor. JNCI *J. Natl. Cancer Inst.* **2006**, 98 (8), 545–556.

96 Berndt, A.; Miller, S.; Williams, O.; Le, D. D.; Houseman, B. T.; Pacold, J. I.; Gorrec, F.; Hon, W.; Ren, P.; Liu, Y.; et al. The P110δ Structure: Mechanisms for Selectivity and Potency of New PI(3)K Inhibitors. *Nat. Chem. Biol.* **2010**, 6 (2), 117–124.

97 Burger, M. T.; Pecchi, S.; Wagman, A.; Ni, Z.-J.; Knapp, M.; Hendrickson, T.; Atallah, G.; Pfister, K.; Zhang, Y.; Bartulis, S.; et al. Identification of NVP-BKM120 as a Potent, Selective, Orally Bioavailable Class I PI3 Kinase Inhibitor for Treating Cancer. *ACS Med. Chem. Lett.* **2011**, 2 (10), 774–779.

98 Burger, M. T.; Knapp, M.; Wagman, A.; Ni, Z.-J.; Hendrickson, T.; Atallah, G.; Zhang, Y.; Frazier, K.; Verhagen, J.; Pfister, K.; et al. Synthesis and in Vitro and in Vivo Evaluation of Phosphoinositide-3-Kinase Inhibitors. *ACS Med. Chem. Lett.* **2011**, 2 (1), 34–38.

99 Pecchi, S.; Renhowe, P. A.; Taylor, C.; Kaufman, S.; Merritt, H.; Wiesmann, M.; Shoemaker, K. R.; Knapp, M. S.; Ornelas, E.; Hendrickson, T. F.; et al. Identification and Structure-Activity Relationship of 2-Morpholino-6-(3-Hydroxyphenyl) Pyrimidines, a Class of Potent and Selective PI3 Kinase Inhibitors. *Bioorg. Med. Chem. Lett.* **2010**, 20 (23), 6895–6898.

100 Brachmann, S. M.; Kleylein-Sohn, J.; Gaulis, S.; Kauffmann, A.; Blommers, M. J. J.; Kazic-Legueux, M.; Laborde, L.; Hattenberger, M.; Stauffer, F.; Vaxelaire, J.; et al. Characterization of the Mechanism of Action of the Pan Class I PI3K Inhibitor NVP-BKM120 across a Broad Range of Concentrations. *Mol. Cancer Ther.* **2012**, 11 (8), 1747–1757.

101 Bohnacker, T.; Prota, A. E.; Beaufils, F.; Burke, J. E.; Melone, A.; Inglis, A. J.; Rageot, D.; Sele, A. M.; Cmiljanovic, V.; Cmiljanovic, N.; et al. Deconvolution of Buparlisib's Mechanism of Action Defines Specific PI3K and Tubulin Inhibitors for Therapeutic Intervention. *Nat. Commun*. **2017**, 8, 1–13.

102 Dehnhardt, C. M.; Venkatesan, A. M.; Delos Santos, E.; Chen, Z.; Santos, O.; Ayral-Kaloustian, S.; Brooijmans, N.; Mallon, R.; Hollander, I.; Feldberg, L.; et al. Lead Optimization of N-3-Substituted 7-Morpholinotriazolopyrimidines as Dual Phosphoinositide 3-Kinase/Mammalian Target of Rapamycin Inhibitors: Discovery of PKI-402. *J. Med. Chem.* **2010**, 53 (2), 798–810.

103 Miller, M. S.; Pinson, J.-A.; Zheng, Z.; Jennings, I. G.; Thompson, P. E. Regioselective Synthesis of 5- and 6-Methoxybenzimidazole-1,3,5-Triazines as Inhibitors of Phosphoinositide 3-Kinase. *Bioorg. Med. Chem. Lett.* **2013**, 23 (3), 802–805.

104 Dugar, S.; Hollinger, F. P.; Mahajan, D.; Sen, S.; Kuila, B.; Arora, R.; Pawar, Y.; Shinde, V.; Rahinj, M.; Kapoor, K. K.; et al. Discovery of Novel and Orally Bioavailable Inhibitors of PI3 Kinase Based on Indazole Substituted Morpholino-Triazines. *ACS Med. Chem. Lett.* **2015**, 6 (12), 1190–1194.

105 Gamage, S. A.; Giddens, A. C.; Tsang, K. Y.; Flanagan, J. U.; Kendall, J. D.; Lee, W. J.; Baguley, B. C.; Buchanan, C. M.; Jamieson, S. M. F.; Shepherd, P. R.; et al. Synthesis and Biological Evaluation of Sulfonamide Analogues of the Phosphatidylinositol 3-Kinase Inhibitor ZSTK474. *Bioorg. Med. Chem.* **2017**, 25 (20), 5859–5874.

106 Ohwada, J.; Ebiike, H.; Kawada, H.; Tsukazaki, M.; Nakamura, M.; Miyazaki, T.; Morikami, K.; Yoshinari, K.; Yoshida, M.; Kondoh, O.; et al. Discovery and Biological Activity of a Novel Class I PI3K Inhibitor, CH5132799. *Bioorg. Med. Chem. Lett.* **2011**, 21 (6), 1767–1772.

107 Kawada, H.; Ebiike, H.; Tsukazaki, M.; Nakamura, M.; Morikami, K.; Yoshinari, K.; Yoshida, M.; Ogawa, K.; Shimma, N.; Tsukuda, T.; et al. Lead Optimization of a Dihydropyrrolopyrimidine Inhibitor against Phosphoinositide 3-Kinase (PI3K) to Improve the Phenol Glucuronic Acid Conjugation. *Bioorg. Med. Chem. Lett.* **2013**, 23 (3), 673–678.

108 Kawada, H.; Ebiike, H.; Tsukazaki, M.; Yamamoto, S.; Koyama, K.; Nakamura, M.; Morikami, K.; Yoshinari, K.; Yoshida, M.; Ogawa, K.; et al. Modification of a Dihydropyrrolopyrimidine Phosphoinositide 3-Kinase (PI3K) Inhibitor to Improve Oral Bioavailability. *Bioorg. Med. Chem.* **2015**, 23 (24), 7650–7660.

109 Kawada, H.; Ebiike, H.; Tsukazaki, M.; Yamamoto, S.; Koyama, K.; Nakamura, M.; Morikami, K.; Yoshinari, K.; Yoshida, M.; Ogawa, K.; et al. Optimization of the Phenylurea Moiety in a Phosphoinositide 3-Kinase (PI3K) Inhibitor to Improve Water Solubility and the PK Profile by Introducing a Solubilizing Group and Ortho Substituents. *Bioorg. Med. Chem.* **2016**, 24 (13), 2897–2906.

110 Staben, S. T.; Siu, M.; Goldsmith, R.; Olivero, A. G.; Do, S.; Burdick, D. J.; Heffron, T. P.; Dotson, J.; Sutherlin, D. P.; Zhu, B.-Y.; et al. Structure-Based Design of Thienobenzoxepin Inhibitors of PI3-Kinase. *Bioorg. Med. Chem. Lett.* **2011**, 21 (13), 4054–4058.

111 Staben, S. T.; Siu, M.; Goldsmith, R.; Olivero, A. G.; Do, S.; Burdick, D. J.; Heffron, T. P.; Dotson, J.; Sutherlin, D. P.; Zhu, B.-Y.; et al. Structure-Based Design of Thienobenzoxepin Inhibitors of PI3-Kinase. *Bioorg. Med. Chem. Lett.* **2011**, 21 (13), 4054–4058.

112 Staben, S. T.; Ndubaku, C.; Blaquiere, N.; Belvin, M.; Bull, R. J.; Dudley, D.; Edgar, K.; Gray, D.; Heald, R.; Heffron, T. P.; et al. Discovery of Thiazolobenzoxepin PI3-Kinase Inhibitors That Spare the PI3-Kinase β Isoform. *Bioorg. Med. Chem. Lett.* **2013**, 23 (9), 2606–2613.

113 Heffron, T. P.; Heald, R. A.; Ndubaku, C.; Wei, B. Q.; Augistin, M.; Do, S.; Edgar, K.; Eigenbrot, C.; Friedman, L.; Gancia, E.; et al. The Rational Design of Selective Benzoxazepin Inhibitors of the α-Isoform of Phosphoinositide 3-Kinase Culminating in the Identification of (S)-2-((2-(1-Isopropyl-1H-1,2,4-Triazol-5-Yl)-5,6-Dihydrobenzo[f]Imidazo[1,2-d][1,4]Oxazepin-9-Yl)Oxy)Propanamide (. *J. Med. Chem.* **2016**, 59 (3), 985–1002.

114 Safina, B. S.; Elliott, R. L.; Forrest, A. K.; Heald, R. A.; Murray, J. M.; Nonomiya, J.; Pang, J.; Salphati, L.; Seward, E. M.; Staben, S. T.; et al. Design of Selective Benzoxazepin PI3Kδ Inhibitors Through Control of Dihedral Angles. *ACS Med. Chem. Lett.* **2017**, 8 (9), 936–940.

115 Bell, K.; Sunose, M.; Ellard, K.; Cansfield, A.; Taylor, J.; Miller, W.; Ramsden, N.; Bergamini, G.; Neubauer, G. SAR Studies around a Series of Triazolopyridines as Potent and Selective PI3Kγ Inhibitors. *Bioorg. Med. Chem. Lett.* **2012**, 22 (16), 5257–5263.

116 Sunose, M.; Bell, K.; Ellard, K.; Bergamini, G.; Neubauer, G.; Werner, T.; Ramsden, N. Discovery of 5-(2-Amino-[1,2,4]Triazolo[1,5-a]Pyridin-7-Yl)-N-(Tert-Butyl)Pyridine-3-Sulfonamide (CZC24758), as a Potent, Orally Bioavailable and Selective Inhibitor of PI3K for the Treatment of Inflammatory Disease. *Bioorg. Med. Chem. Lett.* **2012**, 22 (14), 4613–4618.

117 Bergamini, G.; Bell, K.; Shimamura, S.; Werner, T.; Cansfield, A.; Müller, K.; Perrin, J.; Rau, C.; Ellard, K.; Hopf, C.; et al. A Selective Inhibitor Reveals PI3Kγ Dependence of TH17 *Cell* Differentiation. *Nat. Chem. Biol.* **2012**, 8, 576.

118 Ellard, K.; Sunose, M.; Bell, K.; Ramsden, N.; Bergamini, G.; Neubauer, G. Discovery of Novel PI3Kγ/δ Inhibitors as Potential Agents for Inflammation. *Bioorg. Med. Chem. Lett.* **2012**, 22 (14), 4546–4549.

119 Oka, Y.; Yabuuchi, T.; Fujii, Y.; Ohtake, H.; Wakahara, S.; Matsumoto, K.; Endo, M.; Tamura, Y.; Sekiguchi, Y. Discovery and Optimization of a Series of 2-Aminothiazole-Oxazoles as Potent Phosphoinositide 3-Kinase γ Inhibitors. *Bioorg. Med. Chem. Lett.* **2012**, 22 (24), 7534–7538.

120 Oka, Y.; Yabuuchi, T.; Oi, T.; Kuroda, S.; Fujii, Y.; Ohtake, H.; Inoue, T.; Wakahara, S.; Kimura, K.; Fujita, K.; et al. Discovery of N-{5-[3-(3-Hydroxypiperidin-1-Yl)-1,2,4-Oxadiazol-5-Yl]-4-Methyl-1,3-Thiazol-2-Yl}acetamide (TASP0415914) as an Orally Potent Phosphoinositide 3-Kinase γ Inhibitor for the Treatment of Inflammatory Diseases. *Bioorg. Med. Chem.* **2013**, 21 (24), 7578–7583.

121 Bruce, I.; Akhlaq, M.; Bloomfield, G. C.; Budd, E.; Cox, B.; Cuenoud, B.; Finan, P.; Gedeck, P.; Hatto, J.; Hayler, J. F.; et al. Development of Isoform Selective PI3-Kinase Inhibitors as Pharmacological Tools for Elucidating the PI3K Pathway. *Bioorg. Med. Chem. Lett.* **2012**, 22 (17), 5445–5450.

122 Furet, P.; Guagnano, V.; Fairhurst, R. A.; Imbach-Weese, P.; Bruce, I.; Knapp, M.; Fritsch, C.; Blasco, F.; Blanz, J.; Aichholz, R.; et al. Discovery of NVP-BYL719 a Potent and Selective Phosphatidylinositol-3 Kinase Alpha Inhibitor Selected for Clinical Evaluation. *Bioorg. Med. Chem. Lett.* **2013**, 23 (13), 3741–3748.

123 Collier, P. N.; Martinez-Botella, G.; Cornebise, M.; Cottrell, K. M.; Doran, J. D.; Griffith, J. P.; Mahajan, S.; Maltais, F.; Moody, C. S.; Huck, E. P.; et al. Structural Basis for Isoform Selectivity in a Class of Benzothiazole Inhibitors of Phosphoinositide 3-Kinase γ. *J. Med. Chem.* **2015**, 58 (1), 517–521.

124 Collier, P. N.; Messersmith, D.; Le Tiran, A.; Bandarage, U. K.; Boucher, C.; Come, J.; Cottrell, K. M.; Damagnez, V.; Doran, J. D.; Griffith, J. P.; et al. Discovery of Highly Isoform Selective Thiazolopiperidine Inhibitors of Phosphoinositide 3-Kinase γ. *J. Med. Chem.* **2015**, 58 (14), 5684–5688.

125 Pemberton, N.; Mogemark, M.; Arlbrandt, S.; Bold, P.; Cox, R. J.; Gardelli, C.; Holden, N. S.; Karabelas, K.; Karlsson, J.; Lever, S.; et al. Discovery of Highly Isoform Selective Orally Bioavailable Phosphoinositide 3-Kinase (PI3K)-γ Inhibitors. *J. Med. Chem.* **2018**, 61 (12), 5435–5441.

126 Scott, W. J.; Hentemann, M. F.; Rowley, R. B.; Bull, C. O.; Jenkins, S.; Bullion, A. M.; Johnson, J.; Redman, A.; Robbins, A. H.; Esler, W.; et al. Discovery and SAR of Novel 2,3-Dihydroimidazo[1,2-c]Quinazoline PI3K Inhibitors: Identification of Copanlisib (BAY 80-6946). *ChemMedChem* **2016**, 11 (14), 1517–1530.

127 The European Medicines Agency https://www.ema.europa.eu/en/news/ema-reviews-cancer-medicine-zydelig (accessed December 2018).

128 Winkler, D. G.; Faia, K. L.; DiNitto, J. P.; Ali, J. A.; White, K. F.; Brophy, E. E.; Pink, M. M.; Proctor, J. L.; Lussier, J.; Martin, C. M.; et al. PI3K-δ and PI3K-γ Inhibition by IPI-145 Abrogates Immune Responses and Suppresses Activity in Autoimmune and Inflammatory Disease Models. *Chem. Biol.* **2013**, 20 (11), 1364–1374.

129 Federal Drug Agency https://www.cancer.gov/publications/dictionaries/cancer-drug/def/pi3k-delta-gamma-inhibitor-rp6530 (accessed Dec 2018).

130 Schwehm, C.; Lewis, W.; Blake, A. J.; Kellam, B.; Stocks, M. J. Preparation and Structural Analysis of (±)- Cis -Ethyl 2-Sulfanylidenedecahydro-1,6-Naphthyridine-6-Carboxylate and (±)- Trans -Ethyl 2-Oxooctahydro-1 H -Pyrrolo[3,2- c] Pyridine-5-Carboxylate. *Acta Crystallogr. Sect.* C *Struct. Chem.* **2014**, 70 (12), 1161–1168.

131 Schwehm, C.; Li, J.; Song, H.; Hu, X.; Kellam, B.; Stocks, M. J. Synthesis of New DPP-4 Inhibitors Based on a Novel Tricyclic Scaffold. *ACS Med. Chem. Lett.* **2015**, 6 (3), 324–328.

132 Schwehm, C.; Kellam, B.; Garces, A. E.; Hill, S. J.; Kindon, N. D.; Bradshaw, T. D.; Li, J.; Macdonald, S. J. F.; Rowedder, J. E.; Stoddart, L. A.; et al. Design and Elaboration of a Tractable Tricyclic Scaffold To Synthesize Druglike Inhibitors of Dipeptidyl Peptidase-4 (DPP-4), Antagonists of the C–C Chemokine Receptor Type 5 (CCR5), and Highly Potent and Selective Phosphoinositol-3 Kinase δ (PI3Kδ) Inhib. *J. Med. Chem.* **2017**, 60 (4), 1534–1554.

133 Miyaura, N.; Yamada, K.; Suzuki, A. A New Stereospecific Cross-Coupling by the Palladium-Catalyzed Reaction of 1-Alkenylboranes with 1-Alkenyl or 1-Alkynyl Halides. *Tetrahedron Lett.* **1979**, 20 (36), 3437–3440.

134 Merck Millipore http://www.merckmillipore.com/GB/en/product/PI-3-Kinase-3-step-HTRF-Assay,MM_NF-33-047?ReferrerURL=https%3A%2F%2Fduckduckgo.com%2F (accessed Dec 2018)

135 Lipinski, C. A.; Lombardo, F.; Dominy, B. W.; Feeney, P. J. Experimental and Computational Approaches to Estimate Solubility and Permeability in Drug Discovery and Development Settings1PII of Original Article: S0169-409X(96)00423-1. The Article Was Originally Published in Advanced Drug Delivery Reviews 23 (1997) 3–25.1. *Adv. Drug Deliv. Rev.* **2001**, 46 (1), 3–26.

136 Lipinski, C. A. Lead- and Drug-like Compounds: The Rule-of-Five Revolution. *Drug Discov. Today Technol.* **2004**, 1 (4), 337–341.

137 Veber, D. F.; Johnson, S. R.; Cheng, H.-Y.; Smith, B. R.; Ward, K. W.; Kopple, K. D. Molecular Properties That Influence the Oral Bioavailability of Drug Candidates. *J. Med. Chem.* **2002**, 45 (12), 2615–2623.

138 Waring, M. J.; Arrowsmith, J.; Leach, A. R.; Leeson, P. D.; Mandrell, S.; Owen, R. M.; Pairaudeau, G.; Pennie, W. D.; Pickett, S. D.; Wang, J.; et al. An Analysis of the Attrition of Drug Candidates from Four Major Pharmaceutical Companies. *Nat. Rev. Drug Discov.* **2015**, 14 (7), 475–486.

139 Scott, J. S.; Waring, M. J. Practical Application of Ligand Efficiency Metrics in Lead Optimisation. *Bioorg. Med. Chem.* **2018**, 26 (11), 3006–3015.

140 Hopkins, A. L.; Groom, C. R.; Alex, A. Ligand Efficiency: A Useful Metric for Lead Selection. Drug Discov. Today **2004**, 9 (10), 430–431.

141 Shultz, M. D. Setting Expectations in Molecular Optimizations: Strengths and Limitations of Commonly Used Composite Parameters. *Bioorg. Med. Chem. Lett.* **2013**, 23 (21), 5980–5991.

142 Leeson, P. D.; Springthorpe, B. The Influence of Drug-like Concepts on Decision-Making in Medicinal Chemistry. *Nat. Rev. Drug Discov.* **2007**, 6, 881.

143 Waring, M. J. Defining Optimum Lipophilicity and Molecular Weight Ranges for Drug Candidates—Molecular Weight Dependent Lower LogD Limits Based on Permeability. *Bioorg. Med. Chem. Lett.* **2009**, 19 (10), 2844–2851.

144 Abad-Zapatero, C.; Metz, J. T. Ligand Efficiency Indices as Guideposts for Drug Discovery. *Drug Discov. Today* **2005**, 10 (7), 464–469.

145 Edwards, M. P.; Price, D. A. Chapter 23 - Role of Physicochemical Properties and Ligand Lipophilicity Efficiency in Addressing Drug Safety Risks; Macor, J. E., Ed.; Annual Reports in Medicinal Chemistry; Academic Press, 2010; Vol. 45, pp 380–391.

146 Hughes, J. D.; Blagg, J.; Price, D. A.; Bailey, S.; DeCrescenzo, G. A.; Devraj, R. V; Ellsworth, E.; Fobian, Y. M.; Gibbs, M. E.; Gilles, R. W.; et al. Physiochemical Drug Properties Associated with in Vivo Toxicological Outcomes. *Bioorg. Med. Chem. Lett.* **2008**, 18 (17), 4872–4875.

147 Young, R. J.; Leeson, P. D. Mapping the Efficiency and Physicochemical Trajectories of Successful Optimizations. *J. Med. Chem.* **2018**, 61 (15), 6421–6467.

148 Murray, C. W.; Erlanson, D. a; Hopkins, A. L.; Keserü, G. M.; Leeson, P. D.; Rees, D. C.; Reynolds, C. H.; Richmond, N. J. Validity of Ligand Efficiency Metrics. *ACS Med. Chem. Lett.* **2014**, 5 (6), 616–618.

149 Hopkins, A. L.; Keserü, G. M.; Leeson, P. D.; Rees, D. C.; Reynolds, C. H. The Role of Ligand Efficiency Metrics in Drug Discovery. *Nat. Rev. Drug Discov.* **2014**, 13 (2), 105–121.

150 Schultes, S.; De Graaf, C.; Haaksma, E. E. J.; De Esch, I. J. P.; Leurs, R.; Krämer, O. Ligand Efficiency as a Guide in Fragment Hit Selection and Optimization. *Drug Discov. Today Technol.* **2010**, 7 (3), 157–162.

151 Lovering, F.; Bikker, J.; Humblet, C. Escape from Flatland: Increasing Saturation as an Approach to Improving Clinical Success. *J. Med. Chem.* **2009**, 52 (21), 6752–6756.

152 Ritchie, T. J.; Macdonald, S. J. F. The Impact of Aromatic Ring Count on Compound Developability - Are Too Many Aromatic Rings a Liability in Drug Design? *Drug Discov. Today* **2009**, 14 (21–22), 1011–1020.

153 Ritchie, T. J.; Macdonald, S. J. F.; Young, R. J.; Pickett, S. D. The Impact of Aromatic Ring Count on Compound Developability: Further Insights by Examining Carbo- and Hetero-Aromatic and -Aliphatic Ring Types. *Drug Discov.* Today **2011**, 16 (3), 164–171.

154 Ritchie, T. J.; Macdonald, S. J. F. Physicochemical Descriptors of Aromatic Character and Their Use in Drug Discovery. *J. Med. Chem.* **2014**, 57 (17), 7206–7215.

155 Axten J. M.; Daines R. A.; Davies D. T.; Gallagher T. F.; Jones G. E.; Miller W. H.; Pearson N. D.; Pendrak I. Piperidine derivatives and pharmaceutically acceptable derivatives thereof useful in methods of treatment of bacterial infections in mammals, particularly in man. WO2004002490 (A2), 08 January 2004.

156 Paul, F.; Patt, J.; Hartwig, J. F. Palladium-Catalyzed Formation of Carbon-Nitrogen Bonds. Reaction Intermediates and Catalyst Improvements in the Hetero Cross-Coupling of Aryl Halides and Tin Amides. *J. Am. Chem. Soc*. **1994**, 116 (13), 5969–5970.

157 Eisenberg, D. Three-Dimensional Structure of Membrane and Surface Proteins. *Annu. Rev. Biochem.* **1984**, 53 (1), 595–623.

158 Ullmann, F.; Bielecki, J. Ueber Synthesen in Der Biphenylreihe. *Berichte der Dtsch. Chem. Gesellschaft* 34 (2), 2174–2185.

159 Promega https://www.promega.co.uk/products/cell-signaling/kinase-assays-and-kinase-biology/pi3k-glo-class-i-profiling-kit/ (accessed December 2018).

160 Nepali, K.; Sharma, S.; Sharma, M.; Bedi, P. M. S.; Dhar, K. L. European Journal of Medicinal Chemistry Rational Approaches , Design Strategies , Structure Activity Relationship and Mechanistic Insights for Anticancer Hybrids. *Eur. J. Med. Chem.* **2014**, 77, 422–487.

161 Huang, R.; Martinez-Ferrando, I.; Cole, P. a. Enhanced Interrogation: Emerging Strategies for *Cell* Signaling Inhibition. *Nat. Struct. Mol. Biol.* **2010**, 17 (6), 646–649.

162 Jörg, M.; May, L. T.; Mak, F. S.; Lee, K. C. K.; Miller, N. D.; Scammells, P. J.; Capuano, B. Synthesis and Pharmacological Evaluation of Dual Acting Ligands Targeting the Adenosine A 2A and Dopamine D 2 Receptors for the Potential Treatment of Parkinson's Disease. *J. Med. Chem.* **2015**, 58 (2), 718–738.

163 Wang, K. K.; Stone, L. K.; Lieberman, T. D.; Shavit, M.; Baasov, T.; Kishony, R. A Hybrid Drug Limits Resistance by Evading the Action of the Multiple Antibiotic Resistance Pathway. *Mol. Biol. Evol.* **2015**, 33 (2), 492-500.

164 Hughes, A. D.; Chen, Y.; Hegde, S. S.; Jasper, J. R.; Jaw-Tsai, S.; Lee, T. W.; McNamara, A.; Pulido-Rios, M. T.; Steinfeld, T.; Mammen, M. Discovery of Batefenterol: First-in-Class Dual Pharmacology Multivalent Muscarinic Antagonist and β2 Agonist (MABA) for the Treatment of Chronic Obstructive Pulmonary Disease (COPD). *J. Med. Chem.* **2015**, 58 (6), 2609–2622.

165 Page, C.; Cazzola, M. Bifunctional Drugs for the Treatment of Asthma and Chronic Obstructive Pulmonary Disease. *Eur. Respir. J.* **2014**, 44 (2), 475–482.

166 Chojnacki, J. E.; Liu, K.; Saathoff, J. M.; Zhang, S. Bivalent Ligands Incorporating Curcumin and Diosgenin as Multifunctional Compounds against Alzheimer's Disease. *Bioorg. Med. Chem.* **2015**, 23 (22), 7324–7331.

167 Kolakowski, R. V.; Haelsig, K. T.; Emmerton, K. K.; Leiske, C. I.; Miyamoto, J. B.; Cochran, J. H.; Lyon, R. P.; Senter, P. D.; Jeffrey, S. C. The Methylene Alkoxy Carbamate Self-Immolative Unit: Utilization for the Targeted Delivery of Alcohol-Containing Payloads with Antibody-Drug Conjugates. *Angew. Chemie* **2016**, 128 (28), 8080–8083.

168 Hamada, Y. Novel Prodrugs with a Spontaneous Cleavable Guanidine Moiety. *Bioorg. Med. Chem. Lett.* **2016**, 26 (7), 1685–1689.

169 Parrott, M. C.; Luft, J. C.; Byrne, J. D.; Fain, J. H.; Napier, M. E.; DeSimone, J. M. Tunable Bifunctional Silyl Ether Cross-Linkers for the Design of Acid-Sensitive Biomaterials. *J. Am. Chem. Soc*. **2010**, 132 (50), 17928–17932.

170 Qiao, Z.-Y.; Zhang, R.; Du, F.-S.; Liang, D.-H.; Li, Z.-C. Multi-Responsive Nanogels Containing Motifs of Ortho Ester, Oligo(Ethylene Glycol) and Disulfide Linkage as Carriers of Hydrophobic Anti-Cancer Drugs. *J. Control. Release* **2011**, 152 (1), 57–66.

171 Liu, R.; Zhang, Y.; Zhao, X.; Agarwal, A.; Mueller, L. J.; Feng, P. PH-Responsive Nanogated Ensemble Based on Gold-Capped Mesoporous Silica through an Acid-Labile Acetal Linker. *J. Am. Chem. Soc*. **2010**, 132 (5), 1500–1501.

172 Vinet, L.; Zhedanov, A. A 'Missing' Family of Classical Orthogonal Polynomials. *J. Phys. A Math. Theor.* **2011**, 44 (8), 085201.

173 Stefano, G. Di; Lanza, M.; Kratz, F.; Merina, L.; Fiume, L. A Novel Method for Coupling Doxorubicin to Lactosaminated Human Albumin by an Acid Sensitive Hydrazone Bond: Synthesis, Characterization and Preliminary Biological Properties of the Conjugate. *Eur. J. Pharm. Sci.* **2004**, 23 (4–5), 393–397.

174 Oishi, M.; Nagasaki, Y.; Itaka, K.; Nishiyama, N.; Kataoka, K. Lactosylated Poly(Ethylene Glycol)-SiRNA Conjugate through Acid-Labile β-Thiopropionate Linkage to Construct PH-Sensitive Polyion Complex Micelles Achieving Enhanced Gene Silencing in Hepatoma-Cells. *J. Am. Chem. Soc*. **2005**, 127 (6), 1624–1625.

175 Jeong, J. H.; Kim, S. W.; Park, T. G. Novel Intracellular Delivery System of Antisense Oligonucleotide by Self-Assembled Hybrid Micelles Composed of DNA/PEG Conjugate and Cationic Fusogenic Peptide. *Bioconjug. Chem.* **2003**, 14 (2), 473–479.

176 Jia, Y.; Fei, J.; Cui, Y.; Yang, Y.; Gao, L.; Li, J. PH-Responsive Polysaccharide Microcapsules through Covalent Bonding Assembly. *Chem. Commun.* **2011**, 47 (4), 1175–1177.

177 Zhao, Y.-L.; Li, Z.; Kabehie, S.; Botros, Y. Y.; Stoddart, J. F.; Zink, J. I. PH-Operated Nanopistons on the Surfaces of Mesoporous Silica Nanoparticles. *J. Am. Chem. Soc*. **2010**, 132 (37), 13016–13025.

178 Patel, V. F.; Hardin, J. N.; Mastro, J. M.; Law, K. L.; Zimmermann, J. L.; Ehlhardt, W. J.; Woodland, J. M.; Starling, J. J. Novel Acid Labile COL1 Trityl-Linked Difluoronucleoside Immunoconjugates: Synthesis, Characterization, and Biological Activity. *Bioconjug. Chem.* **1996**, 7 (4), 497–510.

179 Shin, J.; Shum, P.; Thompson, D. H. Acid-Triggered Release via DePEGylation of DOPE Liposomes Containing Acid-Labile Vinyl Ether PEG–Lipids. *J. Control. Release* **2003**, 91 (1–2), 187–200.

180 Sankaranarayanan, J.; Mahmoud, E. a; Kim, G.; Morachis, M.; Almutairi, A. Multiresponse Strategies To Modulate Burst Degradation and Release from Nanoparticles. **2010**, 4 (10), 5930–5936.

181 Heffernan, M. J.; Murthy, N. Polyketal Nanoparticles: A New PH-Sensitive Biodegradable Drug Delivery Vehicle. *Bioconjug. Chem.* **2005**, 16 (6), 1340–1342.

182 Vaupel, P. Tumor Microenvironmental Physiology and Its Implications for Radiation Oncology. *Semin. Radiat. Oncol.* **2004**, 14 (3), 198–206.

183 Vaupel, P.; Kallinowski, F.; Okunieff, P. Blood Flow, Oxygen and Nutrient Supply, and Metabolic Microenvironment of Human Tumors: A Review. *Cancer Res* **1989**, 49, 6449–6465.

184 Larsen, S. W.; Ankersen, M.; Larsen, C. Kinetics of Degradation and Oil Solubility of Ester Prodrugs of a Model Dipeptide (Gly-Ph*e*). *Eur. J. Pharm. Sci.* **2004**, 22 (5), 399–408.

185 MarvinSketch, 16.5.16.0, ChemAxon, 2016

186 Marsilje, T. H.; Pei, W.; Chen, B.; Lu, W.; Uno, T.; Jin, Y.; Jiang, T.; Kim, S.; Li, N.; Warmuth, M.; et al. Synthesis, Structure–Activity Relationships, and in Vivo Efficacy of the Novel Potent and Selective Anaplastic Lymphoma Kinase (ALK) Inhibitor 5-Chloro- N 2-(2-Isopropoxy-5-Methyl-4-(Piperidin-4-Yl)Phenyl)- N 4-(2-(Isopropylsulfonyl)Phenyl)Pyrimidine-2,4-. *J. Med. Chem.* **2013**, 56 (14), 5675–5690.